



Universitat Autònoma de Barcelona

ADVERTIMENT. L'accés als continguts d'aquesta tesi queda condicionat a l'acceptació de les condicions d'ús establertes per la següent llicència Creative Commons:  http://cat.creativecommons.org/?page_id=184

ADVERTENCIA. El acceso a los contenidos de esta tesis queda condicionado a la aceptación de las condiciones de uso establecidas por la siguiente licencia Creative Commons:  <http://es.creativecommons.org/blog/licencias/>

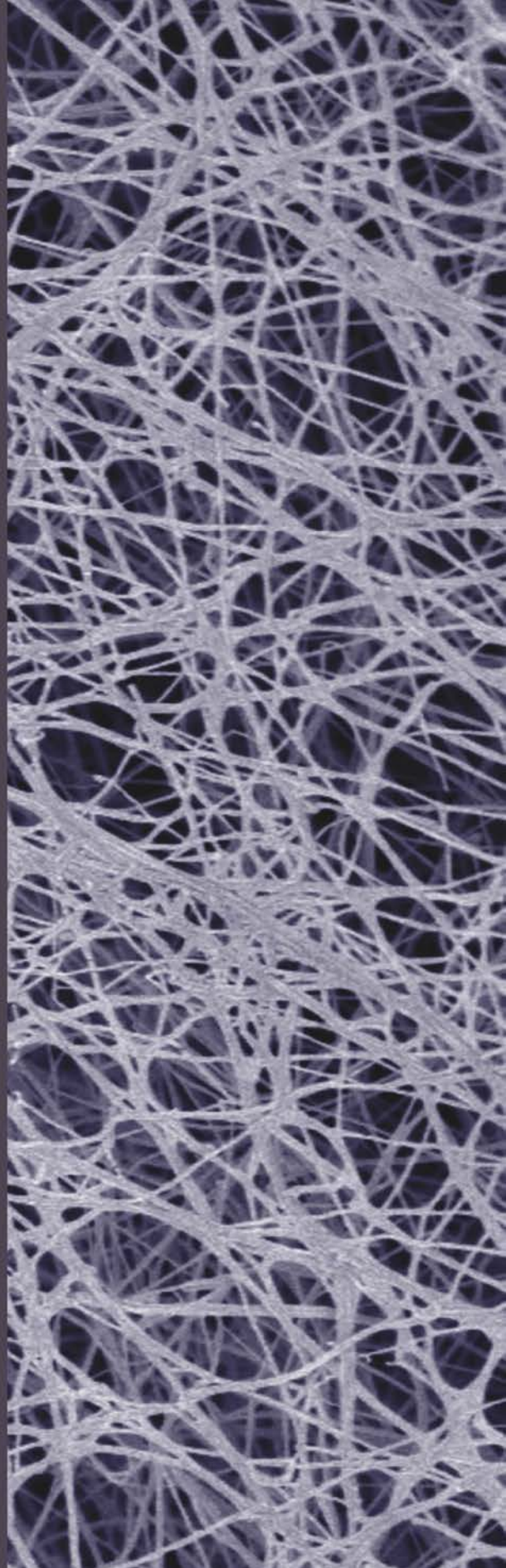
WARNING. The access to the contents of this doctoral thesis it is limited to the acceptance of the use conditions set by the following Creative Commons license:  <https://creativecommons.org/licenses/?lang=en>

Opportunities for bacterial nanocellulose in healthcare

Uses as a cell carrier,
corneal bandage and
tissue reinforcement

Irene Anton-Sales

Doctoral Thesis
2021





Opportunities for bacterial nanocellulose in healthcare.

Uses as a cell carrier, corneal bandage
and tissue reinforcement

Irene Anton-Sales

Doctoral thesis
Doctoral studies in Materials Science

Supervisors: Dr Anna Roig and Dr Anna Laromaine
Tutor: Dr Mercè Capdevila

Departament de Química, Facultat de Ciències
Universitat Autònoma de Barcelona

2021

La **Dra. Anna Roig Serra**, professora d'investigació del CSIC, la **Dra. Anna Laromaine Sagué**, científica titular del CSIC i la **Dra. Mercè Capdevila Vidal** catedràtica de química inorgànica a la UAB

Certifiquen:

Que la **Irene Anton Sales**, graduada en biotecnologia per la Universitat de Barcelona i amb un màster en Recerca Biomèdica per la Universitat Pompeu Fabra ha dut a terme aquesta tesi doctoral sota la seva direcció i que presenta la memòria que porta per títol: "Opportunities for bacterial nanocellulose in helathcare; uses as a cell carrier, corneal bandage and tissue reinforcement" per aspirar al títol de Doctora en Ciència de Materials per la Universitat Autònoma de Barcelona amb menció de Doctorat Internacional.

I perquè així consti, signen el present certificat

Dra. Anna Roig

Dra. Anna Laromaine

Dra. Mercè Capdevila

Bellaterra, 19 d'abril de 2021

Ça fait mé pi pas pi

ROGER FRISON-ROCHE: *Premier de cordée*

A strange expression from the local dialect of Chamonix meaning,
“Obviously, the situation is not the best, but as there is nothing
we can do about it, we must be contented and do our best with it”

Acknowledgements

In 2016, I heard about nanomaterials for the first time in my life. I had never imagined that five years later I would defend my PhD thesis in this subject. By that time, I applied to develop my biomedical research master thesis in the topic of vascular remodelling after stroke at the Vall d’Hebrón Research Institute. Unexpectedly, this project ended up with me, a pure “bio-girl” at that time, preparing polymeric magnetic nanocapsules at the Nanoparticles and Nanocomposites (N&N) group from the Institute of Materials Science of Barcelona (ICMAB), led by Anna Roig. The N&N group kept surprising me when I was offered to continue my education as a PhD candidate. The proposed subject was “bacterial nanocellulose”, a kind of gelatin I had seen around in the lab that apparently had a lot of potential in biomedicine. Now in 2021, I realise that this series of events have shaped my professional identity, giving me the chance to acquire a broad perspective and to become a resourceful researcher. I am sincerely grateful to my supervisors Anna Roig and Anna Laromaine for the opportunity to go through this journey as well as for the freedom to forge my own path. Anna Roig, thank you for being such a great balance between demanding and comprehensive. Anna Laromaine, thank you for all your creative ideas. Big thanks also to all the present and past N&N group members and the rest of ICMABers for the good moments inside and outside the lab. It has been a pleasure to work within such a friendly atmosphere.

This PhD thesis could not have been possible without such fantastic collaborators. Sole, thanks for your non-stop work on keeping our bacterial farm always in good shape. To the SCAC staff, particularly Fran and Olga, huge thanks for your support during my cell culture experiments. I will keep forever with me some of the tricks you showed me. Ralph and Justin, I am deeply grateful to both of you for being the first ones (outside my group) to believe in this project and for introducing me to the exciting world of ophthalmology. Thomas, I am very happy that you have joined “the cornea team”, thanks for keeping me somehow in contact with the lab during this last year. I am also grateful to the other members of the Barraquer clinic, particularly Victor and Jorge, for providing such a valuable clinical perspective. To the Eye Group in Finland goes my sincere gratitude for teaching me how to work with limbal stem cells. Heli, thanks for welcoming me and letting

me be part of your lovely team for a while. Laura, I learnt so much from working with you! Thanks for doing some extra experiments after I left, even if you were on the verge of maternity leave. I also wish to thank the B.Braun researchers, Christine, Kamelia and Pau for their valuable time and for the opportunity to evaluate our materials from a manufacturer's standpoint. Miquel, thanks for your help with "the numbers". Sumi, thanks for all the interesting conversations. Luo, I miss a lot your spontaneity!

Of course, the warm and cheerful atmosphere created by my family, friends and companions of adventures has been crucial for this dissertation; you have been my moral supporters and I feel fortunate for being able to share my free time with you. To my parents, sister and aunties: thank you for your unconditional support and positive energy. To my life-mate Pol: I could not imagine surviving a pandemic and a PhD thesis without you by my side, thanks for being such a wonderful "co-worker". Lluís, I am extremely grateful for your dedication to the layout of this work, you managed to make a 300 page-PhD thesis quite readable!

Finally, I would like to acknowledge the funding received during these years: my PhD scholarship (BE-2017-076734) from the Severo Ochoa Programme for Centres of Excellence in R&D (SEV-2015-0496 and EX2019-000917-S), the Llabor project from AGAUR (2019LLAV00046) that allowed me to broaden my education and the EMBO short-term fellowship (ref 8288) that facilitated my research stay in Finland. Besides, the RTI2018-096273-B-I00 and MAT2015-64442-R projects from the Spanish Ministry of Science and Innovation provided resources for my research.

Attributions

I would like to thank the people that contributed to this thesis:

- Soledad Roig-Sánchez took care of the maintenance of the *K. xylinus* cultures in our lab and provided data about the bacterial nanocellulose/TiO₂ nanocomposites for Publication 2.
- Dr Uwe Beekmann, with whom I worked hand-in-hand in the writing of the review (Publication 1) and Dr Dana Kralisch who reviewed the manuscript.
- All the interviewed experts selflessly shared with me some of their time and knowledge when I was starting this thesis.
- María Jesús Sánchez-Guisado performed the endotoxin tests and initiated the experiments on growth factor delivery from bacterial nanocellulose during her master thesis.
- The master student Natalia Martínez Reyes collaborated in developing the protocol for the controlled delivery of growth factors from bacterial nanocellulose matrices.
- The NANOPTO group from ICMAB allowed me to use their solar simulator for the experiments included in Chapter 2.
- Dr Laura Koivusalo and the rest of the Eye Group members showed me the procedures to culture limbal stem cells. Laura also shared with me her experience with the *ex vivo* corneal organ culture model and conducted some of the immunostainings for Publication 3.
- Dr Justin C. D’Antin –under the supervision of Dr Ralph Michael– organized and conducted with me the experiments with porcine corneas from Publication 4. Justin and Ralph keep involved in the corneal bandage project nowadays.
- Dr Jorge Fernández-Engroba carried out most of the sutures needed for Publication 4 and trained me in the art of suturing.
- Thomas Meslier aided me in the business evaluation of the *Corneal-BNC* project and has been intensively working on the development of bioactive bacterial nanocellulose corneal patches during the last months.
- Kamelia Traeger from B.Braun Surgical performed the mechanical tests from Publication 5.

- Marcos Rosado, from the electron microscopy unit of ICN2, operated the SEM and helped me to interpret the observations of my samples. Marcos is also credited for acquiring the cover image of this thesis.
- The ICMAB technical services: Roberta Ceravola carried out the thermo-gravimetric analysis, the members of the X-ray Diffraction Laboratory acquired the X-ray diffraction patterns of my samples and helped me to interpret the data, Dr Vega Lloveras trained me in spectrophotometric techniques, the technicians from the Scanning Probe Microscopy Laboratory performed the topographical analysis and Dr Judit Oró carried out the TEM analysis.
- Dr Anna May and the team of the Nanoquim Platform of ICMAB helped me with the microwave synthesis.
- Dr Núria Barba and the other members of the microscopy service of UAB thoroughly and patiently trained me in the use of the confocal microscope and the subsequent image analysis.
- The members of SCAC: Fran and Olga taught and assisted me with the cell cultures, Manuela Costa carried out the flow cytometry analysis and Antoni Iborra aided with the plate reader.
- Dr Luis Ruiz from the UPF-Barcelona School of Management guided me through the technology transfer proposal.

Abstract

During the last decades, biomaterials have gained a pivotal role in healthcare, particularly in regenerative medicine. The multidisciplinary field of biomaterials science incessantly innovates towards personalized and bio-interactive platforms able to meet the complex demands of modern medicine. In this framework, biomaterials scientists turn to nature looking for inspiration as well as biofabricated structures to build up the next generation of biomaterials. The recent launch of nanocellulose hydrogels synthesized by bacterial cultures as wound dressings is illustrative of this renewed interest in natural substances intended for medical use. Despite this breakthrough, the potential of bacterial nanocellulose in healthcare remains underexploited as this biological –but animal-free– polymer exhibits a unique combination of properties and unlimited design possibilities.

In this dissertation, novel uses of bacterial nanocellulose in healthcare are investigated. Moreover, we provide insight into the interactions between this emerging biomaterial and a series of biological systems. The doctoral thesis is presented as a compilation of peer-reviewed articles to which I have chiefly contributed. Each of these publications is accompanied by a brief introduction and a critical comment and, occasionally, by unpublished data. Broadly, the thesis is organized in the following sections:

- The *Preface* introduces the general context framing the research and the pursued objectives.
- *Chapter 1* reviews relevant literature related to the use of bacterial nanocellulose to repair diverse tissues and summarizes a series of informative interviews with biomaterial’s end-users.
- *Chapter 2* contains a thorough study on bacterial nanocellulose and bacterial nanocellulose nanocomposites as cryopreservable cell culture supports employing model cells. This section also explores other advanced functionalities of the biomaterials.
- *Chapter 3* describes how bacterial nanocellulose films were conditioned to maintain limbal stem cells cultures, a cell type with high therapeutic potential for ocular surface regeneration.

- *Chapter 4* evaluates bacterial nanocellulose hydrogels as corneal bandages from both a clinical and a commercial perspective.
- *Chapter 5* investigates bacterial nanocellulose patches for tissue reinforcement applications in the context of hernia treatments.
- *Summary* recaps the main findings from the thesis and envisions future horizons.
- The *Annex* includes the *curriculum vitae* of the author and the publications in their original format.

Resum

Durant les últimes dècades, els biomaterials han adquirit un paper decisiu en l'àmbit de la salut, sobretot en el camp de la medicina regenerativa. La recerca en biomaterials engloba coneixements de diferents disciplines i es troba en constant evolució per tal de respondre a les necessitats de la medicina moderna mitjançant solucions personalitzades i bio-interactives. En aquest context, els materials d'origen biològic exerceixen tant de fonts d'inspiració com de punt de partida pel desenvolupament de biomaterials punters. Un bon exemple d'aquesta tendència es troba en la recent entrada al mercat d'apòsits per al tractament de ferides fabricats a partir de nanocel·lulosa d'origen bacterià. Tot i aquest gran avenç, la nanocel·lulosa bacteriana encara té molt de potencial sense explotar en l'àmbit de la salut, ja que aquest polímer biològic (però d'origen no animal) presenta unes propietats molt atractives i infinites possibilitats de modificació.

En aquesta tesi doctoral s'investiguen noves utilitats de la nanocel·lulosa bacteriana en l'àmbit de la salut. En paral·lel, s'aprofundeix en l'estudi de les interaccions entre aquest biomaterial emergent i diversos sistemes biològics. La tesi està presentada com a compendi d'articles acadèmics en els quals l'autora ha tingut un paper fonamental. Cada publicació s'acompanya d'una breu introducció i d'un comentari crític i, ocasionalment, de dades experimentals no publicades. La memòria s'organitza en els apartats següents:

- *Pròleg*: descriu el context general que emmarca aquesta recerca i els objectius de la tesi.
- *Capítol 1*: analitza literatura científica relacionada amb l'ús de la nanocel·lulosa bacteriana per tractar diversos teixits i resumeix una seqüència d'entrevistes fetes a usuaris de biomaterials.
- *Capítol 2*: conté un estudi exhaustiu sobre suports de nanocel·lulosa bacteriana i nanocel·lulosa modificada amb nanopartícules com a plataformes per al cultiu i criopreservació de cèl·lules humanes. Aquesta secció també explora altres funcionalitats dels biomaterials estudiats.
- *Capítol 3*: descriu un mètode per preparar membranes de nanocel·lulosa bacteriana adequades per al cultiu de cèl·lules mare corneals, un tipus

cel·lular amb alt potencial terapèutic en la regeneració de la superfície ocular.

- *Capítol 4:* avalua hidrogels de nanocel·lulosa bacteriana com a nous apòsits corneals tant des d'una perspectiva clínica com comercial.
- *Capítol 5:* investiga malles de nanocel·lulosa bacteriana per a aplicacions de reforç de teixits interns en el context del tractament d'hèrnies abdominals.
- *Resum:* recull les conclusions principals de la tesi i proposa horitzons de futur.
- *Annex:* inclou el currículum de l'autora i les publicacions en el seu format original.

Resumen

Durante las últimas décadas, los biomateriales han jugado un papel decisivo en el ámbito de la salud, especialmente en la medicina regenerativa. La investigación en biomateriales requiere conocimientos de distintos campos y está en constante evolución buscando satisfacer las necesidades de la medicina moderna a través de soluciones personalizadas y bio-interactivas. En este contexto, los materiales de origen biológico se han convertido tanto en fuente de inspiración como en la base para el desarrollo de numerosos biomateriales innovadores. Un buen ejemplo de esta tendencia se encuentra en la reciente entrada en el mercado de vendajes para el tratamiento de heridas fabricados a partir nanocelulosa de origen bacteriano. A pesar de este avance, la nanocelulosa bacteriana todavía tiene mucho potencial sin explotar en el ámbito de la salud, ya que este material biológico (pero de origen no animal) posee propiedades muy atractivas e infinitas posibilidades de modificación.

En esta tesis doctoral se investigan nuevos usos de la nanocelulosa bacteriana en el ámbito de la salud. Al mismo tiempo, se profundiza en el estudio de las interacciones entre este biomaterial emergente y múltiples sistemas biológicos. La tesis se presenta como un compendio de artículos académicos en los que la autora ha desempeñado un papel fundamental. Cada publicación se complementa con una breve introducción y un comentario crítico y, ocasionalmente, con datos experimentales no publicados. La memoria se organiza en los siguientes apartados:

- *Prólogo*: describe el contexto general que enmarca la investigación y los objetivos de la tesis.
- *Capítulo 1*: analiza literatura científica reciente relacionada con el uso de la nanocelulosa bacteriana para tratar diversos tejidos y resume una serie de entrevistas con usuarios de biomateriales.
- *Capítulo 2*: contiene un estudio exhaustivo sobre soportes de nanocelulosa bacteriana y nanocelulosa modificada con nanopartículas como plataformas para el cultivo y criopreservación de células humanas. Esta sección también explora otras funcionalidades de los biomateriales estudiados.
- *Capítulo 3*: describe un método para modificar membranas de nanocelulosa con el fin de facilitar el cultivo de células madre corneales, un tipo

celular con gran potencial terapéutico para la regeneración de la superficie ocular.

- *Capítulo 4:* evalúa hidrogeles de nanocelulosa bacteriana como nuevos apósitos corneales tanto desde una perspectiva clínica como comercial.
- *Capítulo 5:* investiga mallas de nanocelulosa bacteriana para aplicaciones de refuerzo de tejidos internos en el contexto del tratamiento de hernias.
- *Resumen:* incluye las principales conclusiones de la tesis y propone horizontes de futuro.
- *Anexo:* contiene el currículum de la autora y las publicaciones en su formato original.

Glossary

3D	Three-Dimensional
ACS	American Chemical Society
AFM	Atomic Force Microscopy
Ag	Silver
AGAUR	Agència de Gestió d'Ajuts Universitaris i de Recerca
AIDS	Acquired Immuno-Deficiency Syndrome
AM	Amniotic Membrane
ANOVA	ANalysis OfVAriance
API	Active Pharmaceutical Ingredient
ATMP	Advanced Therapy Medicinal Product
ATP	Adenosine TriPhosphate
BC/AA	Bacterial Cellulose/Acrylic acid
BC/COL	Bacterial Cellulose/Collagen
BC/HA	Bacterial Cellulose/Hyaluronic Acid
BC/PCL	Bacterial Cellulose/ PolyCaproLactone
BC	Bacterial Cellulose
BCNC	Bacterial Cellulose NanoCrystals
BNC	Bacterial NanoCellulose
BNC-PP	Bacterial NanoCellulose-PolyPropylene
BSA	Bovine Serum Albumin
CE	Conformité Européenne
CECT	Colección Española de Cultivos Tipo
CGC	Critical Gelation Concentration
CK	Cyto Keratin
CMC (1)	Carboxy Methyl Cellulose
CMC (2)	Critical Micelle Concentration
COB	Centro de Oftalmología Barraquer
Col IV	Collagen IV
CSIC	Consejo Superior de Investigaciones Científicas
Ct	Control
CV	Curriculum Vitae
DAPI	4',6-DiAmidino-2-PhenyIndole di-hydrochloride
DI	DeIonized
DMARD	Disease-Modifying Anti-Rheumatic Drug
DMEM	Dulbecco's Modified Eagle Medium

DMSO	DiMethyl SulfOxide
DNA	Deoxyribo Nucleic Acid
DPBS	Dulbecco's Phosphate Buffered Saline
DS	Degree of Substitution
ECM	Extra Cellular Matrix
EDTA	Ethylene Diamine Tetra-acetic Acid
EDX	Energy-Dispersive X-ray
EMA	European Medicines Agency
EMBO	European Molecular Biology Organization
EtOx	Ethylene Oxide
EU (1)	European Union
EU (2)	Endotoxin Units
FBS	Foetal Bovine Serum
FDA	Food and Drug Administration
FEDER	Fons Europeu de DEsenvolupament Regional
GMPs	Good Manufacturing Practises
HA	Hyaluronic Acid
HBSS	Hank's Balanced Salt Solution
HE	Haematoxylin-Eosin
HEMA	2-HydroxyEthylMethAcrylate
hESC	human Embryonic Stem Cells
hESC-LSC	human Embryonic Stem Cells-derived Limbal Stem Cells
hiPSC	human-induced Pluripotent Stem Cells
hPSC	human Pluripotent Stem Cells
HS	Hestrin-Schramm
ICMAB	Institut de Ciència de MAterials de Barcelona
ICN2	Catalan Institute of Nanoscience and Nanotechnology
ICP-OES	Inductively Coupled Plasma – Optical Emission Spectroscopy
IOBA	Instituto Universitario de OftalmoBiología Aplicada
<i>K. xylinus</i>	<i>Komagataeibacter xylinus</i>
kV	Kilovolt
LAL	Limulus Amebocyte Lysate
LB	Luria-Bertani
LN-521	Laminin-521
LSC	Limbal Stem Cells
M	Molar
MD	Medical Device
Min	Minutes

MQ	Milli-Q
MTT	3-(4,5-diMeThylThiazol-2-yl)-2,5-diphenyltetrazolium bromide
MTX	MeThotreXate
N&N	Nanoparticles and Nanocomposites
N	Newton
N:C ratio	Nuclear-Cytoplasmic ratio
nA	Nano-ampere
NaOH	Sodium hydroxide
NPs	NanoParticles
OEPM	Oficina Española de Patentes y Marcas
PBS	Phosphate Buffered Saline
PCL	PolyCaproLactone
PFA	ParaFormAldehyde
PHEMA	Poly (2-HydroxyEthyl MethAcrylate)
PI	Propidium Iodide
PP	PolyPropylene
PVA	PolyVinyl Alcohol
R+D	Research and Development
RC	Regenerated Chitin
ROCK	Rho-associated coiled-coil containing protein kinase
RPE	Retinal Pigment Epithelium
RSC	Royal Society of Chemistry
RT	Room Temperature
S.A.U.	Sociedad Anónima Unipersonal
SAED	Selected Area Electron Diffraction
SC	Super Critical
SCAC	Servei de Cultius Cel·lulars, Producció d'Anticossos i Citometria
SEM (1)	Scanning Electron Microscope
SEM (2)	Standard Error of the Mean
SMN	Flavonoid Silymarin
SWOT	Strengths, Weaknesses, Opportunities and Threats
TEM	Transmission Electron Microscopy
TEMPO	2,2,6,6-TEtraMethylPiperidine 1-Oxyl radical
TGA	Thermo-Gravimetric Analysis
TiO ₂	Titanium dioxide
TM	Tympanic Membrane
TOBCP	TEMPO-Oxidized Bacterial Cellulose Pellicle
TRL	Technology Readiness Level

TT	Technology Transfer
UAB	Autonomous University of Barcelona
UDPG	Uranyl Diphosphate-Glucose
UPF	Pompeu Fabra University
USA	United States of America
UV	Ultra Violet
UV-Vis-NIR	Ultra Violet-Visible-Near InfraRed
W	Watt
WHO	World Health Organization
XRD	X-Ray Diffraction
ε-PLL	ε-Poly-L-Lysine

Table of contents

• Acknowledgements	IX
• Attributions	XI
• Abstract / Resum / Resumen	XIII
• Glossary	XIX
• Preface: Context and objectives of the PhD thesis	1
o Regenerative medicine	3
o Biomaterials	5
o Polymeric biomaterials	6
o Emerging trends in biomaterials	8
o Cellulosic biomaterials	10
o Bacterial nanocellulose	11
o Objectives of the thesis	15
o Chapter references	16
• Chapter 1: Identifying opportunities for BNC in healthcare	21
o Chapter introduction	23
o Publication 1: Opportunities of Bacterial Cellulose to Treat Epithelial Tissues	25
o On-site interviews with experts	52
o Contributions to the field and critical comment	60
o Chapter references	62
• Chapter 2: Evaluating BNC and BNC/TiO₂ nanocomposites as cell carriers with sunscreen capacity	71
o Chapter introduction	73
o Publication 2: Bacterial Nanocellulose and Titania Hybrids: Cytocompatible and Cryopreservable Cell Carriers	75
o Additional functionality tests of BNC and BNC/TiO ₂ as photo-protectant and antimicrobial agents	101
o Contributions to the field and critical comment	107
o Chapter references	109
• Chapter 3: Bacterial nanocellulose carriers for limbal stem cells	115
o Chapter introduction	117
o Publication 3: Limbal Stem Cells on Bacterial Nanocellulose Carriers for Ocular Surface Regeneration	120
o Preliminary trials on the cryobanking of BNC/LSC constructs	144
o Contributions to the field and critical comment	147
o Chapter references	148
• Chapter 4: Bacterial nanocellulose as a corneal bandage: technical feasibility and business proposal	153
o Chapter introduction	155
o Publication 4: Bacterial Nanocellulose as a Corneal Bandage Material: Comparison with Amniotic Membrane	157

- o Business proposal for the *Corneal-BNC* project 180
 - o Contributions to the field and critical comment 187
 - o Chapter references 189
- **Chapter 5: *In vivo* evaluation of bacterial nanocellulose for hernia repair** 195
 - o Chapter introduction 197
 - o Publication 5: *In vivo* Soft Tissue Reinforcement with Bacterial Nanocellulose 199
 - o Contributions to the field and critical comment 221
 - o Chapter references 223
- **Summary: conclusions and outlook** 227
 - o Conclusions 229
 - o Outlook 232
- **Annex: *Curriculum Vitae* and publications** 235

Preface

Context and objectives of the PhD thesis

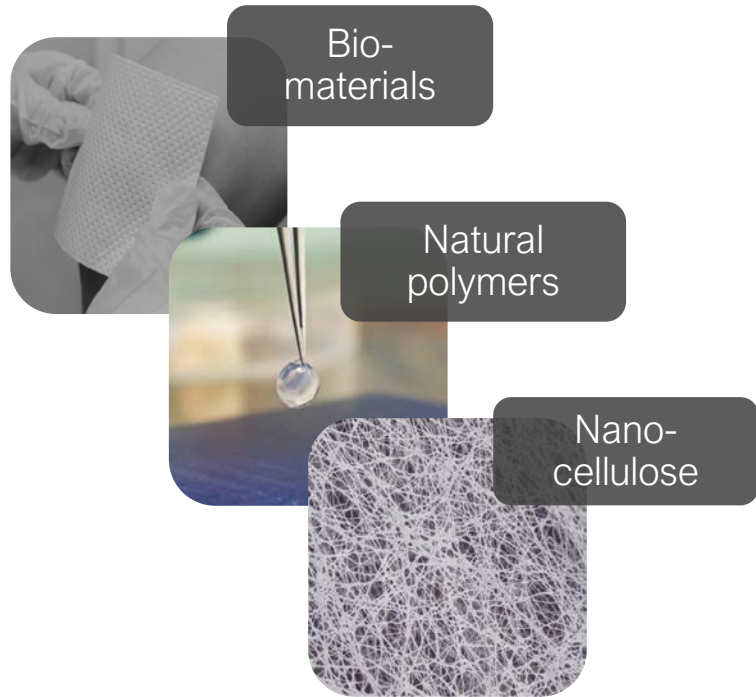


Figure 1: Graphical summary of the general context of the PhD thesis.

Regenerative medicine

Regeneration is described as “the process of growing again”. Regenerative capacity varies dramatically along the animal kingdom being inversely proportional to the level of complexity. While invertebrates like planarians and *Hydra* are able to restore entire organs, humans can only rebuild by natural means the epidermis and small parts of the liver and intestines¹. Current demographic trends toward older populations aggravate this situation as regenerative capability further declines with age.

Interest and concerns about the ageing process are documented since far in the past² and have led humankind to explore procedures to repair deteriorated parts of the body that could not be restored only with medication. Interestingly, attempts of reconstructive interventions *e.g.* dental and bone prosthesis as well as skin grafts, are reported since ancient times³. Nevertheless, it was not until the implementation of aseptic techniques, antibiotics and anaesthesia during the XIX and XX centuries that evidence-based biomedicine was established. The first cell cultures and organ transplants date back to the 1950s and 1960s respectively³. Later, the environment surrounding the cells *i.e.* the extracellular matrix (ECM) was acknowledged as a relevant player in regenerative processes. In 1981, John F. Burke and Ioannis V. Yannas pioneered the use of collagen scaffolds to treat burns and developed the product Integra®⁴.

Embryonic stem cells derived from human blastocysts were characterized in 1998⁵. James A. Thomson and colleagues advocated human stem cells as an extremely powerful tool for basic biological research and envisioned cell transplantation therapies to replace dysfunctional cell populations. The term “regenerative medicine” was coined in 1999 when William Haseltine employed this expression to group several emerging technologies directed to restore lost body functions: tissue engineering, stem cell transplantation and gene therapies among others⁶. Accordingly, regenerative medicine is currently considered an interdisciplinary field aiming at repairing, replacing or regenerating body parts (cells, tissues or organs) with an impaired function due to diseases, trauma or ageing as well as to normalize congenital conditions⁷. The ultimate goal of regenerative medicine is instructing the body to return to its original homeostasis by fostering the natural regenerative capacity of cells and tissues.

In the XXI century, the advancement of regenerative medicine has experienced staggering progress thanks to a huge global scientific effort. However, two remarkable breakthroughs deserve to be singled out; the first 3D bioprinter created in 2003 by Thomas Boland and the reprogramming of somatic cells back to stem cells in 2006 by Shin'ya Yamanaka and co-workers⁸. A timeline of events that hugely influenced the development of regenerative medicine is presented in Figure 2 for better contextualization.

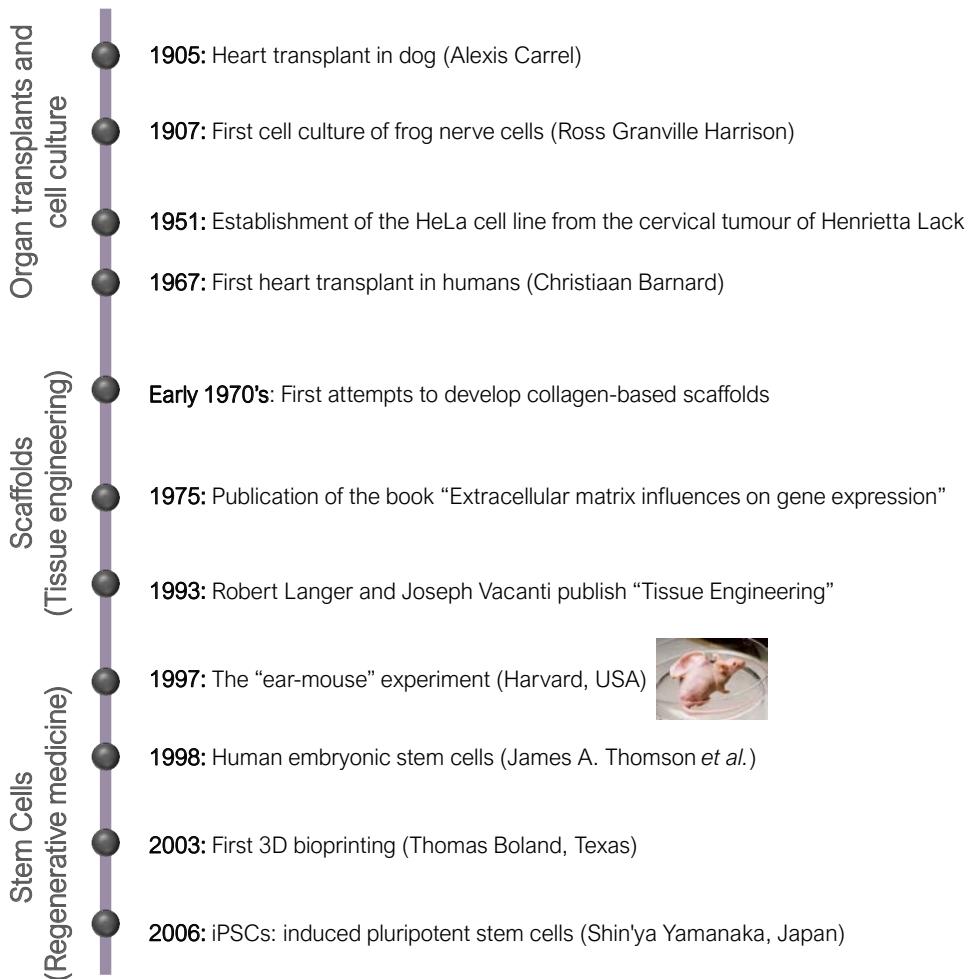


Figure 2: Timeline of remarkable breakthroughs that shaped the development of regenerative medicine.

The widespread implementation of regenerative medicine should no longer be considered just a utopia. It is expected that regenerative approaches will contribute towards healthier ageing, reduced reliance on transplants and more satisfactory recovery after injuries. Naturally, there are still complex scientific challenges to address. Some of them relate to better recapitulating native tissues and organs, modulating the interactions between the bioengineered constructs and the host immune system and developing more bio-interactive solutions^{7,9}. Other obstacles to consider are the high costs usually associated with these therapies and the cumbersome fabrication routes.

Biomaterials

Biomaterials are a fundamental element of regenerative medicine. Biomaterials are utilized alone or in combination with other elements to evaluate, treat, augment, or replace tissues and organs. Despite biomaterials were initially devised to serve mainly structural purposes, they have acquired a high relevance in current regenerative treatments^{10,11}. Illustrative of that is the rapidly growing global market of biomaterials projected to reach \$47.5 billion by 2025 from \$35.5 billion in 2020 at an annual growth rate of 6%¹². Up-to-date biomaterials seek to actively stimulate regeneration by interacting with native tissues. In line with this, stimuli-responsive biomaterials able to react upon temperature or pH variations are under intense investigation, especially for delivery purposes^{13,14}.

Biomaterials can be attained from countless natural and synthetic sources but they must be both functional and biocompatible. Besides, biomaterial's characteristics, mechanical properties and surface chemical moieties among others need to be accurately selected to match the needs of the target tissue and pathology¹⁵. As for implantable biomaterials, another important consideration refers to the degradability rate inside the human body. Frequently, tissue-engineering constructs, *e.g.* collagen scaffolds, are expected to degrade relatively fast leaving no toxic by-products¹⁶. However, there are other circumstances where non-resorbable or slowly degradable options would be preferred. These cases include prosthesis, sutures and surgical meshes^{17,18}.

Medical devices (MD) are generally the final structures where a biomaterial is incorporated. According to the World Health Organization (WHO), a medical device is “any instrument, apparatus, machine, appliance, implant, reagent, software, material or similar intended to be used, alone or in combination, in humans for medical purposes”. In Europe, MDs are stringently regulated by the European Medicines Agency (EMA) and must be CE marked following the recently reviewed 2017/745 regulation. From a regulatory perspective, biomaterials and MDs can also be part of Advanced Therapy Medicinal Products (ATMP) if they are combined with genes, tissues or cells. In the case of combined ATMP, the evaluation procedure is based on Regulation (EC) No 1394/2007.

Polymeric biomaterials

Owing to the vast diversity of biomaterials, the present contextualization is narrowed to polymeric biomaterials and more specifically to naturally sourced polymers. The word "polymer" means "many parts". As such, polymers are high-molar-mass substances formed by chemically reacted monomers. Together with ceramics and metals, polymers are one of the main categories of biomaterials and are generally the preferred option for soft tissue (skin, cartilage, blood vessels, epithelium, eye...) repair. A broad spectrum of natural, synthetic or hybrid polymers have been proposed for biomedical uses in virtually any speciality¹⁹; drug carriers²⁰, cell scaffolds²¹, bio-adhesives²² or surgical implants¹³, to name a few. Even though synthetic polymers are experiencing a fast development^{23,24}, naturally-occurring polymers (a.k.a. biopolymers) are still considered advantageous in terms of biocompatibility and renewability^{25,26}.

Biopolymers

Natural polymers are defined as those that can be found in nature and/or are extracted from plants, animals or other biological sources; the main categories being

polynucleotides, proteins and polysaccharides. The last two have a strong presence in regenerative treatments and some examples are listed in Table 1.

The 3D microenvironment where the cells naturally reside is the ECM. This acellular structure –essentially composed of water, proteins and polysaccharides– serves both as physical support and as a biochemical and biomechanical regulator by constantly exchanging signals with the resident cells²⁷. Due to its ubiquitous presence in biological tissues, ECM components have been extensively harnessed by biomaterials researchers²⁸. Undoubtedly, collagen-based biomaterials dominate the clinically used solutions for skin reconstruction²⁹ while hyaluronic acid (HA) stands out as a lubricating agent and heparin as a linker for growth factors and other molecules^{30,31}. Besides, chitosan and silk are other natural polymers experiencing high popularity as biomaterials²⁶. Chitosan appears as an attractive option because of its abundance and low price allied with an inherent antibacterial activity³². The high mechanical resistance and environmental stability of silk have positioned this natural fibrous material as a great fit for suture manufacturing and more recently silk-made scaffolds have also irrupted in tissue engineering^{33,17}. More information about natural polymers is provided in the next chapter (Publication 1).

Table 1: Commonly used natural polymers in biomedicine, its sources and applications.

Substance name and type	Source	Application examples
Collagen <i>Structural protein</i>	Animal tissues, recombinant	<ul style="list-style-type: none"> • Skin regeneration: Integra®, Matriderm® • Cell culture substrates: PureCol®
Gelatin <i>Protein</i>	Denatured collagen	<ul style="list-style-type: none"> • Haemostatic sponge: Gelfoam® • Cell culture coatings (many options)
Fibrin <i>Blood protein</i>	Animal or human tissues	<ul style="list-style-type: none"> • Sealants: Tissucol® • Cell carriers: Holoclar®
Silk fibroin <i>Fibrous protein</i>	Synthesized by arthropods (spider or silkworm)	<ul style="list-style-type: none"> • Sutures: Perma-Hand® • Microneedles: Ipsylon®
Hyaluronic acid <i>Glycosaminoglycan</i>	Animal tissues, recombinant	<ul style="list-style-type: none"> • Ophthalmic solutions: Ocular Bandage Gel®, Hylo-Vision® • Cell culture substrates: HyStem®

Substance name and type	Source	Application examples
Chitosan <i>Polysaccharide</i>	Crustacean exoskeletons, fungi	<ul style="list-style-type: none"> • Haemostatic patch: (HemCon™) • Soft implant/lubricant: KioMedine®
Alginate <i>Polysaccharide + sodium or calcium</i>	Algae	<ul style="list-style-type: none"> • Wound dressing gels: Phytacare® • Exudating wound dressing sponges: Activheal®
Gellan gum <i>Polysaccharide</i>	Bacterial fermentation	<ul style="list-style-type: none"> • Commercial cosmetic products • Gelrite®: investigated as ocular drug delivery³⁴ • Culture media for microorganisms and plants
Cellulose <i>Polysaccharide</i>	Plants/wood, microorganisms	<ul style="list-style-type: none"> • Wound dressing: Reoxcare® • Cell culture substrates: Grow-Dex® • Resorbable haemostat: Surgicel® (oxidized regenerated cellulose³⁵)

Emerging trends in biomaterials

Aside from the above-mentioned stimuli-responsive biomaterials, two growing tendencies closely related to the scope of this PhD thesis are the nature-inspired designs and the willingness to reduce animal-derived products in medical formulations.

Emulating nature

An overarching trend in current biomaterial research is the attempt to emulate nature a.k.a. biomimetics or biologically-inspired designs³⁶. Hydrogels –water-swollen networks of polymers– have proven suitable for this purpose since they exhibit similarities with native tissues in terms of water content, porosity and physicochemical properties. Thus, hydrogels are largely exploited as biomaterials^{37–39} and hydrogel-based cell culture platforms –like the well-known

Matrigel®– are employed *in vitro* to better recapitulate physiological conditions, as opposed to flat plastic surfaces⁴⁰. Notably, most of the above-mentioned natural polymers can easily be attained in stable hydrogel formats, and this has also boosted its attractiveness as medical materials⁴¹.

On the other hand, accumulated evidence emphasises the critical role of topographical signals in modulating cell responses and maintaining homeostasis^{42–44}. Consequently, emulating the physical cues of the ECM represents another driving force of biomimetic designs. In the ECM, collagen fibrils exhibit a nanometric diameter⁴⁵ and, combined with the water-retaining proteoglycans, form a reticulated structure with specific micro and nanoscale features that scientists have tried to recapitulate^{46,47}. To this end, nanofibrous substrates have been fabricated by replica moulding⁴⁸ and electrospinning⁴⁹. Electrospun biomaterials have shown a high degree of morphological biomimicry⁵⁰ that –allied with the versatility and simplicity of the method⁵¹– situated electrospinning as a principal strategy in biomimetic matrix manufacturing for the last decades.

Towards animal-free treatments

Reducing the current dependency on animal-derived goods concerns many fields. The industrial sector (*e.g.* food and cosmetics) is starting a transition to offer customers animal-free alternatives to traditional products. Similarly, the research community increasingly relies on microfluidic organ-on-a-chip models to evaluate their discoveries reducing the number of test animals⁵². Moreover, human-based animal-free full-thickness skin⁵³ and blood⁵⁴ models are under investigation to better emulate native conditions in preclinical studies.

As for medical biomaterials, minimizing animal products has implications beyond animal welfare and environmental concerns. Animal-derived substances are considered potential immunogens and disease transmitters^{55,56} and therefore must be meticulously scrutinized to comply with safety requirements⁵⁷. For clinical manufacturing, particularly in the field of cell therapies, well-specified compositions and traceable components are in high demand owing to their superior translatability^{58,59}. Thus, clinical-grade reagents are increasingly being harvested

from recombinant bacterial cultures as alternatives to traditional undefined and less-reproducible animal-derived components, *e.g.* foetal serum⁶⁰. As a response to this demand, the market offers already biomimetic, animal origin-free cell culture substrates based on recombinant technologies (*e.g.* Biolaminin™). Similarly, natural but animal origin-free options (*i.e.* fungal chitosan⁶¹, gellan gum⁶² and cellulose⁶³ among others) emerge as promising starting materials for biomaterial development.

Cellulosic biomaterials

Among the palette of emergent biomaterials, cellulose represents one of the most versatile and widely available choices. Cellulose is a linear β -glucose-only polysaccharide synthesized predominantly by plants but also by some animals (tunicates) and microorganisms (oomycetes and acetic acid bacteria), making it one of the most abundant organic compounds in the biosphere. Cellulose differentiates from other glucose carbohydrates (*e.g.* starch) because the monosaccharide units are linked through β -1,4 glycosidic bonds. This β configuration implies that the consecutive β -glucose units are rotated 180° to each other forming long and stable chains. Cellulose organizes hierarchically; monomer chains interact laterally with one another through hydrogen bonds creating insoluble fibrillary structures of increasing diameter and high tensile strength.

Cellulose derivatives have been closely related to human development for millennia (Figure 3). Humankind has used cellulose as a building material for papyrus (Egypt) and paper (China) since antique times, and there is evidence of cotton cloths in the Indus River Valley (Pakistan) from ~3.000 years BC. More recently, environmental awareness has brought a renewed interest in cellulose. This eco-friendly and almost inexhaustible polymer is enjoying popularity to manufacture biodegradable packaging^{64,65}. However, for the fabrication of some added value goods, like medical-grade materials, the presence of impurities (*i.e.* hemicellulose or lignin) and low mechanical stability of common cellulose derivatives are detrimental. This has encouraged research on purified and sturdy forms of cellulose like nanocelluloses⁶⁶, *i.e.* cellulosic materials with one dimension in the

nanoscale. Nanocelluloses synergistically integrate cellulose's and nanomaterial's properties, particularly relevant being the high surface area conferred by the nano-dimensions of the fibres.

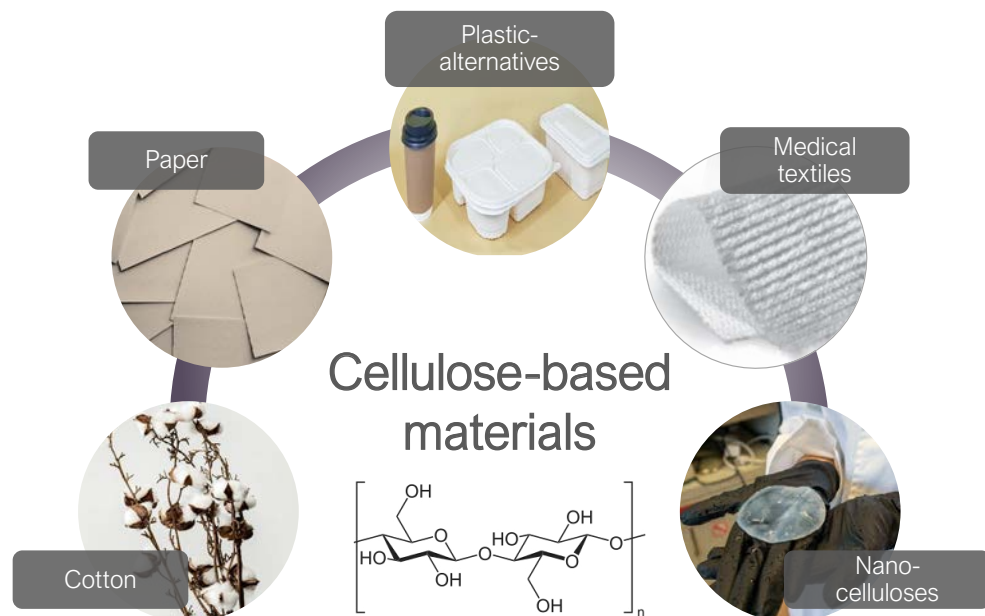


Figure 3: The versatility of cellulose (the chemical formula is shown) is demonstrated by the long-lasting utilities of this material in diverse fields. The bottom right image depicts bacterial nanocellulose produced in our lab. Figure 3 contains adapted content from <https://unsplash.com>.

Bacterial nanocellulose

Differing from the top-down methods to extract nanocellulose from biomass, nanocellulose can be readily obtained from bacterial cultures in a bottom-up approach. The first report on this phenomenon dates from 1886 when A. J. Brown observed a “jelly-like translucent mass on the surface of the culture fluid”⁶⁷. This spontaneous biofabrication method has long been harnessed in the traditional cuisine of Southeast Asia to prepare a dessert named *nata de coco* that is also commercialized worldwide (Figure 4, left). Bacterial nanocellulose (BNC) is secreted by ubiquitous Gram-negative non-pathogenic acetic acid bacteria upon the fermentation of glucose or other carbon sources. The metabolic pathway for BNC

biosynthesis is detailed in the next chapter. *Komagataeibacter xylinus* (*K. xylinus*), previously known as *Acetobacter xylinum*, is one of the most exploited species for BNC harvesting and is the strain employed through this work.

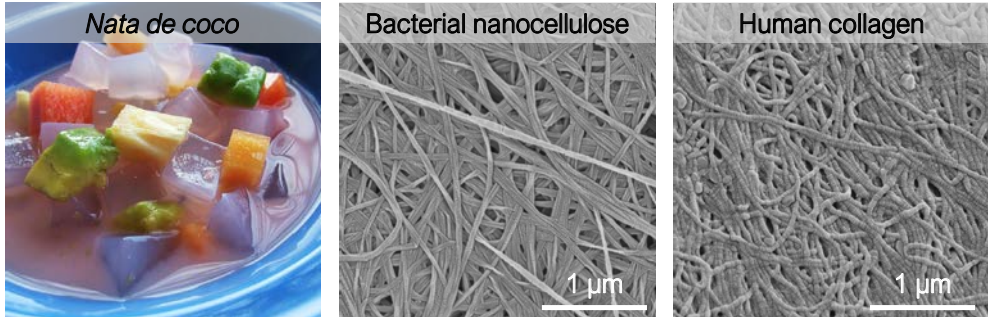


Figure 4: Left: BNC obtained from the fermentation of coconut milk is used to prepare sweet dishes in Southeast Asia, mainly in the Philippines. Middle: BNC is formed exclusively by a reticulated structure of cellulose nanofibers arranged in an ECM-mimetic manner. Right: for comparative purposes, human collagen from the amniotic membrane with an analogous nanofiber organization is depicted.

Properties and uses of BNC

BNC stands out for its unique attributes; some of them are gathered in Figure 5. Most of these features arise from the nano-organization of the BNC fibres, which differentiates BNC from vegetal cellulose despite their common chemical composition. The BNC fibres exhibit elevated molecular weight and crystallinity as well as a high surface area able to retain large amounts of liquid (>99% weight). Such interlaced nano-architecture is stabilized by hydrogen bonds which confer robustness and mechanical resistance while providing flexibility and softness to the biopolymer⁶⁸. Another key characteristic of BNC is its biocompatibility, associated both with its chemical purity and biomimetic organization^{69,70}. Numerous reports emphasize the morphological similarities between nanocellulose and collagen in the ECM in terms of fibre diameter and unorganized distribution (see Figure 4 for illustrative SEM images). These resemblances could be related to the fact that both compounds serve structural purposes in their respective origins⁷¹. The biotechnological origin of BNC enables size, shape and topographical control over the attained materials offering unlimited tailoring opportunities.

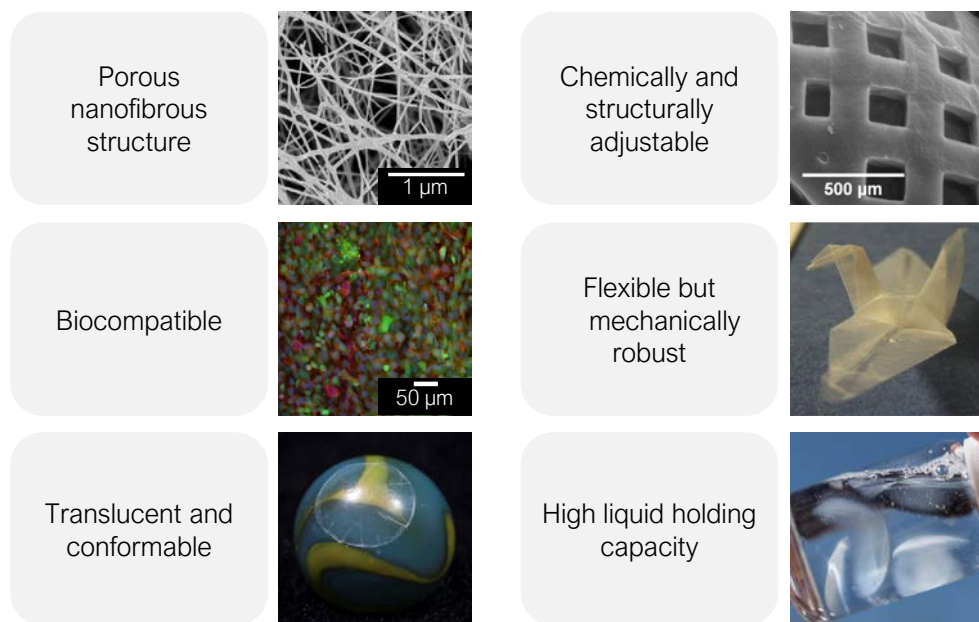


Figure 5: The hallmarks of BNC. Some of the most relevant properties positioning BNC as an appealing candidate for varied biomedical uses.

Another differential trait of BNC refers to its thermal stability. Remarkably, the high temperature resistance of BNC allows sterilization by autoclave (121 °C) and many chemical modifications like the microwave reactions (190 °C) employed in this thesis for BNC functionalization. On the other hand, BNC is also compatible with low-temperature storage methods, a property that is exploited in this work too.

This combination of qualities made BNC an ideal nanomaterial for skin regeneration and prompted an extensive investigation on BNC-based wound healing^{72,73} that has already materialized in commercial BNC wound dressings (e.g. Suprasorb X from Lohmann&Rausche). Nevertheless, the possibilities of this biopolymer can be broadened in a variety of directions to serve other biomedical purposes⁷⁴ as described in the first publication from this compendium.

From a fabrication standpoint, there has been a great deal of innovation too. Rühls and co-workers developed an original method, based on surface roughening and poly-dopamine coating, to grow and immobilize BNC directly on the surface of macroscopic objects envisioning lubricating coatings for implants⁷⁵. Similarly, 3D printing of living materials was accomplished by embedding *K. xylinus* cells

in a hyaluronic acid, κ -carrageenan and fumed silica ink used to attain complex 3D BNC architectures⁷⁶. Other enticing living materials were obtained upon co-culturing genetically engineered yeasts and cellulose-extruding bacteria⁷⁷. Since *Saccharomyces cerevisiae* is a model organism with many accessible genetic modification options, BNC pellicles could be readily functionalized with an array of recombinant proteins endowing the grown living materials with biosensing and bioremediation applicability.

The described general context, from the growing demand for innovating personalized solutions in modern medicine to the novel BNC design routes, settles the basis for a future new wave of BNC-based biomaterials. Moreover, the animal-free, sustainable and simple biofabrication of this nanomaterial could bear competitive advantages over other emerging biomaterials. Accordingly, application-oriented studies on BNC are considered a highly attractive research topic.

Objectives of the thesis

The major goal of the present doctoral thesis is to broaden the applicability landscape of BNC in the healthcare sector. By doing so I seek to contribute towards the advancement of biomaterial-based treatments offering innovative (nano) biotechnological options. More specifically, I aimed at:

1. Identifying niche applications of BNC in biomaterial-enabled regenerative medicine (Publication 1).
2. Gaining insights into the interactions between BNC and human cells and leveraging BNC as a cell carrier for cell transplantation therapies (Publications 2 and 3).
3. Evaluating BNC in clinically relevant settings addressing specific unmet medical needs; namely assessing BNC as an ocular surface bandage and as an anti-adhesive barrier in hernia repair. (Publications 4 and 5).

Chapter references

1. Zhao, A., Qin, H. & Fu, X. What Determines the Regenerative Capacity in Animals? *Bioscience* **66**, 735–746 (2016).
2. Thane, P. What is ‘regeneration’ and who needs it? *Palgrave Commun.* **4**, 8–11 (2018).
3. Marin, E., Boschetto, F. & Pezzotti, G. Biomaterials and biocompatibility: An historical overview. *J. Biomed. Mater. Res. - Part A* **108**, 1617–1633 (2020).
4. Burke, J. F., Yannas, O. V., Quinby, W. C., Bondoc, C. C. & Jung, W. K. Successful use of a physiologically acceptable artificial skin in the treatment of extensive burn injury. *Ann. Surg.* **194**, 413–427 (1981).
5. Thomson, J. A. *et al.* Embryonic stem cell lines derived from human blastocysts. *Science*. **282**, 1145–1147 (1998).
6. Sampogna, G., Guraya, S. Y. & Forgione, A. Regenerative medicine: Historical roots and potential strategies in modern medicine. *J. Microsc. Ultrastruct.* **3**, 101–107 (2015).
7. Mao, A. S. & Mooney, D. J. Regenerative medicine: Current therapies and future directions. *Proc. Natl. Acad. Sci. U. S. A.* **112**, 14452–14459 (2015).
8. Takahashi, K. & Yamanaka, S. Induction of Pluripotent Stem Cells from Mouse Embryonic and Adult Fibroblast Cultures by Defined Factors. *Cell* **126**, 663–676 (2006).
9. Uludag, H. Grand Challenges in Biomaterials. *Front. Bioeng. Biotechnol.* **2**, 43 (2014).
10. HORIZON 2020. *Biomaterials for Health: A Strategic Roadmap for Research and Innovation.* (2020).
11. Huebsch, N. & Mooney, D. J. Inspiration and application in the evolution of biomaterials. *Nature* **462**, 426–432 (2009).
12. MarketsandMarkets. Biomaterials Market – Global Forecast to 2025. *Market research report* (2021). Available at: <https://www.marketsandmarkets.com/Market-Reports/biomaterials-393.html>. (Accessed: 19th February 2021)
13. Lanzalaco, S. *et al.* Toward the New Generation of Surgical Meshes with 4D Response: Soft, Dynamic, and Adaptable. *Adv. Funct. Mater.* **30**, 2004145 (2020).
14. Miotto, M. *et al.* 4D Corneal Tissue Engineering: Achieving Time-Dependent Tissue Self-Curvature through Localized Control of Cell Actuators. *Adv. Funct. Mater.* **29**, 1807334 (2019).
15. D’Este, M. *et al.* Bone Regeneration with Biomaterials and Active Molecules Delivery. *Curr. Pharm. Biotechnol.* **16**, 582–605 (2015).
16. Rafat, M. *et al.* Composite core-and-skirt collagen hydrogels with differential degradation for corneal therapeutic applications. *Biomaterials* **83**, 142–155 (2016).
17. Altman, G. H. *et al.* Silk based biomaterials. *Biomaterials* **24**, 401–416 (2003).
18. De Miguel, I. *et al.* Plasmon-Based Biofilm Inhibition on Surgical Implants. *Nano Lett.* **19**, 2524–2529 (2019).

19. Vasile, C., Pamfil, D., Stoleru, E. & Baican, M. New developments in medical applications of hybrid hydrogels containing natural polymers. *Molecules* **25**, 1539 (2020).
20. Zhang, Y. *et al.* PLGA protein nanocarriers with tailor-made fluorescence/MRI/PET imaging modalities. *Nanoscale* **12**, 4988–5002 (2020).
21. Perez-Puyana, V., Jiménez-Rosado, M., Romero, A. & Guerrero, A. Polymer-based scaffolds for soft-tissue engineering. *Polymers (Basel)*. **12**, 1–21 (2020).
22. Repka, M. *et al.* Formulation and In Vitro Evaluation of Xanthan Gum or Carbopol 934-Based Mucoadhesive Patches, Loaded with Nicotine. *AAPS PharmSciTech* **12**, 1 (2011).
23. Mahdavi, A. *et al.* A biodegradable and biocompatible gecko-inspired tissue adhesive. *Proc. Natl. Acad. Sci. U. S. A.* **105**, 2307–2312 (2008).
24. Sorkio, A. *et al.* Surface modified biodegradable electrospun membranes as a carrier for human embryonic stem cell derived retinal pigment epithelial cells. *Tissue Eng. - Part A* **21**, 2301–2314 (2015).
25. Dieckmann, C., Renner, R., Milkova, L. & Simon, J. C. Regenerative medicine in dermatology: biomaterials, tissue engineering, stem cells, gene transfer and beyond. *Exp. Dermatol.* **19**, 697–706 (2010).
26. Chen, Z. *et al.* Biomaterials for corneal bioengineering. *Biomed. Mater* **13**, 032002 (2018).
27. Frantz, C., Stewart, K. M. & Weaver, V. M. The extracellular matrix at a glance. *J. Cell Sci.* **123**, 4195–4200 (2010).
28. Mogoşanu, G. D. & Grumezescu, A. M. Natural and synthetic polymers for wounds and burns dressing. *Int. J. Pharm.* **463**, 127–136 (2014).
29. MacNeil, S. Biomaterials for tissue engineering of skin. *Mater. Today* **11**, 26–35 (2008).
30. Seal, B. L., Otero, T. C. & Panitch, A. Polymeric biomaterials for tissue and organ regeneration. *Mater. Sci. Eng. R Reports* **34**, 147–230 (2001).
31. K, Y., Liang & L., K. Heparin-functionalized polymeric biomaterials in tissue engineering and drug delivery applications. *Acta Biomater.* **10**, 1588–1600 (2014).
32. Yilmaz Atay, H. Antibacterial activity of chitosan-based systems. in *Functional Chitosan* 457–489 (2020). doi:10.1007/978-981-15-0263-7_15
33. Wang, Y. *et al.* A Biomimetic Silk Fibroin/Sodium Alginate Composite Scaffold for Soft Tissue Engineering. *Sci. Rep.* **6**, 39477 (2016).
34. Liu, Y. *et al.* In situ gelling Gelrite/alginate formulations as vehicles for ophthalmic drug delivery. *AAPS PharmSciTech* **11**, 610–620 (2010).
35. Hutchinson, R. W. *et al.* Hemostatic efficacy and tissue reaction of oxidized regenerated cellulose hemostats. *Cellulose* **20**, 537–545 (2013).
36. Vincent, J. F.V, Bogatyreva, O. A., Bogatyrev, N. R., Bowyer, A. & Pahl, A.-K. Biomimetics: its practice and theory. *J. R. Soc. Interface* **3**, 471–482 (2006).

37. Shirzaei Sani, E. *et al.* Sutureless repair of corneal injuries using naturally derived bioadhesive hydrogels. *Sci. Adv.* **5**, 1281 (2019).
38. Bhat, S. & Kumar, A. Biomaterials in Regenerative Medicine. *J. Postgrad. Med. Educ. Res.* **46**, 81–89 (2012).
39. Ahearne, M., Fernández-Pérez, J., Masterton, S., Madden, P. W. & Bhattacharjee, P. Designing Scaffolds for Corneal Regeneration. *Adv. Funct. Mater.* **30**, 1908996 (2020).
40. Caliari, S. R. & Burdick, J. A. A practical guide to hydrogels for cell culture. *Nat. Methods* **13**, 405–414 (2016).
41. Koivusalo, L. *et al.* Tissue adhesive hyaluronic acid hydrogels for sutureless stem cell delivery and regeneration of corneal epithelium and stroma. *Biomaterials* **225**, 119516 (2019).
42. Xiong, S., Gao, H., Qin, L., Jia, Y.-G. & Ren, L. Engineering topography: Effects on corneal cell behavior and integration into corneal tissue engineering. *Bioact. Mater.* **4**, 293–302 (2019).
43. Geisel, N. *et al.* Microstructured Multilevel Bacterial Cellulose Allows the Guided Growth of Neural Stem Cells. *Small* **12**, 5407–5413 (2016).
44. Reversat, A. *et al.* Cellular locomotion using environmental topography. *Nature* **582**, 582–585 (2020).
45. Kadler, K. E., Baldock, C., Bella, J. & Boot-Handford, R. P. Collagens at a glance. *J. Cell Sci.* **120**, 1955–1958 (2007).
46. Haycock, J. W. *3D cell culture: a review of current approaches and techniques. Methods in molecular biology (Clifton, N.J.)* **695**, (2011).
47. Tavakol, S., Jalili-Firoozinezhad, S., Mashinchian, O. & Mahmoudi, M. *Bioinspired Nanotechnologies for Skin Regeneration. Nanoscience in Dermatology* (2016). doi:10.1016/B978-0-12-802926-8.00026-4
48. Kim, H. N. *et al.* Nanotopography-guided tissue engineering and regenerative medicine. *Adv Drug Deliv Rev* **65**, 536–558 (2013).
49. Sachot, N. *et al.* Towards 4th generation biomaterials: a covalent hybrid polymer–ormoglass architecture. *Nanoscale* **7**, 15349–15361 (2015).
50. Liu, L. *et al.* Nanofibrous gelatin substrates for long-term expansion of human pluripotent stem cells. *Biomaterials* **35**, 6259–6267 (2014).
51. Nguyen, K. N. *et al.* Native and synthetic scaffolds for limbal epithelial stem cell transplantation. *Acta Biomater.* **65**, 21–35 (2018).
52. Musah, S. *et al.* Mature induced-pluripotent-stem-cell-derived human podocytes reconstitute kidney glomerular-capillary-wall function on a chip. *Nat Biomed Eng* **1**, 0069 (2017).
53. Mieremet, A., Rietveld, M., Van Dijk, R., Bouwstra, J. A. & El Ghalbzouri, A. Recapitulation of Native Dermal Tissue in a Full-Thickness Human Skin Model Using Human Collagens. *Tissue Eng. - Part A* **24**, 873–881 (2018).

54. Messerer, D. A. C. *et al.* Animal-Free Human Whole Blood Sepsis Model to Study Changes in Innate Immunity. *Front. Immunol.* **11**, 1–12 (2020).
55. Zeide, D.A. Adverse reactions to collagen implants. *Clin. Dermatol.* **4**, 176–182 (1986).
56. Requena, L. *et al.* Adverse reactions to injectable soft tissue fillers. *J. Am. Acad. Dermatol.* **64**, 1–34 (2011).
57. Ausubel, L. J., Lopez, P. M. & Couture, L. A. GMP Scale-Up and Banking of Pluripotent Stem Cells for Cellular Therapy Applications. in *Human Pluripotent Stem Cells* **11**, 147–159 (2011).
58. Martin, M. J., Muotri, A., Gage, F. & Varki, A. Human embryonic stem cells express an immunogenic nonhuman sialic acid. *Nat. Med.* **11**, 228–232 (2005).
59. Swistowski, A. *et al.* Xeno-free defined conditions for culture of human embryonic stem cells, neural stem cells and dopaminergic neurons derived from them. *PLoS One* **4**, e6233 (2009).
60. Tjin, M. S. *et al.* Biologically relevant laminin as chemically defined and fully human platform for human epidermal keratinocyte culture. *Nat. Commun.* **9**, (2018).
61. D’Almeida, M. *et al.* Chitosan coating as an antibacterial surface for biomedical applications. *PLoS One* **12**, 1–11 (2017).
62. Learmonth, D. A. *et al.* Synthesis and biological evaluation of a bioinspired, tissue-Adhesive gellan gum-based hydrogel designed for minimally invasive delivery and retention of chondrogenic cells. *Biomater. Sci.* **8**, 3697–3711 (2020).
63. Tronser, T., Laromaine, A., Roig, A. & Levkin, P. A. Bacterial Cellulose Promotes Long-Term Stemness of mESC. *ACS Appl. Mater. Interfaces* **10**, 16260–16269 (2018).
64. Narancic, T. & O’Connor, K. E. Plastic waste as a global challenge: Are biodegradable plastics the answer to the plastic waste problem? *Microbiology* **165**, 129–137 (2019).
65. Yang, J., Chee Ching, Y. & Hock Chuah, C. Applications of Lignocellulosic Fibers and Lignin in Bioplastics: A Review. *Polymers (Basel)*. **11**, 751 (2019).
66. Klemm, D. *et al.* Nanocelluloses: A new family of nature-based materials. *Angew. Chemie - Int. Ed.* **50**, 5438–5466 (2011).
67. Brown, A. J. On an acetic ferment which forms cellulose. *J. Chem. Soc., Trans.* **49**, 432–439 (1886).
68. Czaja, W. K., Young, D. J., Kawecky, M. & Brown, R. M. The future prospects of microbial cellulose in biomedical applications. *Biomacromolecules* **8**, 1–12 (2007).
69. Helenius, G. *et al.* In vivo biocompatibility of bacterial cellulose. *J. Biomed. Mater. Res. - Part A* **76**, 431–438 (2006).
70. Abeer, M. M., Mohd Amin, M. C. I. & Martin, C. A review of bacterial cellulose-based drug delivery systems: Their biochemistry, current approaches and future prospects. *J. Pharm. Pharmacol.* **66**, 1047–1061 (2014).

71. Petersen, N. & Gatenholm, P. Bacterial cellulose-based materials and medical devices: Current state and perspectives. *Appl. Microbiol. Biotechnol.* **91**, 1277–1286 (2011).
72. Czaja, W., Krystynowicz, A., Bielecki, S. & Brown, R. M. Microbial cellulose – The natural power to heal wounds. *Biomaterials* **27**, 145–151 (2006).
73. Kwak, M. H. *et al.* Bacterial cellulose membrane produced by *Acetobacter* sp. A10 for burn wound dressing applications. *Carbohydr. Polym.* **122**, 387–398 (2015).
74. Carvalho, T., Guedes, G., Sousa, F. L., Freire, C. S. R. & Santos, H. A. Latest Advances on Bacterial Cellulose-Based Materials for Wound Healing, Delivery Systems, and Tissue Engineering. *Biotechnol. J.* **14**, e1900059 (2019).
75. Rühls, P. A. *et al.* Conformal Bacterial Cellulose Coatings as Lubricious Surfaces. *ACS Nano* **14**, 3885–3895 (2020).
76. Schaffner, M., Rühls, P. A., Coulter, F., Kilcher, S. & Studart, A. R. 3D printing of bacteria into functional complex materials. *Sci. Adv.* **3**, eaao6804 (2017).
77. Gilbert, C. *et al.* Living materials with programmable functionalities grown from engineered microbial co-cultures. *Nat. Mater.* (2021). doi:10.1038/s41563-020-00857-5

Chapter 1

Identifying opportunities for BNC in healthcare



Figure 1: Graphical summary of Chapter 1. Two complementary activities to identify novel medical applications of BNC.

Chapter introduction

The library of materials addressed to the healthcare sector is extensive and assorted. Some biomaterials, such as stents or intraocular lens, play already a vital role in modern medicine; while many others are in advanced stages of development¹⁻³. In such a competitive landscape, detecting specific unmet clinical needs is a complex but essential task when investigating emerging biomaterials like BNC. Therefore, the starting point of this thesis was the identification of application niches in the healthcare sector where BNC could have a competitive edge. Medical applications of BNC mainly spin around patch-like formats intended for wound healing⁴, drug delivery⁵ or repairing soft tissue defects⁶ all having in common a direct contact with epithelial tissues.

The graph in Figure 2 displays the number of scientific publications related to BNC over time. It reflects a steadily growing research interest in this biopolymer, particularly in recent years. Suggested applications of BNC in biomedicine appeared later in the literature, following the seminal work by Fontana *et al.* 1990⁷, and since then have experienced a sharp rise. Accordingly, the first step to identify attractive bio-applications of BNC was an extensive literature search, narrowing our search to usages of BNC related to epithelial regeneration. The insights extracted from this work were captured in a review paper (Publication 1), written in collaboration with the researchers Dr Uwe Beekmann and Dr Dana Kralisch from the Friedrich Schiller University (Jena, Germany) and included in this chapter.

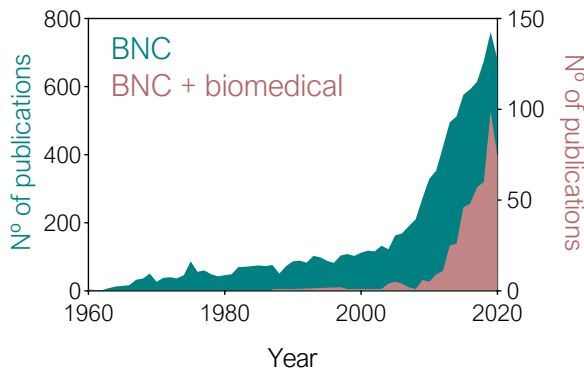


Figure 2: Number of publications in the PubMed database for the search by the keywords “bacterial cellulose” (BNC in green in the graph) and the combination of keywords “bacterial cellulose” AND “biomedical” (BNC+ biomedical in pink) reflecting the growing interest in this biopolymer. The search was performed on 15th January 2021.

On the other hand, we are aware that some unmet clinical needs might be difficult to identify in the scientific literature. Thus, in trying to gain direct insights from the end-users of biomaterials, a parallel strategy was followed; a cohort of local experts –medical doctors, translational medicine researchers and industry workers– was contacted. Those specialists willing to participate in the initiative were on-site interviewed and inquired about their assessments regarding possible applications of BNC in their diverse fields of expertise. The outputs from the set of interviews I conducted comprise the second part of this chapter.

Publication 1: Opportunities of Bacterial Cellulose to Treat Epithelial Tissues

Irene Anton-Sales[‡], Uwe Beekmann[‡], Anna Laromaine, Anna Roig and Dana Kralisch. *Curr. Drug Targets* 20, 808–822 (2019). Published by Bentham Science Publishers (open access). [‡] = authors with equal contribution, note that this publication was also included in the doctoral dissertation of Uwe Beekmann at the Friedrich Schiller University Jena.

<https://www.eurekaselect.com/167837/article>

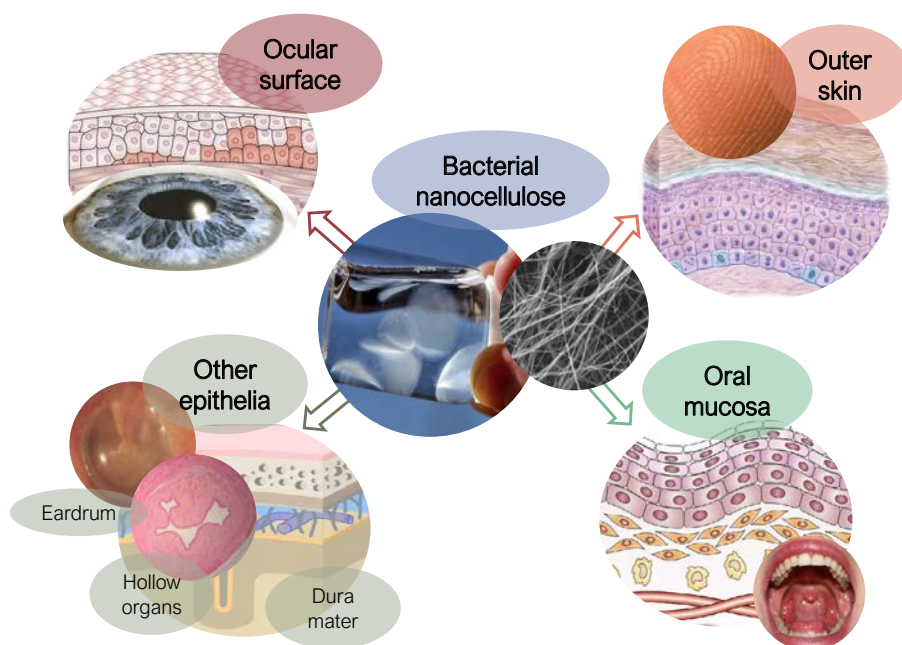


Figure 3: Graphical abstract of Publication 1. Several epithelial surfaces where BNC has been therapeutically applied.

Keywords

Biomaterials, bacterial cellulose, epithelial tissues, wound dressing, cell carrier, drug delivery, epithelial regeneration

Abstract

In this mini-review, we highlight the potential of the biopolymer bacterial cellulose to treat damaged epithelial tissues. Epithelial tissues are continuous cell sheets that delimitate both the external body surfaces and the internal cavities and organs. Epithelia serve as physical protection to underlying organs, regulate the diffusion of molecules and ions, secrete substances and filtrate body fluids among other vital functions. Because of their continuous exposure to environmental stressors, damage to epithelial tissues is highly prevalent.

Here, we first compare the bacterial cellulose properties to the current gold standard, collagen, and then we examine the use of bacterial cellulose patches to heal specific epithelial tissues; the outer skin, the ocular surface, the oral mucosa and other feasible epithelial surfaces. Special emphasis is made on the dermis since, to date, this is the most widespread medical use of bacterial cellulose. It is important to note that some epithelial tissues represent only the outermost layer of complex structures such as the skin or the cornea. In these situations, depending on the penetration of the lesion, bacterial cellulose might also be involved in the regeneration of, for instance, inner connective tissue.

1. Introduction

Epithelial tissues are, essentially, continuous cell sheets that delimitate both the external body surfaces and the internal cavities of organs. Epithelia have a reduced content of extracellular matrix and exhibit strong cell-to-cell adhesions known as tight junctions. Epithelial tissues are not vascularized and receive support from the underlying basement membrane formed by connective tissue. Examples of epithelial tissues are the external linings of the skin, cornea and mouth but also those from the hollow internal organs such as lungs, digestive system, urogenital conducts and spinal cord. Depending on its location in the body, epithelia can be found as single (*e.g.*, intestines, lungs) or multiple cell layers (*e.g.*, skin, cornea, and oesophagus). The glandular epithelium that surrounds the glands in our body is a highly specialized epithelium that will not be addressed here. In this manuscript,

we have used “epithelial tissue” as an umbrella term to refer to diverse body surfaces and barriers.

Epithelial structures physically protect the underlying tissues, regulate the diffusion of molecules and ions, secrete substances and filtrate body fluids among other vital functions. Because of their surface location, epithelia are constantly exposed to environmental stressors ranging from infections caused by microorganisms and mechanical injuries to the exposure to toxic chemicals. Moreover, epithelial tissues are also greatly affected by inflammatory diseases and cancers. Despite the extraordinary regenerative capacity of epithelial tissues, they can be overwhelmed by large-area injuries, surgical scissions, burns or ulcers which result in chronic lesions⁸. Additionally, diabetes, infectious processes, systemic and chronic treatments or other pathological conditions can make epithelial regeneration less efficient⁹. In these specific cases, the use of biomaterials to assist the regeneration of sensitive epithelia becomes vital.

Biomaterials represent a core element of regenerative therapies and are used in multiple ways to treat epithelial defects. Biomaterials are designed to interface with biological systems to evaluate, treat, increase or replace tissues, organs or functions in the body (European Society for Biomaterials, 2nd Consensus Conference on Definition, 1991). The palette of available biomaterials is extensive being polymers, ceramics and metals the main categories. Ceramics and metals are indicated for bioengineering load-bearing structures and are out of the focus of this mini-review. Polymeric biomaterials are often classified into synthetic and natural polymers according to its origin. Because of its superior biocompatibility and bioactivity, naturally occurring polymers (*e.g.* collagen, fibrin, chitosan, keratin, silk, alginate, cellulose) are frequently used for repairing epithelial tissues. Biomaterials based on natural polymers can serve as transitory treatments like wound coverages¹⁰, temporary skin substitutes¹¹, carriers for cell therapy^{12,13} and drug delivery platforms^{14,15} as well as long-term replacements for damaged epithelial tissues^{16,17}.

Despite the broad spectrum of natural polymers and natural-natural¹⁸ or natural-synthetic¹⁹ composites that are being investigated for epithelial regeneration, currently, the main clinical procedures rely on collagen-based solutions²⁰. Collagen is a fibrous structural protein that forms triple helix assemblies; it is a major

constituent of the extracellular matrix and inherently bioactive and biocompatible. It is therefore understandable that collagen has long been considered the gold standard to repair organs and tissues (skin, cornea, oral mucosa etc.) exposed to the environment. Collagen is primarily obtained from livestock sources like cow, pig, rat and more recently also from fish²¹ and typically needs extensive manipulation before attaining the final product. One of the main drawbacks of animal collagen is its moderate immunogenicity²² and its high batch-to-batch variability. On the other hand, religious constraints against animal-derived medical products have also played a role²³. Production of recombinant collagen in bacteria or plants²⁴ can help to overcome these issues but the production is still far from meeting the worldwide increasing collagen demand²⁵. Last but not least, the mechanical properties and degradation kinetics of collagen do not always meet clinical requirements. Thus, novel biomaterials able to fulfil the enormous diversity of conditions and patients' needs are required.

Third generation natural biomaterials are expected to be biocompatible as well as to foster the regeneration of damaged tissues. To achieve this, researchers are screening not only alternative biopolymers²⁶ but also novel architectures of already well-known natural materials²⁷. In line with this, nanostructured biomaterials, typically in the form of nanofibrous hydrogels, have recently attracted much attention²⁸⁻³⁰. Nanostructuring can endow biomaterials with high surface area to volume ratios, enhance cell attachment and proliferation; mechanical stability and adequate porosity³¹. Such nanostructured substrates can be fabricated by electrospinning³². For instance, electrospinning has already allowed forming gelatin and gelatin-alginate nanofibers with improved mechanical properties compared to unstructured hydrogels³³. Silk fibroin electrospun nanomaterials showed reduced inflammation and faster re-epithelization in a rat burn model compared to conventional treatments³⁴. These authors partially ascribed the over-performance of the nanostructured wound dressing to the nanoscale dimensions of the fibres that accurately mimic the properties of soft tissues and retain certain amounts of liquid.

A lesser explored family of natural biopolymers with potential applicability in epithelial regeneration are nanocelluloses³⁵. The term "nanocellulose" refers to cellulose-based materials with at least one dimension in the nanoscale. Nano-

celluloses can be subdivided into bacterial cellulose (BC), cellulose nanofibrils (CNF) and cellulose nanocrystals (CNC). CNF and CNC are commonly obtained from plant/wood cellulose after mechanical and/or chemical treatments and BC is biotechnologically produced by microorganisms using different carbon sources³⁶. The three types of nanocellulose have been proposed for a diversity of medical and/or pharmaceutical applications. Regarding plant-derived nanocellulose hydrogels, recent encouraging applications include renewable and xeno-free wound dressings for skin graft donor sites³⁷ as well as controlled drug release platforms for both low and high molecular weight substances³⁸. As an alternative to CNC and CNF, cellulose produced by microorganisms is emerging as a promising natural source of ready-to-use nanocellulose for medical and pharmaceutical applications.

2. Bacterial cellulose

BC is produced extracellularly by Gram-negative bacterial cultures such as *Glucanacetobacter*, *Acetobacter*, *Agrobacterium*, *Achromobacter*, *Aerobacter*, *Sarcina*, *Azobacter*, *Rhizobium*, *Pseudomonas*, *Salmonella* and *Alcaligenes*. Among them, the most efficient BC producer belongs to the *Komagataeibacter* genus, specifically called *Komagataeibacter xylinus* (*K. xylinus*)^{39,40}. The observation that *Acetobacter xylinus* produces a gelatinous mass on liquid/air interfaces has been known since 1886 by the work of A. J. Brown⁴¹. This gelatinous mass was later identified as BC. The bacterium uses the nanofibrous film to protect itself from environmental stresses such as dehydration, nutrient deficiency and UV radiation. In addition, the BC allows the bacteria to float and to remain at the interface between medium and air thus increasing oxygen supply.

BC can conveniently be produced in laboratories following the process summarized in Figure 4. The biosynthesis starts with the inoculation of a culture medium with a BC-producing bacteria strain (Figure 4 [A]). A typical culture medium contains the following compounds: 2% (w/v) glucose, 0.5% (w/v) yeast extract, 0.5% (w/v) peptone, 0.3% (w/v) sodium hydrogen phosphate and 0.1% (w/v) citric acid (Hestrin-Schramm (HS) culture medium)⁴². At the molecular level, the bi-

osynthesis of BC in the microorganism can be divided into four sub-steps (Figure 4 [B]). First, phosphorylation of glucose by a glucokinase occurs (a) in the nucleus, followed by isomerization of glucose-6-phosphate to glucose-1-phosphate (b). Finally, it reacts with UDPG-pyrophosphorylase to form uranyl diphosphate-glucose (UDPG) (c), followed by the synthesis of BC by cellulose synthase (d). The last step in the cytoplasm is chain growth at the reduced end of the β -1,4-glucan chains by UDPG to form cellulose fibres⁴³.

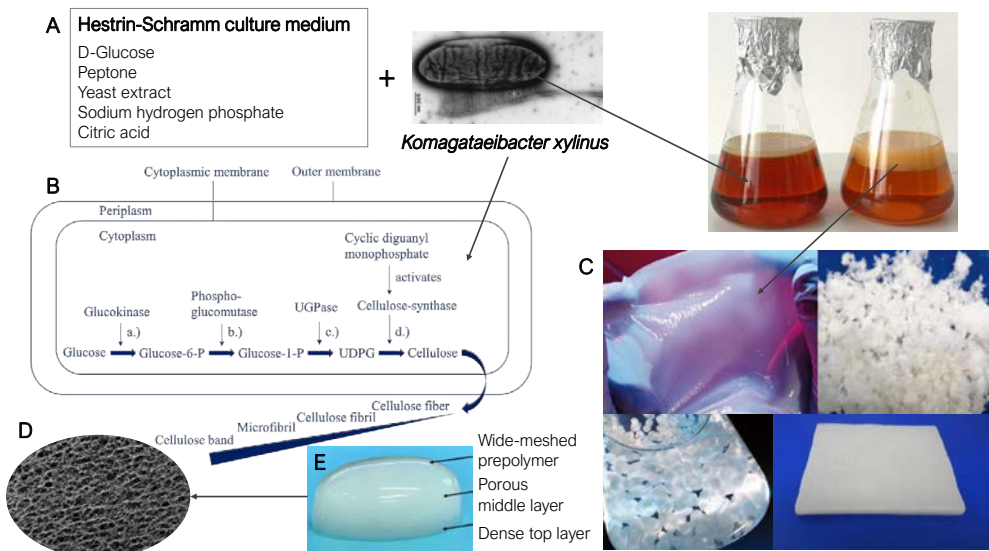


Figure 4. Schematic representation of the basic BC generation process steps. A) Formation process of BC fleece during cultivation of *K. xylinus* in HS medium in Erlenmeyer flasks. B) Metabolic pathway of cellulose formation. C) Different shapes of possible BC production. D) Scanning electron microscopy picture of BC porous middle layer depicting its three-dimensional fibre network. E) Layered structure of a BC pellicle.

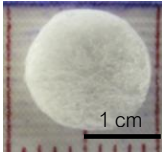
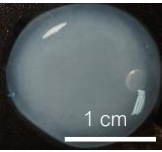
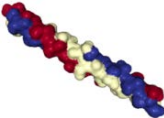
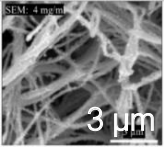
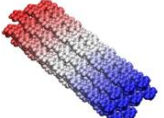
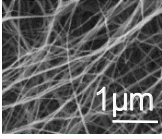
The as-synthesized BC membranes exhibit unique properties proving its adequacy for epithelial regeneration purposes such a high degree of polymerization (4,000 – 10,000)³⁵ and crystallization (up to 90%)⁴⁶. For medical applications, the high mechanical stability, the lack of immunogenicity and the high purity are of particular relevance^{45,47}. The biocompatibility of BC cannot solely be attributed to the high purity of the material but also to its similar organization of the fibres as in native collagen⁴⁸. Despite the identical chemical structure of BC and plant-based cellulose⁴⁹, BC clearly defines itself by its structure and material properties. The

three-dimensional interwoven network of BC is characterized by a high surface area of 35 – 40 m²/g (measured in the freeze-dried form)^{50,51} and a water content of about 99%⁵². The latter characteristic is the reason why BC is also called a “hydropolymer” or “hydrogel”⁴⁶. Moreover, BC exhibits high temperature stability which allows temperature sterilization processes⁵³.

Last but not least, the attractiveness of this innovative biofabricated material has further increased due to its animal and human-free origin⁵⁴. Its biosynthesis opens up the opportunity to develop biotechnological production to significantly influence and control the final BC shape and material features. Shapes, specially designed to come into contact with epithelial tissue, range from thin foils and fleeces used as covering, patch or dressing, tubes for artificial blood vessels⁵⁵ to preformed structures for implantation (*e.g.*, artificial meniscus⁵³ and ear cartilage replacement⁵⁶). In recent years, enormous progress in BC cultivation techniques has been made to provide tailored-made and high-quality BC-based materials. In parallel, the possibility to scale up BC production may broaden BC applicability in the near future³⁵.

To facilitate contextualization, a comparison between the hallmarks of BC and collagen, used here as reference material, can be found in Table 1.

Table 1: Comparison between collagen (as a benchmark material) and bacterial cellulose regarding relevant properties of biomaterials for epithelial regeneration.

Property	Collagen	Bacterial cellulose
Macrostructure	<p>Sponges, hydrogels. Image: Collagen sponge from⁵⁷.</p> 	<p>Hydrogels, aerogels or films mainly with planar forms⁵⁸.</p> 
Micro/nanostructure	<p>Triple helix protein fibres organized in 3D a network.</p>  <p>SEM image of collagen (image from⁵⁹).</p> 	<p>3D network of pure cellulose nanofibers.</p>  
Building blocks	Amino acids, mainly glycine, proline and hydroxyproline.	β-1,4-linked D-glucose units.
Origin	Mainly, livestock animals (cow, pig). Also plants ⁶⁰ and fish ²¹ .	Bacterial cultures, mainly <i>Komagataeibacter xylinus</i> strains
Purity	Variable.	Very high.
Fibre cross-section	≈ 100 nm ⁶¹ .	20-100 nm ³⁵ .
Fibre length	≈ 1 μm ⁶¹ .	> 1 μm, hard to determine precisely.
Interwoven fibres	Yes.	Yes.
Molecular weight	High.	High.
Options for structuration	<ul style="list-style-type: none"> • Fibre alignment^{62,63}. • Sacrificial templates⁶⁴. 	<ul style="list-style-type: none"> • Fibre alignment⁶⁵. • Templates during biosynthesis⁶⁶.

Property	Collagen	Bacterial cellulose
Fibre crystallinity	Non-consensus	High (\approx up to 90% ⁶⁷), mix between α and β cellulose structures.
Porosity	Very variable depending on collagen source and fabrication method 35-99% ^{57,68,69} .	Very variable depending on the drying method and posterior treatments 60% - 95 % ^{58,68,70} .
Pore type and size	Interconnected pores with variable size: 26 ⁶⁸ - 200 μ m (SpongeCol®)	Multi-size in the mesoporous range. Native BC \approx 5 μ m. Can be modified with porogens (40 μ m in ⁷¹) and by in situ-modifications ⁷² .
Water content	98% ⁵⁷ .	99%.
Temperature stability	200 °C ⁷³ .	Up to 300 °C.
Biodegradability	High, \approx 1 month <i>in vitro</i> ⁶⁹ .	Low/none in the body, biodegradable by cellulases.
Biocompatibility	High.	High.
Immunogenicity	Low/moderate	Low.
Bioactivity	High, supports cell attachment and proliferation.	Tunable. Moderate as-synthesized increases after modification ⁷⁴⁻⁷⁶ .
Mechanical stability	Very variable: low in native collagen ²⁰ , increases after crosslinking ¹² .	High in general. Reported to be higher than collagen ⁶⁸ , to be improved after surface modification ⁷⁷ and to recapitulate native cartilage ⁵⁶ .
Price	Variable, high for pure forms.	Variable, depends on the area of application.
Commercial availability/scalability	High.	High in the food form <i>nata de coco</i> (500-1500 tons per year per producer) and cosmetics but still low for high quality/purity (medical-pharmaceutical grade).

3. Applications of BC in epithelial regeneration

3.1. Dermal applications

Skin is the largest and outermost human organ and covers the entire external body surface. Therefore, above all, skin's primary function is to protect the underlying muscles, bones, ligaments and internal organs from external biological and chemical agents as well as physical influences^{78,79}. Furthermore, the skin is also involved in sensation, temperature regulation, immunological surveillance, prevention of dehydration and synthesis of vitamin D₃⁸⁰. The large epithelium of the skin, which is responsible for the barrier function against infection and towards waterproofing, is called the epidermis. This outermost layer of the skin is a stratified squamous epithelium, composed of proliferating basal and differentiated suprabasal keratinocytes. The epidermis contains no blood vessels, and cells in the deepest layers are nourished by diffusion from blood capillaries extending to the upper layers of the dermis⁸¹. The integrity of this organ can be affected by cuts, burns, ulcers, surgical incisions or illnesses, such as diabetes⁸². When the skin integrity is compromised, its structure and functions must be re-established as soon as possible to recover tissue homeostasis. To accomplish that, the wound healing process should begin almost immediately after a skin injury occurs, in order to avoid bacterial infection and dehydration^{83,84}. Due to the properties described above, BC is a promising biomaterial for healing skin injuries. In fact, BC has already been used as a natural polymeric wound care material since the 80s^{85,86}. BC meets many of the requirements of an ideal wound dressing: it acts as a physical barrier against bacterial infections, allows gas exchange, absorbs exudates, keeps a moist environment that enhances reepithelization, and is easy to remove without pain^{87,88}. Furthermore, BC is non-toxic and non-allergenic as described⁴³.

Today, several types of BC-based wound dressings provided by different companies are on the market. The first BC-based medical product on the market was Biofill®, a thin BC film with a water content of 8.5% used as temporary skin substitute and biological wound dressing. It has been successfully applied for the treatment of several skin injuries such as basal cell carcinoma, severe burns, derma-brasions, chronic ulcers as well as at donor and receptor sites in skin grafts. Among other benefits, immediate pain relief, close adhesion to the wound bed, spontane-

ous detachment following reepithelization and reduced treatment times as well as costs have been reported for this product. The only flaw discussed in some reports was the limited elasticity when applied in areas of great mobility⁸⁵. Along with the rising trend for modern moist wound management, clinical investigations of wet, never-dried BC for both, chronic wounds and burns, followed^{89,90}. Moist BC-based dressings such as XCell® were described as more effective than conventional wound dressing materials in promoting autolytic debridement, accelerating granulation and simultaneously donating and absorbing moisture from the wound⁹⁰.

Some recent studies on dermal BC applications focused on the understanding of the accelerated healing observed for both, dry and wet BC wound dressings, and thus contributed to a better understanding of the effects. Kwak and colleagues⁹¹ performed an *in vivo* study on rats and reported on distinct improvements in the thickness of both, epidermis and dermis, as well as the number of blood vessels and inhibition of the infiltration of mast cells at indicated time points in case of BC treated burns compared to gauze. The authors hypothesized that BC may accelerate the process of wound healing in burn injuries through regulation of angiogenesis and connective tissue formation.

Li and colleagues⁹² evaluated the effect of the structure of BC on full-thickness skin wound repair. The hierarchical structure of BC films and their different effects on skin wound healing was studied both *in vitro* (in a wound healing model placed on a microfluidic chip) and *in vivo* (Wistar rats). The results indicated clear benefits of BC in the healing of full-thickness wounds compared to gauze in terms of inflammatory reaction and healing time. The *in vivo* and *ex vivo* experiments on rats also demonstrated a certain difference in the performance of both sides of the BC pellicle. The bottom side of the BC film promoted blood vessel regeneration and collagen production of the wounds more than the top side. The authors argued that a looser BC network also promotes cell migration and proliferation and suggested heterogeneous BC-based biomaterials for complex tissue engineering. However, they did not investigate yet, whether a higher porosity and surface roughness may compromise the easy and pain-free detachment after reepithelization reported for BC wound dressings.

Cavalcanti *et al.* recently published the outcome of a randomized and controlled trial investigating the efficacy of perforated dry BC membranes for the

treatment of lower limbs chronic varicose ulcers⁸⁷. In the BC group, ulcers were more superficial at the end of the observation period (120 days) in more than 80% of the patients (*versus* 60% in the control group treated with triglyceride oil and gauze). The authors suggested that BC dressings could act as an inducer of tissue remodelling, stimulating the granulation process. They stressed the fact that the ulcer healing depends not only on the epidermal proliferation at the margins of the lesion but also on the growth of the granulation tissue from the central area.

Several modifications allow to further increase the functionality of BC as a wound care device while keeping the essential BC properties of biocompatibility and nanofibrillar structuration. Modifications of the cellulose can be obtained during the biofabrication process (*in situ*) e.g. using additives and by post-modification such as drying, chemical functionalization or loading of the BC network with active ingredients. An excellent overview about BC in various modifications developed for wound healing applications can be found in Sulaeva *et al.*⁴⁰. However, some recent findings are highlighted in Table 2 and discussed below.

Table 2: Modifications of BC and properties resulting from the modifications.

Material	Title of the paper	Results obtained by BC modification
BC with structured topography ⁹³	Surface-structured bacterial cellulose with Guided Assembly-Based Biolithography (GAB).	<ul style="list-style-type: none"> • Improved cell alignment • Promotion of fibroblast infiltration and new collagen deposition in the wound bed.
BCNC/RC ⁹⁴	Regenerated chitin fibres reinforced with bacterial cellulose nanocrystals as suture biomaterials.	<ul style="list-style-type: none"> • Biocompatible surgical sutures increasing the strength of BCNC/RC filaments. • Enzymatic degradation possible. • Degradation rate can be tuned by varying concentration of BCNCs in the yarn. • Chitin can promote cell proliferation (<i>in vivo</i>).

Material	Title of the paper	Results obtained by BC modification
TOBCP/AgNP⁹⁵	TEMPO-Oxidized Bacterial Cellulose Pellicle with Silver Nanoparticles for Wound Dressing.	<ul style="list-style-type: none"> • Biocompatible surgical sutures increasing the strength of BCNC/RC filaments. • Enzymatic degradation possible. • Degradation rate can be tuned by varying concentration of BCNCs in the yarn. • Chitin can promote cell proliferation (<i>in vivo</i>).
BC/ZnO⁹⁶	Bacterial cellulose-zinc oxide nanocomposites as a novel dressing system for burn wounds.	<ul style="list-style-type: none"> • Antimicrobial activity against <i>Escherichia coli</i>, <i>Pseudomonas aeruginosa</i>, <i>Staphylococcus aureus</i> and <i>Citrobacter freundii</i>. • Significant healing of 66% after 15 days related to day 0.
BC/TiO₂⁹⁷	Bacterial cellulose-TiO ₂ nanocomposites promote healing and tissue regeneration in burn mice model.	<ul style="list-style-type: none"> • Antimicrobial activity against <i>Escherichia coli</i> (81.0 ± 0.4%) and <i>Staphylococcus aureus</i> (83.0 ± 0%)
BC/SMN-Zein⁹⁸	Drug release and antioxidant/antibacterial activities of silymarin-zein nanoparticle/Bacterial cellulose nanofiber composite films.	<ul style="list-style-type: none"> • Flavonoid silymarin (SMN) and zein loading through nanoparticle adsorbing onto BC nanofibers. • Change of wettability and swelling. • Antioxidant and antibacterial activity. • Air-dried SMN-Zein/BC nanocomposite slowing down the lipid oxidation.

Material	Title of the paper	Results obtained by BC modification
BC/Octenidin⁹⁹	Controlled extended octenidine release from a bacterial nanocellulose/Poloxamer hybrid system.	<ul style="list-style-type: none"> • Long term controlled release of octenidine up to one-week improved mechanical and antimicrobial properties. • Ready-to-use system with Poloxamer loaded BC for advanced treatment of infected wounds. • Toxicity test performed with shell-less hen's egg model.
BC/CMC/MTX¹⁰⁰	Effect of <i>in situ</i> modification of bacterial cellulose with carboxy-methylcellulose on its nano/microstructure and methotrexate release properties.	<ul style="list-style-type: none"> • Impact of DS-CMC on methotrexate loading. • Topical treatment of psoriasis. • Decrease of the elastic modulus as the DS of CMC increased.
BC/PHEMA¹⁰¹	Embedding of Bacterial Cellulose Nanofibers within PHEMA Hydrogel Matrices: Tunable Stiffness Composites with Potential for Biomedical Applications.	<ul style="list-style-type: none"> • New modification: <i>in situ</i> UV radical polymerization of HEMA monomer impregnated into wet BC nanofibrous structure. • Significant improvement in mechanical properties. • Tensile strength increased. • Non-toxic. • rMSCs (rat mesenchymal stem cells) proliferation • Tissue replacement and wound healing.
BC/ε-poly-L-Lysine¹⁰²	Functionalization of bacterial cellulose wound dressings with the antimicrobial peptide ε-poly-L-Lysine.	<ul style="list-style-type: none"> • Antimicrobial activity (broad-spectrum) without affecting the beneficial structural and mechanical properties. • Modification with non-toxic biopolymer. • ε-PLL inhibited the growth of <i>S. epidermidis</i> on the membranes but did not affect the cytocompatibility to cultured human fibroblast.

Material	Title of the paper	Results obtained by BC modification
BC/PVA ¹⁰³	Preparation and <i>in vitro</i> characterization of BC/PVA hydrogel composite for its potential use as artificial cornea biomaterial.	<ul style="list-style-type: none"> • Higher visible light transmittance than plain BC.
ABC/urinary bladder matrix ⁷⁴	Acetylated bacterial cellulose coated with urinary bladder matrix as a substrate for retinal pigment epithelium.	<ul style="list-style-type: none"> • Higher adhesion and proliferation of retinal pigment epithelium cells than uncoated BC. • Closer recapitulation of the <i>in vivo</i> cell phenotype than uncoated BC.
BC/varying porosity ⁷¹	Bacterial Cellulose-Based Biomimetic Nanofibrous Scaffold with Muscle Cells for Hollow Organ Tissue Engineering.	<ul style="list-style-type: none"> • Higher pore size than native BC to allow muscle cell ingrowth. • Higher porosity. • A small decrease in mechanical strength.

3.1.1. Material modifications

Modifications of the BC such as control the water content, surface topography and nanocomposites have been applied to improve wound healing. Rebelo *et al.* recently investigated the effects of varying water content on BC material properties. They demonstrated that the dehydration effects on BCs viscoelastic and electrochemical properties. Lower water contents as 80% and 50% caused increased stiffness and BC resistance to electron transfer became higher with lower electron capacity¹⁰⁴. Those findings have implications for BC wound dressings with different moisture content. They may range from practical aspects such as handling and draping of the dressing to electrolyte exchange through the dressing. However, this should be investigated in further studies. Another group focused on modifications of the surface topography of BC dressings in order to improve wound healing. Botton and colleagues introduced a new approach called guided assembly-based biolithography (GAB) technology⁹³. They developed PDMS moulds with different surface patterns allowing a controlled *in situ* modification of the BC surface topography. The structured surface was shown to influence migratory patterns and alignment of human dermal fibroblasts and keratinocytes. A

full-thickness wound model tested on mice confirmed the promotion of fibroblast infiltration and new collagen deposition in the wound bed by the modified dressing compared to flat BC.

3.1.2. Combination of BC with other biomaterials

In many studies, BC has been combined with other biomaterials known for their beneficial effects on wound healing. To give an example, Moraes and colleagues¹⁰⁵ investigated a self-prepared wound gel made from disintegrated bacterial cellulose and collagen type I (BC/COL). In an animal study, healing of surgical skin wounds in rat dorsum with BC/COL gel was compared with those from animals treated with commercial collagenase ointment and an untreated group. BC/COL hydrogel was found to be more efficient than the collagenase ointment. Wound closure and fully repaired epithelium and dermis with organized collagen fibres and tissue rich in blood vessels were observed at day 15. At the same time, the dermis was thinner in case of the collagenase ointment treatment and still under repair with the presence of numerous inflammatory cells for the untreated group. Especially, the adhesion of the hydrogel on the wound bed was found to be advantageous for the treatment.

Other groups reported about the combination of BC with silk-sericin¹⁰⁶, chitosan¹⁰⁷ and dextran¹⁰⁸. Silk-sericin was selected due to its cytoprotective and mitogenic effects, whereas chitosan and dextran were selected based on their antibacterial efficiency and positive effects on fibroblast cell proliferation, respectively. In all cases, the positive effects of the combination compared to native BC were reported.

H. Wu *et al.* used bacterial cellulose nanocrystals (BCNCs) to reinforce regenerated chitin (RC) fibres to form BCNC/RC filaments for surgical sutures. Mechanical measurements demonstrated that the strength of the BCNC/RC filament increased dramatically over the RC analogue. A yarn made of BCNC-loaded fibres also achieved satisfactory mechanical performance, with a knot-pull tensile strength of 9.8 ± 0.6 N compared to 6.8 ± 0.6 N of RC yarn without BCNC. While obtaining biocompatibility of the surgical suture, the enzymatic degradation rate can be tuned by varying the concentration of BCNCs in the yarn. It has been proven that BCNC/RC promotes cell proliferation (*in vivo* murine skin

wound closure experiments, without any adverse effects. The combination of strength-enhanced fibre and promising *in vivo* experiments qualify BCNC/RC to be a new candidate for application as BC-based medical suture⁹⁴.

3.1.3. Drug-delivery systems

Furthermore, an increasing number of studies report on drug delivery systems based on BC for dermal applications⁵⁴. To avoid the risk of bacterial infections, *e.g.* Amoxicillin loaded BC sponges were examined¹⁰⁹. The functionalized sponges displayed good porosity and swelling, which are beneficial for absorbing wound exudates. Moreover, a wound infection model proved enhanced wound healing ability *in vivo*. In another study, antimicrobial peptides such as ϵ -poly-L-Lysine (ϵ -PLL) were investigated¹⁰². This peptide is a non-toxic biopolymer with broad-spectrum antimicrobial activity. Fürsatz *et al.* cross-linked low molecular weight ϵ -PLL in pristine BC membranes and to carboxymethyl cellulose functionalized BC using carbodiimide chemistry. The functionalization of BC with ϵ -PLL inhibited the growth of *S. epidermidis* on the membranes but did not affect the cytocompatibility to cultured human fibroblasts as compared to native BC. The functionalization had no significant effects neither on the nanofibrous structure nor on the mechanical properties of the BC. Furthermore, there are recently published studies taking advantage of some classical approaches in cellulose chemistry applied to BC. *e.g.* Wu *et al.* used the 2,2,6,6-Tetramethyl-1-piperidinyloxy (TEMPO) oxidation to obtain superficially oxidized bacterial cellulose pellicles (TOBCP) and subsequently loaded them with silver nanoparticles (TOBCP/AgNP)⁹⁵. Through this modification, they established antimicrobial activity by a silver ion release with a rate of 12.2% per day at 37 °C in three days while retaining the biocompatibility of TOBCP.

Following the same purpose, other groups reported about the incorporation of zinc oxide nanoparticles into BC. The nanocomposites exhibited high antibacterial activity against *Escherichia coli*, *Pseudomonas aeruginosa*, *Staphylococcus aureus* and *Citrobacter freundii*. In a burn wound model, animals treated with the BC/ZnO nanocomposite further showed significant healing of 66% after 15 days related to day 0 compared to BC, which showed healing of 50.5% after the same treatment⁹⁶. The incorporation of titanium dioxide nanoparticles (TiO₂) in BC

has also given encouraging results⁹⁷. Khalid *et al.* depicted *in vivo* burn wound healing potential of BC and TiO₂ nanocomposites (BC/TiO₂). Antimicrobial activity of the nanocomposite was against *Escherichia coli* ($81.0 \pm 0.4\%$) and *Staphylococcus aureus* ($83.0 \pm 0.0\%$) was confirmed through agar disc diffusion protocol.

Besides, the combination of BC with natural substances or natural derived Active Pharmaceutical Ingredients (APIs) is becoming more and more notable. Tsai *et al.* investigated a composite film with silymarin-zein nanoparticles and BC nanofibers. They applied adsorption of flavonoid silymarin (SMN) and zein nanoparticles to load them onto the fibres for improving higher antioxidant and antibacterial activity. The authors could also show that air-dried SMN-Zein/BC nanocomposites slowed down lipid oxidation⁹⁸.

Lima Fontes *et al.* have shown the effect of CMC *in situ*-modifications on BC nano/microstructure and methotrexate (MTX) release properties. The degree of substitution of CMC (DS-CMC) has a massive impact on API loading; since carboxymethylcellulose (CMC) is a well-known candidate to change *e.g.* pore-sizes of the three-dimensional network of BC. For topical skin application, MTX is used as a disease-modifying anti-rheumatic drug *e.g.* treatment of psoriasis. However, besides the impact of loading capacity, increasing DS-CMC causes a decrease in the elastic modulus of BC¹⁰⁰.

Remarkable is also a new *in situ*-modification by UV radical polymerization of 2-HydroxyEthyl MethAcrylate (HEMA) monomer impregnated into wet BC nanofibers. The combination of BC with poly(2-hydroxyethyl methacrylate) depicted a significant improvement in the mechanical properties (*e.g.* tensile strength) and the rat mesenchymal stem cells proliferation which qualifies this modification for tissue replacement and wound healing applications¹⁰¹.

Considering all these wound dressings loaded with an API as drug-delivery systems, most of the studies show initial bursts of the API release. Up to now, long-term controlled release systems are still very rare. Nevertheless, Alkhatib *et al.* designed a new delivery system consisting of BC and a Poloxamer developed for the antiseptic API octenidine as a long-term ready-to-use system for dermal wound treatment (Figure 5). This delivery system provides a prolonged retention time for octenidine, up to one week, with improved mechanical and antimicrobial properties as well as a high biocompatibility⁹⁹.

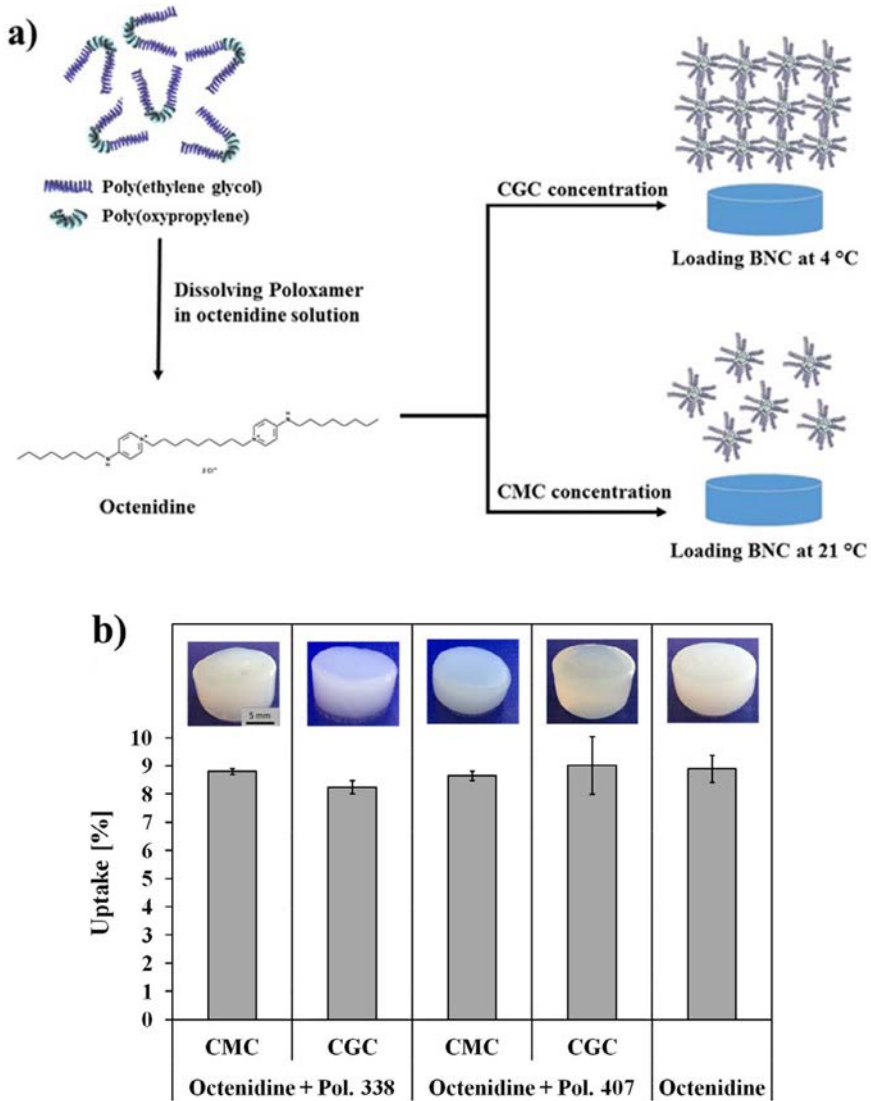


Figure 5. (a) Schematic overview of the loading of BC with Poloxamers forming critical micelle concentration (CMC) and critical gelation concentration (CGC) samples. (b) Photographs of octenidine and octenidine/Poloxamer loaded CMC and CGC BC samples and percentage uptake of octenidine (mean \pm SD, $n = 3$) after incubation of fleeces for 48 h by Alkathib *et al.* reproduced with permission from Elsevier⁹⁹.

3.1.4. BC as a cell carrier

Because of the possibility to support mammalian cell attachment and proliferation, BC films are also investigated as cell carriers in cell transplantation¹¹⁰.

For instance, bacterial cellulose/acrylic acid (BC/AA) wound dressing hydrogels (without cells) enhanced wound healing capacity in nude mice. Interestingly, when the BC/AA hydrogels were loaded with human epidermal keratinocytes and human dermal fibroblasts, the positive effects of the BC/AA in burn recovery were accentuated. The *in vivo* results showed that the cell-loaded hydrogel produces the greatest acceleration on burn wound healing, followed by treatment with the hydrogel alone in comparison to the untreated group. The percentage wound reduction on day 13 in the mice treated with BC/AA hydrogel loaded with cells ($77.3 \pm 6.2\%$) was significantly higher than that in the control-treated mice ($64.8 \pm 6.8\%$) or the hydrogel-treated ones alone (71.5 ± 2.3), respectively. Histological analysis for the expression of collagen type I via immunohistochemistry and transmission electron microscopy indicated a greater deposition of collagen in the mice treated with the hydrogel loaded with cells than in the mice administered with other treatments. Therefore, the BC/AA hydrogel proved promising applicability as a wound dressing and a cell carrier.

In summary, very promising experimental investigations and preclinical studies have been performed suggesting the future application of modified, drug-loaded and/or native BC in an increasing number of dermal applications. The increasing number of BC-based wound dressings on the market follow the same trend and confirm the high commercialization potential of innovative BC-based medical products. Other fields of BC application in damaged epithelial tissues regeneration are still in its infancies, as described below, but show the same promise.

3.2. Ophthalmology

Ophthalmology is a branch of medicine historically linked with the use of biomaterials, exemplified by contact and intraocular lenses. The application of biologically derived materials in regenerative ophthalmology predominantly concentrates on the ocular surface and, to a lesser extent, on the retina¹¹¹. Figure 6 localizes these two tissues in a human eye anatomy representation. To date, for ocular surface wound healing, amniotic membrane patches are regularly applied¹¹² and the most common clinical approach for ocular surface reconstruction relies on corneal transplantation, whereas innovative regenerative medicine approaches are gradually gaining acceptance¹¹³.

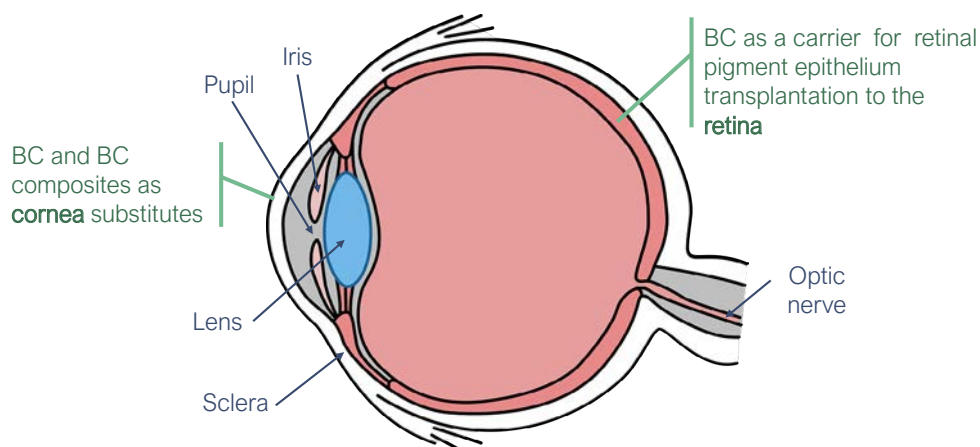


Figure 6. Schematic representation of the human eye anatomy and the targeted tissues treated with BC-based therapies.

The outermost part of the eye comprises two epithelia: the corneal and the conjunctival epithelium. Recently, collagen-based materials have been designed to reconstruct these two structures^{114–116}, while other authors developed silk or keratin-based membranes¹¹⁷. Some previous reviews already pointed out that the innate hydrophilicity, flexibility and mechanical stability of BC suggest a potential application on corneal regeneration^{118,119}. One more strength of BC for this specific application is its conformability, which might facilitate the adaptation of the biomaterial to the dome shape of the ocular surface. BC has been shaped into a contact lens-like form by culturing *K. xylinus* on top of hydrophilic surfaces¹²⁰ and, in parallel, BC has proven to support the growth of human corneal stromal cells¹²¹. However, research papers on this topic are scarce and describe preliminary findings, indicating that the application of BC in ocular surface regeneration is still a field in its infancy that deserves to be explored in more depth.

Native-state BC has a visible light transmittance around 70% due to the dispersive character of the fibres bundles and pores. In order to increase the transparency of BC for long-term applications in corneal regeneration, BC has been combined with other components such as polyvinyl alcohol (PVA)¹⁰³. BC/PVA composites, prepared by a freeze-thaw method, were satisfactorily evaluated in terms of water holding capacity, light transmittance, mechanical properties and thermal stability; important characteristics for a corneal substitute. However, no

biological characterization of those materials has been published at the time of this review. Similarly, BC/Hyaluronic acid composites (BC/HA) were prepared by a physical gelation method with the resulting material displaying 90% of visible light transmittance⁶⁷. Interestingly, this feature was maintained after a drying-re-wetting cycle. According to the authors, biocompatibility tests for the BC/HA composites are in progress.

To our knowledge, the only *in vivo* assessment of BC as a corneal replacement was carried out by R. V. Sepúlveda *et al.*¹²². In this study, dry BC and BC/poly-caprolactone (PCL) hydrogels were implanted into rabbit's eyes to replace the corneas. Both BC and BC/PCL implants remained stable over the 45 days of the study and delayed the manifestation of corneal oedema with respect to the control group that received no treatment. Nevertheless, the authors report chronic inflammation and incomplete re-epithelization in the long term for the rabbits receiving the BC and BC/PCL implants. These results hint that the use of BC as a permanent corneal substitution will be challenging.

Another research direction regarding ophthalmological applications of BC is the repair of retinal pigment epithelium (RPE). The function of this highly specialized epithelium is impaired in patients suffering from age-related macular degeneration, the most common cause of vision loss in Europe¹²³. Gonçalves *et al.* described that acetylated BC supported the attachment and proliferation of RPE cells and envisioned a potential application of BC as a carrier for RPE cell transplantation to the retina¹²⁴. More recently, the same group reported a further functionalization of acetylated-BC (ABC) with urinary bladder matrix⁷⁴. It is encouraging to read that when RPE cells were seeded on these substrates, they recapitulated closer the *in vivo* phenotype than uncoated ABC.

Taken together, these studies set the basis for future research on BC-based biomaterials specifically targeting eye epithelia. The above-summarized results are still immature and, due to the lack of *in vivo* experiments, conclusions must be drawn with caution. Nevertheless, the field of regenerative ophthalmology appears as an opportunity for the BC-based biomaterials to find a potential niche in the health market, which appears as less competitive than *i.e.* the skin.

3.3. Stomatology

Deliberations for potential applications of BC, *e.g.* temporal implants in dental extraction alveoli or wound dressing after mucosal transplantation recently came up, but the testing of BC and specific product developments are still rare. However, the softness of the hydrolymer plus its flexibility and self-attachment to surfaces strongly suggest a broader scope of application in dentistry. Studies of Weyell *et al.* depicted the benefits of doxycycline-loaded hydrated and freeze-dried BC in dental therapies such as dental extraction or mucosal transplantation¹²⁵. Both applications would benefit on the one hand from a material, which degrades under physiological conditions and on the other hand from an antibiotic environment. Consequently, periodate-oxidation of BC was performed to modify its degradation kinetics. In addition, native and oxidized BC loaded with doxycycline were tested for prophylaxis against infection. An *in vitro* toxicity test ensured biocompatibility of oxidized BC, whereas agar diffusion tests of samples loaded with doxycycline against pathogenic oral bacteria proved high antibiotic efficiency. Release studies of the drug from native and oxidized BC confirmed a comparable release behaviour showing an initial burst of 50 – 60% within the first hour and a total release of about 90% after 3–5 h¹²⁶.

Chiaoprakobbkij *et al.* developed freeze-dried composite sponges made from BC fibres and alginate, cross-linked with CaCl₂. This recent *in vitro* study also showed a supported proliferation of human keratinocytes and gingival fibroblasts caused by this composite material¹²⁷. In conclusion, there is still an unmet potential for BC-based products (*e.g.* periodontal dressings, sponges, tamponades, sutures or even drug delivery systems) in dentistry.

3.4. Other epithelial surfaces

Epithelial tissues form part of a myriad of membranes and barriers inside the human body. Some of these structures such as the eardrum, the meninges or the linings of hollow organs are difficult to rebuild after disease or trauma and would largely benefit from new repair approaches based on natural biomaterials. In this last section, we have grouped further applications of BC regarding the regeneration of diverse body surfaces.

The tympanic membrane (TM) separates the external ear from the middle ear and its key function is to amplify air-borne vibrations and transduce them

to the middle ear. TM perforation is a common clinical situation and implies a risk of prolonged damage and hearing reduction, especially if bacterial infection occurs. BC patches have been evaluated as wound healing devices in eardrum perforations to substitute the muscle, fat or cartilage autografts that are conventionally used in TM reconstruction. F. Coelho Alves Silveira *et al.* performed a randomized controlled trial with 40 patients and reported a higher success rate (90 *vs* 80%) when BC films were used as wound dressings respect to autologous temporal fascia (muscle) patches. Notably, the BC treatment reduced the operation time in more than one hour and the total hospitalization costs were 13 times lower. Another study tested the efficiency of BC to solve small but long-lasting TM perforations in 16 ears¹²⁸. The authors conclude that the high rate of recovery of these patients treated with BC (81.3% of the cases) encourages for further investigations of BC in otology. Interestingly, this publication highlights, from a clinical point of view, some advantages of BC respect to other grafting materials for TM reconstruction: no need of general anaesthesia for the surgical procedure, easy shaping of the material to match the defect size, enhancement of cell growth in the damaged area, easy sterilization and short operating time.

Because its limited endogenous regenerative potential, the nervous system is another area where BC patches could be of great interest. In particular, dura mater, the outermost of the three meninges that surround the brain and the spinal cord, is frequently disrupted after neurosurgical interventions or trauma and thus can be regarded as a potential target for BC-based treatments. *In vitro*, patterned BC substrates proved to support and guide the growth of neural stem cells⁶⁶. In line with this, Goldschmidt and co-workers reported the proliferation of human dural fibroblasts (primary cultures) on BC films¹²⁹. These authors propose BC as a conceivable option for dural implants principally because of its mechanical stability and its capability to support the growth and migration of native dural cells. *In vivo*, damage to dura mater has been experimentally treated with BC patches¹³⁰. In this study, sutureless BC implants were inserted in 40 rats and examined after 120 days without noticing any complication such as infection, cerebrospinal fluid leakage, haemorrhages or behaviour disturbance in the animals during the study time. The levels of inflammation were similar between the group that received BC patches and the group implanted with a polytetrafluoroethylene-based material

(positive control). The authors claim a satisfactory level of BC graft acceptance and highlight the potential application of BC in dura mater repair. Actually, in 2014 the commercial product SyntheCel Dura Repair was launched for this specific application after showing equivalent effectiveness compared to other commercially available products for dura replacement¹³¹.

BC native structure in the form of a fibrous hydrogel and some reported BC film thickness⁵⁸ are comparable to those of the mucus layers covering the body's internal cavities^{132,133}. Thus, BC has also been proposed for the reconstruction of hollow organs¹³⁴ that is, urinary, reproductive, respiratory and intestinal tracks, which contain a mucosa on its inner side. To this end, asymmetric BC structures exhibiting one site with densely packed BC fibres and another side with loose BC fibres were generated mimicking the architecture of tubular organs⁷¹. These scaffolds achieved higher porosity than native BC and after being seeded with muscle cells, were implanted in dog urinary systems yielding better outcomes than unmodified BC.

The findings summarized in this section collectively underline the versatility BC and its potential to take part in the regeneration of diverse body surfaces. Likewise, the adaptability of BC in terms of size, shape and porosity will be crucial in the future to conceive tissue-specific biomaterials based on BC.

4. Conclusions

The outstanding properties of BC, in conjunction with its natural origin and sustainable manufacturing, call for many diverse applications in epithelial regeneration. Here, we provide a compact but detailed synopsis about the opportunities for BC-based alternatives to conventional treatments in this field.

Huge progress has been made in the development of novel BC-based materials for dermal applications and the understanding of their positive effects on wound healing. Approaches ranging from modifications of topography, water content and pore structure to combinations with other biopolymers, active ingredients and/or cells have shown that BC is not only an excellent wound dressing material in its native form but also a versatile platform material to tailor-made product design. Along with the increasing comprehension of the reasons for accelerated

wound healing observed for native as well as modified BC, new BC-based medical products, designed for the treatment of specific skin lesions, can be expected to enter the market within the next couple of years.

Besides the well-known example of the outer skin, we pinpointed other epithelial surfaces that could benefit from innovative treatments based on BC. In the field of ophthalmology, the preliminary findings reviewed here should encourage future research on BC-based biomaterials specifically targeting eye epithelia since the field of regenerative ophthalmology appears as a chance for BC to find a niche in the competitive health market. Similarly, the softness of the BC hydrogels together with its flexibility and self-attachment to body surfaces strongly suggest a broader scope of potential application in dentistry, a field that definitely deserves more research efforts. Worth noting are the reports on tympanic membrane reconstruction highlighting important advantages of BC compared to other grafting materials from a clinical perspective: no need of general anaesthesia for the surgical procedure, easy shaping of the material to match the defect size, enhancement of cell growth in the damaged area, easy sterilization and short operating time.

The potential of BC as cell carrier should not be underestimated. In this manuscript, we gathered abundant examples of cell types that can effectively attach and proliferate on BC substrates. These cell types include diverse human cells; epidermal keratinocytes, dermal fibroblasts, corneal stromal cells, retinal pigment epithelium and other mammalian cells like neural stem cells (mouse) and muscle cells (dog). On top of that, BC exhibits potentiality as a substrate for stem cell transplantation as it proved to maintain stemness of mouse mesenchymal stem cells for a longer period of time than traditional culture methods¹³⁵.

Naturally, there are some difficulties that BC-based biomaterials will need to overcome to effectively contribute to epithelial regeneration. When a permanent replacement for epithelial tissue is targeted, BC should allow cell ingrowth to provide proper integration of the biomaterial into the surrounding tissue. So far, this can only be achieved when BC is specifically modified to increase porosity. Moreover, BC-based (implant) materials need to degrade after fulfilling the intended medical purpose. Degradability of BC under physiological conditions can only be achieved after chemical modification or enzymatic treatment and the verification of total degradation and metabolization in *in vivo* studies is still open.

Likewise, for the specific application of long-term corneal replacement, BC will also need to be adapted to improve visible light transmittance.

However, these limitations in some specific fields of medical application are already addressed in current research and will probably be overcome in the next years. The significant progress in controlled production and the successful design of bioreactors suited for industrial-scale production of medical-grade BC⁴⁵ already paved the way for faster commercialization. Together with the profound knowledge gained by young companies worldwide about the production of BC-based products according to current quality management and medical device regulations, this progress will significantly accelerate the market entrance of further BC-based products including an increasing number of implant materials designed for epithelial regeneration.

5. Acknowledgments

The authors IA, AL and AR acknowledge the financial support from the Spanish Ministry of Science, Innovation and Universities through the MAT2015-64442-R project, the ‘Severo Ochoa’ Programme for Centres of Excellence in R&D (SEV-2015-0496) and the PhD scholarship of I.A. (BE-2016-076734) and the Generalitat de Catalunya for the 2017SGR765 project. These authors also express their gratitude to the Centre d’Oftalmologia Barraquer for their helpful suggestions in the elaboration of this manuscript. UB and DK gratefully acknowledge the Free State of Thuringia and the European Social Fund (2016 FGR 0045) as well as the European Commission under an MSCA-ITN award, grant number 675743 (ISPIC), and under an MSCA-RISE award, grant number 777682 (CANCER) for funding.

On-site interviews with experts

While preparing the above mini-review, a relevant consideration was that, to date, the most advanced field of application for BNC is skin tissue regeneration. That presents advantages in terms of success examples and availability of data, yet it involves higher competitiveness and reduced novelty in this area. Hence, in the interviews with specialists, we aimed at:

1. Gaining a well-informed position to decide whether to address the efforts of the current thesis towards skin tissue regeneration with BNC biomaterials.
2. Identifying alternative tissues where the properties of BNC could be appreciated.
3. Hearing the views of end-users regarding the possibilities of BNC in their fields of expertise.

Methodology

Interviewed experts

Approximately forty experts from local institutions (hospitals, universities and private companies) were contacted via email. Out of the totality of the suggestions made, eleven persons from different backgrounds and working sectors (Table 3 lists the details) agreed on arranging an on-site interview. The meetings were conducted face to face in two rounds with a different focus; i) regenerative medicine in general and ii) ophthalmology-related.

Table 3: Number of interviewed specialists classified by the working sector and field of expertise.

Work sector	Number of interviews
Healthcare	4
Veterinarian	3
Academy	2
Industry	2

Field of expertise	Number of interviews
Ophthalmology/optometry	6
Plastic surgery/ dermatology	5

Questions

Roughly, the following questions were posed to the experts:

1. Which are the current strategies used in your field involving biomaterials?
2. Which are the major limitations of the current biomaterials?
3. Which pathologies/tissues cannot be treated satisfactorily with the present solutions?
4. Which characteristics do you think a biomaterial should have to be attractive in your field?
5. Would you be willing to incorporate in your practice novel biomaterials?

The answers provided to these questions and other sporadic comments made by the experts were noted during the interviews and then transcribed and analysed manually.

Results

First-hand, very valuable and practical information was extracted from the interviews. The most agreed opinions from experts regarding i) desirable properties biomaterials should exhibit to be considered attractive and ii) unmet challenges from current solutions where BNC could be valuable are presented in Figure 7 as word clouds. The size of each word matches the frequency a concept appeared in the interviews. Tables 5 and 6 show the quantification of this analysis. Moreover, a summary from each set of meetings is provided below.

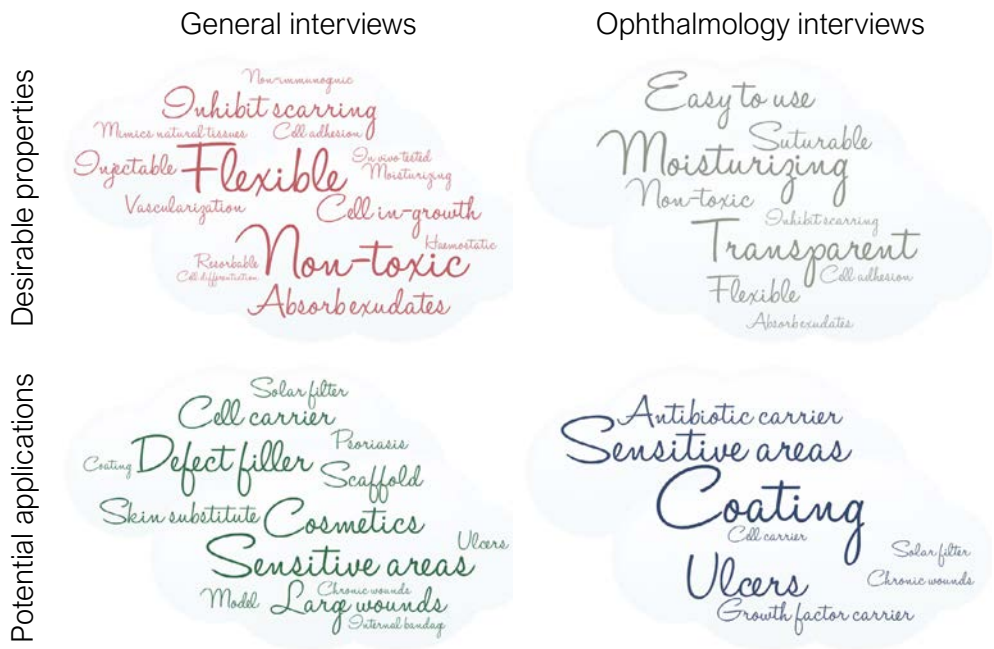


Figure 7. Graphical representation of the interview's outcomes. Word clouds showing the recurrent answers of the interviewees. The size of each word corresponds to the frequency that a concept appeared in the transcripts of the meetings. Top: desirable properties for novel biomaterials. Bottom: attractive applications for BNC. The diagrams were made with <https://wordart.com/>.

General interviews

The first round of interviews sought to acquire an overall view of the regenerative treatments using biomaterials employed in our regional sanitary ecosystem. Interviewed experts included two surgeons, two dermatologists and a regenerative medicine researcher. The main messages extracted from this series of interviews were:

1. Since the skin and other body surfaces are *per se* fast recovering tissues, wounds tend to heal satisfactorily in healthy patients with some exceptions that include: large area wounds like those caused by burns, wounds in particularly sensitive areas such as joints (due to movement and a thin skin layer present on this areas) and cornea (due to lack of irrigation).
2. The second scenario where wound healing might be compromised refers to particularly sensitive patients. Certain patients have impaired wound healing capacity due to pre-existing diseases, like diabetes or Acquired

ImmunoDeficiency Syndrome (AIDS), or systemic treatments like immunosuppression and chemotherapy. Other special patients are those that require a fast recovery such as elite sportspeople.

3. For the standard population, the major complication related to wound healing is the risk of infection. When surgical intervention is required and a biomaterial or a tissue graft is employed, rejection and immune reactions are additional dangers to the always-present risk of microbial contamination.
4. Skin regeneration products are already well standardized and the market offers a vast catalogue of commercial options trusted by the clinicians. Therefore, unless a novel approach provides a ground-breaking improvement, it might be difficult to incorporate BNC-based solutions in this market sector. Examples of some commonly used products in hospitals for severe wound reconstruction are included in Table 4. Accordingly, developing biomaterials have more chances to result attractive if they are directed to treat a specific tissue or pathology still lacking an optimal and/or targeted solution. Some of these situations are gathered in Table 6.
5. BNC inherently meets a fraction of the most sought-after requirements for biomaterials such as flexibility and non-toxicity (see Figure 7 and Table 5) and therefore, it was generally endorsed by the specialists as an option worth exploring in regenerative treatments.

Table 4. Examples of commercial products used in wound management by the interviewed clinicians.

Product name and company	Composition	Recommended use
MatriDerm® MedSkin solutions	Native collagen scaffold mixed with elastin.	Regeneration of full-thickness wounds in a one-step procedure in combination with a split-thickness skin graft from the patient.
Integra® Integra Life	One layer of a porous matrix of cross-linked collagen and glycosaminoglycan + one layer of silicone.	Temporary epidermal substitute for burns or reconstructive procedures.
Sangustop® BBRAUN	High-density collagen sponge supplemented with riboflavin	Control bleeding in internal organs.

Product name and company	Composition	Recommended use
Epicel® Vericel	A sheet of proliferative, autologous keratinocytes attached to a paraffin gauze backing.	Reconstruct large area burs where there are limited suitable harvest sites.
Tissucol® Baxter	Tissue glue based on human fibrin obtained from human plasma.	Seal and prevent bleeding.

Ophthalmology-related interviews

After the first round of interviews, the need for a higher level of specialization became clear. A common observation made by experts was that some tissues *e.g.* cornea or types of lesions *e.g.* chronic wounds require much more attentive and focussed management than conventional wounds thus offering opportunities for novel approaches. Therefore, we selected corneal lesions among the diversity of “sensitive wounds” requiring special healthcare assistance as an alternative to skin regeneration as a plausible target of our BNC-based biomaterials.

To confirm the adequacy of BNC for the regeneration of the cornea, as well as to gain a better understanding of this sector, the second round of interviews targeted professionals dedicated to eyesight including ophthalmologists (both human and veterinarian) and optometrists, extracting the following conclusions:

1. Corneal wounds and ulcers are prevalent and, in some cases, very recurrent and difficult to treat. Similar to skin wounds, excessive scarring and infections are common complications of corneal lesions. Particularly threatening is the risk of vascularization and conjuntivalization of the cornea since it causes opacification and subsequently, corneal blindness.
2. Patient discomfort is a serious complication of current treatments caused by the high sensitivity of the cornea, which is avascular but highly innervated. Another cause of patient discomfort arises from the fact that many ocular surface treatments are administrated as eye drops that require very frequent doses. Therefore, biomaterials incorporating therapeutic agents would be convenient.
3. One of the most desired characteristics for ophthalmology-oriented bio-

materials is its capacity to provide moisture (this attribute was mentioned by 6/6 interviewees) to the ocular surface, *i.e.* high water retention, together with transparency. Biomaterials for corneal regeneration should also be flexible and conformable allowing an easy application onto the dome-shaped ocular surface and should not cause eye irritation.

4. A common approach for corneal wound healing is the application of an amniotic membrane –the innermost layer of the placenta– patch as both physical protection and a source of growth factors and anti-inflammatory molecules. Some collagen-based structures have also been developed but, according to the specialists, this is an underexploited subsector in the health market.
5. If pursuing a corneal bandage application, a key parameter would be the fixation method of the BNC to the ocular surface, which should be minimally invasive but at the same time provide a robust attachment.
6. Overall, the application of a non-toxic and soft hydrogel such as BNC in corneal wound management was perceived as an appealing research line by the interviewed experts.

Table 5: Desirable biomaterial's properties according to the interrogated experts. The figures indicate the number of times a feature was mentioned by the specialists. Categories were added *a posteriori* for comprehension sake.

Category	Property	N° of experts mentioning: GENERAL (out of five)	N° of experts mentioning: OPHTHALMOLOGY (out of six)	Total
Cell-biomaterial interactions	Allows cell in-growth	3	0	3
	Allows cell adhesion and migration	2	1	3
	Induces appropriate differentiation	1	0	1
	Inhibits excessive proliferation and scarring	4	1	5

Category	Property	N° of experts mentioning: GENERAL (out of five)	N° of experts mentioning: OPHTHALMOLOGY (out of six)	Total
Tissue-biomaterial interactions	Non-toxic	4	3	7
	Enhances vascularization	3	0	3
	Mimics natural tissues	2	0	2
	Not immunogenic	2	0	2
	Has been tested <i>in vivo</i>	2	0	2
Properties	Absorbs exudates	4	1	5
	Resorbable	2	0	2
	Moisturizing	2	6	8
	Flexible	4	3	7
	Transparent	0	6	6
	Haemostatic	2	0	2
	Injectable	3	0	3
	Suturable	0	3	3
	Easy to use	0	5	5

Table 6: Potential BNC applications based on the outcomes of the interviews. The specific number of times a prospective use for BNC was cited by the interviewees.

Category	Property	N° of experts mentioning: GENERAL (out of five)	N° of experts mentioning: OPHTHALMOLOGY (out of six)	Total
Long-term use	Tissue substitute	2	0	2
	Defect filler	3	0	3
	Bandage for internal organs	1	0	1
	Resorbable scaffold	2	0	2
Temporary use	Cosmetic patch	3	0	3
	Solar filter	2	1	3
	Ulcers	2	3	5
	Choric wounds	1	1	2
	Sensitive areas (cornea, movement areas...)	4	3	7
	Big area wounds	3	0	3
	Psoriasis treatment	2	0	2
	Coating for sutures, contact lenses...	1	4	5
Carrier	Antibiotics	0	3	3
	Growth factors	0	2	2
	Cells	3	1	4
Model for <i>in vitro</i> studies		2	0	2

Contributions to the field and critical comment

In this non-experimental chapter two activities – a literature review and an array of meetings with experts – have been employed to gain an understanding of the healthcare uses of BNC as well as to identify novel applicability sectors.

Upon reviewing recent literature, we detected abundant reports emphasising the outstanding properties of BNC for tissue regeneration and wound healing. Some of the innate characteristics of BNC are comparable to those of collagen, which we have recognised as the gold standard material for epithelial regeneration. A comprehensive comparison between both biomaterials is provided in Publication 1. Application examples of BNC in the healthcare sector are dominated by skincare products. However, other tissues such as the cornea, the oral mucosa or the dura mater are gradually gaining prominence and we have emphasized these lesser-exploited applications in our mini-review. Besides, BNC was found to stand out on its suitability as a substrate for mammalian cell growth. To my view, this opens a new set of possibilities for BNC in cell transplantation therapies as addressed experimentally in the coming chapters of this thesis. Since the publication of our mini-review in June of 2019, other high-quality bibliographic works have been written regarding uses of BNC in healthcare. To mention a few, Carvalho and colleagues described the latest BNC-based tissue engineering approaches¹³⁶ while Oliveira Barud and co-workers focused on dentistry applications¹³⁷. Interestingly, Klemm *et al.* reviewed process-control methods for BNC production addressed to medical applications¹³⁸.

I believe that the on-site interviews were a successful approach to gain awareness about the use of biomaterials in the local sanitary arena as well as to better comprehend the limitations of the current solutions. Medical doctors confirmed our assessment that, to date, collagen-based materials represent the gold standard in regenerative treatments. Moreover, they shared some examples of products used by themselves, which are gathered in Table 4, offering standards to whom novel biomaterials can be benchmarked. We have also corroborated that BNC exhibits *per se* some of the most sought-after properties for biomaterials according to the consulted experts, namely: biocompatibility, conformability, high water content and manageability while some other desirable attributes could be

attained upon modifications. The reports from the interviews incorporated in this chapter provide a direct and updated picture of the end user's needs and, for this reason, I consider it as a highly relevant and innovative contribution of this chapter. Moreover, the first-hand experiences shared by experts have been of uttermost value in the development of this thesis as they guided our first steps towards problem-oriented approaches and eased later collaborations. Naturally, this interview-based methodology has some limitations that need to be taken into account. First, the number of interviews and the profile of the interviewees were conditioned to the expert's willingness to participate in this research and their availability of time and this might have caused certain bias. Second, even though the starting questionnaire was always the same, in some cases the interviews evolved to different topics and the experts described personal opinions or experiences that were difficult to analyse systematically. Finally, it was challenging to take notes covering the totality of the answers provided by the experts and this might have caused some details to be lost during the transcription of the data. To mitigate this issue, recording the interviews could have been useful.

By integrating the information extracted from the literature and the interviews, and keeping in mind other parameters such as the experimental feasibility, we have been able to identify diverse opportunities for BNC as a biomaterial. In my judgment, some of the most attractive ones are the use of BNC as a carrier for cellular therapies, a biomaterial for corneal wound healing or as a patch to repair internal organs. Moreover, the tunability of BNC has been recognised as a clear advantage to attain tailor-made BNC-based materials for specific unmet clinical demands. Therefore, the coming chapters of this thesis are largely guided by this non-experimental research.

Chapter references

1. Gangadoo, S. & Chapman, J. Emerging biomaterials and strategies for medical applications: A review. *Mater. Technol.* **30**, B3–B7 (2015).
2. Marin, E., Boschetto, F. & Pezzotti, G. Biomaterials and biocompatibility: An historical overview. *J. Biomed. Mater. Res. - Part A* **108**, 1617–1633 (2020).
3. Cicha, I., Singh, R., Garlich, C. D. & Alexiou, C. Nano-biomaterials for cardiovascular applications: Clinical perspective. *J. Control. Release* **229**, 23–36 (2016).
4. Kwak, M. H. *et al.* Bacterial cellulose membrane produced by *Acetobacter* sp. A10 for burn wound dressing applications. *Carbohydr. Polym.* **122**, 387–398 (2015).
5. Silva, N. H. C. S. *et al.* Bacterial cellulose membranes as transdermal delivery systems for diclofenac: In vitro dissolution and permeation studies. *Carbohydr. Polym.* **106**, 264–269 (2014).
6. Stumpf, T. R. *et al.* Design and evaluation of a biosynthesized cellulose drug releasing duraplasty. *Mater. Sci. Eng. C* **110**, 110677 (2020).
7. Fontana, J. D. *et al.* *Acetobacter* cellulose pellicle as a temporary skin substitute. *Appl. Biochem. Biotechnol.* **24–25**, 253–264 (1990).
8. Frykberg, R. G. & Banks, J. Challenges in the Treatment of Chronic Wounds. *Adv. wound care* **4**, (2015).
9. Okonkwo, U. A. & DiPietro, L. A. Diabetes and Wound Angiogenesis. *Int. J. Mol. Sci.* **18**, (2017).
10. Sun, G. *et al.* Dextran hydrogel scaffolds enhance angiogenic responses and promote complete skin regeneration during burn wound healing. *Proc. Natl. Acad. Sci.* **108**, 20976–20981 (2011).
11. MacNeil, S. Biomaterials for tissue engineering of skin. *Mater. Today* **11**, 26–35 (2008).
12. Araña, M. *et al.* Preparation and characterization of collagen-based ADSC-carrier sheets for cardiovascular application. *Acta Biomater.* **9**, 6075–6083 (2013).
13. Qi, C., Yan, X., Huang, C., Melerzanov, A. & Du, Y. Biomaterials as carrier, barrier and reactor for cell-based regenerative medicine. *Protein Cell* **6**, 638–653 (2015).
14. D’Este, M., Eglin, D., Alini, M. & Kyllonen, L. Bone regeneration with biomaterials and active molecules delivery. *Curr. Pharm. Biotechnol.* **16**, 582–605 (2015).
15. Gagner, J. E., Kim, W. & Chaikof, E. L. Designing protein-based biomaterials for medical applications. *Acta Biomater.* **10**, 1542–1557 (2014).
16. Green, J. J. & Elisseeff, J. H. Mimicking biological functionality with polymers for biomedical applications. *Nature* **540**, 386–394 (2016).
17. Wang, Y. *et al.* A Biomimetic Silk Fibroin/Sodium Alginate Composite Scaffold for Soft Tissue Engineering. *Sci. Rep.* **6**, (2016).

18. Wang, Y. *et al.* A Biomimetic Silk Fibroin/Sodium Alginate Composite Scaffold for Soft Tissue Engineering. *Scientific Reports*, **6**, 39477 (2016)
19. Dou, Y. *et al.* Keratin/Polyvinyl Alcohol Blend Films Cross-Linked by Dialdehyde Starch and Their Potential Application for Drug Release. *Polymers*. **7**, 580–591 (2015).
20. Dong, C. & Lv, Y. Application of collagen scaffold in tissue engineering: Recent advances and new perspectives. *Polymers*. **8**, 1–20 (2016).
21. Yamada, S., Yamamoto, K., Ikeda, T., Yanagiguchi, K. & Hayashi, Y. Potency of fish collagen as a scaffold for regenerative medicine. *Biomed Res. Int.* **2014**, 302932 (2014).
22. Mullins, R. J., Richards, C. & Walker, T. Allergic reactions to oral, surgical and topical bovine collagen Anaphylactic risk for surgeons. *Aust. N. Z. J. Ophthalmol.* **24**, (1996).
23. Eriksson, A., Burcharth, J. & Rosenberg, J. Animal derived products may conflict with religious patients' beliefs. *Med. Ethics* **14**, (2013).
24. Willard, J. J. *et al.* Plant-derived human collagen scaffolds for skin tissue engineering. *Tissue Eng. Part A* **19**, 1507–18 (2013).
25. Industry Analysis Report, 2025. Global Collagen Market Size By Source. (2017).
26. A. S. Mundada & J. G. Avari. Novel Biomaterial for Transdermal Application: In vitro and In vivo Characterization. *Drug Deliv.* **18**, 424–431 (2011).
27. Yunoki, S., Hatayama, H., Ebisawa, M., Kondo, E. & Yasuda, K. A novel fabrication method to create a thick collagen bundle composed of uniaxially aligned fibrils: An essential technology for the development of artificial tendon/ligament matrices. *J. Biomed. Mater. Res. - Part A* **103**, 3054–3065 (2015).
28. Baldwin, M., Snelling, S., Dakin, S. & Carr, A. Augmenting endogenous repair of soft tissues with nanofibre scaffolds. *J. R. Soc. Interface* **15**, 20180019 (2018).
29. Mihai, M. M. *et al.* Nanocoatings for Chronic Wound Repair—Modulation of Microbial Colonization and Biofilm Formation. *Int. J. Mol. Sci.* **19**, 1179 (2018).
30. Mofazzal Jahromi, M. A. *et al.* Nanomedicine and advanced technologies for burns: Preventing infection and facilitating wound healing. *Adv. Drug Deliv. Rev.* **123**, 33–64 (2018).
31. Andreu, V., Mendoza, G., Arruebo, M. & Irusta, S. Smart Dressings Based on Nanostructured Fibers Containing Natural Origin Antimicrobial, Anti-Inflammatory, and Regenerative Compounds. *Mater.* **8**, 5154–5193 (2015).
32. Gomes, S. R., Rodrigues, G., Martins, G. G., Henriques, C. M. R. & Silva, J. C. In vitro evaluation of crosslinked electrospun fish gelatin scaffolds. *Mater. Sci. Eng. C* **33**, 1219–1227 (2013).
33. Tonsomboon, K., Butcher, A. L. & Oyen, M. L. Strong and tough nanofibrous hydrogel composites based on biomimetic principles. *Mater. Sci. Eng. C* **72**, 220–227 (2017).

34. Ju, H. W. *et al.* Wound healing effect of electrospun silk fibroin nanomatrix in burn-model. *Int. J. Biol. Macromol.* **85**, 29–39 (2016).
35. Klemm, D. *et al.* Nanocellulose as a natural source for groundbreaking applications in materials science: Today's state. *Mater. Today* **21**, 720–748 (2018).
36. Zeng, M., Laromaine Sagué, A. & Roig Serra, A. Bacterial cellulose: fabrication, characterization and biocompatibility studies. (Autonomous University of Barcelona, 2014).
37. Hakkarainen, T. *et al.* Nanofibrillar cellulose wound dressing in skin graft donor site treatment. *J. Control. Release* **244**, 292–301 (2016).
38. Paukkonen, H. *et al.* Nanofibrillar cellulose hydrogels and reconstructed hydrogels as matrices for controlled drug release. *Int. J. Pharm.* **532**, 269–280 (2017).
39. Picheth, G. F. *et al.* Bacterial cellulose in biomedical applications: A review. *Int. J. Biol. Macromol.* **104**, 97–106 (2017).
40. Sulaeva, I., Henniges, U., Rosenau, T. & Potthast, A. Bacterial cellulose as a material for wound treatment: Properties and modifications. A review. *Biotechnol. Adv.* **33**, 1547–1571 (2015).
41. Brown, A. J. XLIII.—On an acetic ferment which forms cellulose. *J. Chem. Soc. Trans.* **49**, 432–439 (1886).
42. Müller, A. *et al.* The Biopolymer Bacterial Nanocellulose as Drug Delivery System: Investigation of Drug Loading and Release using the Model Protein Albumin. *J. Pharm. Sci.* **102**, 579–592 (2013).
43. Rajwade, J. M., Paknikar, K. M. & Kumbhar, J. V. Applications of bacterial cellulose and its composites in biomedicine. *Appl. Microbiol. Biotechnol.* **99**, 2491–2511 (2015).
44. Lee, K. Y., Buldum, G., Mantalaris, A. & Bismarck, A. More than meets the eye in bacterial cellulose: biosynthesis, bioprocessing, and applications in advanced fiber composites. *Macromol Biosci* **14**, 10–32 (2014).
45. Kralisch, D., Hessler, N., Klemm, D., Erdmann, R. & Schmidt, W. White biotechnology for cellulose manufacturing—the HoLiR concept. *Biotechnol Bioeng* **105**, 740–747 (2010).
46. Klemm, D. *et al.* Nanocelluloses: A new family of nature-based materials. *Angew Chem Int Ed Engl* **50**, 5438–5466 (2011).
47. Chen, L., Hong, F., Yang, X. X. & Han, S. F. Biotransformation of wheat straw to bacterial cellulose and its mechanism. *Bioresour Technol* **135**, 464–468 (2013).
48. Abeer, M. M., Mohd Amin, M. C. I. & Martin, C. A review of bacterial cellulose-based drug delivery systems: Their biochemistry, current approaches and future prospects. *J. Pharm. Pharmacol.* **66**, 1047–1061 (2014).
49. Gardner, K. H. & Blackwell, J. The structure of native cellulose. *Biopolymers* **13**, 1975–2001 (1974).

50. Guo, J. & Catchmark, J. M. Surface area and porosity of acid hydrolyzed cellulose nanowhiskers and cellulose produced by *Gluconacetobacter xylinus*. *Carbohydr. Polym.* **87**, 1026–1037 (2012).
51. Kim, D., Nishiyama, Y. & Kuga, S. Surface acetylation of bacterial cellulose. *Cellulose* **9**, 361–367 (2002).
52. Gatenholm, P. & Klemm, D. Bacterial Nanocellulose as a Renewable Material for Biomedical Applications. *MRS Bull.* **35**, (2010).
53. Bodin, A. *et al.* Influence of cultivation conditions on mechanical and morphological properties of bacterial cellulose tubes. *Biotechnol Bioeng* **97**, 425–434 (2007).
54. Pöttinger, Y., Kralisch, D. & Fischer, D. Bacterial nanocellulose: the future of controlled drug delivery? *Ther. Deliv.* **8**, 753–761 (2017).
55. Klemm, D., Schuhmann, D., Udhardt, U. & Marsch, S. Bacterial synthesized cellulose – artificial blood vessels for microsurgery. *Prog. Polym. Sci.* **26**, 1561–1603 (2001).
56. Nimeskern, L. *et al.* Mechanical evaluation of bacterial nanocellulose as an implant material for ear cartilage replacement. *J. Mech. Behav. Biomed. Mater.* **22**, 12–21 (2013).
57. Chan, E. C. *et al.* Three Dimensional Collagen Scaffold Promotes Intrinsic Vasculari- sation for Tissue Engineering Applications. *PLoS One* **11**, e0149799 (2016).
58. Zeng, M., Laromaine, A. & Roig, A. Bacterial cellulose films: influence of bacterial strain and drying route on film properties. *Cellulose* **21**, 4455–4469 (2014).
59. Reese, S. P. P., Farhang, N., Poulson, R., Parkman, G. & Weiss, J. A. A. Nanoscale Imaging of Collagen Gels with Focused Ion Beam Milling and Scanning Electron Microscopy. *Biophys. J.* **111**, 1797–1804 (2016).
60. Stein, H. *et al.* Production of Bioactive, Post-Translationally Modified, Heterotrimeric, Human Recombinant Type-I Collagen in Transgenic Tobacco. *2640 Biomacromol- ecules* **10**, 2640–2645 (2009).
61. Reese, S. P., Farhang, N., Poulson, R., Parkman, G. & Weiss, J. A. Nanoscale Imaging of Collagen Gels with Focused Ion Beam Milling and Scanning Electron Microscopy. *Biophys. J.* **111**, 1797–1804 (2016).
62. Yunoki, S., Hatayama, H., Ebisawa, M., Kondo, E. & Yasuda, K. A novel fabrication method to create a thick collagen bundle composed of uniaxially aligned fibrils: An essential technology for the development of artificial tendon/ligament matrices. *J. Biomed. Mater. Res. Part A* **103**, 3054–3065 (2015).
63. Kirkwood, J. E. & Fuller, G. G. Liquid Crystalline Collagen: A Self-Assembled Morphology for the Orientation of Mammalian Cells. *Langmuir* **25**, 3200–3206 (2009).
64. Ahn, S., Lee, S., Cho, Y., Chun, W. & Kim, G. Fabrication of three-dimensional col- lagen scaffold using an inverse mould-leaching process. *Bioprocess Biosyst. Eng.* **34**, 903–911 (2011).

65. Wang, S. *et al.* Super-Strong, Super-Stiff Macrofibers with Aligned, Long Bacterial Cellulose Nanofibers. *Adv. Mater.* **29**, 1702498 (2017).
66. Geisel, N. *et al.* Microstructured Multilevel Bacterial Cellulose Allows the Guided Growth of Neural Stem Cells. *Small* **12**, (2016).
67. Jia, Y., Zhu, W., Zheng, M., Huo, M. & Zhong, C. Bacterial cellulose/hyaluronic acid composite hydrogels with improved viscoelastic properties and good thermodynamic stability. *Plast. Rubber Compos.* **47**, 165–175 (2018).
68. Lee, S.-H., Kang, S.-S., Jeong, C.-M. & Huh, J.-B. The effect of bacterial cellulose membrane compared with collagen membrane on guided bone regeneration. *J Adv Prosthodont* **7**, 484–95 (2015).
69. Rafferty, R. M. *et al.* Multifunctional biomaterials from the sea: Assessing the effects of chitosan incorporation into collagen scaffolds on mechanical and biological functionality. *Acta Biomater.* **43**, 160–169 (2016).
70. Pertile, R. A. N., Andrade, F. K., Alves, C. & Gama, M. Surface modification of bacterial cellulose by nitrogen-containing plasma for improved interaction with cells. *Carbohydr. Polym.* **82**, 692–698 (2010).
71. Lv, X. *et al.* Bacterial Cellulose-Based Biomimetic Nanofibrous Scaffold with Muscle Cells for Hollow Organ Tissue Engineering. *ACS Biomater. Sci. Eng.* **2**, 19–29 (2016).
72. Heßler, N. & Klemm, D. Alteration of bacterial nanocellulose structure by in situ modification using polyethylene glycol and carbohydrate additives. *Cellulose* **16**, 899–910 (2009).
73. Madaghiele, M. *et al.* Assessment of collagen crosslinking and denaturation for the design of regenerative scaffolds. *J. Biomed. Mater. Res. Part A* **104**, 186–194 (2016).
74. Gonçalves, S. *et al.* Acetylated bacterial cellulose coated with urinary bladder matrix as a substrate for retinal pigment epithelium. *Colloids Surfaces B Biointerfaces* **139**, 1–9 (2016).
75. Bottan, S. *et al.* Surface-Structured Bacterial Cellulose with Guided Assembly-Based Biolithography (GAB). *ACS Nano* **9**, 206–219 (2014).
76. Pertile, R. A. N., Andrade, F. K., Alves, C. & Gama, M. Surface modification of bacterial cellulose by nitrogen-containing plasma for improved interaction with cells. *Carbohydr. Polym.* **82**, 692–698 (2010).
77. Courtenay Marcus A Johns Fernando Galembeck Christoph Deneke Evandro M Lanzoni Carlos A Costa Janet L Scott Ram I Sharma, J. C. *et al.* Surface modified cellulose scaffolds for tissue engineering. *Cellulose* **24**, 253–267 (2017).
78. Chua, A. W. C. *et al.* Skin tissue engineering advances in severe burns: review and therapeutic applications. *Burn. Trauma* **4**, 3 (2016).
79. Sundaramurthi, D., Krishnan, U. M. & Sethuraman, S. Electrospun Nanofibers as Scaffolds for Skin Tissue Engineering. *Polym. Rev.* **54**, 348–376 (2014).
80. Paul, W. *Advances in Wound Healing Materials.* (Smithers Rapra, 2015).

81. Andonova, M. & Urumova, V. Immune surveillance mechanisms of the skin against the stealth infection strategy of *Pseudomonas aeruginosa*—Review. *Comparative Immunol. Microbiol. Infect. Dis.* **36**, 433–448 (2013).
82. Mühlstädt, M., Thomé, C. & Kunte, C. Rapid wound healing of scalp wounds devoid of periosteum with milling of the outer table and split-thickness skin grafting. *Br. J. Dermatol.* **167**, 343–347 (2012).
83. Siedenbiedel, F. & Tiller, J. C. Antimicrobial Polymers in Solution and on Surfaces: Overview and Functional Principles. *Polymers (Basel)*. **4**, 46–71 (2012).
84. Simões, D. *et al.* Recent advances on antimicrobial wound dressing: A review. *Eur. J. Pharm. Biopharm.* **127**, 130–141 (2018).
85. Fontana, J. D. *et al.* Acetobacter cellulose pellicle as a temporary skin substitute. *Appl. Biochem. Biotechnol.* **24**, 253–264 (1990).
86. Ring, D. F., Nashed, W. & Dow, T. Liquid loaded pad for medical applications. **US4588400**, (1987).
87. Cavalcanti, L. M. *et al.* Efficacy of bacterial cellulose membrane for the treatment of lower limbs chronic varicose ulcers: a randomized and controlled trial. *Rev. Col. Bras. Cir.* **44**, 72–80 (2017).
88. Picheth, G. *et al.* Bacterial cellulose in biomedical applications: a review. *Int. J. Biol. Macromol.* **104**, 97–106 (2017)
89. Czaja, W. *et al.* Biomedical Applications of Microbial Cellulose in Burn Wound Recovery. *Cellul. Mol. Struct. Biol.* 307–321 (2007). doi:10.1007/978-1-4020-5380-1
90. Frankel, V. H., Serafica, G. C. & Damien, C. J. Development and testing of a novel biosynthesized XCell for treating chronic wounds. *Surg. Technol. Int.* **12**, 27–33 (2004).
91. Kwak, M. H. *et al.* Bacterial cellulose membrane produced by *Acetobacter* sp. A10 for burn wound dressing applications. *Carbohydr. Polym.* **122**, 387–398 (2015).
92. Li, Y. *et al.* Evaluation of the Effect of the Structure of Bacterial Cellulose on Full Thickness Skin Wound Repair on a Microfluidic Chip. *Biomacromolecules* **16**, 780–789 (2015).
93. Botton, S. *et al.* Surface-structured bacterial cellulose with guided assembly-based biolithography (GAB). *ACS Nano* **9**, 206–219 (2014).
94. Wu, H. *et al.* Regenerated chitin fibers reinforced with bacterial cellulose nanocrystals as suture biomaterials. *Carbohydr. Polym.* **180**, 304–313 (2018).
95. Wu, C.-N. *et al.* TEMPO-Oxidized Bacterial Cellulose Pellicle with Silver Nanoparticles for Wound Dressing. *Biomacromolecules* **19**, 544–554 (2018).
96. Khalid, A., Khan, R., Ul-Islam, M., Khan, T. & Wahid, F. Bacterial cellulose-zinc oxide nanocomposites as a novel dressing system for burn wounds. *Carbohydr Polym* **164**, 214–221 (2017).

97. Khalid, A. *et al.* Bacterial cellulose–TiO₂ nanocomposites promote healing and tissue regeneration in burn mice model. *RSC Adv.* **7**, 47662–47668 (2017).
98. Tsai, Y.-H., Yang, Y.-N., Ho, Y.-C., Tsai, M.-L. & Mi, F.-L. Drug release and antioxidant/antibacterial activities of silymarin–zein nanoparticle/bacterial cellulose nanofiber composite films. *Carbohydr. Polym.* **180**, 286–296 (2018).
99. Alkhatib, Y. *et al.* Controlled extended octenidine release from a bacterial nanocellulose/Ploxamer hybrid system. *Eur. J. Pharm. Biopharm.* (2017). **112**, 164–176 (2017)
100. de Lima Fontes, M. *et al.* Effect of in situ modification of bacterial cellulose with carboxymethylcellulose on its nano/microstructure and methotrexate release properties. *Carbohydr. Polym.* **179**, 126–134 (2018).
101. Hobzova, R. *et al.* Embedding of Bacterial Cellulose Nanofibers within PHEMA Hydrogel Matrices: Tunable Stiffness Composites with Potential for Biomedical Applications. *J. Nanomater.* **2018**, 1–11 (2018).
102. Fürsatz, M. *et al.* Functionalization of bacterial cellulose wound dressings with the antimicrobial peptide ϵ -poly-L-Lysine. *Biomed. Mater.* **13**, 25014 (2018).
103. Wang, J., Gao, C., Zhang, Y. & Wan, Y. Preparation and in vitro characterization of BC/PVA hydrogel composite for its potential use as artificial cornea biomaterial. *Mater. Sci. Eng. C* **30**, 214–218 (2010).
104. R. Rebelo, A. *et al.* Dehydration of bacterial cellulose and the water content effects on its viscoelastic and electrochemical properties. *Sci. Technol. Adv. Mater.* **19**, 203–211 (2018).
105. Moraes, P. R. F. de S. *et al.* Bacterial Cellulose/Collagen Hydrogel for Wound Healing. *Mater. Res.* **19**, 106–116 (2016).
106. Lamboni, L., Li, Y., Liu, J. & Yang, G. Silk Sericin-Functionalized Bacterial Cellulose as a Potential Wound-Healing Biomaterial. *Biomacromolecules* **17**, 3076–3084 (2016).
107. Lin, W.-C., Lien, C.-C., Yeh, H.-J., Yu, C.-M. & Hsu, S. Bacterial cellulose and bacterial cellulose–chitosan membranes for wound dressing applications. *Carbohydr. Polym.* **94**, 603–611 (2013).
108. Lin, S.-P. *et al.* Novel dextran modified bacterial cellulose hydrogel accelerating cutaneous wound healing. *Cellulose* **24**, 4927–4937 (2017).
109. Ye, S. *et al.* Flexible Amoxicillin-Grafted Bacterial Cellulose Sponges for Wound Dressing: In Vitro and in Vivo Evaluation. *ACS Appl. Mater. Interfaces* **10**, 5862–5870 (2018).
110. Mohamad, N., Loh, E. Y. X., Fauzi, M. B., Ng, M. H. & Mohd Amin, M. C. I. In vivo evaluation of bacterial cellulose/acrylic acid wound dressing hydrogel containing keratinocytes and fibroblasts for burn wounds. *Drug Deliv. Transl. Res.* **9**, 444–452 (2019).
111. Lace, R., Celia, M.-D. & Williams, R. Biomaterials for ocular reconstruction. *J. Mater. Sci.* **50**, 1523–1534 (2015).

112. Alex G. Mcgaughy, BS, and Preeya K. Gupta, M., Edited by Sharon Fekrat, MD, and Ingrid U. Scott, MD, M., McGaughy, A. & Gupta, MD, P. In Office Use of Amniotic Membrane. *Cornea* **3**, 31–32 (2015).
113. Parihar, J. K. S., Parihar, A. S., Jain, V. K., Kaushik, J. & Nath, P. Allogenic cultivated limbal stem cell transplantation versus cadaveric keratolimbal allograft in ocular surface disorder: 1-year outcome. *Int. Ophthalmol.* **37**, 1323–1331 (2017).
114. Wu, Z., Kong, B., Liu, R., Sun, W. & Mi, S. Engineering of Corneal Tissue through an Aligned PVA/Collagen Composite Nanofibrous Electrospun Scaffold. *Nanomaterials* **8**, 124 (2018).
115. Isaacson, A., Swioklo, S. & Connon, C. J. 3D bioprinting of a corneal stroma equivalent. *Exp. Eye Res.* **173**, 188–193 (2018).
116. Yao, Q. *et al.* Electrospun collagen/poly(L-lactic acid-co- ϵ -caprolactone) scaffolds for conjunctival tissue engineering. *Exp. Ther. Med.* **14**, 4141–4147 (2017).
117. Williams, R., Lace, R., Kennedy, S., Doherty, K. & Levis, H. Biomaterials for Regenerative Medicine Approaches for the Anterior Segment of the Eye. *Adv. Healthc. Mater.* **7**, 1701328 (2018).
118. Ullah, H., Wahid, F., Santos, H. A. & Khan, T. Advances in biomedical and pharmaceutical applications of functional bacterial cellulose-based nanocomposites. *Carbohydr. Polym.* **150**, 330–352 (2016).
119. de Oliveira Barud, H. G. *et al.* A multipurpose natural and renewable polymer in medical applications: Bacterial cellulose. *Carbohydr. Polym.* **153**, 406–420 (2016).
120. Laromaine, A. *et al.* Free-standing three-dimensional hollow bacterial cellulose structures with controlled geometry via patterned superhydrophobic–hydrophilic surfaces. *Soft Matter* **14**, 3955–3962 (2018).
121. Cao, J., Zhang, C., Zhao, S., Wan, Y. & Hu, D. Feasibility of bacterial cellulose membrane as biological scaffold for construction of tissue engineering corneal epithelium. *Chinese J. Exp. Ophthalmol.* **34**, 121–124 (2016).
122. Rodrigo V. Sepúlveda, Fabrício L. Valente, Emily C.C. Reis, Fabiana R. Araújo, Renato B. Eleotério, Paulo V.S. Queiroz, A. P. B. B. Bacterial cellulose and bacterial cellulose/polycaprolactone composite as tissue substitutes in rabbits' cornea. *Pesq. Vet. Bras* **36**, 986–992 (2016).
123. Bourne, R. R. A. *et al.* Prevalence and causes of vision loss in high-income countries and in Eastern and Central Europe in 2015: magnitude, temporal trends and projections. *Br J Ophthalmol* **102**, 575–585 (2018).
124. Gonçalves, S. *et al.* Bacterial Cellulose As a Support for the Growth of Retinal Pigment Epithelium. *Biomacromolecules* **16**, 1341–1351 (2015).

125. Beekmann, U., Weyell, P., Küpper, C., Dederichs, M. & Kralisch, D. Modified Bacterial Nanocellulose as biodegradable carrier system for antibiosis in dentistry. *9th Annual Meeting of German Society for Biomaterials* (2017).
126. Weyell, P. *et al.* Tailor-made material characteristics of bacterial cellulose for drug delivery applications in dentistry. *Carbohydr. Polym.* **207**, 1–10 (2019).
127. Chiaoprakobkij, N., Sanchavanakit, N., Subbalekha, K., Pavasant, P. & Phisalaphong, M. Characterization and biocompatibility of bacterial cellulose/alginate composite sponges with human keratinocytes and gingival fibroblasts. *Carbohydr. Polym.* **85**, 548–553 (2011).
128. Biskin, S. *et al.* A new graft material for myringoplasty: bacterial cellulose. *Eur. Arch. Oto-Rhino-Laryngology* **273**, 3561–3565 (2016).
129. Angtika, R. S., Widiyanti, P. & Aminatun. Bacterial Cellulose–Chitosan–Glycerol Biocomposite as Artificial Dura Mater Candidates for Head Trauma. *J. Biomimetics, Biomater. Biomed. Eng.* **36**, 7–16 (2018).
130. Lima, F de M. T. de *et al.* Biocompatible bacterial cellulose membrane in dural defect repair of rat. *J. Mater. Sci. Mater. Med.* **28**, 37 (2017).
131. Rosen, C. L. *et al.* Results of the prospective, randomized, multicenter clinical trial evaluating a biosynthesized cellulose graft for repair of dural defects. *Neurosurgery* **69**, 1093–1103 (2011).
132. Hansson, G. C. Role of mucus layers in gut infection and inflammation. *Curr Opin Microbiol* **15**, 57–62 (2012).
133. Yu, M. *et al.* Rotation-Facilitated Rapid Transport of Nanorods in Mucosal Tissues. *Nano Lett.* **16**, 7176–7182 (2016).
134. de Oliveira Barud, H. G. *et al.* A multipurpose natural and renewable polymer in medical applications: Bacterial cellulose. *Carbohydr. Polym.* **153**, 406–420 (2016).
135. Tronser, T., Laromaine, A., Roig, A. & Levkin, P. A. Bacterial Cellulose Promotes Long-Term Stemness of mESC. *ACS Appl. Mater. Interfaces* **10**, 16260–16269 (2018).
136. Carvalho, T., Guedes, G., Sousa, F. L., Freire, C. S. R. & Santos, H. A. Latest Advances on Bacterial Cellulose-Based Materials for Wound Healing, Delivery Systems, and Tissue Engineering. *Biotechnol. J.* **14**, e1900059 (2019).
137. de Oliveira Barud, H. G. *et al.* Bacterial Nanocellulose in Dentistry: Perspectives and Challenges. *Molecules* **26**, 49 (2020).
138. Klemm, D. *et al.* Biotech nanocellulose: A review on progress in product design and today's state of technical and medical applications. *Carbohydr. Polym.* **15**, 117313 (2020).

Chapter 2

Evaluating BNC and BNC/TiO₂ nanocomposites as cell carriers with sunscreen capacity

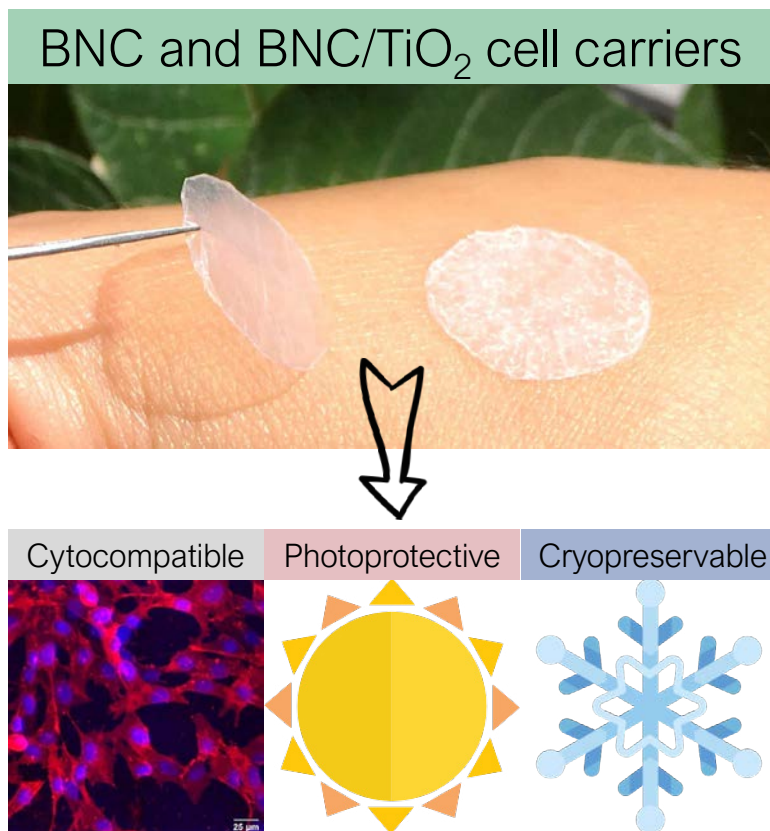


Figure 1: Graphical summary of Chapter 2. The studied BNC and titania hybrids cell carriers (up) and their validated properties (bottom).

Chapter introduction

BNC is broadly considered to be non-toxic and well-tolerated when implanted *in vivo*¹⁻³. These features, coupled with its mechanical properties and nanofibrillary structure mirroring the extracellular matrix (ECM), call for a wide range of uses in the biomedical domain⁴⁻⁶. As commented in Chapter 1, BNC has been advocated as an appealing substrate to grow and expand mammalian cells⁷⁻¹⁰, raising hopes about its value in the blooming field of cellular therapies^{11,12}. Accordingly, assessing BNC as a cell carrier has been one of the main motivations of this thesis.

On the other hand, BNC nanocomposites have gained interest due to the synergies that can be achieved by combining BNC with other functional nanomaterials^{13,14}. A widespread approach has been the incorporation of inorganic nanoparticles (NPs), such as silver (Ag) or titanium dioxide (TiO₂), conferring BNC with antimicrobial properties¹⁵⁻¹⁷. Notably, nano-sized TiO₂ has also been proposed to promote wound healing^{18,19} and to act as a linker between drug molecules and cellulose nanofibers^{20,21}. Besides, nanotitania is regularly used in sunscreens formulations^{22,23} due to its UV-absorption and biocompatibility. Of note is also that photoprotection was mentioned by some interviewed clinicians in the previous chapter as a desirable property for biomaterials used to treat exposed areas of the body.

In the present chapter, I investigate the interactions between pure BNC and modified BNC substrates incorporating TiO₂ NPs with model human cells aiming at:

1. Gaining a better understanding of the cytocompatibility of BNC and its derivatives. This analysis will complement other's publications reporting on the lack of cytotoxicity of BNC through MTT or similar assays²⁴⁻²⁶. Besides, I will focus on cell adhesion, morphology and the possibility to retrieve the cells from the BNC structures.
2. Exploring BNC as a cell culture and transplantation tool.
3. Developing BNC-based substrates with advanced functionalities.

Accordingly, BNC/TiO₂ nanocomposites (anatase phase) were fabricated via an in-house microwave-assisted route^{27,28} and studied together with unmodified BNC. First, an in-depth material and *in vitro* biological characterization of BNC

and the titanium nanocomposites is presented. Then, functionality tests were carried out to evaluate practical applications of these substrates; namely, we focused on three putative uses:

1. BNC and BNC/TiO₂ as supports for adherent cell cryopreservation (reported in Publication 2: I. Anton-Sales *et al.*, *ACS Biomater. Sci. Eng.*, 2020).
2. The photoprotective effects of BNC and the titania hybrids for sunscreen applications
3. The antimicrobial capacity of both substrates towards *Escherichia coli* (*E. coli*).

Publication 2: Bacterial Nanocellulose and Titania Hybrids: Cytocompatible and Cryopreservable Cell Carriers

Irene Anton-Sales, Soledad Roig-Sanchez, Maria Jesus Sánchez-Guisado, Anna Laromaine and Anna Roig. *ACS Biomaterials Science & Engineering* **6**, 4893–4902 (2020).

Reprinted with permission. Copyright: 2020 American Chemical Society.

<https://pubs.acs.org/doi/10.1021/acsbmaterials.0c00492>

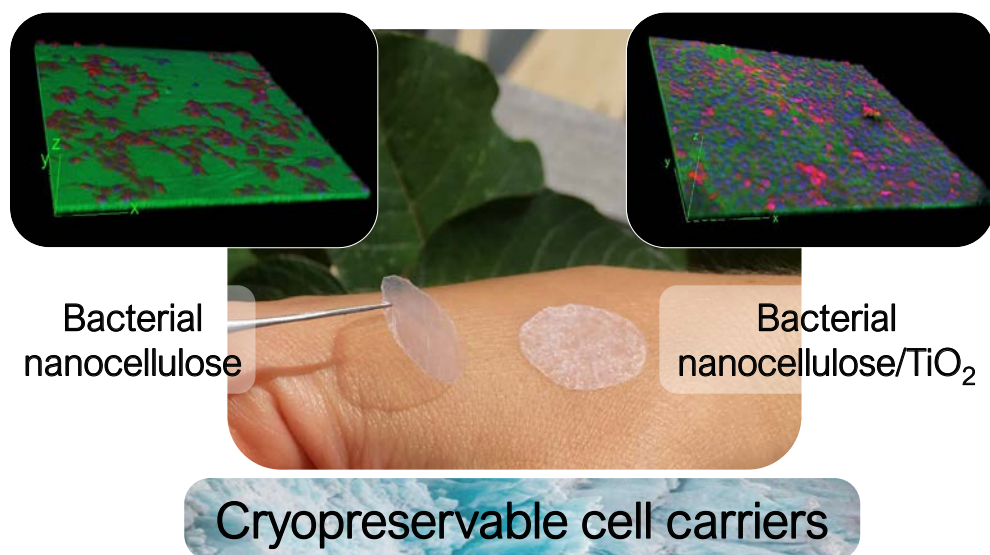


Figure 2: Graphical abstract of Publication 2.

Abstract

Carrier-assisted cell transplantation offers new strategies to improve the clinical outcomes of cellular therapies. Bacterial nanocellulose (BC) is an emerging biopolymer that might be of great value in the development of animal-free, customizable and temperature-stable novel cell carriers. Moreover, BC exhibits a myriad of modification possibilities to incorporate additional functionalities. Here, we have synthesized BC-titanium dioxide (TiO₂) nanocomposites (BC/TiO₂) to evaluate and compare the suitability of not only BC but also a model hybrid nanobiomaterial as cell transplantation supports. This work provides thorough information on

the interactions between BC-based substrates and model human cells in terms of cell attachment, morphology, proliferation rate and metabolic activity. Two methods to partially retrieve the adhered cells are also reported. Both BC and BC/TiO₂ substrates are positively evaluated in terms of cytocompatibility and endotoxin content without detecting major differences between BC and BC nanocomposites. Lastly, the effective cryopreservation of cells-BC and cells-BC/TiO₂ constructs, yielding high cell viability and intact cell carriers after thawing, is demonstrated. Taken together, our results show that both BC and BC/TiO₂ enable to integrate the processes of expansion and long-term storage of human cells in transportable, robust and easy to manipulate supports. We expect these findings to encourage further applications of BC-based biomaterials in cellular therapies and to prompt research on BC-nanocomposites exhibiting advanced functionalities.

Keywords

Microbial cellulose; Nanocomposites; Titania; Cryopreservation; Fibroblasts; Cell culture support

Introduction

Cell transplantation approaches rely on a dual beneficial effect evoked by the administered cells: i) repopulation of the wound bed and ii) contribution towards a favourable microenvironment for tissue repair (*via* secretion of cytokines and growth factors). Cellular therapies in the form of autologous^{29,30} or allogenic³¹ cell transplants exhibit a long-proven efficacy to treat complicated skin lesions; while extending these therapies to other organs³² and developing innovative cell delivery systems³³ represents an active focus of research. Despite some satisfactory clinical outcomes have already been obtained^{34,35}, the complex administration of therapeutic cells *i.e.*, insufficient survival and integration of cells delivered in suspensions or sprays^{36–38}, hinders the widespread implementation of some cell therapies. Moreover, the next generation of cellular products should be provided in a ready-to-use

format to decrease waiting times and be used on-demand. To this end, long-term and reliable storage (*e.g.* cryopreservation) of cellular products needs to be further developed and standardized. The use of cell carriers can contribute to overcoming some of these bottlenecks; specifically by enhancing cell survival, controlling differentiation and retaining the transplanted cells at the target site. Last but not least, cell vehicles can also facilitate cryopreservation and the handling of therapeutic cells³⁹.

Collagen-based biomaterials represent the current gold standard for cell transplantation supports mainly because of its ability to support cell attachment and proliferation^{36,40}. However, collagen presents some disadvantages such as a certain risk of immunogenicity, poor batch-to-batch reproducibility and low availability all due to its animal origin. Nanocellulose synthesized by bacteria (referred here as bacterial nanocellulose, BC) is a biopolymer with potential applicability as an alternative cell carrier. BC inherently presents many of the characteristics sought-after for cell transplantation supports namely; purity, conformability, water holding capacity and porosity¹⁴. Besides, the high thermal and mechanical stability of BC are favourable features for the clinical translation since they enable heat-sterilization, easy handling and fixation by sutures⁴¹. The interwoven nanofibrillar structure of BC is responsible for most of these unique physicochemical properties and the high architectural similarity to collagenous structures. BC was first proposed as a substrate for mammalian cell culture in the 1990s by Watanabe *et al*⁷. Later studies have reported on BC functionalized with the tripeptide motif RGD for the culture of fibroblasts⁴² or surface-modified BC as support for retinal pigment epithelial cells^{43,44}. However, uncoated BC substrates have also been successfully loaded with several cells types^{45–47} and proved to prolong stemness of mouse embryonic stem cells⁴⁸. These findings imply that BC could be deemed as an alternative to collagen in the design of novel carriers for cell transplantation therapies⁴⁹ and *in vitro* studies⁸. On the other hand, BC has been suggested as a cryoprotectant agent⁵⁰ and other cellulosic materials have been employed as substrates to cryopreserve embryos⁵¹ and fungi⁵². However, the possibility to cryopreserve BC-cell constructs has not been addressed so far.

Considering the remarkable functional properties that inorganic nanoparticles (NPs) can endow to BC and the rising research attention on hybrid biomaterials¹³, it is of great interest to investigate the impact of these NPs on cells cultured on

such BC nanocomposites. Because of its widespread use in skin-related applications, titanium dioxide (TiO_2) NPs were selected here as a model NP among the plethora of biocompatible NPs to be combined with BC. Importantly, colloidal TiO_2 NPs have recently been suggested for dermal treatments as antimicrobial and scar-reducing agents^{18,19}. TiO_2 NPs have also been incorporated to plant-derived nanocellulose patches as a linker for drug molecules to modulate release kinetics^{20,21}. In another study, TiO_2 NPs combined with BC films created an efficient wound dressing in a burn mice model⁵³. Nevertheless, the role of TiO_2 on the performance of BC as a cell carrier has never been systematically studied.

Here, we present a thorough study of BC and BC/ TiO_2 nanocomposites as versatile and portable cell culture supports. The two substrates are structurally characterized and proven endotoxin-free and then *in vitro* studies on cell attachment, proliferation, viability and morphology are described. Next, three methods to retrieve the cells adhered to BC and BC/ TiO_2 supports are tested. Finally, we show that cell-BC and cell-BC/ TiO_2 constructs can be effectively cryopreserved yielding highly viable cell populations and intact carriers after thawing.

Experimental section

BC and BC/ TiO_2 substrates: synthesis and characterization

Bacterial nanocellulose production

A commercial *Komagataeibacter xylinus* (*K. xylinus*) strain (NCIMB 5346 from CECT, Valencia, Spain) was initially cultured in Hestrin-Schramm (HS) solid medium consisting of 1.15 g citric acid, 6.8 g $\text{Na}_2\text{HPO}_4 \cdot 12\text{H}_2\text{O}$, 5 g peptone, 5 g yeast extract, 15 g agar and 20 g dextrose all from Condalab for 1 L of Milli-Q water. Next, a bacterial inoculum was picked with a loop and used to inoculate 6 mL of HS liquid medium (same composition as the solid medium but without agar) and this culture was expanded during 7 days at 30° C. Then, 0.5 mL of the previous broth was mixed with 4.5 mL of fresh HS liquid medium and further incubated for 7 days. Finally, a 1:14 dilution of the former bacterial solution was performed with fresh medium and transferred to 24 well-plates (2 mL/well). The culture remained 3 days at 30° C under static conditions and circular BC hydrogels formed

at the air-liquid interface of every well with the same diameter as the container ($\approx 2 \text{ cm}^2$). BC pellicles were picked with plastic tweezers and soaked in a solution of 1:1 Ethanol: deionized water (DI) for 10 min to kill the bacteria.

The exhaustive cleaning process of the BC involved different boiling steps; a) 40 minutes in DI water and b) two periods of 20 minutes in 0.1 M NaOH (Sigma-Aldrich) aqueous solution to remove all organic residues. Lastly, BC films were rinsed with DI water until neutral pH was reached. Then, the films were autoclaved (121 °C, 20 min) and stored in DI water at room temperature until further use. If needed, BC samples were dried at 60 °C between two Teflon plates under a 1 kg weight.

Bacterial nanocellulose functionalization with TiO₂ nanoparticles

For the BC functionalization with TiO₂ NPs, a previously described^{27,28} microwave (CEM Discover Explorer-12 Hybrid reactor operating at a frequency of 2.45 GHz and with a maximum power of 300 W placed in a clean room) assisted method was employed. Briefly, never dry BC films were soaked in benzyl alcohol (99% BA from Scharlau) for approx. 30 minutes to allow solvent exchange and then transferred to a glass tube containing 4 mL of benzyl alcohol and 140 μL of titanium (IV) butoxide (TBOT, 97%, Sigma-Aldrich). All the precursors were mixed immediately before starting the microwave reaction to avoid hydrolysis of the titanium precursor. The reaction vessel was heated in two steps: 1) 5 min at 50 °C 2) 10 min at 190 °C. After the reaction, the BC/TiO₂ films were rinsed once with ethanol to remove the excess of NPs and several times with DI water until reaching a neutral pH. After TiO₂-functionalization, the never dry BC films were dried at 60 °C between two Teflon plates under 1 kg weight.

Endotoxin contamination study

According to the FDA recommendations⁵⁴, the endotoxin extraction was carried out by placing autoclaved BC and BC/TiO₂ never dry samples in depyrogenated falcon tubes with 40 mL of endotoxin-free water during 72 h at 30 °C and under orbital agitation (100 rpm). To evaluate the endotoxin content in the eluates from BC and BC/TiO₂ films, a Pierce™ LAL Chromogenic Endotoxin Quantification Kit was purchased from Thermo Fisher and the assay was performed following the kit's instructions. The products of the reaction were measured for absorbance

at 405 nm in a microplate reader (Infinite 200 PRO, TECAN ®) at 37 °C. The indicated values correspond to the mean \pm standard deviation of two independent experiments obtained from two different endotoxin quantification kits and evaluating each time two samples from two different batches of BC.

Scanning electron microscopy (SEM)

Dry BC and BC/TiO₂ films were fixed flat on top of aluminium SEM sample holders with adhesive carbon tape. The samples were coated with 5 nm of platinum before imaging. A high-resolution scanning electron microscope (FEI Magellan 400L XHR SEM) was used under high vacuum with an acceleration voltage of 2 kV. To image the BC/TiO₂ samples without Pt coating, the same sample preparation without the sputtering step was performed. Energy-dispersive X-ray (EDX) spectroscopy was performed with the same equipment on two BC/TiO₂ samples.

Atomic force microscope (AFM)

To obtain topographical images and roughness measurements of BC and BC/TiO₂ pellicles, a 5100 Agilent Technologies atomic force microscopy was employed on tapping mode and equipped with a FORT tip from AppNano. At least three 30 x 30 μm or 50 x 50 μm images were obtained for four different dry BC and BC/TiO₂ films. The images were processed with Surface analysis software V7.4 (64-bit) - Mountains technology. The indicated roughness values correspond to mean \pm standard deviations.

Thermo-gravimetric analysis (TGA)

Thermal decomposition studies were performed with a NETZSCH -STA 449 F1 Jupiter analyser employing a heating rate of 10 °C per minute from 25 to 600 °C at an air atmosphere. Three dry BC and three dry BC/TiO₂ samples were analysed.

Inductively coupled plasma – optical emission spectroscopy (ICP-OES)

Dry BC/TiO₂ samples were immersed in 8 mL of water during one month under mild agitation and then the eluates were collected for analysis with an ICP-OES Optima 4300DV Perkin-Elmer.

Transmission electron microscopy (TEM)

The nanoparticles characterization was performed through JEOL JEM-1210 electron microscope operating at 120 kv with an ORIUS 831 SC 600 Gatan camera. TEM images were analysed with Image J software and a histogram of 360 nanoparticles was fitted to a Gaussian function. The percentage of standard deviation divided mean value was obtained as the polydispersity value. Selected area electron diffraction (SAED) was used to obtain diffraction patterns from the TiO₂ nanoparticles.

BC and BC/TiO₂ substrates: evaluation as cell carriers

In vitro studies

For the *in vitro* experiments, a human dermal fibroblast cell line was used (1BR3.G cells, ECACC 90020507) as a model. The cultures were maintained in Dulbecco's Modified Eagle Medium (DMEM) supplemented with 2 mM GlutaMax and 10% foetal bovine serum (South American FBS) both from Gibco and monitored with an inverted optical microscope (Nikon Eclipse TS100). 1BR3.G cells were kept in a T75 flask (Sarstedt) at 37° C in 10% CO₂ and split three times per week.

For all the experiments detailed in this section, dry BC and BC/TiO₂ samples were rehydrated in DI water and autoclaved (121 °C, 20 min) before being used as cell supports. To plate the cells, BC and BC/TiO₂ films were preconditioned with warm DMEM and then transferred to 24-well plates using forceps and irradiated with UV light for 30 minutes to ensure sterility. A concentrated cell suspension (50.000 cells/well for the proliferation study and 100.000 cells/well for the rest of the experiments) was carefully pipetted on the middle of the pellicles. When the cell suspension was absorbed by the BC films, 500 µL of fresh culture medium were added to each well. See Figure S2 for an illustration of this process. Controls (uncoated commercial cell culture plates) were seeded with the same procedure and number of cells than the substrates.

Cell proliferation was assessed qualitatively by optical microscope and quantitatively with the CellTiter-Glo® Luminescent Cell Viability Assay (Promega) by measuring ATP levels on the cultures at Day 1, Day 3 and Day 8 after cell seeding.

For this assay, all the elements were accommodated at RT and then the cell-loaded films were transferred to unused culture wells and washed with PBS before adding 100 μL of the CellTiter-Glo® reagent to each well together with 100 μL of DMEM. The 24 multiwell plates were agitated for 2 minutes to lysate the cells and then incubated during 10 minutes at RT to stabilize the luminescence. After careful mixing, 150 μL of the supernatant of each well were transferred to a 96 well plate with an opaque bottom for the luminescent read. Blanks were performed with plain BC films and culture medium without cells. Luminescence was read with a Tecan Spark® multimode microplate reader (LifeSciences) with an integration time of 1000 ms. The experiment was performed three times with three technical replicates at each time point.

Cell viability, distribution and morphology were studied with a confocal laser scanning microscope (Leica SP5) 48 hours after plating the cells. Calcein-AM (BD Pharmingen™) staining was used to monitor the viability of the cells growing on BC and BC/TiO₂ supports since this reagent becomes fluorescent after being cleaved by intracellular esterases that are only present on alive cells. Cell-loaded BC and BC/TiO₂ films were washed with Hank's Balanced Salt Solution (HBSS, Gibco) and then incubated during 15 minutes in the dark with 1 mL/sample of 4 $\mu\text{g}/\text{mL}$ Calcein-AM in HBSS and washed twice with HBSS. Then the cells were fixed with 4% cold paraformaldehyde (Panreac) during 5 minutes. Fixed cells were further stained during 5 minutes with 1 $\mu\text{g}/\text{mL}$ of Hoechst 33342 (Invitrogen, cell nuclei, blue) and 5 $\mu\text{g}/\text{mL}$ CellMask™ Deep Red Plasma Membrane Stain (Invitrogen, cell membranes, red) diluted in PBS and rinsed again. Calcein was excited at a wavelength of 495 nm, Hoesch at 350 nm and Cell Mask at 588 nm. The BC and BC/TiO₂ films were flipped so that the cells faced the surface of Ibidi Glass Bottom dishes to be imaged with 10X (dry), 20X (dry) or 40X (oil) objectives. Several images of different z planes were obtained for each sample so that all the cross-section of the sample was covered. These stacks of images were then used to generate 3D reconstructions with the Fiji package of ImageJ (64-bit version). Cell shape descriptors were analysed with the same software by measuring >60 cells for each condition from images taken from three independent experiments. For the axial ratio, the length of the longer axis of each cell was divided by the length of the shortest axis. Circularity was calculated as $4\pi \cdot (\text{cell area} / \text{cell pe-}$

rimeter²). The nuclear-cytoplasmic ratio (N:C ratio) was obtained by dividing the nuclear area between the total area of the cell. To fluorescently stain the substrates (Images in Figure 3 and 4), rewet BC and BC/TiO₂ films were stained with Safranin-O (Alfa Aesar, 0.01% weight/volume dilution in DI water) overnight and rinsed several times before plating the cells. The Safranin-O dye was excited with a 495 nm laser.

Cryopreservation of cell-biomaterial constructs

For the cryopreservation experiment, 100,000 1BR3.G cells were seeded on triplicates on BC and BC/TiO₂ rewet films and conventional cell culture surfaces (controls) and expanded until highly confluent cultures were achieved; 1 week for BC and BC/TiO₂ substrates and 5 days for controls. Cell-loaded BC and BC/TiO₂ films were transferred to 1.8 mL cryovials (Nunc) containing 1 mL cryopreservation medium consisting of 90% FBS and 10% cell culture grade DMSO. Controls cells were detached from the culture wells using Trypsin-EDTA, centrifuged for 5' at 1400 rpm and then re-suspended in 1 mL of the same cryopreservation medium and transferred to cryovials. The cryovials were kept overnight inside a CoolCell® container at -80 °C to allow a controlled freezing rate of -1 °C/minute. Then, the vials were stored for at least one week at -196 °C on a liquid nitrogen tank. BC and BC/TiO₂ films without cells were included to monitor the material stability upon cryostorage.

All the vials were thawed directly by immersion on a 37 °C water bath. The BC and BC/TiO₂ films were carefully transferred to 24-well plates containing fresh culture medium using tweezers. Control cells were precipitated upon centrifugation and re-suspended in warm DMEM before being transferred to culture well plates. 24 hours later, the medium was changed to remove DMSO remains. Cell recovery was assessed at three time-points: before cryopreservation, 4 and 48 hours after thawing. Cell morphology was monitored with a contrast phase microscope and cell viability was qualitatively evaluated with Calcein-AM staining (described in the previous section) and quantitatively with the CellTiter-Glo® Luminescent Cell Viability Assay also detailed before performing the luminescence reads with a VICTOR 3 plate reader (PerkinElmer). Cell viability after thawing was calculated for each condition relative to the luminescent signal obtained for the not cryopreserved samples.

Cell retrieve

For the trypsin-based cell retrieve experiment, BC, BC/TiO₂ films and controls (cell culture plates) were used as supports to plate 100.000 1BR3.G cells as previously described (triplicates). To estimate the number of cells that attached to the supports, the number of unattached cells, floating on the culture medium, was counted 4 hours after plating as follows: Subsequently to exhaustive homogenization, a sample of 10 µL of the cell suspension was mixed with 10 µL of Trypan Blue Stain (0.4%, Gibco) to count the number of cells that were not attached to the BC and BC/TiO₂ substrates using a Neubauer chamber. 48 hours later, the same cell cultures were washed thoroughly with PBS (Gibco) and trypsinized using 250 µL trypsin-EDTA (0.05%, Gibco)/well during 5 minutes. The enzyme was neutralized with 500 µL of DMEM and the cells that were floating on the medium were counted in the same manner. To estimate the percentage of recovered cells, the initial number of attached cells (100.000 minus the number of not attached cells) was multiplied by the cell proliferation rate calculated for BC and BC/TiO₂ after 48 hours of culture to obtain the theoretical number of cells present on each film. Then the percentage of recovered cells was estimated by dividing the number of detached cells upon trypsinization between the expected numbers of cells for each film. Optical microscopy observations were also conducted to match these calculations. The cell recovery was considered to be 100% for the controls and the experiment was repeated three times.

To study cell retrieve via migration of cells from BC films to other substrates, 100.000 1BR3.G cells were seeded by triplicate on rewet BC and BC/TiO₂ films and cultured for 48 hours. Then, the films were placed upside-down with the cells contacting the new substrates (cell culture plate and never dry BC hydrogels) using tweezers and further incubated for 72 hours. After that, the original films were removed and the migration/transference of cells was qualitatively evaluated with an optical microscope. Migrated-cell's viability was confirmed upon Calcein-AM staining. The experiment was repeated three times.

The third method tested to recover cells from BC and BC/TiO₂ substrates consisted of the enzymatic dissolution of the substrates using cellulase. Three samples of BC and BC/TiO₂ were seeded with 100.000 1BR3.G cells and incubated until reaching high confluence. Then, the samples were rinsed with PBS incubated

with a commercial mix of cellulases (GrowDase™, UPM Biomedicals) at 37 °C until cellulose degradation was observed. Two different concentrations of cellulase were tested: a) 0.45 mg/ sample and 0.675 mg/ sample diluted in culture medium in a total volume of 300 µL. BC degradation was monitored and photographed with an inverted optical microscope (Nikon Eclipse TS100).

Statistical analysis

Quantitative data are expressed as means ± standard deviation. Statistical analyses were performed with Graph Pad Prism 5 software using one-way ANOVA followed by Tukey's multiple comparison test. To compare two different experimental conditions Student's T-tests were conducted. Statistical significance was accepted when obtained P-values were ≤ 0.05 and summarized as * = <0.05, ** = <0.01, *** = <0.001 for the calculated P-values.

Results and discussion

Substrate characterization

BC directly obtained from the *K. xylinus* cultures are hydrogels with a water content of >100 times its own dry weight and a typical thickness of ~800 µm. These samples are semi-transparent after cleaning, sturdy and easy to manipulate and here are referred to as 'never dry BC'. When never dry BC is dried at 60° C under 1 kg weight, its thickness reduces to ~20 micron and samples acquire a paper-like appearance. Upon rehydration, the dry films do not absorb as much water as the never dry BC and exhibited a thickness of ~23 µm⁵⁵. The rehydrated BC samples are referred to as 'rewet BC'. Figure S1 includes digital images of each type of BC and other characteristics of the substrates. To create the BC/TiO₂ nanocomposites, never dry BC films were functionalized with nanotitania via a microwave-assisted thermal decomposition method previously reported²⁷ and summarized in Figure 3A. This one-step (15 min reaction time) hydrothermal reaction allowed uniform nucleation of TiO₂ NPs directly on the BC fibres as evidenced by the whitish colour acquired by the BC samples (See Figure S1). Never dry BC/TiO₂ was dried with the same procedure and its thickness reduced to ~30 microns. Rewet BC/

TiO₂ films were slightly thicker (~35 microns) than rewet BC. The handling of the BC/TiO₂ was comparable to that of plain BC; the samples kept its shape, size and flexibility and we did not observe any sign of deterioration after the microwave reaction.

Before its use as a substrate for cell culture, BC and BC/TiO₂ films were structurally characterized. To get a macroscopic view of the substrates, confocal microscope imaging of fluorescently stained rewet BC and BC/TiO₂ substrates was conducted (Figure 3, B and E). Both samples show continuous, flat and rather smooth surfaces only presenting few wrinkles formed during the drying process. Since surface roughness is reported to impact on cell attachment and growth^{56,57}, Atomic Force Microscopy (AFM) was used to compare the roughness of the substrates in the dry state. BC films showed an average roughness of $0.14 \pm 0.03 \mu\text{m}$ whereas BC/TiO₂ were rougher ($0.33 \pm 0.07 \mu\text{m}$) due to the nanoparticle coating (See Figure 3C and 1F).

Following, scanning electron microscopy (SEM) was used to elucidate fibre organization and nanoparticle distribution on the BC/TiO₂ supports. BC films showed an unorganized interlaced 3D nanofiber distribution (Figure 3D). Interestingly, this 3D network presents a strong architectural similarity to collagen, the current gold standard to devise cell transplantation supports. Insert on Figure 3D shows an SEM image of collagen fibres from amniotic membrane to exemplify this resemblance. BC/TiO₂ exhibits the same nanofibrillar structure than plain BC with a homogenous and dense coating by the TiO₂ NPs (Figure 3G). The insert of Figure 3G shows an SEM image BC/TiO₂ without metal sputtering were the TiO₂ coating is also visible. Energy-dispersive X-ray Spectroscopy revealed that the atomic contribution of titanium on the surface of BC/TiO₂ substrates accounts for $25 \pm 8\%$. Both the atomic percentage of titanium and the density and distribution of the TiO₂ NPs coating was very similar between the two sides of the nanocomposite.

Thermo-gravimetric analysis (TGA) was carried out to determine that nanotitania represents ~6 % of the dry weight of the BC/TiO₂ composites. TGA was also used to study the long-term stability of the nanocomposites; BC/TiO₂ films immersed in water for one month under mild stirring showed no leaching of titanium. That is, the same weight percentage of titanium was detected before

and after the soaking²⁷. Accordingly, inductively coupled plasma–optical emission spectroscopy revealed that the amounts of titanium detected in the eluates BC/TiO₂ samples were < 0.02 mg/ L. These two experiments confirm that the nanoparticles are chemically bonded to the nanocellulose fibres. This should prevent TiO₂ nanoparticles to be released from the substrates and to be internalized by the cells in the next *in vitro* experiments.

Transmission electron microscopy (TEM) was employed to estimate the particle size distribution from the colloidal TiO₂ NPs present on the supernatant of the microwave reaction, being in average 7.1 ± 1.6 nm with a polydispersity of a 23% (Figure S1-C). Finally, TEM on electron diffraction mode was used to determine that the TiO₂ crystallized in the anatase phase, see Figure S1-D.

Together, these observations confirm that the employed microwave synthesis is an effective tool to prepare stable BC/TiO₂ nanocomposites in a fast and reproducible manner, obtaining a uniform coating of the nanocellulosic fibres without compromising the original structural properties of BC.

Endotoxin content

Endotoxin (also known as lipopolysaccharide) contamination induces a variety of negative biological effects such as airway disease, fever, hypotension, coagulopathies, septic shock and even death, and represents a major problem in biomaterial fabrication. Since BC is synthesized by a gram-negative bacterium, the presence of endotoxins could pose a threat. The amount of endotoxins detected in the eluates of sterile never dry BC and BC/TiO₂ films were 0.04 ± 0.01 and 0.05 ± 0.01 Endotoxin Units (EU)/mL respectively. Notably, these values are one order of magnitude below the Food and Drug Administration (FDA) obligatory limit of 0.5 EU/mL applied to medical devices. The low amount of endotoxins detected in the substrates is in accordance with the recent literature^{43,58} and indicates that the cleaning protocol of BC is effective in removing any remains of the *K. xylinus* cell wall.

Cell attachment and morphology

To investigate the suitability of BC and BC/TiO₂ as substrates to expand and transplant adherent cells, a model human dermal fibroblast cell line was employed (1BR3.G). Rewet BC and BC/TiO₂ membranes were selected for the *in vitro* ex-

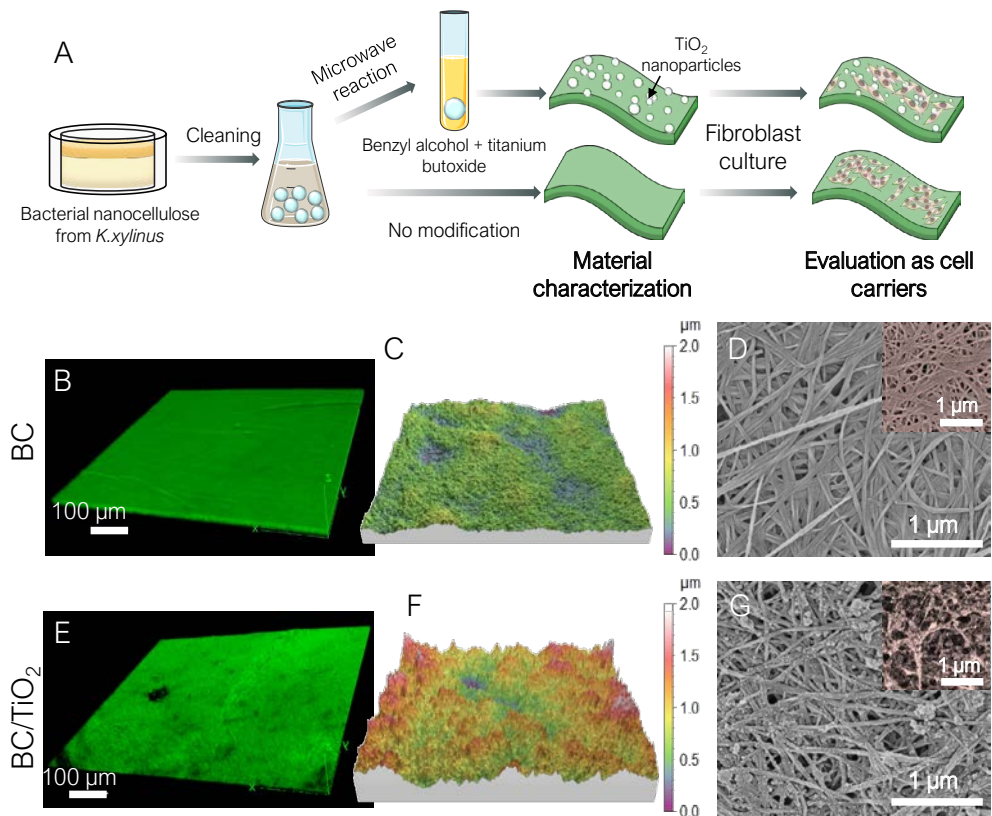


Figure 3: Sample preparation and structural characterization of the BC and BC/TiO₂ substrates A) Schematic representation of the processes adopted to prepare BC and BC/TiO₂ cell carriers. Images B and E show macroscopic confocal microscope images of rewet BC (B) and BC/TiO₂ (E) films fluorescently stained with Safranin-O. AFM images (30x30 μm areas) are shown on C (BC) and F (BC/TiO₂) panels to visualize differences in roughness. Finally, scanning electron microscope (SEM) of BC (D) and BC/TiO₂ (G) illustrates the nanofibrillar structure of the substrates and the TiO₂ coating. Insert on image D corresponds to a collagen-based biological membrane to visualize the high structural similarities with BC. SEM samples were coated with five nm of Pt on images D and G and were left uncoated on the insert in image G. Colour was added to facilitate visualization of the inserts.

periments as the drying-rehydration cycle contributed to reducing the variability between samples and slightly increased the initial cell attachment compared to never dry BC. Accordingly, dry BC and BC/TiO₂ were rehydrated in DI water, autoclaved and then seeded with 1BR3.G cells. This tolerance to heat sterilization represents a clear advantage of BC for future clinical translation. Fibroblasts readily attached to both BC and BC/TiO₂ substrates without the need of any additional treatment, thus greatly facilitating the seeding protocol. Moreover, the

above-mentioned morphological stability of BC and BC/TiO₂ allowed the easy manipulation and portability of the cell cultures. Figure S2 shows the cell plating protocol, the handling of BC-cells constructs and the monitoring of the cell cultures by phase-contrast microscope. By counting the number of cells that were not attached to the substrates 4 hours after seeding, we could assess that $77 \pm 1\%$ of the seeded cells adhered to BC and $73 \pm 9\%$ attached to BC/TiO₂ (not statistically significant differences). Even that the BC and BC/TiO₂ films have the same size as the culture wells, a small portion of the seeded cells still attached to the underneath tissue culture plate instead of the substrates and therefore these numbers are presented as an approximation. After two days of culture, images from Figure 4A were collected with a confocal microscope where fibroblasts attachment to the BC and BC/TiO₂ films (stained in green with Safranin-O) is clearly observed. Optical slicing in the z-direction revealed that 1BR3.G cells grew over the entire surface of the BC and BC/TiO₂ films without penetrating inside the substrates as expected according to the small size of the BC pores. Figure S3 shows large area confocal microscope images ($\sim 40 \text{ mm}^2$) of BC and BC/TiO₂ substrates 48 hours after seeding to further illustrate fibroblast distribution on the surfaces.

Then, we analysed diverse cell shape descriptors to investigate whether BC and BC/TiO₂ films were able to facilitate cell spreading recapitulating the characteristic elongated fibroblast phenotype found *in vivo*. Both supports rendered the expected fibroblast morphology with axial values of 3.9 ± 1.7 for BC/TiO₂ and 3.1 ± 1.3 for plain BC ($n > 60$ cells, $P\text{-value} < 0.005$). Cell shape descriptors measurements are detailed in Figure S4. Notably, the obtained axial ratios are similar to those reported for fibroblasts seeded on collagen and fibrin coated supports⁵⁹. Cells plated on BC/TiO₂ substrates presented statistically significant higher axial ratio compared to cells cultured on plain BC as well as larger total cell area. This indicates an enhanced spreading of the fibroblast on the BC/TiO₂ respect to BC supports (See normalized data on Figure 4B). The nuclear-cytoplasmic ratio (N:C ratio), *i.e.* the relative area of the cytoplasm respect to the nucleus⁶⁰, was significantly smaller for cells seeded on BC/TiO₂ further supporting that cells tend to extend more on the hybrid substrates. We ascribe these effects to the greater roughness of the BC/TiO₂ substrates which might provide more anchoring sites for the fibroblasts^{56,57,61}.

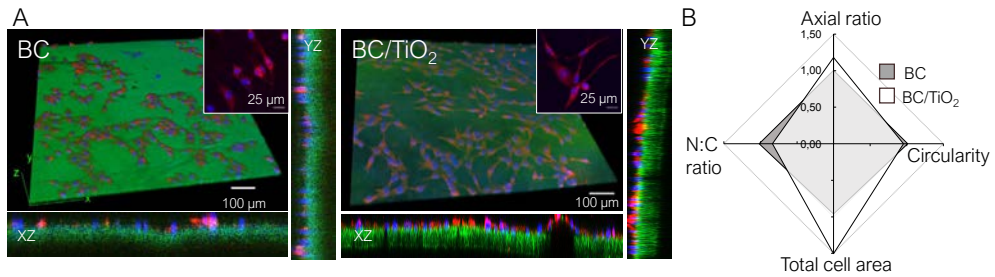


Figure 4: Cell attachment and morphology on BC and BC/TiO₂ substrates. Panel A shows confocal microscope images of human dermal fibroblasts attached to BC and BC/TiO₂ supports 48 hours after plating the cells. Insets display zoom in's to better visualize cell morphology and spreading. Cell nuclei (blue) were stained with Hoechst and cell membranes (red) with Cell Mask while BC and BC/TiO₂ supports were stained with Safranin-O (green). 3D reconstruction of the z stacks revealed that cells distribute over the BC and BC/TiO₂ films surface without penetrating inside the films (see lateral images for the xz and yz planes). B) Radar chart comparing the main cell shape descriptors (normalized) measured 48 hours after seeding 1BR3.G cells on BC and BC/TiO₂ films. N:C ratio refers to the nuclear/cytoplasmic ratio. Statistically significant differences were found for the measurements of axial ratio, total cell area and N:C ratio suggesting a higher fibroblast spreading on BC/TiO₂ than in plain BC.

Cell viability and proliferation

To gain insight into the biological activity of the fibroblasts cultivated on top of BC and BC/TiO₂ substrates, cell viability (Calcein-AM staining) and proliferation kinetics were studied. Figure 5A illustrates that cells seeded on both BC and BC/TiO₂ films exhibit high viability since 98% and 99% of the cells were positive for the Calcein-AM staining respectively at Day 2 after seeding. Fibroblasts plated on control surfaces exhibited analogous Calcein-AM staining. Then, we monitored cell proliferation over 8 days of culture on BC, BC/TiO₂ and cell culture plates as positive controls (Figure 5B). A progressive intensification of the signal was observed for the three conditions finding statistically significant differences at Day 8 respect to Day 1 for the BC and BC/TiO₂ substrates, which correlates with an increasing number of metabolically active cells. Not surprisingly, fibroblasts on the control surfaces exhibit higher absolute values (statistically significant respect to both BC and BC/TiO₂) which we attribute mainly to the higher initial cell attachment to these surfaces compared to the BC and BC/TiO₂ carriers. No statistically significant differences were found when comparing proliferation between plain BC and titania hybrids implying that the TiO₂ NPs coating has a neutral effect over fibroblasts proliferation. After ~one week, the cultures reached 100% confluence

on the three substrates (Figure S2-B) leading to the formation of a continuous cell monolayer. These observations point out that BC and BC/TiO₂ allow not only the adhesion and spreading of fibroblasts but also its metabolic activity and *in vitro* expansion. These findings are relevant for future exploitation of BC and BC/TiO₂ as cells carriers since elevated cell densities are generally required for transplantation.

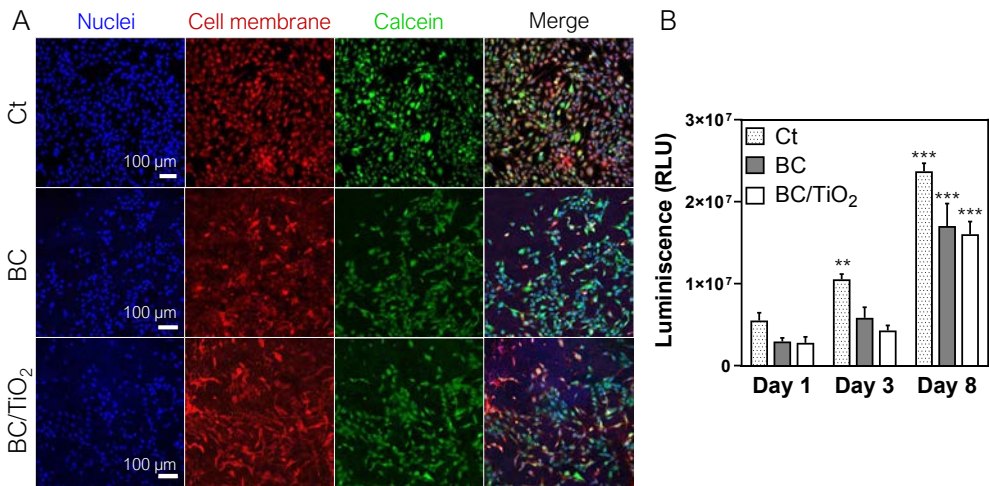


Figure 5: Cell viability and proliferation on BC and BC/TiO₂ supports. A) The study of cell viability was carried out with Calcein-AM staining 48 hours after cell seeding. BC and BC/TiO₂ substrates yielded highly viable cell populations. Confocal microscope images depict cell nuclei (blue) stained with Hoechst and cell membranes (red) with Cell Mask. Viable cells were stained with Calcein-AM (green). The fourth column shows the composite of all pictures. B) Proliferation kinetics of the fibroblasts seeded on BC (grey bars) and BC/TiO₂ (white bars) and controls (dotted bars) monitored with the CellTiter-Glo® assay measuring ATP levels. For the studied cell carriers, statistically significant differences were found for Day 8 compared to Day 1 demonstrating the ability of BC and BC/TiO₂ to support fibroblast proliferation (n=3).

Cell retrieve

To further investigate the properties of BC and BC/TiO₂ substrates as cell culture platforms, we evaluated the possibility to retrieve the cells attached to BC and BC/TiO₂ substrates by three different methods: conventional trypsinization, direct contact with other substrates and degradation of the nanocellulose carriers.

Cells adhered to BC and BC/TiO₂ substrates could partially be harvested upon a five-minute incubation with trypsin-EDTA. To be precise, 55 ± 18% of the cells could be retrieved from BC/TiO₂ substrates while 35 ± 15% of the cells were detached from BC (not statistically significant differences) yielding a suspension of viable cells that could be used for further studies such as flow cytometry (Figure 6A). By

an equivalent trypsinization process of fibroblasts growing on polystyrene plates, virtually the totality of the cells (indicated as 100 % in Figure 6A) was recovered. This observation indicates that both BC and BC/TiO₂ substrates interfere to some extent with the trypsin-EDTA action, making it a partially effective approach to harvest the cells from the investigated substrates. Figure S5 contains optical microscope images of the fibroblasts cultures before and after the trypsin treatment further confirming these results.

Secondly, we placed BC and BC/TiO₂ films loaded with 1BR3.G cells in close contact (turned upside down) with two different substrates: a polystyrene culture plate as an example of a stiff substrate and a never dry BC hydrogel representing a softer surface. With this method, the transference of a fraction of the total adherent cell population (from their initial substrates to the unused ones) was observed (Figure 4B). Remarkably, the fibroblasts that migrated from the BC and BC/TiO₂ films were able to attach to the new supports and were metabolically active as indicated by the positive Calcein-AM staining (inserts in Figure 6B). The migrated cells exhibited a different morphology depending on the substrate where they were transferred; being more spread on the polystyrene plate than on the BC hydrogel. Presumably, this is due to the difference in the acceptor substrate stiffness which is known to influence fibroblast morphology rendering more rounded cell shapes in soft than in stiff substrates⁶². Overall, this preliminary experiment suggests that despite being strongly attached to the BC and BC/TiO₂ supports, the cultured cells keep their migration abilities, which is useful for future cell transplantation therapies.

Finally, we explored the possibility to benefit from cellulase enzymes to dissolve the BC and BC/TiO₂ carriers living a bare cell layer similar to that obtained from the cell-sheet technology that is begin developed with the use of thermo-responsive polymers^{63,64}. However, this option was dismissed because the optimization of the working conditions of the cellulase enzyme was incompatible with the growth of the cells; being the long incubation time required to completely dissolve the nanocellulose carriers the main inconvenience (see Figure S6).

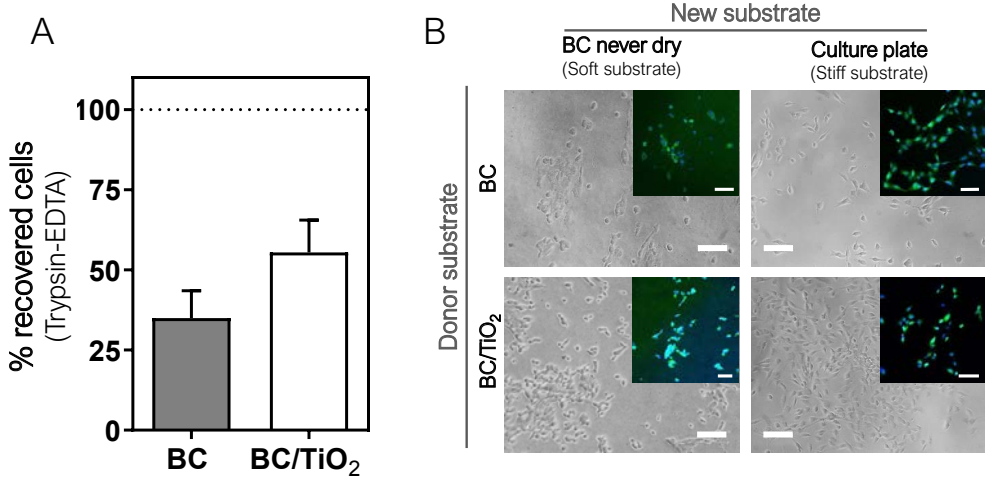


Figure 6: Cell retrieval from BC and BC/TiO₂ supports. A) Percentage of cells that could be harvested upon conventional enzymatic method with trypsin-EDTA. A higher percentage of cells (55 ± 18 vs 35 ± 15 %) was retrieved from the BC/TiO₂ substrates but this difference was not statistically significant (P-value= 0.1965). The dashed line at 100% corresponds to the approximate percentage of cells recovered from polystyrene surfaces by the same procedure. B) Optical microscopy images of the migrated/transferred fibroblasts from the initial substrates (BC and BC/TiO₂) to the new substrates: BNC hydrogels (soft substrate) and polystyrene cell culture surfaces (stiff substrate). Insets correspond to fluorescence microscopy images where cell nuclei are marked in blue (total number of cells) and viable cells are stained green with Calcein-AM. Scale bars = 100 μ m.

Adherent cell cryopreservation

Cryobanking of adherent mammalian cells is challenging because of the need for low-temperature resistant substrates and the high risk of cell detachment after thawing⁶⁵. We hypothesized that the mechanical and thermal stability of BC could be of great value for this application. Accordingly, we evaluated the possibility to directly cryopreserve cell-BC and cell-BC/TiO₂ complexes aiming at facilitating the banking and transport of ready-to-use medical products based on BC⁶⁶. BC-cells constructs were slowly frozen, stored on liquid nitrogen for over one week and thawed to assess cell viability and integrity of the BC and BC/TiO₂ supports.

Figure 7A shows the state of the fibroblast cultures grown on BC, BC/TiO₂ and culture wells before cryopreservation and after thawing. Not surprisingly, 4 hours after defrosting, the cells were visibly stressed on the three tested conditions and decreased its viability down to 20-40 % compared to the not cryopre-

served cultures. However, cells remained attached to the BC and BC/TiO₂ substrates and it was noticeable that, after a recovery time of 48 hours, the fibroblasts cultures became again highly confluent and viable as evidenced by the positive staining for Calcein-AM (see insets in Figure 7A) on the three experimental settings. Accordingly, the ATP levels measured 48 h after thawing (Figure 7B) of the cryopreserved cells were almost identical (no statistically significant differences) to the not cryopreserved samples. This corroborates the successful adherent cell cryopreservation on BC and BC/TiO₂ in a comparable fashion to the conventional cryopreservation method of single cells suspensions (Ct). Notably, the suggested adherent cell cryopreservation process represents even an easier protocol compared to the control method since trypsinization is not required. The flexible nature of BC was helpful to place the substrates inside the cryovials and we speculate it is also convenient to prevent cell detachment as described in⁶⁷ for a poly-urethane nanofibrous supports. Moreover, we assessed the integrity of BC and BC/TiO₂ substrates (without cells) after one-week storage at -196 °C. The films did not undergo any change in shape or consistency and were as easy to manipulate as the non-cryopreserved materials. Accordingly, the SEM micrographs of Figure 7C (BC) and 5D (BC/TiO₂) show intact nanofibrillar structures and NPs coating without the presence of pores or cracks (use SEM images in Figure 3 for comparison). The finding that BC and BC/TiO₂ support the cryopreservation of adherent cells in an off-the-shelf format has important clinical significance as it could reduce the preparation time of cell loaded-biomaterials upon request and boards the possibilities for long-term storage of cellular products⁶⁶.

Conclusions

Here we endorse BC and BC/TiO₂ as endotoxin-free supports to expand human dermal fibroblasts by providing a complete evaluation of cellular responses towards BC and BC/TiO₂. No cytotoxic effects arising from the TiO₂ nanoparticles anchored to the BC fibres have been detected while cell spreading on the hybrids was higher than in plain BC. In this study, TiO₂ NPs were incorporated into the BC substrates to investigate its interactions with cells. However, future studies will examine other reported advantages of TiO₂ NPs such as the positive effect in wound healing and antimicrobial activity. Notably, we also report for the

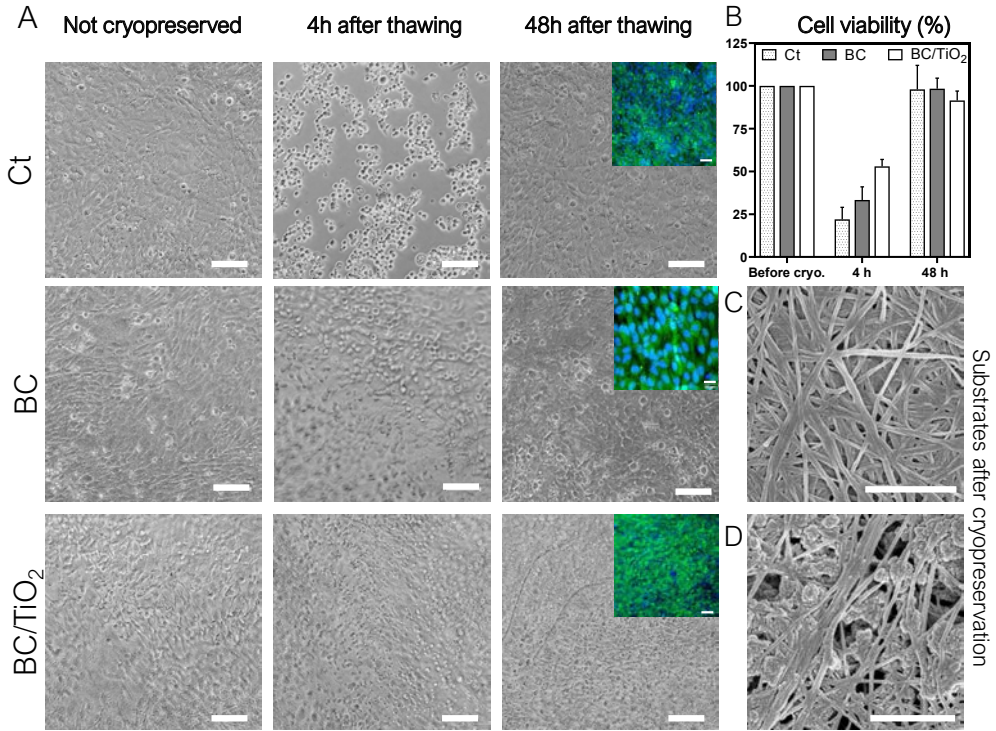


Figure 7: Adherent cell cryopreservation on BC and BC/TiO₂ substrates. A) Phase-contrast and fluorescent (insets showing Calcein-AM staining in green for viable cells) microscope images of fibroblasts grown on BC, BC/TiO₂ and cell culture surfaces at the different evaluated points: before cryopreservation, 4 h and 48 h after thawing where cell recovery can be clearly appreciated. Scale bar = 100 μ m. B) Cell viability after thawing expressed as a percentage of the not cryopreserved cultures. After 48 hours of incubation, the cryopreserved cells recovered almost the same viability values as the not cryopreserved samples on the three assessed methods. C) BC and D) BC/TiO₂ evaluation by scanning electron microscopy of the substrate's integrity after cryostorage. Note that the nanofibrillar structure is totally maintained after thawing on both substrates. Scale bar = 1 μ m.

first time on the cryopreservation of cell-BC and cell-BC/TiO₂ constructs. Viable adherent cell cultures and undamaged carriers were thawed after >one week in liquid nitrogen indicating that BC and its derivatives could be utilized in the fabrication and long-term storage of ready-to-use cellular products. We expect the findings reported here serve as a first step towards the development of BC-based cell transplantation supports paving the way for future uses of BC-nanocomposites as advanced biomaterials.

Acknowledgements

Authors acknowledge financial support from the Spanish Ministry of Science and Innovation through the RTI2018-096273-B-I00, project, the ‘Severo Ochoa’ Programme for Centres of Excellence in R&D (SEV-2015-0496) and the PhD scholarships of I.A.S. (BE-2017-076734) and SRS (BES-2016-077533). The Generalitat de Catalunya with the 2017SGR765 and the 2019LLAV00046 projects are also acknowledged. The authors also express their gratitude to the technical services of ICMAB (Nanoquim, AFM and TGA), UAB (cell culture and microscopy facilities) and ICN2 (electron microscopy). The authors participate in the CSIC Interdisciplinary Platform for Sustainable Plastics towards a Circular Economy, SUSPLAST and in the Aerogels COST ACTION (CA 18125).

Supplementary information included in Publication 2

Figure S1: BC and BC/TiO₂ substrates detailed characterization. Table A gathers information on the characteristics of the BC and BC/TiO₂ supports used to culture 1BR3.G cells. B) Characteristic TGA curves of BC (grey line) and BC/TiO₂ (black line) dry films (n=3 for each type). Remaining masses were $0.7 \pm 0.05\%$ and $6.2 \pm 0.8\%$ respectively. The weight percentage of TiO₂ nanoparticles present on the BC/TiO₂ nanocomposites was estimated by subtracting the remaining mass of the BC substrates to the remaining mass of BC/TiO₂ and was $5.5 \pm 0.8\%$. C) TEM image of the TiO₂ nanoparticles present in the supernatant of the microwave reaction presenting a size of 7.2 ± 1.6 nm. Insert shows the particle size distribution with a polydispersity of 23%. D) Selected area electron diffraction of the TiO₂ nanoparticles anchored to the BC fibres to create the BC/TiO₂ nanocomposites. The crystal structure corresponds to the anatase phase of TiO₂.

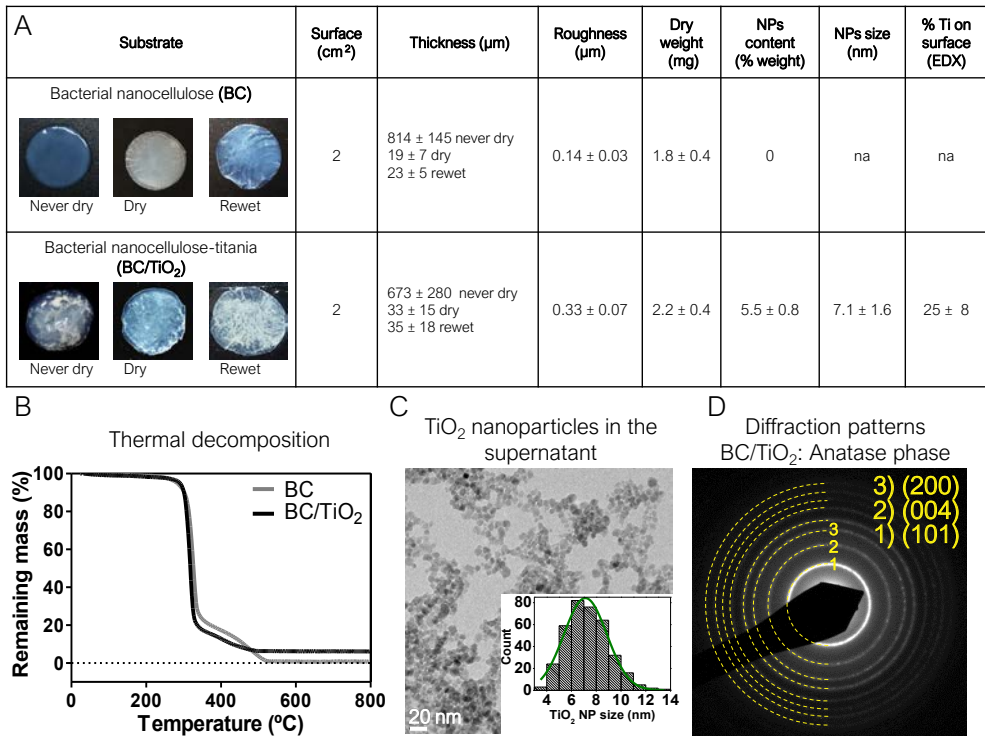


Figure S2: fibroblast culture on BC and BC/TiO₂ substrates. A) Schematic illustration of the process followed to obtain a high percentage of cell adhesion on the BC and BC/TiO₂ substrates. The digital image on the right shows the easy manipulation of the BC-cell composites using tweezers. B) Evolution of the cell cultures (50.000 cells/well as initial cell density) overtime on the

three compared substrates: plain BC, BC-titania hybrids and conventional cell culture surface as a positive control. See the high cell density on day 8 on the three surfaces.

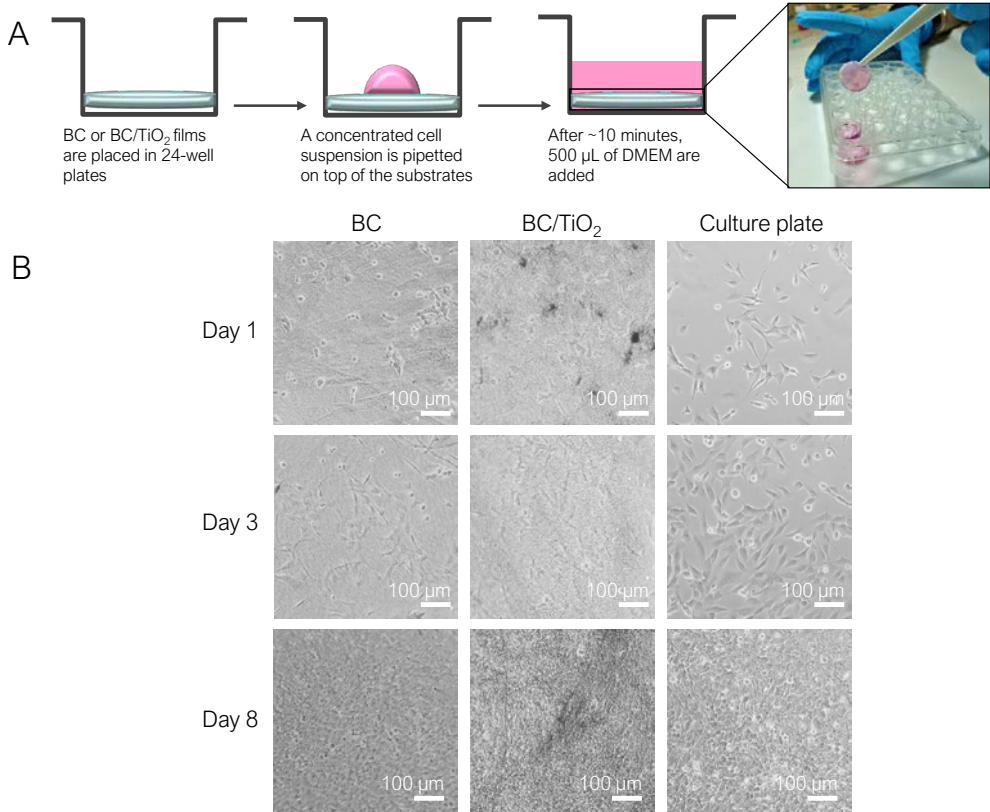


Figure S3: Cell distribution on the BC and BC/TiO₂ substrates. Representative large area ($\approx 40 \text{ mm}^2$) confocal microscope reconstructed images of BC (left) and BC/TiO₂ (right) substrates seeded with human dermal fibroblasts after two days in culture. Fibroblasts distribution all over the surfaces can be observed. Cells were stained with Calcein-AM (green, indicating viable cells), Hoechst (nuclei in blue) and Cell Mask (cell membrane in red).

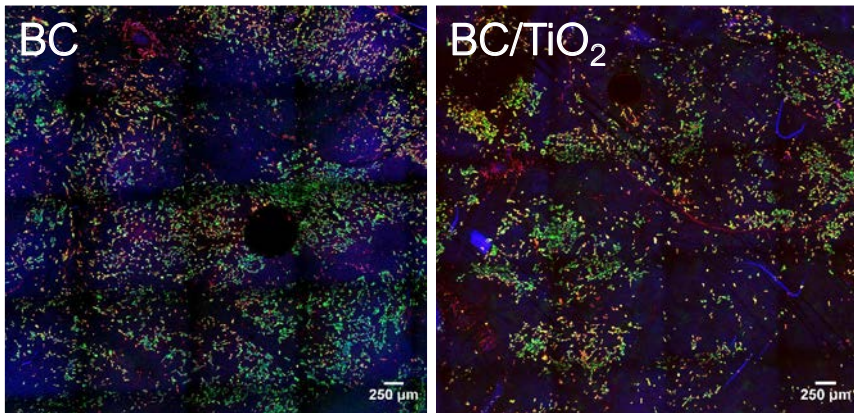


Figure S4: Cell shape descriptors. Box plot graphs showing: A) Fibroblast axial ratio (length of long axis/length of the short axis), B) Circularly ($4\pi/\text{cell perimeter}^2$), C) Nuclear: cytoplasm ratio (N: C ratio) and D) Cell spread area in μm^2 . For all the graphs, boxes illustrate the 25 to the 75 percentile and the whiskers the 5 to 95 percentiles. Black dots correspond to outliers. Statistically significant differences (unpaired T-test) were found for the axial ratio, the N:C ratio and the cell spread area suggesting a better spreading of the cells on the BC/TiO₂ substrates compared to plain BC.

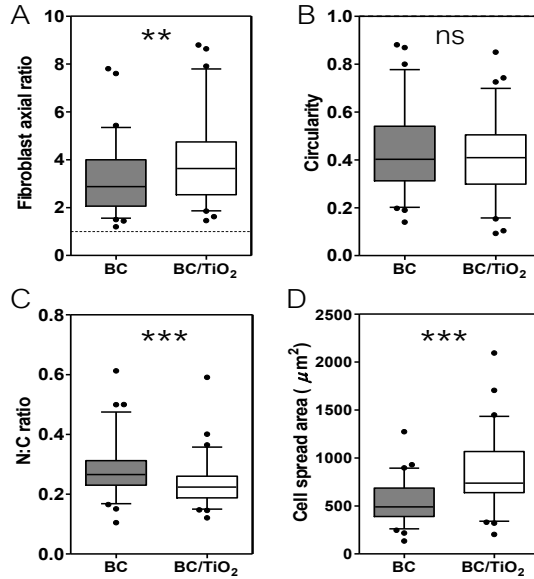


Figure S5: Enzymatic cell recovery. Phase-contrast microscope images from 1BR3.G cells growing on cell culture surfaces (Ct), BC and BC-titania hybrids (BC/TiO₂) before and after incubation with Trypsin-EDTA. Almost the totality of the cells was recovered from controls (considered as 100%) while for BC and BC/TiO₂ some of the cells remained adhered to the substrates. Scale bar = 100 μm .

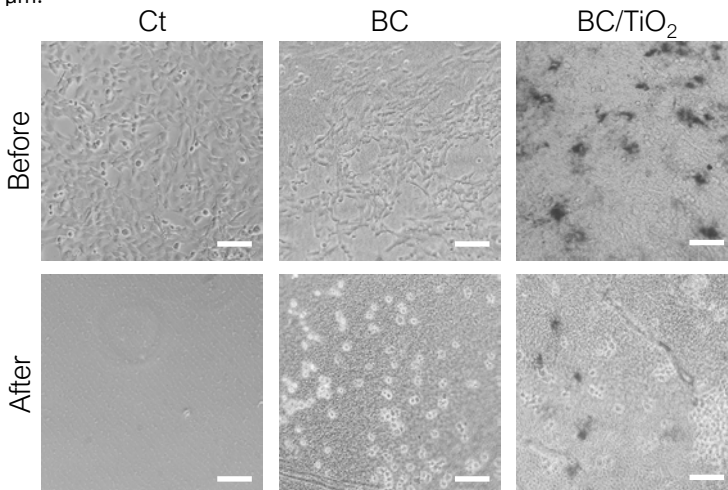
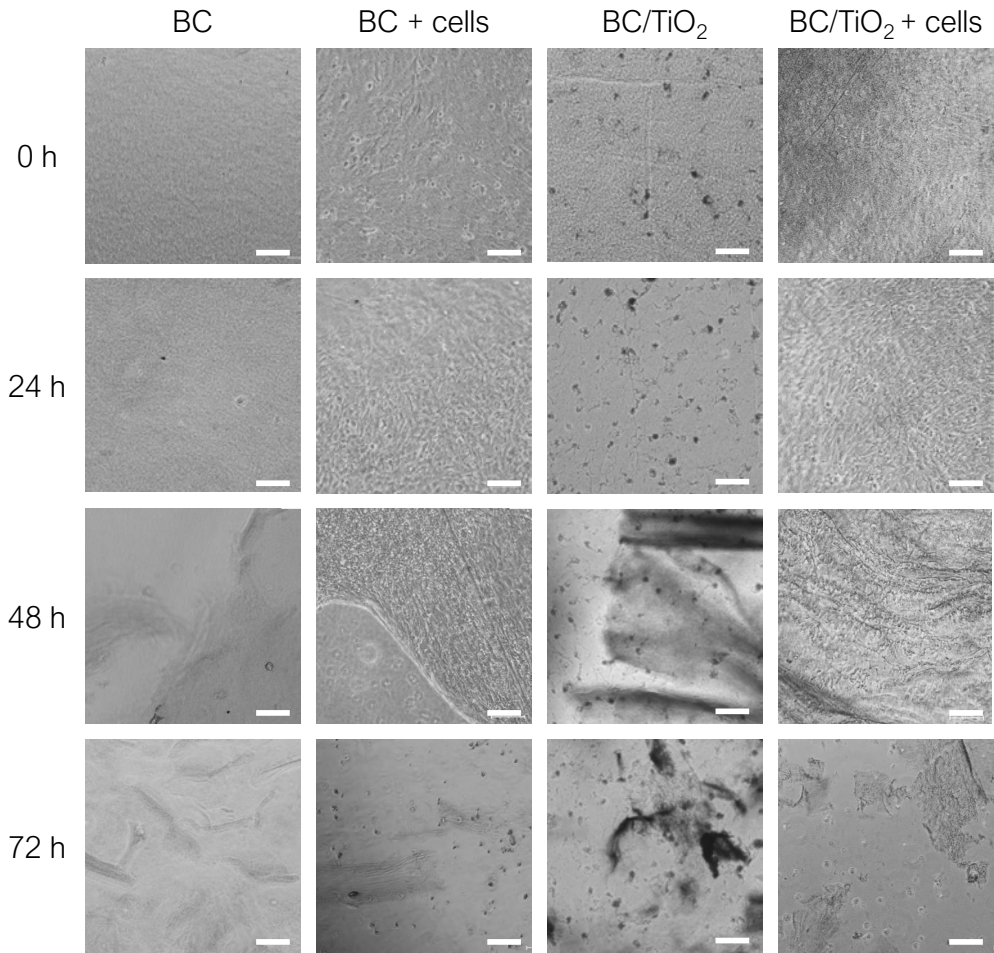


Figure S6: Attempt to recover fibroblasts from BC and BC/TiO₂ substrates by enzymatic nanocellulose dissolution. Phase-contrast microscope images of BC and BC/TiO₂ substrates (with or without 1BR3.G cells as indicated) incubated with cellulase enzyme at different time points. Nanocellulose degradation into small fragments took >48 hours and the cell populations recovered were damaged and many debris from the substrates and the dead cells were observed. A similar degradation rate was perceived on the controls without cells. In light of these results, this option was dismissed as an effective method to recover cells from BC and BC/TiO₂ substrates. Scale bar = 100 μm.



Additional functionality tests of BNC and BNC/TiO₂ as photo-protectant and antimicrobial agents

Publication 2 demonstrates the adequacy of BNC and BNC/TiO₂ as expansion and cryopreservation cell-supports; no major differences between both substrates were detected. To complete this study, the protective effect of BNC and BNC/TiO₂ films against solar radiation was evaluated using human dermal fibroblasts. A preliminary anti-bacterial activity test is also included in this section. Our initial hypothesis was that BNC/TiO₂ would outperform plain BNC in both tests showing advanced features. The results detailed in this section are unpublished to date.

Materials and methods

Ultraviolet-visible (UV-Vis) light spectroscopy

BNC and BNC/TiO₂ membranes were prepared as described in Publication 2. Ultraviolet-visible-near infrared (UV-Vis-NIR) spectra were collected on triplicates with a Varian Cary-5000 UV-Vis-NIR spectrophotometer between 200 and 800 nm for both BNC and BNC/TiO₂ rewet (dried and rehydrated) films. Baseline correction was performed with the glass coverslips that were used to hold the samples and the values were corrected by the thickness of each film. The obtained spectra were compared to the reference solar spectra (ASTM G173-03 Reference Spectra).

Cell exposure to sunlight

To measure the protective capacity of BNC and BNC/TiO₂ films against sun exposure, a solar simulator from ABET Technologies (Model 11016 Sun 2000) with a xenon arc lamp was employed. The power intensity of the solar simulator was fixed at 1000W / m². 1BR3.G cells were plated on triplicates on 24 well-plates at a density of 35.000 cells/well. Two days later, the cultures were irradiated for 5 hours with the solar simulator. An infrared thermometer was employed to monitor that the temperature at the irradiation zone did not surpass ~38 °C. During irradiation, the culture medium was substituted for PBS, the lid of the culture plate was removed and the cells were covered with a plastic foil (previously tested to be not

absorbent in the UV-VIS region). BNC and BNC/TiO₂ films were then placed on top of the plastic foil fully covering the area of the underneath wells containing the cells. A diagram of this setup is shown in Figure 8A. Unprotected cultures and wells covered with aluminium foil (totally opaque to sunlight) were used as negative and positive controls. After irradiation, the cell cultures were incubated in DMEM overnight and evaluated for cell death and apoptosis the following day. The experiment was repeated four times.

Flow cytometry

To quantitatively evaluate the irradiated cultures, the Annexin-V-FLUOS staining kit from Roche was used. Annexin was used to mark apoptotic cells and Propidium Iodide (PI) to spot dead cells. The staining was performed according to manufacturer's protocol before trypsinization and neutralization with fresh culture medium. After centrifugation, the cells were re-suspended in 300 µL of PBS and loaded on 12 x 75 mm tubes for flow cytometry analysis. The number of viable cells (double negative), apoptotic (positive for Annexin, negative for PI) and dead (Positive for Annexin and PI) was measured with a FACSCanto flow cytometer (BD Biosciences).

Agar diffusion assay

500 µL of *E.coli* liquid inoculum were spread on Luria-Bertani (LB) agar plates and left to dry inside a laminar flow cabinet. Then, ~2 cm² rewet plain BNC and BNC/TiO₂ hybrids were blotted with filter paper to remove the excess of water and placed on the surface of the agar using tweezers. 1 mg of TiO₂ NPs, obtained during the same synthesis process as the BNC/TiO₂ substrates, were diluted in 50 µL of Milli-Q water and pipetted on the agar surface too. Finally, 50 µL of Tetracycline were added as a positive control. The agar plates were left closed in an incubator at 30 °C for 48 hours before taking pictures.

Results and discussion

It is well known that excessive exposure to UV radiation induces cellular harm -such as DNA damage⁶⁸ and oxidative stress⁶⁹ - eventually leading to sunburn,

photo-ageing and carcinogenesis^{70,71}. Thus, we anticipated that the UV-blocking capacity of TiO₂ NPs could be valuable if using BNC/TiO₂ as a cell transplantation support to protect both the wound bed and the transplanted cells from the damaging UV radiation.

Compared to plain BNC, BNC/TiO₂ films presented a markedly higher absorption of UV light, especially at shorter wavelengths (250 – 450 nm) corresponding to the most energetic regions (Figure 8B). The obtained spectra were overlapped to the standard solar irradiance power spectrum finding that the peak of absorption of BNC/TiO₂ fell outside the maximum irradiance region (450 – 550 nm).

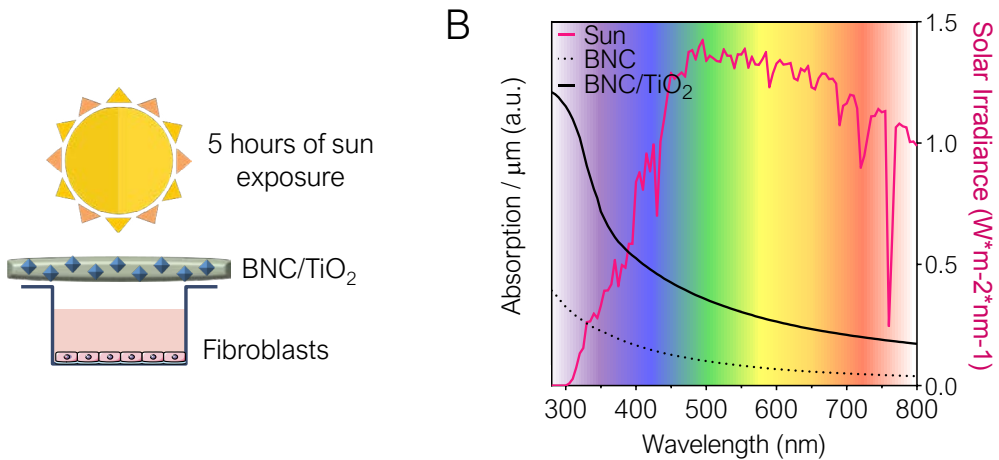


Figure 8: BNC and BNC/TiO₂ as solar filters. A: sketch of the experimental set up devised to evaluate the photoprotective effects of BNC and BNC/TiO₂ films. Human dermal cells were irradiated for 5 hours with a solar simulator while covered with BNC, BNC/TiO₂, aluminium foil (positive control) or left uncovered (negative control). B: UV-Vis absorption spectra of BNC and BNC/TiO₂ overlapped to a reference sun irradiance spectrum.

To evaluate the possible photoprotective effect of BNC and BNC/TiO₂, the experimental setup represented in Figure 8A was implemented using the same substrates and *in vitro* model as in Publication 2. After the exposure, the cultures were harvested and analysed by flow cytometry to evaluate the imparted cell damage in each condition (Figure 9).

Irradiated cultures presented different cell morphologies depending on the filter applied (see microscopy images in Figure 9). Cultures covered with total-

ly opaque foil, BNC or BNC/TiO₂ exhibited the standard elongated fibroblast morphology while round cells were spotted on unprotected wells. To quantify these differences by flow cytometry, an Annexin-Propidium Iodide (PI) staining was carried out. With this procedure death cells appear as double-positive, alive cells as double negative while apoptotic cells stain only positive for Annexin (see representative dot plots in Figure 9A). The distribution of cells between these conditions is represented in Figure 9B. It is noticeable that the number of compromised cells (apoptotic + death) is the highest (representing >50% of the total) in the non-protected cultures followed by cultures covered with BNC or BNC/TiO₂ -presenting a similar pattern- while cultures covered with aluminium foil computed mainly viable cells. Statistical analysis confirmed these observations by showing significant differences in the percentage of dead cells between foil and BNC/TiO₂ substrates compared to unprotected cultures as well as changes in the number of viable cells between covered cultures (regardless of the filter) compared to uncovered wells. Unexpectedly, no statistically significant differences were detected between BNC and BNC/TiO₂ indicating that both substrates are effective in protecting the dermal cells from sun irradiation under the tested conditions. This result could be explained by different factors; firstly, even though plain BNC does not present a marked absorption peak in the UV-Vis range, it is known to scatter light^{72,73} and this effect might be protective for the fibroblasts cultures. In fact, one of the hypothesized reasons for BNC production in nature is its capacity to protect the *K.xylinus* cultures from UV radiation⁷⁴. Secondly, the employed TiO₂ NPs present the maximum light absorption peak at rather short wavelengths (around 250 nm) which corresponds to the UV-C regions that is mainly filtered off by the earth's atmosphere²². Thus, UV-B (290-320 nm) and UV-A (340-400 nm) are the main cellular damage inductors. With this in mind, it is plausible that the increase in UV absorption of BNC/TiO₂ compared to BNC at the UV-A and UV-B wavelength regions is not sufficient as to originate differences in its photoprotective effect with the protocol used here. Thus, tuning the characteristics of the TiO₂ particles and the particle-load on the BNC films for this particular application would be necessary. Note that in commercial sun-care products, the titania nanocrystals are roughly 25 nm in size and exhibit the rutile crystalline phase of TiO₂⁷⁵.

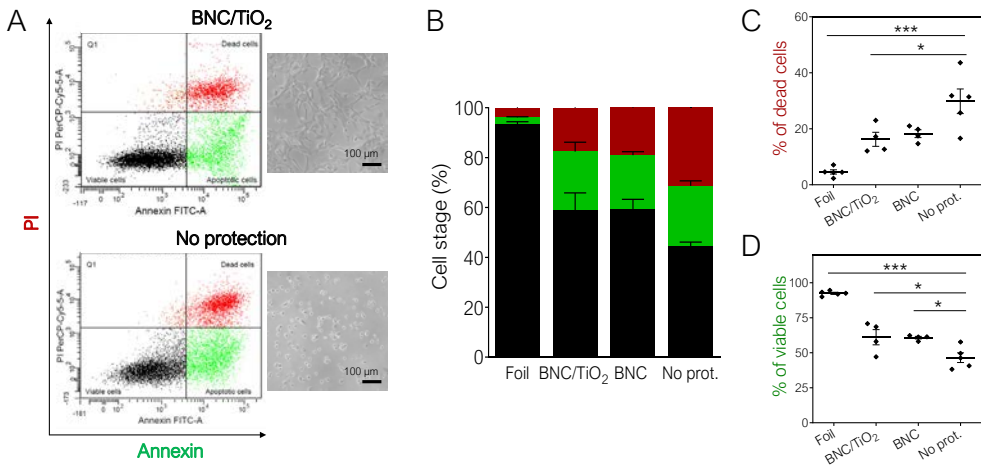


Figure 9: Flow cytometry analysis for cell death and apoptosis of the sun-irradiated cultures. A: Representative colour dot plots from flow cytometry analysis showing subsets of viable (black), apoptotic (green) and dead (red) cells classified based on the Annexin/PI staining for cultures protected with BNC/TiO₂ or left uncovered. Microscope images show the appearance of the cultures after the irradiation. B: Percentages of viable, dead and apoptotic cells for the four tested conditions: aluminium foil (positive control), BNC/TiO₂, BNC and unprotected cultures as negative controls. C: Statistical analysis (one way ANOVA + Tukey's multiple comparison tests) for the percentages of dead and viable cells.

Finally, the antibacterial activity of BNC/TiO₂ towards the common opportunistic pathogen *E.coli* was tested encouraged by several reports describing antimicrobial properties of metal oxide NPs^{17,76,77}. As shown in Figure 10, no inhibition zone was found neither for the BNC and BNC/TiO₂ substrates nor for the suspension of TiO₂ NPs. Different amounts of colloidal TiO₂ NPs were also tested with similar outcomes (results not shown). Only the positive control Tetracycline showed efficacy in preventing bacterial growth. These findings contrast with some reports^{16,17,78,79} on the antimicrobial activity of nano-sized titania incorporated in hybrid materials. We speculate that parameters such as TiO₂ particle size, load, aggregation, surface charge or diffusivity might be responsible for these differences^{77,80}.

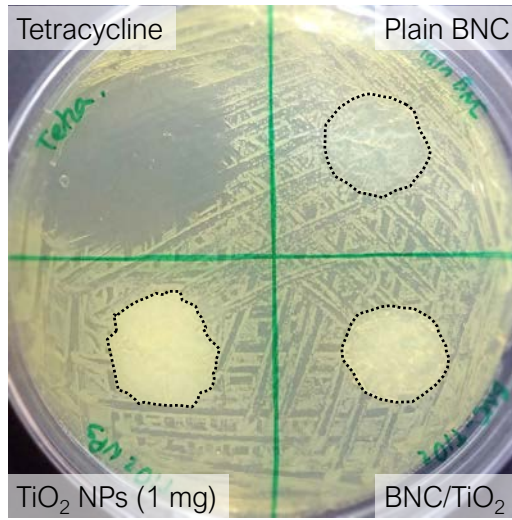


Figure 10: Antibacterial activity test. Agar diffusion assay for ~2 cm² rewet BNC, BNC/TiO₂ membranes and a dispersion TiO₂ NPs towards *E. coli* compared to the positive control Tetracycline, a commonly used antibiotic. No inhibition zone was observed around the tested items (highlighter with a dashed-line).

Contributions to the field and critical comment

In summary, the experimental data presented in Chapter 2 proves the value of BNC as a cell culture substrate and a cryobanking tool and sets the basis for future investigations of BNC as a cell transplantation platform. More specifically I have verified that:

1. Endotoxin-free BNC and BNC/TiO₂ substrates can be obtained after our cleaning process followed by heat sterilization. Since non-pyrogenicity is of paramount importance in the development of medical devices, this finding is highly relevant for our target applications.
2. BNC and TiO₂ NPs-functionalized BNC are not cytotoxic and provide an analogous response in terms of attachment, viability, morphology, proliferation and retrieving of human dermal fibroblasts. Therefore, it is concluded that BNC can be functionalized with TiO₂ NPs without compromising its cytocompatibility, facilitating upcoming applications of these hybrids.
3. BNC and titania hybrids can be used as a support for the cryostorage of ready-made cell-biomaterial composites ensuring their long-term and safe stocking.
4. Both BNC and BNC/TiO₂ are similarly photoprotective as both filters are capable of increasing the number of viable cells in dermal cultures after sun exposure. Our result indicates that the presence of the NPs used here does not significantly boost the sunscreen capacity of native BNC.
5. The employed TiO₂ NPs do not have biocidal/bactericidal activity towards *E.coli* neither in colloidal form nor anchored to BNC nanofibers.

In light of these results, the subsequent experiments to evaluate BNC as a carrier for therapeutic cells (next chapter) were only conducted with plain BNC and the BNC/TiO₂ hybrids were not further investigated. However, we believe that finding a practical application of BNC/TiO₂ deserves future efforts. Due to its photocatalytic activity, TiO₂NPs can generate free radicals (OH· and O²⁻) upon activation with UV light⁸¹. Thus, an interesting line of research would be the UV stimulation of BNC/TiO₂ to foster its antimicrobial activity⁸²⁻⁸⁴. However, this would require intense optimization as the literature of this field is extensive and many parameters and different lab protocols can influence the antimicrobial out-

comes⁸⁰. Regarding the photoprotective capacity of BNC and BNC/TiO₂ nanocomposites, we believe that it represents an interesting addition to the extended list of attractive properties of BNC as a biomaterial. Still, we do not advocate it as a competitive advantage over other biomaterials because, as shown in this chapter, for complete photoprotection the BNC and the titania hybrids were outperformed by opaque surfaces. Therefore, a simpler approach such as covering the treated area with an opaque cotton gauze could be preferred under clinical settings.

Another attractive line of investigation would be the study of cellular responses towards BNC and TiO₂ coated BNC with more specialized cell types such as neural cultures. Reports on BNC substrates enabling the culture of neuron-like cells positioned BNC as a strong candidate in neural tissue engineering⁸⁵⁻⁸⁷. On the other hand, metal oxides such as TiO₂ are under investigation in the design of novel neuroprosthetic platforms^{88,89}. Thus, it is conceivable that the presented cyto-compatible BNC/TiO₂ hybrids could bear specific advantages in this biomedical subspecialty.

Thinking critically on the results presented in Chapter 2, I consider that the most relevant and innovative finding is the BNC and BNC/TiO₂-based adherent cell cryopreservation method. Safe and long-term stocking of biological material is of utmost importance in many medical fields⁹⁰. With this in mind, the cryo-resistance of BNC can be considered a clear strength of BNC-based biomaterials which might be exploited in the future. Furthermore, the utilization of BNC supports for the cryostorage of cells could also be space-saving compared to conventional methods. It is conceivable that cell-loaded BNC films can be piled or rolled up to fit a higher number of cells in a single cryotube and then be retrieved on-demand in small pieces as recently reported for paper-based procedures⁹¹. Last but not least, the *in vitro* biological characterization of BNC and BNC/TiO₂ included in Publication 2 sets a solid basis for the following experiments of this thesis as it discards cytotoxic effects and endorses the potential of BNC as a substrate for the culture of mammalian cells.

Chapter references

1. Mohamad, N., Loh, E. Y. X., Fauzi, M. B., Ng, M. H. & Mohd Amin, M. C. I. In vivo evaluation of bacterial cellulose/acrylic acid wound dressing hydrogel containing keratinocytes and fibroblasts for burn wounds. *Drug Deliv. Transl. Res.* **9**, 444–452 (2019).
2. Piasecka-Zelga, J., Zelga, P., Szulc, J., Wietecha, J. & Ciechańska, D. An in vivo biocompatibility study of surgical meshes made from bacterial cellulose modified with chitosan. *Int. J. Biol. Macromol.* **116**, 1119–1127 (2018).
3. Jeong, S. Il *et al.* Toxicologic evaluation of bacterial synthesized cellulose in endothelial cells and animals. *Mol. Cell. Toxicol.* **6**, 373–380 (2010).
4. Abeer, M. M., Mohd Amin, M. C. I. & Martin, C. A review of bacterial cellulose-based drug delivery systems: Their biochemistry, current approaches and future prospects. *J. Pharm. Pharmacol.* **66**, 1047–1061 (2014).
5. Bacakova, L. *et al.* Versatile application of nanocellulose: From industry to skin tissue engineering and wound healing. *Nanomaterials* **9**, (2019).
6. Shah, N., Ul-Islam, M., Khattak, W. A. & Park, J. K. Overview of bacterial cellulose composites: A multipurpose advanced material. *Carbohydr. Polym.* **98**, 1585–1598 (2013).
7. Watanabe, K. *et al.* A new bacterial cellulose substrate for mammalian cell culture. *Cytotechnology* **13**, 107–114 (1993).
8. Fey, C. *et al.* Bacterial nanocellulose as novel carrier for intestinal epithelial cells in drug delivery studies. *Mater. Sci. Eng. C* **109**, 110613 (2020).
9. Gonçalves, S. *et al.* Acetylated bacterial cellulose coated with urinary bladder matrix as a substrate for retinal pigment epithelium. *Colloids Surfaces B Biointerfaces* **139**, 1–9 (2016).
10. Geisel, N. *et al.* Microstructured Multilevel Bacterial Cellulose Allows the Guided Growth of Neural Stem Cells. *Small* **12**, 5407–5413 (2016).
11. Pellegrini, G. *et al.* Navigating Market Authorization: The Path Holoclar Took to Become the First Stem Cell Product Approved in the European Union. *Stem Cells Transl. Med.* **7**, 146–154 (2018).
12. U.S. Food and Drug Administration. Approved Cellular and Gene Therapy Products | FDA. (2020). Available at: <https://www.fda.gov/vaccines-blood-biologics/cellular-gene-therapy-products/approved-cellular-and-gene-therapy-products>.
13. Ullah, H., Wahid, F., Santos, H. A. & Khan, T. Advances in biomedical and pharmaceutical applications of functional bacterial cellulose-based nanocomposites. *Carbohydr. Polym.* **150**, 330–352 (2016).
14. de Oliveira Barud, H. G. *et al.* A multipurpose natural and renewable polymer in medical applications: Bacterial cellulose. *Carbohydr. Polym.* **153**, 406–420 (2016).

15. Wu, J. *et al.* In situ synthesis of silver-nanoparticles/bacterial cellulose composites for slow-released antimicrobial wound dressing. *Carbohydr. Polym.* **102**, 762–771 (2014).
16. Khalid, A. *et al.* Bacterial cellulose-TiO₂ nanocomposites promote healing and tissue regeneration in burn mice model. *RSC Adv.* **7**, 47662–47668 (2017).
17. Khan, S., Ul-Islam, M., Khattak, W.A., Ullah, M.W. & Park, J. K. Bacterial cellulose-titanium dioxide nanocomposites: nanostructural characteristics, antibacterial mechanism, and biocompatibility. *Cellulose* **22**, 565–579 (2015).
18. Osumi, K. *et al.* Acceleration of wound healing by ultrasound activation of TiO₂ in Escherichia coli-infected wounds in mice. *J Biomed Mater Res Part B* **105**, 2344–2351 (2017).
19. Seisenbaeva, G. A. *et al.* Dispersion of TiO₂ nanoparticles improves burn wound healing and tissue regeneration through specific interaction with blood serum proteins. *Sci. Rep.* **7**, 15448 (2017).
20. Galkina, O. L. *et al.* Antibacterial and photochemical properties of cellulose nanofiber-titania nanocomposites loaded with two different types of antibiotic medicines. *J. Mater. Chem. B* **3**, 7125–7134 (2015).
21. Galkina, O. L., Ivanov, V. K., Agafonov, A.V., Seisenbaeva, G. A. & Kessler, V. G. Cellulose nanofiber-titania nanocomposites as potential drug delivery systems for dermal applications. *J. Mater. Chem. B* **3**, 1688–1698 (2015).
22. Smijs, T. G. & Pavel, S. Titanium dioxide and zinc oxide nanoparticles in sunscreens: Focus on their safety and effectiveness. *Nanotechnol. Sci. Appl.* **4**, 95–112 (2011).
23. Tucci, P. *et al.* Metabolic effects of TiO₂ nanoparticles, a common component of sunscreens and cosmetics, on human keratinocytes. *Cell Death Dis.* **4**, e549–e549 (2013).
24. Fernandes, S. C. M. *et al.* Bioinspired Antimicrobial and Biocompatible Bacterial Cellulose Membranes Obtained by Surface Functionalization with Aminoalkyl Groups. *ACS Appl. Mater. Interfaces* **5**, 3290–3297 (2013).
25. Xiong, G., Luo, H., Zhang, C., Zhu, Y. & Wan, Y. Enhanced biological behavior of bacterial cellulose scaffold by creation of macropores and surface immobilization of collagen. *Macromol. Res.* **23**, 734–740 (2015).
26. Oliveira Barud, H. G. *et al.* Preparation and characterization of a bacterial cellulose/silk fibroin sponge scaffold for tissue regeneration. *Carbohydr. Polym.* **128**, 41–51 (2015).
27. Roig-Sanchez, S. *et al.* Nanocellulose films with multiple functional nanoparticles in confined spatial distribution. *Nanoscale Horizons* **4**, 634–641 (2019).
28. May-Masnou, A. *et al.* Fast and Simple Microwave Synthesis of TiO₂/Au Nanoparticles for Gas-Phase Photocatalytic Hydrogen Generation. *Front. Chem.* **6**, 110 (2018).
29. Boyce, S. T., Kagan, R. J., Meyer, N. A., Yakuboff, K. P. & Warden, G. D. Cultured Skin Substitutes Combined With Integra Artificial Skin to Replace Native Skin Autograft and Allograft for the Closure of Excised Full-Thickness Burns. *J. Burn Care Rehabil.* **20**, 453–461 (1999).

30. O'Connor, N., Mulliken, J., Banks-Schlegel, S., Kehinde, O. & Green, H. Grafting of burns with cultured epithelium prepared from autologous epidermal cells. *Lancet* **317**, 75–78 (1981).
31. Beele, H. *et al.* A prospective multicenter study of the efficacy and tolerability of cryopreserved allogenic human keratinocytes to treat venous leg ulcers. *Int. J. Low. Extrem. Wounds* **4**, 225–33 (2005).
32. Morino, T., Takagi, R., Yamamoto, K., Kojima, H. & Yamato, M. Explant culture of oral mucosal epithelial cells for fabricating transplantable epithelial cell sheet. *Regen. Ther.* **10**, 36–45 (2019).
33. Laurén, P. *et al.* Nanofibrillar cellulose-alginate hydrogel coated surgical sutures as cell-carrier systems. *PLoS One* **12**, e0183487 (2017).
34. Chua, A. W. C. *et al.* From skin allograft coverage to allograft–micrograft sandwich method: A retrospective review of severe burn patients who received conjunctive application of cultured epithelial autografts. *Burns* **44**, 1302–1307 (2018).
35. Carsin, H. *et al.* Cultured epithelial autografts in extensive burn coverage of severely traumatized patients: a five year single-center experience with 30 patients. *Burns* **26**, 379–387 (2000).
36. MacNeil, S. Biomaterials for tissue engineering of skin. *Mater. Today* **11**, 26–35 (2008).
37. ter Horst, B., Chouhan, G., Moiemmen, N. S. & Grover, L. M. Advances in keratinocyte delivery in burn wound care. *Adv. Drug Deliv. Rev.* **123**, 18–32 (2018).
38. Wood, F. M., Kolybaba, M. L. & Allen, P. The use of cultured epithelial autograft in the treatment of major burn injuries: A critical review of the literature. *Burns* **32**, 395–401 (2006).
39. Mitrousis, N., Fokina, A. & Shoichet, M. S. Biomaterials for cell transplantation. *Nat. Rev. Mater.* **3**, 441–456 (2018).
40. Brittberg, M. Cell carriers as the next generation of cell therapy for cartilage repair: A review of the matrix-induced autologous chondrocyte implantation procedure. *Am. J. Sports Med.* **38**, 1259–1271 (2010).
41. Anton-Sales, I. *et al.* Bacterial nanocellulose as a corneal bandage material: A comparison with amniotic membrane. *Biomater. Sci.* **8**, 2921–2930 (2020).
42. Andrade, F. K., Moreira, S. M. G., Domingues, L. & Gama, F. M. P. Improving the affinity of fibroblasts for bacterial cellulose using carbohydrate-binding modules fused to RGD. *J. Biomed. Mater. Res. Part A* **92**, 9–17 (2010).
43. Gonçalves, S. *et al.* Bacterial Cellulose As a Support for the Growth of Retinal Pigment Epithelium. *Biomacromolecules* **16**, 1341–1351 (2015).
44. Gonçalves, S. *et al.* Acetylated bacterial cellulose coated with urinary bladder matrix as a substrate for retinal pigment epithelium. *Colloids Surfaces B Biointerfaces* **139**, 1–9 (2016).
45. Lv, X. *et al.* Bacterial Cellulose-Based Biomimetic Nanofibrous Scaffold with Muscle Cells for Hollow Organ Tissue Engineering. *ACS Biomater. Sci. Eng.* **2**, 19–29 (2016).

46. Svensson, A. *et al.* Bacterial cellulose as a potential scaffold for tissue engineering of cartilage. *Biomaterials* **26**, 419–431 (2005).
47. Khan, S. *et al.* Preparation and structural characterization of surface modified microporous bacterial cellulose scaffolds: A potential material for skin regeneration applications in vitro and in vivo. *Int. J. Biol. Macromol.* **117**, 1200–1210 (2018).
48. Tronser, T., Laromaine, A., Roig, A. & Levkin, P. A. Bacterial Cellulose Promotes Long-Term Stemness of mESC. *ACS Appl. Mater. Interfaces* **10**, 16260–16269 (2018).
49. Anton-Sales, I., Beekmann, U., Laromaine, A., Roig, A. & Kralisch, D. Opportunities of Bacterial Cellulose to Treat Epithelial Tissues. *Curr. Drug Targets* **20**, 808–822 (2019).
50. Jagannath, A., Raju, P. S. & Bawa, A. S. Comparative evaluation of bacterial cellulose (nata) as a cryoprotectant and carrier support during the freeze drying process of probiotic lactic acid bacteria. *LWT - Food Sci. Technol.* **43**, 1197–1203 (2010).
51. Lee, K. H. *et al.* An efficient and mass reproducible method for vitrifying mouse embryos on a paper in cryotubes. *Cryobiology* **66**, 311–317 (2013).
52. Benjamin Stielow, J., Vaas, L. A. I., Göker, M., Hoffmann, P. & Klenk, H. P. Charcoal filter paper improves the viability of cryopreserved filamentous ectomycorrhizal and saprotrophic Basidiomycota and Ascomycota. *Mycologia* **104**, 324–330 (2012).
53. Khalid, A. *et al.* Bacterial cellulose–TiO₂ nanocomposites promote healing and tissue regeneration in burn mice model. *RSC Adv.* **7**, 47662–47668 (2017).
54. U.S. Department of Health and Human Services *et al.* *Guidance for Industry Pyrogen and Endotoxins Testing: Questions and Answers.* (2012).
55. Zeng, M., Laromaine, A. & Roig, A. Bacterial cellulose films: influence of bacterial strain and drying route on film properties. *Cellulose* **21**, 4455–4469 (2014). Zeng, M., Laromaine, A. & Roig, A. Bacterial cellulose films: influence of bacterial strain and drying route on film properties. *Cellulose* **21**, 4455–4469 (2014).
56. Biazar, E., Heidari, M., Asefnejad, A., Asefnezhad, A. & Montazeri, N. The relationship between cellular adhesion and surface roughness in polystyrene modified by microwave plasma radiation. *Int. J. Nanomedicine* **6**, 631–9 (2011).
57. Zareidoost, A., Yousefpour, M., Ghaseme, B. & Amanzadeh, A. The relationship of surface roughness and cell response of chemical surface modification of titanium. *J Mater Sci Mater Med* **23**, 1479–88 (2012).
58. Martínez Ávila, H. *et al.* Novel bilayer bacterial nanocellulose scaffold supports neocartilage formation in vitro and in vivo. *Biomaterials* **44**, 122–133 (2015).
59. Hakkinen, K. M., Harunaga, J. S., Doyle, A. D. & Yamada, K. M. Direct Comparisons of the Morphology, Migration, Cell Adhesions, and Actin Cytoskeleton of Fibroblasts in Four Different Three-Dimensional Extracellular Matrices. *TISSUE Eng. Part A* **17**, (2011).
60. Huber, M. D. & Gerace, L. The size-wise nucleus: nuclear volume control in eukaryotes. *J. Cell Biol.* **179**, 583–4 (2007).

61. Milla, M., Yu, S.-M. & Laromaine, A. Parametrizing the exposure of superparamagnetic iron oxide nanoparticles in cell cultures at different in vitro environments. *Chem. Eng. J.* **340**, 173–180 (2018).
62. Yeung, T. *et al.* Effects of substrate stiffness on cell morphology, cytoskeletal structure, and adhesion. *Cell Motil. Cytoskeleton* **60**, 24–34 (2005).
63. Matsuura, K., Utoh, R., Nagase, K. & Okano, T. Cell sheet approach for tissue engineering and regenerative medicine. *J. Control. Release* **190**, 228–239 (2014).
64. Yamato, M. & Okano, T. Cell sheet engineering. *Mater. Today* **7**, 42–47 (2004).
65. Ng, K. *et al.* Paper-based cell culture platform and its emerging biomedical applications. *Materials Today* **20**, 32–44 (2017).
66. Costa, P. F., Dias, A. F., Reis, R. L. & Gomes, M. E. Cryopreservation of Cell/Scaffold Tissue-Engineered Constructs. *TISSUE Eng. Part C* **18**, (2012).
67. Batnyam, O., Suye, S. & Fujita, S. Direct cryopreservation of adherent cells on an elastic nanofiber sheet featuring a low glass-transition temperature. *RSC Adv.* **7**, 51264–51271 (2017).
68. Callegari, A. J. & Kelly, T. J. UV irradiation induces a postreplication DNA damage checkpoint. *PNAS* **103**, 15877–15882 (2006).
69. Chen, L. L. & Wang, S. Q. *Nanotechnology in Photoprotection. Nanoscience in Dermatology* (Elsevier Inc., 2016). doi:10.1016/B978-0-12-802926-8.00018-5
70. Painter, R. B. DNA DAMAGE AND REPAIR IN EUKARYOTIC CELLS. *Genetics* **78**, 139–148 (1974).
71. Mordorski, B., Landriscina, A. & Friedman, A. An Overview of Nanomaterials in Dermatology. in *Nanoscience in Dermatology* 31–46 (Elsevier Inc., 2016). doi:10.1016/B978-0-12-802926-8.00003-3
72. Hsieh, M., Koga, H., Suganuma, K. & Nogi, M. Hazy Transparent Cellulose Nanopaper. *Sci. Rep.* **7**, 41590 (2017).
73. Wang, S. *et al.* Transparent, Anisotropic Biofilm with Aligned Bacterial Cellulose Nanofibers. *Adv. Funct. Mater* **28**, 1707491 (2018).
74. Williamst, W. S. & Cannon, R. E. Alternative Environmental Roles for Cellulose Produced by *Acetobacter xylinum*. *Appl. Environ. Microbiol.* **55**, 2448–2452 (1989).
75. Lewicka, Z. A. *et al.* The structure, composition, and dimensions of TiO₂ and ZnO nanomaterials in commercial sunscreens. *J. Nanoparticle Res.* **13**, 3607–3617 (2011).
76. Vargas-Reus, M. A., Memarzadeh, K., Huang, J., Ren, G. G. & Allaker, R. P. Antimicrobial activity of nanoparticulate metal oxides against peri-implantitis pathogens. *Int. J. Antimicrob. Agents* **40**, 135–139 (2012).
77. Azizi-Lalabadi, M., Ehsani, A., Divband, B. & Alizadeh-Sani, M. Antimicrobial activity of Titanium dioxide and Zinc oxide nanoparticles supported in 4A zeolite and evaluation the morphological characteristic. *Sci. Rep.* **9**, 1–10 (2019).

78. Evdokimova, O. *et al.* Hybrid Drug Delivery Patches Based on Spherical Cellulose Nanocrystals and Colloid Titania—Synthesis and Antibacterial Properties. *Nanomaterials* **8**, 228 (2018).
79. El-Sayed, N. S., El-Sakhawy, M., Brun, N., Hesemann, P. & Kamel, S. New approach for immobilization of 3-aminopropyltrimethoxysilane and TiO₂ nanoparticles into cellulose for BJ1 skin cells proliferation. *Carbohydr. Polym.* **199**, 193–204 (2018).
80. Kadiyala, U., Kotov, N. A. & VanEpps, J. S. Antibacterial Metal Oxide Nanoparticles: Challenges in Interpreting the Literature. *Curr. Pharm. Des.* **24**, 896–903 (2018).
81. Cho, M., Chung, H., Choi, W. & Yoon, J. Linear correlation between inactivation of *E. coli* and OH radical concentration in TiO₂ photocatalytic disinfection. *Water Res.* **38**, 1069–1077 (2004).
82. SHIRAI, R. *et al.* Antimicrobial effect of titanium dioxide after ultraviolet irradiation against periodontal pathogen. *Dent. Mater. J.* **35**, 511–516 (2016).
83. Motola, M. *et al.* UV light-induced photocatalytic, antimicrobial, and antibiofilm performance of anodic TiO₂ nanotube layers prepared on titanium mesh and Ti sputtered on silicon. *Chem. Pap.* **73**, 1163–1172 (2018).
84. Chawengkijwanich, C. & Hayata, Y. Development of TiO₂ powder-coated food packaging film and its ability to inactivate *Escherichia coli* in vitro and in actual tests. *Int. J. Food Microbiol.* **123**, 288–292 (2008).
85. Pértile, R., Moreira, S., Andrade, F., Domingues, L. & Gama, M. Bacterial cellulose modified using recombinant proteins to improve neuronal and mesenchymal cell adhesion. *Biotechnol. Prog.* **28**, 526–532 (2012).
86. Innala, M. *et al.* 3D Culturing and differentiation of SH-SY5Y neuroblastoma cells on bacterial nanocellulose scaffolds. *Artif. Cells, Nanomedicine Biotechnol.* **42**, 302–308 (2014).
87. Yang, J. *et al.* Reverse Reconstruction and Bioprinting of Bacterial Cellulose-Based Functional Total Intervertebral Disc for Therapeutic Implantation. *Small* **14**, 1702582 (2017).
88. Carballo-Vila, M. *et al.* Titanium oxide as substrate for neural cell growth. *J. Biomed. Mater. Res. - Part A* **90**, 94–105 (2009).
89. Gupta, I. *et al.* Real-time encoding and compression of neuronal spikes by metal-oxide memristors. *Nat. Commun.* **7**, 1–9 (2016).
90. Jang, T. H. *et al.* Cryopreservation and its clinical applications. *integr med res* **6**, 12–18 (2017).
91. Alnemari, R., Sukumar, P., Deliorman, M. & Qasaimeh, M. A. Paper-Based Cell Cryopreservation. *Adv. Biosyst.* **4**, 1–10 (2020).

Chapter 3

Bacterial nanocellulose carriers for limbal stem cells

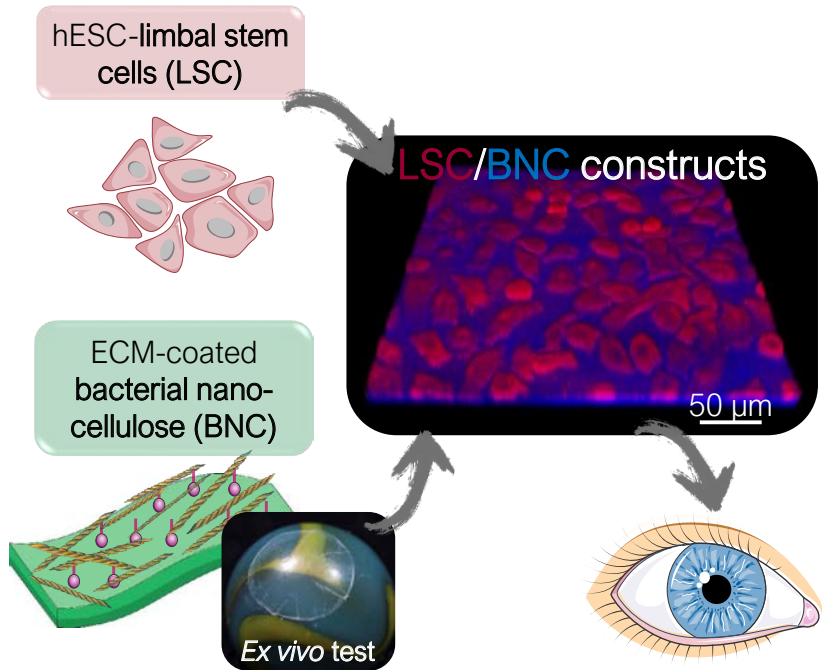


Figure 1: Graphical summary of Chapter 3 (from Publication 3). hESC: human Embryonic Stem Cells indicating the origin of the employed cells and ECM refers to Extra Cellular Matrix.

Chapter introduction

Investigating BNC as an ophthalmologic biomaterial was identified in Chapter 1 as an appealing route to pursue. Consequently, Chapters 3 and 4 are dedicated to corneal regeneration through two complementary approaches.

The cornea is the transparent forefront of the eye and is composed of five layers being a stratified nonkeratinized epithelium the most external one. Apart from the epithelium, there are two other cellular layers; the stroma and the endothelium. The stroma constitutes the bulk of the cornea and is composed of collagen fibrils and sparse corneal fibroblasts so-called keratocytes. The posterior-most layer is the endothelium, formed by a single layer of mitotically inactive cells which nourish and regulate the osmolality of the cornea (see Figure 2)¹. A transparent and healthy cornea is essential for a clear vision and consequently, corneal dysfunctions are greatly feared. Traumas and ulcerations causing corneal opacities are rather common with >1.5 million new cases worldwide every year accounting for a considerable global health issue^{2,3}.

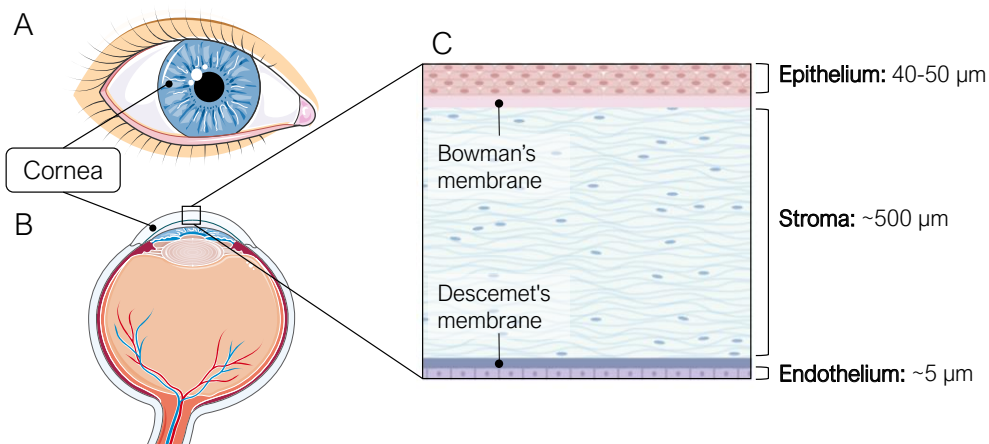


Figure 2: Basic scheme of human ocular anatomy. A) Position of the cornea in a frontal illustration of the eye. B) Corneal localization in a lateral cross-section of the ocular globe. C) The five constituent stratum of the human cornea and the thickness of the three cellular layers. Illustrations have been modified from <https://smart.servier.com/> and <https://biorender.com/>.

Cell transplantation therapies have raised enormous hope for ocular surface reconstruction⁴ particularly since the approval of Holoclar in 2015. Holoclar was

the first Advanced Therapy Medicinal Product (ATMP) containing stem cells ever approved for commercialization in the European Union⁵. This treatment is based on a specific type of epithelial stem cells called Limbal Stem Cells (LSC). These cells are located at the boundary between the cornea and the conjunctiva, in an anatomical area called the limbus (see Figure 3) and are known for their ability to renew the corneal epithelium. The Holoclar procedure consists on transplanting LSC collected from the own patient (autologous) via a limbal biopsy from the less affected eye. The harvested LSC are expanded *ex vivo* and then seeded on a human fibrin membrane that acts as a cell carrier for the administration to the most damaged eye⁶. Then, the fibrin support is rapidly dissolved and a mix of cells containing LSC is released to the ocular surface.

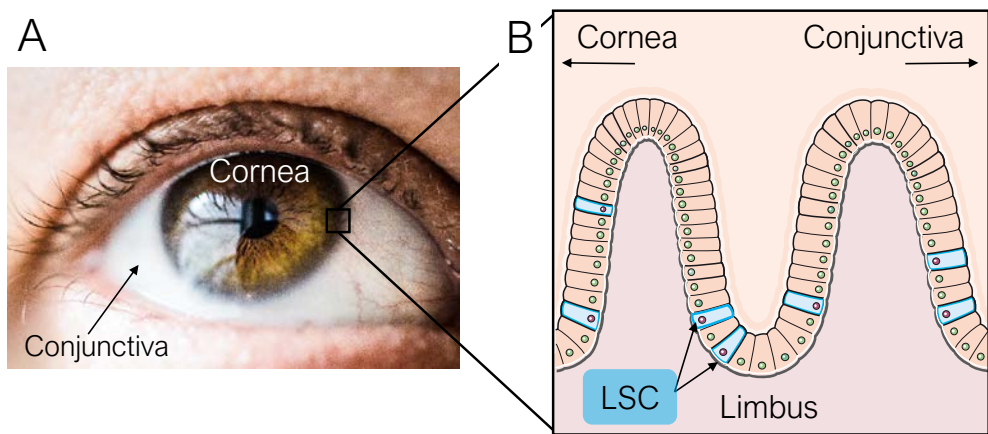


Figure 3: LSC in the human eye. A) The limbus is the circumferential narrow area separating the cornea (transparent) from the conjunctiva (whitish). B) LSC reside in ridges named palisades of Vogt at the corneoscleral junction. This figure contains adapted content from <https://unsplash.com/> and <https://smart.servier.com/>.

This chapter tackles the challenge of expanding the use of BNC as a cell carrier from model cells (as in Chapter 2) to therapeutic cells. For this purpose, I carried out a research stay in the Eye Group led by Prof. Heli Skottman (<https://research.tuni.fi/eye-group/>) at Tampere University (Finland). The stay was supported by a European Molecular Biology Organization (EMBO) short-term scholarship. Skottman's lab is devoted to the development of stem cell-based tools for corneal and retinal repair through cell transplantation. Reproducible and efficient methods to differentiate LSC from human pluripotent stem cells (hPSC) have been developed

in the Eye Group securing LSC availability from allogenic sources without the need for a limbal biopsy.

The experimental work of Chapter 3 encompasses the publication entitled “*Limbal Stem Cells on Bacterial Nanocellulose Carriers for Ocular Surface Regeneration*” and preliminary experiments on the cryopreservation of LSC on BNC carriers.

Publication 3: Limbal Stem Cells on Bacterial Nanocellulose Carriers for Ocular Surface Regeneration

Irene Anton-Sales, Laura Koivusalo, Heli Skottman, Anna Laromaine and Anna Roig. *Small*. 17, e2003937 (2021). <https://onlinelibrary.wiley.com/doi/full/10.1002/sml.202003937>. Reprinted with permission from the copyright holders (John Wiley and Sons).

Abstract

Limbal stem cells (LSC) are already used in cell-based treatments for ocular surface disorders. Clinical translation of LSCs-based therapies critically depends on the successful delivery, survival and retention of these therapeutic cells to the desired region. Such a major bottleneck could be overcome by using an appropriate carrier to provide anchoring sites and structural support to LSC culture and transplantation. Bacterial nanocellulose (BNC) is an appealing, yet unexplored, candidate for this application because of its biocompatibility, animal-free origin and mechanical stability. Here, we investigated BNC as a vehicle for human embryonic stem cells-derived LSC (hESC-LSC). To enhance cell-biomaterial interactions, we implemented a plasma activation followed by a Collagen IV and Laminin coating of the BNC substrates. This surface functionalization with human extracellular matrix proteins greatly improved the attachment and survival of hESC-LSC without compromising the flexible, robust and semi-transparent nature of the BNC. The surface characteristics of the BNC substrates are described and a preliminary *ex vivo* test in simulated transplantation scenarios is provided. Importantly, we show that hESC-LSC retain their self-renewal and stemness characteristics up to 21 days on BNC substrates. These results open the door for future research on hESC-LSC/BNC constructs to treat severe ocular surface pathologies.

Keywords

Microbial cellulose; Corneal epithelium; Human embryonic stem cells; Animal-free; Cell transplantation

Introduction

Limbal stem cells (LSC) are tissue-specific stem cells located at the boundary between the cornea and the bulbar conjunctiva. LSC safeguard ocular surface health by constantly renewing the corneal epithelium and by preventing the opaque conjunctival cells to migrate into the transparent cornea.^{7,8} Acute trauma, burns and inflammatory diseases can disrupt the delicate ocular surface homeostasis and cause opacification, vascularization and scarring of the cornea resulting in impaired vision.^{2,9} LSC transplantation holds enormous therapeutic potential for these incapacitating conditions^{4,10,11} but its implementation is conditioned to the availability of clinically-compliant donor LSC and the effectiveness of the cell delivery strategies.^{12,13} As an alternative to autologous and allogenic primary cell sources, on-demand amounts of LSC can be attained through differentiation from human induced pluripotent (hiPSC) or human embryonic stem cells (hESC) independently from donor ocular tissues. Furthermore, recent protocols ensure the reproducible and well-defined differentiation of LSC offering safer venues for ocular surface reconstruction.¹⁴⁻¹⁶

Finding an optimal carrier for LSC transplantation to the ocular surface would give a firm push to the practical implementation of LSC-based therapies. Ideally, the carrier should be biocompatible and support cell viability while presenting adequate material properties (*e.g.* robustness, conformability, manageability). Human amniotic membrane (AM), the innermost layer of the placenta, is widely used in ophthalmological treatments^{17,18} and it has been advocated as a well-suited substrate for LSC expansion and transplantation.^{19,20} Nevertheless, concerns about the low availability and reproducibility of AM have prompted research on alternative biological substrates such as collagen and fibrin.²¹⁻²³ On this line, we have previously suggested the biopolymer bacterial nanocellulose (BNC) for ocular surface bandaging applications.²⁴ BNC is biosynthesized by non-pathogenic bacterial cultures in the form of an interlaced nanofibrillar structure with high architectonic parallelism to collagen matrices. This nanostructure endows BNC with outstanding material properties regarding mechanical and thermal stability, conformability, water retention and easiness of manipulation.²⁵ In addition, BNC is widely regarded as a cytocompatible substrate owing to its high chemical purity and supported by

numerous *in vitro* investigations^{26–28}. As for immunogenicity, BNC grafts have been found to elicit low to none inflammatory responses *in vivo* and to be generally well tolerated by the surrounding tissues^{29–32}. Production-wise, BNC is equally appealing because of its animal-free origin, tunability and feasible scale-up.^{33,34} All these reasons endorse BNC towards its way through the health market^{35,36} with applications ranging from wound dressings^{37,38} to anti-fibrotic implant coatings.³⁹

Here, we aimed at establishing and characterizing LSC cultures on BNC substrates to assess the potential of BNC as a transplantation vehicle for these cells. BNC has been suggested as a carrier for other cell types,^{40,41} including retinal pigment epithelium,^{42,43} but to the best of our knowledge, this is the first study combining BNC and LSC. Clinical translation being our ultimate goal; we employed LSC differentiated from hESC (hESC-LSC) under feeder- and serum-free conditions¹⁵. Similarly, BNC membranes were thoroughly purified until endotoxin-free before its use as cell support.²⁶ The palette of BNC modifications seeking to enhance cell attachment is particularly diverse^{33,34,36–38}. Thus, our ambition was to find a BNC conditioning rendering a favourable interface for hESC-LSC culture in a simple, well-defined and scalable process.

Materials and methods

Bacterial nanocellulose (BNC) substrates preparation and characterization

BNC production

BNC hydrogels were synthesized by *Komagataeibacter xylinus* (*K. xylinus*, NCIMB 5346 from Colección Española de Cultivos Tipo (CECT), Valencia, Spain) grown on Hestrin-Schramm medium following our previously described protocols.^{24,44} *K. xylinus* cultures were kept on 24-well plates for three days under static conditions at 30 °C to obtain circular BNC fleeces with the same diameter as the containers (~1.6 cm). The as-formed hydrogels were picked with tweezers and immersed in a 1:1 v/v solution of Milli-Q water and ethanol for 10-15 minutes. Then, BNC fleeces were cleaned with boiling Milli-Q water (40 min) and NaOH (2 x 20 min) to remove organic remains. The BNC hydrogels were dried at 60 °C,

between two Teflon plates and 1 Kg weight. Dry films were rehydrated in Milli-Q water, sterilized by autoclave (121 °C, 20 min), and stored at Room Temperature (RT) until experimental use.

BNC surface modification

BNC membranes were placed on 24-well culture plates and incubated overnight at 4 °C with a solution of 0.5 µg/cm² of recombinant human laminin (LN-521, Biolamina) and 5 µg/cm² collagen type IV from human placenta (Col IV, Sigma-Aldrich) in Dulbecco's phosphate-buffered saline (DPBS, Lonza) containing calcium and magnesium. The as-prepared samples are referred to as “ECM coated” BNC. To prepare the “Plasma + ECM coated” samples, dry BNC films were activated for 1 min with oxygen plasma inside a plasma reactor (Diener Electronic GmbH, power=50 W, pressure=0.40 mBar) under vacuum. Then, the activated membranes were immediately coated with the ECM protein solution following the previous procedure. The “plasma” BNC samples were only irradiated with oxygen plasma and the “plain” samples were left untreated.

Light transmittance measurements

Visible light absorption spectra were collected with a JASCO V-570 Ultraviolet-Visible-Near-Infrared spectrophotometer between 400 and 800 nm. Samples were held with a cover glass also used for the baseline correction. Three different samples were analysed for each condition and the obtained values were averaged.

Scanning electron microscopy (SEM)

Fragments of dry BNC films were placed flat on aluminium SEM sample holders with adhesive carbon tape. Metalized samples were sputtered with 5 nm of platinum before imaging. A high-resolution scanning electron microscope (FEI Magellan 400L XHR SEM) was used under a high vacuum and with an acceleration voltage of 2 kV to obtain images at 5.000, 20.000 and 100.000X magnifications. Working distance was 4 mm and the current was 0.1 nA. Energy-dispersive X-ray (EDX) spectroscopy was performed with the same equipment at 1 KeV. At least two areas from four independent BNC samples were imaged on both sides of the films.

Atomic force microscopy (AFM)

Topographical images and roughness values were obtained with a 5100 Agilent Technologies atomic force microscopy on tapping mode and equipped with a FORT tip from AppNano. Three 30 x 30- μm areas were analysed from each sample. Dry BNC samples were fixed flat on the holders with adhesive tape. The images were processed with Surface analysis software V7.4 (64-bit) – Mountains technology.

Ex vivo evaluation of BNC with porcine corneal organ culture

The corneal organ model employed in this study has been described previously^{45,46}. Briefly, fresh porcine eyes from a local abattoir were kept in cold DPBS + 2 % antibiotics for up to 4 h and then disinfected with 2 % povidone-iodine (Betadine®, Leiras). The corneas and part of the sclera were resected under sterile conditions and kept in Dulbecco's Modified Eagle Medium (DMEM) supplemented with 5 % Foetal Bovine Serum (FBS), 1 % Penicillin/Streptomycin (P/S), 0.1 % Amphotericin-B and 1 X GlutaMax at 37 ° C and 5 % CO₂ until BNC implantation. Before the BNC application, epithelial damage was created by an exhaustive scraping of the corneal surface with a scalpel, including the limbal area. BNC membranes were preconditioned with culture medium and 5-mm diameter pieces were cut with a trephine and sutured to the central part of the cornea with the help of a Barron artificial anterior chamber (Katena Products Inc.). Four symmetric sutures (VICRON suture number 7) were made to fix each BNC sample. Then, specimens were moved to 6-well plates and covered with soft contact lenses (EyeQ One-Day Premium, Cooper Vision) to avoid drying. The corneal organ culture was kept in the same culture conditions for two weeks after the implantation. The medium was changed trice per week. Before histological analysis, the porcine corneas were fixed using 4 % paraformaldehyde (PFA) in DPBS for 4 h at RT. Samples were dehydrated in a Tissue-Tek VIP 5 (Sakura Finetek Europe) automatic tissue processor overnight and embedded in paraffin blocks. Following, 7 mm thick tissue sections were cut with a microtome from each sample to cover different areas of the cornea. Histological sections were stained with haematoxylin-eosin (HE) and mounted on TOMO® adhesion microscope slides (Matsunami Glass Ind., Ltd.). Optical microscope images were captured with Nikon Eclipse TE2000-S microscope and DS-Fi1 camera.

***In vitro* experiments**

Human embryonic stem cell-derived limbal stem cells (hESC-LSC) culture

All cell studies were conducted under the ethical approval of the Ethics Committee of Pirkanmaa Hospital District number R05116 to derive, culture and differentiate hESC lines for research. No new cell lines were derived from this study. The hESC-LSCs were differentiated from the hESC line Regea08/17 as described previously.¹⁵ The hESC-LSC cultures were maintained under serum- and feeder cell-free conditions. For the *in vitro* experiments, cryopreserved hESC-LSC in PSC cryopreservation medium (Thermo Fisher Scientific) were thawed at 37°C and directly plated on top of BNC substrates (100.000 cells/ cm²) placed on 24-well plates. Immediately after seeding, the culture plates were centrifuged for one minute at 200 g's to increase the contact between hESC-LSC and the BNC supports. Controls were seeded on Corning® CellBIND 24-well plates with the same ECM coating (5 µg/cm² Col-IV + 0.5 µg/cm² LN-521). The cultures were maintained in defined CnT-30 corneal differentiation medium (CELLnTEC, Advanced Cell Systems) containing 0.5 % antibiotics (P/S) at 37 °C and 5 % CO₂. Cell morphology and attachment were visually evaluated with a phase-contrast microscopy Zeiss Axio Vert A1 (Carl Zeiss) and the medium was changed trice per week.

Cell viability studies

For qualitative cell viability assessment, the LIVE/DEAD® Viability/Cytotoxicity Kit for mammalian cells from Thermo Fisher Scientific was employed following the manufacturer's instructions. Briefly, cell cultures were washed with DPBS and incubated in the dark for 30 min with 500 µL of a 2 µM Calcein-AM and 1 µM Ethidium homodimer solution in DPBS. Then, the samples were rinsed with DPBS and imaged using a fluorescence microscope (Olympus IX51 equipped with a DP71 camera) at 10X. The PrestoBlue™ cell viability reagent (Thermo Fischer Scientific) was used to measure cell proliferation. Triplicate samples were washed with DPBS and incubated with PrestoBlue® reagent diluted 1:10 (v/v) in CnT-30 medium for 30 min at 37 °C and protected from light. Then, the supernatants were pipetted in technical triplicates on a 96-well plate (100 µL/well) and

fluorescence values were read with a Viktor 1420 Multilabel Counter (Wallac) at 544 nm excitation and 590 emission wavelengths. Blanks were made with BNC substrates without cells. The average viability values obtained at Days 3 and 7 were normalized to values from Day 1 and represented as mean \pm standard error repeating the experiment three times.

Immunofluorescence

For specific marker proteins and Collagen IV detection, samples were firstly washed with DPBS, fixed with 4 % PFA for 20 min at RT and washed again three times with DPBS. Triton X-100 was used to permeabilize the cell membranes for 15 min at RT and then samples were blocked for 90 min with a solution of 3 % Bovine Serum Albumin (BSA) in DPBS under mild agitation. Primary antibodies were diluted in 0.5 % BSA and incubated overnight at 4 °C. The next day, specimens were washed three times with DPBS and incubated for one hour at RT under mild agitation with the fluorescently labelled secondary antibodies diluted in 0.5 % BSA. See Table 1 for information regarding the employed antibodies. Finally, samples were rinsed again three times with DPBS, flipped upside down and prepared for imaging with mounting medium containing 4',6-Diamidino-2-phenylindole di-hydrochloride (DAPI) (Vectashield® from Vector Laboratories) under 13 mm Ø coverslips. Pictures were captured using an Olympus IX51 fluorescence microscope with 5X and 10X dry objectives. The stainings were repeated at least three times. Raw images were coloured and adjusted for contrast and brightness using Image-J-Fiji software. Grey values were measured as the average intensity from the whole fluorescent images acquired with the same exposure times using the same software.

Antibody	Host	Supplier	Dilution (v/v)
<i>p63</i> α	Rabbit	Cell Signalling Technology	1:200
<i>p40</i>	Mouse	Biocare Medical	1:100
<i>CK14</i>	Mouse	R&D	1:200
<i>CK15</i>	Mouse	Neomarkers (Thermo Fisher)	1:200
<i>CK12</i>	Goat	Santa Cruz Biotechnology	1:200

Antibody	Host	Supplier	Dilution (v/v)
CK12	Rabbit	Abcam	1:200
Ki-67	Rabbit	Millipore	1:500
Collagen IV	Goat	Millipore	1:100
anti-rabbit Alexa-488	Donkey	Molecular Probes	1:800
anti-rabbit Alexa-568	Donkey	Molecular Probes	1:800
anti-goat Alexa-568	Donkey	Molecular Probes	1:800
anti-mouse Alexa-647	Donkey	Molecular Probes	1:800
anti-mouse-Alexa-568	Donkey	Molecular Probes	1:800

Confocal microscope

Fixed hESC-LSC cultures grown on top of BNC membranes were incubated for 5 min at RT with 1 mL of a solution of 5 µg/mL CellMask™ Deep Red Plasma Membrane Stain (Invitrogen) to dye cellular membranes and 0.25 mg/mL Fluorescent Brightener (Sigma) diluted in DPBS to stain the BNC substrates. Then, samples were rinsed with DPBS and placed with the cells facing down on Ibidi Glass Bottom dishes. Stack images were obtained with a confocal laser-scanning microscope (Leica SP5). Fluorescent Brightener was excited at 350 nm and Cell Mask 588 nm wavelength. Fluorescence images were reconstructed and coloured with the Fiji package of Image-J (64-bit version).

Statistical analysis

Statistically significant differences were determined using Graph Pad Prism 5 software by one-way analysis of variance (ANOVA) and Tukey's multiple comparison *post hoc* test. Significance between groups was established for $P < 0.05$. Values provided correspond to the average \pm standard deviation or standard error of the mean as indicated. P-values on the graphs are summarized as non-significant (ns) for $P \geq 0.05$, * for $P < 0.05$, ** for $P < 0.01$ and *** for $P < 0.001$.

Results

BNC membranes coating and characterization

BNC membranes (*i.e.* dried and rehydrated native BNC hydrogels) were conditioned for hESC-LSC culture following the process summarized in Figure 4A. Typically, hESC-LSC require specific binding moieties present in the extracellular matrix (ECM) for adherence and survival. Therefore, a defined mixture of ECM proteins consisting of human Collagen IV (Col-IV) and recombinant human Laminin-521 (LN-521) was conjugated to endow BNC with specific linkers to favour cell attachment. Col-IV was fluorescently immunostained to investigate the distribution and abundance of the covering (Figure 4, B-E). The conventional method consisting of incubating the BNC membranes with the protein solution rendered an inhomogeneous and incomplete coating of the substrates (Figure 4C) with accumulations of Col-IV in the cavity-like structures of the BNC membranes. To address this issue, a plasma activation step was incorporated before the impregnation with Col-IV and LN-521. The plasma-treated BNC substrates were homogeneously and more profusely covered by Col-IV than the substrates coated without prior plasma activation (Figure 4D). This effect was confirmed by comparing the fluorescence intensity values (Figure 4E) which showed statistically significant differences between the two methods.

Macroscopically, BNC membranes were indistinguishable. All the studied forms of BNC appeared as semi-transparent, thin (~20 microns) flexible and self-standing substrates (Figure 5A). BNC membranes, regardless of the surface treatments, were easily manipulated with tweezers and showed good conformability to a dome-shaped surface (Figure 5A). Moreover, the applied surface treatments had a negligible effect on the light transmittance of the BNC membranes (Figure 5B). All the investigated BNC membranes presented high light transmittance at long wavelengths while showing a gradual decline towards smaller wavelengths. As an example, the average transmittance at 700 nm was 84 % and 70% at 500 nm.

SEM was used to investigate the effect of oxygen plasma on the micro/nanostructure of BNC revealing an altered nanofiber morphology after the plasma treatment (Figure 4, F and H). This is a superficial modification since the reverse side of all the substrates presented the typical BNC nanofibrous organization (see

a representative image in Figure 4). Under SEM, the ECM coating was visually imperceptible on both ECM-coated and plasma-activated + ECM-coated samples (Figure 4, G and H). To discard misinterpretations due to the metallization of the samples, non-metallized substrates were also observed under SEM with comparable outcomes (Figure S1). On the contrary, a nitrogen peak, ascribed to the proteinaceous coating, was detected by EDX only on the samples containing Col-IV and LN-521 (Figure S1). Besides, the surface of the plasma-treated BNC membranes was noticeably rougher than the untreated ones. This observation was confirmed by AFM roughness measurements, which disclosed a 1.4-fold increase in roughness for the plasma-activated samples *vs* the not activated samples (AFM images are shown in Figure S1).

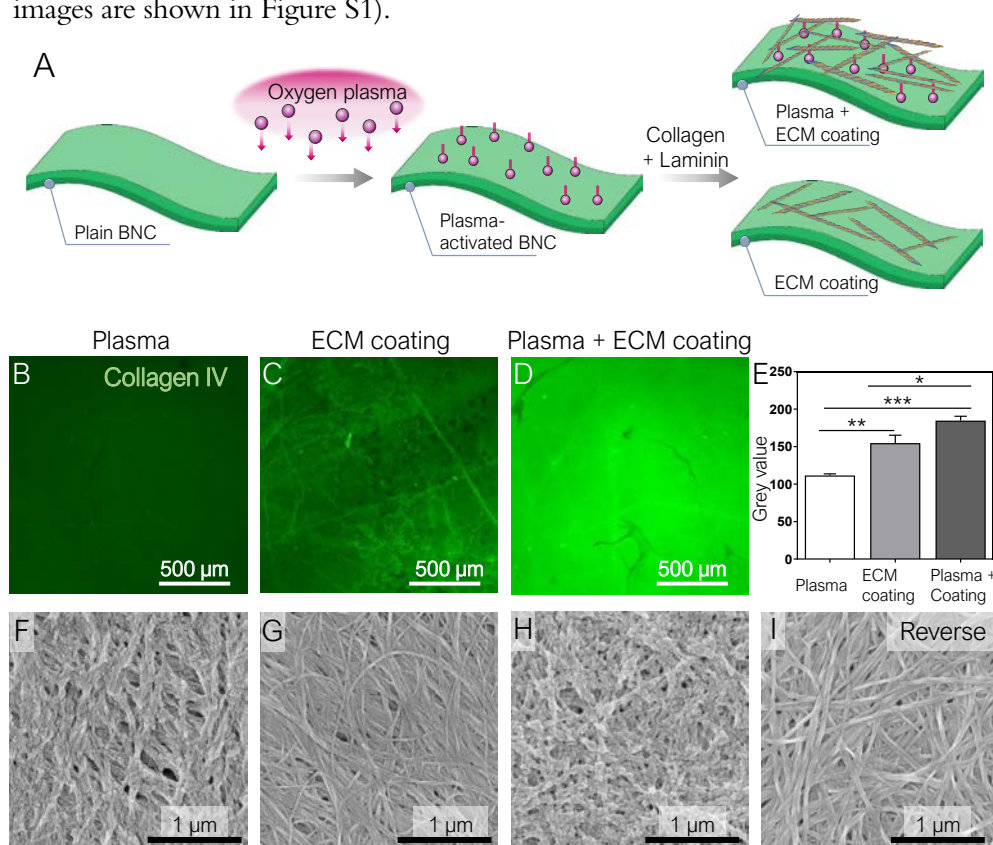


Figure 4: BNC surface treatments. A) Sketch of the different surface modifications of BNC membranes. B-D) Immunofluorescence staining of Collagen IV (green) deposited on BNC substrates. B) BNC activated with plasma but without ECM coating (Blank). C) BNC coated with the standard procedure consisting of pipetting the ECM protein solution on top of the substrates. D) Plasma-activated and ECM-coated BNC substrates where an intense and homogeneous coating

by Collagen IV is observed. E) Fluorescence intensity (grey value \pm standard error) comparison of the Collagen IV staining between the different BNC substrates. Statistically significant differences were detected between all the groups. The lower board (F-I) gathers representative SEM images of the BNC substrates. As seen in images F and H, the plasma treatment altered the BNC nanofibers while the ECM coating was visually undetectable (G). I) The reverse (untreated) side of all the BNC substrates remained unaltered, indicating that the modifications caused by the oxygen plasma are superficial. A representative SEM image is shown.

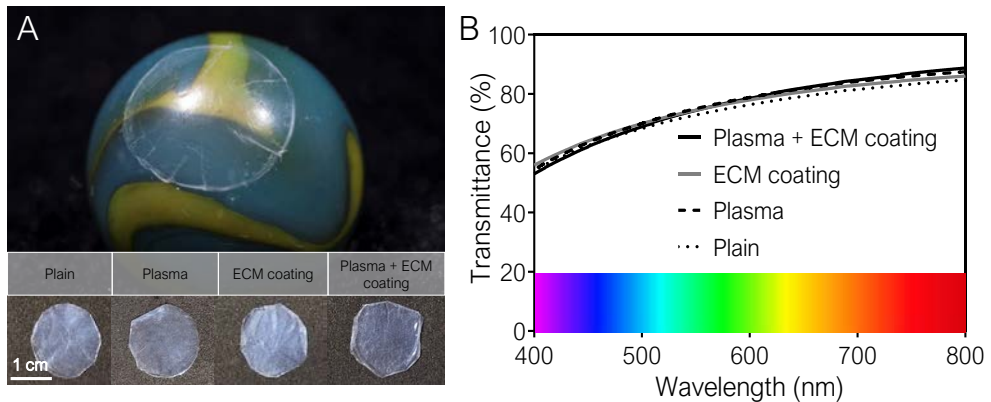


Figure 5: Macroscopic and optical features of BNC substrates. A) Digital images of the tested BNC substrates presenting an analogous appearance. All the membranes could be easily handled, maintained their flexibility and robustness and accommodated well to a curved surface (upper photograph). B) Visible light transmittance of the tested cell carriers. The coatings to enhance hESC-LSC attachment did not alter the optical properties of BNC. All the substrates presented high transmittance at long wavelengths with a progressive decrease towards shorter wavelengths.

Ex vivo BNC evaluation with a corneal organ culture

To assess the applicability of BNC as a support for cell transplantation to the ocular surface, an *ex vivo* organ culture model was used. Epithelial damage was created on excised porcine corneas before BNC implantation. After 14 days in culture, histological analysis was carried out by sectioning the specimens as schematized in Figure 6A. During the sample preparation process, BNC membranes proved excellent conformability to the dome shape of the corneas, could be cut to the desired size and were easily *ex vivo* sutured to the ocular surface (Figure 6B). Imaging of the HE-stained sections showed undamaged BNC membranes in close contact with the corneal surface for some of the tested eyes. Remarkably, a continuous corneal epithelium had re-grown under the BNC patch (Figure 6, C and D). See

Figure S2 for comparison with a control pig cornea without BNC implantation where a similarly regrown pig epithelium is appreciable

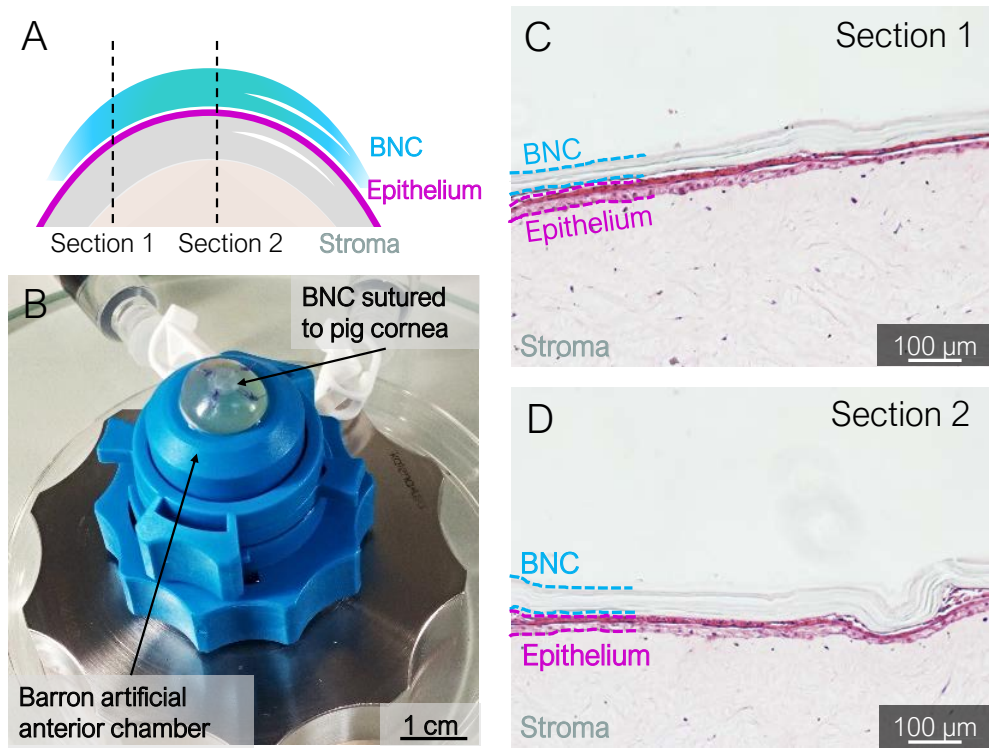


Figure 6: *Ex vivo* evaluation of BNC applicability as a cell delivery vehicle to the ocular surface with a porcine organ culture model. A) and B) depict the experimental setup, a Barron artificial anterior chamber (B) was used to perform the sutures on resected pig eyes. BNC membranes withstood cutting to the desired shape and fixation by suture stitches to porcine corneas with induced epithelial damage. Histological sections were cut as illustrated in A). HE staining of the tissue sections revealed the successful reepithelization of the pig corneas and intimate contact between the BNC and the ocular surface at the two examined cross-sections (C and D). For clarity of the images, BNC has been highlighted in blue and the pig epithelium in pink.

hESC-LSC attachment and viability on BNC substrates

Next, the ability of the BNC to promote hESC-LSC attachment and viability was evaluated and compared for the distinct surface treatments. After 24 h in culture, evident differences could be observed in terms of cell morphology (Figure 7). hESC-LSC plated on plasma activated-ECM coated BNC membranes exhibited a homogeneous distribution on the substrate and the expected epithelial cell appearance (Figure 7D). Oppositely, hESC-LSC seeded on BNC membranes that recei-

ved only plasma activation (Figure 7B) or solely ECM coating (Figure 7C) were round in morphology indicating poor suitability of these substrates for hESC-LSC maintenance. The same outcomes were detected for plain BNC (Figure 7A).

In accordance with these observations, on Day 4 after seeding, Live/Dead staining evidenced a highly viable cell population on the BNC membranes that were plasma-activated and coated with Col IV and LN-521 (Figure 7H). hESC-LSC on plasma-activated as well as plain BNC had mainly detached from the substrates (Figure 7, E and F). On BNC membranes with conventional ECM coating, more hESC-LSC remained adhered but were unable to spread and stained mainly as dead cells (Figure 7G). An additional Live/Dead assay was conducted for BNC with plasma activation and ECM-coating at Day 8 to confirm long-term cell survival observing a highly viable hESC-LSC population (Figure S3). In light of these results, the *in vitro* experiments that follow were only performed with BNC substrates with plasma activation and ECM coating and are referred to as “BNC” from here on.

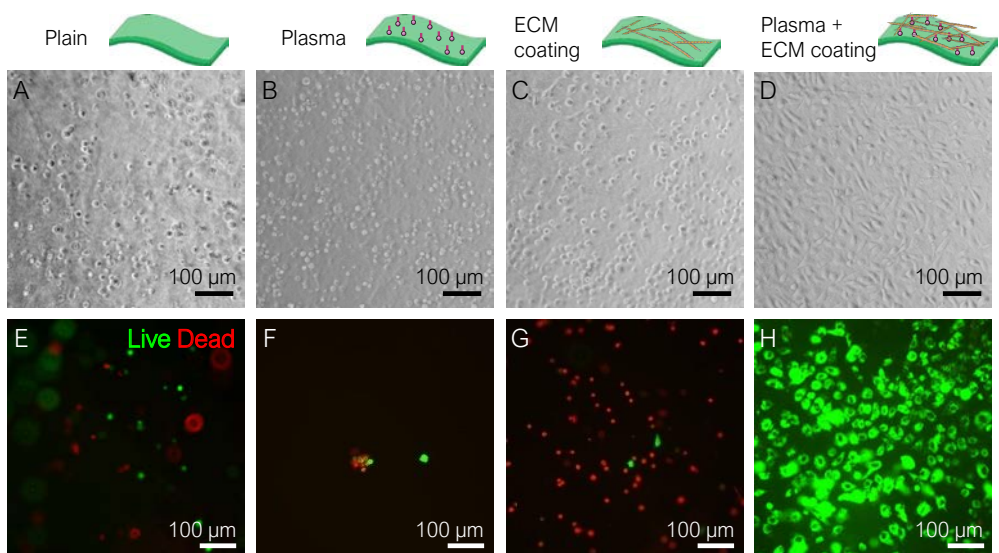


Figure 7: Attachment and viability of hESC-LSC on surface-modified BNC. A-D) Phase-contrast microscope images a Day 1 where, depending on the surface modification of BNC, clear differences in cell morphology can be visualized. Substrates with only one treatment (plasma (B) or ECM coating (C)) rendered rounded hESC-LSC morphologies while the combination of both created a favourable surface for hESC-LSC spreading (D). E-H) Live/Dead staining of hESC-LSC at Day 4 where alive cells are stained in green and dead cells in red. Note the high cell viability in (H) corresponding to BNC substrates with plasma activation followed by ECM protein coating. Viable hESC-LSC on the rest of the substrates were scarce (E-G).

hESC-LSC self-renewing capacity on BNC substrates

Since the capacity to promote cell attachment, proliferation and then further differentiation towards corneal epithelial cells is a valuable characteristic of a cell carrier, we studied the self-renewal properties of hESC-LSC on BNC substrates at three different time points. Visually, an increase in cell number could be observed between Day 1 and 3 while from Day 3 to 7 cell density stabilized and cell size augmented (Figure 8A). hESC-LSC exhibited the expected cobblestone morphology at the three studied time points and tended to form an epithelial monolayer on top of the BNC substrates as observed by confocal microscope (Figure 8B). The metabolic activity was quantitatively analysed with a Presto Blue assay (Figure 8D). An increase in the fluorescence signal was detected at the early stages of the culture but not at the late stages where the fluorescence intensity remained constant (not statistically significant differences). To further confirm these results, immunofluorescence staining of the proliferation marker Ki67 was performed (Figure 8C). Expression of Ki67 was detected at days 1, 3 and 7 in a fraction of the hESC-LSC indicating the presence of a self-renewing cell population. The estimated percentage of Ki67 positive cells was higher on Day 1 than on Day 7. hESC-LSC growing on conventional culture plates coated with Col IV and LN-521 were used for comparison and a similar evolution was observed (See Figure S4).

Protein marker expression

Finally, we investigated whether hESC-LSC cultured on BNC films retain their progenitor phenotype or they start to differentiate towards corneal epithelial cells. The expression of specific LSC markers⁴⁷ was evaluated by immunocytochemistry. Simultaneous p63 α and p40 antibodies were used to detect the presence of the Δ Np63 α isoform of p63 in the cell nuclei, a widely used LSC marker. For further validation of the progenitor phenotype, the presence of distinctive cytokeratins (CK) was also examined. CK14 and CK15 were selected as stemness indicators while CK12 was employed as a differentiated corneal cell marker. Immunofluorescence images shown in Figure 9A illustrate that the majority of hESC-LSC cultured on BNC substrates highly express Δ Np63 α and low to undetectable levels of CK12 at both Days 3 and 7 correlating with the expected LSC phenotype. Control hESC-LSC cultured on ECM-coated plastic exhibited a comparable

marker expression pattern (see Ct in Figure 9A). Notably, the progenitor markers CK14 and CK15 behaved differently. While both keratins presented positive immunofluorescence –less homogeneous than Δ Np63 α – at Day 4, only CK15 remained detectable on hESC-LSC maintained on BNC membranes until Day 7 (Figure 9B). As for controls, a similar trend was observed except for some faint signal still present at Day 7 for CK14.

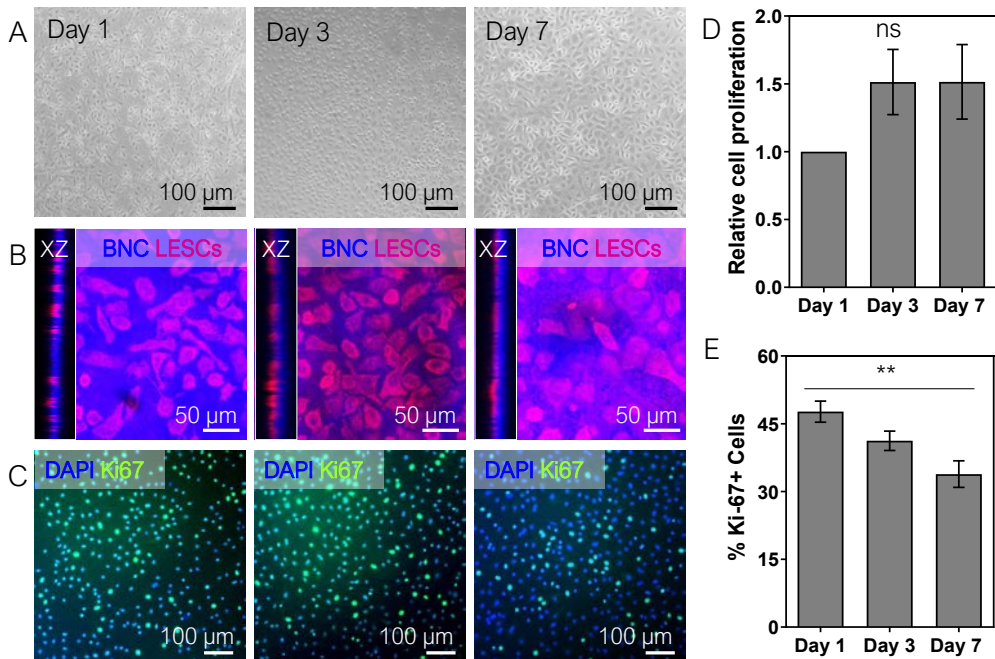


Figure 8: hESC-LSC culture monitoring and proliferation on BNC supports. A) Cell density and distribution vs. time on BNC substrates. B) Confocal microscope and XZ cross-section images where the tendency of hESC-LSC to form an epithelial monolayer on top of the BNC substrates can be observed. hESC-LSC plasma membranes were marked in red and the BNC supports in blue. C) Representative immunofluorescence staining images of the Ki67 proliferation marker expression at diverse time points of hESC-LSC cultures on BNC. D) Presto Blue assay measuring the metabolic activity of hESC-LSC expanded on BNC. Bars show the average value of three independent experiments with standard error. E) Estimation (average and standard error) of the percentage of Ki67-positive cells at three different culture time points.

Furthermore, we examined the long-term maintenance of stemness marker expression. Figure S5 displays immunofluorescence micrographs of hESC-LSC on BNC carriers and control surfaces cultured for 2 and 3 weeks where a sustained LSC phenotype (p40-positive and predominantly CK12 negative) is perceived for both time points and culture surfaces resembling the early time points.

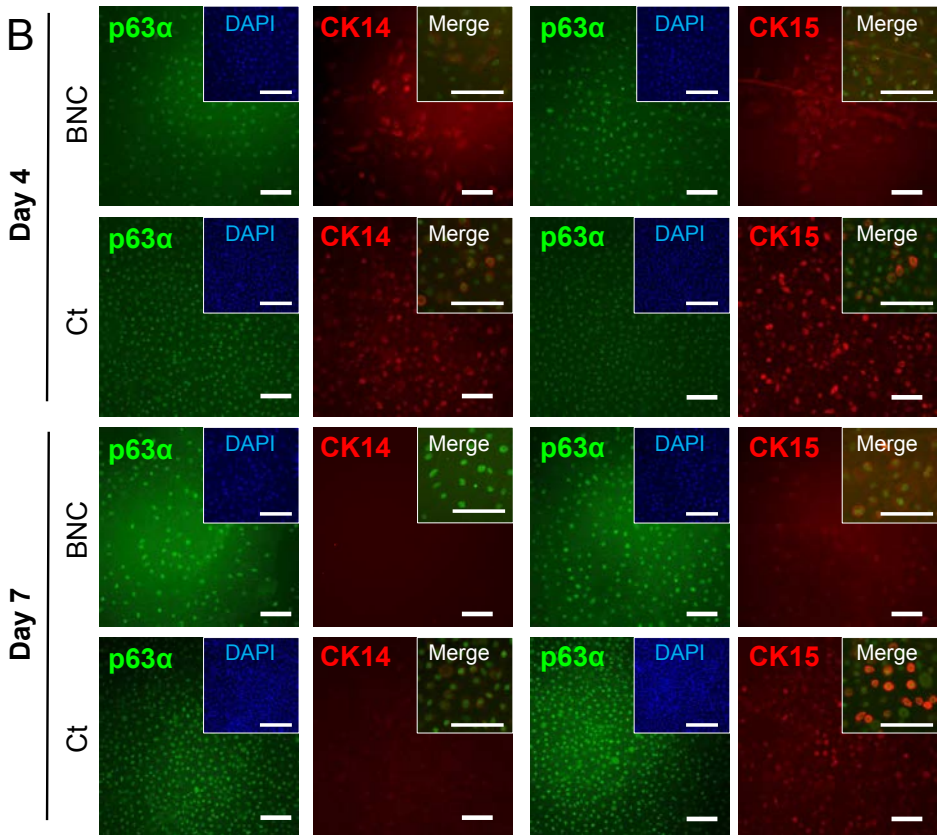
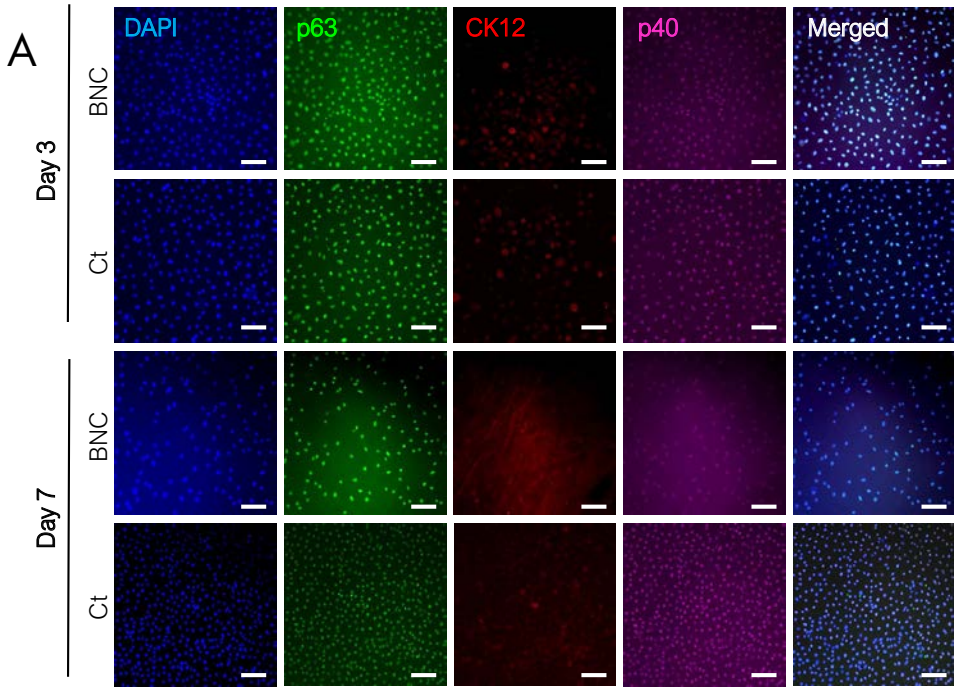


Figure 9: LSC marker expression at early time points. A) Representative immunofluorescence photographs of hESC-LSC cultured on BNC membranes 3 and 7 days after plating. Expression of the well-established limbal stem cell marker Δ Np63 α was confirmed by the simultaneous detection of p63 α and p40. CK12, an epithelial differentiation marker, was identified in low amounts. Merged images confirm the nuclear location of Δ Np63 α and the co-localization of the p63 α and p40 antibodies. Ct refers to conventional ECM-coated cell culture surfaces used for comparison and the scale bar is 100 μ m. B) Cytoplasmic expression of the stemness-associated cytokeratins 14 and 15 (CK14 and CK15) on hESC-LSC cultures grown on top of BNC membranes for 4 and 7 days. The distribution of CK14 and CK15 (red) is compared to p63 α (green) present in the nucleus. Scale bar equals 100 μ m. Inserts: DAPI-stained nuclei (blue) to evidence the total number of cells and details of the localization of the stemness markers. Scale bar of the inserts= 50 μ m.

Discussion

hESC-LSC could revolutionize the management of ocular surface diseases but an optimal cell delivery strategy still needs to be found. This study suggests BNC as a non-animal sourced substrate for hESC-LSC maintenance, manipulation and plausible transplantation. We describe a straightforward plasma-assisted method to anchor ECM proteins on the surface of BNC enabling subsequent hESC-LSC attachment, spreading and viability. Then, we demonstrate that hESC-LSC cultures express the proliferation marker Ki67, especially at the early stages of the culture, and that they retain a LSC phenotype for up to 3 weeks on BNC supports.

A preliminary histological analysis from a corneal organ culture model shows the possibility to achieve intimate contact between BNC and the corneal surface, which is an advantageous situation for cell transplantation. We also observed re-epithelization under the BNC membranes, which hints that BNC does not cause major cytotoxicity or oxygen permeability issues on this *ex vivo* model. These findings, combined with our previous reports on BNC suturability and stability in contact with ocular tissue,²⁴ confirm that the material properties of BNC are adequate for a carrier in ocular surface cell replacement therapies. However, future research is required to assess the migration and integration capabilities of hESC-LSC grown on BNC carriers onto damaged corneas. Likewise, *in vivo* biocompatibility studies about ophthalmological applications of BNC are encouraging but still very scarce⁴⁸ and the interactions between BNC and the host ocular immune system warrant further investigation.

There are a few examples in the literature about the usage of BNC supports in stem cell culture that do not report on the need for coating BNC with ECM proteins to provide cell adhesion moieties.⁴⁹⁻⁵¹ Similarly, in our previous work with human dermal fibroblasts,²⁶ we found that BNC coating was not required to facilitate cell attachment. However, the here presented results prove that the plasma-assisted ECM protein functionalization is crucial for hESC-LSC attachment and survival on the BNC substrates. Neither the plasma activation alone nor the conventional method to coat cell culture surfaces were able to provide a favourable interface between BNC and hESC-LSC. These observations discard that the described enhanced hESC-LSC adhesion is a consequence of the increased roughness of the plasma-treated BNC substrates detected by electronic microscopy and AFM. On the contrary –and backed by the intensified Col IV adsorption on plasma-treated BNC– we ascribe this effect on the presence of specific binding sites for hESC-LSC. Interestingly, an analogous strategy was followed by Sorkio *et al.* to enhance hESC-derived retinal pigment epithelial cells attachment to synthetic electrospun membranes drawing similar conclusions.⁵² Hence, the requirement of surface modifications to use BNC as a cell culture substrate seems to be cell type-dependent. This cell-specificity has also been described by Pertile and colleagues⁵³ who reported that nitrogen plasma activation improved the affinity of microvascular cells and neuroblasts for BNC but had no effect on fibroblasts.

Notably, the plasma treatment (1 min-activation) did not make the hESC-LSC seeding protocol substantially longer, more complex or costlier compared to the standard ECM coating and did not compromise the manageability and the semi-transparency of the BNC membranes. By SEM examination, we encountered morphological changes on the BNC surface which were not present on the bulk of the material again in good agreement with reference.⁵³ Therefore, we conclude that plasma activation offers vast possibilities for BNC functionalization aiming at favouring its interactions with cells without comprising its outstanding materials properties in a fast, simple and scalable manner.⁵⁴

We inferred hESC-LSC cultures progression on BNC by measuring the metabolic activity and by detecting the proliferation marker Ki67 noticing that hESC-LSC can produce new daughter cells on BNC membranes as evidenced

by the presence of Ki67-positive populations. A slowdown in the proliferation rate after Day 3 together with an increase in cell size was detected. These features correlate with a slight maturation of hESC-LSC on BNC, although not complete differentiation since the cultures remained positive for LSC markers and essentially CK12 negative (maturation marker) for up to 3 weeks. The detection of the progenitor marker CK14 at Day 4 but not at Day 7 after plating and the dimmer staining for CK15 at Day 7 compared to Day 4 further supports that a partial maturation of hESC-LSC is occurring on the BNC carriers. We believe that is an interesting finding since cellular therapies expect the progeny of the transplanted cells to mature and become part of a functional corneal epithelium after implantation, mimicking the *in vivo* phenomena.^{8,55} On the other hand, the employed hESC-LSC were previously proved capable of terminal differentiation on porcine collagen matrices by detecting the expression of CK3 and CK12 proteins.²³ However, it remains uncertain if hESC-LSC possess the ability to differentiate towards fully mature corneal epithelial cells on BNC supports indicating a need for future work. Together, these observations lead us to believe that the level of maturation of the hESC-LSC cultures will be an important parameter to consider in upcoming studies on BNC-assisted hESC-LSC delivery to the ocular surface.

Notably, the assumed long-term mode of action of LSC transplantation relies on its capability to repopulate the limbal niche and from there provide constant cell renewal to the corneal epithelium. The expression of multiple stemness markers – Δ Np63 α , CK14 and CK15– on hESC-LSC seeded on BNC carriers corroborates its progenitor phenotype and reinforces the therapeutic expectation that hESC-LSC could act similarly to autologous LSC^{56,57}. Therefore, we venture that the time window between Day 1 and Day 4 after seeding on BNC supports could be an appropriate timing for hESC-LSC transplantation because the cultures exhibit higher proliferation and more stemness characteristics than later time-points; features that have been correlated with greater *in vivo* regenerative potential^{58,22}. Besides, this timing would also reduce the preparation period of the hESC-LSC/BNC constructs. Overall, and considering that biomaterial properties can greatly influence cell differentiation,^{59,60} the ability of BNC membranes to maintain the hESC-LSC phenotype *in vitro* rather than inducing terminal differentiation is encouraging for future implementation. We speculate that this effect could be at least

partially explained by the particular nanotopography of BNC, as already reported for mouse stem cell cultures.^{49,61}

Currently, the library of biomaterials exploited in cell-based corneal regeneration is dominated by AM,^{4,62} collagen^{13,63} and fibrin-derived substrates^{22,64} with successful results already reported.^{22,65} Research efforts are now focused on reducing the inherent risks of these therapies⁶⁶ by switching to well-defined cell culture protocols^{67,68} and non-animal sourced carriers.⁶⁹ In pursuit of clinically-compatible solutions, we employed serum- and feeder-free hESC-LSC cultures containing clinical-grade heparin, from the CnT-30 medium, as the only animal-derived product. BNC fits well into this emerging concept because of its purity and biotechnological animal-free production.⁷⁰ We believe that BNC can be advantageous over the above-mentioned biopolymers because of its mechanical stability, manageability and lack of processing, which are considered as major limiting factors of the current solutions.^{63,1} Moreover, the thermal stability of BNC enables both its sterilization by heat and cryopreservation.²⁶ The latest being of particular significance because it makes the cryobanking of ready-to-use hESC-LSC/BNC constructs a feasible possibility.

Conclusions

Here, we report on the culture of hESC-LSC on BNC membranes. We show that BNC substrates support the formation of new daughter cells and retain the progenitor phenotype of hESC-LSC while providing a self-standing and easy to manipulate mechanical support. Moreover, the non-animal origin of BNC and the well-defined hESC-LSC differentiation and cultivation procedures allowed the formation of cell-biomaterial constructs intended for a prospective clinical application in ocular surface treatments. hESC-LSC attachment and viability were achieved after a plasma-enabled ECM protein functionalization of the BNC substrates. This fast and simple BNC functionalization method could be exploited in the future for the culture of other therapeutic cells and expand the possibilities of BNC as a cell carrier.

Acknowledgements

This collaborative project was mainly funded with a European Molecular Biology Organization (EMBO) short-term fellowship (ref 8288) awarded to IAS and the authors would like to express their gratitude to this institution. Researchers acknowledge financial support from the Spanish Ministry of Science and Innovation through the RTI2018-096273-B-I00 project, the *Severo Ochoa Programme* for Centres of Excellence in R&D (SEV-2015-0496 and CEX2019-000917-S) and the PhD scholarship of IAS (BE-2017-076734) as well as Academy of Finland (326760). We are also grateful to Generalitat de Catalunya for the 2017SGR765 and the 2019LLAV00046 projects. Authors also appreciate Miquel Anton for his assistance with photography, the AFM service of ICMAB, the electron microscopy facility of ICN2 and the optical microscope service of UAB. The ICMAB members (I.A-S., A.L. and A.R.) participate in the CSIC Interdisciplinary Platform for Sustainable Plastics towards a Circular Economy, SUSPLAST, MICINN: “Research Networks” nanoCARE, (RED2018-102469-T) and in the Aerogels COST ACTION (CA 18125). This work has been conducted within the Material Science Doctoral Program of the Autonomous University of Barcelona (I.A-S.).

Authors deeply thank the laboratory staff of Tampere University, especially Outi Melin and Hanna Pekkanen for the production, maintenance and differentiation of the hESCs and hESC-LSC, and Juha Heikkilä for the help with the plasma equipment. The authors acknowledge the Biocenter Finland (BF) and Tampere Imaging Facility (TIF) for their service.

Supplementary information included in Publication 3

Figure S1: Substrate characterization. Table gathering information about surface characterization of BNC membranes undertaking different treatments. Column one shows atomic force microscopy (AFM) topographical pictures and average roughness values \pm standard deviation from three different $30 \times 30\text{-}\mu\text{m}$ images. Column two and three show scanning electron microscopy (SEM) micrographs of non-metallized BNC samples from both sides of the substrates (treated vs untreated). The fourth column shows EDX graphs from the same substrates. Note that a nitrogen peak is only detected on samples with ECM proteins coating.

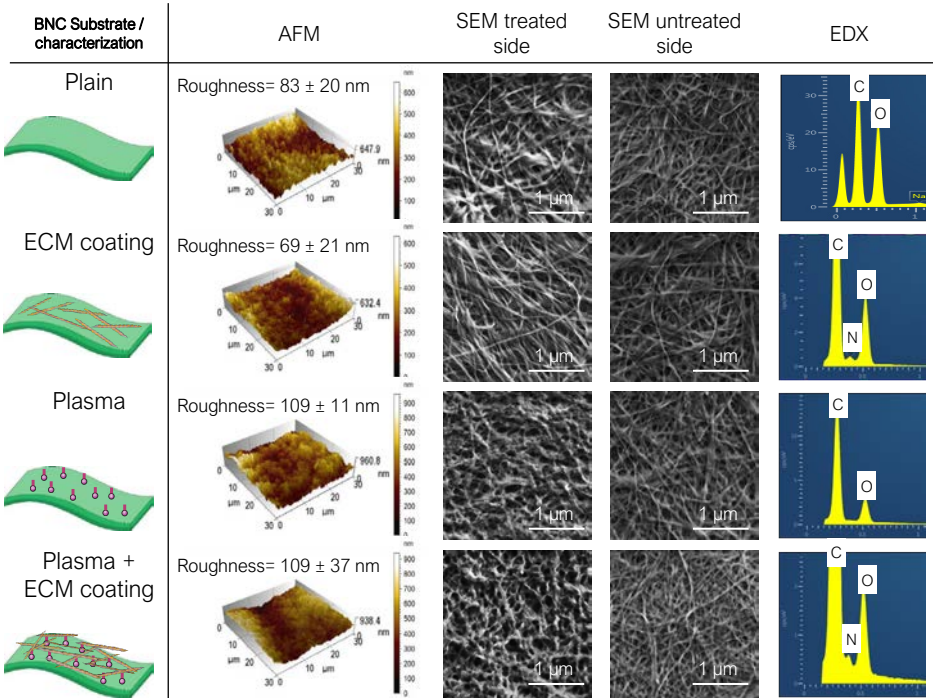


Figure S2: Control pig cornea after epithelial damage. HE-stained tissue section from a cultured porcine cornea one week after inducing epithelial damage and without implanting BNC. The regrown pig epithelium has been highlighted in pink.

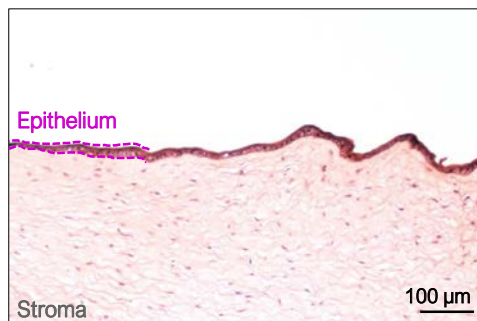


Figure S3: hESC-LSC viability on Day 8. Fluorescent Live/Dead staining of hESC-LSC cultures on control surfaces (ECM-coated commercial culture plate) and BNC coated with ECM proteins after plasma activation. Viable cells are stained green with Calcein-AM and dead cells in red with Propidium Iodide. The right image demonstrates that hESC-LSC keep high viability on BNC supports after 8 days of culture.

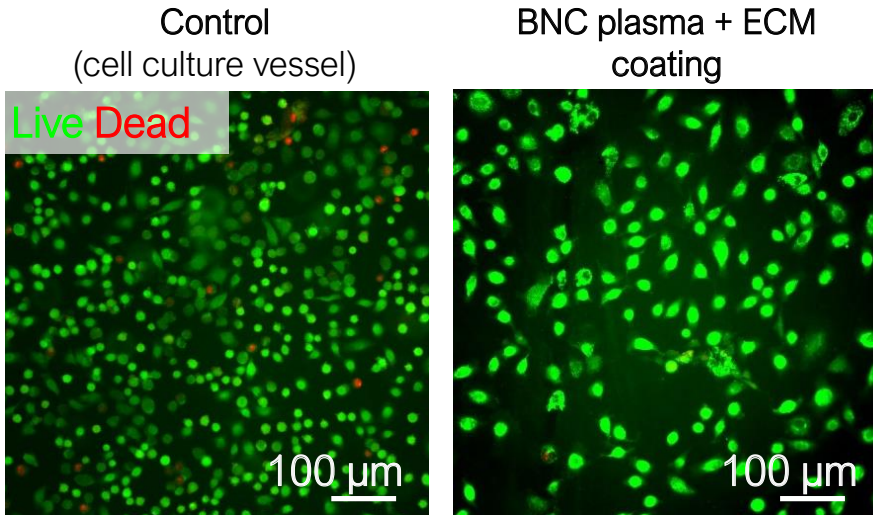


Figure S4: Monitoring of hESC-LSC cultures on control surfaces (ECM-coated cell culture plates). A) Phase-contrast microscope images at different time points. B) Immunofluorescence staining of the proliferation marker Ki67 (green). Cell nuclei are marked in blue (DAPI) to evidence the total number of cells.

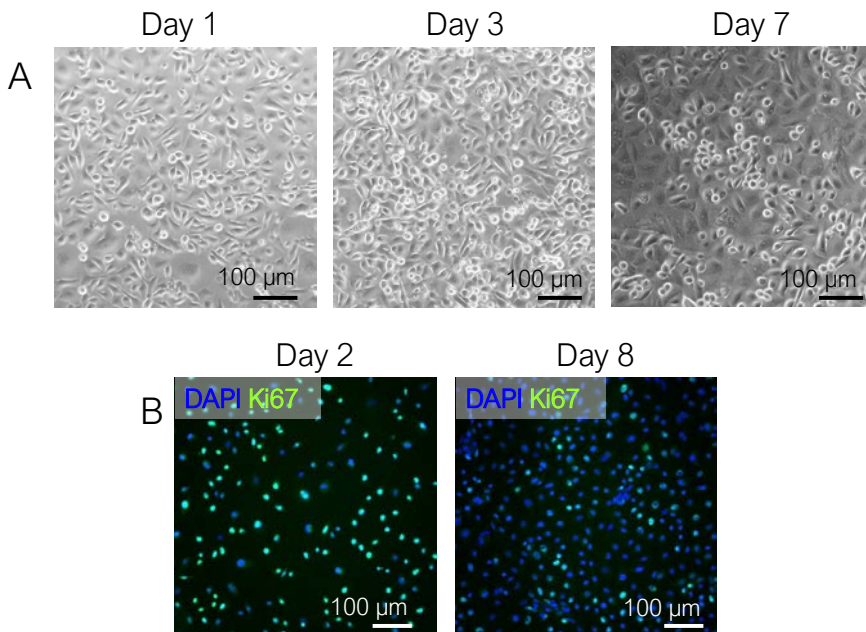
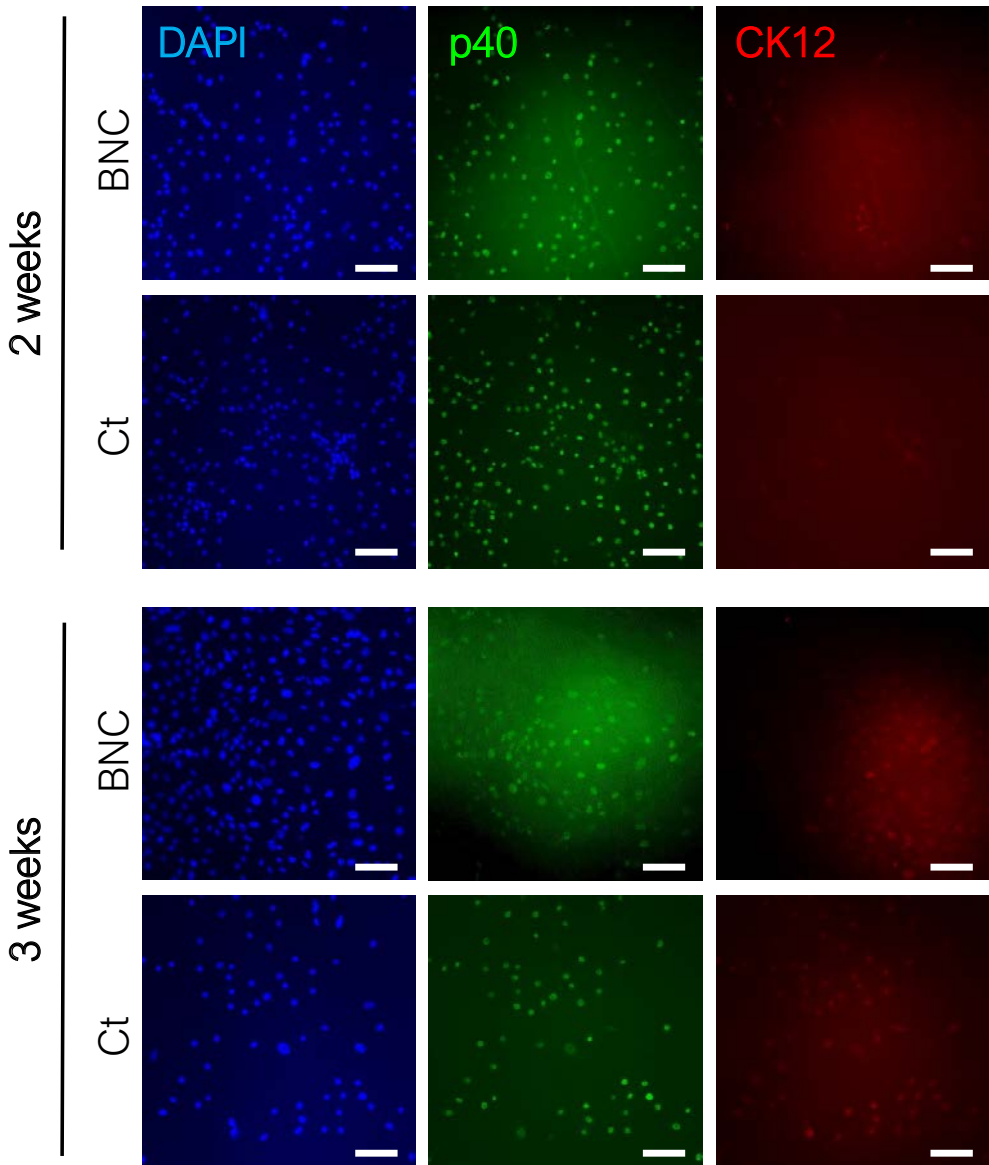


Figure S5: Protein marker expression profile of hESC-LSC after long-term culture. Characteristic immunofluorescence images of hESC-LSC maintained for two and three weeks on plasma-treated + ECM-coated BNC substrates and control surfaces (ECM-coated culture vessels). For all the pictures DAPI marks cell nuclei to show the total cell number, p40-positive cells are considered to exhibit a stemness phenotype and the dim CK12 (corneal maturation marker) signal indicates a predominantly low maturation stage of the cultures on both conditions and time points. Scale bar = 100 μ m.



Preliminary trials on the cryobanking of BNC/LSC constructs

Encouraged by the satisfactory results obtained in Chapter 2 for the cryopreservation of fibroblasts on BNC carriers, a similar approach was adopted for hESC-LSC cultures. The goal of this experiment was to provide safe storage of ready-to-use BNC/LSC constructs causing the minimum cell damage. The results from this section are not published to date.

Materials and methods

Triplicates of hESC-LSCs were cultured on top of plasma-treated and ECM-coated BNC supports as described in Publication 3 and the protocol for cryopreservation was based on that detailed in Publication 2. In short, at Day 3 or 7 after seeding, the BNC/LSC constructs were washed with DPBS and incubated shortly in xeno-free PSC cryopreservation medium (Gibco®) containing 10% DMSO as a cryoprotectant. Then, the samples were placed carefully with tweezers in conventional cryo-tubes containing 1 mL of PSC cryopreservation medium with the cells facing the liquid. Cryovials were frozen in two steps; i) overnight at $-80\text{ }^{\circ}\text{C}$ (cooling rate of $1\text{ }^{\circ}\text{C}/\text{min}$) and ii) moved to a liquid nitrogen tank for one week \pm 2 days. The BNC/LSCs constructs were thawed fast on a warm water bath and examined visually for attachment (phase-contrast microscope) and viability (Live/Dead assay) as described in Publication 3. Not cryopreserved samples prepared from the same batch of cells and BNC were used for comparison.

Results and discussion

Figure 10 shows hESC-LSC/BNC constructs before cryopreservation and after retrieving from the nitrogen tank. Interestingly, soon after thawing (Figure 10B) a large majority of hESC-LSC remained attached to the BNC supports in all samples. However, upon posterior incubation in some specimens hESC-LSC remained adherent, viable and evenly distributed (Figure 10 C and D, showing a

“best-case scenario”) while in other samples, hESC-LSC started to exfoliate from the BNC carriers and the remaining cells stained mainly as dead cells in the Live/Dead assay (see Figure 10 E and F for a “worst-case scenario” example) while other samples exhibited intermediate outcomes. Several attempts to optimize this process were made:

Two parameters related to the freezing step were studied, namely the preculture time and the duration of the plasma activation of the BNC substrates before cell seeding. First, as hESC-LSC experience a partial maturation on the BNC carriers (see Publication 3), Day 3 and Day 7 cultures were cryopreserved and cell viabilities after thawing were compared without detecting remarkable differences. Then, the plasma irradiation time of the BNC samples before ECM coating was raised from one (standard protocol) to two minutes expecting to provide a stronger anchorage of the ECM proteins to the BNC substrates and subsequently mitigate cell detachment after thawing. This approach did not yield the expected results. Even more, the two-minute plasma activation proved to be detrimental for cell attachment and viability as determined by Presto Blue assay where a ~45% reduction in cell viability was observed compared to the one-minute treatment (n=1).

For the next trial, the focus was put on the thawing procedure and only samples activated during one minute and cryopreserved at Day 3 after plating were used. Right after recovering the samples from the nitrogen tank, a selective Rho-associated coiled-coil containing protein kinase (ROCK) inhibitor (10 μ M) was added to the culture medium. Among many other functions, ROCK acts as an apoptosis regulator and ROCK inhibitors have been widely used to enhance cell survival⁷¹. The addition of the ROCK inhibitor was expected to contribute towards increased hESC-LSC viability after cryostorage but, oppositely, this approach did not render noticeable improvements on the reproducibility of the method.

Overall, the results from this section imply that the cryopreservation of ready-to-use BNC/LSC constructs should be feasible but a more exhaustive optimization is needed to obtain reproducible outcomes. Despite the efforts made, there are still several parameters that can influence the cryopreservation protocol, *e.g.* the composition of the cryopreservation medium, the distribution of the cryoprotectant through the sample as well as the sensitivity of the cells to the freeze-thaw cycle⁷², that deserve further investigation. Besides, even though the samples were

manipulated carefully and thawed as fast as possible in small groups (2-3 vials each time), there might be some room for improvement in the technical aspects of the experiment. These results contrast with those obtained in Publication 2 for fibroblasts where the cryopreservation of adherent cells on BNC supports was readily achieved indicating that the present protocol requires fine-tuning depending on the cell type to be cryostored.

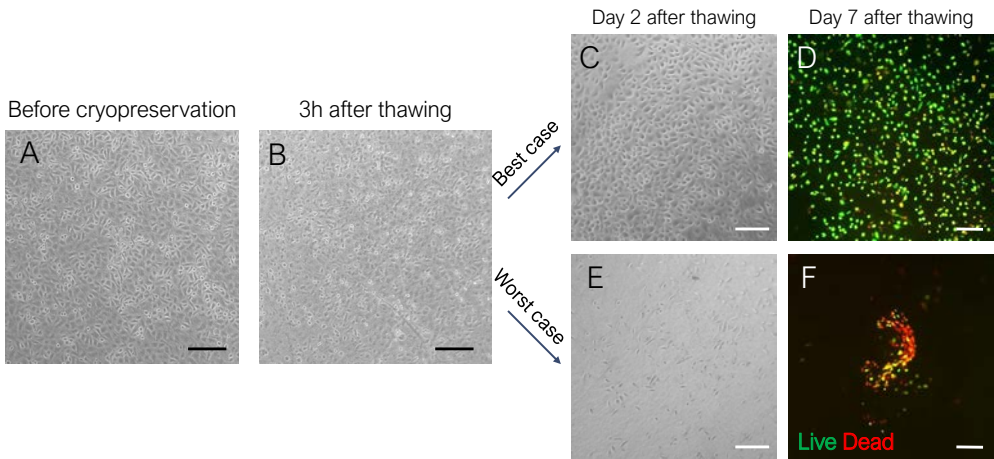


Figure 10: Cryostorage of hESC-LSC precultured on BNC carriers. A) hESC-LSC condition before cryopreservation (Day 3). B) Short after thawing the cells remained attached to the BNC supports in all the cases. C and E) Phase contrast microscope images at day two after thawing where differences between samples became noticeable. D and F) Fluorescence microscopy pictures from Live/Dead staining conducted one week after thawing the cryopreserved BNC/LSC constructs. While in some samples (D) hESC-LSC appeared as highly viable cultures as evidenced by the positive Calcein staining (green) in others (F) most of the cells detached from the substrates. Scale bar = 200 μm for all the images.

Contributions to the field and critical comment

The data provided in Chapter 3 represents a leap forward in this dissertation as it broadens the utility of BNC as a cell carrier from non-therapeutic cells to cells with a clinical significance. This is also relevant for the BNC research community. Previous publications described the culture of animal (rat⁵⁰, mouse⁷³ and rabbit⁷⁴) stem cells on BNC-based substrates however reports on the use of BNC to sustain human stem cell cultures are extremely scarce⁴⁰, adding novelty to Publication 3. Moreover, the employed hESC-LSC cultures are in the pipeline towards product development through a spin-off company (<https://projects.tuni.fi/stemsight/>) which further highlights their therapeutic potential. However, the engraftment and immunogenic properties of hESC-LSC on BNC carriers still need to be investigated before its clinical translation.

A satisfactory outcome on the cryopreservation of hESC-LSC attached to BNC membranes would represent a first step towards the banking of transplantable BNC/LSC constructs readily available upon the patient's needs with minimum preparation times or steps. This situation is still hypothetical but the fast-moving advances in stem cell and BNC research make it a reasonable mid-term goal. Another pivotal activity to advance towards this scenario would be adapting BNC production to Good Manufacturing Practises (GMP's) and ultimately gain the *Conformité Européenne* (CE) mark to meet the requirements of medical devices for human use.

From a technical point of view, the described BNC modification with ECM proteins upon 1-min plasma activation is another worthy contribution from this chapter. It is conceivable that this fast and simple method could be leveraged by other researchers seeking to increase cell attachment to BNC substrates. This chapter also provides a catalogue of biological characterization techniques (Live/Dead assay, Presto Blue assay, immunofluorescence stainings and *ex vivo* transplantation test) which are perfectly compatible with BNC. These methods, together with those described in Chapter 2, encompass a toolkit to study the interplay between BNC and human cells.

Chapter references

1. Chen, Z. *et al.* Biomaterials for corneal bioengineering. *Biomed. Mater* **13**, 032002 (2018).
2. Whitcher, J. P., Srinivasan, M. & Upadhyay, M. P. Corneal blindness: a global perspective. *Bulletin of the World Health Organization*. (2001).
3. HORIZON 2020. *Biomaterials for Health: A Strategic Roadmap for Research and Innovation*. (2020).
4. Zakaria, N. *et al.* Results of a phase I/II clinical trial: Standardized, non-xenogenic, cultivated limbal stem cell transplantation. *J. Transl. Med.* **12**, 58 (2014).
5. Pellegrini, G. *et al.* Navigating Market Authorization: The Path Holoclar Took to Become the First Stem Cell Product Approved in the European Union. *Stem Cells Transl. Med.* **7**, 146–154 (2018).
6. Nowell, C. S. & Radtke, F. Corneal epithelial stem cells and their niche at a glance. *J. Cell Sci.* **130**, 1021–1025 (2017).
7. Ljubimov, A. V. & Saghizadeh, M. Progress in corneal wound healing. *Prog Retin Eye Res* **49**, 17–45 (2015).
8. Ebrahimi, M., Taghi-Abadi, E. & Baharvand, H. Limbal stem cells in review. *J. Ophthalmic Vis. Res.* **4**, 40–58 (2009).
9. Wilson, S. L., El Haj, A. J. & Yang, Y. Control of scar tissue formation in the cornea: strategies in clinical and corneal tissue engineering. *J. Funct. Biomater.* **3**, 642–87 (2012).
10. Menzel-Severing, J., Kruse, F. E. & Schlötzer-Schrehardt, U. Stem cell-based therapy for corneal epithelial reconstruction: present and future. *Can. J. Ophthalmol.* **48**, 13–21 (2013).
11. EuroStemCell. Europe approves Holoclar®, the first stem cell-based medicinal product | Eurostemcell. Available at: <https://www.eurostemcell.org/story/europe-approves-holoclar-first-stem-cell-based-medicinal-product>. (Accessed: 27th October 2020)
12. Harkin, D. G. *et al.* Mounting of Biomaterials for Use in Ophthalmic *Cell Therapies*. *Cell Transplant.* **26**, 1717–1732 (2017).
13. Ahearne, M., Fernández-Pérez, J., Masterton, S., Madden, P. W. & Bhattacharjee, P. Designing Scaffolds for Corneal Regeneration. *Adv. Funct. Mater.* **30**, 1908996 (2020).
14. Hongisto, H., Vattulainen, M., Ilmarinen, T., Mikhailova, A. & Skottman, H. Efficient and scalable directed differentiation of clinically compatible corneal limbal epithelial stem cells from human pluripotent stem cells. *J. Vis. Exp.* **140**, e58279 (2018).
15. Hongisto, H., Ilmarinen, T., Vattulainen, M., Mikhailova, A. & Skottman, H. Xenogenic and feeder-free differentiation of human pluripotent stem cells to two distinct ocular

- epithelial cell types using simple modifications of one method. *Stem Cell Res. Ther.* **8**, 291 (2017).
16. Hayashi, R. *et al.* Generation of Corneal Epithelial Cells from Induced Pluripotent Stem Cells Derived from Human Dermal Fibroblast and Corneal Limbal Epithelium. *PLoS One* **7**, e45435 (2012).
 17. Azuara-Blanco, A., Pillai, C. T., Dua, H. S. & Azuara-Blanco A, Pillai CT, D. H. Amniotic membrane transplantation for ocular surface reconstruction. *Br. J. Ophthalmol.* **83**, 399–402 (1999).
 18. Pires, R. T., Tseng, S. & Prabhasawat, P. Amniotic Membrane Transplantation for Bulbous Keratopathy. *Evidence-Based Eye Care* **1**, 80–81 (2000).
 19. Selver, O. B. *et al.* Corneal recovery in a rabbit limbal stem cell deficiency model by autologous grafts of tertiary outgrowths from cultivated limbal biopsy explants. *Mol. Vis.* **22**, 138–149 (2016).
 20. Chen, S.-Y., Mahabole, M. & Tseng, S. C. G. Optimization of Ex Vivo Expansion of Limbal Epithelial Progenitors by Maintaining Native Niche Cells on Denuded Amniotic Membrane. *Transl. Vis. Sci. Technol.* **2**, 1 (2013).
 21. Mi, S., Chen, B., Wright, B. & Connon, C. J. Ex vivo construction of an artificial ocular surface by combination of corneal limbal epithelial cells and a compressed collagen scaffold containing keratocytes. *Tissue Eng. - Part A* **16**, 2091–2100 (2010).
 22. Rama, P. *et al.* Limbal stem-cell therapy and long-term corneal regeneration. *N. Engl. J. Med.* **363**, 147–155 (2010).
 23. Mikhailova, A. *et al.* Human pluripotent stem cell-derived limbal epithelial stem cells on bioengineered matrices for corneal reconstruction. *Exp. Eye Res.* **146**, 26–34 (2016).
 24. Anton-Sales, I. *et al.* Bacterial nanocellulose as a corneal bandage material: A comparison with amniotic membrane. *Biomater. Sci.* **8**, 2921–2930 (2020).
 25. Anton-Sales, I., Beekmann, U., Laromaine, A., Roig, A. & Kralisch, D. Opportunities of Bacterial Cellulose to Treat Epithelial Tissues. *Curr. Drug Targets* **20**, 808–822 (2019).
 26. Anton-Sales, I., Roig-Sanchez, S., Sánchez-Guisado, M. J., Laromaine, A. & Roig, A. Bacterial nanocellulose and titania hybrids: cytocompatible and cryopreservable cell carriers. *ACS Biomater. Sci. Eng.* **6**, 4893–4902 (2020).
 27. Bacakova, L. *et al.* Versatile Application of Nanocellulose: From Industry to Skin Tissue Engineering and Wound Healing. *Nanomaterials* **9**, 164 (2019).
 28. Fu, L., Zhang, J. & Yang, G. Present status and applications of bacterial cellulose-based materials for skin tissue repair. *Carbohydr. Polym.* **92**, 1432–1442 (2013).
 29. Mendes, P. N. *et al.* In vivo and in vitro evaluation of an Acetobacter xylinum synthesized microbial cellulose membrane intended for guided tissue repair. *Acta Vet. Scand.* **51**, 12 (2009).

30. Almeida, I. F. *et al.* Bacterial cellulose membranes as drug delivery systems: An in vivo skin compatibility study. *Eur. J. Pharm. Biopharm.* **86**, 332–336 (2013).
31. Jeong, S. Il *et al.* Toxicologic evaluation of bacterial synthesized cellulose in endothelial cells and animals. *Mol. Cell. Toxicol.* **6**, 373–380 (2010).
32. Helenius, G. *et al.* In vivo biocompatibility of bacterial cellulose. *J. Biomed. Mater. Res. - Part A* **76**, 431–438 (2006).
33. Beekmann, U. *et al.* Process control and scale-up of modified bacterial cellulose production for tailor-made anti-inflammatory drug delivery systems. *Carbohydr. Polym.* **236**, 116062 (2020).
34. Kralisch, D., Hessler, N., Klemm, D., Erdmann, R. & Schmidt, W. White biotechnology for cellulose manufacturing—the HoLiR concept. *Biotechnol Bioeng* **105**, 740–747 (2010).
35. Klemm, D. *et al.* Nanocellulose as a natural source for groundbreaking applications in materials science: Today’s state. *Mater. Today* **21**, 720–748 (2018).
36. Ferreira, F.V. *et al.* Porous nanocellulose gels and foams: Breakthrough status in the development of scaffolds for tissue engineering. *Mater. Today* **37**, 126–141 (2020).
37. Wu, C.-N. *et al.* TEMPO-Oxidized Bacterial Cellulose Pellicle with Silver Nanoparticles for Wound Dressing. *Biomacromolecules* **19**, 544–554 (2018).
38. Moritz, S. *et al.* Active wound dressings based on bacterial nanocellulose as drug delivery system for octenidine. *Int. J. Pharm.* **471**, 45–55 (2014).
39. Robotti, F. *et al.* Microengineered biosynthesized cellulose as anti-fibrotic in vivo protection for cardiac implantable electronic devices. *Biomaterials* **229**, 119583 (2020).
40. Noh, Y. K. *et al.* Fabrication of bacterial cellulose–collagen composite scaffolds and their osteogenic effect on human mesenchymal stem cells. *Carbohydr. Polym.* **219**, 210–218 (2019).
41. Fey, C. *et al.* Bacterial nanocellulose as novel carrier for intestinal epithelial cells in drug delivery studies. *Mater. Sci. Eng. C* **109**, 110613 (2020).
42. Gonçalves, S. *et al.* Bacterial Cellulose As a Support for the Growth of Retinal Pigment Epithelium. *Biomacromolecules* **16**, 1341–1351 (2015).
43. Gonçalves, S. *et al.* Acetylated bacterial cellulose coated with urinary bladder matrix as a substrate for retinal pigment epithelium. *Colloids Surfaces B Biointerfaces* **139**, 1–9 (2016).
44. Roig-Sanchez, S. *et al.* Nanocellulose films with multiple functional nanoparticles in confined spatial distribution. *Nanoscale Horizons* **4**, 634–641 (2019).
45. Koivusalo, L. *et al.* Hydrazone crosslinked hyaluronan-based hydrogels for therapeutic delivery of adipose stem cells to treat corneal defects. *Mater. Sci. Eng. C* **85**, 68–78 (2018).
46. Sorkio, A. *et al.* Human stem cell based corneal tissue mimicking structures using laser-assisted 3D bioprinting and functional bioinks. *Biomaterials* **171**, 57–71 (2018).

47. Schlötzer-Schrehardt, U. & Kruse, F. E. Identification and characterization of limbal stem cells. *Exp. Eye Res.* **81**, 247–264 (2005).
48. Zhang, C. *et al.* Biocompatibility evaluation of bacterial cellulose as a scaffold material for tissue-engineered corneal stroma. *Cellulose* **27**, 2775–2784 (2020).
49. Tronser, T., Laromaine, A., Roig, A. & Levkin, P. A. Bacterial Cellulose Promotes Long-Term Stemness of mESC. *ACS Appl. Mater. Interfaces* **10**, 16260–16269 (2018).
50. Vielreicher, M. *et al.* Bacterial nanocellulose stimulates mesenchymal stem cell expansion and formation of stable collagen-I networks as a novel biomaterial in tissue engineering. *Sci. Rep.* **8**, 9401 (2018).
51. Laromaine, A. *et al.* Free-standing three-dimensional hollow bacterial cellulose structures with controlled geometry via patterned superhydrophobic–hydrophilic surfaces. *Soft Matter* **14**, 3955–3962 (2018).
52. Li, K.Y. *et al.* Fish-Scale Collagen Membrane Seeded with Corneal Endothelial Cells as Alternative Graft for Endothelial Keratoplasty Transplantation. *ACS Biomater. Sci. Eng.* **6**, 2570–2577 (2020).
53. Pertile, R. A. N., Andrade, F. K., Alves, C. & Gama, M. Surface modification of bacterial cellulose by nitrogen-containing plasma for improved interaction with cells. *Carbohydr. Polym.* **82**, 692–698 (2010).
54. Eswaramoorthy, N. & McKenzie, D. R. Plasma treatments of dressings for wound healing: a review. *Biophysical Reviews* **9**, 895–917 (2017).
55. Yoon, J.J. Limbal stem cells: Central concepts of corneal epithelial homeostasis. *World J. Stem Cells* **6**, 391 (2014).
56. Pellegrini, G. *et al.* Long-term restoration of damaged corneal surfaces with autologous cultivated corneal epithelium. *Lancet* **349**, 990–993 (1997).
57. Pellegrini, G. *et al.* Biological parameters determining the clinical outcome of autologous cultures of limbal stem cells. *Regen. Med.* **8**, 553–567 (2013).
58. Massie, I., Levis, H. J. & Daniels, J. T. Response of human limbal epithelial cells to wounding on 3D RAFT tissue equivalents: Effect of airlifting and human limbal fibroblasts. *Exp. Eye Res.* **127**, 196–205 (2014).
59. Mitrousis, N., Fokina, A. & Shoichet, M. S. Biomaterials for cell transplantation. *Nat. Rev. Mater.* **3**, 441–456 (2018).
60. Masterton, S. & Ahearne, M. Mechanobiology of the corneal epithelium. *Experimental Eye Research* **177**, 122–129 (2018).
61. Geisel, N. *et al.* Microstructured Multilevel Bacterial Cellulose Allows the Guided Growth of Neural Stem Cells. *Small* **12**, 5407–5413 (2016).
62. Loh, E. Y. X. *et al.* Development of a bacterial cellulose-based hydrogel cell carrier containing keratinocytes and fibroblasts for full-thickness wound healing. *Sci. Rep.* **8**, 2875 (2018).

63. Matthyssen, S., Van den Bogerd, B., Dhubhghaill, S. N., Koppen, C. & Zakaria, N. Corneal regeneration: A review of stromal replacements. *Acta Biomater.* **69**, 31–41 (2018).
64. Rama, P. *et al.* Autologous fibrin-cultured limbal stem cells permanently restore the corneal surface of patients with total limbal stem cell deficiency. *Transplantation* **72**, 1478–1485 (2001).
65. Fagerholm, P. *et al.* Stable corneal regeneration four years after implantation of a cell-free recombinant human collagen scaffold. *Biomaterials* **35**, 2420–2427 (2014).
66. Schwab, I. R., Johnson, N. T. & Harkin, D. G. Inherent risks associated with manufacture of bioengineered ocular surface tissue. *Archives of Ophthalmology* **124**, 1734–1740 (2006).
67. Nieto-Nicolau, N. *et al.* Xenofree generation of limbal stem cells for ocular surface advanced cell therapy. *Stem Cell Res. Ther.* **10**, 374 (2019).
68. Nakamura, T. *et al.* The use of autologous serum in the development of corneal and oral epithelial equivalents in patients with Stevens-Johnson syndrome. *Investig. Ophthalmol. Vis. Sci.* **47**, 909–916 (2006).
69. Koivusalo, L. *et al.* Tissue adhesive hyaluronic acid hydrogels for sutureless stem cell delivery and regeneration of corneal epithelium and stroma. *Biomaterials* **225**, 119516 (2019).
70. Cimino, M., Gonçalves, R. M., Barrias, C. C. & Martins, M. C. L. Xeno-Free Strategies for Safe Human Mesenchymal Stem/Stromal Cell Expansion: Supplements and Coatings. *Stem Cells Int.* **2017**, 6597815 (2017).
71. Watanabe, K. *et al.* A ROCK inhibitor permits survival of dissociated human embryonic stem cells. *Nat. Biotechnol.* **25**, 681–686 (2007).
72. Karlsson, J. O. M. & Toner, M. Long-term storage of tissues by cryopreservation: critical issues. *Biomaterials* **17**, 243–256 (1996).
73. Krontiras, P., Gatenholm, P. & Hagg, D. A. Adipogenic differentiation of stem cells in three-dimensional porous bacterial nanocellulose scaffolds. *J. Biomed. Mater. Res. - Part B Appl. Biomater.* **103**, 195–203 (2015).
74. Silva, M. de A. *et al.* Behavior and biocompatibility of rabbit bone marrow mesenchymal stem cells with bacterial cellulose membrane. *PeerJ* **2018**, 1–22 (2018).

Chapter 4

Bacterial nanocellulose as a corneal bandage: technical feasibility and business proposal



Figure 1: Schematic summary of Chapter 4. The proposed BNC corneal bandages on an illustration of the human eye (up) and the two studies included in this chapter (bottom).

Chapter introduction

Chapter 4 describes a new concept of corneal bandage based on BNC hydrogels. This work has been performed in close collaboration with the Barraquer Ophthalmology Centre (COB) –a leading ophthalmological institution located in Barcelona– and represents the second example of BNC applicability in ophthalmology exposed in this thesis.

Several corneal lesions (erosions, abrasions, ulcers...) require the application of an ocular surface dressing to promote efficient and scar-less healing¹. Current corneal bandaging solutions rely on animal or human-derived products like amniotic membrane (AM) grafts² and collagen sponges³. AM is commercialized in different formats: fresh (shipped directly from tissue banks), dehydrated (*e.g.* AmbioDisk®) and cryopreserved (*e.g.* Prokera®). Contact lens-like covers manufactured from bovine collagen are also available under the trademark Collagen Soft Shield®. With the implementation of genetic engineering technologies, recombinant forms of collagen⁴ and hyaluronic acid (HA)⁵ irrupted as donor and animal-free alternatives. Particularly promising seems the “Ocular Bandage Gel” based on cross-linked recombinant HA since this formulation has shown efficacy in promoting corneal re-epithelization in both human^{6,7} and veterinary^{8,9} settings. Synthetic collagen might become another relevant player as implants made from fully-defined collagen-like synthetic peptides¹⁰ have shown long-term regenerative effects in animals¹¹ and humans¹². In this framework, BNC-based biomaterials could result in another family of donor and animal-free ocular bandages with the advantage of requiring minimal processing. See Figure 2 for a schematic summary of the most commonly used biomaterials in corneal regeneration. Among the so-called “consolidated options”, AM represents the most standard choice¹³ and therefore it was selected as a benchmark material for our study.

Chapter 4 encompasses experimental work on the evaluation of BNC as a substitute/complement to AM in corneal bandaging (Publication 4) and a study on the market opportunity of the proposed product. This preliminary business plan has been conducted under the framework of a Llabor (meaning “seed”) grant from AGAUR (*Agència de Gestió d’Ajuts Universitaris i de Recerca, Generalitat de Catalunya*) and FEDER (*Fons Europeu de Desenvolupament Regional*) granted to the project

“Corneal-BNC”. This funding is addressed to innovative projects with potential for being incorporated into the production sector and includes a training program in Technology Transfer (TT) by the UPF-Barcelona School of Management in which I have taken part. The TT proposal was performed in close cooperation with Thomas Meslier from the N&N group of ICMAB.

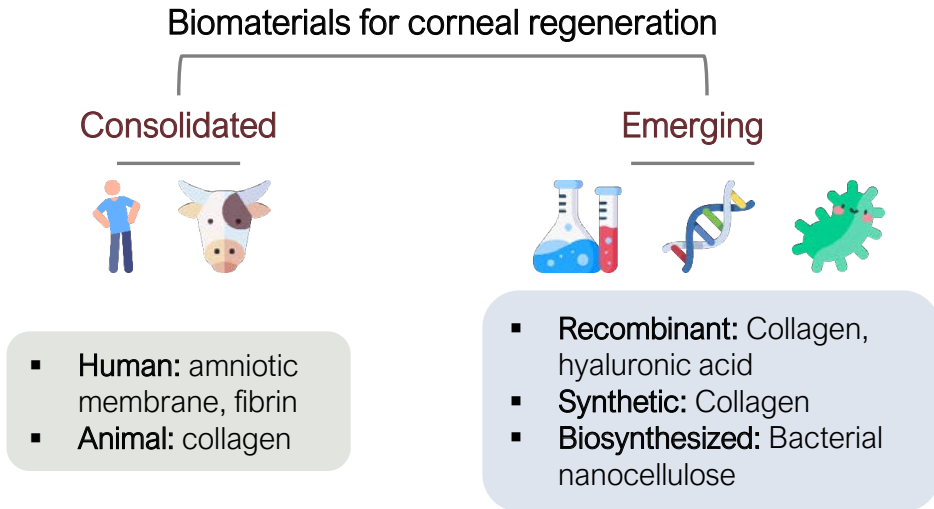


Figure 2: Consolidated and emerging biomaterials exploited to treat ocular surface disorders.

Publication 4: Bacterial Nanocellulose as a Corneal Bandage Material: a Comparison with Amniotic Membrane

Irene Anton-Sales, Justin C. D'Antin, Jorge Fernández-Engroba, Victor Charoenrook, Anna Laromaine, Anna Roig and Ralph Michael. *Biomater. Sci.*, 2020, 8, 2921. Published in open access by The Royal Society of Chemistry (RSC).

<https://pubs.rsc.org/en/content/articlelanding/2020/bm/d0bm00083c#!divAbstract>

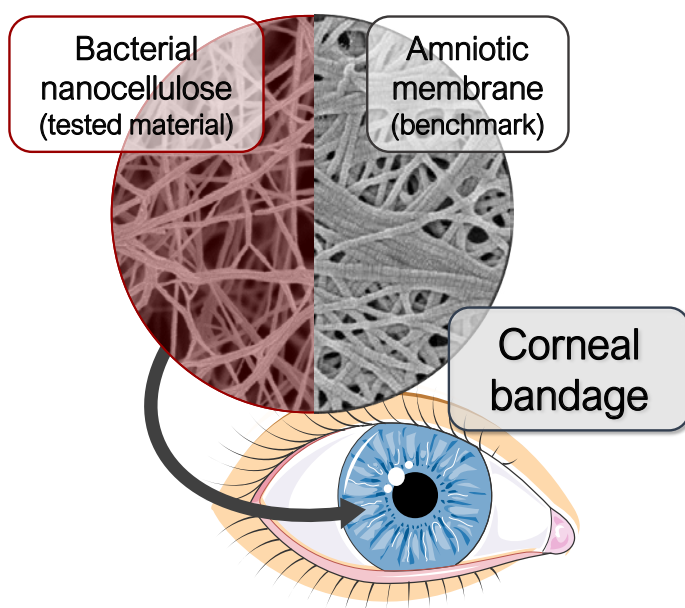


Figure 3: Graphical abstract of Publication 4.

Abstract

Corneal trauma and ulcerations are leading causes of corneal blindness around the world. These lesions require attentive medical monitoring since improper healing or infection has serious consequences on vision and quality of life. Amniotic membrane grafts represent the common solution to treat severe corneal wounds. However, amniotic membrane's availability remains limited by the dependency

on donor tissues, its high price and short shelf life. Consequently, there is an active quest for biomaterials to treat injured corneal tissues. Nanocellulose synthesized by bacteria is an emergent biopolymer with vast clinical potential, namely, for skin tissue regeneration. Bacterial nanocellulose also exhibits appealing characteristics to act as an alternative corneal bandage such as; high liquid holding capacity, biocompatibility, flexibility, natural – but animal-free– origin and a myriad of functionalization opportunities. Here, we present an initial study aiming at testing the suitability of bacterial nanocellulose as a corneal bandage based on diverse preclinical requirements and using amniotic membrane as a benchmark. Bacterial nanocellulose exhibits higher mechanical resistance to sutures and slightly longer stability under *in vitro* and *ex vivo* simulated physiological conditions than amniotic membrane. Additionally, bacterial nanocellulose offers good conformability to the shape of the eye globe and easy manipulation in medical settings. These excellent attributes accompanied by the facts that bacterial nanocellulose is stable at room temperature for long periods, can be heat-sterilized and is easy to produce, reinforce the potential of bacterial nanocellulose as a more accessible ocular surface bandage.

Introduction

Ocular surface disorders, especially those affecting the cornea, can severely disturb vision and quality of life. Yearly, there are approximately 1.5 million worldwide cases of corneal trauma, burns and infectious ulcerations^{14,15}. Conjunctival flap operations have long been performed in these cases^{16–18}, but due to its poor post-operative visual and cosmetic results, during the last decades, human amniotic membrane (AM) patches^{19–21} have been preferred because of their well-known regenerative effects²². The AM has a layered structure with two well-differentiated sides: an epithelial side made of cuboidal cells and a spongy stromal side constituted mainly of collagen fibres²³ which is typically placed in contact with the corneal damage. AM also offers a tectonic pillar for corneal perforations and can be indicated as a temporary treatment prior to a reconstructive technique²⁴. Despite its satisfactory clinical outcomes^{25,26}, AM sometimes degrades faster than the required

healing time²⁷, it is extremely costly and has a short shelf life. Other drawbacks of AM concern its availability, which depends on donors and the presence of tissue banks and medical infrastructure. Therefore, novel biomaterials able to overcome these limitations are currently being investigated^{28–30}.

Bacterial nanocellulose (BNC) is a polysaccharide naturally secreted by several non-pathogenic bacterial strains that has gained a lot of attention for biomedical applications^{31,32}. BNC can easily be produced from *Komagataeibacter xylinus* (*K.xylinus*) cultures as stable water-insoluble hydrogels at the interface between the air and the liquid culture medium. After appropriate cleaning, BNC hydrogels are free of endotoxins and ultra-pure, containing just nanocellulose fibres organized in a similar structure as collagen³³. Furthermore, BNC exhibits a high liquid holding capacity, porosity and conformability together with numerous functionalization opportunities due to its high surface area. All these unique characteristics promote the many valuable applications of BNC as a biomaterial. In fact, BNC has successfully been used for skin tissue regeneration^{34–36} and products like Epicite^{hydro} (JeNaCell) are already available on the market. Similarly, a BNC-based coating for implantable devices (Hylomate Pouch³⁷) is in the final stages of validation as an anti-fibrotic agent. Other studies highlight the potential of BNC as a substrate for *in vitro* models³⁸ and as a drug delivery matrix^{39,40}.

Despite these promising reports, the capability of BNC to heal other body surfaces such as the cornea or the dura mater⁴¹ remain largely unexploited⁴². Therefore, based on the outstanding performance of BNC on skin wound healing, we hypothesize that BNC also holds potential as an ocular surface bandage. In contrast to AM, BNC is stable at room temperature for long periods and its production from diverse carbon sources is sustainable and controllable in terms of size, shape and thickness⁴³. Finally, yet importantly, BNC can be easily sterilized by heat and its animal-free origin might reduce the risk of disease transmission, ethical concerns and dependency on donor tissues. BNC's light transmittance is around 70% due to light scattering caused by fibre bundles and pores⁴⁴. Since this might limit its applicability as a long-term corneal substitute, we focused on a temporal application of BNC similar to that of AM⁴⁵.

Here, we validate BNC as a suitable base material to develop novel corneal bandages. A detailed comparison between physicochemical characteristics of AM

and BNC is provided and then, we demonstrate BNC's mechanical resistance to suture and stability under physiological conditions. Finally, we show preliminary *ex vivo* assays with porcine corneas. Together our results endorse BNC as a strong candidate for future corneal bandaging applications.

Results

Material characterization

Despite the extensive use of AM in ophthalmology, not much has been reported about its micro/nanostructure and material characteristics. Consequently, prior to the stability tests, the main characteristics of BNC and AM were compared. Scanning electron microscopy (SEM) was employed to study the micro and nanostructures of the ocular surface bandages. SEM imaging (Figure 4A) of AM revealed a distinct micro and nanostructure of its two sides. The stromal side, which is generally placed in contact with the corneal surface, exhibits a nanofibrillar structure that highly resembles the BNC's architecture. The mean fibre diameter measured from the SEM images was 57 ± 9 nm for the collagen fibres in AM and 56 ± 13 nm for BNC nanofibers (average value from both sides of BNC). The epithelial side of AM is more unorganized and fibres were not observed. BNC presented a rather similar structure on both sides. However, the top side oriented towards the air during the biosynthesis process shows higher compaction of the fibres than the side facing the liquid bacterial culture (Figure 4A).

BNC hydrogels were investigated as-synthesized, containing high amounts of water (~100 times its own dry weight). A dehydration test revealed that BNC hydrogels exposed to the air under controlled temperature (22 °C) and humidity (45 %) still maintain two-thirds of their initial water content after 6 hours (see supplementary Figure S1). AM membranes were also used as-received from the tissue bank. Thicknesses measured with a micrometre were between 600 and 900 μm for BNC, while AM pieces were much thinner (between 50 and 110 μm). These thickness measurements could be affected by the blotting performed prior to the measurement to remove the excess water of the films and therefore the superficial mass parameter was monitored instead of the thickness on the onward ex-

periments. BNC superficial mass computed was almost 8 times higher than AM (90 vs 12 mg/cm²).

Regarding optical properties, both materials exhibit low visible light absorbance (<1 absorbance from 800 to 400 nm) displaying a progressive increase in light absorbance towards the ultraviolet range. Interestingly, despite the marked difference in thickness, the overall ultraviolet-visible light absorbance was not proportionally higher in BNC. As an example, light absorbance for BNC was 0.38 at 600 nm and 0.29 for AM.

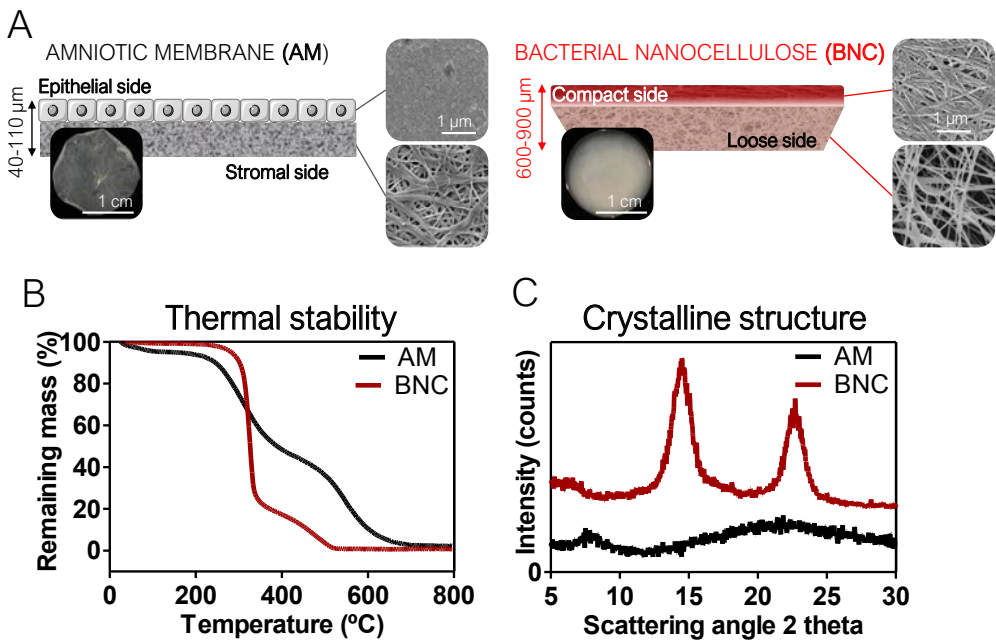


Figure 4: Materials characterization. A) Micro and nanostructure of the bandage materials tested. Each material presents two differentiated sides, which are illustrated schematically and with SEM micrographs. The stromal side of AM and the compact side of BNC were the ones facing the ocular tissues in the experiments detailed below. B) Representative TGA curves of BNC and AM ($n=3$ for each material). The remaining mass of BNC is 0.7 ± 0.1 % and AM is 1.7 ± 0.8 %. C) X-ray diffraction patterns of the ocular surface bandages where BNC shows two broad diffraction peaks while AM appears as an amorphous material.

The thermal stability of the materials was assessed by thermo-gravimetric analysis (TGA) (Figure 4B). The onset of degradation was defined by the position of the peaks from the first derivative function of the TGA curves and happened at ~ 325 °C for BNC and at ~ 250 °C for AM. Both materials decomposed almost

completely (BNC total degradation happened at approx. 500 °C and AM at approx. 650 °C) and show residual masses of 0.7 ± 0.1 % for BNC and 1.7 ± 0.8 % for AM (n=3). This result indicates that both materials are almost entirely constituted by organic matter as expected.

To gain insight into the atomic organization of BNC and AM, their X-Ray diffraction (XRD) patterns were compared (Figure 4C). BNC is a semi-crystalline material that presents two characteristic broad diffraction peaks (at $2\theta = 14.6$ and 22.8) as well as some amorphous background⁴⁶. Contrarily, AM does not show any clear diffraction pattern, indicating an amorphous structure.

Suture stress test

An important specification of an ocular surface bandage material is to enable an easy and durable suturing to the eye surface. Since AM is commonly sutured in ophthalmological procedures, it was used as a benchmark for comparison. BNC has been satisfactorily sutured *in vivo*⁴⁷ but, to the best of our knowledge, not to the ocular tissues and its resistance to suture has never been quantified. A set up was assembled similar to the one reported in⁴⁸ and illustrated in Figure 5A. BNC and AM samples were sutured to small pieces of scleral tissues and clamped. Weights were added until BNC and AM materials torn at the suture point as shown in Figure 5B. BNC films held an average force of 0.47 ± 0.11 N while AM resistance was much lower (0.11 ± 0.02 N). Some of the BNC pieces tolerated higher loads and caused the suture thread to break before BNC (filled dots on the graphs in Figure 5B). Statistical analysis (unpaired T-test) revealed a significant difference between the two maximum forces supported by the compared materials.

Stability under simulated physiological conditions

Another requisite to consider a material for ocular bandaging applications is its durability and stability under the eye's physiological conditions. To gain insight into BNC's bio-stability we performed *in vitro* and *ex vivo* tests. For these tests, native BNC hydrogels were used since dry films have a paper-like appearance that showed poorer conformability to the dome shape of the eye globes. For the *in vitro* study, BNC and AM were maintained in corneal preservation medium to monitor its potential degradation. The integrity of the samples was inferred by measuring

did not present any substantial change whereas incubated BNC showed a small rise in absorbance at 600 nm compared to untreated BNC (from 0.38 to 0.41) (Figure 7A). The material's superficial mass was also characterized after the corneal medium incubation test (Figure 7B). BNC samples reduced their superficial mass by near 12% (from 90 to 79 mg/cm²) while AM samples decreased by 33% its superficial mass (from 12 to 8 mg/cm²). This change of the superficial mass was statistically significant (paired T-test, p-value <0.0001) only for the AM specimens.

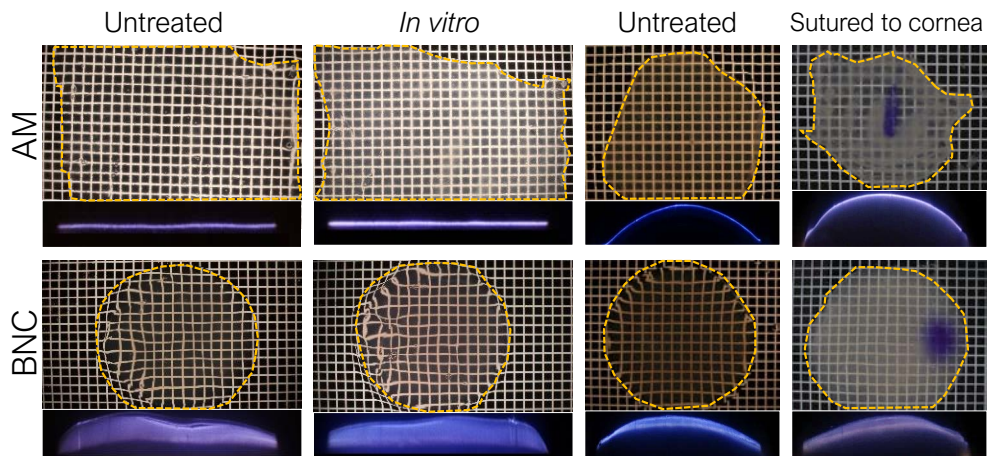


Figure 6: Frontal (white filed + grid) and slit-lamp images of AM and BNC before and after the stability tests. White field photographs were taken with a grid to better visualize the transparency of the materials. Each square of the grid is one mm². Inserts at the bottom of the images correspond to lateral views of the materials captured with a slit lamp. In general, both materials were stable under the tested conditions and incubation times. To mark the orientation of the samples that were sutured to porcine corneas, a tissue marker was used. For clarity in the pictures, corneal bandages were delineated with a yellow-dotted-line.

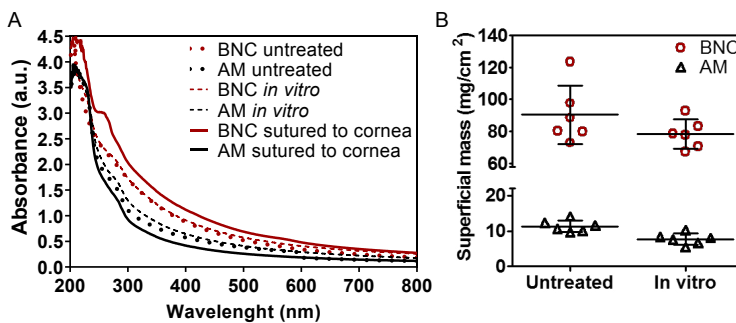


Figure 7: Ultraviolet-visible light absorbance of the materials and superficial mass. A) Ultraviolet and visible light absorbance of BNC and AM materials at different experimental conditions.

Average spectra were obtained from the mean of all the samples for each condition. Each sample was measured at least twice. As for samples sutured to porcine corneas, BNC increased its overall absorbance indicating some acquisition of the tissue/medium components. Oppositely, AM slightly decreases its absorbance, this might be due to a thinning of the material. B) Changes in the superficial mass of the films upon 30-day maintenance *in vitro*. Superficial mass was compared to evaluate degradation and possible changes in thickness. Both materials experienced a reduction in their superficial mass: 12% for BNC and 33% for AM. This change in superficial mass was only statistically significant for AM (P-value <0.0001, paired T-Test) samples.

Finally, SEM investigation revealed that the characteristic nanofibrillar structure of both BNC and AM was retained during the 30-day experiment (Figure 8, see untreated *vs in vitro*) and that the epithelial side of AM presented some crystallizations after the *in vitro* incubation (Supplementary Figure S3). These elongated crystals were undetectable by X-Ray diffraction (data not shown) indicating that its contribution to the total amount of mass of the material should be rather small.

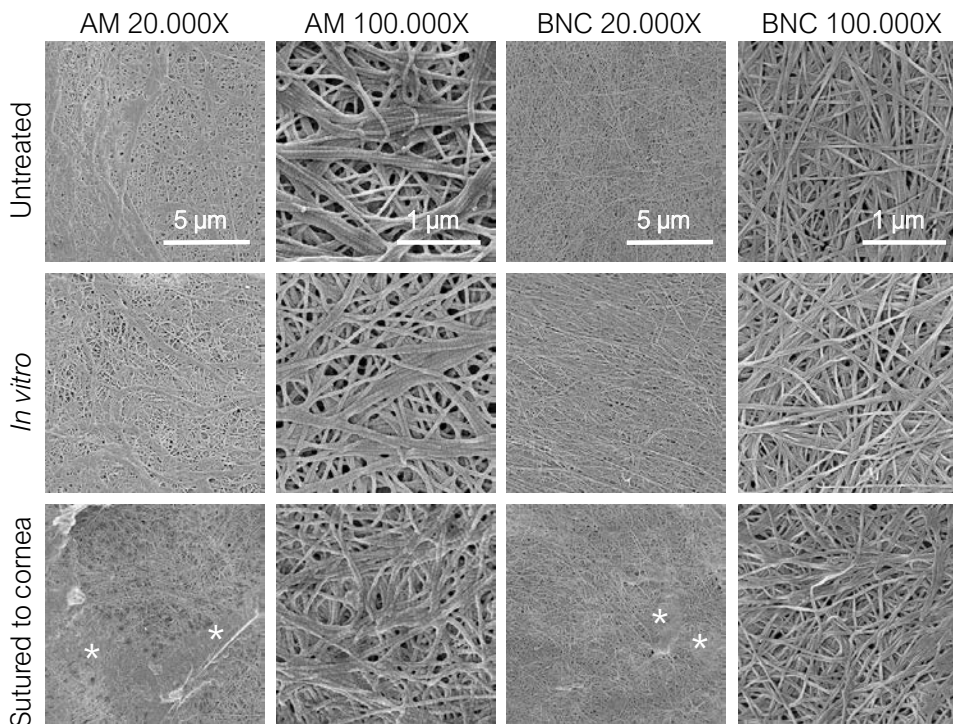


Figure 8: Representative SEM images of the ocular dressing materials before and after the *in vitro* and *ex vivo* stability tests. Three samples were imaged for each material and condition at different magnifications. The side of the material shown here is the one that was in contact with the eye surface, images from the external side are shown as supplementary Figure S3. Under

SEM, no signs of degradation were observed neither for BNC nor for AM samples after any of the two treatments. For the materials sutured to the corneas, both AM and BNC showed some organic deposits (marked with *) that might indicate some transfer of biological matter from the eye surface/culture medium to the ocular surface bandages.

Conformability and adaptability of the materials to the arched shape of the cornea were evaluated by suturing BNC to porcine eyes. BNC films naturally present a flat side (with compact fibres) and a rougher side (loose fibres). After assessing the two possible orientations, the flat side was selected to be in contact with the corneal surface since it showed better adaptability. Importantly, corneal surgeons from our clinic sutured BNC to the cornea of over a score of excised pig eyes and found it easy to handle. BNC maintained its original shape during the process without tearing at the puncture holes. Overall, the suturing of BNC was comparable to that of the AM and the sutured BNC moulded well to the dome-shaped cornea. See supplementary Figure S4 for more details about this process.

Excised porcine corneas were also used for a more realistic *ex vivo* evaluation of the materials under study. Sample preparation for BNC is illustrated in Figure 9 and AM samples were arranged in a similar fashion. After the *ex vivo* culture, the materials were recovered for characterization. Overall, we did not detect major differences in the BNC samples before and after being sutured to the excised porcine corneas; all samples maintained their integrity (size and shape) and did not degrade (for better visualization refer to dark field images in supplementary Figure S2). AM samples also maintained their overall integrity but presented tears at the suture points and some debilitated (*i.e.* more transparent and apparently fragile) areas. Lateral images of the samples taken with a slit lamp showed a continuous layer of material both for AM and BNC after being sutured to the corneas (See third and fourth columns in Figure 6) without detectable defects. Accordingly, SEM imaging revealed that the nanofibrillar structure of BNC and AM was maintained after their incubation (Figure 8, see untreated *vs* sutured to the cornea) in contact with the biological material. Both BNC and AM presented some organic deposits on the side in contact with the corneal surface (indicated with asterisks in Figure 8). The crystals that appeared on the *in vitro* experiments were not detected in these *ex vivo* conditions.

In comparison to untreated samples, BNC increased 26% its absorbance at 600 nm whereas AM samples displayed a reduction of 35% (see Figure 7A). Moreover, BNC samples presented a new absorbance peak at 260 nm. It was not possible to accurately calculate the superficial mass of the samples after the *ex vivo* test since the suture caused deformation of the samples, especially of the AM membranes.

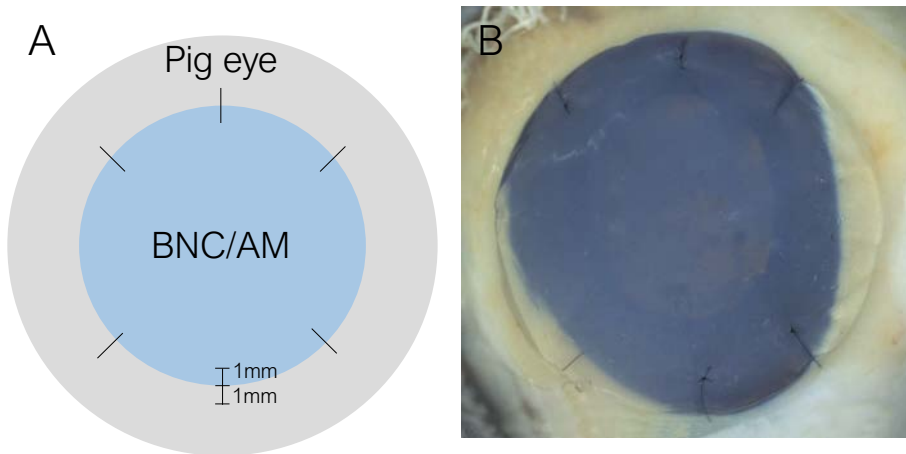


Figure 9: Ex vivo suture test sample preparation. BNC hydrogels and AM were sutured to pig eyes as illustrated schematically in A. The needle easily penetrated the BNC hydrogels and conventional knots were made with surgical instrumentation (B). Both materials adapted well to the dome shape of the eye without forming wrinkles. Then, the cornea and part of the sclera were excised and placed on Petri dishes containing RPMI medium for 20 days. The same sample preparation process was followed for AM.

Discussion

Although BNC possesses attractive intrinsic characteristics to become a new ocular surface bandage material^{31,49}, very few studies have explored this possibility. Here, we present a comparative study between BNC and the most common ocular surface bandage; AM. First, we provide an extensive characterization of BNC and AM and a comparison of their physicochemical characteristics. Then, BNC is positively evaluated regarding: stability under simulated physiological conditions, resistance to the mechanical stress caused by suture, conformability to the eye surface and easiness of manipulation using standard clinical procedures. Compared to AM,

BNC hydrogels resisted a higher force on the suture stress test, did not lose transparency after the *in vitro* test and were less deformed on the *ex vivo* assay.

The present study focused on the suitability of BNC as a new ocular surface bandage from a material point of view. Therefore, data regarding the ability of BNC to promote corneal wound healing is not provided yet. We speculate that BNC corneal bandages can have a protective effect similar to that of collagen corneal shields^{3,50}. Thus, feasible clinical usages of BNC would be as temporary tectonic or multi-layered bandages for patients suffering from non-infectious corneal ulcers, or ulcerative keratitis with a high risk of corneal perforation. Applying a therapeutic contact lens on top of the BNC bandage could be needed, in the same way as when using AM in clinical practice. The contact lens would contribute to decrease friction with the inner surface of the eyelids as well as to maintain moisture by capturing the tears on its concave side.

Importantly, our latest data⁵¹ shows that the amount of endotoxins detected in the eluates of autoclaved BNC are 0.05 ± 0.01 Endotoxin Units (EU)/mL. This value falls well below the Food and Drug Administration limit set at 0.5 EU/mL for medical devices and thus indicates that BNC can be considered a non-pyrogenic material. Regarding inflammatory responses, we expect native BNC to act as an inert biomaterial. That is, BNC hydrogels are expected to be neither pro nor anti-inflammatory as demonstrated in⁵² with *in vitro* tests. It has also been argued that BNC is well tolerated *in vivo* without causing major inflammatory complications^{53,54}. However, the interactions of BNC with the immune system will be addressed in our future investigations.

BNC is a mechanical and thermally stable material. These features are relevant for thermal sterilization (typically performed at 121°C) and for adhering BNC to the ocular surface by suture stitches. AM decomposition takes place at rather high temperatures but its sterilization by heat might compromise its wound healing capabilities. BNC hydrogels used in this study were much thicker than AM, although the thickness of both materials varies considerably due to their biological origin^{55,13}. AM can be up to 200 µm and can be used as a multilayer, an approach that can also be envisioned for BNC. Notably, BNC's thickness can be modulated during the production process⁵⁶ and/or posteriorly by adjusting its water content⁴⁶ to meet specific requirements. Roughly, BNC hydrogels can be obtained with

thicknesses ranging from hundreds of microns to few millimetres while dry BNC membranes exhibit thicknesses of tens of microns.

The Young modulus of BNC is also largely influenced by the water content and biosynthesis method, being in the range of 0.6 to 1.5 GPa^{57,46} in its dry state with considerably lower values for the never dry form. Similarly, tensile strength is in the order of 50 MPa for dry BNC and between 1.5 and 2 MPa for the never dry form. Nevertheless, the BNC hydrogels present higher ductility with elongation at break values up to 20% which might be of interest for the application suggested here⁵⁸. BNC presents a characteristic nanofibrillar structure with great architectural similarity to that of collagen found in the stromal side of AM (see SEM images in Figure 4). Despite the observed similar nanofibrillar organization, BNC and AM differ at the organization level, evidenced by the X-Ray diffraction patterns, being AM non-crystalline and BNC a semi-crystalline material.

On the other hand, BNC's nanofibrillar network can act as a reservoir for diverse molecules^{59,60}. This capability might offer venues for future BNC corneal bandages supplemented with therapeutic agents in order to emulate the anti-scarring and anti-inflammatory effects that AM provides. In fact, the anti-inflammatory effect of BNC hydrogels supplemented with diclofenac has recently been reported⁵². Similarly, in cases of bacterial keratitis, BNC could be impregnated with antibiotics to act as a medication reservoir. In this direction, BNC is also well known to support the culture of several cell types⁶¹⁻⁶³ including retinal pigment epithelial cells^{33,64}. These reports, together with the findings reported here, suggest further uses of BNC as a cell carrier for corneal cell therapies. In the case of a BNC bandage supplemented with sensitive biological material (cells or bioactive molecules), the cryo-storage approach commonly used for preserving AM⁶⁵ could also be considered since our recent data demonstrate that BNC is stable at liquid nitrogen temperatures⁵¹. Other interesting modifications of BNC aim at increasing its optical transparency. This can be achieved by mechanically increasing fibre alignment⁵⁷ or by filling the pores with biocompatible polymers such as polyethylene glycol⁵².

Importantly, we validate that BNC can be sutured to the ocular surface without employing more time or resources than AM while presenting a higher resistance to the mechanical stress caused by the suture. Moreover, its soft and flexible nature confers optimal adaptability to the dome shape of the ocular surface. We also ex-

pect that the high liquid holding capacity of BNC hydrogels will be convenient to keep proper hydration of the ocular surface.

We examined the behaviour of BNC in two simulated physiological environments; *in vitro*, maintained in corneal preservation medium for 30 days, and *ex vivo*, sutured to excised pig corneas during 20 days without observing signs of degradation neither at the macro nor at the micro/nanoscales. *In vitro*, BNC and AM kept their integrity but decreased their superficial mass; this reduction was higher in weight percentage for AM than for BNC. However, it is hard to discern if this shrinking in the superficial mass is due to material deterioration or to loss of water due to osmotic processes. Additionally, AM samples became more opaque after the incubation, possibly due to microcrystals deposits that increased light scattering. BNC hydrogels did not present crystals or opacification but BNC films were coloured by the culture medium and this might be responsible for the slight increase of light absorbance.

Placing the materials in direct contact with ocular tissue on the *ex vivo* test allowed us to discard the degradation of the BNC caused by the interaction with the tissue and to confirm its robustness after suturing. BNC nanofibrillar structure was also intact after the experiment. Contrary to BNC, AM samples were deformed and presented some tears at the suture points but kept their overall integrity. The UV-VIS light absorbance of AM decreased after the treatment and some areas seemed to debilitate as observed on the grid images. This might be attributed to a thinning of the material that needs to be further confirmed. BNC behaved differently, its overall UV-VIS absorbance moderately increased presenting a new peak characteristic of nucleic acids and close to the protein absorbance region. This could be ascribed to the adsorption of biological material on the BNC coming either from the ocular tissues or the culture medium. This observation is also supported by the organic deposits visualized under SEM. Transference of tissue/medium components was also detected visually in the form of opaque areas and with SEM as organic accumulations in the AM samples. Overall, we consider BNC to be stable under the two tested conditions and times.

In summary, corneal damage is a highly prevalent cause of vision reduction and blindness, particularly in rural areas of developing countries. Therefore, there is an evident need for low-cost, accessible, durable and easy to apply ocular sur-

face bandages^{66,67}. In the present study, we aimed at deciphering whether BNC, a biomaterial that shows great promise for skin regeneration, is also suitable as bandage material to treat ocular surface disorders. Using AM as a benchmark, we demonstrated that BNC meets basic preclinical requirements for this purpose. These findings, together with BNC's prolonged shelf life, straightforward and animal-free production and controllability might encourage further investigations of BNC for corneal regeneration.

Methods

The general experimental design of this study is summarized in Supplementary Table 1.

Amniotic membrane

Human amniotic membranes were obtained from the local tissue bank (Barcelona Banc de Sang i Teixits) and stored at $-80\text{ }^{\circ}\text{C}$ until experimental use. The samples were cut into the desired shapes and sizes using a 17 mm \varnothing trephine (circles) or surgical scissors (rectangles).

Production of the bacterial nanocellulose films

Bacterial nanocellulose films were obtained following our established protocol detailed elsewhere⁶⁸. Briefly, a commercial *Komagataeibacter xylinus* (*K. xylinus*) strain (NCIMB 5346 from CECT, Valencia, Spain) was inoculated on 6 mL of Hestrin-Schramm (HS) medium (1.15 g citric acid, 6.8 g $\text{Na}_2\text{HPO}_4 \cdot 12\text{H}_2\text{O}$, 5 g peptone, 5 g yeast, and 20 g dextrose for 1 L of Milli-Q water) and incubated statically for 7 days at $30\text{ }^{\circ}\text{C}$. This bacterial culture was further diluted 1:15 with fresh HS medium and cultured on 24-well plates (2 mL/well) for 3 days. The BNC pellicles that formed at the air-liquid interface were collected and immersed in a solution of 1:1 Ethanol: deionized water (DI) to kill the bacteria. Then, the films were washed 1x40 minutes in boiling DI water and 2x20 minutes in a boiling 0.1 M NaOH solution to remove organic residues. After rinsing several times with DI water, the films were autoclaved ($121\text{ }^{\circ}\text{C}$, 20 min).

Endotoxin contamination study

The endotoxin extraction was carried out by placing clean and autoclaved BNC hydrogels in depyrogenated falcon tubes with 40 mL of endotoxin-free water for 72 h at 30 °C and under orbital agitation (100 rpm), according to FDA recommendations⁶⁹. The endotoxin content in the eluates from BNC samples was measured with a Pierce™ LAL Chromogenic Endotoxin Quantification Kit purchased from Thermo Fisher and the assay was performed following the manufacturer's instructions. The products of the reaction were read for absorbance at 405 nm in a microplate reader (Infinite 200 PRO, TECAN ®) at 37 °C. The indicated values in the results section correspond to the mean \pm standard deviation of two independent experiments obtained from two different endotoxin quantification kits and evaluating each time two samples from two different batches of BNC.

Dehydration test

Three independent BNC hydrogels (12 cm x 12 cm) were left to dehydrate inside a room with controlled humidity (45%) and temperature (22 °C). The materials were weighed every hour with a precision scale. The initial weight of the hydrogels was used to calculate the remaining weight (%) at different time points.

Thickness measurements

The thickness of the AM (n=12) and BNC (n=20) samples were measured with a digital micrometre, placing the samples between two cover slides to keep them flat. A slight blotting of the specimens was made with filter paper prior to the measurement to remove the excess liquid. Five measures were made for each sample at different areas to get an average thickness.

Thermogravimetric analysis

To evaluate the thermal stability of the materials, a TGA-DSC/DTA analyser (NETZSCH STA 449 F1 Jupiter) was used. The covered temperature range was from 25 to 800 °C and the heating rate was 10 °C/minute in air. The first derivative graphs were obtained with the Origin 85 software.

X-Ray diffraction

Dry BNC and AM were fixed flat on a silicon wafer support to acquire X-ray diffraction patterns using a Siemens (Model D-5000) diffractometer. Step size was 0.02°/minute in a 2 θ range from 5° to 30°. A Cu anode was employed. Smoothing of the data was performed with the Savitzky-Golay model included on the Origin 85 software.

Digital images

Digital images were taken with a Canon Eos 550C camera coupled to a microscope with the samples placed on a dark/white field chamber. For the white field images, a grid (squares of 1 mm²) was located under the specimens to better visualize the transparency of the materials. The photographs were acquired with a standardized exposure time of 1/100s. Areas and grey values were measured from these images with the ImageJ-win64 software.

Scanning electron microscopy

Both BNC and AM samples were freeze-dried at -80 °C for 48 hours to preserve their native structure. Small pieces of the films were cut with scissors and immobilized on top of an aluminium sample holder with carbon tape. The samples were sputtered with 5 nm of platinum before being imaged with a high resolution scanning electron microscope Magellan 400L at the following magnifications: 5000X, 20,000X and 100,000X. The employed voltage was 2.00 kV and the current was 100 pA.

Ultraviolet-visible spectroscopy

Ultraviolet-visible (UV-Vis) absorbance spectra of BNC and AM materials were obtained without any sample preparation step. A Varian Cary-5000 UV-Vis-NIR spectrophotometer on transmission mode was employed to obtain a minimum of two spectra (between 200 and 800 nm) from each sample. A baseline correction was performed by subtracting the absorbance of the glass coverslips used to hold the samples. The absorbance of the sample was calculated as: $A = \log_{10}(I_0 / I)$ where I_0 corresponds to the intensity of the light passing through the reference cell (glass) and I to the intensity of the light passing through the sample cell (BNC or AM) at the same wavelength.

In vitro stability test

The *in vitro* stability test evaluated six independent samples of each material. Circular BNC films of $\approx 2 \text{ cm}^2$ and AM rectangles of $\approx 3 \text{ cm}^2$ were used. Every sample was weighed and photographed before the incubation. Each sample was placed individually on sterile glass bottles containing 100 mL of Tissue C (Alchimia) culture medium. The materials were clipped to a CornealFloat to keep them suspended in the liquid. The bottles were kept for 30 days in a CO_2 incubator (5%) at 37°C . Then, the materials were recovered and characterized for: weight, diameter, integrity, micro/nanostructure (SEM) and light absorbance (UV-Vis).

Suture stretch test

To test the mechanical stability of the materials, the device illustrated in Figure 5A was employed. BNC ($n=16$) and AM ($n=5$) samples were sutured (Suture type: Nylon 10/0, Lab Aragón) with a single stitch to small pieces of porcine scleral tissue ($\approx 1 \text{ cm}^2$) using standard suture instruments from Grieshaber (Westcott scissors and Colibrí forceps), a Barraquer needle holder and a Castroviejo Suture forceps. Then, the complex was clamped on the top part (clamp placed on the BNC/AM) and fixed to a support. Another clamp was placed at the scleral tissue (bottom) and a platform was hung from that clamp. 4.5 g weights were added gradually (every two minutes) to the platform until the BNC/AM broke at the suture point. The maximum weight tolerated by each sample before rupture was divided by the normalized thickness of the sample inside each type (BNC and AM). A value of 1 was assigned to the thickest BNC ($986 \mu\text{m}$) and AM ($63 \mu\text{m}$) specimens.

Ex vivo suture test

Eyes globes were obtained from 6-month-old pigs and used within 48 h. BNC and AM films of $\approx 16 \text{ mm}$ diameter were non-invasively characterized (weight and diameter) and then sutured to pig corneas keeping the limbal area intact. 6 symmetric sutures were made for each eye 1 mm away from the BNC/AM border and holding 1 mm of tissue with standard nylon suture 10/0 from Lab Aragón (Barcelona). The knots were not buried. The sutures penetrated $\approx \frac{3}{4}$ of the cornea/sclera thickness. The cornea and part of the sclera were resected from the rest of the eye with scleral scissors. Pictures were also taken at this point. The samples

were decontaminated by immersion into a 5% Povidone-iodine (PI) solution for 2 minutes. Sodium thiosulphate (0.1%) was used to remove the PI and later the samples were rinsed with phosphate-buffered saline. Then, the excised corneas were placed in a closed container (Petri dish) with 13 mL of Roswell Park Memorial Institute (RPMI-1640) culture medium (R8758 Sigma-Aldrich) supplemented with 5% foetal bovine serum (F7524 Sigma-Aldrich) and 1% antibiotic-antimycotic (A5955 Sigma-Aldrich) under sterile conditions. The as-prepared Petri dishes were kept in an incubator at 37°C and 5% CO₂ for 20 days. The medium was changed every 3 to 4 days.

Statistical analysis

For the statistical analysis, GraphPad Prism 5 software was employed. Data is represented by mean \pm standard deviation. Statistical significance was accepted when p-values under 0.05 were obtained in paired (superficial mass) or unpaired (suture stress test) Student's T-tests.

Supplementary information included in Publication 4

Figure S1: Dehydration rate of BNC hydrogels. Graph showing weight losses of BNC hydrogels (water content >99%) over time when exposed to the air under controlled humidity (45%) and temperature (22° C). Water evaporation took place at a constant speed and after 6 hours of exposure, BNC hydrogels still contained 66% of their initial water content. Data were fitted to linear regression ($r^2=0.97$).

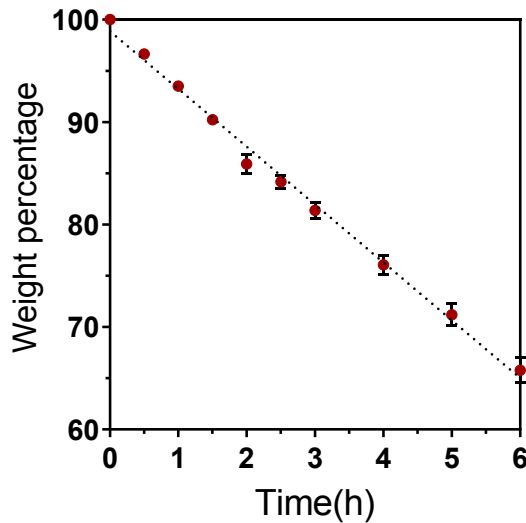


Figure S2: Frontal and slit-lamp images of AM and BNC before and after the *ex vivo* stability tests. Darkfield images are shown on the first and third columns where the integrity of the samples can be visualized. White field photographs were taken with a grid (second and fourth columns) to better visualize the transparency of the materials. Each square of the grid corresponds to one mm². Inserts at the bottom of the grid images correspond to lateral views of the materials captured with a slit lamp. To mark the orientation of the samples a tissue marker was used and for clarity in the pictures, the materials were delineated with a yellow-dotted line.

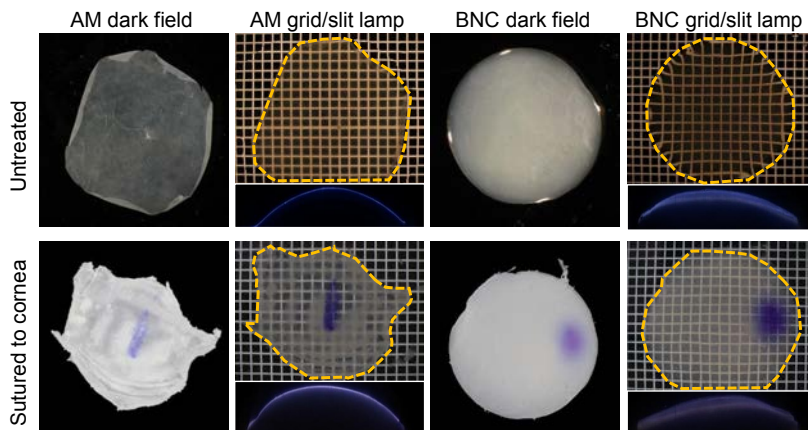


Figure S3: Representative SEM micrographs of the AM and BNC sides expected not to be in contact with the ocular surface. After both *in vitro* and *ex vivo* experiments, the materials did not seem to be degraded and the organic deposits observed on the side placed in contact with the eye surface were not perceived. The only noticeable difference was the presence of elongated crystals on the AM samples of the *in vitro* test (indicated with asterisks). Three samples were imaged for each material at least in three different areas. The mentioned observations were consistent for the three samples that were examined.

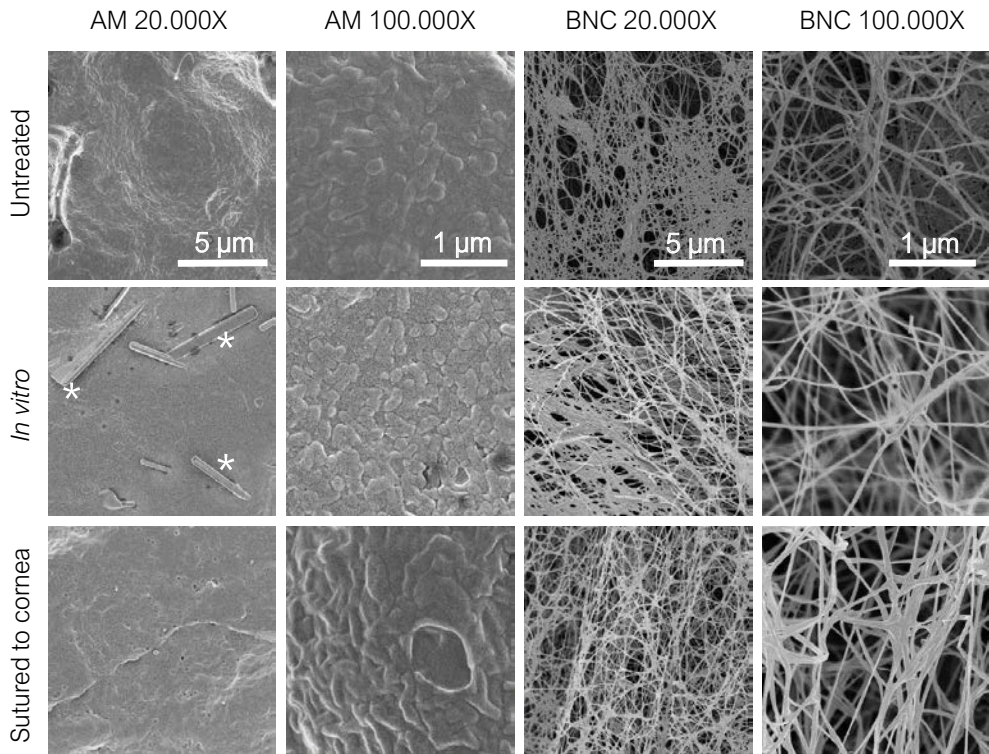


Figure S4: BNC handling and suturing to the ocular surface. BNC hydrogels ($\varnothing=1.6$ cm) were easily manipulated with forceps and maintained their initial shape as illustrated on the left panel. BNC acquired a pink colour from the culture medium components. BNC suture process (right panel) to pig eyes was comparable in terms of time and complexity to that of human AM. The needle penetrated easily on the material without causing tearing and BNC spread and adapted readily on the surface of the cornea.

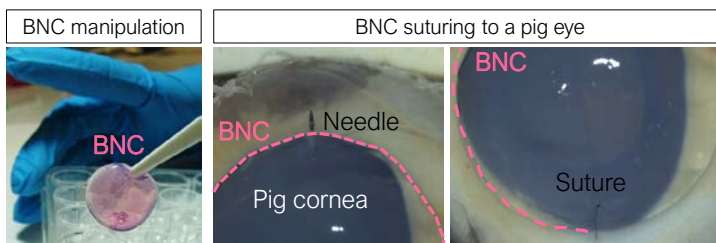


Table S1: Summary of the experimental design.

Experiment	Material characterization	Physiological stability in corneal preservation medium (<i>in vitro</i>)		Physiological stability sutured to the cornea (<i>ex vivo</i>)	
		t=0 (untreated)	t= 30 days	t=0 (untreated)	t= 20 days
Number of samples	Different depending on the characterization technique	n= 6 for BNC n= 6 for AM		n= 3 for BNC n= 3 for AM	
Characterization points and techniques	Untreated	t=0 (untreated)	t= 30 days	t=0 (untreated)	t= 20 days
Thickness Micrometre	X				
Thermal stability Thermo-gravimetric analysis	X				
Atomic structure and crystallinity X-Ray Diffraction	X				
Suture stress resistance Suture stretch test	X				
Macroscopic integrity Digital pictures: darkfield and slit lamp		X	X	X	X
Optical transparency Digital white field pictures with grid		X	X	X	X
Superficial mass Mass and surface		X	X		
Material absorbance UV-Visible spectrophotometry	X		X		X
Micro and nanostructure Scanning electron microscopy	X		X		X

Acknowledgements

Authors acknowledge financial support from the Spanish Ministry of Science and Innovation through the RTI2018-096273-B-I00, project, the ‘Severo Ochoa’ Programme for Centres of Excellence in R&D (SEV-2015-0496) and the PhD scholarship of I.A.S. (BE-2017-076734) and the Generalitat de Catalunya with the 2017SGR765 and the 2019LLAV00046 projects. The authors also thank María Jesús Sánchez-Guisado for her assistance with the endotoxin

study, the ICMAB technical services (TGA and X-Ray) and Marcos Rosado from the ICN2 electron microscopy service. The ICMAB members (IAS, AL, and AR) participate in the CSIC Interdisciplinary Platform for Sustainable Plastics towards a Circular Economy, SUSPLAST and in the Aerogels COST ACTION (CA 18125).

Author Contributions

I.A-S designed experiments, prepared and cultured samples, characterized the samples, acquired data, analysed data, interpreted data, prepared the figures, wrote the manuscript, revised the manuscript; J.C.D designed experiments, prepared and cultured samples, acquired data, interpreted data, revised the manuscript; J. F. E. performed the sutures; provided clinical advice and revised the manuscript; V.C. provided literature, revised experiments, revised the manuscript A. L., A. R. and R.M. designed and supervised experiments, interpreted data, revised the manuscript and obtained funding.

Business proposal for the *Corneal-BNC* project

To truly impact society, research outcomes need to go through a process of technology transfer (TT) to convey academic findings to the market place. The TT pipeline consists of several phases and is a complex and multidisciplinary process that requires skills that are not usually taught in traditional scientific training. This section describes a tentative roadmap for a TT strategy of the BNC corneal bandages.

Market analysis

Problem and target market

A market analysis assesses the attractiveness of an innovation by determining the interest in it of a target market and by estimating the potential market size. As mentioned before, corneal trauma, ulcerations and chronic inflammatory processes are estimated to originate 1.5–2.0 million new cases of vision reduction every year, positioning corneal opacities as the fourth cause of blindness worldwide⁷⁰. Moreover, these numbers are projected to rise due to the growing use of contact lenses (risk factor) as well as the increasing and ageing of the world's population. Irreversible corneal conditions can only be remediated with a corneal transplant but the world's demand surpasses the supply of compliant donor corneas⁷¹. For not so severe cases, a common intervention consists of an AM graft also obtained from donated human tissue (placenta). This approach, although clinically efficacious, suffers from significant limitations *i.e.* the stringent collection and storage conditions of AM, its short shelf life and ethical concerns. This problematic situation leaves a market opportunity for alternative ocular bandages where BNC could find a market share. Thus, our initial market segment would be local ophthalmological institutions, both public and private, that periodically use AM grafts to treat ocular surface pathologies. Typically, the market size is calculated as follows:

$$\text{Market size} = M \times P \times N = 600 \times 335 \times 2 = 402.000\text{€}$$

M corresponds to the target market (number of patients), P to the prize of the product and N the number of times the product is used per year. Based on the registers from COB, the number of patients that could be treated in Catalunya every year is around 600 (total population: 7.5 million). The price of our product is not determined yet and thus the price from fresh AM from the local tissue bank (our benchmark) is used for the calculation (335€/membrane). It is anticipated that for a standard treatment at least two bandages would be required. This estimation computes an estimated market size of 400K€/year only in Catalunya. Naturally, the number of patients to be treated could be expanded to other territories in future endeavours. Thus, by extrapolating the number of patients in Catalunya to other geographies we can anticipate that in Spain there are 3.760 potential patients (total: 47 million), in Europe 59.840 (total: 748 million) and in North America 29.600 (total 370 million).

Competitors

Despite the great supply of products addressed to ocular surface health, not all of them should be considered as direct competitors since their strategies might differ from our positioning. Hence, another pivotal task in market analysis is to identify those products that target a comparable market segment. Table 1 compiles commercial and in-development medical products recognized as the main potential competitors to our suggested BNC corneal bandages. These short-listed products should be monitored for updates, price variations, acquisitions etc. during the development of Corneal-BNC.

Table 1: Details about products addressed to treat ocular pathologies with a similar strategic positioning to the Corneal-BNC.

Product name and company	Therapeutic indication	Composition	Mode of use	Price
Amniotic membrane Banc de Sang i Teixits, BCN	Corneal erosions, ulcerations, chemical/thermal	Fresh human amniotic membrane	Sutured by surgeons in operating room	335€/membrane
AmbioDisk™ IOP Ophthalmic, USA	burns, non-healing epithelial defects, severe dry eye and post-infectious	Dehydrated amniotic membrane	Applied in-office by clinicians	~400€/membrane
Prokera® Biotissue, USA	keratitis	Cryopreserved amniotic membrane	Applied in-office by clinicians	~800€/membrane
Oasis corneal Soft Shield Oasis Medical, USA	Protection after ocular surgery, injections or corneal trauma	Bovine cross-linked collagen	Applied in-office by clinicians	250€/pack of 15
Ocular Bandage Gel Eye Gate pharma, USA	Surgical trauma	Modified and cross-linked hyaluronic acid	Applied by the patient as eye drops	Not determined, product under development
CorNeat EverPatch CorNeat Vision, Israel	Glaucoma and keratoprosthesis	Synthetic non-degradable porous material	Applied by surgeons in the operating room	Not determined, product under development

SWOT analysis

A SWOT (Strengths, Weaknesses, Opportunities and Threats) analysis is a tool used to evaluate a company's competitive position. The SWOT matrix assesses internal and external factors, as well as current and future potential. Figure 10 shows a SWOT analysis of the Corneal-BNC project.

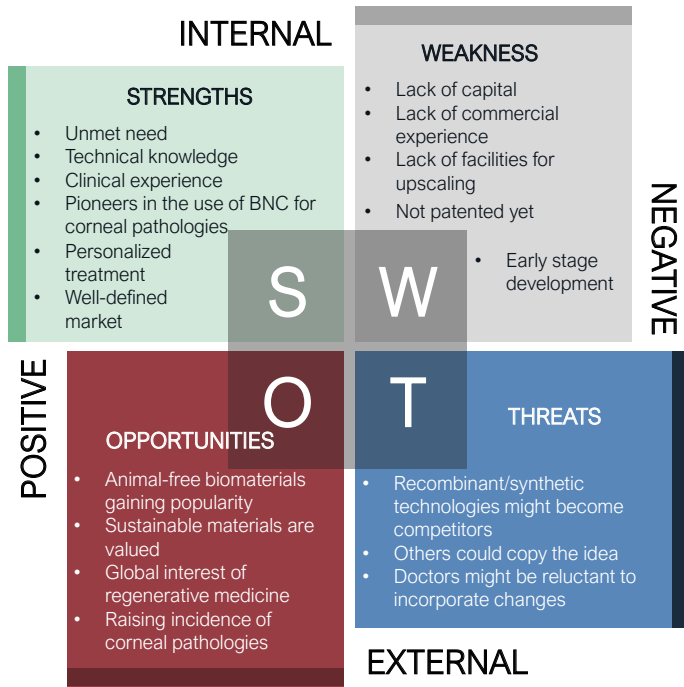


Figure 10: Analysis of the strengths, weaknesses, opportunities and threats (SWOT) of the Corneal-BNC proposal.

Value proposition

A value proposition is a statement that answers 'why' someone should do business with you. It is typically presented as:

1. A single summary statement.
2. A short description of the problem addressed.
3. How the proposed solution is better than current solutions (unique attributes).

A possible value proposition for Corneal-BNC would be:

A biotechnological ocular surface bandage; a novel concept of donor-independent, available, durable and easy to use biomaterial to treat corneal pathologies. Our ophthalmic medical device is based on a naturally produced nanocellulose hydrogel serving also as a reservoir of therapeutic agents.

Business model

A business model is a company’s strategy to achieve revenues. It summarizes how the company creates, delivers and captures value and it is usually visualized as a business model canvas. Figure 11 displays the proposed business model for Corneal-BNC.

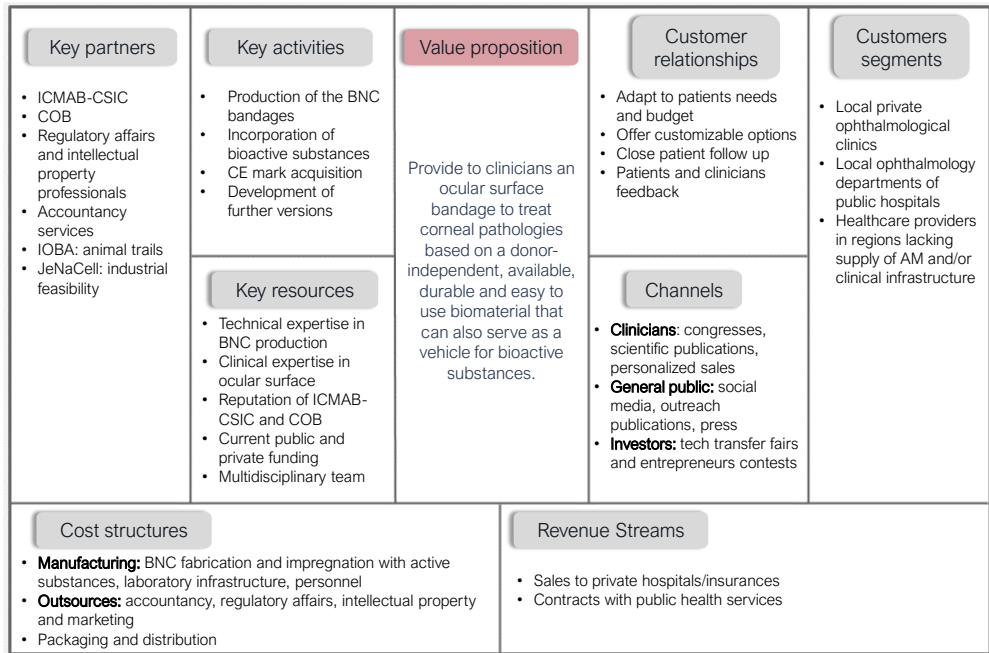


Figure 11: Envisioned business model canvas for the Corneal-BNC project.

Development plan

Early stages

Before the implementation of the business plan, the Technology Readiness Level (TRL) of the Corneal-BNC patches should be increased from the current state, estimated to be around 3 (experimental proof of concept), to a TRL 6 (technology demonstrated in relevant environment). To achieve this milestone, a two-year development plan is presented in Figure 12. The estimated budget provided is based on previous experience from the team as well as inquiries to other organisations (*Instituto Universitario de Oftalmobiología Aplicada (IOBA)*, *Oficina Española de Patentes y Marcas (OEPM)*).

The expenses detailed in the diagram sum up ~33.000€. To this value, personnel (124.000€ for two contracted specialists) and overheads of the research centre (20%) payments should be added together with and a 15% extra for unexpected expenses leaving an approximate budget of 223.000€. In the eventuality of protecting our technology through patenting, the costs of this process should be added. This funding could be reasonably attained through public aids (e.g. *Centro para el Desarrollo Tecnológico Industrial*) or via a seed investment from a private entity (e.g. business angel).

2021		2022			
TRL 3		TRL 6			
Experimental proof of concept		Technology demonstrated in relevant environment			
Activities	<ul style="list-style-type: none"> Final technology validation Corneal wound healing <i>ex vivo</i> test 	<ul style="list-style-type: none"> Research Evaluate suture-less application methods Impregnation with bioactive molecules Refining BNC properties 	<ul style="list-style-type: none"> <i>In vivo</i> preclinical tests Rabbit model Evaluate: efficacy, safety, eye irritation and immune reactions 	<ul style="list-style-type: none"> Intellectual property Patentability study for the new results 	<ul style="list-style-type: none"> Business plan Create a spin off Create an attractive webpage Networking Assist to events
	Budget	<ul style="list-style-type: none"> Current resources (on going) 	<ul style="list-style-type: none"> Material and reagents: ~12.000€ Equipment (incubator) ~5000€ 	<ul style="list-style-type: none"> Protocol: 768€ Eye irritation test: 3600€ Implantation: ~4500€ Histological analysis: ~1500€ 	<ul style="list-style-type: none"> Professional patent study (OEPM): 510€

Figure 12: E Diagram of the early development plan to increase the TRL from 3 to 6. OEPM stands for *Oficina Española de Patentes y Marcas*.

Middle-long term plan

After the proposed creation of the spin-off company at the end of 2022, funding sources are projected to switch to crowdfunding (e.g. <https://capitalcell.es/>) and/or venture capital. The long-term development plan (beyond 2022) appears difficult to predict at the moment. However, one can anticipate that a crucial activity will be the regulatory procedures to attain the CE mark required for commercializing medical devices (MD) in the European Union (EU). After consulting the European requirements (EU regulation 2017/745), we consider that the ocular bandages based solely on BNC should be classified as MD Class IIb as they are expected to contact an injured area of the body. As for the proposed BNC bandages containing ancillary substances, the product would fall into the MD Class III category. Thus,

the conformity assessment of MD Class IIb would be made through a notified body (NB). In the case of the MD Class III, apart from the NB, a Competent Authority (*i.e.* Spanish Agency for Medicines and Health Products) should also be involved. Scaling up the BNC production following Good Manufacturing Practices guideless will represent another challenge. For that, a partnership with JeNaCell (<http://www.jenacell.com/de/>) would be considered as this biotech company already developed industrial-scale production of BNC⁷².

Following our long-term vision, the research activity should be maintained in parallel to the product development process. The product range of Corneal-BNC will spread towards novel formats of ocular bandages (*i.e.* formats that can be applied directly by the patients) and enlarge the portfolio of functionalities to reach other market segments. The packaging, labelling, distribution and marketing steps are also allocated to later stages of the development process.

Ultimately, the spin-off will likely be acquired by a leading medical device group with a global presence to further develop and internationalize the business.

Contributions to the field and critical comment

This chapter combines the preclinical testing of BNC as a novel ocular surface bandage with an initial TT proposal.

The experimental part of Chapter 4 validates the hypothesis that the material properties of BNC that are highly appreciated in the field of skin regeneration (robustness, manageability, conformability, water retention etc.) can also be harnessed in the ophthalmological domains. Moreover, we could identify only a very small number of previous publications pointing towards BNC applicability in corneal regeneration⁷³⁻⁷⁵. Our work differs from these references in the mode of use; *i.e.* we suggest a temporal ocular surface bandage while others pursued the development of a tissue substitute based on BNC or BNC composites.

It is noteworthy that the experimental design for Publication 4 was outlined after several brainstorming sessions with clinicians and researchers from COB (independent from those interviewed in Chapter 1) to always keep in mind the needs of the end-users. The selection of AM as a benchmark further emphasizes our translational intention. Nevertheless, these encouraging results need to be completed with further experiments that are scheduled or already underway. The *ex vivo* test presented in Publication 4 demonstrates the durability and applicability of the BNC bandages yet it does not provide evidence about their capacity to accelerate corneal wound healing, rendering a second round of *ex vivo* tests as a future work priority.

As reported in the literature, BNC matrices have been impregnated with Active Pharmaceutical Ingredients (API) upon simple diffusion methods for topical delivery^{59,76,77}. This approach is currently being investigated in our lab to exploit BNC as an ocular delivery device and accounts for a relevant step in our TT proposal. The possibility to combine BNC with an array of bioactive substances on demand expands the possibilities for medicated ocular bandages. These modifications are expected to emulate the regenerative potential of AM while providing a more controlled and customizable platform. For regulatory compliance sake, the bioactive substances incorporated in the corneal bandages are expected to be compounds commonly used in ophthalmological practice.

Despite its immaturity due to the low TRL, I endorse the valorisation of the BNC corneal bandages as a noteworthy contribution of Chapter 4. The provided guideline can be handy in the future to gradually move from academic results to medical use. Besides, participating in the Llabor program has been beneficial for this thesis as it provided resources to broaden our knowledge in different directions. Finally, I deem the estimated early-stage plan as a realistic horizon. It is expected that when reaching an advanced development phase, more sound decisions would be taken concerning the commercial feasibility of the Corneal-BNC project.

Chapter references

1. Wilson, S. L., El Haj, A. J. & Yang, Y. Control of scar tissue formation in the cornea: strategies in clinical and corneal tissue engineering. *J. Funct. Biomater.* **3**, 642–87 (2012). 1.
2. Lee, S.-H. & Tseng, S. C. G. Amniotic Membrane Transplantation for Persistent Epithelial Defects With Ulceration. *Am. J. Ophthalmol.* **123**, 303–312 (1997).
3. Aquavella, J. V, del Cerro, M., Musco, P. S., Ueda, S. & DePaolis, M. D. The effect of a collagen bandage lens on corneal wound healing: a preliminary report. *Ophthalmic Surg.* **18**, 570–3 (1987).
4. Stein, H. *et al.* Production of Bioactive, Post-Translationally Modified, Heterotrimeric, Human Recombinant Type-I Collagen in Transgenic Tobacco. *Biomacromolecules* **10**, 2640–2645 (2009).
5. Widner, B. *et al.* Hyaluronic Acid Production in *Bacillus subtilis*. *Appl. Environ. Microbiol.* **71**, 3747–3752 (2005).
6. Durrie, D. S. *et al.* Ability of a new crosslinked polymer ocular bandage gel to accelerate reepithelialization after photorefractive keratectomy. *J. Cataract Refract. Surg.* **44**, 369–375 (2018).
7. Wolsey, D. *et al.* Novel cross-linked ocular bandage gel improves reepithelialization after photorefractive keratectomy: A randomized, masked prospective study. *J. Ocul. Pharmacol. Ther.* **36**, 602–608 (2020).
8. Williams, D. L. & Mann, B. K. A crosslinked HA-based hydrogel ameliorates dry eye symptoms in dogs. *Int. J. Biomater.* **2013**, 460437 (2013).
9. Yang, G., Espandar, L., Mamalis, N. & Prestwich, G. D. A cross-linked hyaluronan gel accelerates healing of corneal epithelial abrasion and alkali burn injuries in rabbits. *Vet. Ophthalmol.* **13**, 144–150 (2010).
10. Islam, M. M. *et al.* Self-assembled collagen-like-peptide implants as alternatives to human donor corneal transplantation. *RSC Adv.* **6**, 55745–55749 (2016).
11. McTiernan, C. D. *et al.* LiQD Cornea: Pro-regeneration collagen mimetics as patches and alternatives to corneal transplantation. *Sci. Adv.* **6**, eaba2187 (2020).
12. Fagerholm, P. *et al.* Stable corneal regeneration four years after implantation of a cell-free recombinant human collagen scaffold. *Biomaterials* **35**, 2420–2427 (2014).
13. McGaughy, A. *et al.* In Office Use of Amniotic Membrane. *Am. Acad. Ophthalmol.* **3**, 31–32 (2015).
14. Burton, M. J. Corneal blindness: Prevention, treatment and rehabilitation. *Community eye Heal.* **22**, 33–5 (2009).
15. Whitcher, J. P., Srinivasan, M. & Upadhyay, M. P. *Corneal blindness: a global perspective. Bulletin of the World Health Organization.* (2001).

16. Gundersen T, P. H. Conjunctival flaps for corneal disease: their usefulness and complications. *Trans Am Ophthalmol Soc.* **67**, 78–95 (1969).
17. Arentsen, J. J., Laibson, P. R. & Cohen, E. J. Management of corneal descemetocles and perforations. *Trans. Am. Ophthalmol. Soc.* **82**, 92–105 (1984).
18. Alino, A. M., Perry, H. D., Kanellopoulos, A. J., Donnenfeld, E. D. & Rahn, E. K. Conjunctival flaps. *Ophthalmology* **105**, 1120–3 (1998).
19. Su, C. Y. & Lin, C. P. Combined use of an amniotic membrane and tissue adhesive in treating corneal perforation: a case report. *Ophthalmic Surg. Lasers* **31**, 151–4 (2000).
20. Chen, H.-J., Pires, R. T. & Tseng, S. C. Amniotic membrane transplantation for severe neurotrophic corneal ulcers. *Br. J. Ophthalmol.* **84**, 826–833 (2000).
21. Yildiz, E. H. *et al.* Amniotic Membrane Transplantation: Indications and Results. *Eur. J. Ophthalmol.* **18**, 685–690 (2008).
22. Meller, D. *et al.* Amniotic membrane transplantation for acute chemical or thermal burns. *Ophthalmology* **107**, 980–989 (2000).
23. Bourne, G. THE FOETAL MEMBRANES A Review of the Anatomy of Normal Amnion and Chorion and Some Aspects of Their Function. *POSTGRAD. MED.* **38**, 193– (1962).
24. Solomon, A. *et al.* Amniotic membrane grafts for nontraumatic corneal perforations, descemetocles, and deep ulcers. *Ophthalmology* **109**, 694–703 (2002).
25. Paolin, A. *et al.* Amniotic membranes in ophthalmology: long term data on transplantation outcomes. *Cell Tissue Bank.* **17**, 51–8 (2016).
26. Kaup M, Redbrake, C., Plange, N., Arend, K. . & Remky, A. Amniotic membrane transplantation in severe ocular surface disorders. *Eur. J. Ophthalmol.* **18**, 691–694 (2008).
27. de Farias, C. C., Allemann, N. & Gomes, J. Á. P. Randomized Trial Comparing Amniotic Membrane Transplantation with Lamellar Corneal Graft for the Treatment of Corneal Thinning. *Cornea* **35**, 438–444 (2016).
28. Majumdar, S. *et al.* Cyclodextrin Modulated Type I Collagen Self-Assembly to Engineer Biomimetic Cornea Implants. *Adv. Funct. Mater.* **28**, 1804076 (2018).
29. Sorkio, A. *et al.* Human stem cell based corneal tissue mimicking structures using laser-assisted 3D bioprinting and functional bioinks. *Biomaterials* **171**, 57–71 (2018).
30. Koivusalo, L. *et al.* Tissue adhesive hyaluronic acid hydrogels for sutureless stem cell delivery and regeneration of corneal epithelium and stroma. *Biomaterials* **225**, 119516 (2019).
31. Ullah, H., Wahid, F., Santos, H. A. & Khan, T. Advances in biomedical and pharmaceutical applications of functional bacterial cellulose-based nanocomposites. *Carbohydr. Polym.* **150**, 330–352 (2016).

32. de Oliveira Barud, H. G. *et al.* A multipurpose natural and renewable polymer in medical applications: Bacterial cellulose. *Carbohydr. Polym.* **153**, 406–420 (2016).
33. Gonçalves, S. *et al.* Bacterial Cellulose As a Support for the Growth of Retinal Pigment Epithelium. *Biomacromolecules* **16**, 1341–1351 (2015).
34. Czaja, W., Krystynowicz, A., Bielecki, S. & Brown, R. M. Microbial cellulose - The natural power to heal wounds. *Biomaterials* **27**, 145–151 (2006).
35. Kwak, M. H. *et al.* Bacterial cellulose membrane produced by *Acetobacter* sp. A10 for burn wound dressing applications. *Carbohydr. Polym.* **122**, 387–398 (2015).
36. Li, Y. *et al.* Evaluation of the Effect of the Structure of Bacterial Cellulose on Full Thickness Skin Wound Repair on a Microfluidic Chip. *Biomacromolecules* **16**, 780–789 (2015).
37. Robotti, F. *et al.* Microengineered biosynthesized cellulose as anti-fibrotic in vivo protection for cardiac implantable electronic devices. *Biomaterials* **229**, 119583 (2020).
38. Fey, C. *et al.* Bacterial nanocellulose as novel carrier for intestinal epithelial cells in drug delivery studies. *Mater. Sci. Eng. C* **109**, 110613 (2020).
39. Weyell, P. *et al.* Tailor-made material characteristics of bacterial cellulose for drug delivery applications in dentistry. *Carbohydr. Polym.* **207**, 1–10 (2019).
40. Bacakova, L. *et al.* Versatile Application of Nanocellulose: From Industry to Skin Tissue Engineering and Wound Healing. *Nanomaterials* **9**, 164 (2019).
41. Lima, F. de M. T. de *et al.* Biocompatible bacterial cellulose membrane in dural defect repair of rat. *J. Mater. Sci. Mater. Med.* **28**, (2017).
42. Anton-Sales, I., Beekmann, U., Laromaine, A., Roig, A. & Kralisch, D. Opportunities of Bacterial Cellulose to Treat Epithelial Tissues. *Curr. Drug Targets* **20**, 808–822 (2019).
43. Laromaine, A. *et al.* Free-standing three-dimensional hollow bacterial cellulose structures with controlled geometry via patterned superhydrophobic–hydrophilic surfaces. *Soft Matter* **14**, 3955–3962 (2018).
44. Abol-Fotouh, D. *et al.* Farming thermoelectric paper. *Energy Environ. Sci.* **12**, 716–726 (2019).
45. Azuara-Blanco, A., Pillai, C. T., Dua, H. S. & Azuara-Blanco A, Pillai CT, D. H. Amniotic membrane transplantation for ocular surface reconstruction. *Br. J. Ophthalmol.* **83**, 399–402 (1999).
46. Zeng, M., Laromaine, A. & Roig, A. Bacterial cellulose films: influence of bacterial strain and drying route on film properties. *Cellulose* **21**, 4455–4469 (2014).
47. Pei, Y. *et al.* Effectively promoting wound healing with cellulose/gelatin sponges constructed directly from a cellulose solution. *J. Mater. Chem. B* **3**, 7518–7528 (2015).
48. Küng, F., Schubert, D. W., Stafiej, P., Kruse, F. E. & Fuchsluger, T. A. A novel suture retention test for scaffold strength characterization in ophthalmology. *Mater. Sci. Eng. C* **69**, 941–946 (2016).

49. Jorfi, M. & Foster, E. J. Recent advances in nanocellulose for biomedical applications. *J. Appl. Polym. Sci.* **132**, 1–19 (2015).
50. Willoughby, C. E., Batterbury, M. & Kaye, S. B. Collagen corneal shields. *Surv. Ophthalmol.* **47**, 174–82 (2002).
51. Anton-Sales, I., Roig-Sanchez, S., Sánchez-Guisado, M. J., Laromaine, A. & Roig, A. Bacterial Nanocellulose and Titania Hybrids: Cytocompatible and Cryopreservable Cell Carriers. *ACS Biomater. Sci. Eng.* **6**, 4893–4902 (2020).
52. Beekmann, U. *et al.* Process control and scale-up of modified bacterial cellulose production for tailor-made anti-inflammatory drug delivery systems. *Carbohydr. Polym.* **236**, 116062 (2020).
53. Osorio, M. *et al.* Ex Vivo and In Vivo Biocompatibility Assessment (Blood and Tissue) of Three-Dimensional Bacterial Nanocellulose Biomaterials for Soft Tissue Implants. *Sci. Rep.* **9**, 10553 (2019).
54. Martínez Ávila, H. *et al.* Novel bilayer bacterial nanocellulose scaffold supports neo-cartilage formation in vitro and in vivo. *Biomaterials* **44**, 122–133 (2015).
55. Costa, A. F. S., Almeida, F. C. G., Vinhas, G. M. & Sarubbo, L. A. Production of Bacterial Cellulose by *Gluconacetobacter hansenii* Using Corn Steep Liquor As Nutrient Sources. *Front. Microbiol.* **8**, 2027 (2017).
56. Borzani, W. & de Souza, S. J. Mechanism of the film thickness increasing during the bacterial production of cellulose on non-agitated liquid media. *Biotechnol. Lett.* **17**, 1271–1272 (1995).
57. Wang, S. *et al.* Transparent, Anisotropic Biofilm with Aligned Bacterial Cellulose Nanofibers. *Adv. Funct. Mater.* **28**, 1707491 (2018).
58. Own data, not published.
59. Moritz, S. *et al.* Active wound dressings based on bacterial nanocellulose as drug delivery system for octenidine. *Int. J. Pharm.* **471**, 45–55 (2014).
60. Picheth, G. F. *et al.* Lysozyme-triggered epidermal growth factor release from bacterial cellulose membranes controlled by smart nanostructured films. *J. Pharm. Sci.* **103**, 3958–3965 (2014).
61. Tronser, T., Laromaine, A., Roig, A. & Levkin, P. A. Bacterial Cellulose Promotes Long-Term Stemness of mESC. *ACS Appl. Mater. Interfaces* **10**, 16260–16269 (2018).
62. Taokaew, S., Phisalaphong, M. & Newby, B.-M. Z. Modification of Bacterial Cellulose with Organosilanes to Improve Attachment and Spreading of Human Fibroblasts. *Cellulose* **22**, 2311–2324 (2015).
63. Bodin, A. *et al.* Tissue-engineered conduit using urine-derived stem cells seeded bacterial cellulose polymer in urinary reconstruction and diversion. *Biomaterials* **31**, 8889–8901 (2010).

64. Gonçalves, S. *et al.* Acetylated bacterial cellulose coated with urinary bladder matrix as a substrate for retinal pigment epithelium. *Colloids Surfaces B Biointerfaces* **139**, 1–9 (2016).
65. Jirsova, K. & Jones, G. L. A. Amniotic membrane in ophthalmology: properties, preparation, storage and indications for grafting—a review. *Cell Tissue Bank*. **18**, 193–204 (2017).
66. Shirzaei Sani, E. *et al.* Sutureless repair of corneal injuries using naturally derived bioadhesive hydrogels. *Sci. Adv.* **5**, 1281 (2019).
67. Islam, M. M. *et al.* Biomaterials-enabled cornea regeneration in patients at high risk for rejection of donor tissue transplantation. *npj Regen. Med.* **3**, (2018).
68. Roig-Sanchez, S. *et al.* Nanocellulose films with multiple functional nanoparticles in confined spatial distribution. *Nanoscale Horizons* **4**, 634–641 (2019).
69. U.S. Department of Health and Human Services *et al.* *Guidance for Industry Pyrogen and Endotoxins Testing: Questions and Answers.* (2012).
70. Pascolini, D. & Mariotti, S. P. Global estimates of visual impairment: 2010. *Br. J. Ophthalmol.* **96**, 614–618 (2012).
71. Gain, P. *et al.* Global survey of corneal transplantation and eye banking. *JAMA Ophthalmol.* **134**, 167–173 (2016).
72. Kralisch, D., Hessler, N., Klemm, D., Erdmann, R. & Schmidt, W. White biotechnology for cellulose manufacturing—the HoLiR concept. *Biotechnol Bioeng* **105**, 740–747 (2010).
73. Lewis, J. S., Barani, Z., Magana, A. S. & Kargar, F. Studies on bacterial cellulose/poly vinyl alcohol (BC/PVA) hydrogel composites as tissue-engineered corneal stroma. *Biomed. Mater.* **15**, (2019).
74. Wang, J., Gao, C., Zhang, Y. & Wan, Y. Preparation and in vitro characterization of BC/PVA hydrogel composite for its potential use as artificial cornea biomaterial. *Mater. Sci. Eng. C* **30**, 214–218 (2009).
75. Sepúlveda, R. V. *et al.* Bacterial cellulose and bacterial cellulose/polycaprolactone composite as tissue substitutes in rabbits' cornea. *Pesq. Vet. Bras* **36**, 986–992 (2016).
76. Carvalho, J. P. F. *et al.* Nanocellulose-based patches loaded with hyaluronic acid and diclofenac towards aphthous stomatitis treatment. *Nanomaterials* **10**, (2020).
77. Silva, N. H. C. S. *et al.* Topical drug delivery systems based on bacterial nanocellulose: Accelerated stability testing. *Int. J. Mol. Sci.* **21**, (2020).

Chapter 5

In vivo evaluation of bacterial nanocellulose for hernia repair

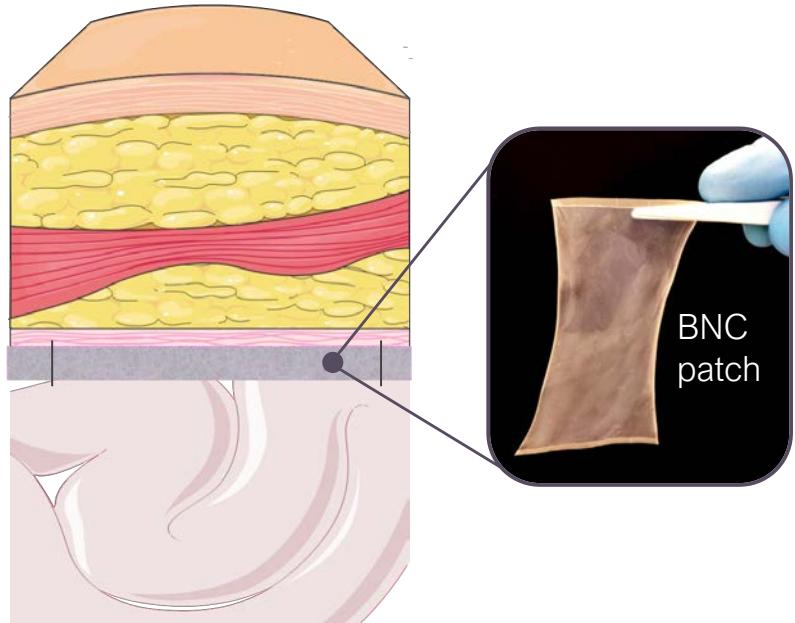


Figure 1: Visual summary of Chapter 5. The proposed use of BNC patches to reinforce the abdominal wall after a hernia repair surgery.

Chapter introduction

This chapter devotes efforts to the applicability of BNC as a non-resorbable patch to repair internal tissues. This possibility was mentioned already in Chapter 1 and could be materialized through a collaboration with the R+D department of B. Braun Surgical in Spain (<https://www.bbraun.es/es.html>) specialized in wound closure technologies.

A tissue reinforcement is often required in the surgical management of abdominal hernias. The term hernia derives from the Greek “hernios” meaning “bud” or “sprout” and refers to a protrusion caused by a part of the bowel or peritoneum –the membrane lining the abdominal cavity– pushing through a gap in the abdominal wall. The prevalence of hernias is extremely high; affecting 5% of the general population at least once during their lifetime¹. Depending on its top-down location in the body, hernias can be classified as²:

- Epigastric: the protrusion occurs between the breastbone and the belly button.
- Umbilical: the weak point appears near the belly button.
- Incisional: the hernia happens in scar tissue caused by a previous surgical incision.
- Inguinal: this is the most common type of hernia and appears above the inguinal ligament, right above the groin.
- Femoral: the internal organs poke through in the upper part of the thigh, below the inguinal ligament.

Strengthening permanently the abdominal wall with a thin surgical mesh –known as hernioplasty– has become the mainstay for hernia repair (Figure 2). Hernioplasty has prevailed over approaches relying on sutures to close the defect, owing to the reduced recurrences achieved with this method.^{3,4} The majority of the implantable meshes are constructed from synthetic non-resorbable polymers and will remain indefinitely inside the body. Nevertheless, hernia repair surgery is not exempt from post-operative complications. Adverse events can be related to infections or hernia reappearances, but also arise from intraperitoneal adhesions which are formed by scar-like tissue sticking together the implanted mesh and the adjacent organs⁵. These adhesions are a major cause of chronic pain after hernia repair and a common trigger of secondary surgeries. Consequently, research and development of anti-adhesive implants⁶ accounts for a pressing need in the field.

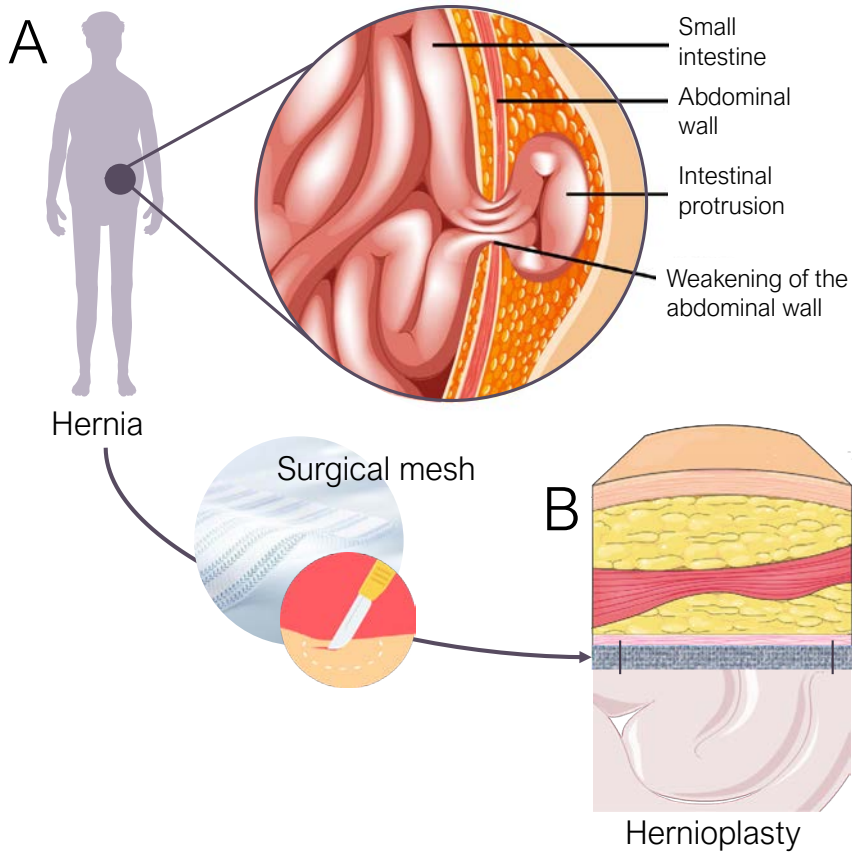


Figure 2: Schematics of hernia management. A) Abdominal hernias appear as protrusions of the internal organs through debilitated areas of the abdominal wall. B) The most common approach for hernia repair is the implantation of a surgical mesh serving as a lifelong tissue reinforcement. The illustration contains modified content from <https://www.freepik.es/> and <https://smart.servier.com/>.

The publication included in this chapter “*In vivo* Soft Tissue Reinforcement with Bacterial Nanocellulose” exposes preclinical data on the assessment of BNC as a candidate biomaterial for hernia repair. This study aimed at mitigating adhesion-related complications employing BNC as an anti-adhesive barrier and is co-authored by the B. Braun Surgical researchers Kamelia Traeger, Dr Christine Weis and Dr Pau Turón. The first part of the work investigates the mechanical properties of different BNC configurations which are discussed in more detail in the doctoral thesis of my colleague Soledad Roig-Sanchez.

Publication 5: *In vivo* Soft Tissue Reinforcement with Bacterial Nanocellulose

Irene Anton-Sales[‡], Soledad Roig-Sanchez[‡], Kamelia Traeger, Christine Weis, Anna Laromaine, Pau Turon and Anna Roig. *Biomat. Sci.* 2021. **9**, 3040–3050 Published in open access by The Royal Society of Chemistry: <https://pubs.rsc.org/en/content/articlelanding/2021/bm/d1bm00025j#!divAbstract>

[‡] Authors with equal contribution

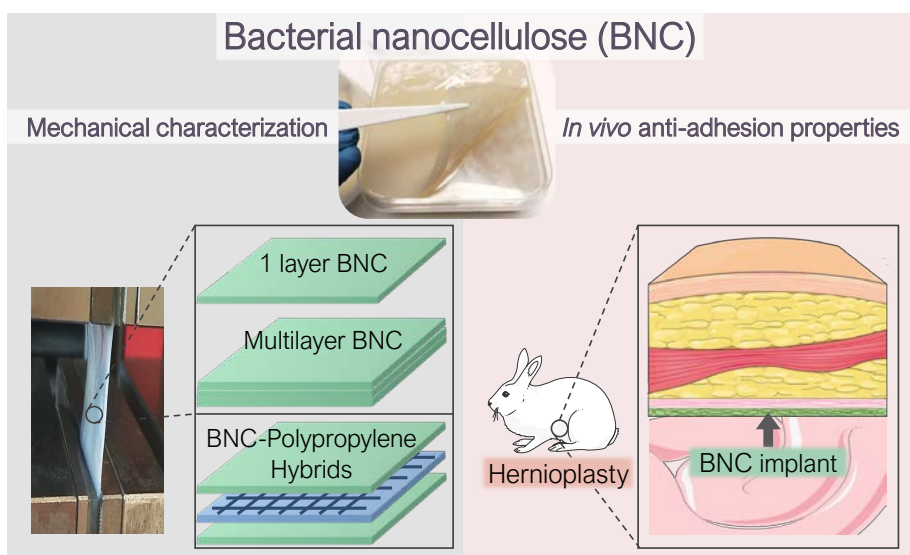


Figure 3: Graphical abstract of Publication 5.

Keywords

Bacterial nanocellulose, abdominal hernia, surgical mesh, mechanical properties, anti-adherent properties.

Abstract

The use of surgical meshes to reinforce damaged internal soft tissues has been instrumental for successful hernia surgery; a highly prevalent condition affecting yearly more than 20 million patients worldwide. Intraperitoneal adhesions be-

tween meshes and viscera are one of the most threatening complications, often implying reoperation or side effects such as chronic pain and bowel perforation. Despite recent advances in the optimization of mesh porous structure, incorporation of anti-adherent coatings or new approaches in the mesh fixation systems, clinicians and manufacturers are still pursuing an optimal material to improve the clinical outcomes at a cost-effective ratio.

Here, bacterial nanocellulose (BNC), a bio-based polymer, is evaluated as a soft tissue reinforcement material regarding mechanical properties and *in vivo* anti-adhesive performance. A double-layer BNC laminate proved sufficient to meet the standards of mechanical resistance for abdominal hernia reinforcement meshes. BNC-polypropylene (BNC-PP) composites incorporating a commercial mesh have also been prepared. The *in vivo* study of implanted BNC patches in a rabbit model demonstrated excellent anti-adherent characteristics of this natural nanofibrous polymer 21-days after implantation and the animals were asymptomatic after the surgery. BNC emerges as a novel and versatile hernioplasty biomaterial with outstanding mechanical and anti-adherent characteristics.

Introduction

Abdominal hernias occur when internal organs protrude through weakened zones of the abdominal cavity. To date, surgical intervention is the only effective approach to repair such a highly prevalent condition that yearly affects more than 20 million patients worldwide⁷. Instrumental for successful hernia surgery has been the use of surgical meshes (*i.e.* hernioplasty) to reinforce the damaged region. Those implants are predominantly manufactured from synthetic polymers, mainly polypropylene (PP), and aim at providing mechanical support to the herniated area. Implantation of a non-resorbable PP-mesh has become the standard procedure for hernia repair, however, complications related to mesh implantation such as seroma, adhesions, chronic severe pain and infections are driving constant innovation in the field^{8,9}.

Adhesions developed between PP-mesh and viscera, as a result of tissue reaction due to foreign body implant, are particularly threatening since they often

cause complicated reoperations in the previously implanted area, increasing the surgical risk and the chances of suffering side effects such as chronic pain and bowel perforation¹⁰. High rates of adhesion are reported in approx. 15% of the cases one year after surgery, resulting in a high burden to healthcare systems¹¹. Aiming to reduce the complications caused by those intraperitoneal adhesions, research efforts have been focused on improving the characteristics of PP meshes. Strategies include the optimization of mesh porous structure¹², incorporation of anti-adherent coatings and improvements of mesh fixation systems (*i.e.* glueing)^{13,14}. Besides, multi-component grafts have been advocated as a well-suited strategy to isolate the PP mesh from the viscera by adding an additional layer of a synthetic^{15,16} or natural biomaterial^{17,18} that acts as an anti-adherent barrier. Despite recent advances, clinicians and manufacturers are still pursuing an optimal mesh to improve the clinical outcome and the cost-effectiveness ratio of hernioplasty procedures by leveraging the selection of materials, porous structure, mechanical resistance, anti-adhesive properties, biocompatibility, long term mechanical stability, tissue integration and conformability¹.

Considering the requirements of hernia repair implants, the bio-based polymer bacterial nanocellulose (BNC) could be deemed as a strong candidate for the above-mentioned tissue reinforcement application¹⁹. BNC is biotechnologically produced as a highly pure, non-soluble nanocellulose fibrillary network entrapping a large amount of liquid and exhibiting excellent mechanical properties^{20–22}. These attributes have enabled an ever-increasing number of bio-applications in wound dressing and drug delivery^{23–25}. Moreover, BNC is emerging as a high-performing alternative to repair other defects where non-biodegradable implants are desirable, such as damage of the dura mater²⁶, the eardrum²⁷ or as an anti-fibrotic agent for cardiac implants²⁸. As for soft tissue reinforcement, a hybrid biomaterial combining BNC with PP-meshes and its *in vitro* low adhesion properties has recently been described²⁹. Besides, Zharikov and co-workers compared the anti-adhesive behaviour of BNC with PP meshes revealing a lower occurrence of adhesion in BNC-implanted dogs together with the absence of infections³⁰. For that study, wet native BNC pellicles were employed and no mechanical tests were carried out. In more recent work, Rauchfuß *et al.* tested two surgical methods to implant wet BNC into the abdominal wall of rats³¹. These authors observed adhe-

sion formation when using BNC as an abdominal wall replacement together with a tissue reaction assessed to be of low clinical significance. Interestingly, this work provides mechanical testing of BNC after explantation showing variable values and calling for future work on the suitability of BNC for hernia repair in terms of mechanical properties. These studies, although preliminary, concur with the absence of major postoperative complications and emphasize the underexploited potential of BNC in herniology.

Our work aims at providing further insight into the prospects of BNC for hernia repair surgery. To expand on the mechanical suitability of BNC for soft tissue reinforcement, the mechanical performance of several types of BNC implants –dry and wet forms as well as single to triple-layered BNC constructs– are evaluated. Furthermore, an *in vivo* study based on a novel animal model (rabbit) and the implantation of dry BNC is presented to demonstrate the anti-adherence properties of BNC.

Materials and Methods

Bacterial nanocellulose (BNC) production

BNC films were obtained as previously described in Roig-Sanchez S. *et al.*³². In brief, the *Komagataeibacter xylinus* (*K. xylinus*) strain (NCIMB 5346, from CECT, Spain) was inoculated on 6 ml of Hestrin-Schramm (HS) fresh medium and expanded for 7 days at 30 °C. HS medium was prepared as follows: 5 g peptone, 5 g yeast, 20 g dextrose (Conda Lab), 1.15 g citric acid and 6.8 g Na₂HPO₄·12H₂O (Sigma-Aldrich) per 1 L of Milli-Q (MQ) water. Then, 0.5 ml of the mixture was transferred to 4.5 ml of fresh HS medium and let to proliferate for another three days. Finally, bacteria were diluted to a proportion 1:14 inoculum: HS medium and 65 ml were cultivated for 6 days in 12x12 cm plates (Labbox polystyrene Petri dishes) at 30 °C. The square BNC pellicles formed at the liquid-air interface of the wells were harvested and cleaned 10 minutes in a 50% ethanol-water solution, twice with boiling water for 20 min and twice with 0.1 M NaOH (Sigma-Aldrich) at 90 °C for 20 min. Lastly, the films were washed with MQ water until neutralization and sterilized by autoclave (121 °C, 20 min). To obtain

the dry and flat BNC films used in the mechanical and *in vivo* tests, BNC hydrogels were placed between two Teflon papers at 60 °C and with a 2 kg weight on top for 12 h as previously described³². Systems with two and three BNC layers were prepared by drying size-matched BNC pellicles in close contact following the same procedure. To achieve a smooth interface between the BNC films, the superficial water was removed by blotting BNC with filter paper and air bubble formation was avoided by applying manual pressure. BNC-PP composites were prepared similarly by placing fragments of PP meshes (Optilene® Mesh Elastic and Optilene® Mesh LP both from B. Braun Surgical, S.A.U., Spain), knitted with different pore sizes, in between two wet BNC films. The size of the BNC layers was larger than the PP meshes to allow the self-adhesion between BNC films to occur during drying.

Scanning Electron Microscopy (SEM)

For the SEM characterization of the native wet BNC structure, BNC hydrogels were supercritically dried (SC). For that, the as-obtained BNC films were placed within filter paper sheets and were subjected to a water-to-ethanol solvent exchange process. After two transfers of 3 h in absolute ethanol, the films were moved to a fresh ethanol bath, kept overnight and the resulting alcogel was dried by SC drying. SC drying was performed on a 300 ml capacity autoclave filled with ethanol which was pressurized to 100 bar at RT. Liquid CO₂ was dispensed for 1.5 h with a flow of 1 kg/h to exchange the solvent. Then, the reactor was heated up to 45 °C to reach supercritical conditions and supercritical CO₂ was pumped for 1 h keeping the same flow rate. Finally, the vessel was slowly depressurized to avoid pore collapse and BNC aerogels were obtained. For the SEM analysis of dry films, BNC hydrogels were dried as described in The previous section.

FEI Magellan 400L XHR SEM under a high vacuum, with an acceleration voltage of 2 kV, current of 0.10 nA and a working distance of 5 mm was used to study the morphology of SC dried and dry BNC. The material was fixed with adhesive carbon tape on top of aluminium SEM holders. Dry BNC was sputtered with 5 nm Pt. BNC fibre diameter was calculated as the mean of 100 measurements obtained using Image-J software.

Cross-section images of multi-layered constructs were obtained with FEI Quanta 650GEG-ESEM under low vacuum conditions, an acceleration voltage of 20 kV, an electron beam spot of 4–5 and a working distance of 10 mm. Samples were cut with a Teflon coated blade (Personna GEM single edge, 3-facet stainless steel, 0.23 mm) and placed on holders with a 90° tilt.

Mechanical studies

Each BNC sheet was cut in 20x50 mm pieces and the weight, size and thickness were measured with an Acculab Atilon ATL-244-1 analytical balance, Stanley Millesimal rule and Mitutoyo 543-250B micrometre respectively. Results were computed from five replicas. Surface weight was calculated as the ratio between weight and area. Wet BNC samples were deposited on a filter paper to remove the excess water and measurements were performed when the material was still wet. The thickness of the films was measured in the middle of the specimens. For wet samples, the plunger of the micrometre was lifted and lowered three times and the thickness was obtained when the value was stable for more than 2 s during the third time.

Zwick Z2.5 dynamometer with a load cell of 2.5 kN was used for tensile experiments. The clamps were metallic with a pneumatic flat rubber part in contact with the sample. The test velocity was 100 mm/min, the pressure of the clamps was 6 bars and the distance between them was 20 mm. The preload applied was 0.05 N. Strain and resistance to tearing (F_{\max}) values were acquired.

Multi-layered systems were immersed in a 0.9% NaCl solution for 5 min for rehydration before the tensile study. Excess of liquid was removed as described before and water uptake (H_2O_{up}) percentage was calculated as $(mw-md)/md \cdot 100$, where mw is the weight of the wet sample after hydration and md is the weight of the dry sample before hydration. Surface weight, calculated as the ratio between dry weight and area, and thickness were obtained before the rehydration.

In vivo study

A scheme of the steps to BNC implantation is depicted in Figure 7A. This study was conducted by FREY-TOX GmbH (Herzberg, Germany), a DAkkS (national

accreditation body of Germany) accredited laboratory according to EN ISO/IEC 17025 and European guidelines 93/42/EWG as well as 90/385/EWG.

BNC implant preparation

Dry BNC patches were cut to a size of 7x3 cm with scissors and sterilized by a routine ethylene oxide (EtOx) cycle from B. Braun Surgical S.A.U. to sterilise non-absorbable meshes. Sterility was confirmed by submerging the EtOx-treated BNC into liquid culture medium for 14 days without detecting the appearance of turbidity. The resistance of the biomaterial to the EtOx cycle was assessed by Fourier-Transform Infrared Spectroscopy (FTIR) (Figure S1).

In vivo model

The *in vivo* implantation study was performed in five female SPF albino rabbits of the stock New Zealand White (Envigo, 58" Venray Netherlands). The animals had a bodyweight from 3.4 to 4.2 kg. An acclimatization period of at least 5 days was allowed. General anaesthesia was induced by intramuscular injection of 35-40 mg/kg ketamine and 5-6 mg/kg xylazine (Serumwerke Bernburg AG, Bernburg, Germany). This rabbit species was chosen because of its convenient body proportion and proved suitability for studying hernia repair materials including meshes³³.

In the literature, it is described that most post-surgical adhesion formation takes place approximately until day 8 post-implantation³⁴. Hence, the follow-up time was set at 21-days based on our previous work endorsing it as a sufficient period to observe mature adhesions in an advanced healing process as well as to infer the integration of the biomaterial within the abdominal wall³⁵.

Surgical procedure

The operation field was shaved, disinfected and the abdomen was covered in a sterile manner. A median laparotomy was performed and the patches were carefully applied onto the left native abdominal wall between the peritoneum and the visceral organs, avoiding folding of the implants. Subsequently, the BNC patches were fixed by 6 suture stitches with PP (Optilene, B. Braun Surgical, S.A.U., USP 3-0) sutures. The wound was closed with a continuous muscle suture and con-

tinuous intracutaneous sutures. The skin was glued with Histoacryl®, a cyanoacrylate-based tissue glue (B. Braun Surgical, S.A.U., Spain). After the follow-up time of 21 days, the rabbits were anaesthetized (Ketamine 40 mg/kg body weight and Xylazine 6 mg/kg body weight) and subsequently euthanized (T61 intravenously).

Once the animals were sacrificed, tissue integration and adhesion formation were macroscopically examined. During explantation, the application site, as well as the abdomen *in toto*, were macroscopically evaluated. Possibly occurring adhesions were evaluated after dissection regarding their area extension in relation (%) to the total abdominal wall area implanted (7x3 cm). Furthermore, adhesions were defined to the following categories following the Zühlke scores as⁶:

Score I: String adhesions that are easy to separate (blunt detachment)

Score II: Adhesions being partially vascularized causing blunt to sharp detachment

Score III: Adhesions having distinct vascularization, with sharp detachment only

Score IV: Tight adhesions requiring sharp detachment causing damage to the organs

The tissue integration was judged descriptively: no integration; mild integration = slight pull for uplifting the patch from the abdominal wall; and distinct integration = distinct pull uplifting from the abdominal wall with visible adhesion and vascularization.

Histological analysis

The central area of the implant (size approximately 1x3 cm) was extirpated and fixed on 4% buffered formalin for histological examination. Tissue sections were cut with a microtome and processed following standard procedures³⁷. Haematoxylin/Eosin (HE) was used as a general staining for judgment of tissue integration.

Statistical analysis

Quantitative data were analysed with GraphPad Prism 8.0.2 software using ordinary one-way ANOVA followed by Tukey's multiple comparison test. Statistical significance was accepted at 0.05 and data are represented as means \pm standard deviation.

Results

Single layered BNC patches

Firstly, single-layer BNC patches intended for hernioplasty applications were produced and characterized in terms of their macroscopic features, thickness and mechanical properties. Figure 4 displays the simultaneous production of seventy-two 12x12 cm-BNC films summing up $>1 \text{ m}^2$ of the biomaterial as a venue to attain increased amounts of BNC at a laboratory level. After 6 days at $30 \text{ }^\circ\text{C}$, continuous BNC pellicles formed at the surface of the liquid culture (Figure 4B). Upon cleaning and removing organic residues, a change in colour (from yellowish to translucent white) was appreciated (Figure 4C).

Macro and microstructure of BNC in wet and dry conditions are depicted in Figure 4 (C-D) and (E-F) respectively. Since the morphology of wet as-synthesized BNC samples could not be observed with enough resolution using SEM, a supercritical (SC) dried film was used as this drying method maintains with high-reliability the architecture of native samples³⁸. As exposed in Figure 4D, SC-dried BNC films are highly porous and composed of entangled cellulose nanofibers of $15 \pm 5 \text{ nm}$ in diameter. Upon drying at $60 \text{ }^\circ\text{C}$, BNC films become more transparent and thinner while the fibres compact and the porosity decreases (see inset in Figure 4F).

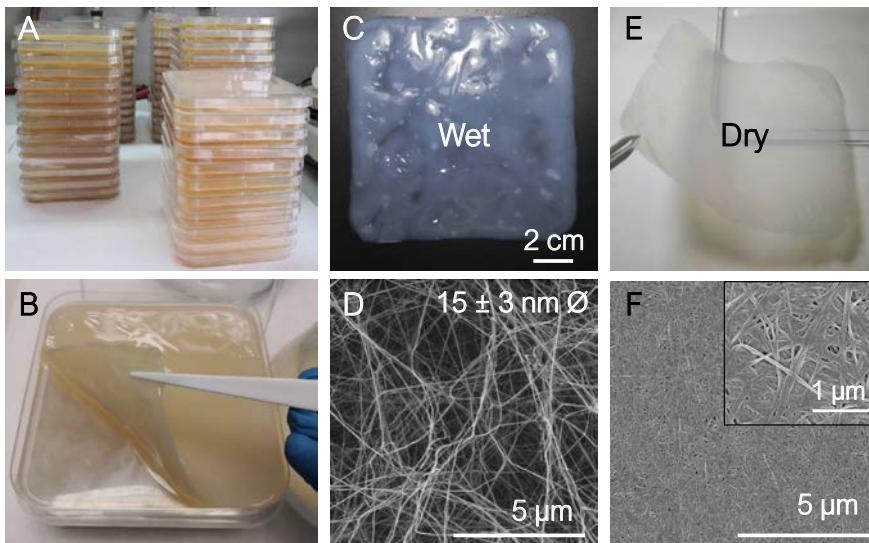


Figure 4. BNC synthesis, wet and dry states and microstructure. A) Numbering up BNC production at laboratory level. B) A native wet BNC pellicle. C) Wet form of BNC after clea-

ning and autoclaving. D) SEM image of an SC dried BNC sample mimicking the microstructure of a wet BNC film. E) Dry BNC film. F) SEM image of the compact nanofiber conformation for dry BNC. Inset: Higher magnification to better visualize the nanofibers arrangement.

High tensile stress is a basic demand for a biomaterial proposed for soft tissue reinforcement applications. Tensile stress $\geq 16\text{N/cm}$ has been used as a benchmark for safe reinforcement of the abdominal wall³⁹. Accordingly, tensile strength experiments were conducted to test the mechanical properties of BNC films using this value as a threshold. Figure 5 shows the mean values obtained from five BNC samples in dry (pink) and wet (blue) conditions. Before mechanical characterization, the original BNC films (12x12 cm) were cut in 20x50 mm samples and their thickness and surface weight (weight per area) were measured in both wet and dry forms. The surface weight is approximately 60 times higher for wet films than for its dried counterparts ($654 \pm 153\text{ g/m}^2$ wet film; $11 \pm 1\text{ g/m}^2$ dry film). Upon drying, 98% of the surface weight is lost as the water is removed, indicating that cellulose nanofibers account for only 2% of the wet BNC mass. These results are in agreement with the thickness measurement as BNC films experience a decrease in thickness of more than 96% when dehydrated (from $445 \pm 91\text{ }\mu\text{m}$ wet film; to $16 \pm 8\text{ }\mu\text{m}$ dry film). For the mechanical characterization, the 20x50 mm BNC pieces were clamped with metallic clips containing a pneumatic flat rubber part to prevent the sliding of the samples (see the image in Figure 5). The resistance to tear (F_{max}) of wet BNC is approximately 60% than that of dry BNC ($5 \pm 1\text{ N/cm}$ and $8 \pm 3\text{ N/cm}$ respectively). On the contrary, the maximum strain increases 12-fold in wet conditions ($24 \pm 2\%$ in comparison to $2.1 \pm 0.5\%$ for dry BNC). These data indicate that our single-layer BNC films (neither in wet nor in the dry state) do not meet the minimum mechanical resistance requirements of 16 N/cm to be used as a PP mesh substitute.

Laminated BNC patches and hybrids

To increase the mechanical resistance of the BNC patches, two strategies were followed: i) preparation of multi-layered BNC meshes and ii) combination of BNC with standard PP meshes. Our previous work showed that robust BNC stacks that endure hard manipulation even upon rehydration can be created by pilling up and drying together (*i.e.* applying weight) several wet BNC films. Upon

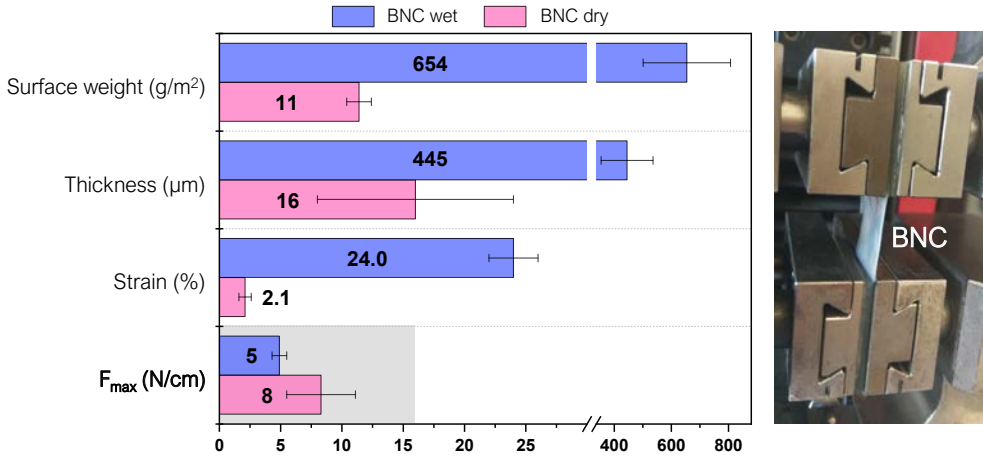


Figure 5: Mechanical properties of single-layer BNC patches in wet and dry conditions and the experimental setup. Single-layered BNC implants did not meet the acceptance criteria of the tensile stress resistance set at $F_{max}=16$ N/cm (grey area). Statistically significant differences between dry and wet BNC samples were found for all the studied parameters except for the F_{max} (P-values <0.001), (n=5).

drying, hydrogen bonding between the fibres of two films confers stability to the stack. The multilayers do not suffer delamination even when immersed in a liquid solution³². Accordingly, laminated patches were created by assembling 2 or 3 wet BNC films and subjected to the same mechanical characterization as the single BNC layers. Figure 6A depicts the results of 2 and 3 layers of BNC (mean values of n=5). All the obtained values were substantially higher than those of a single layer. As expected, thickness and surface weight increased as more layers were added. More precisely, thickness rose from 16 ± 8 µm (1 layer) to 23 ± 2 µm (2 layers) and 34 ± 6 µm (3 layers); and surface weight from 11 ± 1 g/m² (1 layer) to 20 ± 1 g/m² (2 layers) and 28 ± 2 g/m² (3 layers). The multilayers were then rehydrated in a 0.9% NaCl solution for 5 min before performing mechanical studies to better simulate the physiological conditions. As shown in Figure 6A, the laminate BNC presents a maximum strain of 14 ± 1 and 12 ± 3 % and resistance to tearing of 26 ± 6 and 32 ± 9 N/cm for 2 and 3 layers respectively. For the double-layered BNC, the maximum strain increased almost 7-fold compared to a single BNC layer (dry form) while, the resistance to tear increased more than 3-fold. As expected, the triple-layer renders an even higher improvement in mechanical resistance (4-fold compared to a dry single layer). Note that the values of both the double

and triple-layer laminates are above the set threshold of 16 N/cm for abdominal wall reinforcement applications. Improvements in mechanical properties (both the % of strain and the max force tolerated) of the stacked-BNC are statistically significant (P -values <0.001) when compared to the BNC single-layer. Remarkably, during the tensile test, no peeling or separation of the layers was observed. This feature is also exemplified in Figure 6B where a bi-layered sturdy BNC patch is shown. Both images (the macrostructure image and the cross-section SEM picture (inset)) illustrate the homogeneous adhesion between two BNC films. Moreover, the original transparency was maintained without macroscopic air bubbles trapped in the interface and the boundary area between the two BNC films could not be identified by SEM. Figure S2 gathers the values obtained for the mechanical properties of all the studied systems for a clearer comparison.

Finally, BNC hybrid constructs incorporating commercial PP meshes were considered. Figure 6C shows frontal and lateral pictures of a preliminary prototype of a sandwich-like multilayer composite. The construct was prepared by taking advantage of the above-mentioned self-adhesion property of BNC. Note that the BNC-PP composite firmly incorporates PP meshes with different pore sizes. The thickness of the dry composites varied depending on the incorporated PP material between the BNC layers. That is, for a PP mesh with small pores (named SP-PP) a thickness of $332 \pm 8 \mu\text{m}$ was obtained, while when a PP mesh with bigger pores was employed (BP-PP) thickness increased up to $589 \pm 23 \mu\text{m}$. An SEM cross-section study (Figure 6D) showed good integration of the BP-PP mesh in between the BNC layers. Although the synthetic material did not adhere to the BNC layers, it was immobilized in an envelope-like structure due to the BNC self-adhesion in the contact areas in between the pores of the PP mesh and at the composite's contour (inset Figure 6D). The stability of the hybrid structure was tested by rehydration in water. After 5 days, the moist envelope-like structure was flexible and easily handled without noticeable delamination as depicted in Figure S3.

In vivo studies

Besides mechanical validation, a key characteristic required from soft tissue repair materials is their proficiency in minimizing adhesion-related complications

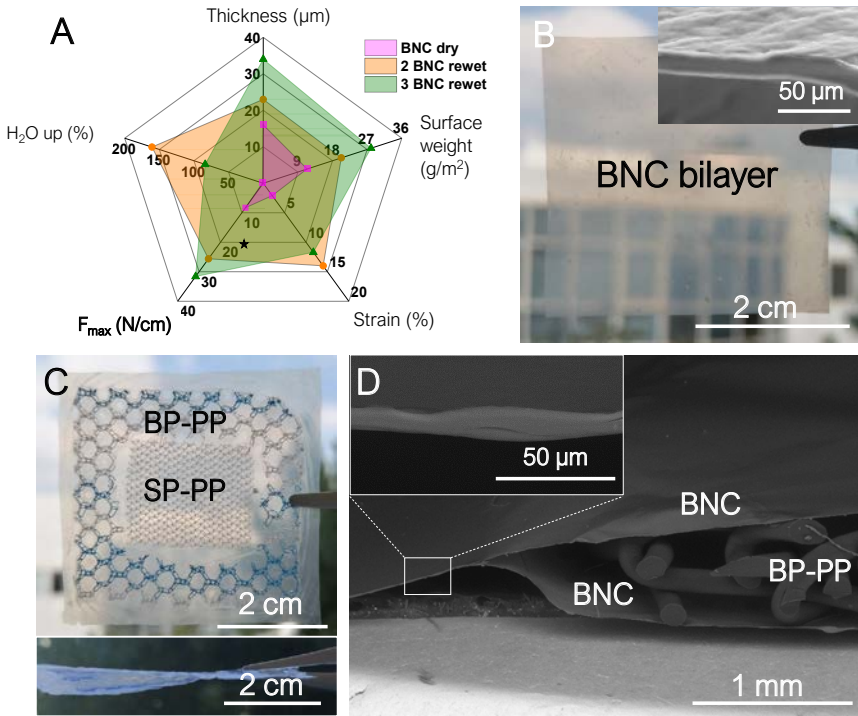


Figure 6: Composite alternatives to increase the mechanical resistance of BNC-based implants. A) Mechanical study of BNC multilayers comprised of 2 or 3 films. ($n=5$) * indicates the resistance to tear threshold for tissue reinforcement materials (16 N/cm). B) Picture of a BNC multilayer formed by 2 dry BNC films. Inset: SEM cross-section image where the interface between the two BNC layers is undetectable. C) Preliminary BNC bilayer combination with PP meshes with different pore sizes. Upper panel: frontal view. Lower panel: a lateral image of the BNC-PP mesh composite. D) SEM cross-section image of the BNC-PP composite. Inset: higher magnification of the cross-section to appreciate the continuous adhesion between BNC layers.

and integration by surrounding tissues. Therefore, the next step was to assess the anti-adhesion properties of BNC with an *in vivo* rabbit model following the implantation process shown in Figure 7A.

Macroscopic evaluation

Dry and sterile single layer BNC patches of 3x7 cm were selected for the *in vivo* study as being the ones with weaker mechanical characteristics and imposing the most stringent conditions. Single-layer BNC patches could be easily handled under operation-room settings, fold-free placing was readily achieved and fixation by suture was performed without complications (Figure 7B). The semi-trans-

parency of BNC was also convenient to avoid unintentional puncturing of blood vessels while suturing. During the application of the BNC patch, careful handling was necessary, nonetheless, the BNC patch allowed the secure application on the abdominal wall; no fracturing of the suture puncture holes was observed and the BNC patches were removable with instruments and repositioned if needed. During the postoperative phase, all animals presented swift recovery. Analgesic treatment was only administered in the first postoperative days and a slight body weight gain was detected.

After the implantation period of 21 days, tissue integration was evaluated using observational criteria during the autopsy. The BNC patches displayed a general good integration to the abdominal wall whereas only marginal areas were not integrated. Adhesion level was examined and scored macroscopically considering prevalence (quantity) and type (quality) of the detected adhesions among BNC implants and the internal organs. In 4 /5 animals adhesions were detected involving approximately 8% of the overall BNC surface. Although some fibrin accumulation and distinct vascularization were observed in all animals, only one rabbit presented a significant adhesion area (20%) as depicted in Figure 7D. Three animals presented adhesions to the greater omentum and one animal to the cecum. Notably, one animal was completely free of adhesions (Figure 7C). The implanted BNC patches were dominated by only one visible layer of fibrin. These macroscopic observations are gathered in Figure S4 and Tables 1 and 2.

Table 1. Individual adhesion observations. Results of the area free of adhesions, adhesion area, adhesion score and tissue integration for each studied animal.

Animal Number	6501	6507	6527	6564	6574
Code	A1	A2	A3	A4	A5
Area free of adhesions approx.	95%	100%	95%	80%	90%
Adhesion area approx.	5% to greater omentum	0%	5% to greater omentum	20% to greater omentum	10% to cecum

Adhesion score (Zühlke scores)	II – blunt to sharp detachment	no adhesions	II – blunt to sharp detachment	IV – sharp detachment	IV – sharp detachment
Tissue integration	mild integration	distinct integration	distinct integration	mild integration	mild integration

Table 2. Overall adhesion observations. Summary of the macroscopic evaluation of adhesions between BNC implants and internal organs.

N°. of animals affected by adhesions	Area (%) free of adhesions	Adhesions area (%)	Organs involved in adhesion processes
4/5	92	8	<ul style="list-style-type: none"> • Greater omentum (3 animals) • Cecum (1 animal)

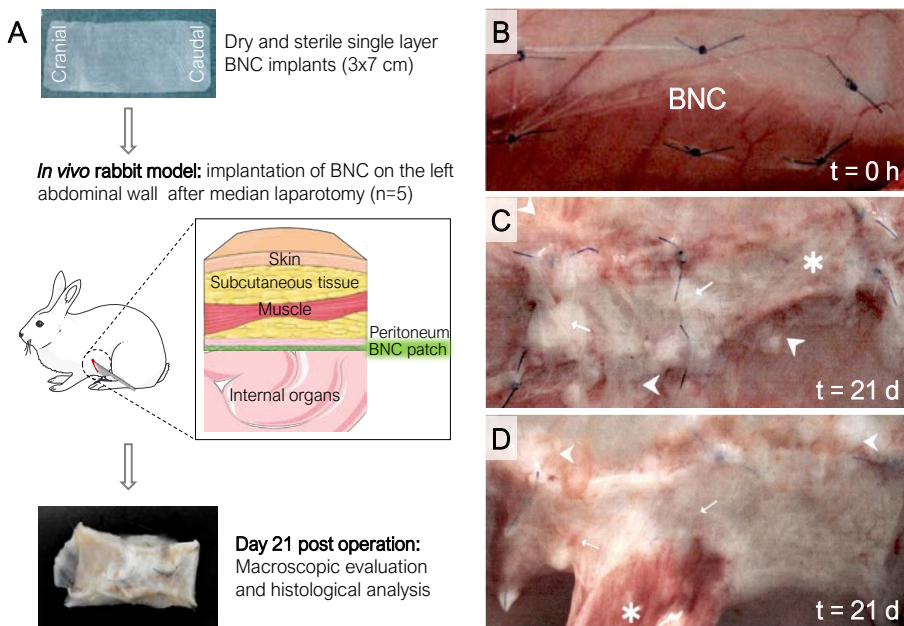


Figure 7. Experimental design, macroscopic evaluation and adhesion assessment for two of the five animals studied. A) Sketch showing the prepared BNC implant, the employed *in vivo* model and the evaluations performed. B) Time 0: BNC patches were applied onto the left abdominal wall and fixed with six suture stitches C) A2 explanted analysis after 21 days (best case scenario). → indicates fibrin accumulation, ▶ the adjacent abdominal wall without adhesions and * marks vascularization. D) A4 explanted analysis after 21 days (worst case scenario). → indicates vascularization, ▶ fibrin accumulations and * corresponds to adhesion.

Histological evaluation

The central area of the implant (size $\sim 1 \times 3$ cm) was extirpated and used for histological examinations. Representative HE-stained tissue sections from the five studied animals are shown in Figure 8. The area surrounding the BNC patches presented a severe diffuse to granulomatous immune cell infiltration involving lymphocytes, heterophilic granulocytes, macrophages and solitary multinucleated giant cells. Also, a moderate active fibroplasia on the implanted zone was noted, as well as a good integration onto the abdominal wall and moderate neovascularization.

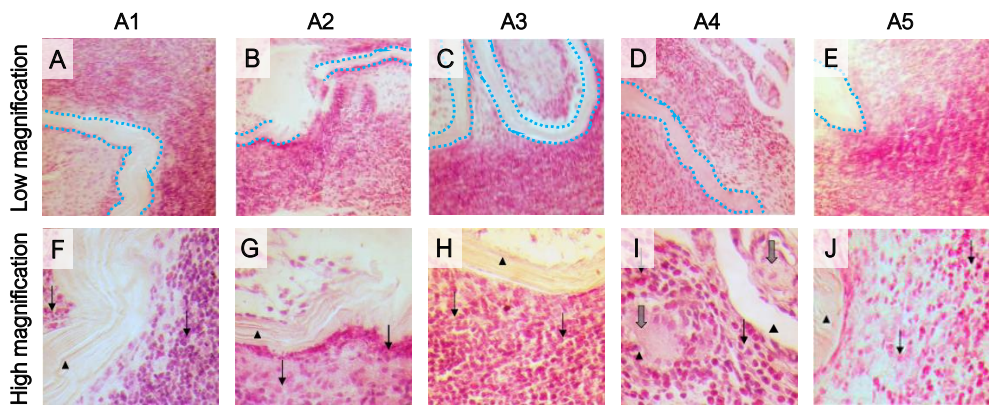


Figure 8. HE-stained tissue sections of the BNC-implanted abdominal walls. A-E: Low magnification images of the five operated rabbits where the BNC implants have been highlighted with a blue dotted line to facilitate interpretation. For all cases, a good integration of the BNC patch together with an inflammatory reaction can be observed. F-J: Zoom-in to better appreciate the BNC implant (▶) and the presence of diverse inflammatory cells (lymphocytes, heterophilic granulocytes and macrophages) surrounding the implant (→). Solitary multinucleated giant cells were observed on A4 (➤).

Discussion

We have investigated BNC patches for soft tissue reinforcement applications by dealing with two clinically relevant parameters; the mechanical resistance of constructs comprising one to three BNC layers and the *in vivo* anti-adherence properties of BNC. Before that, we characterized the BNC patches and present an increased BNC production (up to ~ 1 m²) under laboratory settings to illustrate

the feasibility of an up-scaled fabrication. However, to achieve an industrial manufacturing process, a more advanced system should be implemented such as the pilot-scale production processes reported by Kralisch *et al.*⁴⁰ and Beekmann *et al.*⁴¹

The mechanical characterization of as-synthesized BNC films (wet films) and after drying showed that wet BNC patches are thicker, more brittle but more stretchable than dry BNC patches. This confers to the wet BNC a higher strain but, at the same time, makes the material less resistant to tear. After drying, the water content of BNC decreases drastically and the cellulose nanofibers condense, reducing their porosity²⁰ and their ability to rearrange upon tensile stress application. Thus, the dried form of BNC is stiffer and less stretchable than wet-BNC, making it more suitable for hernioplasty. Although the here studied single-layered BNC did not fulfil the mechanical resistance requirements to be used as a PP mesh substitute, thicker single layer BNC films grown for longer periods (>6 days) are expected to present sufficient mechanical support. We have previously reported that BNC fibres condense upon drying and form strong bonds among the cellulose nanofibers, this characteristic allowed us to arrange robust BNC multilayer laminates consisting of 2 or 3 layers.²⁴ The mechanical studies of those rehydrated BNC laminates have shown that the resistance to tear can be easily improved beyond the required 16 N/cm threshold for abdominal wall reinforcement applications. Even though previous studies confirmed the stability of BNC films in physiological conditions for up to 30 days⁴², the mechanical results of the laminates presented here were obtained after a 5 min-immersion in a saline solution and therefore, we cannot discard that the mechanical properties of the films could be affected by longer hydration times.

Seeking to expand the library of BNC-based configurations for hernia repair patches, a composite patch integrating both BNC films and PP meshes was fabricated. This preliminary proof-of-concept demonstrates the possibility to, not only tune the mechanical properties of BNC but also to combine BNC films and PP meshes with different pore sizes. The sandwich-like BNC-PP structure was easy to prepare and exhibited robustness and good manageability both in dry and rehydrated conditions. This hybrid material shows the potential of BNC in the development of on-demand hybrid biomaterials for reinforcement of the abdominal wall but still requires further validation. The durability

of the BNC-PP composites under physiological conditions is unknown at the moment and the need for additional strengthening of the composite (*i.e.* glueing with a cyanoacrylate-based biocompatible adhesive) could be considered in the future⁴³.

We have recently validated BNC in diverse biological scenarios providing data on its cytocompatibility, lack of endotoxins (0.04 ± 0.01 Endotoxin Units/mL) after its biosynthesis as well as suturability and manageability in preclinical settings^{42,44}. These findings, combined with the appealing mechanical properties reported here, positioned BNC as a suitable candidate for soft tissue repair patches and therefore *in vivo* studies were conducted. The anti-adhesion behaviour, biocompatibility and tissue integration characteristics of the BNC patches have been evaluated with a pilot animal study. BNC presented favourable surgical properties for this specific application in terms of suturability, manageability and accommodation to the implantation site. Moreover, the semi-transparent character of BNC was beneficial to avoid unintentional puncturing of underlying tissues. A general fold-free integration of the BCN material to the abdominal wall was detected in all the rabbits. Regarding adhesions between BNC patches and internal organs, the overall area of the five implanted patches free of adhesions in this study is about 92%. Only a few adhesions were found after BNC implantation in the rabbit model, mostly involving the greater omentum which can be assessed as almost physiological since this organ is typically active in any post-surgical process. We hypothesize that the nanofibrillar microstructure of BNC, similar to that of the collagen networks on the extracellular matrix, favours the non-adherent characteristics of the BNC implants in accordance with the anti-fibrotic effect reported for cardiac implants wrapped with BNC²⁰. The macroscopic evaluation showed that the few adhesion strands detected (overall at about 8% of the implant area) originated mainly on the suture stitches and at the border of the patches. For this pilot test, the BNC patches were fixed with sutures, even though sutures can cause foreign body responses and adhesions; indicating that suture-free administration methods could be worth exploring to diminish the adhesions even more. Overall, the macroscopic observation showed that good biocompatibility can be assumed for the BNC patches *in vivo* and the results indicate that BNC patches might act as a sufficient barrier to prevent

adhesions in this rabbit sidewall model. Systemic tolerability of BNC can also be supposed from the good post-operative recovery of the test animals that occurred without notable complications.

On the histological analysis, all BNC implants appeared to be well integrated onto the abdominal wall, in good agreement with the macroscopic observations. An inflammatory response was observed at the peri-implanted area presenting fibroplasia and infiltration of diverse cell types (lymphocytes, heterophilic granulocytes, macrophages and solitary multinucleated giant cells) indicating a tissue reaction upon BNC. In a similar work, oxidized and laser-perforated BNC was employed in experimental surgery using a rabbit model⁴⁵. One week after subcutaneous suture-free BNC implantation on the animal's back a positive integration of the BNC implants with the surrounding tissues was reported following our observations. Interestingly, Lai and co-workers stated a very low inflammatory response contrasting with the here presented histological analysis. Possibly, the distinct tissue responses arise from the different experimental protocols used (*i.e.* implantation site, use of sutures and longer implantation time, in our case) or the modifications of BNC. On the other hand, the previously cited work from Rauchfuß and colleagues³¹ describes an inflammatory infiltration on the BNC patches judged to be of minimal clinical significance. We endorse that it could also apply to our *in vivo* study based on the witnessed lack of systemic toxicity. Besides, the good integration of the BNC implants –which were only indistinctly noticeable on the surrounding tissue– strengthens this reasoning. Nevertheless, the heterogeneous responses of the host immune system towards BNC implants indicate a need for future work.

Finally, the observation that a single layer of BNC could be sufficient to achieve low adhesions rates further emphasizes the attractiveness of BNC composites. Since a strong mechanical resistance is required for hernioplasty, composite BNC patches (either as multilayers or in combination with PP meshes) should be the mainstay of our future work.

Conclusions

In summary, BNC was investigated as a biomaterial for soft tissue reinforcement applications to tackle the long-lasting challenge of reducing adhesions between implants and internal organs after hernia surgery. While single-layer BNC does not present favourable mechanical properties, BNC laminates with 2 or 3 films are resistant enough to reach the minimal acceptance criteria for abdominal wall reinforcement applications. Notably, this simple stacking methodology supported the integration of commercial PP meshes between the BNC sheets opening future perspectives on BNC-PP hybrid biomaterials. Finally, an *in vivo* study revealed that BNC exhibits favourable surgical features in terms of suturability, manageability and accommodation to the implantation site. Besides, mild adhesion scores involving low percentages of the implant's area together with excellent integration capability on the peri-implant zone could be demonstrated. BNC elicited an inflammatory response that needs to be further investigated. Overall, our work proves that bio-based BNC possesses attractive mechanical and anti-adherent properties that could be valuable in the development of innovative hernia repair solutions.

Acknowledgements

Authors acknowledge financial support from the Spanish Ministry of Science and Innovation through the RTI2018-096273-B-I00 project, the ‘Severo Ochoa’ Programme for Centres of Excellence in R&D (CEX2019-000917-S) and the Generalitat de Catalunya 2017SGR765 grant. The authors are also grateful for the PhD scholarships of I. A-S. (BE-2017-076734) and S. R-S. (BES-2016-077533) and the 2019LLAV00046 project. The ICMAB members participate in the CSIC Interdisciplinary Platform for Sustainable Plastics towards a Circular Economy, SUSPLAST, and in the Aerogels COST ACTION (CA 18125). This work has been performed within the framework of the doctoral program in materials science of UAB (I.A-S. and S.R-S.)

Supplementary information included in Publication 5

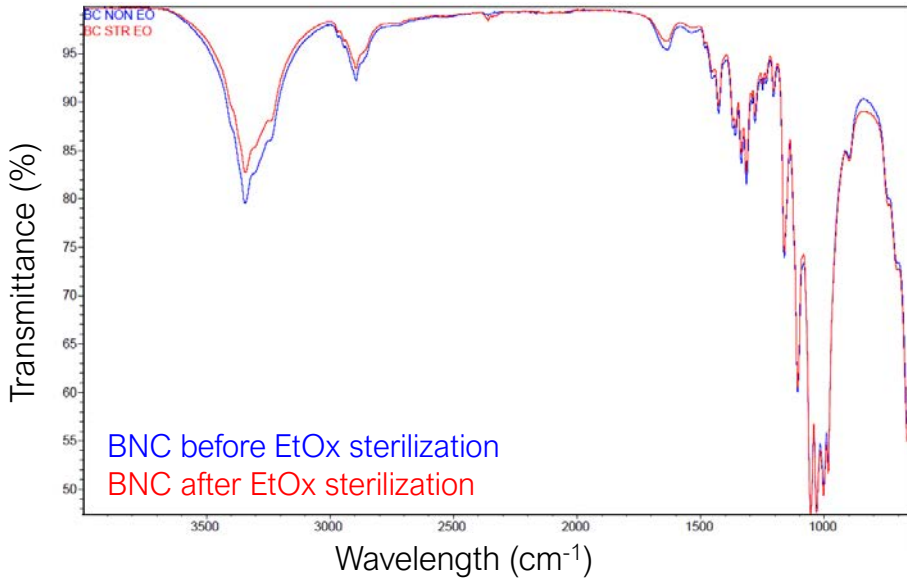


Figure S1: FTIR spectra of BNC samples before (blue line) and after (red line) ethylene oxide sterilization. Note that no major changes are perceived after the treatment indicating the tolerability of BNC to this sterilization method. The FTIR spectra were obtained as the average of 16 scans.

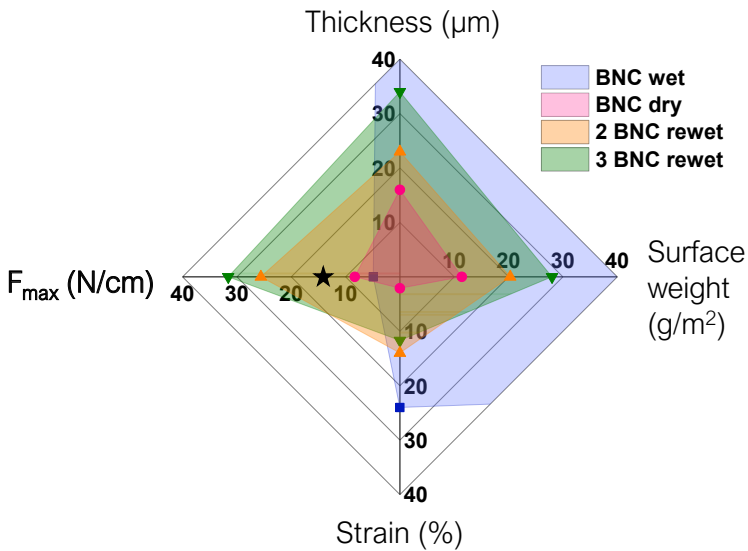


Figure S2: Comparison of the mechanical properties of all the BNC systems studied. * Indicates the resistance to tear threshold for soft tissue reinforcement materials.

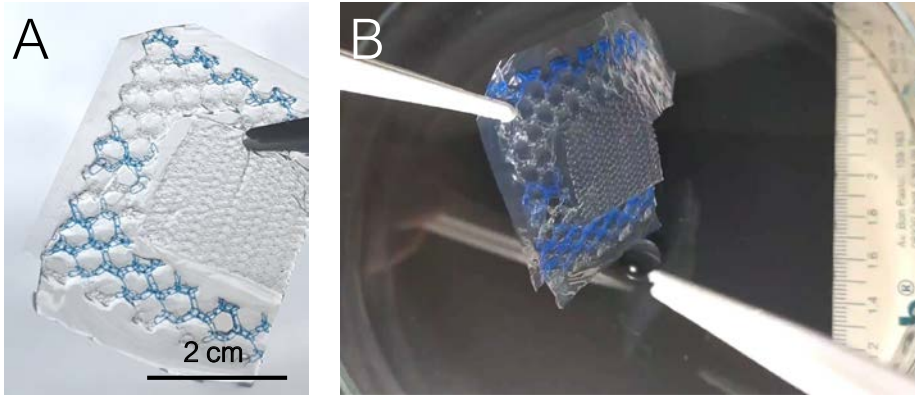


Figure S3: A) Digital image showing the BNC-PP composite after 5-day rehydration in water showing high durability. B) A video is enclosed. See the provided supplementary movie: <http://www.rsc.org/suppdata/d1/bm/d1bm00025j/d1bm00025j2.mp4> to illustrate the manipulation and stability of the hybrid biomaterial.

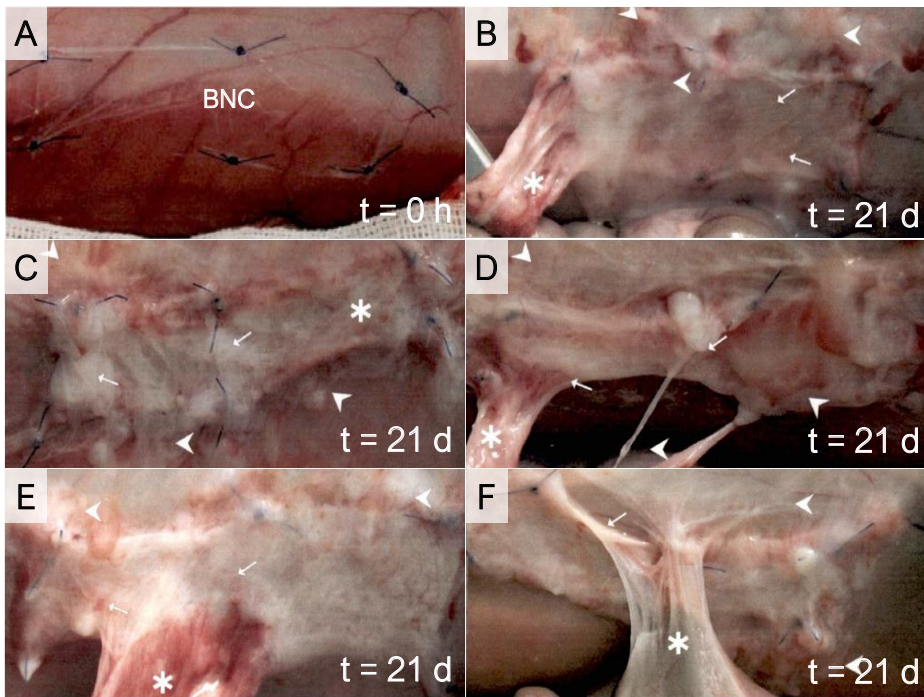


Figure S4: BNC implant's fixation with sutures, macroscopic evaluation and adhesion assessment for the five test animals. A) BNC patch applied onto the abdominal wall and fixed with six suture points at time= 0. Explanted analysis after 21 days; B) A1, * adhesion, ▶ vascularization, → fibrin accumulation, C) A2, * vascularization, ▶ adjacent abdominal wall, → fibrin accumulation. D) A3, * adhesion, ▶ adjacent abdominal wall and vascularization, → thin adhesion strands. E) A4, * big adhesion, ▶ fibrin accumulation, → vascularization, and F) A5, * Adhesion, ▶ fibrin accumulation, → ventral margin turned over.

Contributions to the field and critical comment

Chapter 5 showcases the final healthcare application of BNC from this compendium. In line with the objectives of the thesis, the study incorporates a relevant player in the field of hernia repair to guide our endeavours towards an unmet clinical need. The cooperation with B. Braun –a leading manufacturer of surgical meshes– provided an industrial connection together with a better comprehension of the requirements for biomaterials oriented to soft tissue reinforcement. A good example of this is the selection of dry BNC patches over the wet counterparts. This choice was based not only on better mechanical performance but also on superior manufacturing compliance. That is, dry materials are easier to store, transport and sterilize by gaseous methods such as EtOx. Besides, demonstrating excellent compatibility of BNC with EtOx processes, which is a common technology in the industry but not in research labs, represents another significant input from this chapter.

Publication 5 differs from the temporal treatments exposed in previous sections and explores the possibility of a long-term BNC graft. The notion that BNC can be exploited to design implantable devices is increasingly reported, and specific uses range from meniscus to bile duct prosthesis^{46–49}. The general trend in the literature is to claim low inflammatory reactions and good tissue integration upon BNC implantation⁵⁰. While our observations also point towards a favourable integration, we noted immune cell infiltration in the peri-implant area. Since immune reactions are multifactorial, current data is insufficient to discern the severity and causes of the inflammatory response detected. Despite the need for future investigations, we endorse BNC as a worth considering option in hernia repair because of the advantageous surgical, mechanical and anti-adhesive properties demonstrated in Publication 5.

Interestingly, a promising under development BNC implant (Hylomate®) targets a fairly similar application to that considered here. Hylomate® is designed to interface between prosthesis (*i.e.*, pace-makers and neuro-stimulators) and surrounding host tissues reducing the formation of fibrotic tissue. This BNC biomaterial has been surface engineered with micro-wells to reduce the interactions with immune cells and fibroblasts seeking to enhance its anti-adhesive properties^{28,51}. On the

other hand, some encouraging examples of hernia repair with BNC-derived biomaterials employed perforated BNC films^{45,52}. Cumulatively, these reports suggest that BNC topography and porous structure play an important role in its implantability. Since protocols to microstructure BNC have already been developed in our lab, evaluating the performance of BNC implants with different surface structures emerges as an appealing future work direction.

BNC implants are still finding their way to clinical translation. To the best of our knowledge, the only BNC products that have gained market authorization are intended for topical use (*i.e.*, NanodermTM, Suprasorb[®]). This might be explained, at least partially, by the complexity of the regulatory procedures for implantable devices which are classified as medical devices class III (highest risk). On the other hand, follow-up times of *in vivo* biocompatibility studies rarely surpass 12 months and thus the performance of BNC for devising lifelong prosthesis remains an open question. Nevertheless, the growing interest in naturally-sourced implants⁵³ combined with the development of industrial production of BNC under controlled conditions⁵⁴ are pushing the frontiers of the field. We hope that our work contributes to such progress by emphasising the value of BNC as a robust and anti-adhesive biomaterial and by prompting more public-private collaborations.

Chapter references

1. Basile, F., Biondi, A. & Donati, M. Surgical approach to abdominal wall defects: History and new trends. *Int. J. Surg.* **11**, S20–S23 (2013).
2. Informed Health Organization. *Hernias: Overview*. (Institute for Quality and Efficiency in Health Care (IQWiG), 2020).
3. Kaufmann, R. *et al.* Mesh versus suture repair of umbilical hernia in adults: a randomised, double-blind, controlled, multicentre trial. *Lancet* **391**, 860–869 (2018).
4. Bay-Nielsen, M. *et al.* Quality assessment of 26304 herniorrhaphies in Denmark: A prospective nationwide study. *Lancet* **358**, 1124–1128 (2001).
5. Sanders, D. L. & Kingsnorth, A. N. The modern management of incisional hernias. *Bmj* **344**, 1–9 (2012).
6. Champault, G. & Barrat, C. Inguinal hernia repair with beta glucan-coated mesh: Results at two-year follow up. *Hernia* **9**, 125–130 (2005).
7. Kashyap, A. S., Anand, K. P. & Kashyap, S. Inguinal and incisional hernias. *Lancet* **363**, 84 (2004).
8. Bittner, R. *et al.* Guidelines for laparoscopic (TAPP) and endoscopic (TEP) treatment of inguinal hernia [International Endohernia Society (IEHS)]. *Surg. Endosc.* **25**, 2773–2843 (2011).
9. Köckerling, F. *et al.* Seroma following transabdominal preperitoneal patch plasty (TAPP): incidence, risk factors, and preventive measures. *Surg. Endosc.* **32**, 2222–2231 (2018).
10. Muller, S., Langø, T., Brekken, R. & Ystgaard, B. Degree of Adhesions After Repair of Incisional Hernia. *J. of the Soc. Laparoendosc. Surg.* **14**, 399–404 (2010).
11. Chelala, E. *et al.* Eighty-five redo surgeries after 733 laparoscopic treatments for ventral and incisional hernia: Adhesion and recurrence analysis. *Hernia* **14**, 123–129 (2010).
12. Mirjavan, M., Asayesh, A. & Asgharian Jeddi, A. A. The effect of fabric structure on the mechanical properties of warp knitted surgical mesh for hernia repair. *J. Mech. Behav. Biomed. Mater.* **66**, 77–86 (2017).
13. Hollinsky, C. *et al.* Tensile strength and adhesion formation of mesh fixation systems used in laparoscopic incisional hernia repair. *Surg. Endosc.* **24**, 1318–1324 (2010).
14. Lanzalaco, S. *et al.* Polypropylene mesh for hernia repair with controllable cell adhesion/de-adhesion properties. *J. Mater. Chem. B* **8**, 1049–1059 (2020).
15. Emans, P. J. *et al.* Polypropylene meshes to prevent abdominal herniation. Can stable coatings prevent adhesions in the long term? *Ann. Biomed. Eng.* **37**, 410–418 (2009).
16. Lanzalaco, S. *et al.* Toward the New Generation of Surgical Meshes with 4D Response: Soft, Dynamic, and Adaptable. *Adv. Funct. Mater.* **2004145**, 1–9 (2020).

17. Udpa, N. *et al.* Effects of Chitosan Coatings on Polypropylene Mesh for Implantation in a Rat Abdominal Wall Model. *TISSUE Eng. Part A* **19**, 2713–23 (2013).
18. Pomilio Di Loreto, F. *et al.* Dried human amniotic membrane as an antiadherent layer for intraperitoneal placing of polypropylene mesh in rats. *Surg. Endosc.* **27**, 1435–1440 (2013).
19. Anton-Sales, I., Beekmann, U., Laromaine, A., Roig, A. & Kralisch, D. Opportunities of Bacterial Cellulose to Treat Epithelial Tissues. *Curr. Drug Targets* **20**, 808–822 (2019).
20. Zeng, M., Laromaine, A. & Roig, A. Bacterial cellulose films: influence of bacterial strain and drying route on film properties. *Cellulose* **21**, 4455–4469 (2014).
21. Wang, S. *et al.* Super-Strong, Super-Stiff Macrofibers with Aligned, Long Bacterial Cellulose Nanofibers. *Adv. Mater.* **29**, 1702498 (2017).
22. Chen, S. Q., Lopez-Sanchez, P., Wang, D., Mikkelsen, D. & Gidley, M. J. Mechanical properties of bacterial cellulose synthesised by diverse strains of the genus *Komagataeibacter*. *Food Hydrocoll.* **81**, 87–95 (2018).
23. Ullah, H., Wahid, F., Santos, H. A. & Khan, T. Advances in biomedical and pharmaceutical applications of functional bacterial cellulose-based nanocomposites. *Carbohydr. Polym.* **150**, 330–352 (2016).
24. Klemm, D. *et al.* Nanocellulose as a natural source for groundbreaking applications in materials science: Today's state. *Mater. Today* **21**, 720–748 (2018).
25. Bacakova, L. *et al.* Versatile Application of Nanocellulose: From Industry to Skin Tissue Engineering and Wound Healing. *Nanomaterials* **9**, 164 (2019).
26. Lima, F. de M. T. de *et al.* Biocompatible bacterial cellulose membrane in dural defect repair of rat. *J. Mater. Sci. Mater. Med.* **28**, 37 (2017).
27. Silveira, F. C. A. *et al.* Treatment of tympanic membrane perforation using bacterial cellulose: a randomized controlled trial. *Braz. J. Otorhinolaryngol.* **82**, 203–208 (2016).
28. Robotti, F. *et al.* Microengineered biosynthesized cellulose as anti-fibrotic in vivo protection for cardiac implantable electronic devices. *Biomaterials* **229**, 119583 (2020).
29. Ludwicka, K. *et al.* Stable composite of bacterial nanocellulose and perforated polypropylene mesh for biomedical applications. *J. Biomed. Mater. Res. - Part B Appl. Biomater.* **107**, 978–987 (2019).
30. Zharikov, A. N. *et al.* Early morphological changes in tissues when replacing abdominal wall defects by bacterial nanocellulose in experimental trials. *J. Mater. Sci. Mater. Med.* **29**, (2018).
31. Rauchfuß, F. *et al.* Biocellulose for incisional hernia repair—an experimental pilot study. *Nanomaterials* **9**, 1–11 (2019).

32. Roig-Sanchez, S. *et al.* Nanocellulose films with multiple functional nanoparticles in confined spatial distribution. *Nanoscale Horizons* **4**, 634–641 (2019).
33. Chan, J. C. Y., Burugapalli, K., Huang, Y. S., Kelly, J. L. & Pandit, A. A clinically relevant in vivo model for the assessment of scaffold efficacy in abdominal wall reconstruction. *J. Tissue Eng.* **8**, 1–11 (2017).
34. DiZerega, G. S. & Campeau, J. D. Peritoneal repair and post-surgical adhesion formation. *Hum. Reprod. Update* **7**, 547–555 (2001).
35. Lang, R. A. *et al.* Polyvinyl alcohol gel prevents abdominal adhesion formation in a rabbit model. *Fertil. Steril.* **88**, 1180–1186 (2007).
36. Kataria, H. & Singh, V. P. Liquid Paraffin vs Hyaluronic Acid in Preventing Intraperitoneal Adhesions. *Indian J. Surg.* **79**, 539–543 (2017).
37. Kukleta, J. F., Freytag, C. & Weber, M. Efficiency and safety of mesh fixation in laparoscopic inguinal hernia repair using n-butyl cyanoacrylate: Long-term biocompatibility in over 1,300 mesh fixations. *Hernia* **16**, 153–162 (2012).
38. El-Naggar, M. E., Othman, S. I., Allam, A. A. & Morsy, O. M. Synthesis, drying process and medical application of polysaccharide-based aerogels. *Int. J. Biol. Macromol.* **145**, 1115–1128 (2020).
39. Klinge, U. *et al.* Modified mesh for hernia repair that is adapted to the physiology of the abdominal wall. *Eur. J. Surg.* **164**, 951–960 (1998).
40. Kralisch, D., Hessler, N., Klemm, D., Erdmann, R. & Schmidt, W. White biotechnology for cellulose manufacturing—the HoLiR concept. *Biotechnol Bioeng* **105**, 740–747 (2010).
41. Beekmann, U. *et al.* Process control and scale-up of modified bacterial cellulose production for tailor-made anti-inflammatory drug delivery systems. *Carbohydr. Polym.* **236**, 116062 (2020).
42. Anton-Sales, I. *et al.* Bacterial nanocellulose as a corneal bandage material: A comparison with amniotic membrane. *Biomater. Sci.* **8**, 2921–2930 (2020).
43. Jain, R. & Wairkar, S. Recent developments and clinical applications of surgical glues: An overview. *Int. J. Biol. Macromol.* **137**, 95–106 (2019).
44. Anton-Sales, I., Roig-Sanchez, S., Sánchez-Guisado, M. J., Laromaine, A. & Roig, A. Bacterial nanocellulose and titania hybrids: cytocompatible and cryopreservable cell carriers. *ACS Biomater. Sci. Eng.* **6**, 4893–4902 (2020).
45. Lai, C. *et al.* Anti-Adhesion Mesh for Hernia Repair Based on Modified Bacterial Cellulose. *Starch/Staerke* **70**, 1–10 (2018).
46. de Abreu, G. F. S. *et al.* Use of bacterial cellulose film for repair of bile duct injury in pigs. *J. Biomater. Appl.* **35**, 331–341 (2020).
47. Osorio, M. *et al.* Ex Vivo and In Vivo Biocompatibility Assessment (Blood and Tissue) of Three-Dimensional Bacterial Nanocellulose Biomaterials for Soft Tissue Implants. *Sci. Rep.* **9**, 10553 (2019).

48. Dawidowska, K., Siondalski, P. & Kołaczowska, M. In Vitro Study of a Stentless Aortic Bioprosthesis Made of Bacterial Cellulose. *Cardiovasc. Eng. Technol.* **11**, 646–654 (2020).
49. Bodin, A., Concaro, S., Brittberg, M. & Gatenholm, P. Bacterial cellulose as a potential meniscus implant. *J. Tissue Eng. Regen. Med.* **1**, 406–408 (2007).
50. Helenius, G. *et al.* In vivo biocompatibility of bacterial cellulose. *J. Biomed. Mater. Res. - Part A* **76**, 431–438 (2006).
51. Robotti, F. *et al.* A micron-scale surface topography design reducing cell adhesion to implanted materials. *Sci. Rep.* **8**, 1–13 (2018).
52. Silveira, R. K. *et al.* Bioprosthetic mesh of bacterial cellulose for treatment of abdominal muscle aponeurotic defect in rat model. *J. Mater. Sci. Mater. Med.* **27**, (2016).
53. Gaharwar, A. K., Detamore, M. S. & Khademhosseini, A. Emerging Trends in Biomaterials Research. *Ann. Biomed. Eng.* **44**, 1861–1862 (2016).
54. Klemm, D. *et al.* Biotech nanocellulose: A review on progress in product design and today's state of technical and medical applications. *Carbohydr. Polym.* **15**, 117313 (2020).

Conclusions and outlook

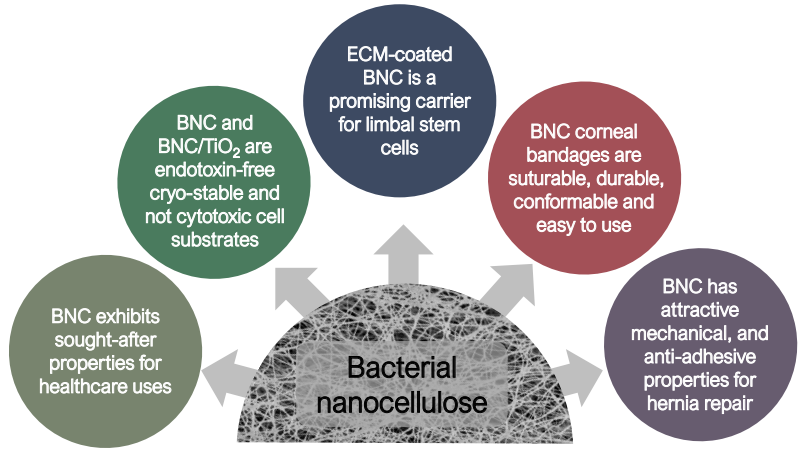


Figure 1: Schematics of the main conclusions of the thesis.

Conclusions

The overarching goal of this PhD thesis was to identify and investigate opportunities for bacterial nanocellulose (BNC) in several healthcare sectors. Based on the gathered scientific data, the following conclusions can be drawn:

1. BNC is an emerging biopolymer with a myriad of underexploited potential in healthcare

- o The distinctive properties of BNC, partially arising from its nano fibrous structure, are highly appreciated in diverse biomedical disciplines, principally for soft tissue (skin, cornea, internal organs, mucosae...) repair and cell-therapies. This is reflected in a growing interest –from both researchers and entrepreneurs– on BNC.
- o The current golden standard for the above applications is collagen-based biomaterials, which can be used to benchmark novel biomaterials, including BNC.
- o Direct interaction with end-users has been proved as an efficient approach to complement bibliographic work and gain a well-informed view about the use of biomaterials in clinical practice and the limitations of the current solutions.
- o Skin regeneration is a competitive field at both the research and the market level. Therefore, we focused on alternative targets like the ocular surface as appealing niches for BNC.
- o According to the interviewees, general pre-requisites for candidate biomaterials are non-toxicity, cell-interactivity and manageability, among others. For ophthalmic biomaterials, flexibility, moisture retention and transparency should be added to this checklist.

2. BNC and BNC/TiO₂ hybrids support the expansion and cryo-preservation of model cells

- o As a starting point, we studied the interactions between two BNC-based substrates with model human cells encountering no signs of

cytotoxicity neither for native BNC films nor for BNC functionalized with TiO₂ nanoparticles.

- o After cleaning and sterilization by autoclave, our BNC hydrogels were found to be endotoxin-free (E.U. values were well below the FDA requirements).
- o Cell viability, proliferation, morphology and retrieval were characterized for both substrates obtaining analogous results.
- o Cell-laden BNC and BNC/TiO₂ were successfully cryopreserved at liquid nitrogen temperature without compromising cell viability and substrate's integrity. This finding opens up venues for fabricating off-the-shelf cell/BNC constructs.
- o Despite being cytocompatible, the BNC/TiO₂ hybrids did not outperform plain BNC substrates in the functionality tests performed; i) sunscreen capacity and ii) anti-microbial activity, and therefore these biomaterials were not further investigated.

3. ECM-coated BNC is a well-suited carrier for limbal stem cell transplantation to the ocular surface

- o The potential of BNC as a cell carrier for therapeutic cells was demonstrated by efficiently culturing human embryonic stem cells-derived limbal stem cells (hESC-LSC) on BNC films.
- o To provide anchoring sites to hESC-LSC, a plasma-enabled collagen and laminin coating of the BNC films was indispensable. This finding indicates that the surface of BNC can be conditioned to match the requirements of the target cells.
- o ECM-coated BNC allowed maintaining a hESC-LSC population with a predominantly stem phenotype for up to three weeks.
- o BNC was evaluated for transplantability with a porcine corneal organ culture model obtaining satisfactory results.
- o The well-defined (feeder- and serum-free) hESC-LSC differentiation and maintenance protocols and the pure and animal product-free nature of BNC are strategic advantages for clinical translation.

- o The cryopreservation of hESC-LSC attached to BNC carriers holds huge potential. However, the cryopreservation protocol requires optimization.
- o The combination of the therapeutic potential of hESC-LSC with the outstanding biomaterial properties of BNC, render the BNC/LSC constructs a worthwhile option for the treatment of blinding corneal pathologies.

4. BNC hydrogels fulfil preclinical requirements to become novel ocular surface bandages

- o In close collaboration with ophthalmologists, BNC hydrogels were positively assessed for basic, but very meaningful demands of biomaterials to treat the ocular surface.
- o BNC was benchmarked against human amniotic membrane as it represents the golden standard for corneal bandaging.
- o The technical feasibility *i.e.* suturability, manageability, adaptability to the implantation site and durability of BNC has been demonstrated using a porcine eye *ex vivo* model.
- o Owing to its versatility, stability and easy production, BNC-based solutions could irrupt as a more widely available option for ocular surface wound healing.
- o The technology transfer potential of BNC as an ophthalmic natural donor-independent material has been assessed detecting an attractive market opportunity.

5. BNC offers possibilities as an anti-adhesive barrier for hernia treatments

- o Together with the R+D department of B.Braun Surgical, we investigated BNC patches as anti-adhesive tissue reinforcements.
- o Rewet double- and triple-layered BNC withstand high tensile stress, making them interesting candidates for hernia repair.

- o BNC membranes displayed great integration and low adhesion scores when placed in contact with internal organs in a rabbit model.
- o The implanted BNC was found to be infiltrated by immune cells, a tissue response that warrants future work.
- o Sterile BNC could be attained upon an ethylene oxide gaseous treatment, demonstrating an additional venue to sterilize dry BNC materials.

Overall, this PhD thesis has identified and paved the way for innovative therapies based on the biopolymer BNC. Three research lines have been initiated; i) the validation of BNC as a resourceful cell carrier ii) the development of BNC-based corneal bandages and iii) the assessment of BNC as a tissue reinforcement. All these new uses of BNC have been rationally addressed grounded on extensive non-experimental research compassing literature review as well as on-site interviews with end-users and validated with robust experimental data. Remarkably, a huge effort has been put into suggesting solutions with high translatability. To this end, collaborations with relevant players have been established and the clinical demands have at all times been taken into consideration.

Outlook

The ultimate goal of the healthcare uses of BNC outlined in this thesis is to reach the clinics, yet there is still a rather long way to go before their implementation.

Regarding the ophthalmological applications, functionality tests are to be conducted. For the limbal stem cell-loaded BNC membranes (Chapter 3), demonstrating the ability of the therapeutic cells to migrate from the BNC carriers and repopulate a damaged limbal stem cells niche would provide convincing evidence about the feasibility of the treatment. As for the BNC corneal bandages (Chapter 4), *ex vivo* tests to elucidate the corneal wound healing capability of BNC are already underway. Notably, apart from native BNC hydrogels, BNC bandages incorporating bioactive substances are being considered in our current work. Moreover, *in vivo* testing using animal models will be required to validate the safety and efficacy

of both approaches. In the long run, the work presented in this thesis could give rise to a BNC-centred therapeutic platform for the ocular surface. Ideally, it will comprise an advanced therapy medicinal product based on BNC carrying limbal stem cells to the ocular surface and a medical device consisting of BNC impregnated with ancillary substances. Tailor-made treatments could be offered by adapting the size, shape and bioactive substances of the final product joining the global trend of personalized medicine.

To reach the full potential of the anti-adhesive BNC implants, future studies are needed to gain insights into the underlying mechanisms of the reported phenomena. Testing BNC implants with different surface properties would probably provide a sound explanation about the low adhesion rates between the BNC implants and the viscera, facilitating the optimisation of the system. Additionally, further experiments with an increased number of animals and follow-up times would be informative about the clinical significance of the observed immune cell infiltration in the peri-implant area.

To conclude, several proof-of-concept's, which are among the first reports of BNC utilization in distinct sectors, are described in this PhD thesis. We expect our findings to push the boundaries of BNC uses in medical care and to support the emergence of BNC-based medical products as biotechnological and customizable biomaterials. This progress should not overlook basic research since understanding the therapeutic action mechanisms and the interplay between biomaterials and host tissues is essential to ensure efficient and safe upcoming treatments.

Annex

Curriculum Vitae and publications



IRENE ANTON SALES

PROFILE

- Soon-to-be PhD in materials science, interested in multidisciplinary projects related to biomaterials and translational research.
- Background in biotechnology and biomedicine.
- **Born in Barcelona on the 24th June of 1993**

SKILLS

- **Lab techniques:** cell culture, microscopy, *ex vivo* biomaterial testing, bacterial nanocellulose production and characterization
- Result analysis, scientific writing and communication
- Problem solving and autonomy

CONTACT

✉ ireneantonsales@gmail.com

☎ +34 661086639

🐦 @ireneantonsales

🌐 Irene Anton-Sales

RESEARCH EXPERIENCE

PhD fellow - Institute of Materials Science of Barcelona, ICMAB-CSIC (Spain)

- December 2016 - Present
- Group of Nanoparticles and Nanocomposites

Project: Opportunities for bacterial nanocellulose in healthcare. Uses as a cell carrier, corneal bandage and tissue reinforcement

Visiting researcher - Tampere University (Finland)

- Setembre 2019- December 2019
- Eye Group

Project: Limbal stem cells on bacterial nanocellulose carriers for ocular surface regeneration

Master Student - Vall d'Hebron Research Institute (Spain)

- December 2015- July 2016
- Neurovascular research group in collaboration with ICMAB-CSIC

Project: Encapsulating endothelial progenitor cells' secretome into magnetic nanocapsules for targeted vascular remodelling

Bachelor Student - Centre for neurogenomics and cognitive research (Netherlands)

- January 2015 - July 2015
- Molecular Neurodegeneration group (ERASMUS+ program)

Project: Targeting the lysosome to reduce Tau pathology. Implications in Alzheimer's disease

CONFERENCES

- 31st Conference of the **European Colloid and Interface Society** + Training on the design of colloidal materials for medical applications (Madrid, 2017)
 - Contribution: two posters
 - Best poster award
- 29th Meeting of the **European Society for Biomaterials** (Maastricht, 2018)
 - Contribution: poster
 - Best poster award
- **NanoBio&Med** Conference (Barcelona, 2018)
 - Contribution: poster + oral
 - Best poster award
- 36th **World Ophthalmology Congress** (Barcelona, 2018)
 - Audience
- 4th **International Symposium on Bacterial Nanocellulose** (Porto, 2019)
 - Contribution: oral
 - Best sharp presentation
- Scientific **Meeting of BNC-b Students** (all the editions between 2016 and 2020, BCN)
 - Contributions: orals and posters
 - Best oral, second oral and 2nd best poster awards
- 3rd **Spanish Conference on Biomedical Applications of Nanomaterials** (online, 2020)
 - Contribution: poster

EDUCATION

Postgraduate course in Technology Transfer. UPF-Barcelona School of Management

- October 2020- March 2021
- Participation in an investment forum
- Grade: 9/10

Master in Biomedical Research. Pompeu Fabra University

- September 2015 - July 2016
- Grade: 9,3/10

Bachelor in Molecular Biotechnology. University of Barcelona

- September 2011 - July 2015
- Grade: 8/10

PUBLICATIONS

1. Irene Anton-Sales‡, Soledad Roig-Sanchez‡, Kamelia Traeger, Christine Weis, Anna Laromaine, Pau Turon and Anna Roig **In vivo soft tissue reinforcement with bacterial nanocellulose.** *Biomater. Sci.* (2021).
2. Irene Anton-Sales, Laura Koivusalo, Heli Skottman, Anna Laromaine and Anna Roig. **Limbic stem cells on bacterial nanocellulose carriers for ocular surface regeneration.** *Small* 17, e2003937 (2021).
3. Irene Anton-Sales, Soledad Roig-Sanchez, Maria Jesus Sánchez-Guisado, Anna Laromaine and Anna Roig. **Bacterial nanocellulose and titania hybrids: cytocompatible and cryopreservable cell carriers.** *ACS Biomater. Sci. Eng* 6, 4893-4902 (2020).
4. Irene Anton-Sales, Justin C. D'Antin, Jorge Fernández-Engroba, Victor Charoenrook, Anna Laromaine, Anna Roig and Ralph Michael. **Bacterial nanocellulose as a corneal bandage material: A comparison with amniotic membrane.** *Biomater. Sci.* 8, 2921 (2020).
5. Irene Anton-Sales‡, Uwe Beekmann‡, Anna Laromaine, Anna Roig and Dana Kralisch. **Opportunities of Bacterial Cellulose to Treat Epithelial Tissues.** *Curr. Drug Targets* 20, 808-822 (2019).
6. Soledad Roig-Sanchez, Erik Jungstedt, Irene Anton-Sales, David C. Malaspina, Jordi Faraudo, Lars A. Berglund, Anna Laromaine and Anna Roig. **Nanocellulose films with multiple functional nanoparticles in confined spatial distribution.** *Nanoscale Horizons* 4, 634-641 (2019).
7. Yajie Zhang, Miguel García-Gabilondo, Alba Grayston, Irene V. J. Feiner, Irene Anton-Sales, Rodrigo A. Loiola, Jordi Llop, Pedro Ramos-Cabrer, Ignasi Barba, David Garcia-Dorado, Fabien Gosselet, Anna Rosell and Anna Roig. **PLGA protein nanocarriers with tailor-made fluorescence/MRI/PET imaging modalities.** *Nanoscale* 12, 4988-5002 (2020).

MERITS

- **Entrepreneur scientist** at the Llabor project *Corneal-BNC*
- Finalist at Expoquimia Awards in Biotechnology R&D&I 2020 for the project *Nanocellulose patches to treat corneal wounds*
- **EMBO short term fellowship** (PhD research stay in 2019)
- Active participation in **science outreach** activities: Pint of Science, press releases...

LANGUAGES

Native: Catalan and Spanish

Bilingual: English

- Certificate of Proficiency in English

MORE ABOUT ME



HOBBIES



COURSES

Responsible research and innovation

- 15 hours, December-January 2017
- Autonomous University of Barcelona

Scientific school on materials for biomedical applications

- 19th - 22nd June 2017
- ICMAB

Technical and conversational English

- 20 hours, March-June 2017
- ICMAB

Neuroscience of emotions and emotional development

- 20 hours, May-June 2017
- ICMAB

Interpersonal relationships in the professional environment

- 16 hours, April-May 2018
- ICMAB

MANAGED PROJECTS

Bacterial nanocellulose for corneal healing

- Supervision of two master students and a research assistant.
- Collaboration with [Barraquer Ophthalmology Centre](#)
- Development of a business plan

PhD thesis: Opportunities for bacterial nanocellulose in healthcare

- 4-year Severo Ochoa PhD Scholarship
- Compendium of five publications
- Application-oriented research with collaborations with the private sector

REVIEW ARTICLE



Opportunities of Bacterial Cellulose to Treat Epithelial Tissues

Irene Anton-Sales^{1,†}, Uwe Beekmann^{2,†}, Anna Laromaine^{1,*}, Anna Roig^{1,*} and Dana Kralisch^{2,3}

¹Institute of Materials Science of Barcelona (ICMAB-CSIC), 08193 Bellaterra, Catalunya, Spain; ²Institute of Pharmacy, Department of Pharmaceutical Technology and Biopharmacy, Friedrich Schiller University Jena, 07743 Jena, Germany; ³JeNaCell GmbH, 07743 Jena, Germany

ARTICLE HISTORY

Received: July 19, 2018
 Revised: October 22, 2018
 Accepted: November 07, 2018

DOI:
 10.2174/1389450120666181129092144



CrossMark

Abstract: In this mini-review, we highlight the potential of the biopolymer bacterial cellulose to treat damaged epithelial tissues. Epithelial tissues are cell sheets that delimitate both the external body surfaces and the internal cavities and organs. Epithelia serve as physical protection to underlying organs, regulate the diffusion of molecules and ions, secrete substances and filtrate body fluids, among other vital functions. Because of their continuous exposure to environmental stressors, damage to epithelial tissues is highly prevalent. Here, we first compare the properties of bacterial cellulose to the current gold standard, collagen, and then we examine the use of bacterial cellulose patches to heal specific epithelial tissues; the outer skin, the ocular surface, the oral mucosa and other epithelial surfaces. Special emphasis is made on the dermis since, to date, this is the most widespread medical use of bacterial cellulose. It is important to note that some epithelial tissues represent only the outermost layer of more complex structures such as the skin or the cornea. In these situations, depending on the penetration of the lesion, bacterial cellulose might also be involved in the regeneration of, for instance, inner connective tissue.

Keywords: Biomaterials, bacterial cellulose, epithelial tissues, wound dressing, cell carrier, drug delivery, epithelial regeneration.

1. INTRODUCTION

Epithelial tissues are, essentially, continuous cell sheets that delimitate both the external body surfaces and the internal cavities. Epithelia have a reduced content of extracellular matrix and exhibit strong cell-to-cell adhesions known as tight junctions. Epithelial tissues are not vascularized and receive support from the underlying basement membrane formed by connective tissue. Examples of epithelial tissues are the external linings of the skin, cornea and mouth but also those from the hollow internal organs such as lungs, digestive system, urogenital conducts and spinal cord. Depending on its location in the body, epithelia can be found as single (e.g., intestines, lungs) or multiple cell layers (e.g., skin, cornea, esophagus). The glandular epithelium that surrounds the glands in our body is a highly specialized epithelium that will not be addressed here. In this manuscript, we have used “epithelial tissue” as an umbrella term to refer to diverse body surfaces and barriers.

Epithelial structures physically protect the underlying tissues, regulate the diffusion of molecules and ions, secrete substances and filtrate body fluids among other vital functions. Because of their surface location, epithelia are

constantly exposed to environmental stressors ranging from infections caused by microorganisms and mechanical injuries to the exposure to toxic chemicals. Moreover, epithelial tissues are also greatly affected by inflammatory diseases and cancers. Despite the extraordinary regenerative capacity of epithelial tissues, they can be overwhelmed by large-area injuries, surgical scissions, burns or ulcers which might result in chronic lesions [1]. Additionally, diabetes, infectious processes, systemic and chronic treatments or other pathological conditions can make epithelial regeneration less efficient [2]. In these specific cases, the use of biomaterials to assist the regeneration of sensitive epithelia becomes vital.

Biomaterials represent a core element of regenerative therapies and are used in multiple ways to treat epithelial defects. Biomaterials are designed to interface with biological systems to evaluate, treat, increase or replace tissues, organs or functions in the body (European Society for Biomaterials, 2nd Consensus Conference on Definition, 1991). The palette of available biomaterials is extensive being polymers, ceramics and metals the main categories. Ceramics and metals are indicated for bioengineering load-bearing structures and are out of the focus of this minireview. Polymeric biomaterials are often classified into synthetic and natural polymers according to its origin. Because of its superior biocompatibility and bioactivity, naturally-occurring polymers (e.g., collagen, fibrin, chitosan, keratin, silk, alginate, cellulose) are frequently used for repairing epithelial tissues. Biomaterials based on natural polymers can serve as transitory

*Address correspondence to these authors at the Institute of Materials Science of Barcelona (ICMAB-CSIC), 08193 Bellaterra, Catalunya, Spain; Tel: +34935801853; E-mails: alaromaine@icmab.es; roig@icmab.es

† These authors contributed equally to this manuscript.

treatments like wound coverages [3], temporary skin substitutes [4], carriers for cell therapy [5, 6] and drug delivery platforms [7, 8] as well as long-term replacements for damaged epithelial tissues [9, 10].

Despite the broad spectrum of natural polymers and natural-natural [11] or natural-synthetic [12] composites that are being investigated for epithelial regeneration, currently, the main clinical procedures rely on collagen-based solutions [13]. Collagen is a fibrous structural protein that forms triple helix assemblies; it is a major constituent of the extracellular matrix and inherently bioactive and biocompatible. It is therefore understandable that collagen has long been considered the gold standard to repair organs and tissues (skin, cornea, oral mucosa *etc.*) exposed to the environment. Collagen is primarily obtained from livestock sources like cow, pig, rat and more recently also from fish [14] and typically needs extensive manipulation prior to attaining the final product. One of the main drawbacks of animal collagen is its moderate immunogenicity [15] and its high batch-to-batch variability. On the other hand, religious constraints against animal derived medical products also have played a role [16]. Recombinant collagen from bacteria or plants [17] can help to overcome these issues but the production is still far from meeting the worldwide increasing collagen demand [18]. Last but not least, the mechanical properties and degradation kinetics of collagen do not always meet clinical requirements. Thus, novel biomaterials able to fulfill the enormous diversity of conditions and patients' needs are required.

Third generation natural biomaterials are expected to be biocompatible as well as to foster the regeneration of damaged tissues. To achieve this, researchers are screening not only alternative biopolymers [19] but also novel architectures of already well-known natural materials [20]. In line with this, nanostructured biomaterials, typically in the form of nanofibrous hydrogels, have recently attracted much attention [21-23]. Nanostructuring can endow biomaterials with high surface area to volume ratios, enhanced cell attachment and proliferation; mechanical stability and adequate porosity [24]. Such nanostructured substrates can be fabricated for instance by electrospinning [25]. Electrospinning has already allowed forming gelatin and gelatin-alginate nanofibers with improved mechanical properties compared to unstructured hydrogels [26]. Silk fibroin electrospun nanomaterials showed reduced inflammation and faster re-epithelization in a rat burn model compared to conventional treatments [27]. These authors partially ascribed the over-performance of the nanostructured wound dressing to the nanoscale dimensions of the fibers that accurately mimic the properties of soft tissues and retain certain amounts of liquid.

A lesser explored family of natural biopolymers with potential applicability in epithelial regeneration are nanocelluloses [28]. The term "nanocellulose" refers to cellulose-based materials with at least one dimension in the nanoscale. Nanocelluloses can be subdivided into bacterial cellulose (BC), cellulose nanofibrils (CNF) and cellulose nanocrystals (CNC). CNF and CNC are commonly obtained from plant/wood cellulose after mechanical and/or chemical treatments while BC is biotechnologically produced by mi-

croorganisms using different carbon sources [29]. The three types of nanocellulose have been proposed for a diversity of medical and/or pharmaceutical applications. Regarding plant-derived nanocellulose hydrogels, recent encouraging applications include renewable and xeno-free wound dressings for skin graft donor sites [30] as well as controlled drug release platforms for both low and high molecular weight substances [31]. As an alternative to CNC and CNF, cellulose produced by microorganisms is emerging as a promising natural source of ready-to-use nanocellulose for medical and pharmaceutical applications.

2. BACTERIAL CELLULOSE

BC is produced extracellularly by Gram-negative bacterial cultures such as *Gluconacetobacter*, *Acetobacter*, *Agrobacterium*, *Achromobacter*, *Aerobacter*, *Sarcina*, *Azobacter*, *Rhizobium*, *Pseudomonas*, *Salmonella* and *Alcaligenes*. Among them, the most efficient BC producer belongs to the *Komagataeibacter* genus, specifically called *Komagataeibacter xylinus* (*K. xylinus*) [32, 33]. The observation that *Acetobacter xylinus* produces a gelatinous mass on liquid/air interfaces has been known since 1886 by the work of A.J. Brown [34]. This gelatinous mass was later identified as BC. The bacterium uses the nanofibrous film to protect itself from environmental stresses such as dehydration, nutrient deficiency and UV radiation. In addition, the BC allows the bacteria to float and to remain at the interface between medium and air thus increasing oxygen supply.

BC can conveniently be produced in laboratories following the process summarized in (Fig. 1). The bio-synthesis starts with the inoculation of a culture medium with a BC-producing bacteria strain (Fig. 1A). A typical culture medium contains the following compounds: 2% (w/v) glucose, 0.5% (w/v) yeast extract, 0.5% (w/v) peptone, 0.3% (w/v) sodium hydrogen phosphate and 0.1% (w/v) citric acid (Hestrin-Schramm (HS) culture medium) [35]. At molecular level, the biosynthesis of BC in the microorganism can be divided into four sub steps (Fig. 1B). First, phosphorylation of glucose by a glucokinase occurs (a) in the nucleus, followed by isomerization of glucose-6-phosphate to glucose-1-phosphate (b). Finally, it reacts with UDPG-pyrophosphorylase to form uranyl diphosphate-glucose (UDPG) (c), followed by the synthesis of BC by a cellulose synthase (d). The last step in the cytoplasm is a chain growth at the reduced end of the β -1,4-glucan chains by UDPG to form cellulose fibers [36].

In the extracellular space, the unassembled cellulose chains aggregate into fibrils. These fibrils usually consist of 10-15 fibers, have an approximate width of 15 nm and form microfibrils, which are arranged in cellulose bands with a width of approximately 80 nm [37]. This mechanism explains the three-dimensional cross-linked BC microstructure depicted in (Fig. 1D). The structure of the cellulose network can be affected by variation of bacteria strain, culture medium, pH value, temperature and mechanical stresses. With static cultivation, BC in form of fleeces or thin films is obtained, whereas agitated cultivation results in irregular aggregated, fibrous structures or spheroidal particles (Fig. 1C) [38].

The as-synthesized BC membranes exhibit unique properties proving its adequacy for epithelial regeneration pur-

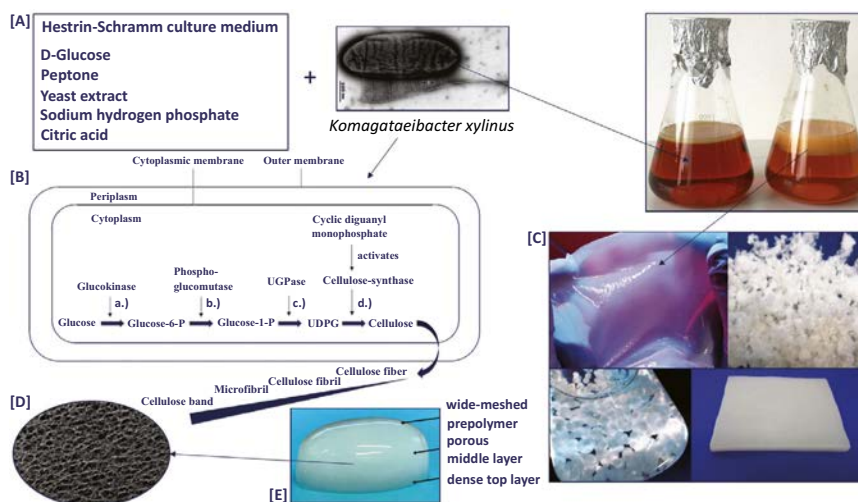


Fig. (1). Schematic representation of the basic BC generation process steps. (A) Formation process of BC fleece during cultivation of *K. xylinus* in HS medium in Erlenmeyer flasks. (B) Metabolic pathway of cellulose formation. (C) BC produced in different shapes. (D) Scanning electron microscopy (SEM) picture of BC porous middle layer depicting its three-dimensional fiber network. (E) Layered structure of a BC pellicle. (The color version of the figure is available in the electronic copy of the article).

poses such a high degree of polymerization (4,000 - 10,000) [28] and crystallization (up to 90%) [39]. For medical applications, the high mechanical stability, the lack of immunogenicity and the high purity are of particular relevance [38, 40]. The biocompatibility of BC cannot solely be attributed to the high purity of the material but also to its similar organization of the fibers as in native collagen [41]. Despite the identical chemical structure of BC and plant-based cellulose [42], BC clearly defines itself by its structure and material properties. The three-dimensional interwoven network of BC is characterized by a high surface area of 35 - 40 m²/g (measured in freeze-dried form) [43, 44] and a water content of about 99% [45]. The latter characteristic is the reason why BC is also called a “hydropolymer” or “hydrogel” [39]. Moreover, BC exhibits high temperature stability which allows temperature sterilization processes [46].

Last but not least, the attractiveness of this innovative biofabricated material has further increased due to its animal and human-free origin [47]. Its biosynthesis opens up the opportunity to develop biotechnological production to significantly influence and control the final BC shape and material features. Shapes, especially designed to come into contact with epithelial tissue, range from thin foils and fleeces used as covering, patch or dressing, tubes for artificial blood vessels [48] to preformed structures for implantation (*e.g.*, artificial meniscus [46] and ear cartilage replacement [49]). In recent years, enormous progress in BC cultivation techniques has been made to provide tailored-made and high-quality BC based materials. In parallel, the possibility to scale up BC production may broaden BC applicability in the near future [28].

To facilitate contextualization, a comparison between the hallmarks of BC and collagen, can be found in Table 1.


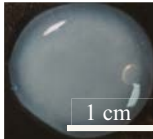
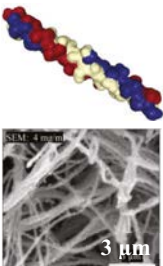
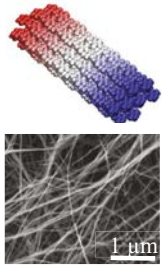
3. APPLICATIONS OF BC IN EPITHELIAL REGENERATION

In this section, several applications of BC in epithelial regeneration are summarized. Special emphasis is made on dermal treatments since, to date, this is the most widespread medical use of BC. Afterward, less studied applications of BC in epithelial regeneration identified as the most promising current research directions are compiled.

3.1. Dermal Applications

Skin is the largest and outermost human organ and covers the entire external body surface. Therefore, above all, the skin's primary function is to protect the underlying muscles, bones, ligaments and internal organs from external biological and chemical agents as well as physical influences [70, 71]. Furthermore, skin is also involved in sensation, temperature regulation, immunological surveillance, prevention of dehydration and synthesis of vitamin D3 [72]. The large epithelium of the skin, which is responsible for the barrier function against infection and waterproofing, is called epidermis. This outermost layer of the skin is a stratified squamous epithelium, composed of proliferating basal and differentiated suprabasal keratinocytes. The epidermis contains no blood vessels, and cells in the deepest layers are nourished by diffusion from blood capillaries extending to the upper layers of the dermis [73]. The integrity of this organ can be affected by cuts, burns, ulcers, surgical incisions or illnesses,

Table 1. Comparison between collagen (as a benchmark material) and bacterial cellulose regarding relevant properties of bio-materials for epithelial regeneration.

Property	Collagen	Bacterial Cellulose
Macrostructure	Sponges, hydrogels Image: Collagen sponge from: [50] 	Hydrogels, aerogels or films mainly with planar forms [51] 
Micro/nano structure	Triple helix protein fibers organized in 3D a network. SEM image of collagen image from [52] 	3D network of pure cellulose nanofibers 
Building blocks	Amino acids, mainly glycine, proline and hydroxyproline	β -1,4-linked D-glucose units
Origin	Mainly, livestock animals (cow, pig). Also plants [53] and fish [14]	Bacterial cultures, mainly <i>Komagataeibacter xylinus</i> strains
Purity	Variable	Very high
Fiber cross-section	≈ 100 nm [54]	20-100 nm [28]
Fiber length	≈ 1 μ m [54]	> 1 μ m, hard to determine precisely
Interwoven fibers	Yes	Yes
Degree of polymerization	> 1400	4,000-10,000 [28]
Molecular weight	High	High
Options for structuration	Fiber alignment [55, 56] Sacrificial templates [57]	Fiber alignment [58] Templates during biosynthesis [59]
Fiber Crystallinity	Non consensus	High (\approx up to 90% [60]), mix between I α and I β cellulose structures
Porosity	Very variable depending on collagen source and fabrication method 35-99% [50, 61, 62]	Very variable depending on the drying method and posterior treatments 60% -95 % [51, 61, 63]
Pore type and size	Interconnected pores with variable size: 26 [61] - 200 μ m (SpongeCol [®])	Multi-size Native BC ≈ 5 μ m. Can be modified with porogens (40 μ m in [64]) and by <i>in situ</i> modifications [65]
Water content	98% [50]	99%

(Table 1) contd....

Property	Collagen	Bacterial Cellulose
Temperature stability	200 °C [66]	Up to 300 °C
Biodegradability	High, \approx 1 month <i>in vitro</i> [62]	Low/none in the body, biodegradable by cellulases
Biocompatibility	High	High
Immunogenicity	Low/moderate	Low
Bioactivity	High, supports cell attachment and proliferation	Tunable Moderate as-synthesized, increases after modification [63, 67, 68]
Mechanical stability	Very variable: low in native collagen [13], increases after crosslinking [5]	High in general. Reported to be higher than collagen [61], to be improved after surface modification [69] and to recapitulate native cartilage [49]
Price	Variable, high for pure forms	Variable, depends on area of application
Commercial availability/scalability	High	High in the food form <i>nata de coco</i> (500-1500 tons per year per producer) and cosmetics but still low for high quality/purity (medical-pharmaceutical grade)

such as diabetes [74]. When the skin integrity is compromised, its structure and functions must be re-established as soon as possible to recover tissue homeostasis. To accomplish that, the wound healing process should begin almost immediately after a skin injury occurs, in order to avoid bacterial infection and dehydration [75, 76]. Due to the properties described above, BC is a promising biomaterial for healing skin injuries. In fact, BC has already been used as a natural polymeric wound care material since the 80s [77, 78]. BC meets many of the requirements of an ideal wound dressing: it acts as a physical barrier against bacterial infections, allows gas exchange, absorbs exudates, keeps a moist environment that enhances reepithelization, and is easy to remove without pain. [79, 80] Furthermore, BC is non-toxic and non-allergenic as described [36].

Today, several types of BC based wound dressings provided by different companies are on the market. The first BC-based medical product on the market was Biofill[®], a thin BC film with a water content of 8.5% used as temporary skin substitute and biological wound dressing. It has been successfully applied for the treatment of several skin injuries such as basal cell carcinoma, severe burns, dermabrasions, chronic ulcers as well as at donor and receptor sites in skin grafts. Among other benefits, immediate pain relief, close adhesion to the wound bed, spontaneous detachment following reepithelization and reduced treatment times as well as costs have been reported for this product. The only flaw discussed in some reports was the limited elasticity, when applied in areas of great mobility [77]. Along with the rising trend for modern moist wound management, clinical investigations of wet, never-dried BC for both, chronic wounds and burns, followed [81, 82]. Moist BC-based dressings such as XCell[®] were described as more effective than conventional wound dressing materials in promoting autolytic debridement, accelerating granulation and simultaneously donating and absorbing moisture from the wound [82].

Some recent studies on dermal BC applications focused on the understanding of the accelerated healing observed for both, dry and wet BC wound dressings, and thus contributed

to a better understanding of the effects. Kwak and colleagues [83] performed an *in vivo* study on rats and reported on distinct improvements in thickness of both, epidermis and dermis, as well as the number of blood vessels and an inhibition of the infiltration of mast cells at indicated time points in case of BC treated burns compared to gauze. The authors hypothesized that BC may accelerate the process of wound healing in burn injuries through regulation of angiogenesis and connective tissue formation.

Li and colleagues [84] evaluated the effect of the structure of BC on full-thickness skin wound repair. The hierarchical structure of BC films and their different effects on skin wound healing were studied both *in vitro* (in a wound healing model placed on a microfluidic chip) and *in vivo* (Wistar rats). The results indicated clear benefits of BC in the healing of full-thickness wounds compared to gauze in terms of inflammatory reaction and healing time. The *in vivo* and *ex vivo* experiments on rats also demonstrated a certain difference in performance of both sides of the BC pellicle. The bottom side of the BC film promoted blood vessel regeneration and collagen production of the wounds more than the top side. The authors argued that a looser BC network also promotes cell migration and proliferation and suggested heterogeneous BC-based biomaterials for complex tissue engineering. However, they did not investigate yet, whether a higher porosity and surface roughness may compromise the easy and pain-free detachment after reepithelization reported for BC wound dressings.

Cavalcanti *et al.* recently published the outcome of a randomized and controlled trial investigating the efficacy of perforated dry BC membranes for the treatment of lower limbs chronic varicose ulcers [79]. In the BC group, ulcers were more superficial at the end of the observation period (120 days) in more than 80% of the patients (*versus* 60% in the control group treated with triglyceride oil and gauze). The authors suggested that BC dressings could act as an inducer of tissue remodeling, stimulating the granulation process. They stressed the fact that the ulcer healing depends not only on the epidermal proliferation at the margins of the

lesion but also on the growth of the granulation tissue from the central area.

Several modifications allow to further increase the functionality of BC as wound care device while keeping the essential BC properties of biocompatibility and nanofibrillar structuration. Modifications of the cellulose can be obtained during the biofabrication process (*in situ*) e.g. using additives and by *post*-modification such as drying, chemical functionalization or loading of the BC network with active ingredients. An excellent overview of BC in various modifications developed for wound healing applications can be found by Sulaeva *et al.* [33]. However, some recent findings are highlighted in (Table 2) and discussed below.

3.1.1. Material Modifications

Modifications of the BC such as control the water content, surface topography and nanocomposites have been applied to improve wound healing. Rebelo *et al.* recently investigated the effects of varying water content on BC material properties. They demonstrated that the dehydration effects on BCs viscoelastic and electrochemical properties. Lower water contents as 80% and 50% caused increased stiffness and BC resistance to electron transfer became higher with lower electron capacity [96]. Those findings have implications for BC wound dressings with different moisture content. They may range from practical aspects such as handling and draping of the dressing to electrolyte exchange through the dressing. However, this should be investigated in further studies. Another group focused on modifications of the surface topography of BC dressings in order to improve wound healing. Botton and colleagues introduced a new approach called guided assembly-based biolithography (GAB) technology [85]. They developed PDMS molds with different surface patterns allowing a controlled *in situ* modification of the BC surface topography. The structured surface was shown to influence migratory patterns and alignment of human dermal fibroblasts and keratinocytes. A full-thickness wound model tested on mice confirmed the promotion of fibroblast infiltration and new collagen deposition in the wound bed by the modified dressing compared to flat BC.

3.1.2. Combination of BC with Other Biomaterials

In many studies, BC has been combined with other biomaterials known for their beneficial effects on wound healing. To give an example, Moraes and colleagues [97] investigated a self-prepared wound gel made from disintegrated bacterial cellulose and collagen type I (BC/COL). In an animal study, healing of surgical skin wounds in rat dorsum with BC/COL gel was compared with those from animals treated with commercial collagenase ointment and an untreated group. BC/COL hydrogel was found to be more efficient than the collagenase ointment. Wound closure and fully repaired epithelium and dermis with organized collagen fibers and tissue rich in blood vessels were observed at day 15. At the same time, the dermis was thinner in case of the collagenase ointment treatment and still under repair with the presence of numerous inflammatory cells for the untreated group. Especially, the adhesion of the hydrogel on the wound bed was found to be advantageous for the treatment.

Other groups reported the combination of BC with silk-sericin [98], chitosan [99] and dextrane [100]. Silk-sericin

was selected due to its cytoprotective and mitogenic effects, whereas chitosan and dextrane were selected based on their antibacterial efficiency and positive effects on fibroblast cell proliferation, respectively. In all cases, positive effects of the combination compared to native BC were reported.

H. Wu *et al.* used bacterial cellulose nanocrystals (BCNCs) to reinforce regenerated chitin (RC) fibers to form BCNC/RC filaments for surgical sutures. Mechanical measurements demonstrated that the strength of the BCNC/RC filament increased dramatically over the RC analogue. A yarn made of 30 BCNC-loaded fibers also achieved satisfactory mechanical performance, with a knot-pull tensile strength of 9.8 ± 0.6 N compared to 6.8 ± 0.6 N of RC yarn without BCNC. While obtaining biocompatibility of the surgical suture, enzymatic degradation rate can be tuned by varying the concentration of BCNCs in the yarn. It has been proven that BCNC/RC promotes cell proliferation (*in vivo*) murine skin wound closure experiments, without any adverse effects. The combination of strength-enhanced fiber and promising *in vivo* experiments qualify BCNC/RC to be a new candidate for application as BC-based medical suture [86].

3.1.3. Drug-delivery Systems

Furthermore, an increasing number of studies report on drug delivery systems based on BC for dermal applications [47]. To avoid the risk of bacterial infections, e.g. Amoxicillin loaded BC sponges were examined [101]. The functionalized sponges displayed good porosity and swelling, which are beneficial for absorbing wound exudates. Moreover, a wound infection model proved enhanced wound healing ability *in vivo*. In another study, antimicrobial peptides such as ϵ -poly-L-Lysine (ϵ -PLL) were investigated [94]. This peptide is a non-toxic biopolymer with broad-spectrum antimicrobial activity. Fürsatz *et al.* cross-linked low molecular weight ϵ -PLL in pristine BC membranes and to carboxymethyl cellulose functionalized BC using carbodiimide chemistry. The functionalization of BC with ϵ -PLL inhibited growth of *S. epidermidis* on the membranes but did not affect the cytocompatibility to cultured human fibroblasts as compared to native BC. The functionalization had no significant effects neither on the nanofibrous structure nor on the mechanical properties of the BC. Furthermore, there are recently published studies taking advantage of some classical approaches in cellulose chemistry applied to BC. e.g. Wu *et al.* used the 2,2,6,6-Tetramethyl-1-piperidinyloxy (TEMPO) oxidation to obtain superficially oxidized bacterial cellulose pellicles (TOBCP) and subsequently loaded them with silver nanoparticles (TOBCP/AgNP) [87]. Through this modification, they established antimicrobial activity by a silver ion release with a rate of 12.2% per day at 37 °C in three days while retaining the biocompatibility of TOBCP.

Following the same purpose, other groups reported about the incorporation of zinc oxide nanoparticles into BC. The nanocomposites exhibited high antibacterial activity against *Escherichia coli*, *Pseudomonas aeruginosa*, *Staphylococcus aureus* and *Citrobacter freundii*. In a burn wound model, animals treated with the BC/ZnO nanocomposite further showed a significant healing of 66% after 15 days related to day 0 compared to BC, which showed a healing of 50.5%

lesion but also on the growth of the granulation tissue from the central area.

Several modifications allow to further increase the functionality of BC as wound care device while keeping the essential BC properties of biocompatibility and nanofibrillar structuration. Modifications of the cellulose can be obtained during the biofabrication process (*in situ*) e.g. using additives and by *post*-modification such as drying, chemical functionalization or loading of the BC network with active ingredients. An excellent overview of BC in various modifications developed for wound healing applications can be found by Sulaeva *et al.* [33]. However, some recent findings are highlighted in (Table 2) and discussed below.

3.1.1. Material Modifications

Modifications of the BC such as control the water content, surface topography and nanocomposites have been applied to improve wound healing. Rebelo *et al.* recently investigated the effects of varying water content on BC material properties. They demonstrated that the dehydration effects on BCs viscoelastic and electrochemical properties. Lower water contents as 80% and 50% caused increased stiffness and BC resistance to electron transfer became higher with lower electron capacity [96]. Those findings have implications for BC wound dressings with different moisture content. They may range from practical aspects such as handling and draping of the dressing to electrolyte exchange through the dressing. However, this should be investigated in further studies. Another group focused on modifications of the surface topography of BC dressings in order to improve wound healing. Botta and colleagues introduced a new approach called guided assembly-based biolithography (GAB) technology [85]. They developed PDMS molds with different surface patterns allowing a controlled *in situ* modification of the BC surface topography. The structured surface was shown to influence migratory patterns and alignment of human dermal fibroblasts and keratinocytes. A full-thickness wound model tested on mice confirmed the promotion of fibroblast infiltration and new collagen deposition in the wound bed by the modified dressing compared to flat BC.

3.1.2. Combination of BC with Other Biomaterials

In many studies, BC has been combined with other biomaterials known for their beneficial effects on wound healing. To give an example, Moraes and colleagues [97] investigated a self-prepared wound gel made from disintegrated bacterial cellulose and collagen type I (BC/COL). In an animal study, healing of surgical skin wounds in rat dorsum with BC/COL gel was compared with those from animals treated with commercial collagenase ointment and an untreated group. BC/COL hydrogel was found to be more efficient than the collagenase ointment. Wound closure and fully repaired epithelium and dermis with organized collagen fibers and tissue rich in blood vessels were observed at day 15. At the same time, the dermis was thinner in case of the collagenase ointment treatment and still under repair with the presence of numerous inflammatory cells for the untreated group. Especially, the adhesion of the hydrogel on the wound bed was found to be advantageous for the treatment.

Other groups reported the combination of BC with silk-sericin [98], chitosan [99] and dextrane [100]. Silk-sericin

was selected due to its cytoprotective and mitogenic effects, whereas chitosan and dextrane were selected based on their antibacterial efficiency and positive effects on fibroblast cell proliferation, respectively. In all cases, positive effects of the combination compared to native BC were reported.

H. Wu *et al.* used bacterial cellulose nanocrystals (BCNCs) to reinforce regenerated chitin (RC) fibers to form BCNC/RC filaments for surgical sutures. Mechanical measurements demonstrated that the strength of the BCNC/RC filament increased dramatically over the RC analogue. A yarn made of 30 BCNC-loaded fibers also achieved satisfactory mechanical performance, with a knot-pull tensile strength of 9.8 ± 0.6 N compared to 6.8 ± 0.6 N of RC yarn without BCNC. While obtaining biocompatibility of the surgical suture, enzymatic degradation rate can be tuned by varying the concentration of BCNCs in the yarn. It has been proven that BCNC/RC promotes cell proliferation (*in vivo*) murine skin wound closure experiments, without any adverse effects. The combination of strength-enhanced fiber and promising *in vivo* experiments qualify BCNC/RC to be a new candidate for application as BC-based medical suture [86].

3.1.3. Drug-delivery Systems

Furthermore, an increasing number of studies report on drug delivery systems based on BC for dermal applications [47]. To avoid the risk of bacterial infections, e.g. Amoxicillin loaded BC sponges were examined [101]. The functionalized sponges displayed good porosity and swelling, which are beneficial for absorbing wound exudates. Moreover, a wound infection model proved enhanced wound healing ability *in vivo*. In another study, antimicrobial peptides such as ϵ -poly-L-Lysine (ϵ -PLL) were investigated [94]. This peptide is a non-toxic biopolymer with broad-spectrum antimicrobial activity. Fürsatz *et al.* cross-linked low molecular weight ϵ -PLL in pristine BC membranes and to carboxymethyl cellulose functionalized BC using carbodiimide chemistry. The functionalization of BC with ϵ -PLL inhibited growth of *S. epidermidis* on the membranes but did not affect the cytocompatibility to cultured human fibroblasts as compared to native BC. The functionalization had no significant effects neither on the nanofibrous structure nor on the mechanical properties of the BC. Furthermore, there are recently published studies taking advantage of some classical approaches in cellulose chemistry applied to BC. e.g. Wu *et al.* used the 2,2,6,6-Tetramethyl-1-piperidinyloxy (TEMPO) oxidation to obtain superficially oxidized bacterial cellulose pellicles (TOBCP) and subsequently loaded them with silver nanoparticles (TOBCP/AgNP) [87]. Through this modification, they established antimicrobial activity by a silver ion release with a rate of 12.2% per day at 37 °C in three days while retaining the biocompatibility of TOBCP.

Following the same purpose, other groups reported about the incorporation of zinc oxide nanoparticles into BC. The nanocomposites exhibited high antibacterial activity against *Escherichia coli*, *Pseudomonas aeruginosa*, *Staphylococcus aureus* and *Citrobacter freundii*. In a burn wound model, animals treated with the BC/ZnO nanocomposite further showed a significant healing of 66% after 15 days related to day 0 compared to BC, which showed a healing of 50.5%

Table 2. Modifications of BC and properties resulting from the modifications.

Material	Title of Paper	Results Obtained by BC Modification
BC with structured topography [85]	Surface-structured bacterial cellulose with Guided Assembly-Based Biolithography (GAB)	Improved cell alignment Promotion of fibroblast infiltration and new collagen deposition in the wound bed
BCNC/RC [86]	Regenerated chitin fibers reinforced with bacterial cellulose nanocrystals as suture biomaterials	Biocompatible surgical sutures increasing strength of BCNC/RC filaments Enzymatic degradation possible Degradation rate can be tuned by varying concentration of BCNCs in the yarn Chitin can promote cell proliferation (<i>in vivo</i>)
TOBCP/AgNP [87]	TEMPO-Oxidized Bacterial Cellulose Pellicle with Silver Nanoparticles for Wound Dressing	Antimicrobial activity Ag ⁺ release with a rate of 12.2%/day at 37°C in 3 days Biocompatible wound dressing
BC/ZnO [88]	Bacterial cellulose-zinc oxide nanocomposites as a novel dressing system for burn wounds	Antimicrobial activity against <i>Escherichia coli</i> , <i>Pseudomonas aeruginosa</i> , <i>Staphylococcus aureus</i> and <i>Citrobacter freundii</i> Significant healing of 66% after 15 days related to day 0
BC/TiO ₂ [89]	Bacterial cellulose-TiO ₂ nanocomposites promote healing and tissue regeneration in burn mice model	Antimicrobial activity against <i>Escherichia coli</i> (81.0 ± 0.4%) and <i>Staphylococcus aureus</i> (83.0 ± 0%)
BC/SMN-Zein [90]	Drug release and antioxidant/antibacterial activities of silymarin-zein nanoparticle/Bacterial cellulose nanofiber composite films	Flavonoid silymarin (SMN) and zein loading through nanoparticle adsorbing onto BC nanofibers Change of wettability and swelling Antioxidant and antibacterial activity air-dried SMN-Zein/BC nanocomposite slow down the lipid oxidation
BC/Octenidin [91]	Controlled extended octenidine release from a bacterial nanocellulose/Poloxamer hybrid system	Long term controlled release of octenidine up to one-week improved mechanical and antimicrobial properties. Ready-to-use system with Poloxamer loaded BC for advanced treatment of infected wounds Toxicity test performed with shell-less hen's egg model
BC/CMC/MTX [92]	Effect of <i>in situ</i> modification of bacterial cellulose with carboxy-methylcellulose on its nano/microstructure and methotrexate release properties	Impact of DS-CMC on methotrexate loading Topical treatment of psoriasis Decrease of the elastic modulus as the DS of CMC increased
BC/PHEMA [93]	Embedding of Bacterial Cellulose Nanofibers within PHEMA Hydrogel Matrices: Tunable Stiffness Composites with Potential for Biomedical Applications	New modification: <i>in situ</i> UV radical polymerization of HEMA monomer impregnated into wet BC nanofibrous structure Significant improvement in mechanical properties Tensile strength increased Non toxic rMSCs (rat mesenchymal stem cells) proliferation tissue replacement and wound healing
BC/ε-poly-L-Lysine [94]	Functionalization of bacterial cellulose wound dressings with the antimicrobial peptide ε-poly-L-Lysine	Antimicrobial activity (broad-spectrum) without affecting the beneficial structural and mechanical properties Modification with non-toxic biopolymer ε-PLL inhibited growth of <i>S. epidermidis</i> on the membranes but did not affect the cytocompatibility to cultured human fibroblast

(Table 2) contd....

Material	Title of Paper	Results Obtained by BC Modification
BC/PVA [95]	Preparation and <i>in vitro</i> characterization of BC/PVA hydrogel composite for its potential use as artificial cornea biomaterial	Higher visible light transmittance than plain BC
BC/HA [60]	Bacterial cellulose/hyaluronic acid composite hydrogels with improved viscoelastic properties and good thermodynamic stability	Higher visible light transmittance than plain BC
ABC/urinary bladder matrix [67]	Acetylated bacterial cellulose coated with urinary bladder matrix as a substrate for retinal pigment epithelium	Higher adhesion and proliferation of retinal pigment epithelium cells than uncoated BC Closer recapitulation of the <i>in vivo</i> cell phenotype than uncoated BC
BC/varying porosity [64]	Bacterial cellulose-based biomimetic nanofibrous scaffold with muscle cells for hollow organ tissue engineering	Higher pore size than native BC to allow muscle cell in-growth Higher porosity Small decrease in mechanical strength

after the same treatment [88]. The incorporation of titanium dioxide nanoparticles (TiO₂) in BC has also given encouraging results [89]. Khalid *et al.* depicted *in vivo* burn wound healing potential of BC and TiO₂ nanocomposites (BC/TiO₂). Antimicrobial activity of the nanocomposite was against *Escherichia coli* (81.0 ± 0.4%) and *Staphylococcus aureus* (83.0 ± 0.0%) was confirmed through agar disc diffusion protocol.

The combination of BC with natural substances or natural derived Active Pharmaceutical Ingredients (APIs) is becoming more and more notable. Tsai *et al.* investigated a composite film with silymarin-zein nanoparticles and BC nanofibers. They applied adsorption of flavonoid silymarin (SMN) and zein nanoparticles to load them onto the fibers for improving higher antioxidant and antibacterial activity. The authors could also show that air-dried SMN-Zein/BC nanocomposites slowed down lipid oxidation [90].

Lima Fontes *et al.* have shown the effect of CMC *in situ*-modifications on BC nano/microstructure and methotrexate (MTX) release properties. The degree of substitution of CMC (DS-CMC) has a massive impact on API loading; since carboxymethylcellulose (CMC) is a well-known candidate to change *e.g.* pore-sizes of the three-dimensional network of BC. For topical skin application, MTX is used as disease-modifying anti-rheumatic drug for *e.g.* treatment of psoriasis. However, besides the impact of loading capacity, increasing DS-CMC causes a decrease of the elastic modulus of BC [92].

Remarkable is also the new *in situ*-modification by UV radical polymerization of HEMA monomer impregnated into wet BC nanofibers. The combination of BC with poly(2-hydroxyethyl methacrylate) depicted a significant improvement in the mechanical properties (*e.g.* tensile strength) and the rat mesenchymal stem cells proliferation which qualifies this modification for tissue replacement and wound healing applications [93].

Considering all these wound dressings loaded with an API as drug-delivery systems, most of the studies show initial bursts of the API release. Up to now, long-term controlled release systems are still very rare. Nevertheless,

Alkhatib *et al.* designed a new delivery system consisting of BC and Poloxamer developed for the antiseptic API octenidine as a long-term ready-to-use system for dermal wound treatment (Fig. 2). This delivery system provides a prolonged retention time for octenidine, up to one week, with improved mechanical and antimicrobial properties as well as a high biocompatibility [91].

3.1.4. BC as Cell Carrier

Because of the possibility to support mammalian cell attachment and proliferation, BC films are also investigated as cell carriers in cell transplantation [102]. For instance, bacterial cellulose/acrylic acid (BC/AA) wound dressing hydrogels (without cells) enhanced wound healing capacity in nude mice. Interestingly, when the BC/AA hydrogels were loaded with human epidermal keratinocytes and human dermal fibroblasts, the positive effects of the BC/AA in burn recovery were accentuated. The *in vivo* results showed that the cell-loaded hydrogel produces the greatest acceleration on burn wound healing, followed by treatment with the hydrogel alone in comparison to the untreated group. The percentage wound reduction on day 13 in the mice treated with BC/AA hydrogel loaded with cells (77.3 ± 6.2%) was significantly higher than that in the control-treated mice (64.8 ± 6.8%) or the hydrogel-treated ones alone (71.5 ± 2.3), respectively. Histological analysis for the expression of collagen type I *via* immunohistochemistry and transmission electron microscopy indicated a greater deposition of collagen in the mice treated with the hydrogel loaded with cells than in the mice administered with other treatments. Therefore, the BC/AA hydrogel proved promising applicability as a wound dressing and as a cell carrier.

In summary, very promising experimental investigations and preclinical studies have been performed suggesting the future application of modified, drug-loaded and/or native BC in an increasing number of dermal applications. The increasing number of BC-based wound dressings on the market follow the same trend and confirm the high commercialization potential of innovative BC based medical products. Other fields of BC application in damaged epithelial tissues regeneration are still in its infancies, as described below, but show the same promise.

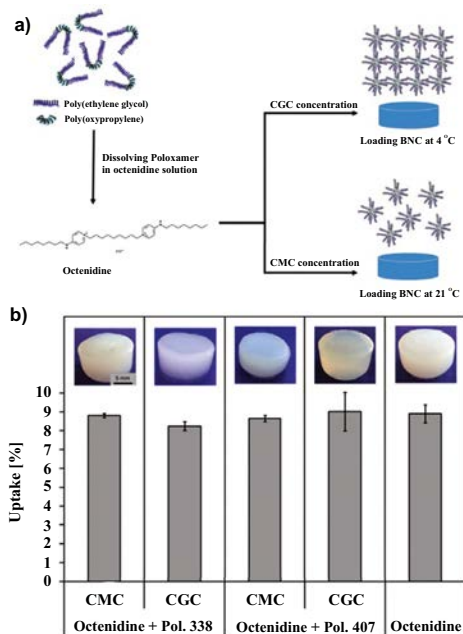


Fig. (2). (a) Schematic overview of the loading of BC with Poloxamers forming critical micelle concentration (CMC) and critical gelation concentration (CGC) samples. (b) Photographs of octenidine and octenidine/Poloxamer loaded CMC and CGC BC samples and percentage uptake of octenidine (mean \pm SD, $n = 3$) after incubation of fleeces for 48 h by Alkathib *et al.* reproduced with permission from Elsevier [91]. (The color version of the figure is available in the electronic copy of the article).

3.2. Ophthalmology

Ophthalmology is a branch of medicine historically linked with the use of biomaterials, exemplified by contact and intraocular lenses. The application of biologically derived materials in regenerative ophthalmology predominantly concentrates on the ocular surface and, to a lesser extent, on the retina. [103] (Fig. 3) localizes these two tissues in a 3D human eye anatomy representation. To date, for ocular surface wound healing, amniotic membrane patches are regularly applied [104] and the most common clinical approach for ocular surface reconstruction relies on corneal transplantation, whereas innovative regenerative medicine approaches are gradually gaining acceptance [105].

The outermost part of eye comprises two epithelia: The corneal and the conjunctival epithelium. Recently, collagen based materials have been designed to reconstruct these two structures [106-109], while other authors developed silk or keratin-based membranes [110]. Some previous reviews already pointed out that the innate hydrophilicity, flexibility and mechanical stability of BC suggest a potential application on corneal regeneration [111, 112]. One more strength of BC for this specific application is its conformability, which might facilitate the adaptation of the biomaterial to the

dome shape of the ocular surface. BC has been shaped into a contact lens-like form by culturing *K. xylinus* on top of hydrophilic surfaces [113] and, in parallel, BC has proven to support the growth of human corneal stromal cells [114]. However, research papers on this topic are scarce and describe preliminary findings, indicating that the application of BC in ocular surface regeneration is still a field in its infancy that deserves to be explored in more depth.

Native-state BC has a visible light transmittance around 70% due to the dispersive character of the fibers bundles and pores. In order to increase the transparency of BC for long-term applications in corneal regeneration, BC has been combined with other components such polyvinyl alcohol (PVA) [95]. BC/PVA composites, prepared by a freeze-thaw method, were satisfactorily evaluated in terms of water holding capacity, light transmittance, mechanical properties and thermal stability; important characteristics for a corneal substitute. However, no biological characterization of those materials have been published at the time of this review. Similarly, BC/Hyaluronic acid composites (BC/HA) were prepared by a physical gelation method with the resulting material displaying 90% of visible light transmittance [60]. Interestingly, this feature was maintained after a drying-rewetting cycle. According to the authors, biocompatibility tests for the BC/HA composites are in progress.

To our knowledge, the only *in vivo* assessment of BC as a corneal replacement was carried out by R. V. Sepúlveda *et al.* [115]. In this study, dry BC and BC/polycaprolactone (PCL) hydrogels were implanted into rabbit's eyes to replace the corneas. Both BC and BC/PCL implants remained stable over the 45 days of the study and delayed the manifestation of corneal edema with respect to the control group that received no treatment. Nevertheless, the authors report chronic inflammation and incomplete re-epithelization in the long term for the rabbits receiving the BC and BC/PCL implants. These results hint that the use of BC as a permanent corneal substitution will be challenging.

Another research direction regarding ophthalmological applications of BC is the repair of retinal pigment epithelium (RPE). The function of this highly specialized epithelium is impaired in patients suffering from age related macular degeneration, the most common cause of vision loss in Europe [116]. Gonçalves *et al.* described that acetylated BC supported the attachment and proliferation of RPE cells and envisioned a potential application of BC as a carrier for RPE cell transplantation to the retina [117]. More recently, the same group reported a further functionalization of acetylated-BC (ABC) with urinary bladder matrix [67]. It is encouraging to read that when RPE cells were seeded on these substrates, they recapitulated closer the *in vivo* phenotype than on uncoated ABC.

Taken together, these studies set the basis for future research on BC-based biomaterials specifically targeting eye epithelia. The above-summarized results are still immature and, due to the lack of *in vivo* experiments, conclusions must be drawn with caution. Nevertheless, the field of regenerative ophthalmology appears as an opportunity for the BC-based biomaterials to find a potential niche in the health market, which appears as less competitive than *i.e.* the skin.

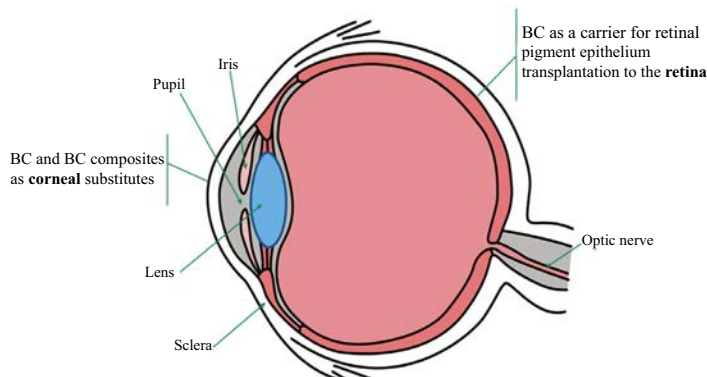


Fig. (3). Schematic representation of the human eye anatomy and the targeted tissues treated with BC-based therapies. Image modified from [106]. (The color version of the figure is available in the electronic copy of the article).

3.3. Stomatology

Deliberations for potential applications of BC, e.g. temporal implants in dental extraction alveoli or wound dressing after mucosal transplantation recently came up, but the testing of BC and specific product developments are still rare. However, the softness of the hydropolymer plus its flexibility and self-attachment to surfaces strongly suggest a broader scope of application in dentistry. Studies of Weyell *et al.* depicted the benefits of doxycycline-loaded hydrated and freeze-dried BC in dental therapies such as dental extraction or mucosal transplantation [118]. Both applications would benefit on the one hand from a material, which degrades under physiological conditions and on the other hand from an antibiotic environment. Consequently, periodate-oxidation of BC was performed to modify its degradation kinetics. In addition, native and oxidized BC loaded with doxycycline were tested for prophylaxis against infection. An *in vitro* toxicity test ensured biocompatibility of oxidized BC, whereas agar diffusion tests of samples loaded with doxycycline against pathogenic oral bacteria proved high antibiotic efficiency. Release studies of the drug from native and oxidized BC confirmed a comparable release behavior showing an initial burst of 50-60% within the first hour and a total release of about 90% after 3-5 h [119].

Chiaoprakobbkij *et al.* developed freeze-dried composite sponges made from BC fibers and alginate, crosslinked with CaCl_2 . This recent *in vitro* study also showed a supported proliferation of human keratinocytes and gingival fibroblasts caused by this composite material [120]. In conclusion, there is still an unmet potential for BC-based products (e.g. periodontal dressings, sponges, tamponades, sutures or even drug delivery systems) in dentistry.

3.4. Other Epithelial Surfaces

Epithelial tissues form part of a myriad of membranes and barriers inside the human body. Some of these structures such as the eardrum, the meninges or the linings of hollow organs are difficult to rebuild after disease or trauma and would largely benefit from new repair approaches based on

natural biomaterials. In this last section, we have grouped further applications of BC regarding the regeneration of diverse body surfaces.

The tympanic membrane (TM) separates the external ear from the middle ear and its key function is to amplify airborne vibrations and transduce them to the middle ear. TM perforation is a common clinical situation and implies a risk of prolonged damage and hearing reduction, especially if bacterial infection occurs. BC patches have been evaluated as wound healing devices in eardrum perforations to substitute the muscle, fat or cartilage autografts that are conventionally used in TM reconstruction. F. Coelho Alves Silveira *et al.* performed a randomized controlled trial with 40 patients and reported a higher success rate (90 vs 80%) when BC films were used as wound dressings respect to autologous temporal fascia (muscle) patches. Notably, the BC treatment reduced the operation time in more than one hour and the total hospitalization costs were 13 times lower. Another study tested the efficiency of BC to solve small but long-lasting TM perforations in 16 ears [121]. The authors conclude that the high rate of recovery of these patients treated with BC (81.3% of the cases) encourages for further investigations of BC in otology. Interestingly, this publication highlights, from a clinical point of view, some advantages of BC respect to other grafting materials for TM reconstruction: no need of general anesthesia for the surgical procedure, easy shaping of the material to match the defect size, enhancement of cell growth in the damaged area, easy sterilization and short operating time.

Because its limited endogenous regenerative potential, the nervous system is another area where BC patches could be of great interest. In particular, dura mater, the outermost of the three meninges that surround the brain and the spinal cord, is frequently disrupted after neurosurgical interventions or trauma and thus can be regarded as a potential target for BC-based treatments. *In vitro*, patterned BC substrates proved to support and guide the growth of neural stem cells [59]. In line with this, Goldschmidt and coworkers reported the proliferation of human dural fibroblasts (primary cul-

tures) on BC films [122]. These authors propose BC as a conceivable option for dural implants principally because of its mechanical stability and its capability to support the growth and migration of native dural cells. *In vivo*, damage to dura mater has been experimentally treated with BC patches [123]. In this study, sutureless BC implants were inserted in 40 rats and examined after 120 days without noticing any complication such as infection, cerebrospinal fluid leakage, hemorrhages or behavior disturbance in the animals during the study time. The levels of inflammation were similar between the group that received BC patches and the group implanted with a polytetrafluoroethylene-based material (positive control). The authors claim a satisfactory level of BC graft acceptance and highlight the potential application of BC in dura mater repair. Actually, in 2014 the commercial product SYNTHACEL Dura Repair was launched for this specific application after showing an equivalent effectiveness compared to other commercially available products for dura replacement [124].

BC native structure in the form of a fibrous hydrogel and some reported BC film thickness [51] are comparable to those of the mucus layers covering the body's internal cavities [125, 126]. Thus, BC has also been proposed for reconstruction of hollow organs [112] that is, urinary, reproductive, respiratory and intestinal tracks, which contain a mucosa on its inner side. To this end, asymmetric BC structures exhibiting one site with densely packed BC fibers and another side with loose BC fibers were generated mimicking the architecture of tubular organs [64]. These scaffolds achieved higher porosity than native BC and after being seeded with muscle cells, were implanted in dog urinary systems yielding better outcomes than unmodified BC.

The findings summarized in this section collectively underline the versatility BC and its potential to take part in the regeneration of diverse body surfaces. Likewise, the adaptability of BC in terms of size, shape and porosity will be crucial in the future to conceive tissue-specific biomaterials based on BC.

CONCLUSION

The outstanding properties of BC, in conjunction with its natural origin and sustainable manufacturing call for many diverse applications in epithelial regeneration. Here, we provide a compact but detailed synopsis about the opportunities for BC-based alternatives to conventional treatments in this field.

Huge progress has been made in the development of novel BC-based materials for dermal applications and in the understanding of their positive effects on wound healing. Approaches ranging from modifications of topography, water content and pore structure to combinations with other biopolymers, active ingredients and/or cells have shown that BC is not only an excellent wound dressing material in its native form but also a versatile platform material to tailor-made product design. Along with the increasing comprehension of the reasons for accelerated wound healing observed for native as well as modified BC, new BC-based medical products, designed for the treatment of specific skin lesions, can be expected to enter the market within the next couple of years.

Besides the well-known example of the outer skin, we pinpointed other epithelial surfaces that could benefit from innovative treatments based on BC. In the field of ophthalmology, the preliminary findings reviewed here should encourage future research on BC-based biomaterials specifically targeting eye epithelia since the field of regenerative ophthalmology appears as an opportunity for BC to find a niche in the competitive health market. Similarly, the softness of the BC hydrogels together with its flexibility and self-attachment to body surfaces strongly suggest a broader scope of potential application in dentistry, a field that definitely deserves more research efforts. Worth noting are the reports on tympanic membrane reconstruction highlighting important advantages of BC compared to other grafting materials from a clinical perspective: no need of general anesthesia for the surgical procedure, easy shaping of the material to match the defect size, enhancement of cell growth in the damaged area, easy sterilization and short operating time.

The potential of BC as cell carrier should not be underestimated. In this manuscript we gathered abundant examples of cell types that can effectively attach and proliferate on BC substrates. These cell types include diverse human cells; epidermal keratinocytes, dermal fibroblasts, corneal stromal cells, retinal pigment epithelium and other mammalian cells like neural stem cells (mouse) and muscle cells (dog). On top of that, BC exhibits potentiality as a substrate for stem cell transplantation as it proved to maintain stemness of mouse mesenchymal stem cells for a longer period of time than traditional culture methods [127].

Naturally, there are some difficulties that BC-based biomaterials will need to overcome to effectively contribute to epithelial regeneration. When permanent replacement for epithelial tissue is targeted, BC should allow cell ingrowth to provide a proper integration of the biomaterial into the surrounding tissue. So far, this can only be achieved when BC is specifically modified to increase porosity. Moreover, BC based (implant) materials need to degrade after fulfilling the intended medical purpose. Degradability of BC under physiological conditions can only be achieved after chemical modification or enzymatic treatment and the verification of total degradation and metabolization in *in vivo* studies is still open. Likewise, for the specific application of long-term corneal replacement, BC will also need to be adapted to improve visible light transmittance.

However, these limitations in some specific fields of medical application are already addressed in current research and will probably be overcome in the next years. The significant progress in controlled production and the successful design of bioreactors suited for industrial scale production of medical grade BC [38] already paved the way for faster commercialization. Together with the profound knowledge gained by young companies world-wide about the production of BC based products according to current quality management and medical device regulations, this progress will significantly accelerate the market entrance of further BC based products including an increasing number of implant materials designed for epithelial regeneration.

LIST OF ABBREVIATIONS

API	= Active Pharmaceutical Ingredient
BC	= Bacterial Cellulose

BC/AA	=	Bacterial Cellulose/Acrylic acid
BC/COL	=	Bacterial Cellulose/Collagen
BC/HA	=	Bacterial Cellulose/Hyaluronic Acid
BC/PCL	=	Bacterial Cellulose/ PolyCaproLactone
BCNC	=	Bacterial Cellulose NanoCrystals
CGC	=	Critical Gelation Concentration
CMC (1)	=	Carboxymethylcellulose
CMC (2)	=	Critical Micelle Concentration
DMARD	=	Disease-Modifying Anti-Rheumatic Drug
DS	=	Degree of Substitution
HA	=	Hyaluronic Acid
HEMA	=	2-HydroxyEthyl MethAcrylate
K. xylinus	=	Komagataeibacter xylinus
MTX	=	Methotrexate
PCL	=	PolyCaproLactone
PHEMA	=	Poly (2-HydroxyEthyl MethAcrylate)
PVA	=	Poly Vinyl Alcohol
RC	=	Regenerated Chitin
RPE	=	Retinal Pigment Epithelium
SEM	=	Scanning Electron Microscope
SMN	=	Flavonoid Silymarin
TEMPO	=	2,2,6,6-Tetramethylpiperidine 1-oxyl radical
TM	=	Tympanic Membrane
TOBCP	=	TEMPO-Oxidized Bacterial Cellulose Pellicle
UDPG	=	Uranyl Diphosphate-Glucose
ε-PLL	=	ε-Poly-L-Lysine

CONSENT FOR PUBLICATION

Not applicable.

FUNDING

UB and DK gratefully acknowledge the Free State of Thuringia and the European Social Fund (2016 FGR 0045) as well as the European Commission under a MSCA-ITN award, grant number 675743 (ISPIC), and under a MSCA-RISE award, grant number 777682 (CANCER) for funding.

CONFLICT OF INTEREST

The authors declare no conflict of interest, financial or otherwise.

ACKNOWLEDGEMENTS

The authors IA, AL and AR acknowledge the financial support from the Spanish Ministry of Science, Innovation and Universities through the MAT2015-64442-R project, the ‘Severo Ochoa’ Programme for Centers of Excellence in R&D (SEV-2015-0496) and the PhD scholarship of I.A. (BE-2016-076734) and the Generalitat de Catalunya for the 2017SGR765 project. These authors also express their gratitude to the Centre d’Oftalmologia Barraquer for their helpful suggestions in the elaboration of this manuscript.

REFERENCES

- [1] Frykberg RG, Banks J. Challenges in the treatment of chronic wounds. *Adv wound care*. 2015; 4(9): 560-82.
- [2] Okonkwo UA, DiPietro LA. Diabetes and wound angiogenesis. *Int J Mol Sci* 2017; 3; 18(7).
- [3] Sun G, Zhang X, Shen Y-I, *et al.* Dextran hydrogel scaffolds enhance angiogenic responses and promote complete skin

- regeneration during burn wound healing. *Proc Natl Acad Sci* 2011; 108(52): 20976-81.
- [4] MacNeil S. Biomaterials for tissue engineering of skin. *Mater Today* 2008; 11(5): 26-35.
- [5] Araña M, Peña E, Abizanda G, *et al.* Preparation and characterization of collagen-based ADSC-carrier sheets for cardiovascular application. *Acta Biomater* 2013; 9(4): 6075-83.
- [6] Qi C, Yan X, Huang C, Melzerzanov A, Du Y. Biomaterials as carrier, barrier and reactor for cell-based regenerative medicine. *Protein Cell* 2015; 6(9): 638-53.
- [7] D’Este M, Eglin D, Alini M, Kyllonen L. Bone regeneration with biomaterials and active molecules delivery. *Curr Pharm Biotechnol* 2015; 16(7): 582-605.
- [8] Gagner JE, Kim W, Chaikof EL. Designing protein-based biomaterials for medical applications. *Acta Biomater* 2014; 10(4): 1542-57.
- [9] Green JJ, Elisseff JH. Mimicking biological functionality with polymers for biomedical applications. *Nature* 2016; 540(7633): 386-94.
- [10] Sugihara H, Toda S, Miyabara S, Fujiyama C, Yonemitsu N. Reconstruction of alveolus-like structure from alveolar type II epithelial cells in three-dimensional collagen gel matrix culture. *AMJ Pathol* 1993; 142: 783-92.
- [11] Wang Y, Wang X, Shi J, *et al.* A biomimetic silk fibroin/sodium alginate composite scaffold for soft tissue engineering. *Nat Publ Gr* 2016; 6: 39477; doi: 10.1038/srep39477 (2016)
- [12] Dou Y, Zhang B, He M, *et al.* Keratin/polyvinyl alcohol blend films cross-linked by dialdehyde starch and their potential application for drug release. *Polymers (Basel)* 2015; 7(3): 580-91.
- [13] Dong C, Lv Y. Application of collagen scaffold in tissue engineering: Recent advances and new perspectives. *Polymers (Basel)* 2016; 8(2): 1-20.
- [14] Yamada S, Yamamoto K, Ikeda T, Yanagiguchi K, Hayashi Y. Potency of fish collagen as a scaffold for regenerative medicine. *Biomed Res Int* 2014; 2014: 302932.
- [15] Mullins RJ, Richards C, Walker T. Allergic reactions to oral, surgical and topical bovine collagen Anaphylactic risk for surgeons. *Aust N Z J Ophthalmol* 1996; 24(3): 257-60.
- [16] Eriksson A, Burcharth J, Rosenberg J. Animal derived products may conflict with religious patients’ beliefs. *Med Ethics* 2013; 1: 14-8.
- [17] Willard JJ, Drexler JW, Das A, *et al.* Plant-derived human collagen scaffolds for skin tissue engineering. *Tissue Eng Part A* 2013; 19(13-14): 1507-18.
- [18] Industry Analysis Report 2025. Global Collagen Market Size By Source. *Grand View Research*; 2017.
- [19] Mundada AS, Avari JG. Novel biomaterial for transdermal application: *in vitro* and *in vivo* characterization. *Drug Deliv* 2011; 18(6): 424-31.
- [20] Yunoki S, Hatayama H, Ebisawa M, Kondo E, Yasuda K. A novel fabrication method to create a thick collagen bundle composed of uniaxially aligned fibrils: An essential technology for the development of artificial tendon/ligament matrices. *J Biomed Mater Res-Part A* 2015; 103(9): 3054-65.
- [21] Baldwin M, Snelling S, Dakin S, Carr A. Augmenting endogenous repair of soft tissues with nanofibre scaffolds. *J R Soc Interface* 2018; 15(141): 20180019.
- [22] Mihai MM, Preda M, Lungu I, *et al.* Nanocoatings for chronic wound repair-modulation of microbial colonization and biofilm formation. *Int J Mol Sci* 2018; 19(4): 1179.
- [23] Mofazzal Jahromi MA, Sahandi Zangabad P, Moosavi Basri SM, *et al.* Nanomedicine and advanced technologies for burns: Preventing infection and facilitating wound healing. *Adv Drug Deliv Rev* 2018; 123: 33-64.
- [24] Andreu V, Mendoza G, Arruebo M, Irueta S. Smart dressings based on nanostructured fibers containing natural origin antimicrobial, anti-inflammatory, and regenerative compounds. *Mater* 2015; 8(8): 5154-93.
- [25] Gomes SR, Rodrigues G, Martins GG, Henriques CMR, Silva JC. *In vitro* evaluation of crosslinked electrospun fish gelatin scaffolds. *Mater Sci Eng C* 2013; 33: 1219-27.
- [26] Tonsomboon K, Butcher AL, Oyen ML. Strong and tough nanofibrous hydrogel composites based on biomimetic principles. *Mater Sci Eng C* 2017; 72: 220-7.
- [27] Ju HW, Lee OJ, Lee JM, *et al.* Wound healing effect of electrospun silk fibroin nanomatrix in burn-model. *Int J Biol Macromol* 2016;

- 85: 29-39.
- [28] Klemm D, Cranston ED, Fischer D, *et al.* Nanocellulose as a natural source for groundbreaking applications in materials science: Today's state. *Mater Today* 2018; 21(7): 720-48.
- [29] Zeng M, Laromaine Sagué A, Roig Serra A. Bacterial cellulose: fabrication, characterization and biocompatibility studies. Autonomous University of Barcelona; 2014; 148.
- [30] Hakkarainen T, Koivuniemi R, Kosonen M, *et al.* Nanofibrillar cellulose wound dressing in skin graft donor site treatment. *J Control Release* 2016; 244: 292-301.
- [31] Paukkonen H, Kunnari M, Laurén P, *et al.* Nanofibrillar cellulose hydrogels and reconstructed hydrogels as matrices for controlled drug release. *Int J Pharm* 2017; 532(1): 269-80.
- [32] Piecheth GF, Pirich CL, Sierakowski MR, *et al.* Bacterial cellulose in biomedical applications: A review. *Int J Biol Macromol* 2017; 104: 97-106.
- [33] Sulaeva I, Hennigs U, Rosenau T, Potthast A. Bacterial cellulose as a material for wound treatment: Properties and modifications. A review. *Biotechnol Adv* 2015; 33(8): 1547-71.
- [34] Brown AJ. XLIII.-On an acetic ferment which forms cellulose. *J Chem Soc Trans* 1886; 49: 432-9.
- [35] Müller A, Ni Z, Hessler N, *et al.* The biopolymer bacterial nanocellulose as drug delivery system: investigation of drug loading and release using the model protein albumin. *J Pharm Sci* 2013; 102(2): 579-92.
- [36] Rajwade JM, Paknikar KM, Kumbhar JV. Applications of bacterial cellulose and its composites in biomedicine. *Appl Microbiol Biotechnol* 2015; 99(6): 2491-511.
- [37] Lee KY, Buldum G, Mantalaris A, Bismarck A. More than meets the eye in bacterial cellulose: Biosynthesis, bioprocessing, and applications in advanced fiber composites. *Macromol Biosci* 2014; 14(1): 10-32.
- [38] Kralisch D, Hessler N, Klemm D, Erdmann R, Schmidt W. White biotechnology for cellulose manufacturing-the HoLiR concept. *Biotechnol Bioeng* 2010; 105(4): 740-7.
- [39] Klemm D, Kramer F, Moritz S, *et al.* Nanocelluloses: A new family of nature-based materials. *Angew Chem Int Ed Engl* 2011; 50(24): 5438-66.
- [40] Chen L, Hong F, Yang XX, Han SF. Biotransformation of wheat straw to bacterial cellulose and its mechanism. *Bioresour Technol* 2013; 135: 464-8.
- [41] Aber MM, Mohd Amin MCL, Martin C. A review of bacterial cellulose-based drug delivery systems: Their biochemistry, current approaches and future prospects. *J Pharm Pharmacol* 2014; 66(8): 1047-61.
- [42] Gardner KH, Blackwell J. The structure of native cellulose. *Biopolymers* 1974; 13(10): 1975-2001.
- [43] Guo J, Catchmark JM. Surface area and porosity of acid hydrolyzed cellulose nanowhiskers and cellulose produced by *Gluconacetobacter xylinus*. *Carbohydr Polym* 2012; 87(2): 1026-37.
- [44] Kim D, Nishiyama Y, Kuga S. Surface acetylation of bacterial cellulose. *Cellulose* 2002; 9(3): 361-7.
- [45] Gatenholm P, Klemm D. Bacterial nanocellulose as a renewable material for biomedical applications. *MRS Bull* 2010; 35: 208-13.
- [46] Bodin A, Backdahl H, Fink H, *et al.* Influence of cultivation conditions on mechanical and morphological properties of bacterial cellulose tubes. *Biotechnol Bioeng* 2007; 97(2): 425-34.
- [47] Pöttinger Y, Kralisch D, Fischer D. Bacterial nanocellulose: The future of controlled drug delivery? 2017; 8(9): 753-61.
- [48] Klemm D, Schuhmann D, Udhardt U, Marsch S. Bacterial synthesized cellulose-artificial blood vessels for microsurgery. *Prog Polym Sci* 2001; 26(9): 1561-603.
- [49] Nimeskern L, Martinez Ávila H, Sundberg J, *et al.* Mechanical evaluation of bacterial nanocellulose as an implant material for ear cartilage replacement. *J Mech Behav Biomed Mater* 2013; 22: 12-21.
- [50] Chan EC, Kuo S-M, Kong AM, *et al.* Three dimensional collagen scaffold promotes intrinsic vascularisation for tissue engineering applications. Lai J-Y, editor. *PLoS One*. 2016; 11(2): e0149799.
- [51] Zeng M, Laromaine A, Roig A. Bacterial cellulose films: Influence of bacterial strain and drying route on film properties. *Cellulose* 2014; 21(6): 4455-69.
- [52] Reese SPP, Farhang N, Poulson R, Parkman G, Weiss JAA. Nanoscale imaging of collagen gels with focused ion beam milling and scanning electron microscopy. *Biophys J* 2016; 111(8): 1797-804.
- [53] Stein H, Wilensky M, Tsafir Y, *et al.* Production of bioactive, post-translationally modified, heterotrimeric, human recombinant type-I collagen in transgenic tobacco. *Biomacromol* 2009; 10: 2640-5.
- [54] Reese SP, Farhang N, Poulson R, Parkman G, Weiss JA. Nanoscale imaging of collagen gels with focused ion beam milling and scanning electron microscopy. *Biophys J* 2016; 111: 1797-804.
- [55] Yunoki S, Hatayama H, Ebisawa M, Kondo E, Yasuda K. A novel fabrication method to create a thick collagen bundle composed of uniaxially aligned fibrils: An essential technology for the development of artificial tendon/ligament matrices. *J Biomed Mater Res Part A* 2015; 103(9): 3054-65.
- [56] Kirkwood JE, Fuller GG. Liquid crystalline collagen: A self-assembled morphology for the orientation of mammalian cells. *Langmuir* 2009; 25: 3200-6.
- [57] Ahn S, Lee S, Cho Y, Chun W, Kim G. Fabrication of three-dimensional collagen scaffold using an inverse mould-leaching process. *Bioprocess Biosyst Eng* 2011; 34(7): 903-11.
- [58] Wang S, Jiang F, Xu X, *et al.* Super-Strong, super-stiff macrofibers with aligned, long bacterial cellulose nanofibers. *Adv Mater* 2017; 29(35): 1702498.
- [59] Geisel N, Clasohm J, Shi X, *et al.* Microstructured multilevel bacterial cellulose allows the guided growth of neural stem cells. *Small* 2016; 12(39): 5407-13.
- [60] Jia Y, Zhu W, Zheng M, Huo M, Zhong C. Bacterial cellulose/hyaluronic acid composite hydrogels with improved viscoelastic properties and good thermodynamic stability. *Plast Rubber Compos* 2018; 47(4): 165-75.
- [61] Lee S-H, Kang S-S, Jeong C-M, Huh J-B. The effect of bacterial cellulose membrane compared with collagen membrane on guided bone regeneration. *J Adv Prosthodont* 2015; 7: 484-95.
- [62] Raftery RM, Woods B, Marques ALPP, *et al.* Multifunctional biomaterials from the sea: Assessing the effects of chitosan incorporation into collagen scaffolds on mechanical and biological functionality. *Acta Biomater* 2016; 43: 160-9.
- [63] Pertile RAN, Andrade FK, Alves C, Gama M. Surface modification of bacterial cellulose by nitrogen-containing plasma for improved interaction with cells. *Carbohydr Polym* 2010; 82(3): 692-8.
- [64] Lv X, Yang J, Feng C, *et al.* Bacterial cellulose-based biomimetic nanofibrous scaffold with muscle cells for hollow organ tissue engineering. *ACS Biomater Sci Eng* 2016; 2(1): 19-29.
- [65] Heßler N, Klemm D. Alteration of bacterial nanocellulose structure by *in situ* modification using polyethylene glycol and carbohydrate additives. *Cellulose* 2009; 16(5): 899-910.
- [66] Madaghiele M, Calò E, Salvatore L, *et al.* Assessment of collagen crosslinking and denaturation for the design of regenerative scaffolds. *J Biomed Mater Res (Part A)* 2016; 104(1): 186-94.
- [67] Gonçalves S, Rodrigues IP, Padrao J, *et al.* Acetylated bacterial cellulose coated with urinary bladder matrix as a substrate for retinal pigment epithelium. *Colloids Surfaces B Biointerfaces* 2016; 139: 1-9.
- [68] Bontan S, Robotti F, Jayathissa P, *et al.* Surface-structured bacterial cellulose with guided assembly-based biolithography (GAB). *ACS Nano* 2014; 9(1): 206-19.
- [69] James CC, Marcus AJ, Fernando G, *et al.* Surface modified cellulose scaffolds for tissue engineering. *Cellulose* 2017; 24: 253-67.
- [70] Chua AWC, Khoo YC, Tan BK, *et al.* Skin tissue engineering advances in severe burns: Review and therapeutic applications. *Burn Trauma* 2016; 4(1): 3.
- [71] Sundaramurthi D, Krishnan UM, Sethuraman S. Electrospun nanofibers as scaffolds for skin tissue engineering. *Polym Rev* 2014; 54(2): 348-76.
- [72] Paul W. Advances in wound healing materials. *Smithers Rapra*; 2015.
- [73] Andonova M, Urumova V. Immune surveillance mechanisms of the skin against the stealth infection strategy of *Pseudomonas aeruginosa*-Review. *Comparative Immunol Microbiol Infect Dis* 2013; 36: 433-48.
- [74] Mühlstädt M, Thomé C, Kunte C. Rapid wound healing of scalp wounds devoid of periosteum with milling of the outer table and split-thickness skin grafting. *Br J Dermatol* 2012; 167(2): 343-7.
- [75] Siedenbiedel F, Tiller JC. Antimicrobial polymers in solution and on surfaces: Overview and functional principles. *Polymers (Basel)* 2012; 4(1): 46-71.

- [76] Simões D, Miguel SP, Ribeiro MP, *et al.* Recent advances on antimicrobial wound dressing: A review. *Eur J Pharm Biopharm* 2018; 127: 130-41.
- [77] Fontana JD, De Souza AM, Fontana CK, *et al.* Acetobacter cellulose pellicle as a temporary skin substitute. *Appl Biochem Biotechnol* 1990; 24(1): 253-64.
- [78] Ring DF, Nashed W, Dow T. Liquid loaded pad for medical applications. Vol. US4588400. Google Patents; 1987.
- [79] Cavalcanti LM, Pinto FCM, Oliveira GM de, *et al.* Efficacy of bacterial cellulose membrane for the treatment of lower limbs chronic varicose ulcers: A randomized and controlled trial. *Rev Col Bras Cir* 2017; 44(1): 72-80.
- [80] Picheth G, Pirich C, Sierakowski M, *et al.* Bacterial cellulose in biomedical applications: A review. *Int J Biol Macromol* 2017; 114: 97-106.
- [81] Czaja W, Krystynowicz A, Kawecki M, *et al.* Biomedical applications of microbial cellulose in burn wound recovery. Brown Jr. RM, Saxena I, editors. *Cellul Mol Struct Biol* 2007; 307-21.
- [82] Frankel VH, Serafica GC, Damien CJ. Development and testing of a novel biosynthesized XCell for treating chronic wounds. *Surg Technol Int* 2004; 12: 27-33.
- [83] Kwak MH, Kim JE, Go J, *et al.* Bacterial cellulose membrane produced by *Acetobacter* sp. A10 for burn wound dressing applications. *Carbohydr Polym* 2015; 122: 387-98.
- [84] Li Y, Wang S, Huang R, *et al.* Evaluation of the effect of the structure of bacterial cellulose on full thickness skin wound repair on a microfluidic chip. *Biomacromolecules* 2015; 16(3): 780-9.
- [85] Botton S, Robotti F, Jayathissa P, *et al.* Surface-structured bacterial cellulose with guided assembly-based biolithography (GAB). *ACS Nano* 2014; 9(1): 206-19.
- [86] Wu H, Williams GR, Wu J, *et al.* Regenerated chitin fibers reinforced with bacterial cellulose nanocrystals as suture biomaterials. *Carbohydr Polym* 2018; 180: 304-13.
- [87] Wu C-N, Fuh S-C, Lin S-P, *et al.* TEMPO-oxidized bacterial cellulose pellicle with silver nanoparticles for wound dressing. *Biomacromolecules* 2018; 19(2): 544-54.
- [88] Khalid A, Khan R, Ul-Islam M, Khan T, Wahid F. Bacterial cellulose-zinc oxide nanocomposites as a novel dressing system for burn wounds. *Carbohydr Polym* 2017; 164: 214-21.
- [89] Khalid A, Ullah H, Ul-Islam M, *et al.* Bacterial cellulose-TiO₂ nanocomposites promote healing and tissue regeneration in burn mice model. *RSC Adv* 2017; 7(75): 47662-8.
- [90] Tsai Y-H, Yang Y-N, Ho Y-C, Tsai M-L, Mi F-L. Drug release and antioxidant/antibacterial activities of silymarin-zinc nanoparticle/bacterial cellulose nanofiber composite films. *Carbohydr Polym* 2018; 180: 286-96.
- [91] Alkhatib Y, Dewaldt M, Moritz S, *et al.* Controlled extended octenidine release from a bacterial nanocellulose/Poloxamer hybrid system. *Eur J Pharm Biopharm* 2017; 12: 164-76.
- [92] de Lima Fontes M, Meneguim AB, Tercjak A, *et al.* Effect of *in situ* modification of bacterial cellulose with carboxymethylcellulose on its nano/microstructure and methotrexate release properties. *Carbohydr Polym* 2018; 179: 126-34.
- [93] Hobzova R, Hrib J, Sirc J, *et al.* Embedding of bacterial cellulose nanofibers within PHEMA hydrogel matrices: Tunable Stiffness composites with potential for biomedical applications. *J Nanomater* 2018; 2018: 1-11.
- [94] Fürsatz M, Skog M, Sivlér P, *et al.* Functionalization of bacterial cellulose wound dressings with the antimicrobial peptide ϵ -poly-L-Lysine. *Biomed Mater* 2018; 13(2): 25014.
- [95] Wang J, Gao C, Zhang Y, Wan Y. Preparation and *in vitro* characterization of BC/PVA hydrogel composite for its potential use as artificial cornea biomaterial. *Mater Sci Eng C* 2010; 30(1): 214-8.
- [96] Rebelo RA, Archer AJ, Chen X, *et al.* Dehydration of bacterial cellulose and the water content effects on its viscoelastic and electrochemical properties. *Sci Technol Adv Mater* 2018; 19(1): 203-11.
- [97] Moraes PRF de S, Saska S, Barud H, *et al.* Bacterial cellulose/collagen hydrogel for wound healing. *Mater Res* 2016; 19: 106-16.
- [98] Lamboni L, Li Y, Liu J, Yang G. Silk sericin-functionalized bacterial cellulose as a potential wound-healing biomaterial. *Biomacromolecules* 2016; 17(9): 3076-84.
- [99] Lin W-C, Lien C-C, Yeh H-J, Yu C-M, Hsu S. Bacterial cellulose and bacterial cellulose-chitosan membranes for wound dressing applications. *Carbohydrate Polymers* 2013; 94: 603-11.
- [100] Lin S-P, Kung H-N, Tsai Y-S, *et al.* Novel dextran modified bacterial cellulose hydrogel accelerating cutaneous wound healing. *Cellulose* 2017; 24(11): 4927-37.
- [101] Ye S, Jiang L, Wu J, *et al.* Flexible amoxicillin-grafted bacterial cellulose sponges for wound dressing: *In Vitro* and *In Vivo* Evaluation. *ACS Appl Mater Interfaces* 2018; 10(6): 5862-70.
- [102] Mohamad N, Loh EYX, Fauzi MB, Ng MH, Mohd Amin MCI. *In vivo* evaluation of bacterial cellulose/acrylic acid wound dressing hydrogel containing keratinocytes and fibroblasts for burn wounds. *Drug Deliv Transl Res* 2018; 4: 1-9.
- [103] Lacey R, Celia M-D, Williams R. Biomaterials for ocular reconstruction. *J Mater Sci* 2015; 50: 1523-34.
- [104] Alex G, Mcgaughy, BS, Preeya K, Gupta M, Edited by Sharon Fekrat, MD, and Ingrid U. Scott, MD M, McGaughy A, Gupta, MD P. In Office Use of Amniotic Membrane. *Cornea* 2015; 3(3): 31-2.
- [105] Parihar JKS, Parihar AS, Jain VK, Kaushik J, Nath P. Allogenic cultivated limbal stem cell transplantation *versus* cadaveric keratolimbal allograft in ocular surface disorder: 1-year outcome. *Int Ophthalmol* 2017; 37(6): 1323-31.
- [106] e_l_o_j_o_h_u_m_a_n_o_d_r_s_o_l_e_r_c_o_m_j_p_g (800x592) [Internet]. [cited 2018 Jul 18]. Available from: https://drsoler.com/blog/wp-content/uploads/2013/06/el_ojo_humano_drsoler.com_jpg
- [107] Wu Z, Kong B, Liu R, Sun W, Mi S. Engineering of corneal tissue through an aligned pva/collagen composite nanofibrous electrospun scaffold. *Nanomaterials* 2018; 8(2): 124.
- [108] Isaacson A, Swioklo S, Connon CJ. 3D bioprinting of a corneal stroma equivalent. *Exp Eye Res* 2018; 173: 188-93.
- [109] Yao Q, Zhang W, Hu Y, *et al.* Electrospun collagen/poly(L-lactic acid-co- ϵ -caprolactone) scaffolds for conjunctival tissue engineering. *Exp Ther Med* 2017; 14(5): 4141-7.
- [110] Williams R, Lacey R, Kennedy S, Doherty K, Levis H. Biomaterials for regenerative medicine approaches for the anterior segment of the eye. *Adv Healthc Mater* 2018; 7(10): 1701328.
- [111] Ullah H, Wahid F, Santos HA, Khan T. Advances in biomedical and pharmaceutical applications of functional bacterial cellulose-based nanocomposites. *Carbohydr Polym* 2016; 150: 330-52.
- [112] de Oliveira Barud HG, da Silva RR, da Silva Barud H, *et al.* A multipurpose natural and renewable polymer in medical applications: Bacterial cellulose. *Carbohydr Polym* 2016; 153: 406-20.
- [113] Laromaine A, Tronser T, Pini I, *et al.* Free-standing three-dimensional hollow bacterial cellulose structures with controlled geometry *via* patterned superhydrophobic-hydrophilic surfaces. *Soft Matter* 2018; 14(19): 3955-62.
- [114] Cao J, Zhang C, Zhao S, Wan Y, Hu D. Feasibility of bacterial cellulose membrane as biological scaffold for construction of tissue engineering corneal epithelium. *Chinese J Exp Ophthalmol* 2016; 34(2): 121-4.
- [115] Rodrigo VS, Fabricio LV, Emily CCR, *et al.* Bacterial cellulose and bacterial cellulose/polycaprolactone composite as tissue substitutes in rabbits' cornea. *Pesq Vet Bras* 2016; 36(10): 986-92.
- [116] Bourne RRA, Jonas JB, Bron AM, *et al.* Prevalence and causes of vision loss in high-income countries and in Eastern and Central Europe in 2015: Magnitude, temporal trends and projections. *Br J Ophthalmol* 2018; 102(5): 575-85.
- [117] Gonçalves S, Padrão J, Rodrigues IP, *et al.* Bacterial cellulose as a support for the growth of retinal pigment epithelium. *Biomacromolecules* 2015; 16(4): 1341-51.
- [118] Beekmann U, Weyell P, Küpper C, Dederichs M, Kralisch D. Modified bacterial nanocellulose as biodegradable carrier system for antibiotic in dentistry. In *Würzburg*; 2017.
- [119] Weyell P, Beekmann U, Kuepper C, *et al.* Tailor-made material characteristics of bacterial cellulose for drug delivery applications in dentistry. *Carbohydr Polym* 2019; 207: 1-10.
- [120] Chiaoarakobkij N, Sanchavanakit N, Subbalekha K, Pavasant P, Phisalaphong M. Characterization and biocompatibility of bacterial cellulose/alginate composite sponges with human keratinocytes and gingival fibroblasts. *Carbohydr Polym* 2011; 85(3): 548-53.
- [121] Biskin S, Damar M, Oktem SN, *et al.* A new graft material for myringoplasty: Bacterial cellulose. *Eur Arch Oto-Rhino-Laryngology* 2016; 273(11): 3561-5.
- [122] Angtika RS, Widiyanti P, Aminatun. Bacterial cellulose-chitosan-glycerol biocomposite as artificial dura mater candidates for head trauma. *J Biomimetics Biomater Biomed Eng* 2018; 36: 7-16.
- [123] Lima F de MT de, Pinto FCM, *et al.* Biocompatible bacterial

- cellulose membrane in dural defect repair of rat. *J Mater Sci Mater Med* 2017; (28): 37.
- [124] Rosen CL, Steinberg GK, Demonte F, *et al.* Results of the prospective, randomized, multicenter clinical trial evaluating a biosynthesized cellulose graft for repair of dural defects. *Neurosurgery* 2011; 69(5): 1093-103.
- [125] Hansson GC. Role of mucus layers in gut infection and inflammation. *Curr Opin Microbiol* 2012; 15(1): 57-62.
- [126] Yu M, Wang J, Yang Y, *et al.* Rotation-facilitated rapid transport of nanorods in mucosal tissues. *Nano Lett* 2016; 16: 7176-82.
- [127] Tronser T, Laromaine A, Roig A, Levkin PA. Bacterial cellulose promotes long-term stemness of meso. *ACS Appl Mater Interfaces* 2018;10(19): 16260-9.

PMID: 30488795

Bacterial Nanocellulose and Titania Hybrids: Cytocompatible and Cryopreservable Cell Carriers

Irene Anton-Sales, Soledad Roig-Sanchez, María Jesús Sánchez-Guisado, Anna Laromaine,* and Anna Roig*



Cite This: *ACS Biomater. Sci. Eng.* 2020, 6, 4893–4902



Read Online

ACCESS |



Metrics & More



Article Recommendations



Supporting Information

ABSTRACT: Carrier-assisted cell transplantation offers new strategies to improve the clinical outcomes of cellular therapies. Bacterial nanocellulose (BC) is an emerging biopolymer that might be of great value in the development of animal-free, customizable, and temperature-stable novel cell carriers. Moreover, BC exhibits a myriad of modification possibilities to incorporate additional functionalities. Here, we have synthesized BC-titanium dioxide (TiO₂) nanocomposites (BC/TiO₂) to evaluate and compare the suitability of not only BC but also a model hybrid nanobiomaterial as cell transplantation supports. This work provides thorough information on the interactions between BC-based substrates and model human cells in terms of cell attachment, morphology, proliferation rate, and metabolic activity. Two methods to partially retrieve the adhered cells are also reported. Both BC and BC/TiO₂ substrates are positively evaluated in terms of cytocompatibility and endotoxin content without detecting major differences between BC and BC nanocomposites. Lastly, the effective cryopreservation of cells-BC and cells-BC/TiO₂ constructs, yielding high cell viability and intact cell carrier's characteristics after thawing, is demonstrated. Taken together, our results show that both BC and BC/TiO₂ enable to integrate the processes of expansion and long-term storage of human cells in transportable, robust and easy to manipulate supports.

KEYWORDS: *microbial cellulose, nanocomposites, titania, cryopreservation, fibroblasts, cell culture support*



INTRODUCTION

Cell transplantation approaches rely on a dual beneficial effect evoked by the administered cells: (i) repopulation of the wound bed and (ii) contribution toward a favorable micro-environment for tissue repair (via secretion of cytokines and growth factors). Cellular therapies in the form of autologous^{1,2} or allogenic³ cell transplants exhibit a long-proven efficacy to treat complicated skin lesions; while extending these therapies to other organs⁴ and developing innovative cell delivery systems⁵ represents an active focus of research. Despite some satisfactory clinical outcomes have already been obtained,^{6,7} the complex administration of therapeutic cells, i.e., insufficient survival and integration of cells delivered in suspensions or sprays,^{8–10} hinders the widespread implementation of some cell therapies. Moreover, the next generation of cellular products should be provided in a ready-to-use format to decrease waiting times and be used on-demand. To this end, long-term and reliable storage (e.g., cryopreservation) of cellular products needs to be further developed and standardized. The use of cell carriers can contribute to overcoming some of these bottlenecks; specifically by enhancing cell survival, controlling differentiation and retaining the transplanted cells at the target site. Last but not least, cell vehicles can also facilitate cryopreservation and the handling of therapeutic cells.¹¹

Collagen-based biomaterials represent the current gold standard for cell transplantation supports mainly because of its ability to support cell attachment and proliferation.^{8,12} However, collagen presents some disadvantages such as a certain risk of immunogenicity, poor batch-to-batch reproducibility and low availability, all due to its animal origin. Nanocellulose synthesized by bacteria (referred here as bacterial nanocellulose, BC) is a biopolymer with potential applicability as an alternative cell carrier. BC inherently presents many of the characteristics sought-after for cell transplantation supports, namely; purity, conformability, water holding capacity, and porosity.¹³ Besides, the high thermal and mechanical stability of BC are favorable features for the clinical translation since they enable heat-sterilization, easy handling and fixation by suturing.¹⁴ The interwoven nanofibrillar structure of BC is responsible for most of these unique physicochemical properties and for the high architectural similarity to collagenous structures. BC was first proposed as a

Received: April 7, 2020

Accepted: August 11, 2020

Published: August 11, 2020



substrate for mammalian cell culture in the 1990s by Watanabe *et al.*¹⁵ Later studies have reported on BC functionalized with the tripeptide motif RGD for the culture of fibroblasts¹⁶ or surface-modified BC as support for retinal pigment epithelial cells.^{17,18} However, uncoated BC substrates have also been successfully loaded with several cells types^{19–21} and proved to prolong stemness of mouse embryonic stem cells.²² These findings imply that BC could be deemed as an alternative to collagen in the design of novel carriers for cell transplantation therapies²³ and *in vitro* studies.²⁴ On the other hand, BC has been suggested as a cryoprotectant agent²⁵ and other cellulosic materials have been employed as substrates to cryopreserve embryos²⁶ and fungi.²⁷ However, the possibility to cryopreserve BC-cell constructs has not been addressed so far.

Considering the remarkable functional properties that inorganic nanoparticles (NPs) can endow to BC and the rising research attention on hybrid biomaterials,²⁸ it is of great interest to investigate the impact of these NPs on cells cultured on such BC nanocomposites. Because of its widespread use in skin-related applications, titanium dioxide (TiO₂) NPs were selected here as a model NP among the plethora of biocompatible NPs to be combined with BC. Importantly, colloidal TiO₂ NPs have recently been suggested for dermal treatments as antimicrobial and scar-reducing agents.^{29,30} TiO₂ NPs have also been incorporated to plant-derived nanocellulose patches as a linker for drug molecules to modulate release kinetics.^{31,32} In another study, TiO₂ NPs combined with BC films created an efficient wound dressing in a burn mice model.³³ Nevertheless, the role of TiO₂ on the performance of BC as a cell carrier has never been systematically studied.

Here, we present a thorough study of BC and BC/TiO₂ nanocomposites as versatile and portable cell culture supports. The two substrates are structurally characterized and proven endotoxin-free and then *in vitro* studies on cell attachment, proliferation, viability and morphology are described. Next, three methods to retrieve the cells adhered to BC and BC/TiO₂ supports are tested. Finally, we show that cell-BC and cell-BC/TiO₂ constructs can be effectively cryopreserved yielding highly viable cell populations and intact carriers after thawing.

EXPERIMENTAL SECTION

BC and BC/TiO₂ Substrates: Synthesis and Characterization.

Bacterial Nanocellulose Production. A commercial *Komagataeibacter xylinus* (*K. xylinus*) strain (NCIMB 5346 from CECT, Valencia, Spain) was initially cultured in Hestrin-Schramm (HS) solid medium consisting of 1.15 g of citric acid, 6.8 g of Na₂HPO₄·12H₂O, 5 g of peptone, 5 g of yeast extract, 15 g of agar, and 20 g of dextrose all from Condalab for 1 L of Milli-Q water. Next, a bacterial inoculum was picked with a loop and used to inoculate 6 mL of HS liquid medium (same composition as the solid medium but without agar), and this culture was expanded during 7 days at 30 °C. Then, 0.5 mL of the previous broth was mixed with 4.5 mL of fresh HS liquid medium and further incubated for 7 days. Finally, a 1:14 dilution of the former bacterial solution was performed with fresh medium and transferred to 24 well-plates (2 mL/well). The culture remained 3 days at 30 °C under static conditions and circular BC hydrogels formed at the air–liquid interface of every well with the same diameter as the container (~2 cm²). BC pellicles were picked with plastic tweezers and soaked in a solution of 1:1 Ethanol: deionized water (DI) for 10 min to kill the bacteria.

The exhaustive cleaning process of the BC involved different boiling steps; (i) 40 min in DI water and (ii) two periods of 20 min in 0.1 M NaOH (Sigma-Aldrich) aqueous solution to remove all organic

residues. Lastly, BC films were rinsed with DI water until neutral pH was reached. Then, the films were autoclaved (121 °C, 20 min) and stored in DI water at RT until further use. BC samples were dried at 60 °C between two Teflon plates under a 1 kg weight.

Bacterial Nanocellulose Functionalization with TiO₂ Nanoparticles. For the BC functionalization with TiO₂ NPs, a previously described^{34,35} microwave (CEM Discover Explorer-12 Hybrid reactor operating at a frequency of 2.45 GHz and with a maximum power of 300 W placed in a clean room) assisted method was employed. Briefly, ever dry BC films were soaked in benzyl alcohol (99% BA from Scharlau) for approximately 30 min to allow solvent exchange and then transferred to a glass tube containing 4 mL of benzyl alcohol and 140 μL of titanium(IV) butoxide (TBOT, 97%, Sigma-Aldrich). All of the precursors were mixed immediately before starting the microwave reaction to avoid hydrolysis of the titanium precursor. The reaction vessel was heated in two steps: (1) 5 min at 50 °C and (2) 10 min at 190 °C. After the reaction, the BC/TiO₂ films were rinsed once with ethanol to remove the excess of NPs and several times with DI water until reaching a neutral pH. After TiO₂-functionalization, the never dry BC films were dried at 60 °C between two Teflon plates under 1 kg weight.

Endotoxin Contamination Study. According to the FDA recommendations,³⁶ the endotoxin extraction was carried out by placing autoclaved BC and BC/TiO₂ never dry samples in depyrogenated falcon tubes with 40 mL of endotoxin-free water during 72 h at 30 °C and under orbital agitation (100 rpm). To evaluate the endotoxin content in the eluates from BC and BC/TiO₂ films, a Pierce LAL Chromogenic Endotoxin Quantification Kit was purchased from Thermo Fisher and the assay was performed following the kit's instructions. The products of the reaction were measured for absorbance at 405 nm in a microplate reader (Infinite 200 PRO, TECAN) at 37 °C. The indicated values correspond to the mean ± standard deviation of two independent experiments obtained from two different endotoxin quantification kits and evaluating each time two samples from two different batches of BC.

Scanning Electron Microscopy (SEM). Dry BC and BC/TiO₂ films were fixed flat on top of aluminum SEM sample holders with adhesive carbon tape. The samples were coated with 5 nm of platinum before imaging. A high-resolution scanning electron microscope (FEI Magellan 400L XHR SEM) was used under high vacuum with an acceleration voltage of 2 kV. To image the BC/TiO₂ samples without Pt coating, the same sample preparation without the sputtering step was performed. Energy-dispersive X-ray (EDX) spectroscopy was performed with the same equipment on two BC/TiO₂ samples.

Atomic Force Microscope (AFM). To obtain topographical images and roughness measurements of BC and BC/TiO₂ pellicles, a 5100 Agilent Technologies atomic force microscope was employed on tapping mode and equipped with a FORT tip firm AppNano. At least three 30 × 30 μm or 50 × 50 μm images were obtained for four different dry BC and BC/TiO₂ films. The images were processed with surface analysis software V7.4 (64-bit) - mountains technology. The indicated roughness values correspond to mean ± standard deviations.

Thermogravimetric Analysis (TGA). Thermal decomposition studies were performed with a NETZSCH -STA 449 F1 Jupiter analyzer employing a heating rate of 10 °C per minute from 25 to 600 °C at an air atmosphere. Three dry BC and three dry BC/TiO₂ samples were analyzed.

Inductively Coupled Plasma–Optical Emission Spectroscopy (ICP-OES). Dry BC/TiO₂ samples were immersed in 8 mL of water during 1 month under mild agitation and then the eluates were collected for analysis with an ICP-OES Optima 4300DV PerkinElmer.

Transmission Electron Microscopy (TEM). The nanoparticles characterization was performed through JEOL JEM-1210 electron microscope operating at 120kV with an ORIUS 831 SC 600 Gatan camera. TEM images were analyzed with ImageJ software and a histogram of 360 nanoparticles was fitted to a Gaussian function. The percentage of standard deviation divided mean value was obtained as the polydispersity value. Selected area electron diffraction (SAED) was used to obtain diffraction patterns from the TiO₂ nanoparticles.

BC and BC/TiO₂ Substrates: Evaluation As Cell Carriers. *In Vitro* Studies. For the *in vitro* experiments, a human dermal fibroblast cell line was used (1BR3.G cells, ECACC 90020507) as a model. The cultures were maintained in Dulbecco's Modified Eagle Medium (DMEM) supplemented with 2 mM GlutaMax and 10% fetal bovine serum (South American FBS) both from Gibco and monitored with an inverted optical microscope (Nikon Eclipse TS100). 1BR3.G cells were kept in a T75 flask (Sarstedt) at 37 °C in 10% CO₂ and split three times per week.

For all of the experiments detailed in this section, dry BC and BC/TiO₂ samples were rehydrated in DI water and autoclaved (121 °C, 20 min) before being used as cell supports. To plate the cells, BC and BC/TiO₂ films were preconditioned with warm DMEM and then transferred to 24-well plates using forceps and irradiated with UV light for 30 min to ensure sterility. A concentrated cell suspension (50,000 cells/well for the proliferation study and 100,000 cells/well for the rest of the experiments) was carefully pipetted on the middle of the pellicles. When the cell suspension was absorbed by the BC films, 500 μ L of fresh culture medium were added to each well. See Figure S2 for an illustration of this process. Controls (uncoated commercial cell culture plates, Nunc) were seeded with the same procedure and number of cells than the substrates.

Cell proliferation was assessed qualitatively by optical microscope and quantitatively with the CellTiter-Glo Luminescent Cell Viability Assay (Promega) by measuring ATP levels on the cultures at Day 1, Day 3 and Day 8 after cell seeding. For this assay, all the elements were accommodated at RT and then the cell-loaded films were transferred to unused culture wells and washed with PBS before adding 100 μ L of the CellTiter-Glo reagent to each well together with 100 μ L of DMEM. The 24 multiwell plates were agitated for 2 min to lyse the cells and then incubated during 10 min at RT to stabilize the luminescence. After careful mixing, 150 μ L of the supernatant of each well were transferred to a 96-well plate with an opaque bottom for the luminescent read. Blanks were performed with plain BC films and culture medium without cells. Luminescence was read with a Tecan Spark multimode microplate reader (LifeSciences) with an integration time of 1000 ms. The experiment was performed three times with three technical replicates for each time point.

Cell viability, distribution, and morphology were studied with a confocal laser scanning microscope (Leica SP5) 48 h after plating the cells. Calcein-AM (BD Pharmingen) staining was used to monitor the viability of the cells growing on BC and BC/TiO₂ supports since this reagent becomes fluorescent after being cleaved by intracellular esterases that are only present on alive cells. Cell-loaded BC and BC/TiO₂ films were washed with Hank's Balanced Salt Solution (HBSS, Gibco) and then incubated during 15 min in the dark with 1 mL/sample of 4 μ g/mL Calcein-AM in HBSS and washed twice with HBSS. Then the cells were fixed with 4% cold paraformaldehyde (Panreac) during 5 min. Fixed cells were further stained during 5 min with 1 μ g/mL of Hoechst 33342 (Invitrogen, cell nuclei) and 5 μ g/mL CellMask Deep Red Plasma Membrane Stain (Invitrogen, cell membranes, red) diluted in PBS and rinsed again. Calcein was excited at a wavelength of 495 nm, Hoechst at 350 nm and Cell Mask at 588 nm. The BC and BC/TiO₂ films were flipped so that the cells faced the surface of Ibidi Glass Bottom dishes to be imaged with 10 \times (dry), 20 \times (dry), or 40 \times (oil) objectives. Several images of different z planes were obtained for each sample so that all the cross-section off the sample was covered. These stacks of images were then used to generate 3D reconstructions with the Fiji package of ImageJ (64-bit version). Cell shape descriptors were analyzed with the same software by measuring >60 cells for each condition from images taken from three independent experiments. For the axial ratio, the length of the longer axis of each cell was divided by the length of the shortest axis. Circularity was calculated as $4\pi^*$ (cell area/cell perimeter²). The nuclear-cytoplasmic ratio (N:C ratio) was obtained by dividing the nuclear area between the total area of the cell. To fluorescently stain the substrates (images in Figures 1 and 2), rewet BC and BC/TiO₂ films were stained with Safranin-O (Alfa Aesar, 0.01% weight/volume dilution in DI water) overnight and rinsed several times before plating the cells. The Safranin-O dye was excited with a 495 nm laser.

Cryopreservation of Cell-Biomaterial Constructs. For the cryopreservation experiment, 100,000 1BR3.G cells were seeded on triplicates on BC and BC/TiO₂ rewet films and conventional cell culture surfaces (controls) and expanded until highly confluent cultures were achieved; 1 week for BC and BC/TiO₂ substrates and 5 days for controls. Cell-loaded BC and BC/TiO₂ films were transferred to 1.8 mL cryovials (Nunc) containing 1 mL cryopreservation medium consisting of 90% FBS and 10% cell culture grade DMSO. Controls cells were detached from the culture wells using Trypsin-EDTA, centrifuged for 5 min at 1400 rpm and then resuspended in 1 mL of the same cryopreservation medium and transferred to cryovials. The cryovials were kept overnight inside a CoolCell container at -80 °C to allow a controlled freezing rate of -1 °C/min. Then, the vials were stored for at least 1 week at -196 °C on a liquid nitrogen tank. BC and BC/TiO₂ films without cells were included to monitor the material stability upon cryostorage.

All of the vials were thawed directly by immersion on a 37 °C water bath. The BC and BC/TiO₂ films were carefully transferred to 24 well plates containing fresh culture medium using tweezers. Control cells were precipitated upon centrifugation and resuspended in warm DMEM before being transferred to culture well plates. Twenty-four hours later, the medium was changed to remove DMSO remains. Cell recovery was assessed at three time-points: before cryopreservation, 4 and 48 h after thawing. Cell morphology was monitored with a contrast phase microscope and cell viability was qualitatively evaluated with Calcein-AM staining (described in the previous section) and quantitatively with the CellTiter-Glo Luminescent Cell Viability Assay also detailed before performing the luminescence reads with a VICTOR 3 plate reader (PerkinElmer). Cell viability after thawing was calculated for each condition relative to the luminescent signal obtained for the not cryopreserved samples.

Cell Retrieve. For the trypsin-based cell retrieve experiment, BC, BC/TiO₂ films and controls (cell culture plates) were used as supports to plate 100,000 1BR3.G cells as previously described (triplicates). To estimate the number of cells that attached to the supports, the number of unattached cells, floating on the culture medium, was counted 4 h after plating as follows: Subsequently to exhaustive homogenization, a sample of 10 μ L of the cell suspension was mixed with 10 μ L of Trypan Blue Stain (0.4%, Gibco) to count the number of cells that were not attached to the BC and BC/TiO₂ substrates using a Neubauer chamber. 48 h later, the same cell cultures were washed thoroughly with PBS (Gibco) and trypsinized using 250 μ L trypsin-EDTA (0.05%, Gibco)/well during 5 min. The enzyme was neutralized with 500 μ L of DMEM and the cells that were floating on the medium were counted in the same manner. To estimate the percentage of recovered cells, the initial number of attached cells (100,000 minus the number of not attached cells) was multiplied by the cell proliferation rate calculated for BC and BC/TiO₂ after 48 h of culture to obtain the theoretical number of cells present on each film. Then the percentage of recovered cells was estimated by dividing the number of detached cells upon trypsinization between the expected numbers of cells for each film. Optical microscopy observations were also conducted to match these calculations. The cell recovery was considered to be 100% for the controls and the experiment was repeated three times.

To study cell retrieve via migration of cells from BC films to other substrates, 100,000 1BR3.G cells were seeded by triplicate on rewet BC and BC/TiO₂ films and cultured for 48 h. Then, the films were placed upside-down with the cells contacting the new substrates (cell culture plate and never dry BC hydrogels) using tweezers and further incubated for 72 h. After that, the original films were removed and the migration/transference of cells was qualitatively evaluated with an optical microscope. Migrated-cell's viability was confirmed upon Calcein-AM staining. The experiment was repeated three times.

The third method tested to recover cells from BC and BC/TiO₂ substrates consisted of the enzymatic dissolution of the substrates using cellulase. Three samples of BC and BC/TiO₂ were seeded with 100,000 1BR3.G cells and incubated until reaching high confluence. Then, the samples were rinsed with PBS incubated with a commercial mix of cellulases (GrowDase, UPM Biomedicals) at 37 °C until

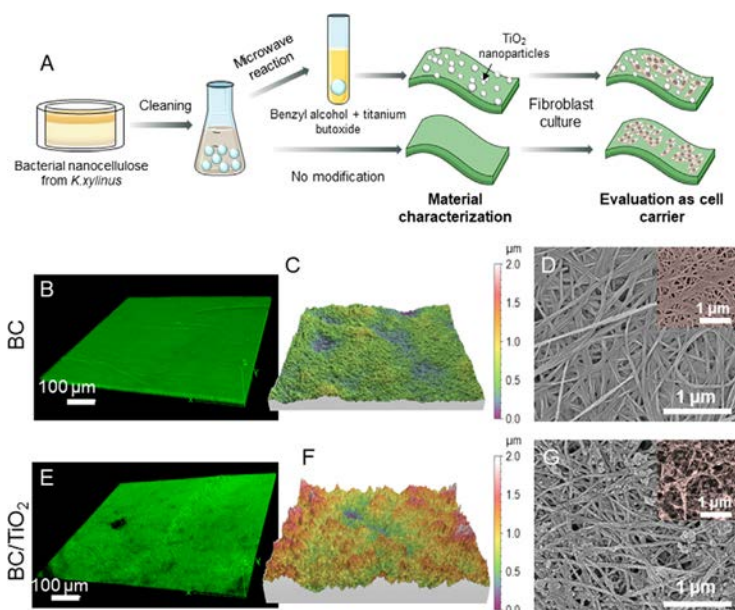


Figure 1. Preparation and structural characterization of the BC and BC/TiO₂ substrates. (A) Schematic representation of the processes adopted to prepare BC and BC/TiO₂ cell carriers. Images B and E show macroscopic confocal microscope images of rewet BC (B) and BC/TiO₂ (E) films fluorescently stained with Safranin-O. AFM images (30 × 30 μm areas) are shown on C (BC) and F (BC/TiO₂) panels to visualize differences in roughness. Finally, scanning electron microscope (SEM) of BC (D) and BC/TiO₂ (G) illustrates the nanofibrillar structure of the substrates and the TiO₂ coating. Insert on image D corresponds to a collagen-based biological membrane to visualize the high structural similarities with BC. SEM samples were coated with five nm of Pt on images D and G and were left uncoated on the inset in image G. Color was added to facilitate visualization of the insets.

cellulose degradation as observed. Two different concentrations of cellulase were tested: (i) 0.45 mg/sample and 0.675 mg/sample diluted in culture medium in a total volume of 300 μL. BC degradation was monitored and photographed with an inverted optical microscope (Nikon Eclipse TS100).

Statistical Analysis. Quantitative data are expressed as means ± standard deviation. Statistical analyses were performed with Graph Pad Prism 5 software using one-way ANOVA followed by Tukey's multiple comparison test. To compare two different experimental conditions Student's *t* tests were conducted. Statistical significance was accepted when obtained *P*-values were ≤0.05 and summarized as * = <0.05, ** = <0.01, *** = <0.001 for the calculated *P*-values.

RESULTS AND DISCUSSION

Substrate Characterization. BC directly obtained from the *K. xylinus* cultures are hydrogels with a water content of >100 times its own dry weight and a typical thickness of ~800 μm. These samples are semitransparent after cleaning, sturdy and easy to manipulate, and here are referred to as “never dry BC”. When never dry BC is dried at 60 °C under 1 kg weight, its thickness reduces to ~20 μm, and samples acquire a paper-like appearance. Upon rehydration, the dry films do not absorb as much water as the never dry BC and exhibited a thickness of ~23 μm.³⁷ The rehydrated BC samples are referred to as “rewet BC”. Figure S1 includes digital images of each type of BC and other characteristics of the substrates. To create the BC/TiO₂ nanocomposites, never dry BC films were functionalized with nanotitania via a microwave-assisted thermal

decomposition method previously reported³⁴ and summarized in Figure 1A. This one-step (15 min reaction time) hydrothermal reaction allowed uniform nucleation of TiO₂ NPs directly on the BC fibers as evidenced by the whitish color acquired by the BC samples (see Figure S1). Never dry BC/TiO₂ was dried with the same procedure and its thickness reduced to ~30 μm. Rewet BC/TiO₂ films were slightly thicker (~35 μm) than rewet BC. The handling of the BC/TiO₂ was comparable to that of plain BC; the samples kept its shape, size, and flexibility, and we did not observe any sign of deterioration after the microwave reaction.

Before its use as a substrate for cell culture, BC and BC/TiO₂ films were structurally characterized. To get a macroscopic view of the substrates, confocal microscope imaging of fluorescently stained rewet BC and BC/TiO₂ substrates was conducted (Figure 1B,E). Both samples show continuous, flat, and rather smooth surfaces only presenting few wrinkles formed during the drying process. Since surface roughness is reported to impact on cell attachment and growth,^{38,39} atomic force microscopy (AFM) was used to compare the roughness of the substrates in the dry state. BC films showed an average roughness of 0.14 ± 0.03 μm whereas BC/TiO₂ were rougher (0.33 ± 0.07 μm) due to the nanoparticle coating (see Figure 1C,F).

Following, scanning electron microscopy (SEM) was used to elucidate fiber organization and nanoparticle distribution on the BC/TiO₂ supports. BC films showed an unorganized

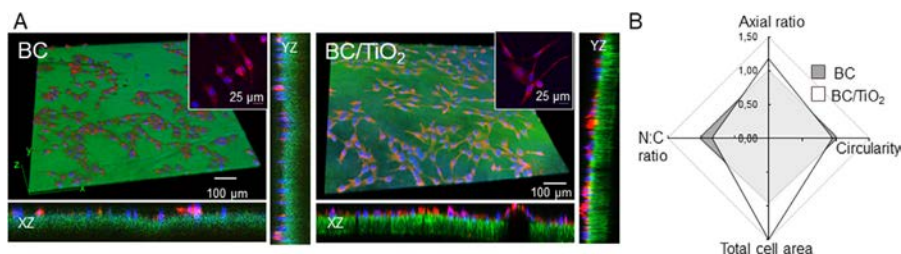


Figure 2. Cell attachment and morphology on BC and BC/TiO₂ substrates. Panel A shows confocal microscope images of human dermal fibroblasts attached to BC and BC/TiO₂ supports 48 h after plating the cells. Insets display enlargements to better visualize cell morphology and spreading. Cell nuclei (blue) were stained with Hoechst and cell membranes (red) with Cell Mask while BC and BC/TiO₂ supports were stained with Safranin-O (green). 3D reconstruction of the z stacks revealed that cells distribute over the BC and BC/TiO₂ films surface without penetrating inside the films (see lateral images for the xz and yz planes). (B) Radar chart comparing the main cell shape descriptors (normalized) measured 48 h after seeding 1BR3.G cells on BC and BC/TiO₂ films. N:C ratio refers to the nuclear/cytoplasmic ratio. Statistically significant differences were found for the measurements of axial ratio, total cell area and N:C ratio suggesting a higher fibroblast spreading on BC/TiO₂ than in plain BC.

interlaced 3D nanofiber distribution (Figure 1D). Interestingly, this 3D network presents a strong architectural similarity to collagen, the current gold standard to devise cell transplantation supports. Insert on Figure 1D shows an SEM image of collagen fibers from the amniotic membrane to exemplify this resemblance. BC/TiO₂ exhibits the same nanofibrillar structure than plain BC with a homogeneous and dense coating by the TiO₂ NPs (Figure 1G). The inset of Figure 1G shows an SEM image BC/TiO₂ without metal sputtering where the TiO₂ coating is also visible. Energy-dispersive X-ray Spectroscopy revealed that the atomic contribution of titanium on the surface of BC/TiO₂ substrates accounts for 25 ± 8%. Both the atomic percentage of titanium and the density and distribution of the TiO₂ NPs coating was very similar between the two sides of the nanocomposite.

Thermogravimetric analysis (TGA) was carried out to determine that nanotitania represents ~6% of the dry weight of the BC/TiO₂ composites. TGA was also used to study the long-term stability of the nanocomposites; BC/TiO₂ films immersed in water for one month under mild stirring showed no leaching of titanium. That is, the same weight percentage of titanium was detected before and after the soaking.³⁴ Accordingly, inductively coupled plasma-optical emission spectroscopy revealed that the amounts of titanium detected in the eluates BC/TiO₂ samples were <0.02 mg/L. These two experiments confirm that the nanoparticles are chemically bonded to the nanocellulose fibers. This should prevent TiO₂ nanoparticles to be released from the substrates and to be internalized by the cells in the next *in vitro* experiments.

Transmission electron microscopy (TEM) was employed to estimate the particle size distribution from the colloidal TiO₂ NPs present on the supernatant of the microwave reaction, being in average 7.1 ± 1.6 nm with a polydispersity of a 23% (Figure S1–C). Finally, TEM on electron diffraction mode was used to determine that the TiO₂ crystallized in the anatase phase, see Figure S1–D.

Together, these observations confirm that the employed microwave synthesis is an effective method to prepare stable BC/TiO₂ nanocomposites in a fast and reproducible manner, obtaining a uniform coating of the nanocellulosic fibers without compromising the original structural properties of BC.

Endotoxin Content. Endotoxin (also known as lipopolysaccharide) contamination induces a variety of negative

biological effects such as airway disease, fever, hypotension, coagulopathies, septic shock and even death, and represents a major problem in biomaterial fabrication. Since BC is synthesized by a Gram-negative bacterium, the presence of endotoxins could pose a threat. The amount of endotoxins detected in the eluates of sterile never dry BC and BC/TiO₂ films were 0.04 ± 0.01 and 0.05 ± 0.01 endotoxin units (EU)/mL respectively. Notably, these values are 1 order of magnitude below the Food and Drug Administration (FDA) obligatory limit of 0.5 EU/mL applied to medical devices. The low amount of endotoxins detected in the substrates is in accordance with the recent literature^{17,40} and indicates that the cleaning protocol of BC is effective in removing any remains of the *K. xylinus* cell wall.

Cell Attachment and Morphology. To investigate the suitability of BC and BC/TiO₂ as substrates to expand and transplant adherent cells, a model human dermal fibroblast cell line was employed (1BR3.G). Rewet BC and BC/TiO₂ membranes were selected for the *in vitro* experiments as the drying-rehydration cycle contributed to reducing the variability between samples and slightly increased the initial cell attachment compared to never dry BC. Accordingly, dry BC and BC/TiO₂ were rehydrated in DI water, autoclaved and then seeded with 1BR3.G cells. This tolerance to heat sterilization represents a clear advantage of BC for future clinical translation. Fibroblasts readily attached to both BC and BC/TiO₂ substrates without the need of any additional treatment, thus greatly facilitating the seeding protocol. Moreover, the above-mentioned morphological stability of BC and BC/TiO₂ allowed the easy manipulation and portability of the cell cultures. Figure S2 shows the cell plating protocol, the handling of BC-cells constructs, and the monitoring of the cell cultures by phase-contrast microscope. By counting the number of cells that were not attached to the substrates 4 h after seeding, we could assess that 77 ± 1% of the seeded cells adhered to BC and 73 ± 9% attached to BC/TiO₂ (not statistically significant differences). Even that the BC and BC/TiO₂ films have the same size as the culture wells, a small portion of the seeded cells still attached to the underneath tissue culture plate instead of the substrates and therefore these numbers are presented as an approximation. After 2 days of culture, images from Figure 2A were collected with a confocal microscope where fibroblasts attachment to the

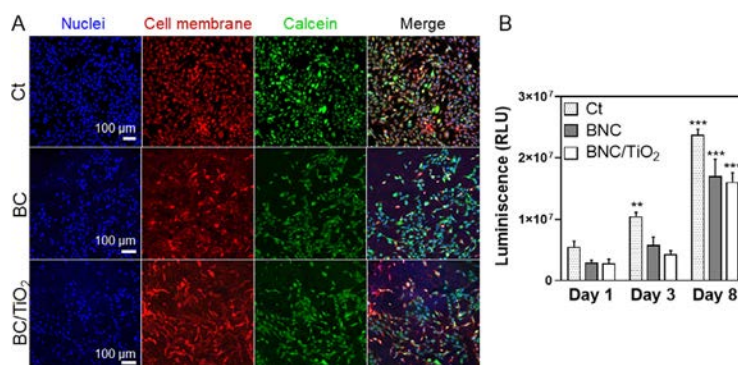


Figure 3. Cell viability and proliferation on BC and BC/TiO₂ supports. (A) The study of cell viability was carried out with Calcein-AM staining 48 h after cell seeding. BC and BC/TiO₂ substrates yielded highly viable cell populations. Confocal microscope images depict cell nuclei (blue) stained with Hoechst and cell membranes (red) colored with Cell Mask. Viable cells were stained with Calcein-AM (green). The fourth column shows the composite of all pictures. (B) Proliferation kinetics of the fibroblasts seeded on BC (gray bars) and BC/TiO₂ (white bars) and controls (dotted bars) monitored with the CellTiter-Glo assay measuring ATP levels. For the studied cell carriers, statistically significant differences were found for day 8 compared to day 1 demonstrating the ability of BC and BC/TiO₂ to support fibroblast proliferation ($n = 3$).

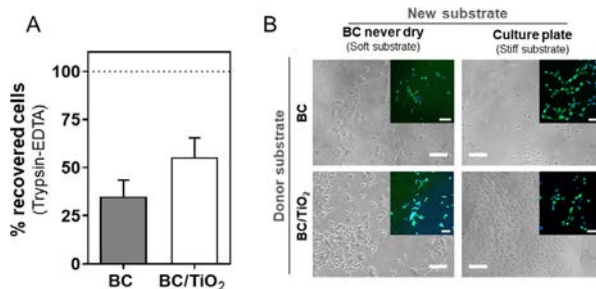


Figure 4. Cell retrieval from BC and BC/TiO₂ supports. (A) Percentage of cells that could be harvested upon conventional enzymatic method with trypsin-EDTA. A higher percentage of cells (55 ± 18 vs $35 \pm 15\%$) was retrieved from the BC/TiO₂ substrates but this difference was not statistically significant (P -value = 0.1965). The dashed line at 100% corresponds to the approximate percentage of cells recovered from polystyrene surfaces by the same procedure. (B) Optical microscopy images of the migrated/transferred fibroblasts from the initial substrates (BC and BC/TiO₂) to the new substrates: BC hydrogels (soft substrate) and polystyrene cell culture surfaces (stiff substrate). Insets correspond to fluorescence microscopy images where cell nuclei are marked in blue (total number of cells) and viable cells are stained green with Calcein-AM. Scale bars = 100 μ m.

BC and BC/TiO₂ films (stained in green with Safranin-O) is clearly observed. Optical slicing in the z direction revealed that 1BR3.G cells grew over the entire surface of the BC and BC/TiO₂ films without penetrating inside the substrates as expected according to the small size of the BC pores. Figure S3 shows large area confocal microscope images ($\sim 40 \text{ mm}^2$) of BC and BC/TiO₂ substrates 48 h after seeding to further illustrate fibroblast distribution on the surfaces.

Then, we analyzed diverse cell shape descriptors to investigate whether BC and BC/TiO₂ films were able to facilitate cell spreading recapitulating the characteristic elongated fibroblast phenotype found *in vivo*. Both supports rendered the expected fibroblast morphology with axial values of 3.9 ± 1.7 for BC/TiO₂ and 3.1 ± 1.3 for plain BC ($n > 60$ cells, P -value < 0.005). Cell shape descriptors measurements are detailed in Figure S4. Notably, the obtained axial ratios are similar to those reported for fibroblasts seeded on collagen and

fibrin coated supports.⁴¹ Cells plated on BC/TiO₂ substrates presented statistically significant higher axial ratio compared to cells cultured on plain BC as well as larger total cell area. This indicates an enhanced spreading of the fibroblast on the BC/TiO₂ respect to BC supports (See normalized data on Figure 2B). The nuclear-cytoplasmic ratio (N:C ratio), i.e. the relative area of the cytoplasm respect to the nucleus,⁴² was significantly smaller for cells seeded on BC/TiO₂ further supporting that cells tend to extend more on the hybrid substrates. We ascribe these effects to the greater roughness of the BC/TiO₂ substrates which might provide more anchoring sites for the fibroblasts.^{38,39,43}

Cell Viability and Proliferation. To gain insight into the biological activity of the fibroblasts cultivated on top of BC and BC/TiO₂ substrates, cell viability (Calcein-AM staining) and proliferation kinetics were studied. Figure 3A illustrates that cells seeded on both BC and BC/TiO₂ films exhibit high

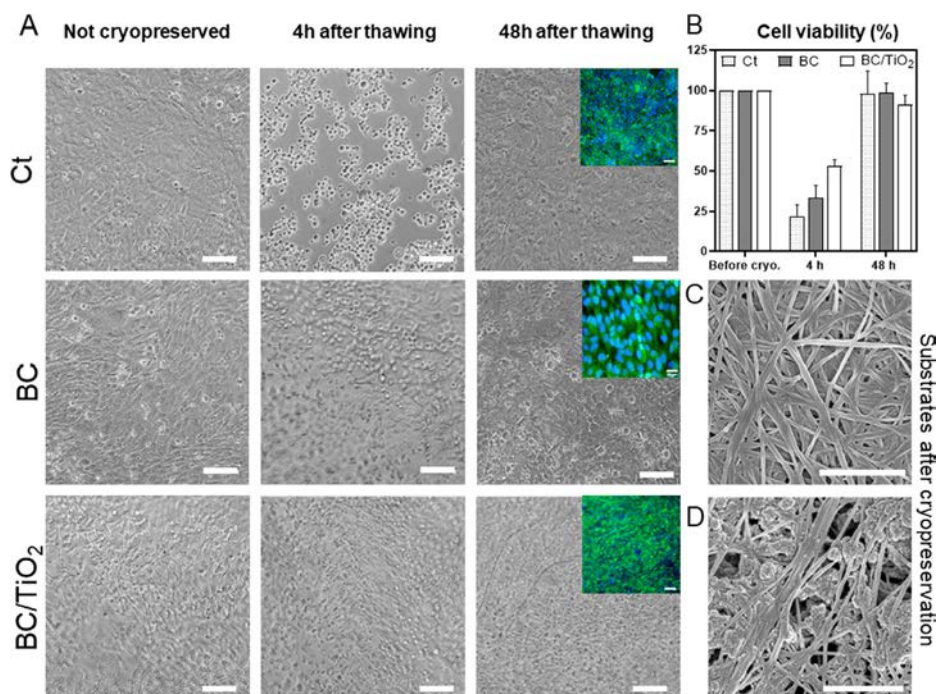


Figure 5. Adherent cell cryopreservation in BC and BC/TiO₂ substrates. (A) Phase-contrast and fluorescent (insets showing Calcein-AM staining in green for viable cells) microscope images of fibroblasts grown on BC, BC/TiO₂ and cell culture surfaces at the different evaluated points: before cryopreservation, 4 and 48 h after thawing where cell recovery can be clearly appreciated. Scale bar = 100 μ m. (B) Cell viability after thawing expressed as a percentage of the not cryopreserved cultures. After 48 h of incubation, the cryopreserved cells recovered almost the same viability values as the not cryopreserved samples on the three assessed methods (No statistically significant differences). (C) BC and (D) BC/TiO₂ evaluation by scanning electron microscopy of the substrate's integrity after cryostorage. Note that the nanofibrillar structure is totally maintained after thawing on both substrates. Scale bar = 1 μ m.

viability since 98% and 99% of the cells were positive for the Calcein-AM staining respectively at day 2 after seeding. Fibroblasts plated on control surfaces exhibited analogous Calcein-AM staining. Then, we monitored cell proliferation over 8 days of culture on BC, BC/TiO₂ and cell culture plates as positive controls (Figure 3B). A progressive intensification of the signal was observed for the three conditions finding statistically significant differences at day 8 with respect to day 1 for the BC and BC/TiO₂ substrates, which correlates with an increasing number of metabolically active cells. Not surprisingly, fibroblasts on the control surfaces exhibit higher absolute values (statistically significant respect to both BC and BC/TiO₂) which we attribute mainly to the higher initial cell attachment to these surfaces compared to the BC and BC/TiO₂ carriers. No statistically significant differences were found when comparing proliferation between plain BC and titania hybrids implying that the TiO₂ NPs coating has a neutral effect over fibroblasts proliferation. After \sim 1 week, the cultures reached 100% confluence on the three substrates (Figure S2–B) leading to the formation of a continuous cell monolayer. These observations point out that BC and BC/TiO₂ allow not only the adhesion and spreading of fibroblasts but also its

metabolic activity and *in vitro* expansion. These findings are relevant for future exploitation of BC and BC/TiO₂ as cells carriers since elevated cell densities are generally required for transplantation.

Cell Retrieve. To further investigate the properties of BC and BC/TiO₂ substrates as cell culture platforms, we evaluated the possibility to retrieve the cells attached to BC and BC/TiO₂ substrates by three different methods: conventional trypsinization, direct contact with other substrates and degradation of the nanocellulose carriers.

Cells adhered to BC and BC/TiO₂ substrates could partially be harvested upon a 5 min incubation with trypsin-EDTA. To be precise, $55 \pm 18\%$ of the cells could be retrieved from BC/TiO₂ substrates while $35 \pm 15\%$ of the cells were detached from BC (not statistically significant differences) yielding a suspension of viable cells that could be used for further studies such as flow cytometry (Figure 4A). By an equivalent trypsinization process of fibroblasts growing on polystyrene plates, virtually the totality of the cells (indicated as 100% in Figure 4A) was recovered. This observation indicates that both BC and BC/TiO₂ substrates interfere to some extent with the trypsin-EDTA action, making it a partially effective approach

to harvest the cells from the investigated substrates. Figure S-5 contains optical microscope images of the fibroblasts cultures before and after the trypsin treatment further confirming these results.

Second, we placed BC and BC/TiO₂ films loaded with 1BR3.G cells in close contact (turned upside down) with two different substrates: a polystyrene culture plate as an example of a stiff substrate and a never dry BC hydrogel representing a softer surface. With this method, the transference of a fraction of the total adherent cell population (from their initial substrates to the unused ones) was observed (Figure 4B). Remarkably, the fibroblasts that migrated from the BC and BC/TiO₂ films were able to attach to the new supports and were metabolically active as indicated by the positive Calcein-AM staining (inserts in Figure 4B). The migrated cells exhibited a different morphology depending on the substrate where they were transferred; being more spread on the polystyrene plate than on the BC hydrogel. Presumably, this is due to the difference in the acceptor substrate stiffness which is known to influence fibroblast morphology rendering more rounded cell shapes in soft than in stiff substrates.⁴⁴ Overall, this preliminary experiment suggests that despite being strongly attached to the BC and BC/TiO₂ supports, the cultured cells keep their migration abilities, which is useful for future cell transplantation therapies.

Finally, we explored the possibility to benefit from cellulase enzymes to dissolve the BC and BC/TiO₂ carriers living a bare cell layer similar to that obtained from the cell-sheet technology that is begin developed with the use of thermoresponsive polymers.^{45,46} However, this option was dismissed because the optimization of the working conditions of the cellulase enzyme was incompatible with the growth of the cells; being the long incubation time required to completely dissolve the nanocellulose carriers the main inconvenience (see Figure S-6).

Adherent Cell Cryopreservation. Cryobanking of adherent mammalian cells is challenging because of the need for low-temperature resistant substrates and the high risk of cell detachment after thawing.⁴⁷ We hypothesized that the mechanical and thermal stability of BC could be of great value for this application. Accordingly, we evaluated the possibility to directly cryopreserve cell-BC and cell-BC/TiO₂ complexes aiming at facilitating the banking and transport of ready-to-use medical products based on BC.⁴⁸ BC-cells constructs were slowly frozen, stored on liquid nitrogen for over 1 week and thawed to assess cell viability and integrity of the BC and BC/TiO₂ supports.

Figure 5A shows the state of the fibroblast cultures grown on BC, BC/TiO₂ and culture wells before cryopreservation and after thawing. Not surprisingly, 4 h after defrosting, the cells were visibly stressed on the three tested conditions and decreased its viability down to 20–40% compared to the not cryopreserved cultures. However, cells remained attached to the BC and BC/TiO₂ substrates and it was noticeable that, after a recovery time of 48 h, the fibroblasts cultures became again highly confluent and viable as evidenced by the positive staining for Calcein-AM (see insets in Figure 5A) on the three experimental settings. Accordingly, the ATP levels measured 48 h after thawing (Figure 5B) of the cryopreserved cells were almost identical (no statistically significant differences) to the not cryopreserved samples. This corroborates the successful adherent cell cryopreservation on BC and BC/TiO₂ in a comparable fashion to the conventional cryopreservation

method of single cells suspensions (Ct). Notably, the suggested adherent cell cryopreservation process represents even an easier protocol compared to the control method since trypsinization is not required. The flexible nature of BC was helpful to place the substrates inside the cryovials and we speculate it is also convenient to prevent cell detachment as described in⁴⁹ for a poly urethane nanofibrous supports. Moreover, we assessed the integrity of BC and BC/TiO₂ substrates (without cells) after one-week storage at −196 °C. The films did not undergo any change in shape or consistency and were as easy to manipulate as the noncryopreserved materials. Accordingly, the SEM micrographs of Figure 5C (BC) and 5D (BC/TiO₂) show intact nanofibrillar structures and NPs coating without the presence of pores or cracks (use SEM images in Figure 1 for comparison). The finding that BC and BC/TiO₂ support the cryopreservation of adherent cells in an off-the-shelf format has important clinical significance as it could reduce the preparation time of cell loaded-biomaterials and boards the possibilities for long-term storage of cellular products.⁴⁸

CONCLUSIONS

Here, we endorse BC and BC/TiO₂ as endotoxin-free supports to expand human dermal fibroblasts by providing a complete evaluation of cellular responses toward BC and BC/TiO₂. No cytotoxic effects arising from the TiO₂ nanoparticles anchored to the BC fibers have been detected while cell spreading on the hybrids was higher than in plain BC. In this study, TiO₂ NPs were incorporated into the BC substrates to investigate its interactions with cells. However, future studies will examine other reported advantages of TiO₂ NPs such as the positive effect in wound healing and antimicrobial activity. Notably, we also report for the first time on the successful cryopreservation of cell-BC and cell-BC/TiO₂ constructs. Viable adherent cell cultures and undamaged carriers were thawed after being stored >1 week in liquid nitrogen. This indicates that BC and its derivatives could be utilized in the fabrication and long-term storage of ready-to-use cellular products. We expect the findings reported here serve as a first step toward the development of BC-based cell transplantation supports paving the way for future uses of BC-nanocomposites as advanced biomaterials.

ASSOCIATED CONTENT

Supporting Information

The Supporting Information is available free of charge at <https://pubs.acs.org/doi/10.1021/acsbomaterials.0c00492>.

Supporting Information includes: Detailed characterization of the BC and BC/TiO₂ substrates; phase contrast microscope images to illustrate cell proliferation; images before and after trypsinization; BC degradation by cellulase enzymes; large area confocal microscope images and details about the cell shape descriptors analysis (PDF)

AUTHOR INFORMATION

Corresponding Authors

Anna Laromaine – *Institute of Materials Science of Barcelona (ICMAB-CSIC), 08193 Bellaterra, Catalonia, Spain;*
 ● orcid.org/0000-0002-4764-0780; Email: alaromaine@icmab.es

Anna Roig – Institute of Materials Science of Barcelona (ICMAB-CSIC), 08193 Bellaterra, Catalonia, Spain;
 ● orcid.org/0000-0001-6464-7573; Email: roig@icmab.es

Authors

Irene Anton-Sales – Institute of Materials Science of Barcelona (ICMAB-CSIC), 08193 Bellaterra, Catalonia, Spain;
 ● orcid.org/0000-0003-3511-2574

Soledad Roig-Sanchez – Institute of Materials Science of Barcelona (ICMAB-CSIC), 08193 Bellaterra, Catalonia, Spain

María Jesús Sánchez-Guisado – Institute of Materials Science of Barcelona (ICMAB-CSIC), 08193 Bellaterra, Catalonia, Spain

Complete contact information is available at:
<https://pubs.acs.org/10.1021/acsbmaterials.0c00492>

Notes

The authors declare no competing financial interest.

ACKNOWLEDGMENTS

Authors acknowledge financial support from the Spanish Ministry of Science and Innovation through the RTI2018-096273-B-I00, project, the “Severo Ochoa” Programme for Centres of Excellence in R&D (SEV-2015-0496) and the PhD scholarships of I.A.S. (BE-2017-076734) and S.R.S. (BES-2016-077533). The Generalitat de Catalunya with the 2017SGR765 and the 2019LLAV00046 projects are also acknowledged. The authors also express their gratitude to the technical services of ICMAB (Nanoquim, AFM and TGA), UAB (cell culture and microscopy facilities), and ICN2 (electron microscopy). The authors participate in the CSIC Interdisciplinary Platform for Sustainable Plastics towards a Circular Economy, SUSPLAST, in the Aerogels COST ACTION (CA 18125) and in the Research network NANOCARE from MICINN (RED2018-102469-T).

REFERENCES

- Boyce, S. T.; Kagan, R. J.; Meyer, N. A.; Yakuboff, K. P.; Warden, G. D. Cultured Skin Substitutes Combined With Integra Artificial Skin to Replace Native Skin Autograft and Allograft for the Closure of Excised Full-Thickness Burns. *J. Burn Care Rehabil.* **1999**, *20*, 453–461.
- O'Connor, N.; Mulliken, J.; Banks-Schlegel, S.; Kehinde, O.; Green, H. Grafting of burns with cultured epithelium prepared from autologous epidermal cells. *Lancet* **1981**, *317*, 75–78.
- Beele, H.; de la Brassine, M.; Lambert, J.; Suys, E.; De Cuyper, C.; Decroix, J.; Boyden, B.; Tobback, L.; Hulstaert, F.; Schepper, S. D.; Brissinck, J.; Delaey, B.; Draye, J.-P.; Deene, A. D.; Waele, P. D.; Verbeken, G. A prospective multicenter study of the efficacy and tolerability of cryopreserved allogenic human keratinocytes to treat venous leg ulcers. *Int. J. Lower Extremity Wounds* **2005**, *4*, 225–233.
- Morino, T.; Takagi, R.; Yamamoto, K.; Kojima, H.; Yamato, M. Explant culture of oral mucosal epithelial cells for fabricating transplantable epithelial cell sheet. *Regen. Ther.* **2019**, *10*, 36–45.
- Lauren, P.; Somersalo, P.; Pitkanen, I.; Lou, Y.-R.; Urtti, A.; Partanen, J.; Seppala, J.; Madetoja, M.; Laaksonen, T.; Makitie, A.; Yliperttula, M. Nanofibrillar cellulose-alginate hydrogel coated surgical sutures as cell-carrier systems. *PLoS One* **2017**, *12*, No. e0183487.
- Chua, A. W. C.; Khoo, I. K.; Truong, T. T. A.; Woo, E.; Tan, B. K.; Chong, S. J. From skin allograft coverage to allograft-micrograft sandwich method: A retrospective review of severe burn patients who received conjunctive application of cultured epithelial autografts. *Burns* **2018**, *44*, 1302–1307.

- Carsin, H.; Ainaud, P.; Le Bever, H.; Rives, J.-M.; Lakhel, A.; Stephanazzi, J.; Lambert, F.; Perrot, J. Cultured epithelial autografts in extensive burn coverage of severely traumatized patients: a five year single-center experience with 30 patients. *Burns* **2000**, *26*, 379–387.
- MacNeil, S. Biomaterials for tissue engineering of skin. *Mater. Today* **2008**, *11*, 26–35.
- ter Horst, B.; Chouhan, G.; Moiemien, N. S.; Grover, L. M. Advances in keratinocyte delivery in burn wound care. *Adv. Drug Delivery Rev.* **2018**, *123*, 18–32.
- Wood, F. M.; Kolybaba, M. L.; Allen, P. The use of cultured epithelial autograft in the treatment of major burn injuries: A critical review of the literature. *Burns* **2006**, *32*, 395–401.
- Mitrousis, N.; Fokina, A.; Shoichet, M. S. Biomaterials for cell transplantation. *Nat. Rev. Mater.* **2018**, *3*, 441–456.
- Brittberg, M. Cell carriers as the next generation of cell therapy for cartilage repair: A review of the matrix-induced autologous chondrocyte implantation procedure. *Am. J. Sports Med.* **2010**, *38*, 1259–1271.
- de Oliveira Barud, H.; da Silva, R.; da Silva Barud, H.; Terçjak, A.; Gutierrez, J.; Lustrri, W.; de Oliveira, O.; Ribeiro, S. A multipurpose natural and renewable polymer in medical applications: Bacterial cellulose. *Carbohydr. Polym.* **2016**, *153*, 406–420.
- Anton-Sales, I.; D'Antin, C. J.; Fernández-Engroba, J.; Charoenrook, V.; Laromaine, A.; Roig, A.; Michael, R. Bacterial nanocellulose as a corneal bandage material: A comparison with amniotic membrane. *Biomater. Sci.* **2020**, *8*, 2921.
- Watanabe, K.; et al. A new bacterial cellulose substrate for mammalian cell culture. *Cytotechnology* **1993**, *13*, 107–114.
- Andrade, F. K.; Moreira, S. M. G.; Domingues, L.; Gama, F. M. P. Improving the affinity of fibroblasts for bacterial cellulose using carbohydrate-binding modules fused to RGD. *J. Biomed. Mater. Res., Part A* **2010**, *92A*, 9–17.
- Gonçalves, S.; Padrão, J.; Rodrigues, I. P.; Silva, J. P.; Sencadas, V.; Lanceros-Mendez, S.; Girão, H.; Dourado, F.; Rodrigues, L. R. Bacterial Cellulose As a Support for the Growth of Retinal Pigment Epithelium. *Biomacromolecules* **2015**, *16*, 1341–1351.
- Gonçalves, S.; Rodrigues, I. P.; Padrao, J.; Silva, J. P.; Sencadas, V.; Lanceros-Mendez, S.; Girao, H.; Gama, F. M.; Dourado, F.; Rodrigues, L. R. Acetylated bacterial cellulose coated with urinary bladder matrix as a substrate for retinal pigment epithelium. *Colloids Surf., B* **2016**, *139*, 1–9.
- Lv, X.; Yang, J.; Feng, C.; Li, Z.; Chen, S.; Xie, M.; Huang, J.; Li, H.; Wang, H.; Xu, Y. Bacterial Cellulose-Based Biomimetic Nanofibrous Scaffold with Muscle Cells for Hollow Organ Tissue Engineering. *ACS Biomater. Sci. Eng.* **2016**, *2*, 19–29.
- Svensson, A.; Nicklasson, E.; Harrah, T.; Panilaitis, B.; Kaplan, D. L.; Brittberg, M.; Gatenholm, P. Bacterial cellulose as a potential scaffold for tissue engineering of cartilage. *Biomaterials* **2005**, *26*, 419–431.
- Khan, S.; Ul-Islam, M.; Ikram, M.; Islam, S. U.; Ullah, M. W.; Israr, M.; Jang, J. H.; Yoon, S.; Park, J. K. Preparation and structural characterization of surface modified microporous bacterial cellulose scaffolds: A potential material for skin regeneration applications in vitro and in vivo. *Int. J. Biol. Macromol.* **2018**, *117*, 1200–1210.
- Tronser, T.; Laromaine, A.; Roig, A.; Levkin, P. A. Bacterial Cellulose Promotes Long-Term Stemness of mESC. *ACS Appl. Mater. Interfaces* **2018**, *10*, 16260–16269.
- Anton-Sales, I.; Beekmann, U.; Laromaine, A.; Roig, A.; Kralisch, D. Opportunities of Bacterial Cellulose to Treat Epithelial Tissues. *Curr. Drug Targets* **2019**, *20*, 808–822.
- Fey, C.; Betz, J.; Rosenbaum, C.; Kralisch, D.; Vielreicher, M.; Friedrich, O.; Metzger, M.; Zdzienb, D. Bacterial nanocellulose as novel carrier for intestinal epithelial cells in drug delivery studies. *Mater. Sci. Eng., C* **2020**, *109*, 110613.
- Jagannath, A.; Raju, P. S.; Bawa, A. S. Comparative evaluation of bacterial cellulose (nata) as a cryoprotectant and carrier support during the freeze drying process of probiotic lactic acid bacteria. *LWT - Food Sci. Technol.* **2010**, *43*, 1197–1203.

- (26) Lee, K. H.; Sun, J. C.; Chuang, C. K.; Guo, S. F.; Tu, C. F.; Ju, J. C. An efficient and mass reproducible method for vitrifying mouse embryos on a paper in cryotubes. *Cryobiology* **2013**, *66*, 311–317.
- (27) Stielow, J. B.; Vaas, L. A. I.; Goker, M.; Hoffmann, P.; Klenk, H.-P. Charcoal filter paper improves the viability of cryopreserved filamentous ectomycorrhizal and saprotrophic Basidiomycota and Ascomycota. *Mycologia* **2012**, *104*, 324–330.
- (28) Ullah, H.; Wahid, F.; Santos, H. A.; Khan, T. Advances in biomedical and pharmaceutical applications of functional bacterial cellulose-based nanocomposites. *Carbohydr. Polym.* **2016**, *150*, 330–352.
- (29) Osumi, K.; Matsuda, S.; Fujimura, N.; Matsubara, K.; Kitago, M.; Itano, O.; Ogino, C.; Shimizu, N.; Obara, H.; Kitagawa, Y. Acceleration of wound healing by ultrasound activation of TiO₂ in *Escherichia coli*-infected wounds in mice. *J. Biomed. Mater. Res., Part B* **2017**, *105*, 2344–2351.
- (30) Seisenbaeva, G. A.; Fromell, K.; Vinogradov, V. V.; Terekhov, A. N.; Pakhomov, A. V.; Nilsson, B.; Ekdahl, K. N.; Vinogradov, V. V.; Kessler, V. G. Dispersion of TiO₂ nanoparticles improves burn wound healing and tissue regeneration through specific interaction with blood serum proteins. *Sci. Rep.* **2017**, *7*, 15448.
- (31) Galkina, O. L.; Ivanov, V. K.; Agafonov, A. V.; Seisenbaeva, G. A.; Kessler, V. G. Cellulose nanofiber–titania nanocomposites as potential drug delivery systems for dermal applications. *J. Mater. Chem. B* **2015**, *3*, 1688–1698.
- (32) Galkina, O. L.; Öneby, K.; Huang, P.; Ivanov, V. K.; Agafonov, A. V.; Seisenbaeva, G. A.; Kessler, V. G. Antibacterial and photochemical properties of cellulose nanofiber–titania nanocomposites loaded with two different types of antibiotic medicines. *J. Mater. Chem. B* **2015**, *3*, 7125–7134.
- (33) Khalid, A.; Ullah, H.; Ul-Islam, M.; Khan, R.; Khan, S.; Ahmad, F.; Khan, T.; Wahid, F. Bacterial cellulose–TiO₂ nanocomposites promote healing and tissue regeneration in burn mice model. *RSC Adv.* **2017**, *7*, 47662–47668.
- (34) Roig-Sanchez, S.; Jungstedt, E.; Anton-Sales, I.; Malaspina, D. C.; Faraudo, J.; Berglund, L. A.; Laromaine, A.; Roig, A. Nanocellulose films with multiple functional nanoparticles in confined spatial distribution. *Nanoscale Horizons* **2019**, *4*, 634–641.
- (35) May-Masnou, A.; Soler, L.; Torras, M.; Salles, P.; Llorca, J.; Roig, A. Fast and Simple Microwave Synthesis of TiO₂/Au Nanoparticles for Gas-Phase Photocatalytic Hydrogen Generation. *Front. Chem.* **2018**, *6*, 110.
- (36) U.S. Department of Health and Human Services, *Guidance for Industry Pyrogen and Endotoxins Testing: Questions and Answers* (2012).
- (37) Zeng, M.; Laromaine, A.; Roig, A. Bacterial cellulose films: influence of bacterial strain and drying route on film properties. *Cellulose* **2014**, *21* (6), 4455–4469.
- (38) Biazar, E.; Heidari, M.; Asefnejad, A.; Asefnejad, A.; Montazeri, N. The relationship between cellular adhesion and surface roughness in polystyrene modified by microwave plasma radiation. *Int. J. Nanomed.* **2011**, *6*, 631–9.
- (39) Zareidoost, A.; Yousefpour, M.; Ghaseme, B.; Amanzadeh, A. The relationship of surface roughness and cell response of chemical surface modification of titanium. *J. Mater. Sci.: Mater. Med.* **2012**, *23*, 1479–88.
- (40) Martínez Ávila, H.; Feldmann, E. M.; Pleumeekers, M. M.; Nimeskern, L.; Kuo, W.; de Jong, W. C.; Schwarz, S.; Müller, R.; Hendriks, J.; Rotter, N.; van Osch, G. J. V. M.; Stok, K. S.; Gatenholm, P. Novel bilayer bacterial nanocellulose scaffold supports neocartilage formation in vitro and in vivo. *Biomaterials* **2015**, *44*, 122–133.
- (41) Hakkinen, K. M.; Harunaga, J. S.; Doyle, A. D.; Yamada, K. M. Direct Comparisons of the Morphology, Migration, Cell Adhesions, and Actin Cytoskeleton of Fibroblasts in Four Different Three-Dimensional Extracellular Matrices. *Tissue Eng., Part A* **2011**, *17* (2011), 713.
- (42) Huber, M. D.; Gerace, L. The size-wise nucleus: nuclear volume control in eukaryotes. *J. Cell Biol.* **2007**, *179*, 583–4.
- (43) Milla, M.; Yu, S.-M.; Laromaine, A. Parametrizing the exposure of superparamagnetic iron oxide nanoparticles in cell cultures at different in vitro environments. *Chem. Eng. J.* **2018**, *340*, 173–180.
- (44) Yeung, T.; Georges, P. C.; Flanagan, L. A.; Marg, B.; Ortiz, M.; Funaki, M.; Zahir, N.; Ming, W.; Weaver, V.; Janmey, P. A. Effects of substrate stiffness on cell morphology, cytoskeletal structure, and adhesion. *Cell Motil. Cytoskeleton* **2005**, *60*, 24–34.
- (45) Matsuura, K.; Utoh, R.; Nagase, K.; Okano, T. Cell sheet approach for tissue engineering and regenerative medicine. *J. Controlled Release* **2014**, *190*, 228–239.
- (46) Yamato, M.; Okano, T. Cell sheet engineering. *Mater. Today* **2004**, *7*, 42–47.
- (47) Ng, K.; Gao, B.; Yong, K. W.; Li, Y.; Shi, M.; Zhao, X.; Li, Z.; Zhang, X. H.; Pingguan-Murphy, B.; Yang, H.; Xu, F. Paper-based cell culture platform and its emerging biomedical applications. *Mater. Today* **2017**, *20*, 32–44.
- (48) Costa, P. F.; Dias, A. F.; Reis, R. L.; Gomes, M. E. Cryopreservation of Cell/Scaffold Tissue-Engineered Constructs. *Tissue Eng., Part C* **2012**, *18* (2012), 852.
- (49) Batnyam, O.; Suye, S.; Fujita, S. Direct cryopreservation of adherent cells on an elastic nanofiber sheet featuring a low glass-transition temperature. *RSC Adv.* **2017**, *7*, S1264–S1271.

Limbal Stem Cells on Bacterial Nanocellulose Carriers for Ocular Surface Regeneration

Irene Anton-Sales, Laura Koivusalo, Heli Skottman,* Anna Laromaine,* and Anna Roig*

Limbal stem cells (LSCs) are already used in cell-based treatments for ocular surface disorders. Clinical translation of LSCs-based therapies critically depends on the successful delivery, survival, and retention of these therapeutic cells to the desired region. Such a major bottleneck could be overcome by using an appropriate carrier to provide anchoring sites and structural support to LSC culture and transplantation. Bacterial nanocellulose (BNC) is an appealing, yet unexplored, candidate for this application because of its biocompatibility, animal-free origin and mechanical stability. Here, BNC as a vehicle for human embryonic stem cells-derived LSC (hESC-LSC) are investigated. To enhance cell-biomaterial interactions, a plasma activation followed by a Collagen IV and Laminin coating of the BNC substrates is implemented. This surface functionalization with human extracellular matrix proteins greatly improved the attachment and survival of hESC-LSC without compromising the flexible, robust and semi-transparent nature of the BNC. The surface characteristics of the BNC substrates are described and a preliminary ex vivo test in simulated transplantation scenarios is provided. Importantly, it is shown that hESC-LSC retain their self-renewal and stemness characteristics up to 21 days on BNC substrates. These results open the door for future research on hESC-LSC/BNC constructs to treat severe ocular surface pathologies.

impaired vision.^[3,4] LSC transplantation hold enormous therapeutic potential for these incapacitating conditions^[5-7] but its implementation is conditioned to the availability of clinically compliant donor LSC and the effectiveness of the cell delivery strategies.^[8,9] As an alternative to autologous and allogenic primary cell sources, on-demand amounts of LSC can be attained through differentiation from human induced pluripotent (hiPSC) or human embryonic stem cells (hESC) independently from donor ocular tissues. Furthermore, recent protocols ensure the reproducible and well-defined differentiation of LSC offering safer venues for ocular surface reconstruction.^[10-12]

Finding an optimal carrier for LSC transplantation to the ocular surface would give a firm push to the practical implementation of LSC-based therapies. Ideally, the carrier should be biocompatible and support cell viability while presenting adequate material properties (e.g., robustness, conformability, manageability). Human amniotic membrane

(AM), the innermost layer of the placenta, is widely used in ophthalmological treatments^[13,14] and it has been advocated as a well-suited substrate for LSC expansion and transplantation.^[15,16] Nevertheless, concerns about the low availability and reproducibility of AM have prompted research on alternative biological substrates such as collagen and fibrin.^[17-19] On this line, we have previously suggested the biopolymer bacterial nanocellulose (BNC) for ocular surface bandaging applications.^[20] BNC is biosynthesized by nonpathogenic bacterial cultures in the form of an interlaced nanofibrillar structure with high architectonic parallelism to collagen matrices. This nanostructure endows BNC with outstanding material properties regarding mechanical and thermal stability, conformability, water retention and easiness of manipulation.^[21] In addition, BNC is widely regarded as a cytocompatible substrate owing it to its high chemical purity and supported by numerous in vitro investigations.^[22-24] As for immunogenicity, BNC grafts have been found to elicit low to none inflammatory responses in vivo and to be generally well tolerated by the surrounding tissues.^[25-28] Productionwise, BNC is equally appealing because of its animal-free origin, tunability and feasible scale-up.^[29,30] All these reasons endorse BNC toward its way through the health market^[31,32] with applications ranging from wound dressings^[33,34] to antifibrotic implant coatings.^[35]

1. Introduction

Limbal stem cells (LSC) are tissue-specific stem cells located at the boundary between the cornea and the bulbar conjunctiva. LSC safeguard ocular surface health by constantly renewing the corneal epithelium and by preventing the opaque conjunctival cells to migrate into the transparent cornea.^[1,2] Acute trauma, burns, and inflammatory diseases can disrupt the delicate ocular surface homeostasis and cause opacification, vascularization, and scarring of the cornea resulting in

I. Anton-Sales, Dr. A. Laromaine, Prof. A. Roig
 Institute of Materials Science of Barcelona (ICMAB-CSIC)
 Campus UAB
 Bellaterra 08193, Spain
 E-mail: alaromaine@icmab.es; roig@icmab.es
 Dr. L. Koivusalo, Prof. H. Skottman
 Faculty of Medicine and Health Technology
 Tampere University
 Arvo Ylpön katu 34, Tampere 33520, Finland
 E-mail: heli.skottman@tuni.fi

The ORCID identification number(s) for the author(s) of this article can be found under <https://doi.org/10.1002/smll.202003937>.

DOI: 10.1002/smll.202003937

Here, we aimed at establishing and characterizing LSC cultures on BNC substrates to assess its potential as a transplantation vehicle for these cells. BNC has been suggested as a carrier for other cell types,^[36,37] including retinal pigment epithelium,^[38,39] but to the best of our knowledge, this is the first study combining BNC and LSC. Clinical translation being our ultimate goal; we employed LSC differentiated from hESC (hESC-LSC) under feeder- and serum-free conditions.^[11] Similarly, BNC membranes were thoroughly purified until endotoxin-free before its use as cell support.^[22] The palette of BNC modifications seeking to enhance cell attachment is particularly diverse.^[29,30,40–42] Thus, our ambition was to find a BNC conditioning rendering a favorable interface for hESC-LSC culture in a simple, well-defined and scalable process.

2. Experimental Section

2.1. BNC Substrates Preparation and Characterization

2.1.1. BNC Production

BNC hydrogels were synthesized by *Komagataeibacter xylinus* (*K. xylinus*, NCIMB 5346 from Colección Española de Cultivos Tipo, Valencia, Spain) grown on Hestrin-Schramm medium following previously described protocols.^[20,43] *K. xylinus* cultures were kept on 24-well plates for 3 d under static conditions at 30 °C to obtain circular BNC fleeces with the same diameter as the containers (≈1.6 cm). The as-formed hydrogels were picked with tweezers and immersed in a 1:1 v/v solution of Milli-Q water and ethanol for 10–15 min. Then, BNC fleeces were cleaned with boiling Milli-Q water (40 min) and NaOH (2 × 20 min) to remove organic remains. The BNC hydrogels were dried at 60 °C, between two Teflon plates and 1 kg weight. Dry films were rehydrated in Milli-Q water, sterilized by autoclave (121 °C, 20 min), and stored at room temperature (RT) until experimental use.

2.1.2. BNC Surface Modification

BNC membranes were placed on 24-well culture plates and incubated overnight at 4 °C with a solution of 0.5 μg cm⁻² of recombinant human laminin (LN-521, Biolamina) and 5 μg cm⁻² collagen type IV from human placenta (Col IV, Sigma-Aldrich) in Dulbecco's phosphate-buffered saline (DPBS, Lonza) containing calcium and magnesium. The as-prepared samples are referred to as “extracellular matrix (ECM) coated” BNC. To prepare the “Plasma + ECM coated” samples, dry BNC films were activated for 1 min with oxygen plasma inside a plasma reactor (Diener Electronic GmbH, power = 50 W, pressure = 0.40 mBar) under vacuum. Then, the activated membranes were immediately coated with the ECM protein solution following the previous procedure. The “plasma” BNC samples were only irradiated with oxygen plasma and the “plain” samples were left untreated.

2.1.3. Light Transmittance Measurements

Visible light absorption spectra were collected with a JASCO V-570 ultraviolet–visible–near infrared spectrophotometer between 400

and 800 nm. Samples were held with a cover glass also used for the baseline correction. Three different samples were analyzed for each condition and the obtained values were averaged.

2.1.4. Scanning Electron Microscopy (SEM)

Fragments of dry BNC films were placed flat on aluminum SEM sample holders with adhesive carbon tape. Metalized samples were sputtered with 5 nm of platinum before imaging. A high-resolution scanning electron microscope (FEI Magellan 400L XHR SEM) was used under a high vacuum and with an acceleration voltage of 2 kV to obtain images at 5,000, 20,000, and 100,000X magnifications. Working distance was 4 mm and the current was 0.1 nA. Energy-dispersive X-ray (EDX) spectroscopy was performed with the same equipment at 1 KeV. At least two areas from four independent BNC samples were imaged on both sides of the films.

2.1.5. Atomic Force Microscopy (AFM)

Topographical images and roughness values were obtained with a 5100 Agilent Technologies atomic force microscopy on tapping mode and equipped with a FORT tip from AppNano. Three 30 μm × 30 μm areas were analyzed from each sample. Dry BNC samples were fixed flat on the holders with adhesive tape. The images were processed with Surface analysis software V7.4 (64-bit)—Mountains technology.

2.1.6. Ex Vivo Evaluation of BNC with Porcine Corneal Organ Culture

The corneal organ model employed in this study has been described previously.^[44,45] Briefly, fresh porcine eyes from a local abattoir were kept in cold DPBS + 2% antibiotics for up to 4 h and then disinfected with 2% povidone-iodine (Betadine, Leiras). The corneas and part of the sclera were resected under sterile conditions and kept in Dulbecco's modified Eagle medium supplemented with 5% fetal bovine serum, 1% Penicillin/Streptomycin (P/S), 0.1% Amphotericin-B and 1 X GlutaMax at 37 °C and 5% CO₂ until BNC implantation. Before the BNC application, epithelial damage was created by an exhaustive scraping of the corneal surface with a scalpel, including the limbal area. BNC membranes were preconditioned with culture medium and 5 mm diameter pieces were cut with a trephine and sutured to the central part of the cornea with the help of a Barron artificial anterior chamber (Katena products Inc.). Four symmetric sutures (VICRON suture number 7) were made to fix each BNC sample. Then, specimens were moved to six-well plates and covered with soft contact lenses (EyeQ One-Day Premium, Cooper Vision) to avoid drying. The corneal organ culture was kept in the same culture conditions for 2 weeks after the implantation. The medium was changed twice per week. Before histological analysis, the porcine corneas were fixed using 4% paraformaldehyde (PFA) in DPBS for 4 h at RT. Samples were dehydrated in a Tissue-Tek VIP 5 (Sakura Finetek Europe) automatic tissue processor overnight

and embedded in paraffin blocks. Following, 7 mm thick tissue sections were cut with a microtome from each sample to cover different areas of the cornea. Histological sections were stained with hematoxylin-eosin (HE) and mounted on TOMO adhesion microscope slides (Matsunami Glass Ind., Ltd.). Optical microscope images were captured with Nikon Eclipse TE2000-S microscope and DS-Fi1 camera.

2.2. In Vitro Experiments

2.2.1. Human Embryonic Stem Cell-Derived Limbal Stem Cells (hESC-LSC) Culture

All cell studies were conducted under the ethical approval of the Ethics Committee of Pirkanmaa Hospital District number R05116 to derive, culture, and differentiate hESC lines for research. No new cell lines were derived from this study. The hESC-LSCs were differentiated from the hESC line Regea08/17 as described previously.^[11] The hESC-LSC cultures were maintained under serum- and feeder cell-free conditions. For the in vitro experiments, cryopreserved hESC-LSC in PSC cryopreservation medium (Thermo Fisher Scientific) were thawed at 37 °C and directly plated on top of BNC substrates (100,000 cells cm⁻²) placed on 24-well plates. Immediately after seeding, the culture plates were centrifuged for 1 min at 200 g's to increase the contact between hESC-LSC and the BNC supports. Controls were seeded on Corning CellBIND 24-well plates with the same ECM coating (5 µg cm⁻² Col-IV + 0.5 µg cm⁻² LN-521). The cultures were maintained in defined CnT-30 corneal differentiation medium (CELLnTEC, Advanced Cell Systems) containing 0.5% antibiotics (P/S) at 37 °C and 5% CO₂. Cell morphology and attachment were visually evaluated with a phase-contrast microscopy Zeiss Axio Vert A1 (Carl Zeiss) and the medium was changed twice per week.

2.2.2. Cell Viability Studies

For qualitative cell viability assessment, the LIVE/DEAD Viability/Cytotoxicity Kit for mammalian cells from Thermo Fisher Scientific was employed following the manufacturer's instructions. Briefly, cell cultures were washed with DPBS and incubated in the dark for 30 min with 500 µL of a 2 × 10⁻⁶ M Calcein-AM and 1 × 10⁻⁶ M Ethidium homodimer solution in DPBS. Then, the samples were rinsed with DPBS and imaged using a fluorescence microscope (Olympus IX51 equipped with a DP71 camera) at 10X. PrestoBlue cell viability reagent (Thermo Fischer Scientific) was used to measure cell proliferation. Triplicate samples were washed with DPBS and incubated with PrestoBlue reagent diluted 1:10 v/v in CnT-30 medium for 30 min at 37 °C and protected from light. Then, the supernatants were pipetted in technical triplicates on a 96-well plate (100 µL per well) and fluorescence values were read with a Viktor 1420 Multilabel Counter (Wallac) at 544 nm excitation and 590 nm emission wavelengths. Blanks were made with BNC substrates without cells. The average viability values obtained at Days 3 and 7 were normalized to values from Day 1 and represented as mean ± standard error repeating the experiment three times.

Table 1. Antibodies employed in the immunofluorescence staining.

Antibody	Host	Supplier	Dilution (v/v)
p63α	Rabbit	Cell Signaling Technology	1:200
p40	Mouse	Biocare Medical	1:100
CK14	Mouse	R&D	1:200
CK15	Mouse	Neomarkers (Thermo Fisher)	1:200
CK12	Goat	Santa Cruz Biotechnology	1:200
CK12	Rabbit	Abcam	1:200
Ki-67	Rabbit	Millipore	1:500
Collagen IV	Goat	Millipore	1:100
Antirabbit Alexa-488	Donkey	Molecular Probes	1:800
Antirabbit Alexa-568	Donkey	Molecular Probes	1:800
Antigoat Alexa-568	Donkey	Molecular Probes	1:800
Antimouse Alexa-647	Donkey	Molecular Probes	1:800
Antimouse Alexa-568	Donkey	Molecular Probes	1:800

2.2.3. Immunofluorescence

For specific marker proteins and Collagen IV detection, samples were first washed with DPBS, fixed with 4% PFA for 20 min at RT and washed again three times with DPBS. Triton X-100 was used to permeabilize the cell membranes for 15 min at RT and then samples were blocked for 90 min with a solution of 3% bovine serum albumin (BSA) in DPBS under mild agitation. Primary antibodies were diluted in 0.5% BSA and incubated overnight at 4 °C. The next day, specimens were washed three times with DPBS and incubated for 1 h at RT under mild agitation with the fluorescently labeled secondary antibodies diluted in 0.5% BSA. See Table 1 for information regarding the employed antibodies. Finally, samples were rinsed again three times with DPBS, flipped upside down and prepared for imaging with mounting medium containing 4',6-diamidino-2-phenylindole dihydrochloride (DAPI) (Vectashield from Vector Laboratories) under 13 mm Ø coverslips. Pictures were captured using an Olympus IX51 fluorescence microscope with 5X and 10X dry objectives. The stainings were repeated at least three times. Raw images were colored and adjusted for contrast and brightness using Image-J-Fiji software. Gray values were measured as the average intensity from the whole fluorescent images acquired with the same exposure times using the same software.

2.2.4. Confocal Microscope

Fixed hESC-LSC cultures grown on top of BNC membranes were incubated for 5 min at RT with 1 mL of a solution of 5 µg mL⁻¹ CellMask Deep Red Plasma Membrane Stain (Invitrogen) to dye cellular membranes and 0.25 mg mL⁻¹ Fluorescent Brightener (Sigma) diluted in DPBS to stain the BNC substrates. Then, samples were rinsed with DPBS and placed with the cells facing down on Ibidi Glass Bottom dishes. Stack images were obtained with a confocal laser-scanning microscope (Leica SP5). Fluorescent Brightener was excited at 350 nm and Cell Mask 588 nm wavelengths. Fluorescence images were reconstructed and colored with the Fiji package of Image-J (64-bit version).

2.3. Statistical Analysis

Statistically significant differences were determined using Graph Pad Prism 5 software by one-way analysis of variance and Tukey's multiple comparison post hoc test. Significance between groups was established for $P < 0.05$. Values provided correspond to the average \pm standard deviation or standard error of the mean as indicated. P -values on the graphs are summarized as nonsignificant (ns) for $P \geq 0.05$, * for $P < 0.05$, ** for $P < 0.01$, and *** for $P < 0.001$.

3. Results

3.1. BNC Membranes Coating and Characterization

BNC membranes (i.e., dried and rehydrated native BNC hydrogels) were conditioned for hESC-LSC culture following the process summarized in Figure 1A. Typically, hESC-LSC require specific binding moieties present in the ECM for adherence and survival. Therefore, a defined mixture of ECM proteins consisting of human Collagen IV (Col-IV) and recombinant human Laminin-521 (LN-521) was conjugated to endow BNC with specific linkers to favor cell attachment. Col-IV was fluorescently immunostained to investigate the distribution and abundance of the covering (Figure 1B–E). The conventional method consisting of incubating the BNC membranes with the protein solution rendered an inhomogeneous and incomplete coating of the substrates (Figure 1C) with accumulations of Col-IV in the cavity-like structures of the BNC membranes. To address this issue, a plasma activation step was incorporated before the impregnation with Col-IV and LN-521. The plasma-treated BNC substrates were homogeneously and more profusely covered by Col-IV than the substrates coated without prior plasma activation (Figure 1D). This effect was confirmed by comparing the fluorescence intensity values (Figure 1E) which showed statistically significant differences between the two methods.

Macroscopically, BNC membranes were indistinguishable. All the studied forms of BNC appeared as semi-transparent, thin ($\approx 20 \mu\text{m}$), flexible, and self-standing substrates (Figure 2A). BNC membranes, regardless of the surface treatments, were easily manipulated with tweezers and showed good conformability to a dome-shaped surface (Figure 2A). Moreover, the applied surface treatments had a negligible effect on the light transmittance of the BNC membranes (Figure 2B). All the investigated BNC membranes presented high light transmittance at long wavelengths while showing a gradual decline toward smaller wavelengths. As an example, the average transmittance at 700 nm was 84% and 70% at 500 nm.

SEM was used to investigate the effect of oxygen plasma on the micro/nanostructure of BNC revealing an altered nanofiber morphology after the plasma treatment (Figure 1F,H). This is a superficial modification since the reverse side of all the substrates presented the typical BNC nanofibrous organization (see a representative image in Figure 1I). Under SEM, the ECM coating was visually imperceptible on both ECM-coated and plasma-activated + ECM-coated samples (Figure 1G,H). To discard misinterpretations due to the metallization of the

samples, nonmetallized substrates were also observed under SEM with comparable outcomes (Figure S1, Supporting Information). On the contrary, a nitrogen peak, ascribed to the proteinaceous coating, was detected by EDX only on the samples containing Col-IV an LN-521 (Figure S1, Supporting Information). Besides, the surface of the plasma-treated BNC membranes was noticeably rougher than the untreated ones. This observation was confirmed by AFM roughness measurements, which disclosed a 1.4-fold increase in roughness for the plasma-activated samples versus the not activated samples (AFM images are shown in Figure S1, Supporting Information).

3.2. Ex Vivo BNC Evaluation with a Corneal Organ Culture

To assess the applicability of BNC as a support for cell transplantation to the ocular surface, an ex vivo organ culture model was used. Epithelial damage was created on excised porcine corneas before BNC implantation. After 14 d in culture, histological analysis was carried out by sectioning the specimens as schematized in Figure 3A. During the sample preparation process, BNC membranes proved excellent conformability to the dome shape of the corneas, could be cut to the desired size and were easily ex vivo sutured to the ocular surface (Figure 3B). Imaging of the HE-stained sections showed undamaged BNC membranes in close contact with the corneal surface for some of the tested eyes. Remarkably, a continuous corneal epithelium had regrown under the BNC patch (Figure 3C,D). See Figure S2 in the Supporting Information for comparison with a control pig cornea without BNC implantation where a similarly regrown pig epithelium is appreciable.

3.3. hESC-LSC Attachment and Viability on BNC Substrates

Next, the ability of the BNC to promote hESC-LSC attachment and viability was evaluated and compared for the distinct surface treatments. After 24 h in culture, evident differences could be observed in terms of cell morphology (Figure 4). hESC-LSC plated on plasma activated-ECM coated BNC membranes exhibited a homogeneous distribution on the substrate and the expected epithelial cell appearance (Figure 4D). Oppositely, hESC-LSC seeded on BNC membranes that received only plasma activation (Figure 4B) or solely ECM coating (Figure 4C) were round in morphology indicating poor suitability of these substrates for hESC-LSC maintenance. The same outcomes were detected for plain BNC (Figure 4A).

In accordance with these observations, at Day 4 after seeding, Live/Dead staining evidenced a highly viable cell population on the BNC membranes that were plasma-activated and coated with Col IV and LN-521 (Figure 4H). hESC-LSC on plasma-activated as well as plain BNC had mainly detached from the substrates (Figure 4E,F). On BNC membranes with conventional ECM coating, more hESC-LSC remained adhered but were unable to spread and stained mainly as dead cells (Figure 4G). An additional Live/Dead assay was conducted for BNC with plasma activation and ECM-coating at Day 8 to confirm long-term cell survival observing a highly

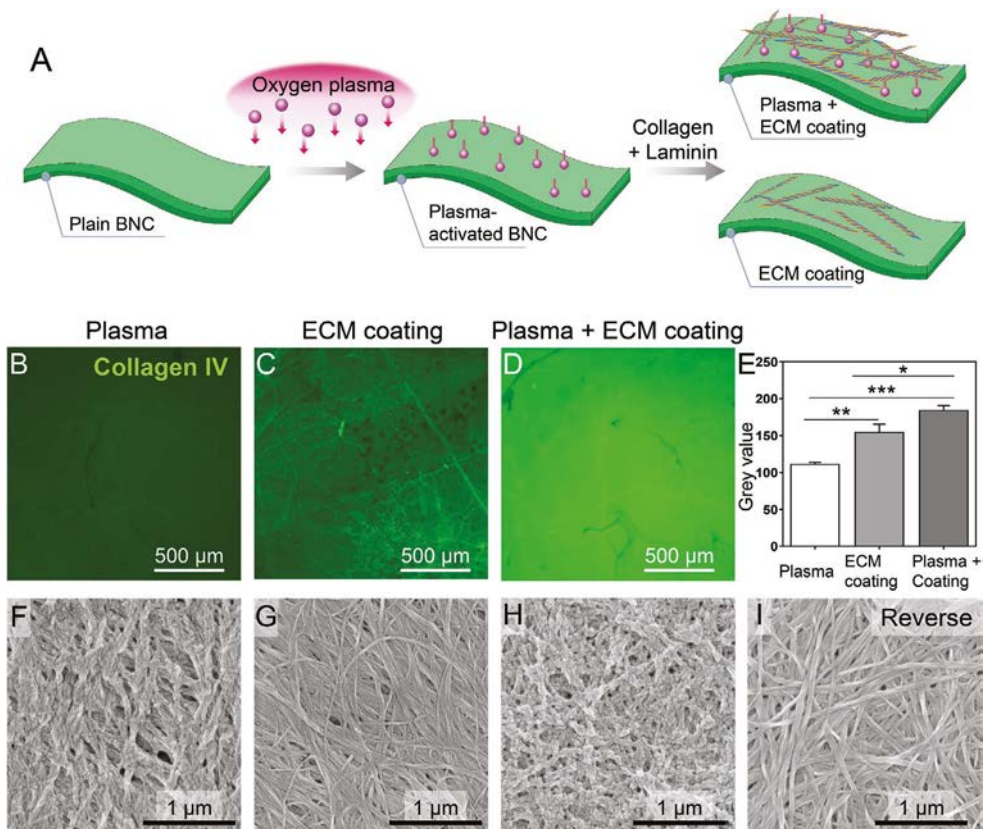


Figure 1. BNC surface treatments. A) Sketch of the different surface modifications of BNC membranes. B–D) Immunofluorescence staining of Collagen IV (green) deposited on BNC substrates. B) BNC activated with plasma but without ECM coating (Blank). C) BNC coated with the standard procedure consisting of pipetting the ECM protein solution on top of the substrates. D) Plasma-activated and ECM-coated BNC substrates where an intense and homogeneous coating by Collagen IV is observed. E) Fluorescence intensity (grey value \pm standard error) comparison of the Collagen IV staining between the different BNC substrates. Statistically significant differences were detected between all the groups. The lower board (F)–(I) gathers representative SEM images of the BNC substrates. As seen in images (F)–(H), C) the plasma treatment altered the BNC nanofibers while the ECM coating was visually undetectable. I) The reverse (untreated) side of all the BNC substrates remained unaltered, indicating that the modifications caused by the oxygen plasma are superficial. A representative SEM image is shown.

viable hESC-LSC population (Figure S3, Supporting Information). In light of these results, the *in vitro* experiments that follow were only performed with BNC substrates with plasma activation and ECM coating and are referred to as “BNC” from here on.

3.4. hESC-LSC Self-Renewing Capacity on BNC Substrates

Since the capacity to promote cell attachment, proliferation and then further differentiation toward corneal epithelial cells is a valuable characteristic of a cell carrier, we studied

the self-renewal properties of hESC-LSC on BNC substrates at three different time points. Visually, an increase in cell number could be observed between Days 1 and 3 while from Days 3 to 7 cell density stabilized and cell size augmented (Figure 5A). hESC-LSC exhibited the expected cobblestone morphology at the three studied time points and tended to form an epithelial monolayer on top of the BNC substrates as observed by confocal microscope (Figure 5B). The metabolic activity was quantitatively analyzed with a Presto Blue assay (Figure 5D). An increase in the fluorescence signal was detected at the early stages of the culture but not at the late stages where the fluorescence intensity remained constant

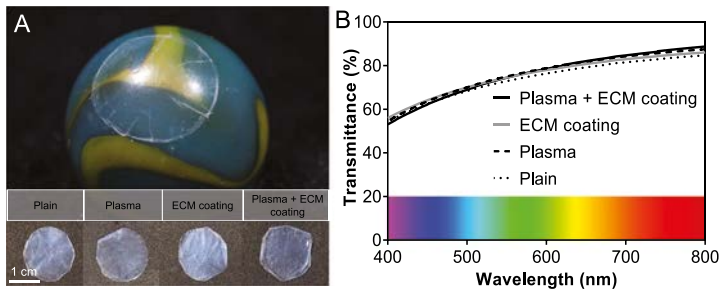


Figure 2. Macroscopic and optical features of BNC substrates. A) Digital images of the tested BNC substrates presenting an analogous appearance. All the membranes could be easily handled, maintained its flexibility and robustness, and accommodated well to a curved surface (upper photograph). B) Visible light transmittance of the tested cell carriers. The coatings to enhance hESC-LSC attachment did not alter the optical properties of BNC. All the substrates presented high transmittance at long wavelengths with a progressive decrease toward shorter wavelengths.

(not statistically significant differences). To further confirm these results, immunofluorescence staining of the proliferation marker Ki67 was performed (Figure 5C). Expression of Ki67 was detected at Days 1, 3, and 7 in a fraction of the hESC-LSC indicating the presence of a self-renewing cell population. The estimated percentage of Ki67 positive cells was higher on Day 1 than on Day 7. hESC-LSC growing on conventional culture plates coated with Col IV and LN-521 were used for comparison and a similar evolution was observed (see Figure S4, Supporting Information).

3.5. Protein Marker Expression

Finally, we investigated whether hESC-LSC cultured on BNC films retain their progenitor phenotype or they start to differentiate toward corneal epithelial cells. The expression of specific LSC markers^[46] was evaluated by immunocytochemistry. Simultaneous p63 α and p40 antibodies were used to detect the presence of the Δ Np63 α isoform of p63 in the cell nuclei, a widely used LSC marker. For further validation of the progenitor phenotype, the presence of distinctive cytokeratins (CK)

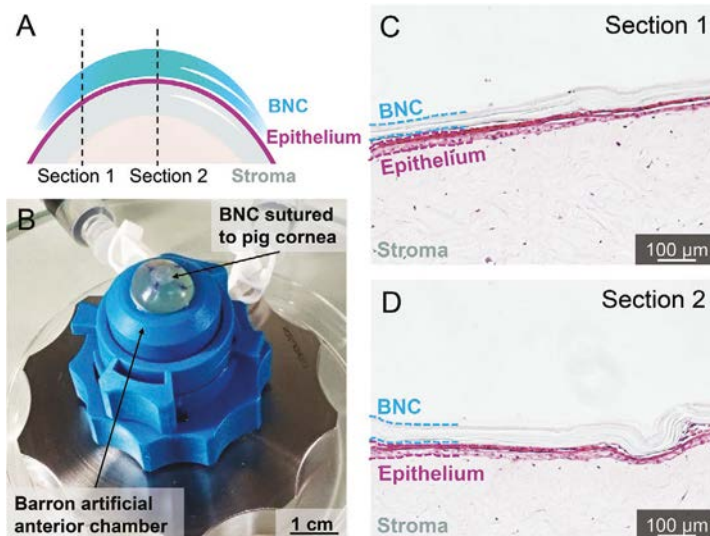


Figure 3. Ex vivo evaluation of BNC applicability as a cell delivery vehicle to the ocular surface with a porcine organ culture model. (A) and (B) depict the experimental setup, a Barron artificial anterior chamber (B) was used to perform the sutures on resected pig eyes. BNC membranes withstood cutting to the desired shape and fixation by suture stitches to porcine corneas with induced epithelial damage. Histological sections were cut as illustrated in (A). C,D) HE staining of the tissue sections revealed the successful re-epithelization of the pig corneas and intimate contact between the BNC and the ocular surface at the two examined cross-sections. For clarity of the images, BNC has been highlighted in blue and the pig epithelium in pink.

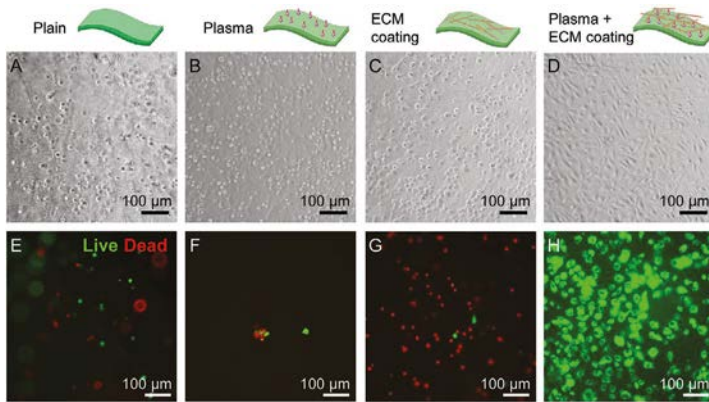


Figure 4. Attachment and viability of hESC-LSC on surface-modified BNC. A–D) Phase-contrast microscope images a Day 1 where, depending on the surface modification of BNC, clear differences in cell morphology can be visualized. Substrates with only one treatment (plasma (B) or ECM coating (C)) rendered rounded hESC-LSC morphologies while the combination of both created a favorable surface for hESC-LSC spreading (D). E–H) Live/Dead staining of hESC-LSC at Day 4 where alive cells are stained in green and dead cells in red. Note the high cell viability in (H) corresponding to BNC substrates with plasma activation followed by ECM protein coating. E–C) Viable hESC-LSC on the rest of the substrates were scarce.

was also examined. CK14 and CK15 were selected as stemness indicators while CK12 was employed as a differentiated corneal cell marker. Immunofluorescence images shown in **Figure 6A** illustrate that the majority of hESC-LSC cultured on BNC substrates highly express Δ Np63 α and low to undetectable levels

of CK12 at both Days 3 and 7 correlating with the expected LSC phenotype. Control hESC-LSC cultured on ECM-coated plastic exhibited a comparable marker expression pattern (see Ct in **Figure 6A**). Notably, the progenitor markers CK14 and CK15 behaved differently. While both keratins presented positive

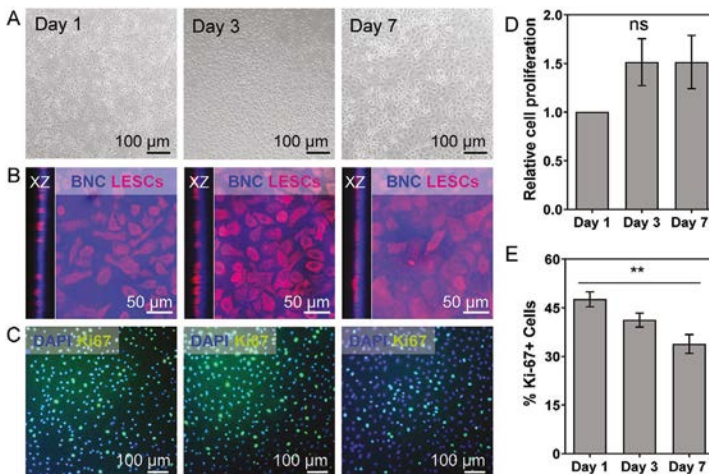


Figure 5. hESC-LSC culture monitoring and proliferation on BNC supports. A) Cell density and distribution versus time on BNC substrates. B) Confocal microscope and XZ cross-section images where the tendency of hESC-LSC to form an epithelial monolayer on top of the BNC substrates can be observed. hESC-LSC plasma membranes were marked in red and the BNC supports in blue. C) Representative immunofluorescence staining images of the Ki67 proliferation marker expression at diverse time points of hESC-LSC cultures on BNC. D) Presto Blue assay measuring the metabolic activity of hESC-LSC expanded on BNC. Bars show the average value of three independent experiments with standard error. E) Estimation (average and standard error) of the percentage of Ki67-positive cells at three different culture time points.

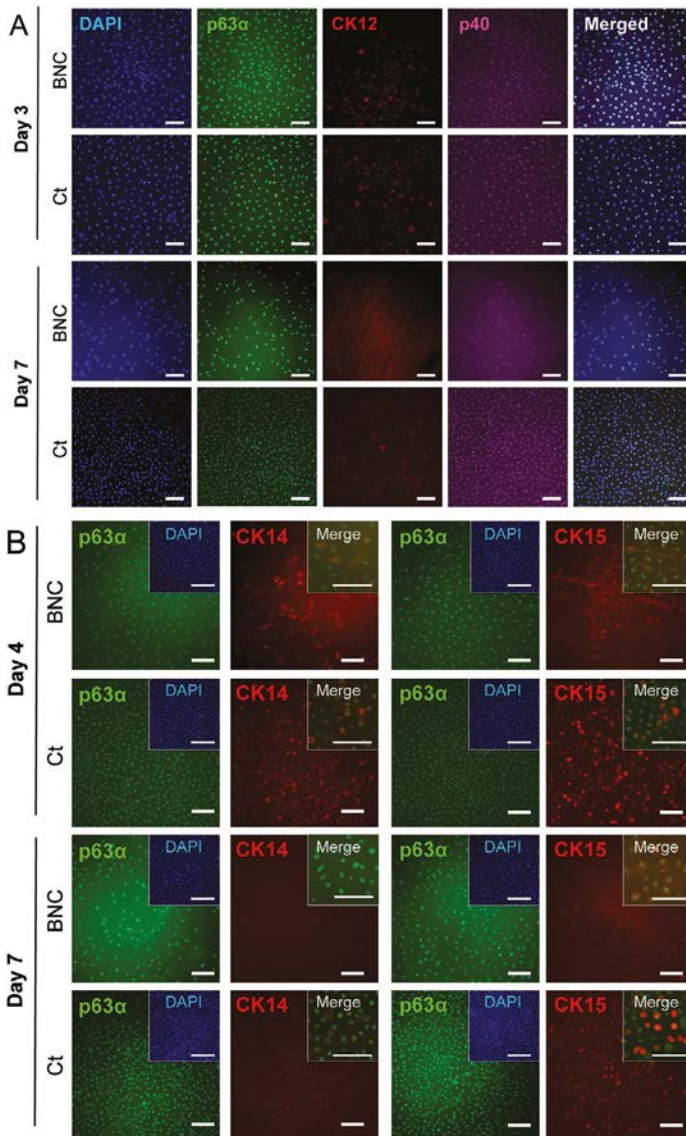


Figure 6. LSC marker expression at early time points. A) Representative immunofluorescence photographs of hESC-LSC cultured on BNC membranes 3 and 7 d after plating. Expression of the well-established limbal stem cell marker $\Delta Np63\alpha$ was confirmed by the simultaneous detection of p63 α and p40. CK12, an epithelial differentiation marker, was identified in low amounts. Merged images confirm the nuclear location of $\Delta Np63\alpha$ and the colocalization of the p63 α and p40 antibodies. Ct refers to conventional ECM-coated cell culture surfaces used for comparison and the scale bar is 100 μm . B) Cytoplasmic expression of the stemness-associated cytokeratins 14 and 15 (CK14 and CK15) on hESC-LSC cultures grown on top of BNC membranes for 4 and 7 d. The distribution of CK14 and CK15 (red) is compared to p63 α (green) present in the nucleus. Scale bar equals to 100 μm . Insets: DAPI-stained nuclei (blue) to evidence the total number of cells and details of the localization of the stemness markers. Scale bar of the insets = 50 μm .

immunofluorescence—less homogeneous than $\Delta\text{Np63}\alpha$ —at Day 4, only CK15 remained detectable on hESC-LSC maintained on BNC membranes until Day 7 (Figure 6B). As for controls, a similar trend was observed except for some faint signal still present at Day 7 for CK14.

Furthermore, we examined the long-term maintenance of stemness marker expression. Figure S5 in the Supporting Information displays immunofluorescence images of hESC-LSC on BNC carriers and control surfaces cultured for 2 and 3 weeks where a sustained LSC phenotype (p40-positive and predominantly CK12 negative) is perceived for both time points and culture surfaces resembling the early time points.

4. Discussion

hESC-LSC could revolutionize the management of ocular surface diseases but an optimal cell delivery strategy still needs to be found. This study suggests BNC as a nonanimal sourced substrate for hESC-LSC maintenance, manipulation, and plausible transplantation. We describe a straightforward plasma-assisted method to anchor ECM proteins on the surface of BNC enabling subsequent hESC-LSC attachment, spreading, and viability. Then, we demonstrate that hESC-LSC cultures express the proliferation marker Ki67, especially at the early stages of the culture and that they retain a LSC phenotype for up to 3 weeks on BNC supports.

A preliminary histological analysis from a corneal organ culture model shows the possibility to achieve intimate contact between BNC and the corneal surface, which is an advantageous situation for cell transplantation. We also observed reepithelization under the BNC membranes, which hints that BNC does not cause major cytotoxicity or oxygen permeability issues on this *ex vivo* model. These findings, combined with our previous reports on BNC suturability and stability in contact with ocular tissue,^[20] confirm that the material properties of BNC are adequate for a carrier in ocular surface cell replacement therapies. However, future research is required to assess the migration and integration capabilities of hESC-LSC grown on BNC carriers onto damaged corneas. Likewise, *in vivo* biocompatibility studies about ophthalmological applications of BNC are encouraging but still very scarce^[47] and the interactions between BNC and the host ocular immune system warrant further investigation.

There are a few examples in the literature about the usage of BNC supports in stem cell culture that do not report on the need for coating BNC with ECM proteins to provide cell adhesion moieties.^[48–50] Similarly, in our previous work with human dermal fibroblasts,^[22] we found that BNC coating was not required to facilitate cell attachment. However, the here presented results prove that the plasma-assisted ECM protein functionalization is crucial for hESC-LSC attachment and survival on the BNC substrates. Neither the plasma activation alone nor the conventional method to coat cell culture surfaces was able to provide a favorable interface between BNC and hESC-LSC. These observations discard that the described enhanced hESC-LSC adhesion is a consequence of the increased roughness of the plasma-treated BNC substrates detected by electronic microscopy and AFM. On the

contrary—and backed by the intensified Col IV adsorption on plasma-treated BNC—we ascribe this effect on the presence of specific binding sites for hESC-LSC. Interestingly, an analogous strategy was followed by Sorkio et al. to enhance hESC-derived retinal pigment epithelial cells attachment to synthetic electrospun membranes drawing similar conclusions.^[51] Hence, the requirement of surface modifications to use BNC as a cell culture substrate seems to be cell type-dependent. This cell-specificity has also been described by Pertile and colleagues^[52] who reported that nitrogen plasma activation improved the affinity of microvascular cells and neuroblasts for BNC but had no effect on fibroblasts.

Notably, the plasma treatment (1 min activation) did not make the hESC-LSC seeding protocol substantially longer, more complex or costlier compared to the standard ECM coating and did not compromise the manageability and the semi-transparency of the BNC membranes. By SEM examination, we encountered morphological changes on the BNC surface which were not present on the bulk of the material again in good agreement with reference.^[52] Therefore, we conclude that plasma activation offers vast possibilities for BNC functionalization aiming at favoring its interactions with cells without comprising its outstanding materials properties in a fast, simple, and scalable manner.^[53]

We inferred hESC-LSC cultures progression on BNC by measuring the metabolic activity and by detecting the proliferation marker Ki67 noticing that hESC-LSC can produce new daughter cells on BNC membranes as evidenced by the presence of Ki67-positive populations. A slowdown on the proliferation rate after Day 3 together with an increase in cell size was detected. These features correlate with a slight maturation of the hESC-LSC on BNC, although not complete differentiation since cultures remained positive for LSC markers and essentially CK12 negative (maturation marker) for up to 3 weeks. The detection of the progenitor marker CK14 at Day 4 but not at Day 7 after plating and the dimmer staining for CK15 at Day 7 compared to Day 4 further supports that a partial maturation of hESC-LSC is occurring on the BNC carriers. We believe that is an interesting finding since cellular therapies expect the progeny of the transplanted cells to mature and become part of a functional corneal epithelium after implantation, mimicking the *in vivo* phenomena.^[2,54] On the other hand, the employed hESC-LSC were previously proved capable of terminal differentiation on porcine collagen matrices by detecting the expression of CK3 and CK12 proteins.^[19] However, it remains uncertain if hESC-LSC possess the ability to differentiate toward fully mature corneal epithelial cells on BNC supports indicating a need for future work. Together, these observations lead us to believe that the level of maturation of the hESC-LSC cultures will be an important parameter to consider in upcoming studies on BNC-assisted hESC-LSC delivery to the ocular surface.

Notably, the assumed long-term mode of action of LSC transplantation relies on its capability to repopulate the limbal niche and from there provide constant cell renewal to the corneal epithelium. The expression of multiple stemness markers— $\Delta\text{Np63}\alpha$, CK14, and CK15—on hESC-LSC seeded on BNC carriers corroborates its progenitor phenotype and reinforces the therapeutic expectation that hESC-LSC could act similarly

to autologous LSC.^[55,56] Therefore, we venture that the time window between Day 1 and Day 4 after seeding on BNC supports could be an appropriate timing for hESC-LSC transplantation because the cultures exhibit higher proliferation and more stemness characteristics than later time-points; features that have been correlated with greater in vivo regenerative potential.^[57,18] Besides, this timing would also reduce the preparation period of the hESC-LSC/BNC constructs. Overall, and considering that biomaterial properties can greatly influence cell differentiation,^[58,59] the ability of BNC membranes to maintain the hESC-LSC phenotype in vitro rather than inducing terminal differentiation is encouraging for future implementation. We speculate that this effect could be at least partially explained by the particular nanotopography of BNC, as already reported for mouse stem cell cultures.^[48,60]

Currently, the library of biomaterials exploited in cell-based corneal regeneration is dominated by AM,^[5,61] collagen,^[9,62] and fibrin-derived substrates^[18,63] with successful results already reported.^[18,64] Research efforts are now focused on reducing the inherent risks of these therapies^[65] by switching to well-defined cell culture protocols^[66,67] and nonanimal sourced carriers.^[68] In pursuit of clinically compatible solutions, we employed serum- and feeder-free hESC-LSC cultures containing clinical-grade heparin, from the CnT-30 medium, as the only animal-derived product. BNC fits well into this emerging concept because of its purity and biotechnological animal-free production.^[69] We believe that BNC can be advantageous over the above mentioned biopolymers because of its mechanical stability, manageability, and lack of processing, which are considered as major limiting factors of the current solutions.^[62,70] Moreover, the thermal stability of BNC enables both its sterilization by heat and cryopreservation.^[22] The latest being of particular significance because it makes the cryobanking of ready-to-use hESC-LSC/BNC constructs a feasible possibility.

5. Conclusions

Here, we report on the culture of hESC-LSC on BNC membranes. We show that BNC substrates support the formation of new daughter cells and retain the progenitor phenotype of hESC-LSC while providing a self-standing and easy to manipulate mechanical support. Moreover, the nonanimal origin of BNC and the well-defined hESC-LSC differentiation and cultivation procedures allowed the formation of cell-biomaterial constructs intended for a prospective clinical application in ocular surface treatments. hESC-LSC attachment and viability were achieved after a plasma-enabled ECM protein functionalization of the BNC substrates. This fast and simple BNC functionalization method could be exploited in the future for the culture of other therapeutic cells and expand the possibilities of BNC as a cell carrier.

Supporting Information

Supporting Information is available from the Wiley Online Library or from the author.

Acknowledgements

This collaborative project was mainly funded with an European molecular biology organization short-term fellowship (ref 8288) awarded to I.A.-S. and the authors would like to express their gratitude to this institution. Researchers acknowledge financial support from the Spanish Ministry of Science and Innovation through the RTI2018-096273-B-I00 project, the Severo Ochoa Programme for Centres of Excellence in R&D (SEV-2015-0496 and CEX2019-000917-S) and the Ph.D. scholarship of I.A.-S. (BE-2017-076734) as well as Academy of Finland (326760). The authors are also grateful to Generalitat de Catalunya for the 2017SGR765 and the 2019LLAV00046 projects. Authors also appreciate Miquel Anton for his assistance with photography, the AFM service of ICMAB, the electron microscopy facility of ICN2, and the optical microscope service of UAB. The ICMAB members (I.A.-S., A.L., and A.R.) participate in the CSIC Interdisciplinary Platform for Sustainable Plastics toward a Circular Economy, SUSPLAST, MICINN: "Research Networks" nanoCARE, (RED2018-102469-T) and in the Aerogels COST ACTION (CA 18125). This work was conducted within the Material Science Doctoral Program of the Autonomous University of Barcelona (I.A.-S.). The authors deeply thank the laboratory staff of Tampere University, especially Outi Melin and Hanna Pekkanen for the production, maintenance and differentiation of the hESCs and hESC-LSC, and Juha Heikkilä for the help with the plasma equipment. The authors acknowledge the Biocenter Finland (BF) and Tampere Imaging Facility (TIF) for their service.

Conflict of Interest

The authors declare no conflict of interest.

Data Availability Statement

Research data are not shared.

Keywords

animal-free production, cell transplantation, corneal epithelium, human embryonic stem cells, microbial cellulose

Received: June 29, 2020

Revised: December 18, 2020

Published online: February 15, 2021

- [1] A. V. Ljubimov, M. Saghizadeh, *Prog. Retinal Eye Res.* **2015**, *49*, 17.
- [2] M. Ebrahimi, E. Taghi-Abadi, H. Baharvand, *J. Ophthalmic Vision Res.* **2009**, *4*, 40.
- [3] J. P. Whitcher, M. Srinivasan, M. P. Upadhyay, Corneal Blindness: A Global Perspective, *Bulletin of the World Health Organization* **2001**.
- [4] S. L. Wilson, A. J. El Haj, Y. Yang, *J. Funct. Biomater.* **2012**, *3*, 642.
- [5] N. Zakaria, T. Possemiers, S. Dhubhghaill, I. Leysen, J. Rozema, C. Koppen, J.-P. Timmermans, Z. Berneman, M.-J. Tassignon, *J. Transl. Med.* **2014**, *12*, 58.
- [6] J. Menzel-Severing, F. E. Kruse, U. Schlötzer-Schrehardt, *Can. J. Ophthalmol.* **2013**, *48*, 13.
- [7] EuroStemCell, <https://www.eurostemcell.org/story/europe-approves-holoclar-first-stem-cell-based-medicinal-product> (accessed: October 2020).
- [8] D. G. Harkin, S. E. Dunphy, A. M. A. Shadforth, R. A. Dawson, J. Walshe, N. Zakaria, *Cell Transplant.* **2017**, *26*, 1717.

- [9] M. Ahearne, J. Fernández-Pérez, S. Masterton, P. W. Madden, P. Bhattacharjee, *Adv. Funct. Mater.* **2020**, *30*, 1908996.
- [10] H. Hongisto, M. Vattulainen, T. Ilmarinen, A. Mikhailova, H. Skottman, *J. Visualized Exp.* **2018**, *140*, 58279.
- [11] H. Hongisto, T. Ilmarinen, M. Vattulainen, A. Mikhailova, H. Skottman, *Stem Cell Res. Ther.* **2017**, *8*, 291.
- [12] R. Hayashi, Y. Ishikawa, M. Ito, T. Kageyama, K. Takashiba, T. Fujioka, M. Tsujikawa, H. Miyoshi, M. Yamato, Y. Nakamura, K. Nishida, *PLoS One* **2012**, *7*, e45435.
- [13] A. Azuara-Blanco, C. T. Pillai, H. S. Dua, *Br. J. Ophthalmol.* **1999**, *83*, 399.
- [14] R. T. Pires, S. Tseng, P. Prabhasawat, *Evidence-Based Eye Care* **2000**, *1*, 80.
- [15] O. B. Selver, I. Durak, M. Gürdal, K. Baysal, H. Ates, Z. Ozbek, Z. Wang, A. Wu, J. M. Wolosin, *Mol. Vision* **2016**, *22*, 138.
- [16] S.-Y. Chen, M. Mahabole, S. C. G. Tseng, *Transl. Vision Sci. Technol.* **2013**, *2*, 1.
- [17] S. Mi, B. Chen, B. Wright, C. J. Connon, *Tissue Eng., Part A* **2010**, *16*, 2091.
- [18] P. Rama, S. Matuska, G. Paganoni, A. Spinelli, M. De Luca, G. Pellegrini, *N. Engl. J. Med.* **2010**, *363*, 147.
- [19] A. Mikhailova, T. Ilmarinen, A. Ratnayake, G. Petrovski, H. Uusitalo, H. Skottman, M. Rafat, *Exp. Eye Res.* **2016**, *146*, 26.
- [20] I. Anton-Sales, J. C. D'antin, J. Fernández-Engroba, V. Charoerook, A. Laromaine, A. Roig, R. Michael, *Biomater. Sci.* **2020**, *8*, 2921.
- [21] I. Anton-Sales, U. Beekmann, A. Laromaine, A. Roig, D. Kralisch, *Curr. Drug Targets* **2019**, *20*, 808.
- [22] I. Anton-Sales, S. Roig-Sanchez, M. J. Sánchez-Guisado, A. Laromaine, A. Roig, *ACS Biomater. Sci. Eng.* **2020**, *6*, 4893.
- [23] L. Bacakova, J. Pajorova, M. Bacakova, A. Skogberg, P. Kallio, K. Kolarova, V. Svorcik, *Nanomaterials* **2019**, *9*, 164.
- [24] L. Fu, J. Zhang, G. Yang, *Carbohydr. Polym.* **2013**, *92*, 1432.
- [25] P. Mendes, S. Rahal, O. Pereira-Junior, V. Fabris, S. Lenharo, J. De Lima-Neto, F. Da Cruz Landim-Alvarenga, *Acta Vet. Scand.* **2009**, *51*, 12.
- [26] I. F. Almeida, T. Pereira, N. H. C. S. Silva, F. P. Gomes, A. J. D. Silvestre, C. S. R. Freire, J. M. Sousa Lobo, P. C. Costa, *Eur. J. Pharm. Biopharm.* **2013**, *86*, 332.
- [27] S. I. Jeong, S. E. Lee, H. Yang, Y.-H. Jin, C.-S. Park, Y. S. Park, *Mol. Cell. Toxicol.* **2010**, *6*, 370.
- [28] G. Helenius, H. Bäckdahl, A. Bodin, U. Nannmark, P. Gatenholm, B. Risberg, *J. Biomed. Mater. Res., Part A* **2006**, *76A*, 431.
- [29] U. Beekmann, L. Schmözl, S. Lorkowski, O. Wertz, J. Thamm, D. Fischer, D. Kralisch, *Carbohydr. Polym.* **2019**, *236*, 116062.
- [30] D. Kralisch, N. Hessler, D. Klemm, R. Erdmann, W. Schmidt, *Biotechnol. Bioeng.* **2010**, *105*, 740.
- [31] D. Klemm, E. D. Cranston, D. Fischer, M. Gama, S. A. Kedzior, D. Kralisch, F. Kramer, T. Kondo, T. Lindström, S. Nietzsche, K. Petzold-Welcke, F. Rauchfuß, *Mater. Today* **2018**, *21*, 720.
- [32] F. V. Ferreira, C. G. Otoni, K. J. De France, H. S. Barud, L. M. F. Lona, E. D. Cranston, O. J. Rojas, *Materials Today* **2020**, *37*, 126.
- [33] C.-N. Wu, S.-C. Fuh, S.-P. Lin, Y.-Y. Lin, H.-Y. Chen, J.-M. Liu, K.-C. Cheng, *Biomacromolecules* **2018**, *19*, 544.
- [34] S. Moritz, C. Wiegand, F. Wesarg, N. Hessler, F. A. Müller, D. Kralisch, U.-C. Hippler, D. Fischer, *Int. J. Pharm.* **2014**, *471*, 45.
- [35] F. Robotti, I. Sterner, S. Botton, J. M. Monné Rodríguez, G. Pellegrini, T. Schmidt, V. Falk, D. Poulikakos, A. Ferrari, C. Starck, *Biomaterials* **2020**, *229*, 119583.
- [36] Y. K. Noh, A. Dos Santos Da Costa, Y. S. Park, P. Du, I.-H. Kim, K. Park, *Carbohydr. Polym.* **2019**, *219*, 210.
- [37] C. Fey, J. Betz, C. Rosenbaum, D. Kralisch, M. Vielreicher, O. Friedrich, M. Metzger, D. Zdzienko, *Mater. Sci. Eng., C* **2020**, *109*, 110613.
- [38] S. Gonçalves, J. Padrão, I. P. Rodrigues, J. P. Silva, V. Sencadas, S. Lancerso-Mendez, H. Girão, F. Dourado, L. R. Rodrigues, *Biomacromolecules* **2015**, *16*, 1341.
- [39] S. Gonçalves, I. P. Rodrigues, J. Padrão, J. P. Silva, V. Sencadas, S. Lancerso-Mendez, H. Girão, F. M. Gama, F. Dourado, L. R. Rodrigues, *Colloids Surf., B* **2016**, *139*, 1.
- [40] S. Taokaew, M. Phisalaphong, B.-M. Z. Newby, *Cellulose* **2015**, *22*, 2311.
- [41] F. K. Andrade, S. M. G. Moreira, L. Domingues, F. M. P. Gama, *J. Biomed. Mater. Res., Part A* **2010**, *92A*, 9.
- [42] R. Pêtille, S. Moreira, F. Andrade, L. Domingues, M. Gama, *Biotechnol. Prog.* **2012**, *28*, 526.
- [43] S. Roig-Sanchez, E. Jungstedt, I. Anton-Sales, D. C. Malaspina, J. Faraud, L. A. Berglund, A. Laromaine, A. Roig, *Nanoscale Horiz.* **2019**, *4*, 634.
- [44] L. Koivusalo, J. Karvonen, E. Sorsa, I. Jönkkäri, J. Väliaho, P. Kallio, T. Ilmarinen, S. Miettinen, H. Skottman, M. Kellomäki, *Mater. Sci. Eng., C* **2018**, *85*, 68.
- [45] A. Sorkio, L. Koch, L. Koivusalo, A. Deiwick, S. Miettinen, B. Chichkov, H. Skottman, *Biomaterials* **2018**, *171*, 57.
- [46] U. Schlötzer-Schrehardt, F. E. Kruse, *Exp. Eye Res.* **2005**, *81*, 247.
- [47] C. Zhang, J. Cao, S. Zhao, H. Luo, Z. Yang, M. Gama, Q. Zhang, D. Su, Y. Wan, *Cellulose* **2020**, *27*, 2775.
- [48] T. Tronser, A. Laromaine, A. Roig, P. A. Levkin, *ACS Appl. Mater. Interfaces* **2018**, *10*, 16260.
- [49] M. Vielreicher, D. Kralisch, S. Völkl, F. Sternal, A. Arkudas, O. Friedrich, *Sci. Rep.* **2018**, *8*, 9401.
- [50] A. Laromaine, T. Tronser, I. Pini, S. Parets, P. A. Levkin, A. Roig, *Soft Matter* **2018**, *14*, 3955.
- [51] K.-Y. Li, H.-A. Pan, K.-H. Chen, T.-L. Kuo, C.-H. Chou, Y.-J. Liang, F.-H. Lin, *ACS Biomater. Sci. Eng.* **2020**, *6*, 2570.
- [52] R. A. N. Pertile, F. K. Andrade, C. Alves, M. Gama, *Carbohydr. Polym.* **2010**, *82*, 692.
- [53] N. Eswaramoorthy, D. R. McKenzie, *Biophys Rev.* **2017**, *9*, 895.
- [54] J. J. Yoon, *World J. Stem Cells* **2014**, *6*, 391.
- [55] G. Pellegrini, C. E. Traverso, A. T. Franzini, M. Zingirian, R. Cancedda, M. De Luca, *Lancet* **1997**, *349*, 990.
- [56] G. Pellegrini, P. Rama, S. Matuska, A. Lambiase, S. Bonini, A. Pocobelli, R. G. Colabelli, L. Spadea, R. Fasciani, E. Balestrazzi, P. Vinciguerra, P. Rosetta, A. Tortori, M. Nardi, G. Gabbriellini, C. E. Traverso, C. Macaluso, L. Losi, A. Percesepe, B. Venturi, F. Corradini, A. Panaras, A. Di Rocco, P. Guatelli, M. De Luca, *Regener. Med.* **2013**, *8*, 553.
- [57] I. Massie, H. J. Levis, J. T. Daniels, *Exp. Eye Res.* **2014**, *127*, 196.
- [58] N. Mitrousis, A. Fokina, M. S. Shoichet, *Nat. Rev. Mater.* **2018**, *3*, 441.
- [59] S. Masterton, M. Ahearne, *Exp. Eye Res.* **2018**, *177*, 122.
- [60] N. Geisel, J. Clasohm, X. Shi, L. Lamboni, J. Yang, K. Mattern, G. Yang, K.-H. Schäfer, M. Saumer, *Small* **2016**, *12*, 5407.
- [61] E. Y. X. Loh, N. Mohamad, M. B. Fauzi, M. H. Ng, S. F. Ng, M. C. I. Mohd Amin, *Sci. Rep.* **2018**, *8*, 2875.
- [62] S. Matthyssen, B. Van Den Bogerd, S. N. Dhubbhghail, C. Koppen, N. Zakaria, *Acta Biomater.* **2018**, *69*, 31.
- [63] P. Rama, S. Bonini, A. Lambiase, O. Golisano, P. Paterna, M. De Luca, G. Pellegrini, *Transplantation* **2001**, *72*, 1478.
- [64] P. Fagerholm, N. S. Lagali, J. A. Ong, K. Merrett, W. B. Jackson, J. W. Polarek, E. J. Suuronen, Y. Liu, I. Brunette, M. Griffith, *Biomaterials* **2014**, *35*, 2420.
- [65] I. R. Schwab, *Arch. Ophthalmol.* **2006**, *124*, 1734.
- [66] N. Nieto-Nicolau, E. M. Martínez-Conesa, A. M. Velasco-García, C. Aloy-Reverte, A. Vilarrodona, R. P. Casaroli-Marano, *Stem Cell Res. Ther.* **2019**, *10*, 374.
- [67] T. Nakamura, L. P. K. Ang, H. Rigby, E. Sekiyama, T. Inatomi, C. Sotozono, N. J. Fullwood, S. Kinoshita, *Invest. Ophthalmol. Visual Sci.* **2006**, *47*, 909.
- [68] L. Koivusalo, M. Kauppi, S. Samanta, V. S. Parihar, T. Ilmarinen, S. Miettinen, O. P. Oommen, H. Skottman, *Biomaterials* **2019**, *225*, 119516.
- [69] M. Cimino, R. M. Gonçalves, C. C. Barrias, M. C. L. Martins, *Stem Cells Int.* **2017**, *2017*, 1.
- [70] Z. Chen, J. You, X. Liu, S. Cooper, C. Hodge, G. Sutton, J. M. Crook, G. G. Wallace, *Biomed. Mater.* **2018**, *13*, 032002.

Cite this: *Biomater. Sci.*, 2020, **8**, 2921

Bacterial nanocellulose as a corneal bandage material: a comparison with amniotic membrane†

Irene Anton-Sales,^a Justin Christopher D'Antin,^{b,c} Jorge Fernández-Engroba,^{b,c} Victor Charoenrook,^{b,c} Anna Laromaine,^{b,*a} Anna Roig^{b,*a} and Ralph Michael^{b,c}

Corneal trauma and ulcerations are leading causes of corneal blindness around the world. These lesions require attentive medical monitoring since improper healing or infection has serious consequences in vision and quality of life. Amniotic membrane grafts represent the common solution to treat severe corneal wounds. However, amniotic membrane's availability remains limited by the dependency on donor tissues, its high price and short shelf life. Consequently, there is an active quest for biomaterials to treat injured corneal tissues. Nanocellulose synthesized by bacteria (BNC) is an emergent biopolymer with vast clinical potential for skin tissue regeneration. BNC also exhibits appealing characteristics to act as an alternative corneal bandage such as; high liquid holding capacity, biocompatibility, flexibility, natural – but animal free–origin and a myriad of functionalization opportunities. Here, we present an initial study aiming at testing the suitability of BNC as corneal bandage regarding preclinical requirements and using amniotic membrane as a benchmark. Bacterial nanocellulose exhibits higher mechanical resistance to sutures and slightly longer stability under *in vitro* and *ex vivo* simulated physiological conditions than amniotic membrane. Additionally, bacterial nanocellulose offers good conformability to the shape of the eye globe and easy manipulation in medical settings. These excellent attributes accompanied by the facts that bacterial nanocellulose is stable at room temperature for long periods, can be heat-sterilized and is easy to produce, reinforce the potential of bacterial nanocellulose as a more accessible ocular surface bandage.

Received 15th January 2020,
Accepted 3rd April 2020

DOI: 10.1039/d0bm00083c

rsc.li/biomaterials-science

Introduction

Ocular surface disorders, especially those affecting the cornea, can severely disturb vision and quality of life. Yearly, there are approximately 1.5 million worldwide cases of corneal trauma, burns and infectious ulcerations.^{1,2} Conjunctival flap operations have long been performed in these cases,^{3–5} but due to its poor post-operative visual and cosmetic results, during the last decades, human amniotic membrane (AM) patches^{6–8} have been preferred because of their well-known regenerative effects.⁹ The AM has a layered structure with two well differentiated sides: an epithelial side made of cuboidal cells and a spongy stromal side constituted mainly of collagen fibres¹⁰ which is typically placed in contact with the corneal damage. AM also offers a tectonic pillar for corneal perforations and

can be indicated as a temporary treatment prior to a reconstructive technique.¹¹ Despite its satisfactory clinical outcomes,^{12,13} AM sometimes degrades faster than the required healing time,¹⁴ it is extremely costly and it has a short shelf life. Other drawbacks of AM concern its availability, which depends on donors and the presence of tissue banks and medical infrastructure. Therefore, novel biomaterials able to overcome these limitations are currently being investigated.^{15–17}

Bacterial nanocellulose (BNC) is a polysaccharide naturally secreted by several non-pathogenic bacterial strains that has gained a lot of attention for biomedical applications.^{18,19} BNC can easily be produced from *Komagataeibacter xylinus* (*K. xylinus*) cultures as stable water-insoluble hydrogels at the interface between the air and the liquid culture medium. After appropriate cleaning, BNC hydrogels are free of endotoxins and ultra-pure, containing just nanocellulose fibres organized in a similar structure as collagen.²⁰ Furthermore, BNC exhibits a high liquid holding capacity, porosity and conformability together with numerous functionalization opportunities due to its high surface area. All these unique characteristics promote the many valuable applications of BNC as a biomaterial. In fact, BNC has successfully been used for skin tissue

^aInstitute of Materials Science of Barcelona (ICMAB-CSIC), Spain.

E-mail: alaromaine@icmab.es, anna.roig@csic.es

^bInstitut Universitari Barraquer, Universitat Autònoma de Barcelona, Barcelona, Spain^cCentro de Oftalmología Barraquer, Barcelona, Spain

†Electronic supplementary information (ESI) available. See DOI: 10.1039/d0bm00083c



regeneration^{21–23} and products like Epicite^{hydro} (JenaCell) are already available on the market. Similarly, a BNC-based coating for implantable devices (Hylomate Pouch²⁴) is in the final stages of validation as an anti-fibrotic agent. Other studies highlight the potential of BNC as substrate for *in vitro* models²⁵ and as a drug delivery matrix.^{26,27}

Despite these promising reports, the capability of BNC to heal other body surfaces such as the cornea or the dura mater²⁸ remain largely unexploited.²⁹ Therefore, based on the outstanding performance of BNC on skin wound healing, we hypothesize that BNC also holds potential as an ocular surface bandage. In contrast to AM, BNC is stable at room temperature for long periods of time and its production from diverse carbon sources is sustainable and controllable in terms of size, shape and thickness.³⁰ Finally, yet importantly, BNC can be easily sterilized by heat and its animal-free origin might reduce the risk of disease transmission, ethical concerns and dependency on donor tissues. BNC's light transmittance is around 70% due to light scattering caused by fibre bundles and pores.³¹ Since this might limit its applicability as a long-term corneal substitute, we focused on a temporal application of BNC similar to that of AM.³²

Here, we validate BNC as suitable base material to develop novel corneal bandages. A detailed comparison between physicochemical characteristics of AM and BNC is provided and then, we demonstrate BNC's mechanical resistance to suture and stability under physiological conditions. Finally, we show preliminary *ex vivo* assays with porcine corneas. Together our results endorse BNC as a strong candidate for future corneal bandaging applications.

Results

Material characterization

Despite the extensive use of AM in ophthalmology, not much has been reported about its micro/nanostructure and material characteristics. Consequently, prior to the stability tests, the main characteristics of BNC and AM were compared. Scanning electron microscopy (SEM) was employed to study the micro and nanostructures of the ocular surface bandages. SEM imaging (Fig. 1A) of AM revealed a distinct micro and nanostructure of its two sides. The stromal side, which is generally placed in contact to the corneal surface, exhibits a nanofibrillar structure that highly resembles the BNC's architecture. The mean fibre diameter measured from the SEM images was 57 ± 9 nm for the collagen fibres in AM and 56 ± 13 nm for BNC nanofibres (average value from both sides of BNC). The epithelial side of AM is more unorganized and fibres were not observed. BNC presented a rather similar structure at both sides. However, the top side oriented towards the air during the biosynthesis process shows higher compaction of the fibres than the side facing the liquid bacterial culture (Fig. 1A).

BNC hydrogels were investigated as-synthesized, containing high amounts of water (≈ 100 times its own dry weight). A dehydration test revealed that BNC hydrogels exposed to the air under controlled temperature (22 °C) and humidity (45%) still maintain two thirds of their initial water content after 6 hours (see ESI Fig. S1†). AM membranes were also used as-received from the tissue bank. Thicknesses measured with a micrometer were between 600 and 900 μm for BNC, while AM pieces were much thinner (between 50 and 110 μm). These

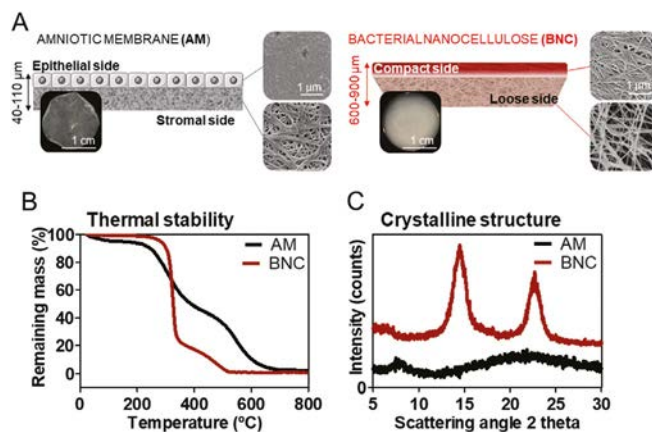


Fig. 1 Materials characterization. (A) Micro and nano structure of the bandage materials tested. Each material presents two differentiated sides, which are illustrated schematically and with SEM micrographs. The stromal side of AM and the compact side of BNC were the ones facing the ocular tissues in the experiments detailed below. (B) Representative TGA curves of BNC and AM ($n = 3$ for each material). Remaining mass of BNC is $0.7 \pm 0.1\%$ and AM is $1.7 \pm 0.8\%$. (C) X-ray diffraction patterns of the ocular surface bandages where BNC shows two broad diffraction peaks while AM appears as an amorphous material.



thickness measurements can be slightly affected by the blotting performed prior to the measurement to remove the excess water of the films and therefore the superficial mass parameter was monitored instead of the thickness on the onward experiments. BNC superficial mass computed was almost 8 times higher than AM (90 vs. 12 mg cm^{-2}).

Regarding optical properties, both materials exhibit low visible light absorbance (<1 absorbance from 800 to 400 nm) displaying a progressive increase in light absorbance towards the ultraviolet range. Interestingly, despite the marked difference in thickness, the overall ultraviolet-visible light absorbance was not proportionally higher in BNC. As an example, light absorbance for BNC was 0.38 at 600 nm and 0.29 for AM.

The thermal stability of the materials was assessed by thermo-gravimetric analysis (TGA) (Fig. 1B). The onset of degradation was defined by the position of the peaks from the first derivative function of the TGA curves and happened at $\approx 325 \text{ }^\circ\text{C}$ for BNC and at $\approx 250 \text{ }^\circ\text{C}$ for AM. Both materials decomposed almost completely (BNC total degradation happened at approx. $500 \text{ }^\circ\text{C}$ and AM at approx. $650 \text{ }^\circ\text{C}$) and show residual masses of $0.7 \pm 0.1\%$ for BNC and $1.7 \pm 0.8\%$ for AM ($n = 3$). This result indicates that both materials are almost entirely constituted by organic matter as expected.

To gain insight into the atomic organization of BNC and AM, their X-Ray diffraction (XRD) patterns were compared (Fig. 1C). BNC is a semi-crystalline material that presents two characteristic broad diffraction peaks (at $2\theta = 14.6$ and 22.8) as well as some amorphous background.³³ Contrarily, AM does not show any clear diffraction pattern, indicating an amorphous structure.

Suture stress test

An important specification of an ocular surface bandage material is to enable an easy and durable suturing to the eye surface. Since AM is commonly sutured in ophthalmological procedures, it was used as a benchmark for comparison. BNC has been satisfactorily sutured *in vivo*³⁴ but, to the best of our knowledge, not to the ocular tissues and its resistance to suture has never been quantified. A set up was assembled similar to the one reported in ref. 35 and illustrated in Fig. 2A. BNC and AM samples were sutured to small pieces of scleral tissues and clamped. Weights were added until BNC and AM materials teared at the suture point as shown in Fig. 2B. BNC films held an average force of $0.47 \pm 0.11 \text{ N}$ while AM resistance was much lower ($0.11 \pm 0.02 \text{ N}$). Some of the BNC pieces tolerated higher loads and caused the suture thread to break before BNC (filled dots on the graphs in Fig. 2B). Statistical analysis (unpaired *T*-test) revealed a significant difference between the two maximum forces supported by the compared materials.

Stability under simulated physiological conditions

Another requisite to consider a material for ocular bandaging applications is its durability and stability under the eye's physiological conditions. To gain insight on BNC's bio-stability we performed *in vitro* and *ex vivo* tests. For these tests, native BNC

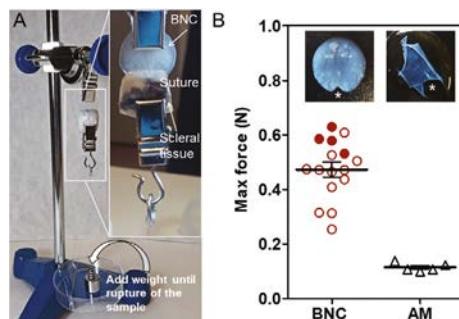


Fig. 2 Suture stress resistance test. (A) Set up of the device for the suture stress resistance test. The insert image shows a BNC sample sutured to a piece of scleral tissue. Same procedure was employed to evaluate AM. (B) Force (N) that caused the breakage of the materials. Filled circles indicate that BNC tolerated a higher weight than the suture thread. That is to say, the complex collapsed because the suture broke before the BNC. *P*-Value (unpaired *T*-test): <0.0001 . Max forces were normalized for the maximum thickness sample of each group ($986 \mu\text{m}$ for BNC and $63 \mu\text{m}$ for AM). Images inside the graph show the fracture of the material (indicated with asterisk) at the suture point.

hydrogels were used since dry films have a paper-like appearance that showed poorer conformability to the dome shape of the eye globes. For the *in vitro* study, BNC and AM were maintained in corneal preservation medium to monitor its potential degradation. The integrity of the samples was inferred by measuring their superficial mass and by visual observation. No indications of degradation were noticed for any of the two materials as depicted in Fig. 3. The materials did not show any substantial change in diameter or thickness (see slit lamp pictures). In addition, no disintegration features or holes were observed in any of the samples. Visually, AM samples became more opaque after the 30-day incubation while BNC samples maintained their transparency but acquired some shading from the culture medium. These visual observations were confirmed by measuring the grey values of the dark field images taken for each sample before and after incubation (dark field pictures are shown in Fig. S2†). The grey values of AM samples considerably increased upon incubation (from 77 ± 7 to 162 ± 7) while similar grey values for BNC were conserved after the incubation period (79 ± 18 prior to incubation and 73 ± 17 after incubation). As for the UV-VIS absorbance, AM did not present any substantial change whereas incubated BNC showed a small rise in absorbance at 600 nm compared to untreated BNC (from 0.38 to 0.41) (Fig. 4A). The material's superficial mass was also characterized after the corneal medium incubation test (Fig. 4B). BNC samples reduced its superficial mass near 12% (from 90 to 79 mg cm^{-2}) while AM samples decreased 33% its superficial mass (from 12 to 8 mg cm^{-2}). This change of the superficial mass was statistically significant (paired *T*-test, *p*-value < 0.0001) only for the AM specimens.



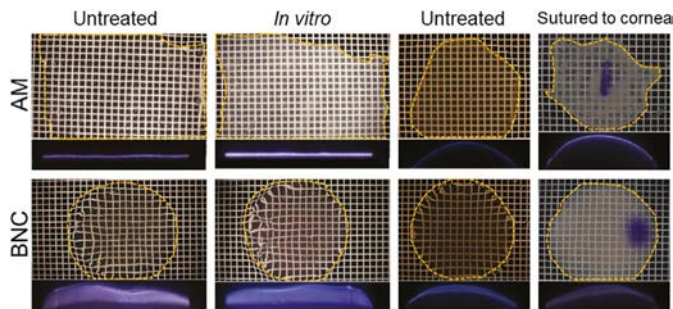


Fig. 3 Frontal (white filed + grid) and slit lamp images of AM and BNC before and after the stability tests. White field photographs were taken with a grid to better visualize transparency of the materials. Each square of the grid is one mm^2 . Inserts at the bottom of the images correspond to lateral views of the materials captured with a slit lamp. In general, both materials were stable under the tested conditions and incubation times. To mark the orientation of the samples that were sutured to porcine corneas, a tissue marker was used. For clarity in the pictures, corneal bandages were delineated with a yellow-dotted-line.

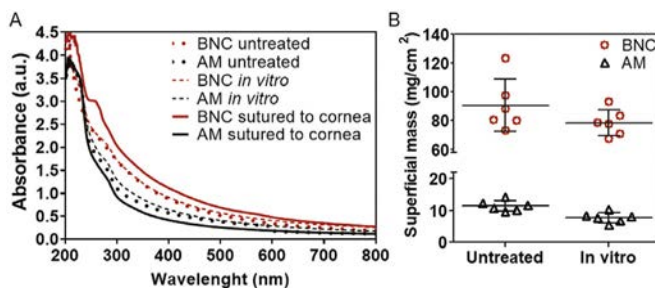


Fig. 4 Ultra violet-visible light absorbance of the materials and superficial mass. (A) Ultraviolet and visible light absorbance of BNC and AM materials at different experimental conditions. Average spectra were obtained from the mean of all the samples for each condition. As for samples sutured to porcine corneas, BNC increased its overall absorbance indicating some acquisition of the tissue/medium components. Oppositely, AM slightly decreases its absorbance, this might be due to a thinning of the material. (B) Changes in the superficial mass of the films upon 30-day maintenance *in vitro*. Superficial mass was compared to evaluate degradation and possible changes in thickness. Both materials experienced a reduction on its superficial mass: 12% for BNC and 33% for AM. This change in superficial mass was only statistically significant for AM (P -value < 0.0001, paired T -test) samples.

Finally, SEM investigation revealed that the characteristic nanofibrillar structure of both BNC and AM was retained during the 30-day experiment (Fig. 5, see untreated *vs.* *in vitro*) and that the epithelial side of AM presented some crystallizations after the *in vitro* incubation (ESI Fig. S3†). These elongated crystals, were undetectable by X-ray diffraction (data not shown) indicating that its contribution to the total amount of mass of the material should be rather small.

Conformability and adaptability of the materials to the arched shape of the cornea were evaluated by suturing BNC to porcine eyes. BNC films naturally present a flat side (with compact fibres) and a rougher side (loose fibres). After assessing the two possible orientations, the flat side was selected to

be in contact with the corneal surface since it showed better adaptability. Importantly, corneal surgeons from our clinic sutured BNC to the cornea of over a score of excised pig eyes and found it easy to handle. BNC maintained its original shape during the process without tearing at the puncture holes. Overall, the suturing of BNC was comparable to that of AM and the sutured BNC molded well to the dome-shaped cornea. See ESI Fig. S4† for more details about this process.

Excised porcine corneas were also used for a more realistic *ex vivo* evaluation of the materials under study. Sample preparation for BNC is illustrated in Fig. 6 and AM samples were arranged in a similar fashion. After the *ex vivo* culture, the materials were recovered for characterization. Overall, we did



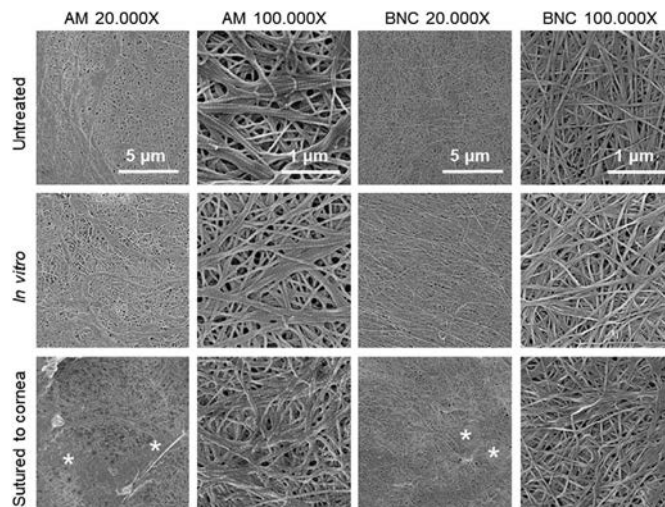


Fig. 5 Representative SEM images of the corneal bandage materials before and after the *in vitro* and *ex vivo* stability tests. The side of the material shown here is the one that was in contact with the eye surface, images from the external side are shown as ESI Fig. S3.† Under SEM, no signs of degradation were observed neither for BNC nor for AM samples after any of the two treatments. For the materials sutured to the corneas, both AM and BNC showed some organic deposits (marked with *) that might indicate some transfer of biological matter from the eye surface/culture medium to the ocular surface bandages.

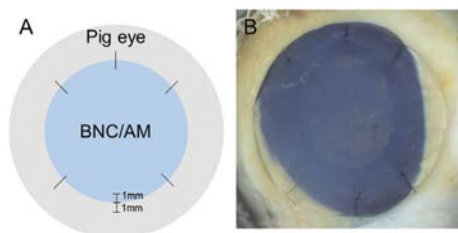


Fig. 6 *Ex vivo* suture test sample preparation. BNC hydrogels and AM were sutured to pig eyes as illustrated schematically in (A). The needle easily penetrated the BNC hydrogels and conventional knots were made with surgical instrumentation (B). Both materials adapted well to the dome shape of the eye without forming wrinkles. Then, the cornea and part of the sclera were excised and placed on Petri dishes containing RPMI medium for 20 days. Same sample preparation process was followed for AM.

Lateral images of the samples taken with a slit lamp showed a continuous layer of material both for AM and BNC after being sutured to the corneas (see third and fourth columns in Fig. 3) without detectable defects. Accordingly, SEM imaging revealed that the nanofibrillar structure of BNC and AM was maintained after their incubation (Fig. 5, see untreated vs. sutured to cornea) in contact with the biological material. Both BNC and AM presented some organic deposits on the side in contact with the corneal surface (indicated with asterisks in Fig. 5). The crystals that appeared on the *in vitro* experiment were not detected in these *ex vivo* conditions.

In comparison to untreated samples, BNC increased 26% its absorbance at 600 nm whereas AM samples displayed a reduction of 35% (see Fig. 4A). Moreover, BNC samples presented a new absorbance peak at 260 nm. It was not possible to accurately calculate the superficial mass of the samples after the *ex vivo* test since the suture caused deformation of the samples, especially of the AM membranes.

not detect major differences in the BNC samples before and after being sutured to the excised porcine corneas; all samples maintained their integrity (size and shape) and did not degrade (for better visualization refer to dark field images in ESI Fig. S2†). AM samples also maintained their overall integrity but presented tears at the suture points and some debilitated (*i.e.* more transparent and apparently fragile) areas.

Discussion

Although BNC possesses attractive intrinsic characteristics to become a new ocular surface bandage material,^{18,36} very few studies have explored this possibility. Here, we present a comparative study between BNC and the most common ocular surface bandage; AM. First, we provide an extensive character-



ization of BNC and AM and a comparison of their physico-chemical characteristics. Then, BNC is positively evaluated regarding: stability under simulated physiological conditions, resistance to the mechanical stress caused by suture, conformability to the eye surface and easiness of manipulation using standard clinical procedures. Compared to AM, BNC hydrogels resisted a higher force on the suture stress test, did not lose transparency after the *in vitro* test and where less deformed on the *ex vivo* assay.

The present study focused on the suitability of BNC as a new ocular surface bandage from a material point of view. Therefore, data regarding the ability of BNC to promote corneal wound healing is not provided yet. We speculate that BNC corneal bandages can have a protective effect similar to that of collagen corneal shields.^{37,38} Thus, feasible clinical usages of BNC would be as temporary tectonic or multi-layered bandages for patients suffering from non-infectious corneal ulcers, or ulcerative keratitis with high risk of corneal perforation. Applying a therapeutic contact lens on top of the BNC bandage could be needed, in the same way as when using AM in clinical practice. The contact lens would contribute to decrease friction with the inner surface of the eyelids as well as to maintain moisture by capturing the tears on its concave side.

Importantly, our latest data³⁹ shows that the amount of endotoxins detected in the eluates of autoclaved BNC are 0.05 ± 0.01 Endotoxin Units (EU) mL^{-1} . This value falls well below the Food and Drug Administration limit set at 0.5 EU mL^{-1} for medical devices and indicates that BNC can be considered a non-pyrogenic material. Regarding inflammatory responses, we expect native BNC to act as an inert biomaterial. That is, BNC hydrogels are expected to be neither pro nor anti-inflammatory as demonstrated in ref. 40 with *in vitro* tests. It has also been argued that BNC is well tolerated *in vivo* without causing major inflammatory complications.^{41,42} However, the interactions of BNC with the immune system will be addressed on our future investigations.

BNC is a mechanical and thermally stable material. These features are relevant for thermal sterilization (typically performed at 121 °C) and for adhering BNC to the ocular surface by suture stitches. AM decomposition takes place at rather high temperatures but its sterilization by heat might compromise its wound healing capabilities. BNC hydrogels used in this study were much thicker than AM, although the thickness of both materials varies considerable due to its biological origin.^{43,44} AM can be up to 200 μm and can be used as a multilayer, an approach that can also be envisioned for BNC. Notably, BNC's thickness can be modulated during the production process⁴⁵ and/or posteriorly by adjusting its water content³³ to meet specific requirements. Roughly, BNC hydrogels can be obtained with thicknesses ranging from hundreds of microns to few millimetres while dry BNC membranes exhibit thicknesses of tens of microns.

The Young modulus of BNC is also largely influenced by the water content and biosynthesis method, being in the range of 0.6 to 1.5 GPa^{33,46} in its dry state with considerably lower

values for the never dry form. Similarly, tensile strength is in the order of 50 MPa for dry BNC and between 1.5 and 2 MPa for the never dry form. Nevertheless, the BNC hydrogels present higher ductility with elongation at break values up to 20% which might be of interest for the application suggested here.⁴⁷ BNC presents a characteristic nanofibrillar structure with a great architectural similarity to that of collagen found in the stromal side of AM (see SEM images in Fig. 1). Despite the observed similar nanofibrillar organization, BNC and AM differ at the organization level, evidenced by the X-ray diffraction patterns, being AM non-crystalline and BNC a semi-crystalline material.

On the other hand, BNC's nanofibrillar network can act as a reservoir for diverse molecules.^{48,49} This capability might offer venues for future BNC corneal bandages supplemented with therapeutic agents in order to emulate the anti-scarring and anti-inflammatory effects that AM provides. In fact, the anti-inflammatory effect BNC hydrogels supplemented with diclofenac has recently been reported.⁴⁰ Similarly, in cases of bacterial keratitis, BNC could be impregnated with antibiotics to act as a medication reservoir. In this direction, BNC is also well known to support the culture of several cell types⁵⁰⁻⁵² including retinal pigment epithelial cells.^{20,53} These reports, together with the findings presented here, suggest further uses of BNC as a cell carrier for corneal cell therapies. In the case of a BNC bandage supplemented with sensitive biological material (cells or bioactive molecules), the cryo-storage approach commonly used for preserving AM⁵⁴ could also be considered since our recent data demonstrate that BNC is stable at liquid nitrogen temperatures.³⁹ Other interesting modifications of BNC aim at increasing its optical transparency. This can be achieved by mechanically increasing fibre alignment⁴⁶ or by filling the pores with biocompatible polymers such as polyethylene glycol.⁴⁰

Importantly, we validate that BNC can be sutured to the ocular surface without employing more time or resources than AM while presenting a higher resistance to the mechanical stress caused by the suture. Moreover, its soft and flexible nature confers optimal adaptability to the dome shape of the ocular surface. We also expect that the high liquid holding capacity of BNC hydrogels will be convenient to keep proper hydration of the ocular surface.

We examined the behaviour of BNC in two simulated physiological environments; *in vitro*, maintained in corneal preservation medium for 30 days, and *ex vivo*, sutured to excised pig corneas during 20 days without observing signs of degradation neither at the macro nor at the micro/nano scales. *In vitro*, BNC and AM kept its integrity but decreased its superficial mass; this reduction was higher in weight percentage for AM than for BNC. However, it is hard to discern if this shrinking in the superficial mass is due to material deterioration or to loss of water due to osmotic processes. Additionally, AM samples became more opaque after the incubation, possibly due to microcrystals deposits that increased light scattering. BNC hydrogels did not present crystals or opacification but BNC films were coloured by the culture medium and this



might be responsible of the slight increase of light absorbance.

Placing the materials in direct contact with ocular tissue on the *ex vivo* test allowed us to discard degradation of the BNC caused by the interaction with the tissue and to confirm its robustness after suturing. BNC nanofibrillar structure was also intact after the experiment. Contrary to BNC, AM samples were deformed and presented some tears at the suture points but kept its overall integrity. The UV-VIS light absorbance of AM was decreased after the treatment and some areas seemed to debilitate as observed on the grid images. This might be attributed to a thinning of the material that needs to be further confirmed. BNC behaved differently, its overall UV-VIS absorbance moderately increased presenting a new peak characteristic of nucleic acids and close to the protein absorbance region. This could be ascribed to the adsorption of biological material on the BNC coming either from the ocular tissues or the culture medium. This observation is also supported by the organic deposits visualized under SEM. Transference of tissue/medium components was also detected visually in the form of opaque areas and with SEM as organic accumulations in the AM samples. Overall, we consider BNC to be stable under the two tested conditions and times.

In summary, corneal damage is a highly prevalent cause of vision reduction and blindness, particularly in rural areas of developing countries. Therefore, there is an evident need for low-cost, accessible, durable and easy to apply ocular surface bandages.^{55,56} In the present study, we aimed to elucidate whether BNC, a biomaterial that shows great promise for skin regeneration, is also suitable as bandage material to treat ocular surface disorders. Using AM as a benchmark, we demonstrated that BNC meets basic preclinical requirements for this purpose. These findings, together with BNC's prolonged shelf life, straightforward and animal-free production and controllability might encourage further investigations of BNC for corneal regeneration.

Methods

The general experimental design of this study is summarized on ESI Table 1.†

Amniotic membrane

Human AM were obtained from the local tissue bank (Barcelona Banc de Sang i Teixits) and stored at $-80\text{ }^{\circ}\text{C}$ until experimental use. The samples were cut into the desired shapes and sizes using a 17 mm \varnothing trephine (circles) or surgical scissors (rectangles).

Production of the bacterial nanocellulose films

Bacterial nanocellulose films were obtained following our established protocol detailed elsewhere.⁵⁷ Briefly, a commercial *Komagataeibacter xylinus* (*K. xylinus*) strain (NCIMB 5346 from CECT, Valencia, Spain) was inoculated on 6 mL of Hestrin-Schramm (HS) medium (1.15 g citric acid, 6.8 g

$\text{Na}_2\text{HPO}_4 \cdot 12\text{H}_2\text{O}$, 5 g peptone, 5 g yeast, and 20 g dextrose for 1 L of Milli-Q water) and incubated statically for 7 days at $30\text{ }^{\circ}\text{C}$. This bacterial culture was further diluted 1:15 with fresh HS medium and cultured on 24-well plates (2 mL per well) during 3 days. The BNC pellicles that formed at the air-liquid interface were collected and immersed in a solution of 1:1 ethanol:deionized water (DI) to kill the bacteria. Then, the films were washed 1×40 minutes in boiling DI water and 2×20 minutes in a boiling 0.1 M NaOH solution to remove organic residues. After rinsing several times with DI water, the films were autoclaved ($121\text{ }^{\circ}\text{C}$, 20 min).

Endotoxin contamination study

The endotoxin extraction was carried out by placing clean and autoclaved BNC hydrogels in depyrogenated falcon tubes with 40 mL of endotoxin free water during 72 h at $30\text{ }^{\circ}\text{C}$ and under orbital agitation (100 rpm), according to FDA recommendations.⁵⁸ The endotoxin content in the eluates from BNC samples was measured with a Pierce™ LAL Chromogenic Endotoxin Quantification Kit purchased from Thermo Fisher and the assay was performed following the manufacture's instructions. The products of the reaction were read for absorbance at 405 nm in a microplate reader (Infinite 200 PRO, TECAN®) at $37\text{ }^{\circ}\text{C}$. The indicated values in the results section correspond to mean \pm standard deviation of two independent experiments obtained from two different endotoxin quantification kits and evaluating each time two samples from two different batches of BNC.

Dehydration test

Three independent BNC hydrogels (12 cm \times 12 cm) were left to dehydrate inside a room with controlled humidity (45%) and temperature ($22\text{ }^{\circ}\text{C}$). The materials were weighed every hour with a precision scale. The initial weight of the hydrogels was used to calculate the remaining weight (%) at different time points.

Thickness measurements

Thickness of the AM ($n = 12$) and BNC ($n = 20$) samples was measured with a digital micrometre, placing the samples between two cover slides to keep them flat. A slight blotting of the specimens was made with filter paper prior to the measurement to remove the excess of liquid. Five measures were made for each sample at different areas to get an average thickness.

Thermogravimetric analysis

To evaluate the thermal stability of the materials, a TGA-DSC/DTA analyser (NETZSCH STA 449 F1 Jupiter) was used. The covered temperature range was from 25 to $800\text{ }^{\circ}\text{C}$ and the heating rate was $10\text{ }^{\circ}\text{C}$ per minute in air. The first derivative graphs were obtained with the Origin 85 software. Three samples were analysed from each material.



X-Ray diffraction

Dry BNC and AM were fixed flat on a silicon wafer support to acquire X-ray diffraction patterns using a Siemens (Model D-5000) diffractometer. Step size was 0.02° per minute in a 2θ range from 5° to 30° . A Cu anode was employed. Smoothing of the data was performed with the Savitzky–Golay model included on the Origin 85 software.

Digital images

Digital images were taken with a Canon Eos 550C camera coupled to a microscope with the samples placed on a dark/white field chamber. For the white field images, a grid (squares of 1 mm^2) was located under the specimens to better visualize transparency of the materials. The photographs were acquired with a standardized exposure time of 1/100 s. Areas and grey values were measured from these images with the ImageJ-win64 software.

Scanning electron microscopy

Both BNC and AM samples were freeze dried at -80°C for 48 hours to preserve its native structure. Small pieces of the films were cut with scissors and immobilized on top of aluminium sample holder with a carbon tape. The samples were sputtered with 5 nm of platinum before being imaged with a high resolution scanning electron microscope Magellan 400L at the following magnifications: 5000X, 20 000X and 100 000X. The employed voltage was 2.00 kV and the current was 100 pA.

Ultraviolet visible spectroscopy

Ultraviolet-visible (UV-Vis) absorbance spectra of BNC and AM materials were obtained without any sample preparation step. A Varian Cary-5000 UV-Vis-NIR spectrophotometer on transmission mode was employed to obtain a minimum of two spectra (between 200 and 800 nm) from each sample. A baseline correction was performed by subtracting the absorbance of the glass coverslips used to hold the samples. The absorbance of the sample was calculated as: $A = \log_{10}(I_0/I)$ where I_0 corresponds to the intensity of the light passing through the reference cell (glass) and I to the intensity of the light passing through the sample cell (BNC or AM) at the same wavelength.

In vitro stability test

The *in vitro* stability test evaluated six independent samples of each material. Circular BNC films of $\approx 2\text{ cm}^2$ and AM rectangles of $\approx 3\text{ cm}^2$ were used. Every sample was weighed and photographed before the incubation. Each sample was placed individually on sterile glass bottles containing 100 mL of Tissue C (Alchimia) culture medium. The materials were clipped to a CornealFloat to keep them suspended in the liquid. The bottles were kept during 30 days in a CO_2 incubator (5%) at 37°C . Then, the materials were recovered and characterized for: weight, diameter, integrity, micro/nano structure (SEM) and light absorbance (UV-Vis).

Suture stretch test

To test the mechanical stability of the materials, the device illustrated in Fig. 2A was employed. BNC ($n = 16$) and AM ($n = 5$) samples were sutured (Suture type: Nylon 10/0, Lab Aragón) with a single stitch to small pieces of porcine scleral tissue ($\approx 1\text{ cm}^2$) using standard suture instruments from Grieshaber (Westcott scissors and Colibri forceps), a Barraquer needle holder and a Castroviejo Suture forceps. Then, the complex was clamped on the top part (clamp placed on the BNC/AM) and fixed to a support. Another clamp was placed at the scleral tissue (bottom) and a platform was hung from that clamp. 4.5 g weights were added gradually (every two minutes) to the platform until the BNC/AM broke at the suture point. The maximum weight tolerated by each sample before rupture was divided by the normalized thickness of the sample inside each type (BNC and AM). A value of 1 was assigned to the thickest BNC (986 μm) and AM (63 μm) specimens.

Ex vivo suture test

Eyes globes were obtained from 6 month old pigs and used within 48 h. BNC and AM films of $\approx 16\text{ mm}$ diameter were non-invasively characterized (weight and diameter) and then sutured to pig corneas keeping the limbal area intact. 6 symmetric sutures were made for each eye 1 mm away from the BNC/AM border and holding 1 mm of tissue with standard nylon suture 10/0 from Lab Aragón (Barcelona). The knots were not buried. The sutures penetrated $\approx \frac{2}{3}$ of the cornea/sclera thickness. The cornea and part of the sclera were resected from the rest of the eye with scleral scissors. Pictures were also taken at this point. The samples were decontaminated by immersion into a 5% Povidone-iodine (PI) solution during 2 minutes. Sodium thiosulphate (0.1%) was used to remove the PI and later the samples were rinsed with phosphate-buffered saline. Then, the excised corneas were placed in a closed container (Petri dish) with 13 mL of Roswell Park Memorial Institute (RPMI-1640) culture medium (R8758 Sigma-Aldrich) supplemented with 5% fetal bovine serum (F7524 Sigma-Aldrich) and 1% antibiotic-antimycotic (A5955 Sigma-Aldrich) under sterile conditions. The as-prepared Petri dishes were kept in an incubator at 37°C and 5% CO_2 for 20 days. Medium was changed every 3 to 4 days.

Statistical analysis

For the statistical analysis, GraphPad Prism 5 software was employed. Data is represented by mean \pm standard deviation. Statistical significance was accepted when p -values under 0.05 were obtained in paired (superficial mass) or unpaired (suture stress test) Student's T -tests.

Author contributions

I.A.S designed experiments, prepared and cultured samples, characterized the samples, acquired data, analysed data, interpreted data, prepared the figures, wrote the manuscript, revised the manuscript; J.C.D designed experiments, prepared



and cultured samples, acquired data, interpreted data, revised the manuscript; J. F. E. performed the sutures; provided clinical advice and revised the manuscript; V.C. provided literature, revised experiments, revised the manuscript A. L., A. R. and R. M. designed and supervised experiments, interpreted data, revised the manuscript and obtained funding.

Data availability

The data generated during and/or analysed during the current study are available from the corresponding author on reasonable request.

Conflicts of interest

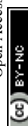
The author(s) declare no competing interests.

Acknowledgements

Authors acknowledge financial support from the Spanish Ministry of Science and Innovation through the RTI2018-096273-B-I00, project, the 'Severo Ochoa' Programme for Centers of Excellence in R&D (SEV-2015-0496) and the PhD scholarship of I. A. S. (BE-2017-076734) and the Generalitat de Catalunya with the 2017SGR765 and the 2019LLAV00046 projects. Authors also thank María Jesús Sánchez-Guisado for her assistance with the endotoxin study. The ICMAB technical services (TGA and X-Ray) and Marcos Rosado from the ICN2 electron microscopy service are acknowledged. The ICMAB members (IAS, AL, AR) participate in the CSIC Interdisciplinary Platform for Sustainable Plastics towards a Circular Economy, SUSPLAST and in the Aerogels COST ACTION (CA 18125). We acknowledge support of the publication fee by the CSIC Open Access Publication Support Initiative through its Unit of Information Resources for Research (URICI).

References

- 1 M. J. Burton, Corneal blindness: Prevention, treatment and rehabilitation, *Community Eye Health*, 2009, **22**, 33–35.
- 2 J. P. Whiteher, M. Srinivasan and M. P. Upadhyay, *Corneal blindness: a global perspective*, 2001.
- 3 T. P. H. Gundersen, Conjunctival flaps for corneal disease: their usefulness and complications, *Trans. Am. Ophthalmol. Soc.*, 1969, **67**, 78–95.
- 4 J. J. Arentsen, P. R. Laibson and E. J. Cohen, Management of corneal descemetocoeles and perforations, *Trans. Am. Ophthalmol. Soc.*, 1984, **82**, 92–105.
- 5 A. M. Alino, H. D. Perry, A. J. Kanellopoulos, E. D. Donnenfeld and E. K. Rahn, Conjunctival flaps, *Ophthalmology*, 1998, **105**, 1120–1123.
- 6 C. Y. Su and C. P. Lin, Combined use of an amniotic membrane and tissue adhesive in treating corneal perforation: a case report, *Ophthalmic Surg. Lasers*, 2000, **31**, 151–154.
- 7 H.-J. Chen, R. T. Pires and S. C. Tseng, Amniotic membrane transplantation for severe neurotrophic corneal ulcers, *Br. J. Ophthalmol.*, 2000, **84**, 826–833.
- 8 E. H. Yildiz, *et al.*, Amniotic Membrane Transplantation: Indications and Results, *Eur. J. Ophthalmol.*, 2008, **18**, 685–690.
- 9 D. Meller, *et al.*, Amniotic membrane transplantation for acute chemical or thermal burns, *Ophthalmology*, 2000, **107**, 980–989.
- 10 G. Bourne, THE FOETAL MEMBRANES A Review of the Anatomy of Normal Amnion and Chorion and Some Aspects of Their Function, *Postgrad. Med.*, 1962, **38**, 193–201.
- 11 A. Solomon, *et al.*, Amniotic membrane grafts for nontraumatic corneal perforations, descemetocoeles, and deep ulcers, *Ophthalmology*, 2002, **109**, 694–703.
- 12 A. Paolin, *et al.*, Amniotic membranes in ophthalmology: long term data on transplantation outcomes, *Cell Tissue Banking*, 2016, **17**, 51–58.
- 13 M. Kaup, C. Redbrake, N. Plange, K. Arend and A. Remky, Amniotic membrane transplantation in severe ocular surface disorders, *Eur. J. Ophthalmol.*, 2008, **18**, 691–694.
- 14 C. C. de Farias, N. Allemann and J.Á.P. Gomes, Randomized Trial Comparing Amniotic Membrane Transplantation with Lamellar Corneal Graft for the Treatment of Corneal Thinning, *Cornea*, 2016, **35**, 438–444.
- 15 S. Majumdar, *et al.*, Cyclodextrin Modulated Type I Collagen Self-Assembly to Engineer Biomimetic Cornea Implants, *Adv. Funct. Mater.*, 2018, **28**, 1804076.
- 16 A. Sorkio, *et al.*, Human stem cell based corneal tissue mimicking structures using laser-assisted 3D bioprinting and functional bioinks, *Biomaterials*, 2018, **171**, 57–71.
- 17 L. Koivusalo, *et al.*, Tissue adhesive hyaluronic acid hydrogels for sutureless stem cell delivery and regeneration of corneal epithelium and stroma, *Biomaterials*, 2019, **225**, 119516.
- 18 H. Ullah, F. Wahid, H. A. Santos and T. Khan, Advances in biomedical and pharmaceutical applications of functional bacterial cellulose-based nanocomposites, *Carbohydr. Polym.*, 2016, **150**, 330–352.
- 19 H. G. de Oliveira Barud, *et al.*, A multipurpose natural and renewable polymer in medical applications: Bacterial cellulose, *Carbohydr. Polym.*, 2016, **153**, 406–420.
- 20 S. Gonçalves, *et al.*, Bacterial Cellulose As a Support for the Growth of Retinal Pigment Epithelium, *Biomacromolecules*, 2015, **16**, 1341–1351.
- 21 W. Czaja, A. Krystynowicz, S. Bielecki and R. M. Brown, Microbial cellulose - The natural power to heal wounds, *Biomaterials*, 2006, **27**, 145–151.
- 22 M. H. Kwak, *et al.*, Bacterial cellulose membrane produced by *Acetobacter* sp. A10 for burn wound dressing applications, *Carbohydr. Polym.*, 2015, **122**, 387–398.
- 23 Y. Li, *et al.*, Evaluation of the Effect of the Structure of Bacterial Cellulose on Full Thickness Skin Wound Repair on a Microfluidic Chip, *Biomacromolecules*, 2015, **16**, 780–789.



- 24 F. Robotti, *et al.*, Microengineered biosynthesized cellulose as anti-fibrotic in vivo protection for cardiac implantable electronic devices, *Biomaterials*, 2020, **229**, 119583.
- 25 C. Fey, *et al.*, Bacterial nanocellulose as novel carrier for intestinal epithelial cells in drug delivery studies, *Mater. Sci. Eng., C*, 2020, **109**, 110613.
- 26 P. Weyell, *et al.*, Tailor-made material characteristics of bacterial cellulose for drug delivery applications in dentistry, *Carbohydr. Polym.*, 2019, **207**, 1–10.
- 27 L. Bacakova, *et al.*, Versatile Application of Nanocellulose: From Industry to Skin Tissue Engineering and Wound Healing, *Nanomaterials*, 2019, **9**, 164.
- 28 F. d. M. T. Lima, F. C. M. Pinto, B. L. d. S. Andrade-da-Costa, *et al.*, Biocompatible bacterial cellulose membrane in dural defect repair of rat, *J. Mater. Sci.: Mater. Med.*, 2017, **28**, 37.
- 29 I. Anton-Sales, U. Beekmann, A. Laromaine, A. Roig and D. Kralisch, Opportunities of Bacterial Cellulose to Treat Epithelial Tissues, *Curr. Drug Targets*, 2018, **20**, 808–822.
- 30 A. Laromaine, *et al.*, Free-standing three-dimensional hollow bacterial cellulose structures with controlled geometry via patterned superhydrophobic-hydrophilic surfaces, *Soft Matter*, 2018, **14**, 3955–3962.
- 31 D. Abol-Fotouh, *et al.*, Farming thermoelectric paper, *Energy Environ. Sci.*, 2019, **12**, 716–726.
- 32 A. Azuara-Blanco and D. H. Pillai CT, Amniotic membrane transplantation for ocular surface reconstruction, *Br. J. Ophthalmol.*, 1999, **83**, 399–402.
- 33 M. Zeng, A. Laromaine and A. Roig, Bacterial cellulose films: influence of bacterial strain and drying route on film properties, *Cellulose*, 2014, **21**, 4455–4469.
- 34 Y. Pei, *et al.*, Effectively promoting wound healing with cellulose/gelatin sponges constructed directly from a cellulose solution, *J. Mater. Chem. B*, 2015, **3**, 7518–7528.
- 35 F. Küng, D. W. Schubert, P. Staffej, F. E. Kruse and T. A. Fuchsluger, A novel suture retention test for scaffold strength characterization in ophthalmology, *Mater. Sci. Eng., C*, 2016, **69**, 941–946.
- 36 M. Jorfi and E. J. Foster, Recent advances in nanocellulose for biomedical applications, *J. Appl. Polym. Sci.*, 2015, **132**, 1–19.
- 37 J. V. Aquavella, M. del Cerro, P. S. Musco, S. Ueda and M. D. DePaolis, The effect of a collagen bandage lens on corneal wound healing: a preliminary report, *Ophthalmic Surg.*, 1987, **18**, 570–573.
- 38 C. E. Willoughby, M. Batterbury and S. B. Kaye, Collagen corneal shields, *Surv. Ophthalmol.*, 2002, **47**, 174–182.
- 39 I. Anton-Sales, S. Roig-Sánchez, M.-J. Sánchez-Guisado, A. Laromaine and A. Roig, *Bacterial Nanocellulose and Titania Hybrids: Cytocompatible and Cryopreservable Cell Carriers*, 2020, submitted.
- 40 U. Beekmann, *et al.*, Process control and scale-up of modified bacterial cellulose production for tailor-made anti-inflammatory drug delivery systems, *Carbohydr. Polym.*, 2020, **236**, 116062.
- 41 U. Osorio, *et al.*, Ex Vivo and In Vivo Biocompatibility Assessment (Blood and Tissue) of Three-Dimensional Bacterial Nanocellulose Biomaterials for Soft Tissue Implants, *Sci. Rep.*, 2019, **9**, 10553.
- 42 H. Martínez Ávila, *et al.*, Novel bilayer bacterial nanocellulose scaffold supports neocartilage formation in vitro and in vivo, *Biomaterials*, 2015, **44**, 122–133.
- 43 A. F. S. Costa, F. C. G. Almeida, G. M. Vinhas and L. A. Sarubbo, Production of Bacterial Cellulose by *Gluconacetobacter hansenii* Using Corn Steep Liquor As Nutrient Sources, *Front. Microbiol.*, 2017, **8**, 2027.
- 44 A. McGaughy, *et al.*, In Office Use of Amniotic Membrane, *Cornea*, 2015, 31–32.
- 45 W. Borzani and S. J. de Souza, Mechanism of the film thickness increasing during the bacterial production of cellulose on non-agitated liquid media, *Biotechnol. Lett.*, 1995, **17**, 1271–1272.
- 46 S. Wang, *et al.*, Transparent, Anisotropic Biofilm with Aligned Bacterial Cellulose Nanofibers, *Adv. Funct. Mater.*, 2018, **28**, 1707491.
- 47 Own data, not published.
- 48 S. Moritz, *et al.*, Active wound dressings based on bacterial nanocellulose as drug delivery system for octenidine, *Int. J. Pharm.*, 2014, **471**, 45–55.
- 49 G. F. Picheth, *et al.*, Lysozyme-triggered epidermal growth factor release from bacterial cellulose membranes controlled by smart nanostructured films, *J. Pharm. Sci.*, 2014, **103**, 3958–3965.
- 50 T. Tronser, A. Laromaine, A. Roig and P. A. Levkin, Bacterial Cellulose Promotes Long-Term Stemness of mESC, *ACS Appl. Mater. Interfaces*, 2018, **10**, 16260–16269.
- 51 S. Taokaew, M. Phisalaphong and B.-M. Z. Newby, Modification of Bacterial Cellulose with Organosilanes to Improve Attachment and Spreading of Human Fibroblasts, *Cellulose*, 2015, **22**, 2311–2324.
- 52 A. Bodin, *et al.*, Tissue-engineered conduit using urine-derived stem cells seeded bacterial cellulose polymer in urinary reconstruction and diversion, *Biomaterials*, 2010, **31**, 8889–8901.
- 53 S. Gonçalves, *et al.*, Acetylated bacterial cellulose coated with urinary bladder matrix as a substrate for retinal pigment epithelium, *Colloids Surf., B*, 2016, **139**, 1–9.
- 54 K. Jirsava and G. L. A. Jones, Amniotic membrane in ophthalmology: properties, preparation, storage and indications for grafting—a review, *Cell Tissue Banking*, 2017, **18**, 193–204.
- 55 E. Shirzaei Sani, *et al.*, Sutureless repair of corneal injuries using naturally derived bioadhesive hydrogels, *Sci. Adv.*, 2019, **5**, 1281.
- 56 M. M. Islam, *et al.*, Biomaterials-enabled cornea regeneration in patients at high risk for rejection of donor tissue transplantation, *npj Regen. Med.*, 2018, **3**, DOI: 10.1038/s41536-017-0038-8.
- 57 S. Roig-Sanchez, *et al.*, Nanocellulose films with multiple functional nanoparticles in confined spatial distribution, *Nanoscale Horiz.*, 2019, **4**, 634–641.
- 58 U.S. Department of Health and Human Services, *et al.* *Guidance for Industry Pyrogen and Endotoxins Testing: Questions and Answers*, 2012.





Cite this: DOI: 10.1039/d1bm00025j

In vivo soft tissue reinforcement with bacterial nanocellulose†

 Irene Anton-Sales,  ‡^a Soledad Roig-Sanchez,  ‡^a Kamelia Traeger,  ^b
Christine Weis,  *^b Anna Laromaine,  ^a Pau Turon  ^b and Anna Roig  *^a

The use of surgical meshes to reinforce damaged internal soft tissues has been instrumental for successful hernia surgery; a highly prevalent condition affecting yearly more than 20 million patients worldwide. Intraperitoneal adhesions between meshes and viscera are one of the most threatening complications, often implying reoperation or side effects such as chronic pain and bowel perforation. Despite recent advances in the optimization of mesh porous structure, incorporation of anti-adherent coatings or new approaches in the mesh fixation systems, clinicians and manufacturers are still pursuing an optimal material to improve the clinical outcomes at a cost-effective ratio. Here, bacterial nanocellulose (BNC), a bio-based polymer, is evaluated as a soft tissue reinforcement material regarding mechanical properties and *in vivo* anti-adhesive performance. A double-layer BNC laminate proved sufficient to meet the standards of mechanical resistance for abdominal hernia reinforcement meshes. BNC-polypropylene (BNC-PP) composites incorporating a commercial mesh have also been prepared. The *in vivo* study of implanted BNC patches in a rabbit model demonstrated excellent anti-adherent characteristics of this natural nanofibrous polymer 21-days after implantation and the animals were asymptomatic after the surgery. BNC emerges as a novel and versatile hernioplasty biomaterial with outstanding mechanical and anti-adherent characteristics.

 Received 7th January 2021,
Accepted 23rd February 2021
DOI: 10.1039/d1bm00025j

rsc.li/biomaterials-science

1. Introduction

Abdominal hernias occur when internal organs protrude through weakened zones of the abdominal cavity. To date, surgical intervention is the only effective approach to repair such a highly prevalent condition that yearly affects more than 20 million patients worldwide.¹ Instrumental for successful hernia surgery has been the use of surgical meshes (*i.e.* hernioplasty) to reinforce the damaged region. Those implants are predominantly manufactured from synthetic polymers, mainly polypropylene (PP), and aim at providing mechanical support to the herniated area. Implantation of a non-resorbable PP-mesh has become the standard procedure for hernia repair, however, complications related to mesh implantation such as seroma, adhesions, chronic severe pain and infections are driving constant innovation in the field.^{2,3}

Adhesions developed between PP-mesh and viscera, as a result of tissue reaction due to foreign body implant, are particularly threatening since they often cause complicated reoperations in the previously implanted area, increasing the surgical risk and the chances of suffering side effects such as chronic pain and bowel perforation.⁴ High rates of adhesion are reported in approx. 15% of the cases one year after surgery, resulting in a high burden to healthcare systems.⁵ Aiming to reduce the complications caused by those intraperitoneal adhesions, research efforts have been focused on improving the characteristics of PP meshes. Strategies include the optimization of mesh porous structure,⁶ incorporation of anti-adherent coatings and improvements of mesh fixation systems (*i.e.* glueing).^{7,8} Besides, multi-component grafts have been advocated as a well-suited strategy to isolate the PP mesh from the viscera by adding an additional layer of a synthetic^{9,10} or natural biomaterial^{11,12} that acts as an anti-adherent barrier. Despite recent advances, clinicians and manufacturers are still pursuing an optimal mesh to improve the clinical outcome and the cost-effectiveness ratio of hernioplasty procedures by leveraging the selection of materials, porous structure, mechanical resistance, anti-adhesive properties, biocompatibility, long term mechanical stability, tissue integration and conformability.¹³

Considering the requirements of hernia repair implants, the bio-based polymer bacterial nanocellulose (BNC) could be

^aInstitute of Materials Science of Barcelona (ICMAB-CSIC), Campus UAB, 08193 Bellaterra, Catalonia, Spain. E-mail: anna.roig@csic.es

^bDepartment of Research and Development, B. Braun Surgical, S.A.U., Carretera de Terrassa 121, Rubí, 08191 Barcelona, Spain. E-mail: christine.weis@bbraun.com

† Electronic supplementary information (ESI) available. See DOI: 10.1039/d1bm00025j

‡ Authors with equal contribution



deemed as a strong candidate for the above-mentioned tissue reinforcement application.¹⁴ BNC is biotechnologically produced as a highly pure, non-soluble nanocellulose fibrillary network entrapping a large amount of liquid and exhibiting excellent mechanical properties.^{15–17} These attributes have enabled an ever-increasing number of bio-applications in wound dressing and drug delivery.^{18–20} Moreover, BNC is emerging as a high-performing alternative to repair other defects where non-biodegradable implants are desirable, such as damage of the dura mater,²¹ the eardrum²² or as an anti-fibrotic agent for cardiac implants.²³ As for soft tissue reinforcement, a hybrid biomaterial combining BNC with PP-meshes and its *in vitro* low adhesion properties has recently been described.²⁴ Besides, Zharikov and co-workers compared the anti-adhesive behaviour of BNC with PP meshes revealing a lower occurrence of adhesion in BNC-implanted dogs together with the absence of infections.²⁵ For that study, wet native BNC pellicles were employed and no mechanical tests were carried out. In more recent work, Rauchfuß *et al.* tested two surgical methods to implant wet BNC into the abdominal wall of rats.²⁶ These authors observed adhesion formation when using BNC as an abdominal wall replacement together with a tissue reaction assessed to be of low clinical significance. Interestingly, this work provides mechanical testing of BNC after explantation showing variable values and calling for future work on the suitability of BNC for hernia repair in terms of mechanical properties. These studies, although preliminary, concur with the absence of major postoperative complications and emphasize the underexploited potential of BNC in herniology.

Our work aims at providing further insight into the prospects of BNC for hernia repair surgery. To expand on the mechanical suitability of BNC for soft tissue reinforcement, the mechanical performance of several types of BNC implants –dry and wet forms as well as single to triple-layered BNC constructs– are evaluated. Furthermore, an *in vivo* study based on a novel animal model (rabbit) and the implantation of dry BNC is presented to demonstrate the anti-adherent properties of BNC.

2. Materials and methods

2.1 Bacterial nanocellulose (BNC) production

BNC films were obtained as previously described in Roig-Sanchez *S. et al.*²⁷ In brief, *Komagataeibacter xylinus* (*K. xylinus*) strain (NCIMB 5346, from CECT, Spain) was inoculated on 6 mL of Hestrin-Schramm (HS) fresh medium and expanded for 7 days at 30 °C. HS medium was prepared as follows: 5 g peptone, 5 g yeast, 20 g dextrose (Conda Lab), 1.15 g citric acid and 6.8 g Na₂HPO₄·12H₂O (Sigma-Aldrich) per 1 L of Milli-Q (MQ) water. Then, 0.5 mL of the mixture was transferred to 4.5 mL of fresh HS medium and let to proliferate for another three days. Finally, bacteria were diluted to a proportion 1:14 inoculum:HS medium and 65 mL were cultivated for 6 days in 12 × 12 cm plates (Labbox polystyrene Petri

dishes) at 30 °C. The square BNC pellicles formed at the liquid-air interface of the wells were harvested and cleaned 10 minutes in a 50% ethanol-water solution, twice with boiling water for 20 min and twice with 0.1 M NaOH (Sigma-Aldrich) at 90 °C for 20 min. Lastly, the films were washed with MQ water until neutralization and sterilized by autoclave (121 °C, 20 min). To obtain the dry and flat BNC films used in the mechanical and *in vivo* tests, BNC hydrogels were placed between two Teflon papers at 60 °C and with a 2 kg weight on top for 12 h as previously described.²⁷ Systems with two and three BNC layers were prepared by drying size-matched BNC pellicles in close contact following the same procedure. To achieve a smooth interface between the BNC films, the superficial water was removed by blotting BNC with filter paper and air bubble formation was avoided by applying manual pressure. BNC-PP composites were prepared similarly by placing fragments of PP meshes (Optilene® Mesh Elastic and Optilene® Mesh LP both from B. Braun Surgical, S.A.U., Spain), knitted with different pore sizes, in between two wet BNC films. The size of the BNC layers was larger than the PP meshes to allow the self-adhesion between BNC films to occur during drying.

2.2 Scanning electron microscopy (SEM)

For the SEM characterization of the native wet BNC structure, BNC hydrogels were supercritically dried (SC). For that, the as-obtained BNC films were placed within filter paper sheets and were subjected to a water-to-ethanol solvent exchange process. After two transfers of 3 h in absolute ethanol, the films were moved to a fresh ethanol bath, kept overnight and the resulting alcogel was dried by SC drying. SC drying was performed on a 300 mL capacity autoclave filled with ethanol which was pressurized to 100 bar at room temperature. Liquid CO₂ was dispensed for 1.5 h with a flow of 1 kg h⁻¹ to exchange the solvent. Then, the reactor was heated up to 45 °C to reach supercritical conditions and supercritical CO₂ was pumped for 1 h keeping the same flow rate. Finally, the vessel was slowly depressurized to avoid pore collapse and BNC aerogels were obtained. For the SEM analysis of dry films, BNC hydrogels were dried as described in section 2.1.

FEI Magellan 400L XHR SEM under a high vacuum, with an acceleration voltage of 2 kV, current of 0.10 nA and a working distance of 5 mm was used to study the morphology of SC dried and dry BNC. The material was fixed with adhesive carbon tape on top of aluminium SEM holders. Dry BNC was sputtered with 5 nm Pt. BNC fibre diameter was calculated as the mean of 100 measurements obtained using Image-J software.

Cross-section images of multi-layered constructs were obtained with FEI Quanta 650GEG-ESEM under low vacuum conditions, an acceleration voltage of 20 kV, an electron beam spot of 4–5 and a working distance of 10 mm. Samples were cut with a PTFE coated blade (Personna GEM single edge, 3-facet stainless steel, 0.23 mm) and placed on holders with a 90° tilt.



2.3 Mechanical studies

Each BNC sheet was cut in 20 × 50 mm pieces and the weight, size and thickness were measured with an Acculab Atilon ATL-244-1 analytical balance, Stanley Millesimal rule and Mitutoyo 543-250B micrometer respectively. Results were computed from five replicas. Surface weight was calculated as the ratio between weight and area. Wet BNC samples were deposited on a filter paper to remove the excess of water and measurements were performed when the material was still wet. The thickness of the films was measured in the middle of the specimens. For wet samples, the plunger of the micrometer was lifted and lowered three times and the thickness was obtained when the value was stable for more than 2 s during the third time.

Zwick Z2.5 dynamometer with a load cell of 2.5 kN was used for tensile experiments. The clamps were metallic with a pneumatic flat rubber part in contact with the sample. The test velocity was 100 mm min⁻¹, the pressure of the clamps was 6 bars and the distance between them was 20 mm. The preload applied was 0.05 N. Strain and resistance to tearing (F_{max}) values were acquired.

Multi-layered systems were immersed in a 0.9% NaCl solution for 5 min for rehydration before the tensile study. Excess of liquid was removed as described before and water uptake (H_2O_{up}) percentage was calculated as $(m_w - m_d)/m_d \times 100$, where m_w is the weight of the wet sample after hydration and m_d is the weight of the dry sample before hydration. Surface weight, calculated as the ratio between dry weight and area, and thickness were obtained before the rehydration.

2.4 *In vivo* study

A scheme of the steps to BNC implantation is depicted in Fig. 4A. This study was conducted by FREY-TOX GmbH (Herzberg, Germany), a DAkkS (national accreditation body of Germany) accredited laboratory according to EN ISO/IEC 17025 and European guidelines 93/42/EWG as well as 90/385/EWG.

2.4.1. BNC implant preparation. Dry BNC patches were cut to a size of 7 × 3 cm with scissors and sterilized by a routine ethylene oxide (EtOx) cycle from B. Braun Surgical S.A.U. to sterilise non-absorbable meshes. Sterility was confirmed by submerging the EtOx-treated BNC into liquid culture medium for 14 days without detecting the appearance of turbidity. The resistance of the biomaterial to the EtOx cycle was assessed by Fourier-Transform Infrared Spectroscopy (FTIR) (Fig. S1†).

2.4.2. *In vivo* model. The *in vivo* implantation study was performed in five female SPF albino rabbits of the stock New Zealand White (Envigo, 58" Venray Netherlands). The animals had a bodyweight from 3.4 to 4.2 kg. An acclimatization period of at least 5 days was allowed. General anaesthesia was induced by intramuscular injection of 35–40 mg kg⁻¹ ketamine and 5–6 mg kg⁻¹ xylazine (Serumwerke Bernburg AG, Bernburg, Germany). This rabbit species was chosen because of its convenient body proportion and proved suitability for studying hernia repair materials including meshes.²⁸

In the literature, it is described that most post-surgical adhesion formation takes place approximately until day 8 post-

implantation.²⁹ Hence, the follow-up time was set at 21-days based on our previous work endorsing it as a sufficient period to observe mature adhesions in an advanced healing process as well as to infer the integration of the biomaterial within the abdominal wall.³⁰

2.4.3 Surgical procedure. The operation field was shaved, disinfected and the abdomen was covered in a sterile manner. A median laparotomy was performed and the patches were carefully applied onto the left native abdominal wall between the peritoneum and the visceral organs, avoiding folding of the implants. Subsequently, the BNC patches were fixed by 6 suture stitches with polypropylene (Optilene, B. Braun Surgical, S.A.U., USP 3-0) sutures. The wound was closed with a continuous muscle suture and continuous intracutaneous sutures. The skin was glued with Histoacryl®, a cyanoacrylate-based tissue glue (B. Braun Surgical, S.A.U., Spain). After the follow-up time of 21 days, the rabbits were anaesthetized (Ketamine 40 mg per kg body weight and Xylazine 6 mg per kg body weight) and subsequently euthanized (T61 intravenously).

Once the animals were sacrificed, tissue integration and adhesion formation were macroscopically examined. During explantation, the application site, as well as the abdomen *in toto*, were macroscopically evaluated. Possibly occurring adhesions were evaluated after dissection regarding their area extension in relation (%) to the total abdominal wall area implanted (7 × 3 cm). Furthermore, adhesions were defined to the following categories following the Zühlke scores as follows:³¹

Score I: String adhesions that are easy to separate (blunt detachment).

Score II: Adhesions being partially vascularized causing blunt to sharp detachment.

Score III: Adhesions having distinct vascularization, with sharp detachment only.

Score IV: Tight adhesions requiring sharp detachment causing damage to the organs.

The tissue integration was judged descriptively: no integration; mild integration = slight pull for uplifting the patch from the abdominal wall; and distinct integration = distinct pull uplifting from the abdominal wall with visible adhesion and vascularization.

2.5. Histological analysis

The central area of the implant (size approximately 1 × 3 cm) was extirpated and fixed on 4% buffered formalin for histological examination. Tissue sections were cut with a microtome and processed following standard procedures.³² Haematoxylin/eosin (HE) was used as a general staining for judgment of tissue integration.

2.6 Statistical analysis

Quantitative data were analysed with GraphPad Prism 8.0.2 software using ordinary one-way ANOVA followed by Tukey's multiple comparison test. Statistical significance was accepted



at 0.05 and data are represented as means \pm standard deviation.

3. Results

3.1 Single layered BNC patches

Firstly, single-layer BNC patches intended for hernioplasty applications were produced and characterized in terms of their macroscopic features, thickness and mechanical properties. Fig. 1A displays the simultaneous production of seventy-two 12×12 cm-BNC films summing up >1 m² of the biomaterial as a venue to attain increased amounts of BNC at a laboratory level. After 6 days at 30 °C, continuous BNC pellicles formed at the surface of the liquid culture (Fig. 1B). Upon cleaning and removing organic residues, a change in colour (from yellowish to translucent white) was appreciated (Fig. 1C).

Macro and microstructure of BNC in wet and dry conditions are depicted in Fig. 1(C, D) and (E, F) respectively. Since the morphology of wet as-synthesized BNC samples could not be observed with enough resolution using SEM, a supercritical (SC) dried film was used as this drying method maintains with high-reliability the architecture of native samples.³³ As exposed in Fig. 1D, SC-dried BNC films are highly porous and composed of entangled cellulose nanofibers of 15 ± 5 nm in diameter. Upon drying at 60 °C, BNC films become more transparent and thinner while the fibres compact and the porosity decreases (see inset in Fig. 1F).

High tensile stress is a basic demand for a biomaterial proposed for soft tissue reinforcement applications. Tensile stress ≥ 16 N cm⁻¹ has been used as a benchmark for safe reinforcement of the abdominal wall.³⁴ Accordingly, tensile strength experiments were conducted to test the mechanical properties of BNC films using this value as a threshold. Fig. 2 shows the mean values obtained from five BNC samples in dry (pink) and wet (blue) conditions. Before mechanical characterization, the original BNC films (12×12 cm) were cut in 20×50 mm samples and their thickness and surface weight (weight per area) were measured in both wet and dry forms. The surface weight is approximately 60 times higher for wet films than for its dried counterparts (654 ± 153 g m⁻² wet film; 11 ± 1 g m⁻² dry film). Upon drying, 98% of the surface weight is lost as the water is removed, indicating that cellulose nanofibers account for only 2% of the wet BNC mass. These results are in agreement with the thickness measurement as BNC films experience a decrease in thickness of more than 96% when dehydrated (from 445 ± 91 μ m wet film; to 16 ± 8 μ m dry film). For the mechanical characterization, the 20×50 mm BNC pieces were clamped with metallic clips containing a pneumatic flat rubber part to prevent the sliding of the samples (see the image in Fig. 2). The resistance to tear (F_{max}) of wet BNC is approximately 60% that of dry BNC (5 ± 1 N cm⁻¹ and 8 ± 3 N cm⁻¹ respectively). On the contrary, the maximum strain increases 12-fold in wet conditions ($24 \pm 2\%$ in comparison to $2.1 \pm 0.5\%$ for dry BNC). These data indicate that our single-layer BNC films (neither in wet nor in the dry state) do not meet the minimum mechanical resistance requirements of 16 N cm⁻¹ to be used as a PP mesh substitute.

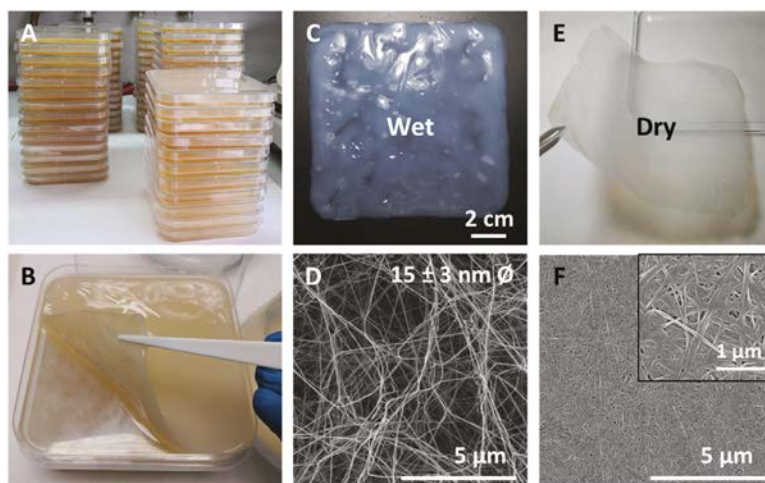


Fig. 1 BNC synthesis, wet and dry states and microstructure. (A) Numbering up BNC production at laboratory level. (B) A native wet BNC pellicle. (C) Wet form of BNC after cleaning and autoclaving. (D) SEM image of an SC dried BNC sample mimicking the microstructure of a wet BNC film. (E) Dry BNC film. (F) SEM image of the compact nanofiber conformation for dry BNC. Inset: higher magnification to better visualize the nanofibers arrangement.



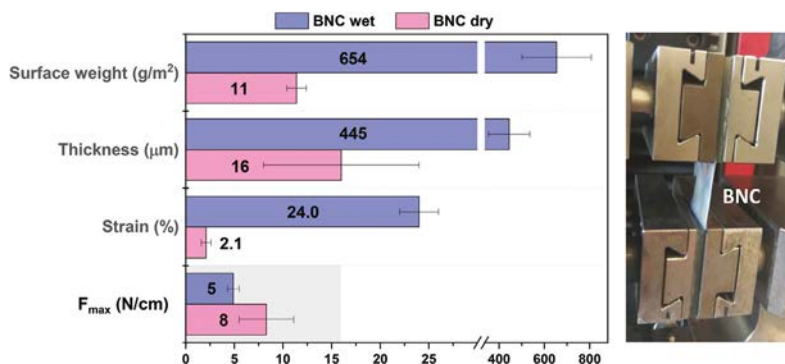


Fig. 2 Mechanical properties of single-layer BNC patches in wet and dry conditions and the experimental setup. Single-layered BNC implants did not meet the acceptance criteria of tensile stress resistance set at $F_{\max} = 16 \text{ N cm}^{-1}$ (grey area). Statistically significant differences between dry and wet BNC samples were found for all the studied parameters except for the F_{\max} (P -values < 0.001) ($n = 5$).

3.2 Laminated BNC patches and hybrids

To increase the mechanical resistance of the BNC patches, two strategies were followed: (i) preparation of multi-layered BNC meshes and (ii) combination of BNC with standard PP meshes. Our previous work showed that robust BNC stacks that endure hard manipulation even upon rehydration can be created by pilling up and drying together (*i.e.* applying weight) several wet BNC films. Upon drying, hydrogen bonding between the fibres of two films confers stability to the stack. The multilayers do not suffer delamination even when immersed in a liquid solution.²⁷ Accordingly, laminated patches were created by assembling 2 or 3 wet BNC films and subjected to the same mechanical characterization as the single BNC layers. Fig. 3A depicts the results of 2 and 3 layers of BNC (mean values of $n = 5$). All the obtained values were substantially higher than those of a single layer. As expected, thickness and surface weight increased as more layers were added. More precisely, thickness raised from $16 \pm 8 \mu\text{m}$ (1 layer) to $23 \pm 2 \mu\text{m}$ (2 layers) and $34 \pm 6 \mu\text{m}$ (3 layers); and surface weight from $11 \pm 1 \text{ g m}^{-2}$ (1 layer) to $20 \pm 1 \text{ g m}^{-2}$ (2 layers) and $28 \pm 2 \text{ g m}^{-2}$ (3 layers). The multilayers were then rehydrated in a 0.9% NaCl solution for 5 min before performing mechanical studies to better simulate the physiological conditions. As shown in Fig. 3A, the laminate BNC presents a maximum strain of 14 ± 1 and $12 \pm 3\%$ and resistance to tearing of 26 ± 6 and $32 \pm 9 \text{ N cm}^{-1}$ for 2 and 3 layers respectively. For the double-layered BNC, the maximum strain increased almost 7-fold compared to a single BNC layer (dry form) while, the resistance to tear increased more than 3-fold. As expected, the triple-layer renders an even higher improvement in mechanical resistance (4-fold compared to a dry single layer). Note that the values of both the double and triple-layer laminates are above the set threshold of 16 N cm^{-1} for abdominal wall reinforcement applications. Improvements

in mechanical properties (both the % of strain and the max force tolerated) of the stacked-BNC are statistically significant (P -values < 0.001) when compared to the BNC single-layer. Remarkably, during the tensile test, no peeling or separation of the layers was observed. This feature is also exemplified in Fig. 3B where a bi-layered sturdy BNC patch is shown. Both images –the macrostructure image and the cross-section SEM picture (inset)– illustrate the homogeneous adhesion between two BNC films. Moreover, the original transparency was maintained without macroscopic air bubbles trapped in the interface and the boundary area between the two BNC films could not be identified by SEM. Fig. S2† gathers the values obtained for the mechanical properties of all the studied systems for a clearer comparison.

Finally, BNC hybrid constructs incorporating commercial PP meshes were considered. Fig. 3C shows frontal and lateral pictures of a preliminary prototype of a sandwich-like multi-layer composite. The construct was prepared by taking advantage of the above-mentioned self-adhesion property of BNC. Note that the BNC-PP composite firmly incorporates PP meshes with different pore sizes. The thickness of the dry composites varied depending on the incorporated PP material between the BNC layers. That is, for a PP mesh with small pores (named SP-PP) a thickness of $332 \pm 8 \mu\text{m}$ was obtained, while when a PP mesh with bigger pores was employed (BP-PP) thickness increased up to $589 \pm 23 \mu\text{m}$. An SEM cross-section study (Fig. 3D) showed good integration of the BP-PP mesh in between the BNC layers. Although the synthetic material did not adhere to the BNC layers, it was immobilized in an envelop-like structure due to the BNC self-adhesion in the contact areas in between the pores of the PP mesh and at the composite's contour (inset Fig. 3D). The stability of the hybrid structure was tested by rehydration in water. After 5 days, the moist envelope-like structure was flexible and easily handled without noticeable delamination as depicted in Fig. S3.†



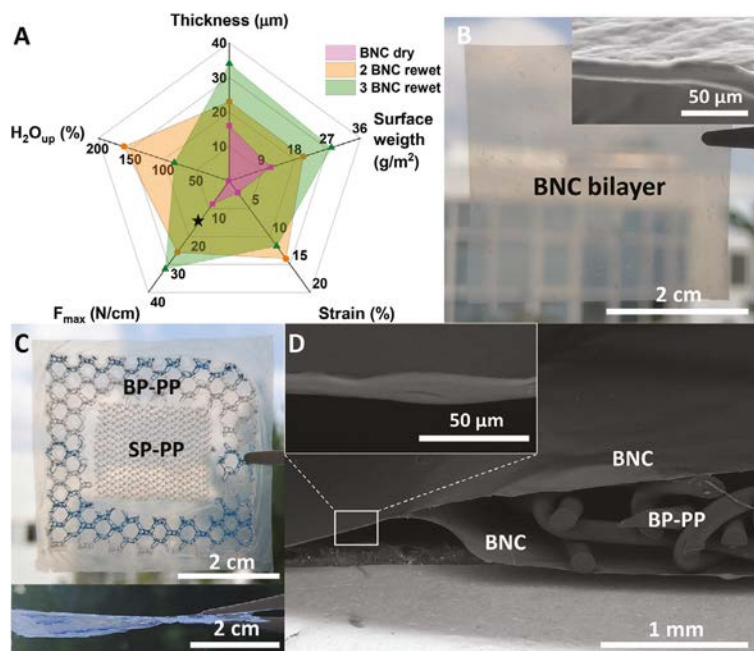


Fig. 3 Composite alternatives to increase the mechanical resistance of BNC-based implants. (A) Mechanical study of BNC multilayers comprised of 2 or 3 films. ($n = 5$) \star indicates the resistance to tear threshold for tissue reinforcement materials (16 N cm^{-3}). (B) Picture of a BNC multilayer formed by 2 dry BNC films. Inset: SEM cross-section image where the interface between the two BNC layers is undetectable. (C) Preliminary BNC bilayer combination with PP meshes with different pore sizes. Upper panel: frontal view. Lower panel: a lateral image of the BNC-PP mesh composite. (D) SEM cross-section image of the BNC-PP composite. Inset: higher magnification of the cross-section to appreciate the continuous adhesion between BNC layers.

3.3 *In vivo* studies

Besides mechanical validation, a key characteristic required from soft tissue repair materials is their proficiency in minimizing adhesion-related complications and integration by surrounding tissues. Therefore, the next step was to assess the anti-adhesion properties of BNC with an *in vivo* rabbit model following the implantation process shown in Fig. 4A.

3.3.1 Macroscopic evaluation. Dry and sterile single layer BNC patches of $3 \times 7 \text{ cm}$ were selected for the *in vivo* study as being the ones with weaker mechanical characteristics and imposing the most stringent conditions. Single-layer BNC patches could be easily handled under operation-room settings, fold-free placing was readily achieved and fixation by suture was performed without complications (Fig. 4B). The semi-transparency of BNC was also convenient to avoid unintentional puncturing of blood vessels while suturing. During the application of the BNC patch, careful handling was necessary, nonetheless, the BNC patch allowed the secure application on the abdominal wall; no fracturing of the suture puncture

holes was observed and the BNC patches were removable with instruments and repositioned if needed. During the postoperative phase, all animals presented swift recovery. Analgesic treatment was only administered in the first postoperative days and a slight body weight gain was detected.

After the implantation period of 21 days, tissue integration was evaluated using observational criteria during the autopsy. The BNC patches displayed a general good integration to the abdominal wall whereas only marginal areas were not integrated. Adhesion level was examined and scored macroscopically considering prevalence (quantity) and type (quality) of the detected adhesions among BNC implants and the internal organs. In 4/5 animals adhesions were detected involving approximately 8% of the overall BNC surface. Although some fibrin accumulation and distinct vascularization were observed in all animals, only one rabbit presented a significant adhesion area (20%) as depicted in Fig. 4D. Three animals presented adhesions to the greater omentum and one animal to the cecum. Notably, one animal was completely free of adhesions (Fig. 4C). The implanted BNC patches were dominated



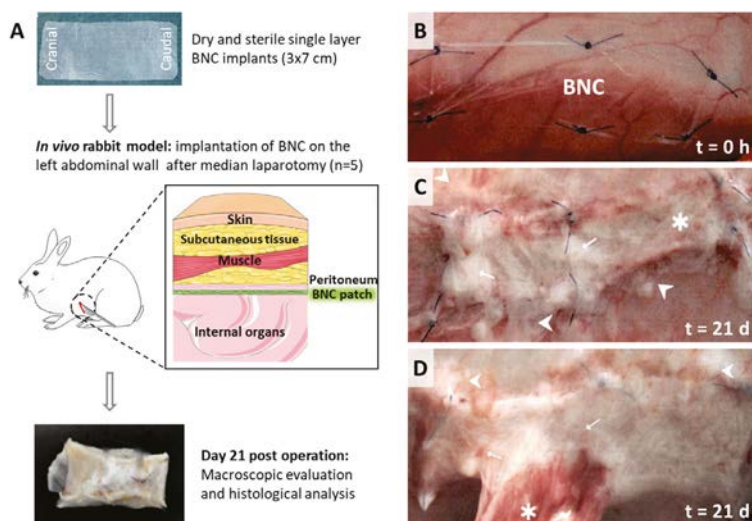


Fig. 4 Experimental design, macroscopic evaluation and adhesion assessment for two of the five animals studied. (A) Sketch showing the prepared BNC implant, the employed *in vivo* model and the evaluations performed. (B) Time 0: BNC patches were applied onto the left abdominal wall and fixed with six suture stitches (C) A2 explanted analysis after 21 days (best case scenario). → indicates fibrin accumulation, ► adjacent abdominal wall without adhesions and * marks vascularization. (D) A4 explanted analysis after 21 days (worst case scenario). → indicates vascularization, ► fibrin accumulations and * corresponds to adhesion.

by only one visible layer of fibrin. These macroscopic observations are gathered in Fig. S4† and Tables 1 and 2.

3.3.2. Histological evaluation. The central area of the implant (size $\sim 1 \times 3$ cm) was extirpated and used for histological examinations. Representative HE-stained tissue sections from the five studied animals are shown in Fig. 5. The area surrounding the BNC patches presented a severe diffuse to granulomatous immune cell infiltration involving lymphocytes, heterophilic granulocytes, macrophages and solitary

multinucleated giant cells. Also, a moderate active fibroplasia on the implanted zone was noted, as well as a good integration onto the abdominal wall and moderate neovascularization.

4. Discussion

We have investigated BNC patches for soft tissue reinforcement applications by dealing with two clinically relevant para-

Table 1 Individual adhesion observations. Results of the area free of adhesions, adhesion area, adhesion score and tissue integration for each studied animal

Animal number Code	6501 A1	6507 A2	6527 A3	6564 A4	6574 A5
Area free of adhesions approx.	95%	100%	95%	80%	90%
Adhesion area approx.	5% to greater omentum	0%	5% to greater omentum	20% to greater omentum	10% to cecum
Adhesion score (Zühlke scores)	II – blunt to sharp detachment	No adhesions	II – blunt to sharp detachment	IV – sharp detachment	IV – sharp detachment
Tissue integration	Mild integration	Distinct integration	Distinct integration	Mild integration	Mild integration

Table 2 Overall adhesion observations. Summary of the macroscopic evaluation of adhesions between BNC implants and internal organs

No. of animals affected by adhesions	Area (%) free of adhesions	Adhesions area (%)	Organs involved in adhesion processes
4/5	92	8	Greater omentum (3 animals) Cecum (1 animal)



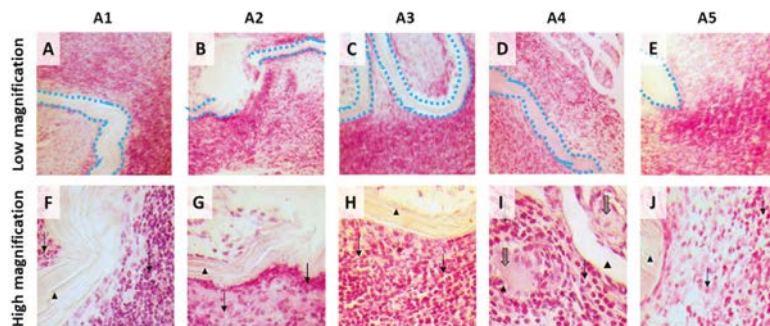


Fig. 5 HE-stained tissue sections of the BNC-implanted abdominal walls. A–E: Low magnification images of the five operated rabbits where the BNC implants have been highlighted with a blue dotted line to facilitate interpretation. For all cases, a good integration of the BNC patch together with an inflammatory reaction can be observed. F–J: Zoom-in to better appreciate the BNC implant (►) and the presence of diverse inflammatory cells (lymphocytes, heterophilic granulocytes and macrophages) surrounding the implant (→). Solitary multinucleated giant cells were observed on A4 (I) (⇒).

meters; the mechanical resistance of constructs comprising one to three BNC layers and the *in vivo* anti-adherence properties of BNC. Before that, we characterized the BNC patches and present an increased BNC production (up to $\sim 1 \text{ m}^2$) under laboratory settings to illustrate the feasibility of an up-scaled fabrication. However, to achieve an industrial manufacturing process, a more advanced system should be implemented such as the pilot-scale production processes reported by Kralisch *et al.*³⁵ and Beekmann *et al.*³⁶

The mechanical characterization of as-synthesized BNC films (wet films) and after drying showed that wet BNC patches are thicker, more brittle but more stretchable than dry BNC patches. This confers to the wet-BNC a higher strain but, at the same time, makes the material less resistant to tear. After drying, the water content of BNC decreases drastically and the cellulose nanofibers condense, reducing their porosity¹⁵ and their ability to rearrange upon tensile stress application. Thus, the dried form of BNC is stiffer and less stretchable than wet-BNC, making it more suitable for hernioplasty. Although the here studied single-layered BNC did not fulfil the mechanical resistance requirements to be used as a PP mesh substitute, thicker single layer BNC films grown for longer periods (>6 days) are expected to present sufficient mechanical support. We have previously reported that BNC fibres condense upon drying and form strong bonds among the cellulose nanofibers, this characteristic allowed us to arrange robust BNC multilayer laminates consisting of 2 or 3 layers.²⁴ The mechanical studies of those rehydrated BNC laminates have shown that the resistance to tear can be easily improved beyond the required 16 N cm^{-1} threshold for abdominal wall reinforcement applications. Even though previous studies confirmed the stability of BNC films in physiological conditions for up to 30 days,³⁷ the mechanical results of the laminates presented here were obtained after a 5 min-immersion in a saline solution and therefore, we cannot discard that the

mechanical properties of the films could be affected by longer hydration times.

Seeking to expand the library of BNC-based configurations for hernia repair patches, a composite patch integrating both BNC films and PP meshes was fabricated. This preliminary proof-of-concept demonstrates the possibility to, not only tune the mechanical properties of BNC but also to combine BNC films and PP meshes with different pore sizes. The sandwich-like BNC-PP structure was easy to prepare and exhibited robustness and good manageability both in dry and rehydrated conditions. This hybrid material shows the potential of BNC in the development of on-demand hybrid biomaterials for reinforcement of the abdominal wall but still requires further validation. The durability of the BNC-PP composites under physiological conditions is unknown at the moment and the need for additional strengthening of the composite (*i.e.* glueing with a cyanoacrylate-based biocompatible adhesive) could be considered in the future.³⁸

We have recently validated BNC in diverse biological scenarios providing data on its cytocompatibility, lack of endotoxins (0.04 ± 0.01 Endotoxin Units per mL) after its biosynthesis as well as suturability and manageability in preclinical settings.^{37,39} These findings, combined with the appealing mechanical properties reported here, positioned BNC as a suitable candidate for soft tissue repair patches and therefore *in vivo* studies were conducted. The anti-adhesion behaviour, biocompatibility and tissue integration characteristics of the BNC patches have been evaluated with a pilot animal study. BNC presented favourable surgical properties for this specific application in terms of suturability, manageability and accommodation to the implantation site. Moreover, the semi-transparent character of BNC was beneficial to avoid unintentional puncturing of underlying tissues. A general fold-free integration of the BNC material to the abdominal wall was detected in all the rabbits. Regarding adhesions between BNC



patches and internal organs, the overall area of the 5 implanted patches free of adhesions in this study is about 92%. Only a few adhesions were found after BNC implantation in the rabbit model, mostly involving the greater omentum which can be assessed as almost physiological since this organ is typically active in any post-surgical process. We hypothesize that the nanofibrillar microstructure of BNC, similar to that of the collagen networks on the extracellular matrix, favours the non-adherent characteristics of the BNC implants in accordance with the anti-fibrotic effect reported for cardiac implants wrapped with BNC.²⁰ The macroscopic evaluation showed that only a few adhesion strands were detected (overall at about 8% of the implant area) originated mainly on the suture stitches and at the border of the patches. For this pilot test, the BNC patches were fixed with sutures, even though sutures can cause foreign body responses and adhesions; indicating that suture-free administration methods could be worth exploring to diminish the adhesions even more. Overall, the macroscopic observation showed that good biocompatibility can be assumed for the BNC patches *in vivo* and the results indicate that BNC patches might act as a sufficient barrier to prevent adhesions in this rabbit sidewall model. Systemic tolerability of BNC can also be supposed from the good post-operative recovery of the test animals that occurred without notable complications.

On the histological analysis, all BNC implants appeared to be well integrated onto the abdominal wall, in good agreement with the macroscopic observations. An inflammatory response was observed at the *peri*-implanted area presenting fibroplasia and infiltration of diverse cell types (lymphocytes, heterophilic granulocytes, macrophages and solitary multinucleated giant cells) indicating a tissue reaction upon BNC. In a similar work, oxidized and laser-perforated BNC was employed in experimental surgery using a rabbit model.⁴⁰ One week after subcutaneous suture-free BNC implantation on the animal's back a positive integration of the BNC implants with the surrounding tissues was reported following our observations. Interestingly, Lai and co-workers stated a very low inflammatory response contrasting with the here presented histological analysis. Possibly, the distinct tissue responses arise from the different experimental protocols used (*i.e.* implantation site, use of sutures and longer implantation time, in our case) or the modifications of BNC. On the other hand, the previously cited work from Rauchfuß and colleagues²⁶ describes an inflammatory infiltration on the BNC patches judged to be of minimal clinical significance. We endorse that it could also apply to our *in vivo* study based on the witnessed lack of systemic toxicity. Besides, the good integration of the BNC implants – which were only indistinctly noticeable on the surrounding tissue – strengthens this reasoning. Nevertheless, the heterogeneous responses of the host immune system towards BNC implants indicate a need for future work.

Finally, the observation that a single layer of BNC could be sufficient to achieve low adhesions rates further emphasizes the attractiveness of BNC composites. Since a strong mechanical resistance is required for hernioplasty, composite BNC

patches (either as multilayers or in combination with PP meshes) should be the mainstay of our future work.

5. Conclusions

In summary, BNC was investigated as a biomaterial for soft tissue reinforcement applications to tackle the long-lasting challenge of reducing adhesions between implants and internal organs after hernia surgery. While single-layer BNC does not present favourable mechanical properties, BNC laminates with 2 or 3 films are resistant enough to reach the minimal acceptance criteria for abdominal wall reinforcement applications. Notably, this simple stacking methodology supported the integration of commercial PP meshes between the BNC sheets opening future perspectives on BNC-PP hybrid biomaterials. Finally, an *in vivo* study revealed that BNC exhibits favourable surgical features in terms of suturability, manageability and accommodation to the implantation site. Besides, mild adhesion scores involving low percentages of the implant's area together with excellent integration capability on the *peri*-implant zone could be demonstrated. BNC elicited an inflammatory response that needs to be further investigated. Overall, our work proves that bio-based BNC possesses attractive mechanical and anti-adherent properties that could be valuable in the development of innovative hernia repair solutions.

Ethical statement

All animal procedures were performed according to Good Laboratory Guidelines and were carried out in accordance with the guidelines of EN ISO/IEC 17025 and European guidelines 93/42/EWG and 90/385/EWG as accredited by the national accreditation body of Germany (DAkkS, accreditation scope of records: D-PL-20600-01-00).

Author contributions

Irene Anton-Sales: conceptualization, methodology, validation, formal analysis, writing – original draft. Soledad Roig-Sanchez: conceptualization, methodology, validation, formal analysis, writing – original draft. Kamelia Traeger: methodology, validation, writing – review & editing. Christine Weis: conceptualization, resources, project administration, supervision, writing – review & editing. Anna Laromaine: conceptualization, funding acquisition, supervision, writing – review & editing. Pau Turon: conceptualization, resources, supervision, writing – review & editing. Anna Roig: conceptualization, project administration, funding acquisition, supervision, writing – review & editing.

Conflicts of interest

There are no conflicts to declare.



Acknowledgements

Authors acknowledge financial support from the Spanish Ministry of Science and Innovation through the RTI2018-096273-B-I00 project, the 'Severo Ochoa' Programme for Centres of Excellence in R&D (CEX2019-000917-S) and the Generalitat de Catalunya 2017SGR765 grant. Authors are also grateful for the PhD scholarships of I. A-S. (BE-2017-076734) and S. R-S. (BES-2016-077533) and the 2019LLAV00046 project. The ICMAB members participate in the CSIC Interdisciplinary Platform for Sustainable Plastics towards a Circular Economy, SUSPLAST, and in the Aerogels COST ACTION (CA 18125). This work has been performed within the framework of the doctoral program in materials science of UAB (I. A-S. and S. R-S.). We acknowledge the support by the CSIC Open Access Publication Support Initiative through its Unit of Information Resources for Research (URICI) to cover the publication fee.

References

- 1 A. S. Kashyap, K. P. Anand and S. Kashyap, Inguinal and incisional hernias, *Lancet*, 2004, **363**(9402), 84.
- 2 R. Bittner, M. E. Arregui, T. Bisgaard, M. Dudai, G. S. Ferzli, R. J. Fitzgibbons, *et al.*, Guidelines for laparoscopic (TAPP) and endoscopic (TEP) treatment of inguinal hernia, *Surg. Endosc.*, 2011, **25**(9), 2773–2843.
- 3 F. Köckerling, R. Bittner, D. Adolf, R. Fortelny, H. Niebuhr, F. Mayer, *et al.*, Seroma following transabdominal preperitoneal patch plasty (TAPP): incidence, risk factors, and preventive measures, *Surg. Endosc.*, 2018, **32**(5), 2222–2231.
- 4 S. Muller, T. Langø, R. Brekken and B. Ystgaard, Degree of Adhesions After Repair of Incisional Hernia, *J. Soc. Laparoendosc. Surg.*, 2010, **14**, 399–404.
- 5 E. Chelala, Y. Debardemaeker, B. Elias, F. Charara, M. Dessily and J. L. Allé, Eighty-five redo surgeries after 733 laparoscopic treatments for ventral and incisional hernia: Adhesion and recurrence analysis, *Hernia*, 2010, **14**(2), 123–129.
- 6 M. Mirjavan and A. Asayesh, Asgharian Jeddi AA. The effect of fabric structure on the mechanical properties of warp knitted surgical mesh for hernia repair, *J. Mech. Behav. Biomed. Mater.*, 2017, **66**, 77–86.
- 7 C. Hollinsky, T. Kolbe, I. Walter, A. Joachim, S. Sandberg, T. Koch, *et al.*, Tensile strength and adhesion formation of mesh fixation systems used in laparoscopic incisional hernia repair, *Surg. Endosc.*, 2010, **24**(6), 1318–1324.
- 8 S. Lanzalaco, L. J. del Valle, P. Turon, C. Weis, F. Estrany, C. Alemán, *et al.*, Polypropylene mesh for hernia repair with controllable cell adhesion/de-adhesion properties, *J. Mater. Chem. B*, 2020, **8**(5), 1049–1059.
- 9 P. J. Emans, M. H. F. Schreinemacher, M. J. J. Gijbels, G. L. Beets, J. W. M. Greve, L. H. Koole, *et al.*, Polypropylene meshes to prevent abdominal herniation. Can stable coatings prevent adhesions in the long term?, *Ann. Biomed. Eng.*, 2009, **37**(2), 410–418.
- 10 S. Lanzalaco, P. Turon, C. Weis, C. Mata, E. Planas, C. Alemán, *et al.*, Toward the New Generation of Surgical Meshes with 4D Response: Soft, Dynamic, and Adaptable, *Adv. Funct. Mater.*, 2020, **2004145**, 1–9.
- 11 N. Udpa, S. R. Iyer, R. Rajoria, K. E. Breyer, H. Valentine, B. Singh, *et al.*, Effects of Chitosan Coatings on Polypropylene Mesh for Implantation in a Rat Abdominal Wall Model, *Tissue Eng., Part A*, 2013, **19**(23), 2713–2723.
- 12 F. Pomilio Di Loreto, A. Mangione, E. Palmisano, J. I. Cerda, M. J. Dominguez, G. Ponce, *et al.*, Dried human amniotic membrane as an antiadherent layer for intraperitoneal placing of polypropylene mesh in rats, *Surg. Endosc.*, 2013, **27**(4), 1435–1440.
- 13 F. Basile, A. Biondi and M. Donati, Surgical approach to abdominal wall defects: History and new trends, *Int. J. Surg.*, 2013, **11**(S1), S20–S23.
- 14 I. Anton-Sales, U. Beekmann, A. Laromaine, A. Roig and D. Kralisch, Opportunities of Bacterial Cellulose to Treat Epithelial Tissues, *Curr. Drug Targets*, 2019, **20**(8), 808–822.
- 15 M. Zeng, A. Laromaine and A. Roig, Bacterial cellulose films: influence of bacterial strain and drying route on film properties, *Cellulose*, 2014, **21**(6), 4455–4469.
- 16 S. Wang, F. Jiang, X. Xu, Y. Kuang, K. Fu, E. Hitz, *et al.*, Super-Strong, Super-Stiff Macrofibers with Aligned, Long Bacterial Cellulose Nanofibers, *Adv. Mater.*, 2017, **29**(35), 1702498.
- 17 S. Q. Chen, P. Lopez-Sanchez, D. Wang, D. Mikkelsen and M. J. Gidley, Mechanical properties of bacterial cellulose synthesised by diverse strains of the genus *Komagataeibacter*, *Food Hydrocolloids*, 2018, **81**, 87–95.
- 18 H. Ullah, F. Wahid, H. A. Santos and T. Khan, Advances in biomedical and pharmaceutical applications of functional bacterial cellulose-based nanocomposites, *Carbohydr. Polym.*, 2016, **150**, 330–352.
- 19 D. Klemm, E. D. Cranston, D. Fischer, M. Gama, S. A. Kedzior, D. Kralisch, *et al.*, Nanocellulose as a natural source for groundbreaking applications in materials science: Today's state, *Mater. Today*, 2018, **21**(7), 720–748.
- 20 L. Bacakova, J. Pajorova, M. Bacakova, A. Skogberg, P. Kallio, K. Kolarova, *et al.*, Versatile Application of Nanocellulose: From Industry to Skin Tissue Engineering and Wound Healing, *Nanomaterials*, 2019, **9**(2), 164.
- 21 F. M. Lima, F. C. M. Pinto, B. L. Andrade-da-Costa, J. G. Silva, O. Campos Júnior and J. L. Aguiar, Biocompatible bacterial cellulose membrane in dural defect repair of rat, *J. Mater. Sci.: Mater. Med.*, 2017, **28**(37).
- 22 F. C. A. Silveira, F. C. M. Pinto, S. Caldas Neto Sda, M. de C. Leal, J. Cesário and J. L. Aguiar, Treatment of tympanic membrane perforation using bacterial cellulose: a randomized controlled trial, *Braz. J. Otorhinolaryngol.*, 2016, **82**(2), 203–208.
- 23 F. Robotti, I. Sterner, S. Botta, J. M. Monné Rodríguez, G. Pellegrini, T. Schmidt, *et al.*, Microengineered biosynthesized cellulose as anti-fibrotic in vivo protection for cardiac implantable electronic devices, *Biomaterials*, 2020, **229**, 119583.
- 24 K. Ludwicka, M. Kolodziejczyk, E. Gendaszewska-Darmach, M. Chrzanowski, M. Jedrzejczak-Krzepkowska, P. Rytczak,



- et al.*, Stable composite of bacterial nanocellulose and perforated polypropylene mesh for biomedical applications, *J. Biomed. Mater. Res., Part B*, 2019, **107**(4), 978–987.
- 25 A. N. Zharikov, V. G. Lubyansky, E. K. Gladysheva, E. A. Skiba, V. Budaeva, E. N. Semyonova, *et al.*, Early morphological changes in tissues when replacing abdominal wall defects by bacterial nanocellulose in experimental trials, *J. Mater. Sci. Mater. Med.*, 2018, **29**(7).
 - 26 F. Rauchfuß, J. Helble, J. Bruns, O. Dirsch, U. Dahmen, M. Ardelt, *et al.*, Biocellulose for incisional hernia repair—an experimental pilot study, *Nanomaterials*, 2019, **9**(2), 1–11.
 - 27 S. Roig-Sanchez, E. Jungstedt, I. Anton-Sales, D. C. Malaspina, J. Faraudo, L. A. Berglund, *et al.*, Nanocellulose films with multiple functional nanoparticles in confined spatial distribution, *Nanoscale Horiz.*, 2019, **4**, 634–641.
 - 28 J. C. Y. Chan, K. Burugapalli, Y. S. Huang, J. L. Kelly and A. Pandit, A clinically relevant in vivo model for the assessment of scaffold efficacy in abdominal wall reconstruction, *J. Tissue Eng.*, 2017, **8**, 1–11.
 - 29 G. S. DiZerega and J. D. Campeau, Peritoneal repair and post-surgical adhesion formation, *Hum. Reprod. Update*, 2001, **7**(6), 547–555.
 - 30 R. A. Lang, P. M. Grüntzig, C. Weisgerber, C. Weis, E. K. Odermatt and M. H. Kirschner, Polyvinyl alcohol gel prevents abdominal adhesion formation in a rabbit model, *Fertil Steril*, 2007, **88**(4 suppl.), 1180–1186.
 - 31 H. Kataria and V. P. Singh, Liquid Paraffin vs Hyaluronic Acid in Preventing Intraperitoneal Adhesions, *Indian J. Surg.*, 2017, **79**(6), 539–543.
 - 32 J. F. Kukleta, C. Freytag and M. Weber, Efficiency and safety of mesh fixation in laparoscopic inguinal hernia repair using n-butyl cyanoacrylate: Long-term biocompatibility in over 1, 300 mesh fixations, *Hernia*, 2012, **16**(2), 153–162.
 - 33 M. E. El-Naggar, S. I. Othman, A. A. Allam and O. M. Morsy, Synthesis, drying process and medical application of polysaccharide-based aerogels, *Int. J. Biol. Macromol.*, 2020, **145**, 1115–1128.
 - 34 U. Klinge, B. Klosterhalfen, J. Conze, W. Limberg, B. Obolenski, A. P. Öttinger, *et al.*, Modified mesh for hernia repair that is adapted to the physiology of the abdominal wall, *Eur. J. Surg.*, 1998, **164**(12), 951–960.
 - 35 D. Kralisch, N. Hessler, D. Klemm, R. Erdmann and W. Schmidt, White biotechnology for cellulose manufacturing—the HoLiR concept, *Biotechnol. Bioeng.*, 2010, **105**(4), 740–747.
 - 36 U. Beekmann, L. Schmölz, S. Lorkowski, O. Werz, J. Thamm, D. Fischer, *et al.*, Process control and scale-up of modified bacterial cellulose production for tailor-made anti-inflammatory drug delivery systems, *Carbohydr. Polym.*, 2020, 116062.
 - 37 I. Anton-Sales, J. C. D'Antin, J. Fernández-Engroba, V. Charoenrook, A. Laromaine, A. Roig, *et al.*, Bacterial nanocellulose as a corneal bandage material: A comparison with amniotic membrane, *Biomater. Sci.*, 2020, **8**(10), 2921–2930.
 - 38 R. Jain and S. Wairkar, Recent developments and clinical applications of surgical glues: An overview, *Int. J. Biol. Macromol.*, 2019, **137**, 95–106.
 - 39 I. Anton-Sales, S. Roig-Sanchez, M. J. Sánchez-Guisado, A. Laromaine and A. Roig, Bacterial nanocellulose and titania hybrids: cytocompatible and cryopreservable cell carriers, *ACS Biomater. Sci. Eng.*, 2020, **6**(9), 4893–4902.
 - 40 C. Lai, K. S. Hu, Q. L. Wang, L. Y. Sheng, S. J. Zhang and Y. Zhang, Anti-Adhesion Mesh for Hernia Repair Based on Modified Bacterial Cellulose, *Starch/Staerke*, 2018, **70**(11–12), 1–10.



